

CRANFIELD UNIVERSITY

SCHOOL OF AEROSPACE, TRANSPORT and MANUFACTURING

PhD THESIS

Academic Year 2015 - 2018

Chana GOLDBERG

Techno-economic, Environment and Risk Analysis of an Aircraft  
Concept with Turbo-electric Distributed Propulsion

Supervisor: DR. Devaiah NALIANDA  
DECEMBER 2017

This thesis is submitted in partial fulfilment of the requirements for  
the degree of Doctor of Philosophy

© Cranfield University 2018. All rights reserved. No part of this  
publication may be reproduced without the written permission of the  
copyright owner.



## Executive Summary

The commercial aviation industry has always been driven by the need to grow and increase profitability. This has led to the evolution of aircraft from the early jets capable of carrying tens of passengers to current large airliners capable of carrying hundreds of passengers across the globe. Whilst these aircraft look superficially similar to their predecessors, they are significantly more efficient, thanks to the continuous evolution of technology. However, new aircraft are bound to increasingly stricter targets that aim to develop an environmentally sustainable industry for the future. Previous technological development has largely focused on reducing fuel consumption through iterative improvements. However, new emissions and noise targets have been set that necessitate dramatic leaps in technology. To achieve these goals, revolutionary technologies are the subject of research in the aerospace sector.

Research focus predominantly focuses on proving the technological viability of these novel concepts. The aim is generally to ensure that concepts are feasible and capable of meeting performance targets. However, commercial aviation is a profit-oriented industry. It is therefore vital to ensure that concepts are economically as well as environmentally sustainable. This form of study is more rarely seen but is vital in ensuring that aviation remains both environmentally and economically sustainable. This research presents the development of a techno-economic and environmental risk assessment (TERA) framework that combines the performance and economic aspects of an aircraft in order to inform a conclusion as to the aircraft's viability. The methodology addresses two key questions. How can an operator differentiate competing concepts when they are designed for similar performance targets? How can the economic viability of a novel aircraft concept be predicted when there is no historical data on which cost estimates can be based?

The research focuses on a case study of NASA's N3-X, a blended wing body aircraft concept with a turbo-electric distributed propulsion system and boundary layer ingestion. In order to quantify economic viability, it was first necessary to identify the performance benefits offered by the novel aircraft configuration. Modelling methodologies were therefore developed to simulate novel propulsion systems that utilise boundary layer ingestion and distributed propulsion. In particular, a methodology was developed to address a gap in literature with respect to simulating the off-design performance of such propulsion systems.

Performance simulation demonstrates that the aircraft is able to meet the 60% fuel saving target versus the baseline aircraft for the design mission. The high fuel saving of the N3-X in comparison to the baseline aircraft has the potential to provide direct operating cost saving of up to 21% versus the baseline aircraft. This enables the manufacturer to offer the aircraft at a higher acquisition price, whilst retaining an attractive product for customers. Economic viability of the aircraft is more limited for short haul mission ranges, as fuel is a less dominant factor for the aircraft's direct operating cost. Acquisition cost estimation suggests that the aircraft could achieve the cost target for an economically viable aircraft. This cost estimate is associated with a reasonable number of aircraft sales that could feasibly be supported by the future aircraft market for large widebodies. However, viability is closely tied to the economic environment, especially factors such as the current fuel price or environmental taxation levels. In particular, low fuel price reduces the financial value of high efficiency technology, and hence the maximum economical viable price of the aircraft is lower.

The research also performs a design space exploration for the case study aircraft. This included the assessment of liquid hydrogen as an alternative to conventional kerosene and the exploration of alternative configurations for the propulsion system. As the final stage of the TERA analysis of the aircraft, a risk assessment was also performed to identify those technologies and factors that may have the greatest influence over the aircraft's viability.

The methods developed in this research open up a wide range of activities for further work in both the performance and techno-economic aspects of the research. Further design space exploration is possible, particularly with respect to the propulsion system design. In addition, the TERA framework may be used to assess alternative novel aircraft concepts to identify aircraft and technology combinations that may benefit most from further investment.

## **Acknowledgements**

Work of this scale cannot take place in isolation. There are countless people who are owed thanks for the part they have played during the course of this research, be it feedback following presentations, technical discussions, or providing support and understanding over the past three years. Whilst I will call out a few here, there are numerous others who played some part.

First and foremost, a big thank you is owed to my supervisor, Dr. Devaiah Nalianda. From when this project started in the Thermal Power MSc and throughout the duration of my PhD, the support has been invaluable. I have genuinely appreciated being given the chance to conduct this research and the countless other opportunities, small and large, over the past three years. This research would not have been possible without the many discussions we have had.

This research owes a debt of gratitude to NASA for providing the opportunity to conduct the study as part of NASA Grant NNX13AI78G. In particular, many thanks to Mr. James Felder and Dr. Rubén del Rosario from NASA Glenn Research Center and Dr. Nateri Madavan from NASA Ames Research Center. It was a pleasure to have the chance to meet and have discussions with you and others during the course of the research grant. I would also like to thank the Principal Investigator for the grant, Prof. Riti Singh, for his valuable insights.

Many thanks to other staff members at Cranfield University. for the valuable assistance provided over the course of the research: Dr. Panos Laskaridis for the assistance and opportunities in the Hybrid Electric Propulsion group, Dr. David MacManus for valuable feedback, Dr. Theoklis Nikolaidis for advice on Turbomatch, Prof. Periclis Pilidis for the opportunities provided over the course of my PhD, and Dr. Bobby Sethi. Many thanks also to Mr. Darrell Williams for the valuable discussion and advice during the development of the method for modelling a BLI propulsion system.

Whilst I may not have been around very often, thanks are also owed to my fellow PhD students. It was always nice to catch up whenever I was in university.

Last but certainly not least, a big thanks to my parents and siblings for their endless support and understanding over the past three years.



# Contents

<b>Executive Summary</b>	<b>i</b>
<b>Acknowledgements</b>	<b>iii</b>
<b>Table of Contents</b>	<b>vii</b>
<b>List of Figures</b>	<b>xiii</b>
<b>List of Tables</b>	<b>xv</b>
<b>Abbreviations</b>	<b>xvi</b>
<b>Symbols</b>	<b>xviii</b>
<b>1 Introduction</b>	<b>1</b>
<b>2 Literature Review</b>	<b>3</b>
2.1 Growth and Development in the Aviation Industry . . . . .	3
2.2 Technology Research for High Efficiency Aircraft . . . . .	6
2.2.1 Boundary Layer Ingestion . . . . .	7
2.2.2 Distributed, Turbo-electric, Electric, and Hybrid Propulsion . . . . .	9
2.2.3 Electrical Systems and Superconductivity . . . . .	13
2.2.4 Blended Wing Bodies . . . . .	15
2.3 Alternative Aviation Fuels . . . . .	16
2.4 Techno-economic Analysis . . . . .	18
2.5 Emerging Markets in Aerospace . . . . .	21
2.6 Work Scope . . . . .	23
2.7 Contributions from the Research . . . . .	24
<b>3 Propulsion System Modelling</b>	<b>27</b>
3.1 Boundary Layer Ingestion . . . . .	27
3.1.1 Performance Benefits from BLI . . . . .	30
3.1.2 Thrust and Drag Accounting . . . . .	33
3.1.3 Boundary Layer Flow Characteristics . . . . .	35
3.1.4 Inlet Flow Characteristics for a BLI System . . . . .	37
3.1.5 Design Point Sizing . . . . .	39
3.1.6 Off-Design Extension . . . . .	43
3.1.7 Intake Duct Total Pressure Loss . . . . .	47
3.1.8 Fan/Compressor Efficiency . . . . .	48
3.1.9 Representing the Efficiency of a BLI System . . . . .	48
3.2 N3-X Propulsion System Simulation Methodology . . . . .	50
3.2.1 N3-X Propulsion System Definition . . . . .	50

3.2.2	Main Engines . . . . .	51
3.2.3	Propulsor Array and Propulsors . . . . .	53
3.2.4	Combined Propulsion System . . . . .	54
3.2.5	BLI Model Validation . . . . .	55
3.3	Propulsor Array Design Variables . . . . .	56
3.3.1	Individual Propulsor Design . . . . .	57
3.3.2	Boundary layer-related Losses . . . . .	58
3.3.3	Propulsor Location . . . . .	60
3.3.4	Whole Array Design . . . . .	62
3.4	Weight Estimation . . . . .	65
3.4.1	Turbomachinery . . . . .	65
3.4.2	Superconducting Electrical System . . . . .	65
3.5	Baseline Propulsion System . . . . .	66
3.5.1	Final Design Conclusions . . . . .	67
3.6	Propulsor Array Performance . . . . .	69
3.6.1	Individual Propulsors . . . . .	69
3.6.2	Whole Array . . . . .	71
<b>4</b>	<b>Aircraft Modelling</b>	<b>76</b>
4.1	Aircraft Performance Model Development . . . . .	77
4.1.1	Aircraft Drag . . . . .	77
4.1.2	Propulsion System Thrust . . . . .	83
4.1.3	Mission Performance . . . . .	84
4.2	Liquid Hydrogen Implementation . . . . .	89
4.2.1	Liquid Hydrogen Tank Requirements . . . . .	90
4.2.2	Tank Configuration . . . . .	92
4.2.3	Mechanical Sizing . . . . .	92
4.2.4	Thermal Sizing . . . . .	93
4.2.5	Tank Liner . . . . .	95
4.3	Liquid Hydrogen Tank Sizing Results . . . . .	95
4.3.1	Tank Boil-off . . . . .	96
4.3.2	Tank Dimensions . . . . .	96
4.3.3	Tanks for the N3-X . . . . .	97
4.4	Aircraft Case Study Definition . . . . .	99
4.4.1	Baseline Aircraft . . . . .	100
4.4.2	N3-X . . . . .	100
4.5	Maximum Take-off Weight Estimates . . . . .	102
4.6	Performance Model Validation . . . . .	105
4.7	Aircraft Performance Results . . . . .	107
4.7.1	Payload Range Assessment . . . . .	108
4.7.2	Mission Performance . . . . .	109
4.7.3	Cruise-climb . . . . .	112
<b>5</b>	<b>Alternative Propulsion System Configurations</b>	<b>116</b>
5.1	Array Configurations . . . . .	117
5.1.1	Thrust Split . . . . .	117
5.1.2	Boundary-Layer Only . . . . .	121
5.2	Propulsion System Optimisation . . . . .	126
5.2.1	Array Fan Pressure Ratio . . . . .	128



5.2.2	Array Weight . . . . .	129
5.2.3	Optimisation for Fuel . . . . .	131
5.2.4	Combining Propulsion System Options . . . . .	132
5.3	Alternative LH <sub>2</sub> Aircraft Configurations . . . . .	133
5.3.1	Resized Propulsion System . . . . .	134
5.3.2	Extended Payload Capacity . . . . .	136
5.3.3	Removable Tanks . . . . .	137
5.3.4	Dual Fuel . . . . .	138
5.4	Alternative Integration Architectures . . . . .	140
<b>6</b>	<b>Cost and Techno-economic Modelling</b>	<b>144</b>
6.1	Operating Cost in a Novel Aircraft . . . . .	145
6.2	Direct Operating Cost . . . . .	146
6.3	Investment Cost Analysis . . . . .	147
6.4	Acquisition Cost Estimation . . . . .	152
6.4.1	Cost Model Classification . . . . .	153
6.4.2	Airframe Acquisition Cost Model Selection . . . . .	157
6.4.3	Engine Acquisition Cost Model Selection . . . . .	160
6.4.4	Cost Model Validation . . . . .	162
6.5	Maintenance Cost Estimation . . . . .	166
6.5.1	Maintenance Cost Model Selection . . . . .	169
6.5.2	Maintenance Cost Model Validation . . . . .	172
6.6	Application to the N3-X . . . . .	174
6.6.1	Acquisition Price . . . . .	174
6.6.2	Maintenance Cost . . . . .	175
<b>7</b>	<b>Techno-economic Analysis</b>	<b>177</b>
7.1	Direct Operating Cost . . . . .	178
7.2	Investment Cost Analysis . . . . .	182
7.2.1	Alternative Scenarios . . . . .	184
7.2.2	Average Aircraft Mission . . . . .	188
7.2.3	Yearly DOC Variation . . . . .	189
7.3	Aircraft Price & Market . . . . .	193
<b>8</b>	<b>Technology Roadmap and Risk Assessment</b>	<b>196</b>
8.1	Overview of Possible Risk Factors . . . . .	197
8.1.1	Airframe Performance and Operating Empty Weight . . . . .	199
8.1.2	Airframe Material Composition . . . . .	200
8.1.3	Aircraft Internal Configuration and Compatibility . . . . .	201
8.1.4	Superconducting Propulsion System . . . . .	201
8.1.5	Electrical System Architecture & Safety . . . . .	202
8.1.6	Engine Intake Total Pressure Recovery . . . . .	202
8.1.7	Propulsor Array Design and Location . . . . .	203
8.1.8	Boundary Layer Distortion . . . . .	203
8.1.9	Safety Factors . . . . .	204
8.2	SWOT Analysis . . . . .	205
<b>9</b>	<b>Conclusions</b>	<b>211</b>
<b>10</b>	<b>Further Work</b>	<b>214</b>

<b>11 Publications</b>	<b>220</b>
<b>Bibliography</b>	<b>221</b>
<b>Appendices</b>	<b>235</b>
<b>A Related Research</b>	<b>236</b>
A.1 Liquid Hydrogen Tank Sizing . . . . .	236
A.2 Leasing Model . . . . .	237
A.3 CFD Analysis of the N3-X Airframe . . . . .	240
A.3.1 Boundary Layer and Velocity Profile Assumptions . . . . .	241
<b>B BLI Simulation Method</b>	<b>246</b>
<b>C Flow Profile over the N3-X</b>	<b>248</b>
<b>D Atmospheric Properties</b>	<b>250</b>
<b>E Acquisition Cost Models</b>	<b>251</b>
E.1 Airframe . . . . .	251
E.2 Engine . . . . .	255
E.2.1 Birkler <i>et al.</i> . . . . .	255
E.2.2 Younossi <i>et al.</i> . . . . .	255
E.2.3 Regression Model . . . . .	256
<b>F Maintenance Cost Models</b>	<b>258</b>
F.1 Airframe . . . . .	258
F.2 Engine . . . . .	259

# List of Figures

2.1	Growth in the commercial aviation passenger market over time . . . . .	3
2.2	Influence of jet fuel price on airline profits . . . . .	4
2.3	Industry measures for reducing global aviation CO <sub>2</sub> emissions . . . . .	5
2.4	Representation of boundary layer ingestion in comparison to a free-stream propulsion system . . . . .	8
2.5	Cruise thermodynamic and propulsive efficiencies for a simple cycle gas turbine engine with projections of potential maximum efficiency . . . . .	10
2.6	Example turbo-, hybrid-, or all-electric propulsion system architectures . . . . .	12
2.7	Electric machine power levels required for different aircraft classes . . . . .	14
2.8	The double bubble fuselage planform . . . . .	15
2.9	Main market groupings for the commercial passenger aircraft market with future concepts marked . . . . .	21
2.10	Hub and spoke versus point to point airline network . . . . .	22
2.11	The N3-X . . . . .	23
2.12	Research phases . . . . .	25
3.1	Example cases comparing conventional and boundary layer ingesting propulsion systems . . . . .	29
3.2	Simple propulsor performance calculations . . . . .	30
3.3	Boundary layer ingestion with an added plate versus fuselage boundary layer . . . . .	32
3.4	Comparison sketch of two propulsion system control volumes for a BLI propulsion system . . . . .	34
3.5	Propulsion system control volume and station definition. . . . .	35
3.6	BLI propulsor simulation method at design point . . . . .	40
3.7	Propulsor performance flowchart . . . . .	41
3.8	Nacelle sizing flowchart to provide an estimate of nacelle dimensions, NACA-1 forebody and circular arc afterbody, with assumptions . . . . .	42
3.9	Definition of key intake areas . . . . .	43
3.10	Generic scaled fan/compressor map with peak efficiency running line . . . . .	44
3.11	BLI propulsor simulation method at off-design . . . . .	46
3.12	Boundary layer function for inlet total pressure loss . . . . .	48
3.13	N3-X airframe Mach number profile and BL thickness. . . . .	51
3.14	Representative general engine configurations for the N3-X main engine . . . . .	53
3.15	Simulation procedure for N3-X propulsion system operating modes . . . . .	55
3.16	Validation of stream flow characteristics against NASA data . . . . .	56
3.17	Validation of BLI propulsor inlet height against NASA data . . . . .	56
3.18	Design charts for a propulsor at M0.84 and 30,000 ft. . . . .	57
3.19	Influence of efficiency loss on specific power consumption for a propulsor on the N3-X airframe centreline at M0.84 and 30,000 ft (neglecting nacelle drag). . . . .	59
3.20	Influence of efficiency loss on power saving coefficient for a propulsor on the N3-X airframe centreline at M0.84 and 30,000 ft (neglecting nacelle drag). . . . .	59

3.21	Inlet total pressure recovery as a function of $h/\delta$ (CAR = 0.8)	60
3.22	Propulsor specific power consumption as a function of distance from the airframe centreline	61
3.23	Propulsor intake total pressure recovery using Seddon's method	61
3.24	Influence of span-wise flow characteristic variation on power requirement of an array with 15 fans at M0.84 and 30,000 ft (neglecting nacelle drag)	63
3.25	Sketch indicating propulsor array size and local flow conditions for a 15 fan array with fan pressure ratio of 1.3 and length of 20.1 m	63
3.26	Influence of fan pressure ratio on individual performance of propulsors in an array (20.1 m array, neglecting nacelle drag)	63
3.27	Influence of array length on power requirement of an array with 15 fans at M0.84 and 30,000 ft (neglecting nacelle drag)	64
3.28	Weight of superconducting equipment as a function of power	66
3.29	ADP performance of propulsors at the centreline and end of the propulsor array as a function of rotational speed	70
3.30	Sea level static performance of propulsors at the centreline and end of the propulsor array as a function of rotational speed	71
3.31	Performance of propulsors at the centreline and end of the propulsor array at 30,000ft as a function of Mach number	72
3.32	Mass flow-average total pressure and velocity of inlet stream as a function of mass flow ratio (85% chord)	72
3.33	Power deficit in MW between propulsor array and main engines at ADP power setting as a function of altitude and Mach number	74
3.34	Propulsor array performance as a function of altitude and Mach number at 100% rotational speed	75
3.35	Propulsion system performance as a function of altitude and Mach number (ADP engine power setting: TET = 1811 K)	75
3.36	Propulsion system performance as a function of altitude and Mach number (Array capped at 100% design rotational speed, ADP engine power setting until propulsor array speed cap)	75
4.1	Mission segments in the aircraft performance model	77
4.2	Simplified planforms for a tube and wing and blended wing body airframe	78
4.3	Aerodynamic equivalent planform for a blended wing body	81
4.4	Simplified approximation for the wave drag coefficient	82
4.5	Correlations for $M_{DD0}$ and $LF_{DD}$	82
4.6	Take-off segments	85
4.7	Forces on an aircraft during steady climb and descent	87
4.8	Landing segments	88
4.9	LH <sub>2</sub> tube-and-wing aircraft concepts from previous research	90
4.10	Liquid hydrogen tank structure	92
4.11	Heat transfer through tank insulation layer	94
4.12	Iterative process to solve for the required LH <sub>2</sub> tank insulation thickness	95
4.13	Influence of insulation thickness on insulation weight and boil off rate (example tank with $r = 2\text{m}$ and $W = 5\text{m}$ )	96
4.14	Unit of LH <sub>2</sub> fuel carried per unit of tank mass for varying tank capacities	97
4.15	Breakdown of components of tank weight for a tank with a 2500 kg LH <sub>2</sub> capacity	98
4.16	Potential internal configuration for the N3-X showing locations for the passenger cabin and fuel tank hold	98

4.17	Diagram of tank dimensions for the larger N3-X liquid hydrogen tank . . . . .	99
4.18	Plan drawing of the B777-200LR . . . . .	100
4.19	Plan drawing of the N3-X . . . . .	103
4.20	Operating empty weight estimate for the baseline aircraft as a function of the ratio of operating empty weight to the maximum take-off weight . . . . .	105
4.21	Operating empty weight estimate for the N3-X as a function of the maximum take-off weight (using an assumed ratio of OEW/MTOW) . . . . .	105
4.22	Example payload-range chart . . . . .	106
4.23	Aircraft model validation using payload range chart data . . . . .	107
4.24	Flight duration for B777-200LR flights in three 24-hour periods . . . . .	107
4.25	Payload-range chart prediction for the baseline aircraft and N3-X . . . . .	109
4.26	Fuel burn of the baseline aircraft and N3-X variants up to the 7500 nautical mile design range (maximum payload) . . . . .	110
4.27	Aircraft energy-to-revenue-work ratio as a function of mission range (maximum payload) . . . . .	110
4.28	N3-X energy saving versus the baseline aircraft as a function of range with 60% savings target marked (maximum payload) . . . . .	111
4.29	N3-X energy saving versus the baseline aircraft as a function of payload with 60% savings target marked (Kerosene aircraft, 7500 nmi range) . . . . .	111
4.30	Aircraft energy-to-revenue-work ratio as a function of payload (7500 nmi range) . . . . .	111
4.31	N3-X performance as a function of operating empty weight (where OEW is a function of OEW/MTOW) . . . . .	113
4.32	N3-X lift to drag ratio as a function of altitude for varying values of fuel on board (maximum payload, 7500 nmi mission) . . . . .	114
4.33	N3-X lift to drag ratio as a function of aircraft weight at a fixed altitude of 35,000 ft . . . . .	114
4.34	Cruise climb comparison to fixed altitude cruise . . . . .	115
5.1	Specific fuel consumption as a function of thrust split and turbomachinery bypass ratio . . . . .	118
5.2	Bypass ratio influence over optimum thrust split and effective specific fuel consumption . . . . .	118
5.3	Effective specific fuel consumption as a function of thrust split and electrical transmission efficiency for a turbojet configuration . . . . .	119
5.4	Total propulsion system weight as a function of thrust split . . . . .	120
5.5	Fuel saving for a 7500 nmi mission as a function of thrust split . . . . .	120
5.6	Performance of an array sized to ingest the boundary layer only compared to a fixed thrust array (20.1 m array) . . . . .	123
5.7	Individual fan performance for an array sized to ingest the boundary layer only (20.1 m array) . . . . .	123
5.8	Effective specific fuel consumption for a fixed height array equal to boundary layer thickness . . . . .	125
5.9	Fuel saving versus the baseline configuration for a fixed height array equal to boundary layer thickness . . . . .	125
5.10	Optimum fan pressure ratio for individual fans and a 100% TS array in comparison to the baseline configuration and an optimum array fan pressure ratio configuration . . . . .	129
5.11	Influence of array fan pressure ratio on propulsion system weight . . . . .	130
5.12	Influence of array fan pressure ratio on mission fuel consumption for a 7500 nmi flight . . . . .	130

5.13	Pareto front of individual propulsor fan pressure ratio optimisation for minimum eSFC and array weight . . . . .	131
5.14	Pareto front of individual propulsor fan pressure ratio and fuel saving versus baseline N3-X configuration . . . . .	132
5.15	Fan pressure ratio for individual fans for a minimum fuel configuration in comparison to an eSFC minimum configuration . . . . .	133
5.16	Fan pressure ratio for individual fans for a minimum fuel configuration in comparison to minimum weight and minimum eSFC configuration from the pareto front . . . . .	133
5.17	Payload-range chart prediction for the extended payload LH <sub>2</sub> N3-X . . . . .	136
5.18	Aircraft energy-to-revenue-work ratio as a function . . . . .	137
5.19	Sketch of removable tank configurations for the LH <sub>2</sub> N3-X . . . . .	137
5.20	Energy to revenue work ratio for a removable LH <sub>2</sub> tank aircraft configuration . . . . .	138
5.21	Energy saving versus the baseline aircraft for a dual fuel N3-X variant in comparison to the baseline N3-X . . . . .	139
5.22	Energy to revenue work ratio for a dual fuel N3-X variant in comparison to LH <sub>2</sub> only and baseline N3-X (inapplicable ranges marked) . . . . .	140
5.23	Influence of nacelle drag and engine inlet total pressure loss on specific fuel consumption of the baseline N3-X configuration . . . . .	141
5.24	Representative sketch of embedded engine location and duct for the N3-X . . . . .	142
5.25	Fuel saving of the N3-I versus the baseline aircraft . . . . .	143
6.1	Sketch of operating costs for a novel aircraft . . . . .	145
6.2	Breakdown of direct operating cost model components for an aircraft ownership model . . . . .	148
6.3	Flight cycles per year for the Boeing 777-200LR . . . . .	151
6.4	Flowchart for direct operating cost sensitivity analysis . . . . .	151
6.5	Example output from the economic sensitivity analysis. . . . .	152
6.6	Aircraft list price versus operating empty weight . . . . .	154
6.7	Example learning curves for the manufacturing cost of an airframe . . . . .	158
6.8	Engine price correlation with thrust and weight . . . . .	160
6.9	Motor cost correlations for three commercial motor classes . . . . .	162
6.10	Cost model validation on the baseline aircraft, including standard error of estimate . . . . .	163
6.11	Cost model validation on the baseline aircraft's engines, including standard error of estimate . . . . .	164
6.12	Probability and cumulative distribution functions for the baseline aircraft cost estimate (normal distribution) . . . . .	164
6.13	Probability and cumulative distribution functions for the baseline aircraft cost estimate (lognormal distribution, $\text{Var}(X) = \sigma^2$ ) . . . . .	165
6.14	Probability and cumulative distribution functions for the baseline aircraft cost estimate (lognormal distribution, $\text{Var}(X) = 2\sigma^2$ ) . . . . .	165
6.15	Engine maintenance cost per flight hour as an engine ages . . . . .	167
6.16	Engine ageing and age factor . . . . .	167
6.17	Engine severity factor as a function of engine flight hours per flight cycle . . . . .	168
6.18	Airframe maintenance severity curve estimate for the baseline aircraft . . . . .	173
6.19	Engine maintenance severity curve estimate for the baseline aircraft . . . . .	173
6.20	Probability and cumulative distribution functions for the N3-X aircraft cost estimate (normal distribution) . . . . .	174
6.21	N3-X gas turbine engine cost estimates, including standard error of estimate . . . . .	175

6.22	Airframe maintenance severity curve estimate for the N3-X versus the baseline aircraft . . . . .	175
6.23	Engine maintenance severity curve estimate for the N3-X versus the baseline aircraft . . . . .	176
7.1	Direct operating cost comparison for the N3-X and baseline aircraft (assuming acquisition and maintenance equal to the baseline) . . . . .	179
7.2	Breakdown of direct operating cost components as a function of mission range .	179
7.3	Breakdown of direct operating cost components for the baseline aircraft as a function of payload (7500 nmi) . . . . .	180
7.4	Influence of historical fuel price changes on the fuel and direct operating cost estimates for a 7500 nmi mission (Fuel price data source: IndexMundi) . . . . .	181
7.5	Hydrogen fuel price for which LH <sub>2</sub> N3-X DOC is equal to DOC for the baseline aircraft and kerosene N3-X (7500 nmi mission) . . . . .	181
7.6	Direct operating cost sensitivity analysis for the kerosene N3-X in comparison to the baseline aircraft . . . . .	183
7.7	Direct operating cost sensitivity analysis for the kerosene N3-X in comparison to the baseline aircraft – Alternative fuel price scenarios (7500 nmi) . . . . .	185
7.8	Direct operating cost sensitivity analysis for the kerosene N3-X in comparison to the baseline aircraft – Carbon tax \$27/mt, Fuel price \$477.2/mt (7500 nmi) . . .	185
7.9	Direct operating cost sensitivity analysis for the kerosene N3-X in comparison to the baseline aircraft for the ‘average’ aircraft mission (5000 nmi, 90% max. payload) . . . . .	188
7.10	Sample fuel datasets over time . . . . .	191
7.11	Direct operating cost time snapshot for a rising fuel price scenario . . . . .	192
7.12	Direct operating cost time snapshot for a falling fuel price scenario . . . . .	192
7.13	Direct operating cost time snapshot for an increasing carbon tax scenario . . . .	193
7.14	N3-X acquisition price versus the baseline aircraft as a function of the number of aircraft in the first lot . . . . .	195
8.1	Key aircraft design factors with an influence over fuel consumption . . . . .	198
8.2	Key aircraft design factors with an influence over direct operating cost . . . . .	199
8.3	Influence of intake total pressure recovery in the BLI propulsors on SFC . . . . .	204
8.4	Strengths, weaknesses, opportunities & threats (SWOT) analysis matrix . . . . .	206
10.1	Approximate running line for a sample BLI propulsor with a fixed area nozzle . .	216
A.1	Example internal configuration layout for the N3-X . . . . .	237
A.2	Breakdown of direct operating cost model components for the leasing model . .	238
A.3	Net present value comparison of N3-X leasing and purchase options as a function of operating period for the design mission range . . . . .	239
A.4	Net present value comparison of N3-X leasing and purchase options as a function of range (19 year operating period) . . . . .	240
A.5	Mach contours over the N3-X nacelle with comparison to previous research by Kim & Liou . . . . .	241
A.6	CFD for different flight conditions and propulsors with approximate interface point	243
A.7	Comparison of CFD data displaying the Mach number over the N3-X fuselage versus N2A fuselage data (Flight Mach number 0.84) . . . . .	245
A.8	Mach number as a fraction of free-stream Mach number for each propulsor in the array . . . . .	245

A.9	Boundary layer profile comparison to data extracted from CFD analysis . . . . .	245
C.1	N2A centreline boundary layer and Mach number profiles . . . . .	248
C.2	N3-X airframe Mach number profile and BL thickness at centreline extracted from reference data . . . . .	249
C.3	Correction factor $k$ for the turbulent boundary layer equation . . . . .	249



# List of Tables

3.1	N3-X engine design parameters . . . . .	53
3.2	Performance parameters for individual fans in the baseline N3-X propulsor array at the aerodynamic design point . . . . .	67
3.3	Performance of the baseline N3-X propulsion system configuration . . . . .	68
3.4	Performance of the LH <sub>2</sub> variant propulsion system configuration . . . . .	68
3.5	Overall weight of the baseline propulsion system configuration . . . . .	69
4.1	Interference and form factors for profile drag calculation . . . . .	79
4.2	Heat transfer terms for cylinders and spheres . . . . .	94
4.3	Key design parameters for the N3-X LH <sub>2</sub> fuel tanks . . . . .	99
4.4	Key dimensions for the B777-200LR . . . . .	101
4.5	Key design and performance parameters for engine model approximating the configuration of the GE90-115B . . . . .	102
4.6	Key dimensions for the N3-X . . . . .	103
4.7	Aircraft model validation data for the B777-200LR . . . . .	106
4.8	Aircraft model validation data for the B777-200LR . . . . .	106
5.1	Performance of a sample thrust split propulsion system (Turbofan BPR = 4.0, Array FPR = 1.3) . . . . .	121
5.2	Overall weight of a thrust split propulsion system (Turbofan BPR = 4.0, Array FPR = 1.3) . . . . .	121
5.3	Performance parameters for individual fans in a propulsor array sized to equal the boundary layer thickness, FPR = 1.7, at the aerodynamic design point . . . . .	126
5.4	Performance of a propulsion system configuration with array sized to equal the boundary layer thickness (Turbofan BPR = 4.0, Array FPR = 1.7) . . . . .	127
5.5	Overall of a propulsion system configuration with array sized to equal the boundary layer (Turbofan BPR = 4.0, Array FPR = 1.7) . . . . .	127
5.6	Performance parameters for individual fans in the resized propulsor array at the aerodynamic design point for the LH <sub>2</sub> variant . . . . .	135
5.7	Performance of the resized propulsion system configuration for the LH <sub>2</sub> N3-X variant . . . . .	135
5.8	Overall weight of the baseline propulsion system configuration . . . . .	135
5.9	Fuel capacity and tank weight for removable tank configurations . . . . .	138
6.1	Example net present value analysis with a 10% discount factor and \$500 initial investment . . . . .	149
6.2	Aircraft unit cost estimates for the baseline aircraft (2017 US\$mil) . . . . .	163
6.3	Engine unit cost estimates for the baseline aircraft (2017 US\$mil) . . . . .	163
6.4	Inputs for the selected cost estimating relationships . . . . .	170

7.1	Example net present value analysis with a 10% discount factor, \$500 initial investment and changing yearly costs . . . . .	190
D.1	Atmosphere layers . . . . .	250
E.1	Labour rate and learning exponents for aircraft manufacturing and development cost . . . . .	253
E.2	Influence of material on cost components . . . . .	254
E.3	Factors, $S_m$ , for calculating the materials cost weighting factor . . . . .	254
E.4	Engine data for regression analysis . . . . .	257

# Abbreviations

<b>ADP</b>	Aerodynamic design point
<b>AF</b>	Ageing factor
<b>AR</b>	Aspect ratio
<b>BL</b>	Boundary layer
<b>BLC</b>	Boundary layer control
<b>BLI</b>	Boundary layer ingestion
<b>BWB</b>	Blended wing Body
<b>CDF</b>	Cumulative distribution function
<b>CAR</b>	Capture area ratio
<b>CER</b>	Cost estimating relationship
<b>DOC</b>	Direct operating cost
<b>EIS</b>	Entry into service
<b>EGT</b>	Exhaust gas temperature
<b>FC</b>	Flight cycles
<b>FH</b>	Flight hours
<b>FoS</b>	Factor of safety
<b>FPR</b>	Fan pressure ratio
<b>FS</b>	Free-stream
<b>IRR</b>	Internal rate of return
<b>KE</b>	Kinetic energy
<b>KEG</b>	Kinetic energy non-dimensional group
<b>LLP</b>	Life limited part
<b>LTO</b>	Landing and take-off
<b>MAG</b>	Mass flow non-dimensional group
<b>MFR</b>	Mass flow ratio
<b>MOG</b>	Momentum non-dimensional group
<b>MPCM</b>	Manufacturing process cost model
<b>mom</b>	Momentum
<b>NPF</b>	Net propulsive force
<b>NPV</b>	Net present value
<b>PCM</b>	Parametric cost model
<b>PDF</b>	Probability distribution function
<b>PSC</b>	Power saving coefficient
<b>RoC</b>	Rate of climb
<b>RTO</b>	Rolling take-off
<b>SF</b>	Severity factor
<b>SLS</b>	Sea-level static
<b>SWOT</b>	Strengths, weaknesses, opportunities & threats
<b>TRL</b>	Technology Readiness Level

**TS** Thrust Split  
**WACC** Weighted average cost of capital  
**WMCF** Weighted material cost factor

# Symbols

**Note:** By necessity, a number of symbols have multiple meanings. The context of the text will make clear which meaning is relevant.

$\gamma$	Specific heat capacity of air	-
$\gamma_c$	Climb angle	°
$\gamma_a$	Approach angle	°
$\delta$	Boundary layer thickness	m
$\delta^*$	Displacement thickness	m
$\Delta\%$	Percentage point change	-
$\varepsilon$	Emissivity of material	-
$\eta_{\text{inlet}}$	Intake efficiency	-
$\rho$	Density	kg/m <sup>3</sup>
$\tau_w$	Shear stress	N/m <sup>2</sup>
$\theta$	Momentum thickness	m
$\theta^*$	Energy thickness	m
$\lambda$	Taper ratio	-
$\lambda_{\text{fan}}$	Fan hub-to-tip ratio	-
$\Lambda$	Sweep	°
$\Lambda_{0.5c}$	Half-chord sweep	°
$\sigma$	Stefan-Boltzmann constant	kg/s <sup>3</sup> .K <sup>4</sup>
$\sigma_y$	Material yield strength	MPa
$A$	Area	m <sup>2</sup>
$b$	Learning exponent	-
$b$	Wing span	m
$c$	Chord length	m
$C$	Specific fuel consumption	g/kN.s
$C_{\text{CO}_2}$	Carbon tax	US\$/kg
$C_{\text{crew}}$	Yearly crew salary	US\$
$C_D$	Drag coefficient	-
$C_{D0}$	Profile drag coefficient	-
$C_{\text{depreciation}}$	Depreciation cost	US\$
$C_{Di}$	Lift induced drag coefficient	-
$C_{Dw}$	Transonic wave drag / parasitic drag coefficient	-
$C_{\text{fuel}}$	Fuel price	US\$/kg
$C_{\text{maint}/\text{FH}}$	Maintenance cost per flight hour	US\$/FH
$C_f$	Skin friction coefficient	-
$C_L$	Lift coefficient	-
$C_n$	Cash flow in year $n$	US\$

$C_p$	Specific heat of gas	J/kg.K
$d$	Distance	m
$D$	Drag	N
$D$	Diameter	m
$F_G$	Gross thrust	N
$F_N$	Net thrust	N
$g$	Gravitational acceleration	m/s <sup>2</sup>
$h$	Stream height above surface / stream thickness	m
$h$	Convection coefficient	W/m.K
$h_{fg}$	Latent heat of vaporisation	J/kg
$i$	Inflation rate	-
$K$	Thermal conductivity of material	W/m.K
$K_g$	Thermal conductivity of air	W/m.K
$L$	Length	m
$L$	Lift	N
$L_{array}$	Array total length	m
$\dot{m}$	Mass flow rate	kg/s
$M$	Mach number	-
$M_{CO_2}$	CO <sub>2</sub> emissions total	kg
$M_f$	Fuel mass	kg
$N_{fan}$	Number of fans/propulsors	-
$Nu$	Nusselt number	-
$p$	Static pressure	Pa
$P$	Total pressure	Pa
$P_{BLI}$	BLI propulsion system power	MW
$P_{ref}$	Reference propulsion system power	MW
$Pr$	Prandtl number	-
$q$	Dynamic pressure	Pa
$Q$	Heat	J
$Q_{cond}$	Heat conduction	J
$Q_{conv}$	Heat convection	J
$Q_{rad}$	Heat radiation	J
$r$	Discount factor	-
$r_d$	Rate of debt	-
$r_e$	Rate of equity	-
$R$	Range / distance	nmi or m
$R$	Specific gas constant for air	J/kg.K
$R_{ad}$	Rayleigh number	-
$R_e$	Reynolds number	-
$R_{th}$	Thermal resistance	Km/W
$S_{ref}$	Reference aerodynamic area	m <sup>2</sup>
$S_{wet}$	Wetted surface area	m <sup>2</sup>
$t$	Thickness	m
$t$	Static temperature	K
$T$	Total temperature	K
$u$	Axial velocity	m/s
$V$	Flight velocity	m/s
$V$	Volume	m <sup>3</sup>
$w$	Stream width	m

$W$	Weight	kg
$W$	Tank cylinder length	m
$y$	Vertical distance above aircraft surface	m
$x$	Chordwise distance from leading edge	m
$x_0$	Chordwise distance from aircraft nose	m
$X$	Acquisition price	US\$

### Subscripts

0	Free-stream
$0i$	Local free-stream
1	Inlet (Highlight)
2	Fan face
3	Fan exit
9	Nozzle exhaust
$i$	Interface plane
$j$	Exhaust jet

# 1. Introduction

Commercial aviation has rapidly grown from the earliest commercial flights of the early 20<sup>th</sup> century to the multi-billion dollar industry of today. Aviation has been a key aspect of global growth and supports the tourism, business, and transportation industries across the globe, in addition to directly creating jobs within the industry [1]. In reflection of this growth, aircraft have rapidly developed from single seater vehicles able to travel for only a few tens of meters to modern aircraft capable of transporting hundreds of passengers across the globe. Whilst modern aircraft may appear superficially similar to their predecessors from the past half century, the designs and technology within the airframe and propulsion system have led to large improvements in efficiency.

The industry has experienced a steady increase in revenue passenger kilometres of close to 5% per year, with much of the growth occurring in emerging markets such as Asia Pacific and Latin America [2]. To support this demand, Boeing and Airbus estimate that the global commercial aircraft fleet will more than double by 2035 [3, 4]. Despite growth in the market, airlines typically operate with a low profit margin due to high operating costs, strong industry competition and high customer bargaining power [5]. Commercial airlines are profit-oriented entities, and it is therefore inevitable that they will be influenced by economic factors. As fuel contributes to a significant proportion of the total operating cost for an airline, the primary driver behind most new technology developments is the saving in cost that may be obtained through reductions in fuel consumption. However, the modern industry is subject to a new driver for development. Global environmental awareness has led to pressure for technology that reduces the global community's impact on the environment. Development in the aviation industry is typically iterative, with improvements in efficiency achieved via incremental technology upgrades. However, environmental goals necessitate dramatic reductions in emissions that cannot be achieved without a revolution in the design of aerospace vehicles.

In a commercial industry, it is vital to ensure that new concepts are both economically and environmentally sustainable. As profit margins for operators are generally low relative to revenue, any investment must be well justified. From a manufacturer's perspective, the development cycle of a new aircraft generally spans a number of years and requires billion dollar research and development programs. Investment in new technology entails risk, and given the sums involved, new technology must be able to prove that it is a worthwhile investment. To invest in an aircraft or concept that fails can prove very costly to a commercial entity, and any avenue of research that is able to reduce risk for the manufacturer or operator can be beneficial. This is especially key in the current development environment, where numerous new technology avenues are being proposed. Cost is the only way to differentiate aircraft concepts that may otherwise be designed with very similar goals in mind. It is therefore vital to integrate cost analysis within the research process at a reasonably early stage. However, it is difficult to develop an economic assessment of a novel aircraft at preliminary design stage, as there is little data on which the analysis can be based. A process is therefore required that can first predict the technical performance of a novel aircraft and then identify whether a performance



## 1. Introduction

---

improvement would translate into an economic benefit for an operator. As a part of this analysis, it is important to be able to account for uncertainty in the design process, as novel concepts entail a high degree of risk.

This research presents a methodology and work-flow for assessing the viability of a novel aircraft from a techno-economic perspective. The framework combines simulation methods for a novel aircraft with an investment cost analysis to present a financier's perspective on the cost benefits and hence financial value of a high efficiency aircraft concept. The analysis can be used to provide both a manufacturer's view on what will make an attractive product for a customer, and an operator's view on whether there is value to investing in a novel aircraft concept. The end goal is to provide a framework that can be used to rank and compare different aircraft concepts on a consistent basis and identify those factors that may have the greatest influence over a concept's viability. The present research focuses on the N3-X, NASA's blended wing body aircraft with a turbo-electric distributed propulsion system. However, the methods developed within the research are applicable to alternative configurations.

Chapter 2 presents a literature review that sets the scene of development for novel and high efficiency aircraft. Key technologies and concepts for such novel aircraft are described, providing a view on the path of development and the new markets that may emerge in the future. Finally, the section summarises previous techno-economic research and identifies the main aim and work scope of the research. Chapters 3 and 4 present the development of modelling procedures for the propulsion system and aircraft with performance results for the case study aircraft. Subsequently, Chapter 5 explores the design space for the N3-X to identify the most useful design variables to improve the performance of the aircraft. Chapter 6 then presents the cost modelling procedure for the direct operating cost, maintenance cost, and acquisition price of an aircraft. In addition, it details the development of an investment cost and direct operating cost analysis for a novel aircraft. The results of the techno-economic analysis under a number of scenarios are shown Chapter 7, with a risk analysis of the aircraft presented in Chapter 8. Finally, conclusions and suggestions for further work are presented in Chapters 9 and 10.

Chapter 11 summarises publications that have resulted from this research. Appendix A presents highlights from MSc research that has been conducted in relation to the grant research. Further appendices are also included to provide more detail on select modelling procedures, methods, and assumptions.

# 2. Literature Review

## 2.1 Growth and Development in the Aviation Industry

The commercial aviation market has grown consistently and rapidly since its inception. Despite a number of crises, data shows that air traffic in terms of revenue passenger kilometres (RPK) doubles every 15 years [4] (Figure 2.1). In addition to established markets, emerging markets in Asia and Africa suggest there is still significant potential for growth. To support this growth, Airbus and Boeing predict there is a market for 34,170 or 41,030 new aircraft by 2036, respectively [4, 6]. Whilst approximately 40% of these are expected to serve as replacements for older, less efficient aircraft, others are new aircraft for the increasing market.

Technological growth in the industry predominantly focuses on reducing cost and increasing profits. A large aspect of development is therefore to increase fuel economy, as fuel is typically a large percentage of an airline’s operating cost. The International Air Transport Association (IATA) predicts that aviation’s fuel bill for 2017 will be \$129 billion, 17.4% of the average airline operating costs. Depending on current fuel price, fuel consumption can be account for upwards of 30% of an airline’s operating cost [7]. In addition, the price of crude oil, and hence jet fuel, is volatile and changes on a weekly and even daily basis. The profitability of the industry is therefore closely tied to the price of fuel (Figure 2.2). As a result, technologies that offer increases in fuel economy and a lower fuel burn per seat are generally attractive to operators looking to increase their profit margins, especially when fuel price is high.

Reducing fuel consumption has historically been a common goal of new technology. However, with the increase in global environmental awareness, lessening the impact of aviation on the environment has become a new dominant driver in research. Growth in the industry is matched with an increase in aviation emissions. Whilst Carbon Dioxide (CO<sub>2</sub>) emissions are growing much more slowly than RPKs (1.8% per year versus 5.0% per year [6]) the goal is

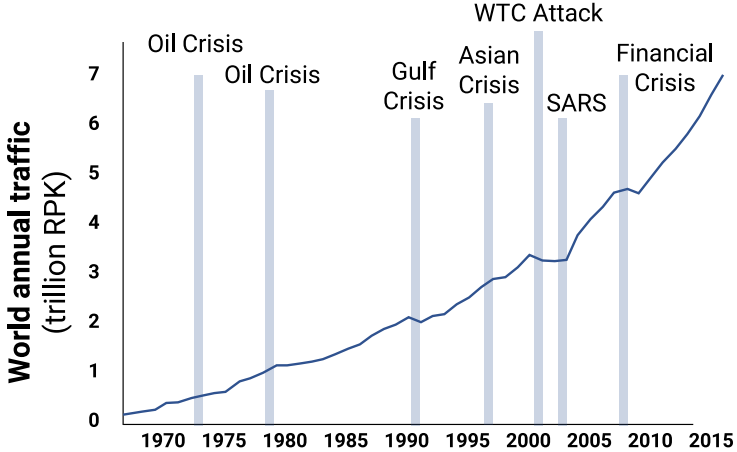
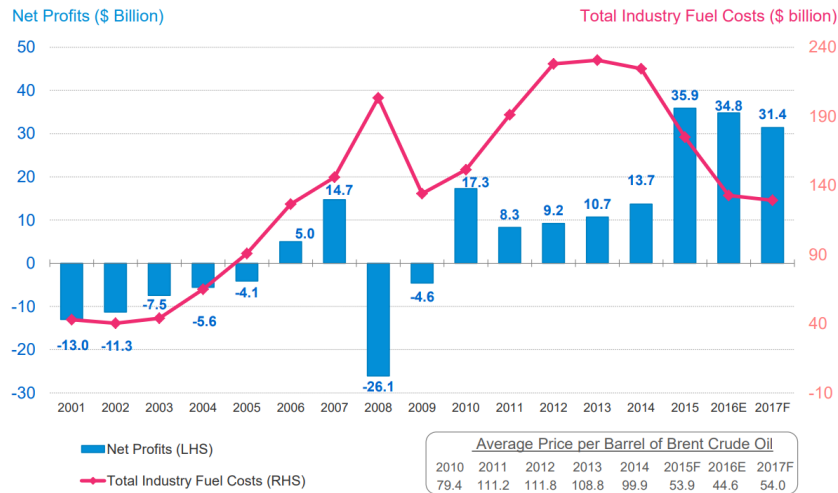


Figure 2.1: Growth in the commercial aviation passenger market over time (Data Source: Airbus [4])

## 2. Literature Review



**Figure 2.2:** Influence of jet fuel price on airline profits (Image Source: IATA [7])

to slow and eventually decrease current CO<sub>2</sub> emissions levels. Aviation bodies have set challenging goals for development of future aircraft that target a number of key factors: emissions (primarily CO<sub>2</sub> and oxides of nitrogen, NO<sub>x</sub>), energy/fuel consumption, and noise. The aviation industry has committed to a set of three goals to achieve sustainable future development [6] (Figure 2.3):

**Goal 1:** 1.5% average annual fleet efficiency improvement from **2009 to 2020**

- New aircraft and engine technologies
- More efficient operations
- Improvements to air traffic management

**Goal 2:** Stabilise net aviation CO<sub>2</sub> emissions at **2020** levels (carbon neutral growth)

- As with Goal 1
- Carbon Offsetting and Reduction Scheme for International Aviation (CORSIA)

**Goal 3:** Reduce aviation net CO<sub>2</sub> emissions to 50% of 2005 levels by **2050**

- As with Goals 1 & 2
- Development of sustainable alternative fuels
- Research into future design concepts by aircraft and engine manufacturers

The International Civil Aviation Organization (ICAO) expects global CO<sub>2</sub> emissions reductions to be achieved through a combination of four routes: aircraft technology, operational improvement, market based measures, and sustainable alternative fuels [8]. One such market measure is the Carbon Offsetting and Reduction Scheme for International Aviation (CORSIA) introduced by ICAO in 2016. The scheme is intended to cover any annual CO<sub>2</sub> emissions from international civil aviation and is a part of the move towards a carbon neutral industry. ICAO also defines technology standards that must be met by aircraft through the Committee on Aviation Environmental Protection (CAEP). This defines efficiency, noise, and emissions level that must be met in order for new technology to gain certification. Over time, these standards have enforced more stringent levels to minimize the effect of global civil aviation on the environment. ICAO also coordinates action plans for states to communicate information on their activities to

## 2. Literature Review

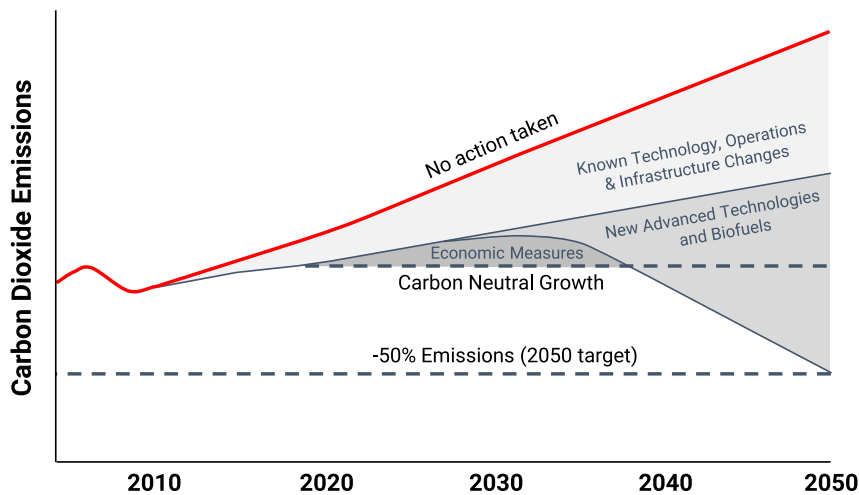


Figure 2.3: Industry measures for reducing global aviation CO<sub>2</sub> emissions [9]

address CO<sub>2</sub> emissions from international civil aviation to ICAO. They note that actions plans have been submitted by 104 States, representing 90.1% of global Revenue Tonne Kilometres (representing both passenger and cargo utilisation). This co-ordination represents a strong drive towards a more environmentally friendly industry across the globe.

Some of the move towards a sustainable industry will be achieved by improving operations and air traffic management. However, the majority of the move towards an environmentally friendly industry must originate from new developments in aircraft technology. Reducing emissions lies partially in line with the original development drive for increasing fuel economy, as a reduction in fuel burn implies a reduction in CO<sub>2</sub>. The first developmental goal for a 1.5% annual increase in efficiency can and is being achieved with incremental improvements in technology. However, further goals necessitate dramatic reductions in fuel consumption and CO<sub>2</sub> emissions that cannot be met with the current evolutionary development model. Revolutionary new technologies and policies are therefore required for future aircraft [9]. These technologies are generally at a low technology readiness level (TRL), and therefore imply a significant amount of a risk in the future. There is therefore a large body of research focusing on the development of new technology for the industry to bring it to a level where it can be implemented on aircraft.

In reflection of the challenging developmental targets for aviation, national and international research programs are assessing the technologies that will be required to meet each level of the developmental goals. The Clean Sky program in Europe (part of the European Union's Horizon 2020) has funded research into a range of projects aimed at two target concepts; Ultra Green Air Transport System, for technologies that reduce the impact of air transport on the environment, and Highly Cost-efficient Air Transport Systems [10]. The program covers research by industry, academia, and research institutes that intends to develop revolutionary technology for low CO<sub>2</sub>, low emissions, and low noise. In the USA, NASA has proposed emissions and energy consumption goals for aviation, including a 60% reduction in energy consumption by 2035 (versus a 2005 EIS aircraft). A wide body of research has been conducted by NASA, academia, and industry that investigates novel technologies, with the aim of reducing NO<sub>x</sub>, CO<sub>2</sub>, energy consumption, and noise [11].

Whilst much of the research is focused on developing technology that is able to meet developmental goals, it is vital to ensure that the industry is both environmentally and economically sustainable. High risk and novel technologies suggest that costs may increase for operators. However, profit margins in aviation are low (4.2% of revenue for 2017 [12]) due to high operating costs, strong industry competition and high customer bargaining power [5]. Large increases in

cost will therefore not be economically sustainable.

Commercial airlines are profit-oriented entities, and it is therefore inevitable that they will be influenced by economic factors. Fuel cost has already been identified as a key aspect of operating costs. It is also an influencing factor in determining investment in new technologies. In a high fuel price scenario, the cost penalty for operating older, less efficient aircraft is high. Operators are therefore more likely to invest in newer aircraft. In contrast, in a low fuel price scenario operators are more likely to expand capacity by utilising older aircraft, as the operating cost is lower than purchasing a new aircraft [13]. This can also influence the development of new technology. In the 1980s, fuel costs and hence airline operating costs were high. During this period of time, propfan concepts were developed that offered operators reasonable fuel savings in comparison to the then current engines. As fuel prices dropped back to previous levels, operators no longer showed any interest in the technology, despite the demonstration of the concept on an experimental aircraft in 1988 [14]. The case demonstrates the close link between research & development and the economic market and the importance of economic factors in success of a concept. Therefore, both historically and in the future, the technologies that progress to market are those for which a business case can be found. Future research must keep an eye on economics in order to identify the technologies that are both most promising and most profitable.

In response to the need for revolutionary new technology in the industry, there is a wide spectrum of research that investigates new concepts for the aviation industry. These can be split into two pillars for the purposes of this research: propulsion (including distributed propulsion, engine technology evolution, and electrical transmission system) and airframe technologies (including propulsion system integration and novel airframe configurations). Given their novelty, the associated risk is high, from both technological and economic perspectives. There are nevertheless numerous promising technologies in development for the future of the aviation industry.

### 2.2 Technology Research for High Efficiency Aircraft

Over time, developments have been introduced to aerospace technology to achieve improvements in fuel consumption and to increase the range and size of aircraft. The original driver for the development of these technologies was the constant goal of a commercial industry: to drive down costs and improve profitability. In the modern aviation industry, environmentally friendly technologies are now necessary, following the introduction of challenging goals for reductions in energy consumption and emissions.

ICAO identifies a number of key research areas to achieve developmental goals [8]:

**Aerodynamics** Reducing the two main components of airframe drag, lift-induced and profile drag, is a route to increasing the aerodynamic efficiency of airframes. Reductions in lift-induced drag can be achieved by increasing wing aspect ratio and wing span. Technologies such as wingtip devices are one option currently used on aircraft. Improvements in materials and structures also support the implementation of larger wingspans. Folding wingtips are an alternative proposal for increasing wingspan that works around current airport limits on the maximum wingspan of an aircraft.

The main challenge with respect to skin friction drag is to avoid or mitigate the drag of turbulent flow. Riblets and surface texturing can be used to reduce drag from turbulent flow. Encouraging laminar flow is also a route to avoid turbulent skin friction drag. Research is assessing the possibility of Natural Laminar Flow technologies to encourage laminar

## 2. Literature Review

---

rather than turbulent flow over the aircraft. Alternatively, active flow control or boundary layer suction can be used to maintain laminar flow over the aircraft surface.

**Structural Design and Materials** Reducing the structural weight of the aircraft is a direct route to reducing fuel consumption. Composites and advanced alloys can be used to produce lighter, more resilient structures. Additive manufacturing is a major topic of research which may support the implementation of more efficiently designed components that reduce weight and part count. The potential of programmable materials that are able to change shape is also being explored.

**Propulsion** Developments in engine technology will be able to directly reduce an aircraft's fuel consumption. Improvements in thermal efficiency, propulsive efficiency, and installed weight and drag are all possible research paths for propulsion. Engine development focuses on higher bypass ratio turbofan engines. Novel configurations are also being assessed that diverge from current turbofan designs. Some of the concepts being considered will be presented in the sections 2.2.1 and 2.2.2.

Numerous bodies have identified the necessity for revolutionary technologies to achieve these goals. A wide range of novel concepts are therefore under development that have the potential to dramatically change the industry. A common theme is the need for more integration between the airframe and propulsion system both during development and on the aircraft. This is particularly apparent with the introduction of numerous novel concepts that make use of integrated or coupled configurations (e.g. boundary layer ingestion, embedded engines, distributed propulsion systems, and integration of high bypass turbofans on aircraft). In NASA's N+3 Aircraft Concept Designs and Trade Studies report, propulsion system-airframe integration is identified as a "critical technology challenge" that must be resolved [15]. Similarly, the Committee on Propulsion and Energy Systems to Reduce Commercial Aviation Carbon Emissions from the National Academies of Sciences, Engineering, and Medicine identifies advances in aircraft-propulsion system integration as a high priority research task [16].

Significant research effort is being focused on concepts that will diverge from the design requirements of the conventional airframe with podded engine configuration that characterises most large commercial aircraft. Whilst concepts can be broadly split into propulsion and airframe groups, it will become increasingly difficult to entirely separate the two in a more integrated design. Nevertheless, given the current configuration of large commercial aircraft development it is still useful to differentiate technologies into airframe and thrust groups. The following section presents a number of key concepts and technology themes relevant to this research. Many of the propulsion concepts presented in this section have been combined in various forms in a number of aircraft concepts and bodies of research. Whilst it is not a comprehensive list of novel technologies in aerospace, it reflects some of the dominant themes that are emerging in response to developmental targets.

### 2.2.1 Boundary Layer Ingestion

In general, the boundary layer is considered to be detrimental to the performance of a conventional aircraft, as it contributes to drag and results in a momentum deficit, or wake. In the propulsion system, an ingested turbulent boundary layer can give rise to total pressure and swirl non-uniformities, which can have a negative impact on the performance of an engine. To avoid such problems with the quality of the ingested flow, the typical commercial aircraft planform is powered by podded engines. These are positioned to ingest free-stream air without any influence from the aircraft wake or boundary layer. Aircraft with more closely integrated engines, such as military configurations, often include some form of boundary layer bleed or

## 2. Literature Review

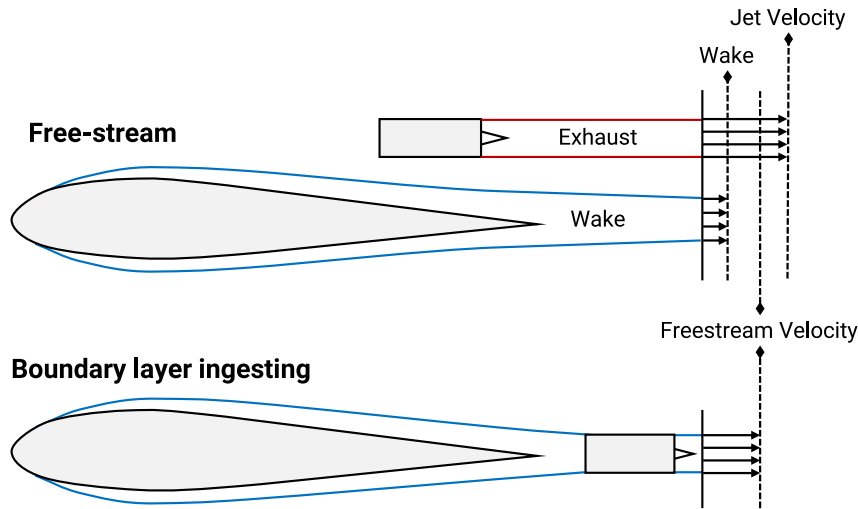


**Figure 2.4:** Representation of boundary layer ingestion in comparison to a free-stream propulsion system

diversion which modifies the boundary layer before it enters the inlet. As momentum deficit is one of the sources of aircraft drag, it follows that technologies to control or reduce the impact of the boundary layer are a potential route to an improvement in aircraft performance. Lower aircraft drag corresponds to lower thrust requirements, and hence has the potential to reduce the fuel consumption of the aircraft. The continuous increase in environmental awareness, coupled with the volatility of fuel price, means that reductions in fuel consumption are one of the primary drivers of aircraft development. As such, boundary layer control is one of the possible technological routes that can be taken during the design of an aircraft. Passive management of the boundary layer induced drag on an aircraft can be obtained through modification of the micro-scale nature of the aircraft surface. An option that may be applied without an extensive aircraft redesign is the application of sharkskin paint, which reduces turbulence perpendicular to the flow along the airframe [17]. Alternatively, highly smooth coatings on the surface of the aircraft can be used to reduce the airframe skin friction coefficient [18].

The concept of boundary layer control is not a new one. Early research suggested that the application of constant suction on the aircraft surface could reduce the drag of the aircraft through removal of the boundary layer [19]. The boundary layer also has the potential to be of benefit to the propulsion system through the application of boundary layer ingestion (BLI). BLI can re-energise the wake of the aircraft by accelerating ingested boundary layer flow back up to the free stream velocity (Figure 2.4). By ingesting the boundary layer, less power is used by the propulsion system than for a propulsion system that produces the same thrust with free-stream air [20]. However, ingestion of the boundary layer is not entirely beneficial to a propulsion system. The boundary layer is an inherently distorted flow, which will almost certainly have some impact on the performance of the system. The engine may be subject to distorted flow from the bottom to the top of the inlet, or radially along the fan blade, such as in the case of a propulsive fuselage [21]. Significant distortion can negate the power or fuel consumption benefits of a BLI system, such that a free-stream system is the more efficient option [20]. Boundary layers are prone to separation in an adverse pressure gradient, which is compounded by the development of classical secondary flows associated with the turning through an S-duct bend [22, 23]. Nonetheless, S-ducts have been considered as an option for a BLI system, as they support the application of embedded engines to reduce the profile of the aircraft. The use of passive, active or hybrid boundary layer flow control (BLC) can contribute towards a significant reduction in the distortion in intakes such as an S-duct [22].

## 2. Literature Review

---

A number of aircraft concepts apply boundary layer ingestion to provide improvements in fuel burn. Aircraft such as NASA's N3-X make use of a distributed propulsor array mounted on the upper surface of a blended wing body (BWB) fuselage [24]. The high-aspect ratio spanwise or 'mail-slot' inlet allows for the ingestion of a significant proportion of the boundary layer. Similarly, the Silent Aircraft Initiative's SAX-40 BWB makes use of three boundary layer ingesting engine clusters [25] which ingest 16.6% of the airframe boundary layer [20]. Boundary layer ingestion has also been applied to conventional tube-and-wing configurations. These configurations integrate a boundary-layer ingesting fan at the rear of the fuselage that ingests and re-energises the fuselage wake. Research on the Propulsive fuselage concept by Bauhaus Luftfahrt e.V. suggests that this configuration can lead to a 9.9% improvement in efficiency versus a projected 2035 EIS aircraft baseline [21]. The NASA STARC-ABL concept presented by Welstead and Felder employs a similar configuration and expects a 12% block fuel burn reduction for the design mission versus a 2035 EIS aircraft baseline [26].

### 2.2.2 Distributed, Turbo-electric, Electric, and Hybrid Propulsion

Modern aircraft are at least 70% more efficient than early aircraft, gained through a combination of advancements in airframe and propulsion technology [1]. To achieve this improvement, engine design has evolved from turbojet engines to turbofans with increasingly high bypass ratios and very low specific thrust. Higher bypass ratio engines imply an improvement in propulsive efficiency and hence in overall efficiency. However, there are a number of challenges that must be addressed with regards to the increase in engine size. Higher bypass ratios can be achieved by maintaining the same fan outer diameter and shrinking the engine core, which leads to a reduction in thermal efficiency. One avenue of research is therefore to improve the efficiency of small core engines. Alternatively, bypass ratios can be increased by increasing the size of the fan. This too has a number of downsides, as large fans may need a gearbox to step the rotational speed down to a level that avoids high fan tip speeds. In addition, a large diameter engine will run into ground clearance issues, as the distance between the underside of the wing and the ground is limited, and may require thicker casing for blade-off containment.

This difficulty may be addressed by changing the engine location or wing configuration and by moving to a more integrated layout. An alternative solution is to move to a distributed propulsion system. Distributed propulsion can be defined as a propulsion configuration where thrust originates from a number of sources [27]. Typical commercial aircraft can therefore be defined as distributed propulsion configurations, as thrust is generally produced by between two and four engines. This distribution can act as a solution to the large turbofan challenge, as a single engine core can be linked to a number of fans, mechanically or otherwise. A large number of distributed fans can therefore provide a large effective bypass ratio with resulting benefits to the overall efficiency of the propulsion system. As these fans would be smaller than a single high bypass turbofan, tip speed and ground clearance issues can potentially be avoided. Other benefits are also available from a distributed propulsion system, including noise reduction (potential for very low specific thrust and noise shielding from fuselage), safety (redundancy in case of failure), enhanced aerodynamics (using the exhaust to favourably influence air over the wing or by flap blowing), and enhanced in-flight control (with individual control of propulsors or thrust vectoring) [27–29]. Distributed propulsion can also be combined with boundary layer ingestion by integrating the system within the airframe, as a distributed propulsion system allows a greater proportion of the airframe boundary layer to be ingested. Whilst many concepts focus on distributed propulsors, other distributed applications are possible, such as cross flow fans [30].

Despite the requirement for revolutionary technology, conventional simple cycle turboma-



## 2. Literature Review

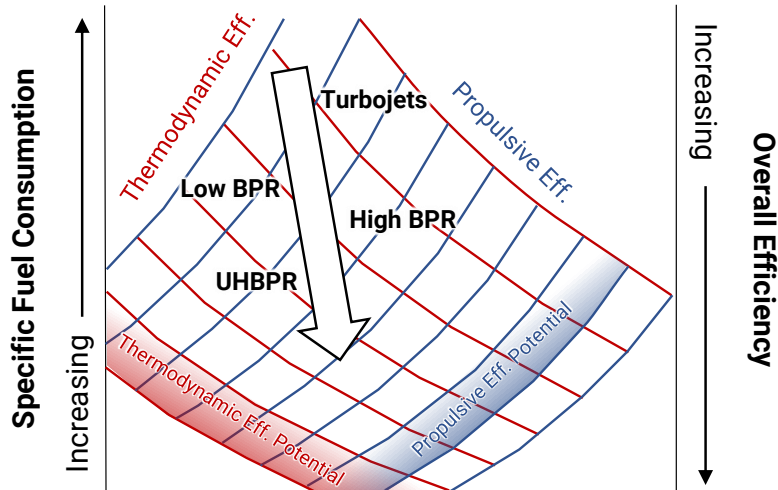


**Figure 2.5:** Cruise thermodynamic and propulsive efficiencies for a simple cycle gas turbine engine with projections of potential maximum efficiency (adapted from [31] and [16])

chinery is by no means obsolete. Projections suggest that the gas turbine has yet to reach its maximum potential efficiency and that efficiency improvements can still be made on modern technology [31] (Figure 2.5). These improvements will be the result of incremental improvements from optimising the engine cycle, rather than a single large leap [16]. The requirement for a dramatic increase in efficiency has led to a move in research towards novel configurations. Some avenues of research consider combined cycle propulsion systems that apply processes such as reheat or intercooling to gain an increase in efficiency. Parallel advances in materials and manufacturing technology will also enable improvements in the operating temperature limits of gas turbines and propulsion system weight.

Another avenue is to break the propulsion system into a number of building blocks: sources of energy, sources of thrust, and transmission of thrust to power. In a conventional turbofan, the source of energy is fuel, the source of thrust is the turbomachinery (fan and core thrust), and the transmission of energy to thrust is through the turbomachinery. More flexibility is possible by separating these factors to be addressed by different components and subsystems. Further flexibility is available by introducing stored power or electrical motors and generators in addition to conventional fuel sources. Breaking the systems down into building blocks does not guarantee a more efficient system, but it does provide a wider design space to explore. This can support the development of high efficiency and low emissions propulsion system configurations.

Propulsion systems that use this building block form of design come under a number of headings that can make it difficult to easily categorise or label. Distributed propulsion is one such modular design outlook, with the source of thrust spread over a number of subsystems or subcomponents. Other design outlooks or groups include turbo-electric, all-electric and hybrid electric propulsion systems. Each of these shares a common theme of applying electrical subsystems in the design of the propulsion system. Whilst Turbo-electric, electric or hybrid propulsion systems are not necessarily distributed propulsion systems, the concepts can be easily combined.

The definition of turbo-electric versus hybrid versus electric systems depends on the source of energy. In a turbo-electric system, energy is stored in fuel and converted to useful energy in the turbomachinery. In an electric system, all energy is stored in batteries. A hybrid system combines both sources of power. It is likewise possible to split the source of thrust between

## 2. Literature Review

---

turbomachinery, propulsors, or a combination of both. Figure 2.6 presents a selection of different architectures using electrical transmission system that demonstrate the flexibility available once the system is broken down into its constituent parts. Note that a configuration in the top right of the sketch would be along the lines of a conventional turbofan, with all thrust produced in the turbomachinery. In addition, a battery storage only configuration would not be combined with turbomachinery thrust sources, as the turbomachinery is applied only where a fuel such as kerosene is used. Whilst the presented configurations use electrical transmission systems, distributed or modular propulsion configurations are not required to be exclusively electric. Once considering the efficiency of each subsystem in the transmission of electrical power (e.g. generator to converter to wire to motor), overall efficiency can be low, despite reasonably high efficiency for each subsystem [16]. In some configurations, it may therefore be advantageous to transmit power mechanically and avoid losses in the electrical transmission system. One such configuration with mechanical transmission is the multi-fan turbofan configuration considered for the Silent Aircraft, with power transferred from the engine core to adjacent fans through a drive shaft and gearbox [25]. Further configurations become available when electrical and mechanical transmission systems are combined. With such a wide design space, it is highly unlikely that there is any one perfect solution. Instead, it is likely that a whole suite of different configurations will arise, each suited to a different application or requirement.

Novel propulsion system concepts and technologies are also enablers for new markets. Distributed propulsion covers the multi-rotor configurations already commonly seen on hobby drone aircraft. Many of these concepts have also created a new market for local air taxis to address the increase in urban road traffic. Distributed electric propulsion is being applied on light aircraft concepts including the Airbus Vahana [32], Lilium's VTOL concepts [33], and the VoloCopter [34]. Larger scale applications are also being considered for distributed propulsion in the commercial aircraft sector. Many of the new aircraft concepts apply some form of distributed propulsion system, generally in combination with electrical propulsion. Isikverin *et al.* investigate a number of distributed propulsion configurations [35]. In combination with boundary layer ingesting propulsion systems, they expect a fuel burn improvement of at least 8% for their Distributed Multiple-Fans Concept versus evolutionary 2036 entry into service aircraft and 37% versus a 2000 entry into service aircraft.

Hybrid propulsion may also be a promising technology. The SUGAR Volt hybrid electric aircraft concept, one of a number of novel concepts developed in the Subsonic Ultra Green Aircraft Research project, expects a fuel saving of 63.4% versus a reference 2008 entry into service aircraft in combination with other technologies [36]. Lents *et al.* developed a conceptual parallel hybrid turbofan configuration for a single aisle aircraft application [37]. The rationale behind the design was to size the turbofan for cruise rather than take-off or top of climb. Additional power to achieve a suitable thrust level during climb or take-off could then be obtained from an external power source through a motor driving the low pressure spool. The resulting configuration reduces fuel burn for the design mission by 6% (given the assumptions made for energy density of the energy storage). The flexibility of such designs has led to a wide range of additional concepts, all of which expect significant reductions in fuel burn of anywhere between 6–70% depending on the defined mission and baseline for comparison [38]. This highlights a challenge in the comparison of novel concepts, as there is no consistent baseline against which performance can be measured. Distributed, hybrid or electric concepts are nonetheless expected to lead to reasonable improvements in efficiency versus evolutionary technology.

The next phase for implementation on aircraft is the demonstration of concepts on experimental aircraft. NASA's X-57 Maxwell is intended to test a distributed electric propulsion system and expands on previous ground tests of a similar system, the Hybrid-Electric Integrated Systems Testbed [39]. The goal is to prove the viability of the technology and the potential for

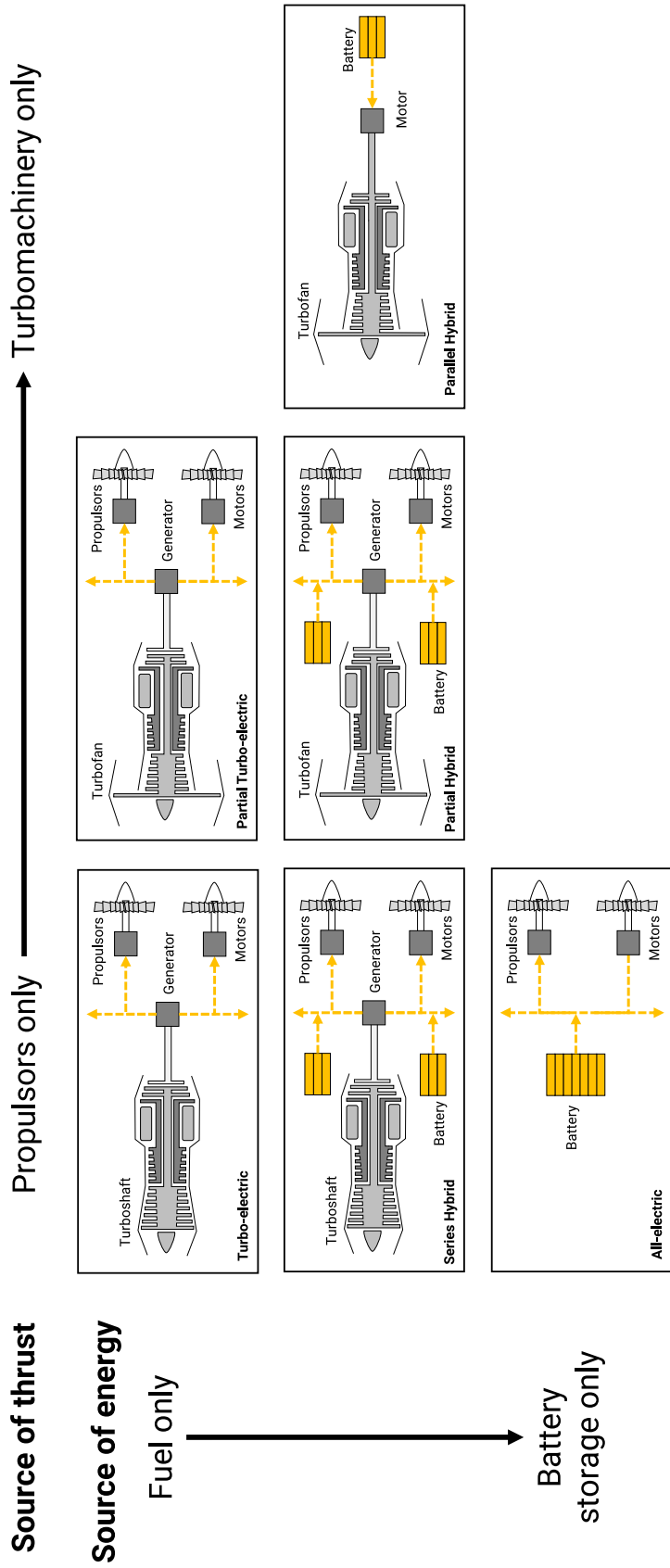


Figure 2.6: Example turbo-, hybrid-, or all-electric propulsion system architectures (adapted from [16])

reductions in noise, emissions, cost, in addition to providing short take-off capability. Similarly, the XV-24A Lightning Strike by Aurora Flight Sciences with partners Rolls-Royce and Honeywell is a concept designed to demonstrate an aircraft using distributed hybrid-electric propulsion ducted fans [40].

Whilst distributed electric propulsion is expected to provide performance benefits, it is important to highlight that conclusions about efficiency will necessarily change if the end-to-end energy usage and emissions are considered. The parallel hybrid study by Lents *et al.* identifies that there is no net fuel benefit if the energy required to charge on-board batteries is included [37]. In addition, the price of electricity varies on both a time and location basis, similar to jet fuel. Therefore, even where there may be a net energy benefit through the use of novel technologies, there is a possibility that costs will remain high [41]. At current levels, and into the near future, jet fuel has a higher energy density than batteries [16], even when taking into account the efficiency of converting the fuel's chemical energy through the gas turbine. In addition, a gas turbine at altitude is able to produce power more efficiently than current ground-based (hydrocarbon) power plants. Therefore, without the introduction of an entirely green electricity grid, gas turbines at altitude may be the more environmentally friendly option in the near term [42]. It is worth highlighting that a similar conclusion arises for alternative fuel sources, as the cost of producing the fuel may outweigh the associated benefits.

A key challenge that must be addressed for all electric aircraft is the weight on board the aircraft. Unlike a conventional fuel source, the weight of the aircraft does not reduce over the course of the flight. There is therefore no performance improvement over the course of a flight as weight reduces. This is especially problematic for long haul applications, where flight time is long and hence energy consumption may be significantly higher. Battery storage technology will be required to reach a much higher energy density level before it can be implemented on long haul aircraft. Additional costs will also be associated with battery powered aircraft, such as infrastructure costs at airports and CO<sub>2</sub> costs from electricity generation [16]. Configurations that rely on conventional fuel as an energy source avoid the challenges associated with battery storage. Long haul aircraft concepts therefore focus predominantly on turbo- or hybrid-electric configurations rather than all electric.

Despite a number of challenges that must be addressed, the potential benefits of distributed, turbo-electric, electric, and hybrid propulsion make it a very promising avenue of research. This is reflected by the large number of concepts and demonstrators expected in the near future. The flexibility of configurations offered by such systems is not only a route towards more efficient aircraft, but is also an enabler for new applications in the aerospace industry. Whilst further advancements to an appropriate technology level are needed to support implementation on large commercial applications, it is probable that distributed, turbo-electric, electric, or hybrid propulsion will be seen on future aircraft.

### 2.2.3 Electrical Systems and Superconductivity

Given the current power density of electrical components and the projected improvement in energy density over time, it is unlikely that an all-electric aircraft concept would be feasible in the near term for large commercial aircraft (Figure 2.7). Current state of the art in the field of electric motors suggests a power level in the 250–300kW range [16, 43], well below the >1 MW power level required for large long-haul aircraft applications. However, power densities are already at a level that makes it feasible to apply the technology on current light aircraft concepts. In 2014, Airbus flew an electrical aircraft demonstrator, the E-Fan, with two 30kW electrical motors. Two years later in 2016, Siemens flew an aircraft equipped with a 300kW motor, ten times the power level of the Airbus demonstrator [43]. One key boundary that is typically quoted is to

## 2. Literature Review

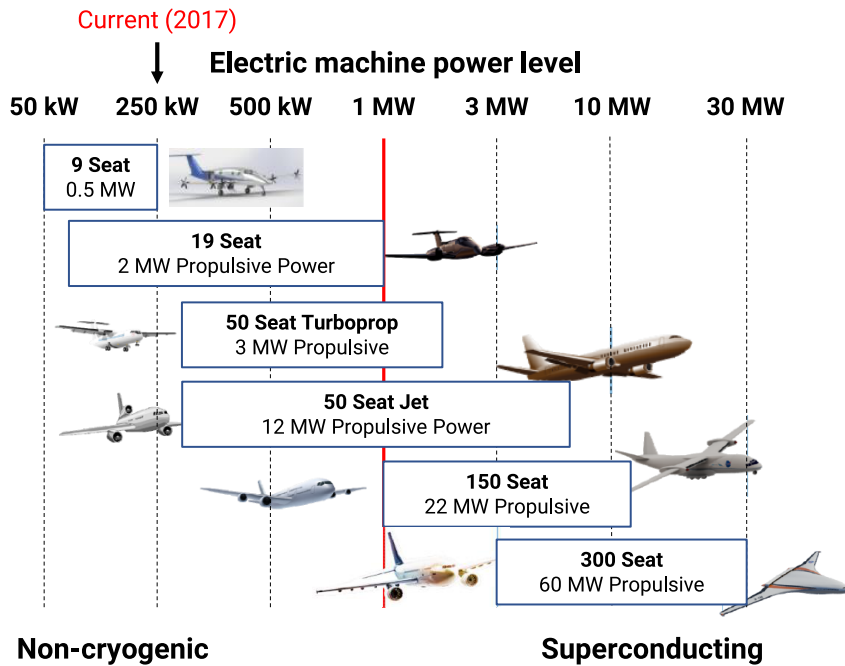


**Figure 2.7:** Electric machine power levels required for different aircraft classes (Adapted from [44])

break 1MW power levels for motors. This will be an enabler for large scale turbo-electric and electric, and hybrid propulsion systems [38]. High power electrical systems are therefore a key subcomponent of the described novel propulsion systems, with manufacturers such as Airbus and Siemens focusing on demonstrating the feasibility of hybrid electric aircraft propulsion by 2020 [43]. Whilst current electrical components power densities are at an adequate level for small scale applications, it is not yet feasible for large scale applications.

The previous section introduced a wide range of novel propulsion system configurations, some of which rely on the transmission of electrical power from a power source to the propulsion source. Introducing an electrical transmission system implies losses from the generator, through the cabling and into motors. A loss in power leads to two major challenges for a more electric aircraft: waste heat management, and a loss in efficiency that leads to an increase in fuel or energy required by the aircraft. However, some concepts consider the application of superconducting electrical systems, rather than conventional electrical systems. Superconducting systems have the potential to dramatically increase efficiency, as large currents can be carried with minimal loss [45]. In addition, superconducting systems are lighter than conventional motors and therefore have a higher power density than conventional electric motors or generators [46]. However, superconducting systems must be cooled to cryogenic temperatures, necessitating either cryocoolers or a cryogen to maintain superconductivity, which increases weight. A superconducting electrical system nevertheless has the potential to be a low-loss option for aircraft that rely on electrical systems and electrical transmission.

The Airbus Group Innovations and Rolls-Royce have developed a distributed electric propulsion aircraft concept, the E-Thrust [47]. The configuration is a partial hybrid system and it therefore uses both turbomachinery and battery storage, with superconductivity as an enabler for a system that is reliant on electrical power. To support the concept, the Programmable Alternating current Superconducting Machine (PSAM) project plans to develop superconducting electrical machines for the six wake re-energising fans that form the distributed propulsion system. These machines are intended to be bi-directional, and can therefore act as both motors and generators. NASA's N3-X concept first presented by Felder *et al.* applies superconductivity in a turbo-electric distributed propulsion system [24]. A number of studies were conducted to

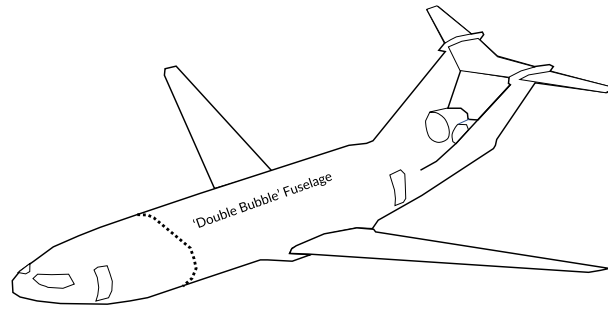


**Figure 2.8:** The double bubble fuselage planform [15]

assess the system components, including a study on the system architecture by Armstrong *et al.* [48] and target system weights and cryocoolant options by Brown [46]. The expectation is for the superconducting system to provide a transmission efficiency of up to 99.8%. Superconductivity was also implemented on a concept by Berg *et al.* to assess the possible implementation on an aircraft and the technology targets that should be met for superconductivity to be beneficial [49]. Key targets were identified in machine power density and component losses for the concept considered, a tube-and-wing with two turbofans and an electrically driven BLI fan at the end of the fuselage. Both the N3-X studies and the study by Berg *et al.* suggest that a cryocoolant such as  $\text{LH}_2$  would prove beneficial to reduce weight and increase efficiency.

Whilst superconductivity is promising, it has not yet been implemented on the aircraft. Projections suggest that superconducting power systems will not be implemented on aircraft within the next 30 years [16]. It is nevertheless considered an enabler for electric and turbo-electric technology, particularly on larger aircraft applications [45]. As the technology is yet to be implemented, concepts do consider the use of conventional electric machines. The ECO-150 concept originally utilised superconducting electric machines, however, following iterations utilised conventional electric machines, as superconductivity was considered out of reach for a near term application [50]. Given the assumptions made, the research found that the aircraft turbo-electric distributed propulsion system with conventional electric machines had a similar efficiency level to a conventional aircraft, despite the high weight of the electrical system. Further advances in electrical system technology will improve the viability of turbo-/hybrid-/all-electric aircraft concepts.

### 2.2.4 Blended Wing Bodies

Historically, the dominant configuration for commercial aircraft has been a tube-and-wing with podded engines. Therefore, whilst significant improvements have been made to the airframe's performance, modern aircraft are superficially similar to their predecessors. One of the key factors that has influenced the prevalence of this configuration is that a cylinder is a good pressure vessel, a vital aspect of an aircraft that cruises at altitude. Further improvements are being researched for the tube-and-wing configuration, such as strut bracing to support high wingspans or laminar flow wings [36]. Alternatively, a 'double bubble' fuselage has been assessed that combines two cylindrical fuselage cross-sections into a single body [15] (Figure 2.8). Conventional configurations can also incorporate some of the previously identified novel propulsion system concepts. The STARC-ABL is a tube-and-wing concept that integrates a boundary layer ingesting fan at the rear of a fuselage [26]. This provides performance benefits on a conventional configuration without dramatically changing the aircraft planform. However, further performance benefits may be possible by moving entirely away from concepts derived from the tube-and-wing configuration.

Removing the cylindrical pressure vessel design perspective opens up the potential for new

configurations. The study by Liebeck [51] attempted to address a key question: “Is there a renaissance for the longhaul transport?”. The results of the study produced a blended / hybrid wing body concept, one such novel configuration. Blended wing bodies are comparable to flying wing designs, as the wings transition smoothly into a lifting body fuselage. Rather than a separate fuselage, passengers can be accommodated within the useful volume of a lifting fuselage. This configuration has a number of advantages. A non-cylindrical fuselage has the potential to reduce the surface area to volume ratio of the aircraft, reducing wetted surface area and hence resulting in a lower drag and an increase in lift to drag ratio. In addition, the configuration removes the requirement for a horizontal tail, further reducing wetted surface area [52]. As the fuselage is a lifting body it can also be used to favourably influence the lift distribution of the aircraft [53].

The aircraft design produced by Liebeck predicted a 27% reduction in fuel burn as a result of the change in airframe configuration alone [54]. The large upper surface area of the airframe fuselage also enables it to be used as a noise shield. A blended wing body was therefore utilised in the SAX-40 silent aircraft's design, leading to a 28% reduction in noise in comparison to a similarly sized conventional aircraft [55]. The primary goal was to produce a low-noise design, nevertheless benefits in fuel economy of at least 22% were expected in comparison to conventional aircraft, in part thanks to the airframe design enabling the use of distributed boundary layer ingesting propulsors. NASA's N3-X also makes use of a blended wing body design to achieve the 60% fuel savings target. In the design, it was predicted that the blended wing body planform alone would achieve 14% fuel savings versus the baseline aircraft [56]. The SUGAR Ray hybrid wing body is an additional concept developed for NASA's N+3 goals. The configuration achieves a 43.3% improvement in fuel consumption versus a reference 2008 EIS aircraft [36].

There are a number of challenges that must be addressed in a blended wing body design. Many of the concepts do not include vertical surfaces, necessitating multi-purpose control surfaces. In addition, the stability characteristics of the airframe may necessitate fly by wire systems [54]. As the fuselage is a lifting body, cabin angle during cruise may be higher than is ideal [52]. Additionally, high volume and longer distance from fuselage exits may make safe egress more difficult. This may also reduce passenger comfort, as there will likely be fewer windows per passenger.

The blended wing body airframe has the potential to both improve efficiency and support the implementation of other novel technologies. The greatest challenge for such a configuration will be on the implementation side. The cost to a manufacturer of the facilities and tools necessary for a dramatically new airframe may be prohibitive. Similarly, the cost of new airport infrastructure may be high.

### 2.3 Alternative Aviation Fuels

In the power generation industry, the search for alternative and renewable power sources has led to the increasing use of tidal, solar or wind power generation. However, many of the more environmentally friendly options used in power generation are challenging or impossible to implement for aircraft applications. Weight, volume, safety and availability of the resource are all important factors in the selection of an alternative fuel sources for an aircraft, and rule out many power sources as direct elements of an aircraft design.

One of the routes towards a low emissions industry is to move to alternative low or zero carbon fuels. Kerosene has historically been a good fuel for aviation, due to a reasonably high energy density. However, alternative options are being investigated that may offer lower CO<sub>2</sub> emissions. Biofuels have been identified as one of the future industry measures to reach

## 2. Literature Review

---

the -50% CO<sub>2</sub> by 2050 target. They have been demonstrated on a number of flights using fuels blending conventional Jet-A with biofuels such as Jatropha and Algae [57].

In order to achieve a sustainable biofuel industry, it would also be important to ensure that biofuel production does not negatively impact the environment, such as through deforestation. Whilst biofuels are being considered for the 2050 goals, they are still hydrocarbon fuels and hence will still lead to CO<sub>2</sub> emissions as with conventional kerosene. Liquid natural gas (LNG) is also another alternative hydrocarbon that offers a higher energy density than conventional kerosene [58].

In the long term, a zero carbon emissions option may be to consider alternative fuel source such as liquid hydrogen (LH<sub>2</sub>) for aviation applications. At a first glance, liquid hydrogen is an ideal replacement for hydrocarbon fuels. In comparison to kerosene and other hydrocarbon fuel sources, LH<sub>2</sub> has a significantly higher Specific Energy (energy per unit mass), which suggests that, for a fixed mission length, an aircraft would be required to carry less LH<sub>2</sub> than kerosene. This provides benefits to the aircraft's energy consumption requirement, as the in-flight weight of the aircraft is reduced [59]. In addition to lower fuel mass, the water products of hydrogen combustion eliminate any CO<sub>2</sub> emissions. However, this water exhaust results in a greater incidence of contrails with their associated influence over the climate. Despite the high specific energy, hydrogen's low density results in a concurrent low energy density per unit volume. Therefore, the maximum LH<sub>2</sub> that may be carried on the aircraft is limited by the volume available, as opposed to the maximum structural load of the airframe. The combustion characteristics of LH<sub>2</sub> also necessitates the development of combustion chambers suitable for the fuel. The chambers must be designed to ensure complete combustion of the fuel by considering all aspects of the combustion process. Two such concepts for LH<sub>2</sub> fuel are the Lean Direct Injection and Micro-mix concepts [60]. The low residence time of these combustor designs also supports a reduction in NO<sub>x</sub> emissions. Safety is a key concern with the use of LH<sub>2</sub> as fuel, especially due to public perception of hydrogen as a dangerous substance. Although the fuel has a good safety record, the different characteristics of hydrogen in comparison to hydrocarbon fuels will require new industry standards for transportation, storage and use [61].

The primary requirement for commercial viability as a fuel source for aviation is to ensure that the fuel price is economically sustainable. ICAO identifies that one of the main barriers to the implementation of biofuels is the price gap between conventional aviation fuels and biofuels [8]. This will also be a challenge for LH<sub>2</sub>, as there is no infrastructure for the large scale production of LH<sub>2</sub> for aviation. Ideally, the price per unit energy of LH<sub>2</sub> should reach a similar point to the price per unit energy of kerosene. The future cost of liquid hydrogen as an aviation fuel is unknown, with targets lying at around \$2.00 per kilogram by 2020. Estimates of the price per kilogram LH<sub>2</sub> for the aviation industry are currently significantly higher than the price of kerosene at around \$6.90 per kilogram LH<sub>2</sub> [62, 63]. At the 2017 fuel price, LH<sub>2</sub> is close to five times the cost per unit energy of kerosene. However, the price of LH<sub>2</sub> may be expected to reduce, particularly if industry focus is moved towards LH<sub>2</sub> as a fuel. In addition to reducing production cost, it would be necessary to ramp up LH<sub>2</sub> production rate to an amount sufficient for aviation's requirements [64].

Synthetic and biofuels have the advantage of being roughly the same density and having similar performance characteristics to conventional fuel. Storage requirements are therefore similar and no major design changes are required to accommodate the fuel. Fuel sources such as liquid natural gas and LH<sub>2</sub> differ noticeably from kerosene, and will have a corresponding impact on aircraft design [65]. In particular, these cryogenic and compressed fuels would require specialised tanks able to maintain the correct pressure and volume for the fuel [66]. However, cryogenic liquids can also be used as cryocoolants in advanced propulsion concepts such as intercooling and superconducting electrical system.



## 2. Literature Review

---

There have been a number of aircraft concepts that utilise LH<sub>2</sub> as a fuel source. Silverstein and Hall proposed LH<sub>2</sub> as a fuel source for a number of different military aircraft applications, including a subsonic bomber. Although the proposed applications were military, they noted that the fuel could support higher endurance missions than with conventional hydrocarbon fuel [67]. The Cryoplane project developed a LH<sub>2</sub> fuelled passenger aircraft concept with the aim of assessing the feasibility of a zero CO<sub>2</sub> emissions aircraft. The project found that implementing LH<sub>2</sub> would increase operating empty weight by 20–25% due to structural changes and the addition of LH<sub>2</sub> fuel tanks. As a result, energy consumption increased versus a conventional aircraft [64]. More recently, LH<sub>2</sub> was implemented on the Boeing Phantom Eye, a high altitude long endurance unmanned aerial vehicle. The high energy density of LH<sub>2</sub> fuel was seen as an enabler for high endurance and high efficiency in all these concepts. Hydrogen may also be implemented in fuel cells in electric aircraft, such as on the HY4, a 4-seat passenger aircraft demonstrator [68].

In general, LH<sub>2</sub> would appear to be a promising option for a fuel source in the aviation industry. High energy density by weight will lead to a lower aircraft weight during the course of a flight, and therefore a reduction in mission energy consumption. This lower aircraft weight can also support design changes such as reducing wing area, leading to further reductions in take-off weight or aircraft wetted surface area [65]. Although incorporating LH<sub>2</sub> tanks may necessitate an increase in airframe size, LH<sub>2</sub> has the potential to reduce the energy consumption of commercial aircraft. In addition, LH<sub>2</sub> is a zero carbon fuel and is therefore ideally suited to a more environmentally aware industry in the future.

Although not strictly an alternative fuel source, all-electric aircraft are also an option for zero carbon emissions. In this case, CO<sub>2</sub> emissions may still result on ground from the production of electrical power. In addition, electrical systems cannot currently achieve the energy density of fuel sources such as kerosene or hydrogen. The use of more conventional chemical fuel sources is therefore still the best option for long haul commercial applications.

### 2.4 Techno-economic Analysis

For the greatest performance benefits, it is necessary to move away from conventional technology towards revolutionary concepts. The associated risk for revolutionary technology is high, as performance is based on projections. In addition, the economic risk is high as costs for novel technologies are almost entirely unknown. This leads to a corresponding risk that the technologies will not be commercial viable and hence will not be adopted by the industry. The necessity for economical aircraft in combination with the high risk of novel technology lead towards the final pillar of the research: proving or predicting the economic benefits of novel concepts.

As a commercial product, economic considerations are a crucial component of the aircraft design process. Fuel cost contributes a significant amount to the operating cost of an aircraft and has been a key driver in aircraft development. However, there are other costs to consider, as fuel is only a percentage of overall costs. In addition, the concept should be viable for both the operator and the manufacturer. Naturally, the cost of both developing and manufacturing the aircraft technology will be key factors in a concept's final economic viability as a commercial product. Costs should ideally be factored into the decision making process at a reasonably early stage. The general expectation is that 70-80% of program costs are committed at the early concept phase [69]. For example, fundamental decisions such as the size and capacity of an aircraft will fix a certain cost level for manufacture. A long-haul airliner will never cost the same as a light aircraft, if only because of the costs of material for an aircraft that is significantly larger. Once the preliminary design phase is complete, it can be more difficult to reverse design decisions that are later found to result in high costs of development or manufacture. In addition,

## 2. Literature Review

---

costs incurred by a manufacturer are relatively low in the preliminary phase. The best scope for mitigating or avoiding high costs in a new design is therefore at the preliminary concept phase.

Design optimisation can be used during the development of a new concept to ensure costs are kept low. However, there are generally conflicting goals for a commercial aircraft. An aircraft optimised for fuel consumption will be very different from an aircraft optimised for flight time, noise, emissions, or life cycle costs [70]. Optimisation must therefore account for a number of variables, meaning there is no perfect solution but there may instead be a selection of options that attempt to address conflicting design drivers and that weight each variable differently [71]. It is important to highlight that viability is not only influenced by internal project costs, but also by external factors. An individual concept may therefore be optimised, but nevertheless not be an attractive investment. Section 2.1 identified that fuel price has a dominant role in determining whether a concept will be attractive to potential customers. Competing options, both internally (i.e. a number of proposed concepts) and externally (from other manufacturers) will also influence viability. Other factors such as governmental policy and environmental taxation will play a role, in addition to factors such as airport infrastructure or whether there is a market that may be served by the new aircraft. These factors may lead to a concept that is less attractive to customers, regardless of its state of completion.

Goel and Rich [72] studied the incentives that drive the adoption of new innovations, using a sample set of US airlines. The main conclusion from the study was that more competition in the market led to a higher likelihood for new innovations to be adopted. The study highlighted the point that a significant operating cost difference between existing and new technology was an incentive for adoption. The greater the magnitude of difference, the higher the likelihood of adoption. The study highlights the importance of comparative frameworks in assessing the viability of the aircraft. A dominant factor in the adoption of new technology is whether the benefits offered outweigh the cost versus current technology.

Given all these factors, it is vital to have a framework for assessing the economic aspects of a design at the preliminary phase. This combines both technological aspects, in terms of the ability to meet performance targets such as fuel burn, emissions, or noise levels, and the economic viability, in terms of manufacturer and operator costs. This techno-economic perspective is then used to inform design decisions or determine viability.

A techno-economic and environmental risk assessment (TERA) framework has been used in numerous bodies of research at Cranfield University to assess concepts and policies including performance (aircraft and/or engine), economics, environmental impact, noise, emissions and cost in a modular framework [73]. This framework has been used on a number of research projects, including ULTIMATE (Ultra Low emission Technology Innovations for Mid-century Aircraft Turbine Engines) [74], LEMCOTEC (Low Emissions Core-Engine Technologies) [75], and DREAM (validation of Radical Engine Architecture systems) [76].

Rolt and Kyprianidis [77] performed a design space exploration of new engine core technologies to rank and compare the specific fuel consumption and direct operating cost changes for each option. This was then used to identify the most promising technologies. The framework was also applied to the previously described propfan case by Nalianda *et al.* [78]. Two key unknown costs were identified for a novel technology: maintenance cost and acquisition price, and the sensitivity of operating cost to these unknowns was predicted. Fuel was identified as a key factor in determining viability, reinforcing the historical case of the propfan.

The TOSCA study (Technology Opportunities and Strategies towards Climate friendly transport) presented a techno-economic analysis of various options for reducing CO<sub>2</sub> emissions in Europe for two aircraft types [79]. The goal was to assess the technical, economic and societal issues of the technology, rather than performance aspects alone. The study identified both technologies and changes to operation that would achieve the best reductions in CO<sub>2</sub> emis-

## 2. Literature Review

---

sions and the oil price for which these options would be economically feasible.

Techno-economic perspectives can be used to assist in the decision-making process and when identifying the best combination of design variables and technologies. Mavris *et al.* produced a number of studies that assess the impact of various technology options on an aircraft concept in order to determine economic viability [80]. Probability curves are included that account for uncertainty in the design and are used to determine feasibility and the likelihood of a design reaching target design goals. Each technology infusion is presented as a 'technology metric', with a corresponding impact on performance and cost, amongst other factors. More recently, Burgaud *et al.* considers the different divisions in a manufacturer and their influence on an aircraft development program [81]. The study proposes a number of tools that can be used to compare and select different technology options for the 'ideal solution'. The study focuses on the fact that the different divisions of a manufacturer should be able to make risk-aware decisions in an multi-objective environment with a high level of risk and uncertainty.

Techno-economics can also be used to help determine aviation policies that will encourage investment in an aviation concept. Dray *et al.* [82] used the Aviation Integrated Model (AIM) to perform a study on the CO<sub>2</sub> taxation level required to encourage operators to retire aircraft over 20 years old and to invest in new, more efficient aircraft. The study also included wider perspective of the aviation industry by accounting for the influence of taxation on demand, fares, and fleet composition. The study highlights the interdependencies of different factors, as a change in policy or the introduction of new technology may have a wider ranging effect. The wider effect of technology infusion was also assessed in the study on the silent aircraft by Tam *et al.* [83]. The study predicted regional economic influence of the introduction of a low noise aircraft for both the aviation sector and the wider effects on the economy. In particular, a low noise aircraft was found to boost the local economy, suggesting there may be larger benefits to the introduction of revolutionary aircraft technology. The study also assessed the costs for which the silent aircraft concept may be economically attractive to operator. In particular, the trade-off between purchase price and maintenance cost was identified. This perspective was used to identify where their novel aircraft was more or less attractive than alternative technologies. The study highlighted that policy decisions will influence profitability and that there is a wider context that may need to be considered in the course of developing a revolutionary aircraft. In particular, policy makers must consider the need to maintain a profitable and sustainable industry when setting taxation levels. The TERA study by Nalianda *et al.* [78] was also used to identify the taxation scenario that could be used to incentivise investment in a technology such as the propfan. In general, emissions taxation incentivises investment in more efficient technology where an operating cost benefit alone is not sufficient. However, the necessary taxation level may be high, which may unreasonably penalise the industry.

The studies presented here cover a range of perspectives on the aspects that are required for a techno-economic analysis and a viability assessment. Some focus on how design decisions influence a concept's direct operating cost. Other studies use a techno-economic framework to identify the policy or economic environment that is most favourable for a concept's viability. Others take a wider perspective and assess how an aircraft may influence the wider industry or aircraft market. Whilst the approaches to techno-economics are different, each study consistently highlights the importance of cost and economics in aircraft design. In addition to assessing whether a concept is able to meet performance targets, it is necessary to assess the economic risk that a concept will not be viable. A techno-economic and environmental risk assessment therefore provides a view of risk from an investment rather than performance perspective.

## 2. Literature Review

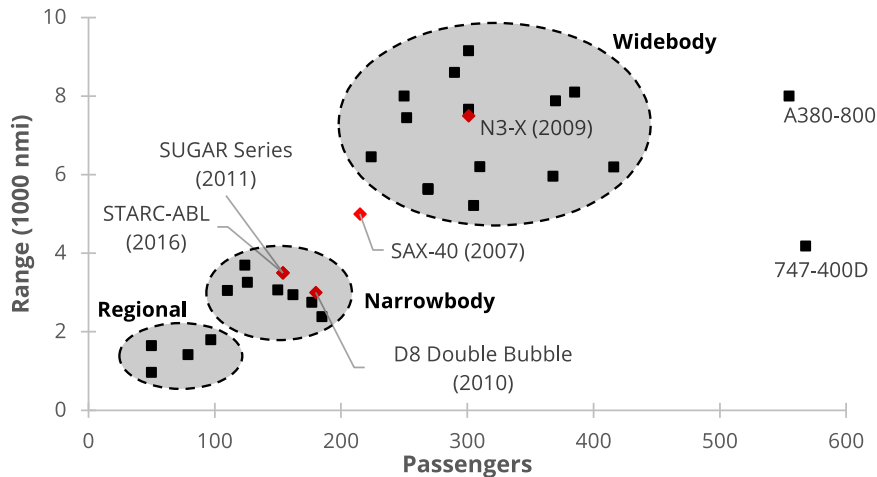


**Figure 2.9:** Main market groupings for the commercial passenger aircraft market with future concepts marked [84]

### 2.5 Emerging Markets in Aerospace

Commercial passenger aircraft can be split into some distinct groupings: Large widebody aircraft for long haul flights, narrowbodies for shorter distance, and small regional jets. There are also additional aircraft types covered in the private class such as business jets and small general aviation aircraft. The general trend for public transportation aircraft is that a high capacity aircraft is associated with long range, whilst low capacity aircraft are associated with shorter range (Figure 2.9). Much focus has been applied to developing highly efficient aircraft options to replace aircraft in these existing markets, as these are the main segments of the industry covered by developmental targets. The early concepts developed for future aircraft have therefore typically fallen into one of the three passenger aircraft groupings. The narrow body market is the largest segment in the commercial passenger aircraft market (66% of total 2015 fleet, and 71% of the predicted 2035 fleet [3]). It therefore follows that most focus is aimed at the narrow body market grouping, with aircraft like the SUGAR series, the D8 Double Bubble and the E-Thrust aimed at the 100-passenger market [15, 36, 47]. However, there are also concepts intended for larger applications in the 300-passenger market, such as the N3-X [24].

The identified commercial aircraft groups suit the 'hub and spoke' typical of many airlines, rather than point to point network. In this hub and spoke network, passengers are concentrated in large hubs and then distribute out towards the final destination (Figure 2.10). However, aircraft are occasionally used well outside of their design mission to suit the needs of the market. Large aircraft have very high capacities that can reduce the number of flights that must be operated on very high density routes. One such example is the use of Boeing 747 aircraft on short domestic routes in Japan. Despite a design range for the B747 series of over 7,000 nautical miles, the airline used the aircraft on routes up to 4,170 nautical miles [85]. This use necessitated modifications to the design to suit very high payload short range flights. The airline therefore made use of a '747-400 Domestic' version of the aircraft with a high passenger capacity and reinforced structure, amongst other design changes, to suit the different mode of operation [84]. This high capacity, short haul aircraft is a market that is not covered by current aircraft. However, it is a market that may become increasingly common as the global aviation market grows. Other aircraft such as the A380 seek to stretch the boundaries of the widebody market group to very high capacity long haul applications. The opposite end of the spectrum for low capacity long haul aircraft is the focus of private or business type applications where a

## 2. Literature Review

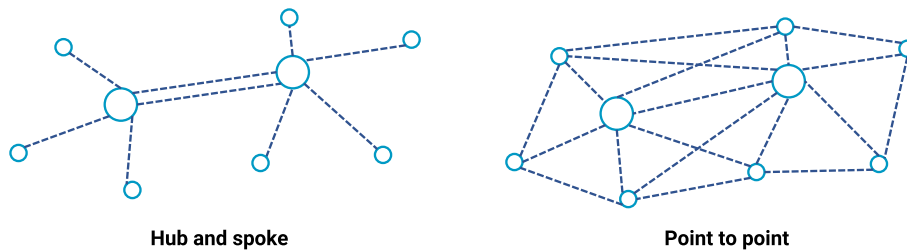


**Figure 2.10:** Hub and spoke versus point to point airline network

more economical option for the operator is less important. There are other possible markets that may emerge for aircraft. For example, Figure 2.9 demonstrates that there is a gap in the 200–300 passenger capacity group. With the current spread of commercial aircraft, this is not currently a major aircraft market. However, it is possible that this may emerge as a new market in the future.

Major airline operators serve relatively larger airports with anything from short haul services up to ultra long-haul, depending on the airport. However, Harish *et al.* identify that only 10% of public airports in the United States are served by major commercial airlines [41]. This is due to the hub and spoke nature of the current airline network, with airlines serving only those airports that are able to handle a larger volume of passengers in the 100+ passenger segments of the market. The remainder of the airports have much lower utilisation and are instead covered by a ‘thin haul’ network of aircraft with capacities in the region of 10 passengers. This thin haul segment of the aviation market has lower demand and a higher operating cost per seat than large commercial airlines. It has therefore not seen the same growth as the 100+ passenger market. However, recent research into high efficiency aircraft propulsion technologies has led to an increase in focus on this market. With the current technology level of electric motors, it is highly unlikely that turbo-/hybrid-/all-electric propulsion systems will be applied to large aircraft in the near future. However, many of the technologies proposed for aircraft such as the N3-X are now being leveraged for new aircraft applications in the 10 seat or less range which are better suited to the current technology level (Figure 2.7). As the propulsive and electric power requirements are lower for a thin haul aircraft, current technology can be used to create hybrid or all-electric propulsion systems for a thin-haul aircraft. A study by Stoll and Mikić concluded that significant energy savings are possible for a thin haul aircraft utilising a distributed electric propulsion system [86]. Although the operating cost saving is lower, due to an increase in aircraft size and hence cost, there is still a net benefit in comparison to a conventional aircraft.

Entirely new markets are also emerging in the aviation industry. Companies such as Uber are looking to introduce air taxi type services providing an on demand transportation service similar to current ground taxis [87]. The requirements of these air taxis are dramatically different to the requirements of large scale commercial transportation, and hence will have a very different set of design drivers.

The concepts being developed for air taxi and thin-haul applications predominantly leverage the novel technologies that were initially applied as part of developing an environmentally friendly commercial aviation industry. Whilst early research may have focused on larger aircraft applications, the current level of technology has opened up the potential for new advancements in the industry. The current technology level already enables the use of electric machines on smaller aircraft, which has led to many of the demonstrator aircraft identified in these sections and flown in recent years. Whilst this research focuses on the application of technology on a larger scale commercial aircraft, current trends suggest that many of the technologies considered will first be seen for an entirely different aircraft segment. Over time, the development of high power density electric machines will enable their application on larger commercial aircraft,



**Figure 2.11:** The N3-X (Image Credit: [NASA](#))

building on progress made for small scale applications.

### 2.6 Work Scope

The present research focuses on a case-study of the NASA N3-X conceptual aircraft, developed by Felder *et al.* [24, 56] (Figure 2.11). The N3-X is designed to reduce energy consumption by at least 60% relative to a conventional ‘best in class’ aircraft with a 2005 EIS. For the purposes of research on the N3-X, the baseline aircraft is the Boeing 777-200LR. Given the current level of technologies such as electric motors, long range concepts are not being actively pursued. In the short term, it is more likely that the tube-and-wing concepts presented in the previous sections will be developed to an advanced technology readiness level. However, the N3-X incorporates a wide range of novel technologies on both the propulsion system and airframe aspects of the aircraft. It is therefore the ideal candidate for studying the potential performance and economic benefits of a wide range of novel technologies. In addition, the N3-X is one of the few configurations that would not need an airframe change to integrate LH<sub>2</sub> tanks. It is therefore well suited to assessing the possible benefits of a LH<sub>2</sub> fuelled aircraft in comparison to conventional kerosene.

Following the established performance characteristics of the selected baseline aircraft, mission level goals have been set for the N3-X aircraft in terms of payload and range requirements. The N3-X is therefore required to achieve a mission range of at least 7500 nautical miles at Mach 0.84 with a full payload (payload mass equal to the aircraft maximum of 53,570 kg). In order to achieve the required efficiency improvements, the aircraft makes use of a number of novel technologies in both the airframe and the propulsion system. The aircraft propulsive power is provided by a distributed propulsion system consisting of an array of propulsor fans which ingest the boundary layer of the airframe, along with free stream air. Electrical power for the propulsor fans is produced by a pair of turbojet/turbogenerator type engines through a superconducting system cooled by liquid hydrogen. The N3-X airframe is a blended wing body planform with main engines assumed to be embedded within the airframe. The embedded engine and propulsor array location provide noise shielding to achieve target noise levels [88]. Fuel burn and CO<sub>2</sub> emissions targets are achieved through a combination of the boundary layer ingesting distributed and turbo-electric propulsion system and a blended wing body airframe. Subsequent chapters cover relevant details and the data available for the propulsion system configuration (Chapter 3) and airframe design (Chapter 4).

Previous research on the N3-X has focused on the design of the airframe and propulsion system [24, 56, 89]. Additional research has also been published on possible architectures for the electrical system [48]. The research has been used to assess the performance of the

## 2. Literature Review

---

N3-X configuration and identify whether the aircraft will be able to achieve the 60% energy saving goal versus the baseline aircraft. However, this chapter has identified the importance of incorporating economics in research for revolutionary technology, as this can be used to inform or guide design decisions and research paths. As previous research has focused on performance and design, there is a key gap in research to determine the economic viability of such an aircraft. The previous sections have identified that establishing the economic viability of a concept is vital to ensure a sustainable industry. Two key questions must therefore be answered for the N3-X: What is the financial value of efficiency improvements offered by the novel technologies of the aircraft? Secondly, in what situations or scenarios would the aircraft be financially viable?

This research will therefore address the techno-economic and environmental risk assessment aspects of a novel aircraft such as the N3-X. As a part of this process, a design space exploration was conducted to identify possible alternative configurations that it may be useful to consider as research progresses on the N3-X or similar concepts. Two main aspects of the design were considered. First was the option for liquid hydrogen as a fuel source. LH<sub>2</sub> has already been proposed as a potential cryocoolant for the aircraft. However, LH<sub>2</sub> has been identified as a low weight, low CO<sub>2</sub> emissions alternative to current hydrocarbon fuels. LH<sub>2</sub> is therefore ideally suited for a more environmentally aware industry. The research also explores the design space for the novel propulsion system design utilised by the N3-X. Distributed and turbo-electric propulsion systems have been identified as a configuration that provides significant design flexibility. It is therefore useful to assess promising avenues for further research. This then contributes towards a technology roadmap for the aircraft and its constituent technologies.

To achieve the stated aims, the research was split into three phases (Figure 2.12):

1. Develop models to simulate a novel aircraft and propulsion system
  - Novel aircraft planform (blended wing body)
  - Novel propulsion system configurations including boundary layer ingestion, distributed propulsion, and turbo-electric propulsion
2. Develop a framework to predict the economic viability of novel aircraft concepts
  - Direct operating cost and investment cost analysis
  - Identify and account for cost uncertainty in the direct operating cost of a novel aircraft
  - Develop a comparative framework for the economic viability of novel aircraft
3. Perform a risk assessment and identify a technology roadmap for the aircraft

Throughout this research, simulations and model development has taken place to a level of fidelity suitable for preliminary design. The aircraft and technologies assessed in this research are at an early conceptualisation stage. Therefore, by making use of preliminary design tools, the design search space can be more fully explored. This can then be used to more easily identify the design parameters that may be most useful and the greatest risk factors. Further research may then be conducted to narrow down options for the aircraft design and reduce the uncertainty inherent in a novel aircraft. Design conclusions made in this research therefore provide an insight and prediction of performance.

### 2.7 Contributions from the Research

The literature review has presented an overview of emerging trends in aircraft technology and the aviation industry. Developmental goals for aviation have set challenging targets with the

## 2. Literature Review

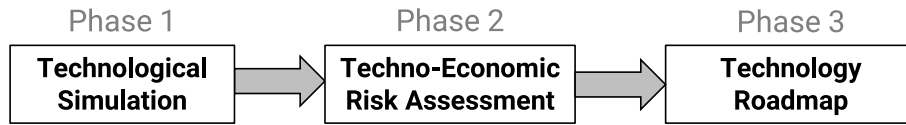


Figure 2.12: Research phases

aim of establishing a more environmentally sustainable industry. This has necessitated the development of revolutionary new technologies with lower emissions and energy consumption. Despite constant growth in the industry, profit margins remain low. It is therefore vital to ensure that the aviation industry remains economically sustainable. In a commercial industry, cost is the dominant decision factor. This can be easily demonstrated using the historical case of the propfan engine concepts of the 1980s [14]. The propfan offered an efficiency increase ideal for the then high fuel price market. However, a drop in fuel price reduced the attractiveness of investment in expensive, novel technologies, despite a demonstrable efficiency increase. Development of propfan engines was subsequently halted, following a lack of interest by airline operators. The reduction in fuel consumption offered by the propfan no longer justified cost of investment in novel technology [78]. Cost is therefore a vital decision factor in the selection of future investment in the aviation industry. This is especially true where risk is high.

The technologies presented in the previous sections are promising from a performance standpoint, but their economic viability is unknown. A wide range of concepts are currently being researched to achieve developmental goals. *If it can be assumed that each competing concept is designed for the same performance level, then the only method to differentiate between options is cost.* In a profit-oriented industry, decisions cannot be made from an altruistic perspective. As the end goal is for the industry to adopt environmentally friendly technologies, it is vital to ensure that the technologies selected for further development are those that will be financially attractive or profitable. The cost of a concept must be considered at an early stage in order to determine its economic viability and rule out those technologies that may not be attractive. This highlights the necessity for a techno-economic analysis, even when aircraft concepts are at an early development stage. Otherwise, the industry runs the risk of developing technologies that will not be adopted by manufacturers or operators as costs would be prohibitive.

The work scope identifies a number of aspects that must be addressed to develop a techno-economic and environmental risk assessment of a novel aircraft. The previous sections have presented a number of different perspectives on how a techno-economic assessment can be performed. However, two key gaps in research have been identified that this research attempts to address. When dealing with evolutionary technology, cost estimates can be made with reasonable accuracy, as there is historical data on which estimates can be based. It is therefore relatively simple to determine whether a new technology is likely to be profitable. *For revolutionary or novel technologies, estimating cost is more difficult and hence it can be challenging to make conclusions regarding an aircraft's viability without including a large number of assumptions. It is nevertheless useful to have some way of predicting the viability of a concept in order to ensure financial viability and encourage investment.* This is particularly important for revolutionary concepts, where the perception of high risk may deter the investment necessary for the technology's implementation. Another key gap is the *need for comparative assessments, including the influence of policy and external economic factors.* An aircraft can be optimised for minimum cost or for a certain performance target, however, the concept will fail if a competitor offers a more cost effective option. Techno-economic modelling generally focuses on optimising or assessing a single aircraft, without comparing its viability to alternatives. The study by Goel and Rich [72] highlighted that a significant operating cost difference between existing and



## 2. Literature Review

---

new technology was an incentive for adoption. Comparative assessments that identify whether there is a significant operating cost difference are therefore a vital aspect of determining a concept's viability. Similarly, investment cannot be justified if the savings offered by the new technology are not significant. This comparative assessment can be used to view development from the airline customer perspective, in order to identify whether technologies will be attractive investments.

This research addresses the two identified gaps in research and presents a framework for assessing the viability of a novel aircraft concept. The framework used by Nalianda *et al.* [78] was extended to be applied to novel aircraft. This research presents the application of a comparative framework of assessment that is intended to present a operator's perspective for the manufacturer on determining whether a concept is economically viable and suitable for investment. The main aim of this research can be summarised as follows:

TO DEVELOP A TECHNO-ECONOMIC METHODOLOGY TO ASSESS, COMPARE, AND SELECT ENVIRONMENTALLY OPTIMISED AIRCRAFT CONCEPTS UTILISING NOVEL TECHNOLOGIES

During the course of the research, a further gap in literature was identified. Modelling procedures were required for boundary layer ingesting propulsion systems as an element of modelling a novel aircraft configuration. Previous models published in literature focus on proving the potential benefits of BLI propulsion. These studies therefore focus on design point sizing and performance. As research on aircraft with BLI propulsion progresses, it becomes necessary to develop tools that are able to simulate the performance of such systems at a wide range of operating points. A generic off-design modelling procedure that can be consistently applied to different configurations was therefore required as a component of the research. A workflow and tool for modelling BLI propulsion systems was developed during the course of the research to address this gap in current research. Subsequently, an aircraft performance modelling tool was developed to integrate the BLI propulsion system modelling workflow. The secondary aim of the research may therefore be summarised as follows:

TO DEVELOP A GENERIC WORKFLOW TO DESIGN AND SIMULATE THE PERFORMANCE OF A BOUNDARY LAYER INGESTING PROPULSION SYSTEM AT OFF-DESIGN, SUITABLE FOR USE WITH AIRCRAFT PERFORMANCE SIMULATION METHODS

# 3. Propulsion System Modelling

This research focuses on the analysis of the N3-X aircraft. In the performance modelling phase of research, models were required to suitably simulate the performance of the aircraft in order to estimate fuel consumption and CO<sub>2</sub> emissions. This chapter details the development of models to simulate the novel propulsion system of the N3-X. Section 3.1 details the development of a new workflow for simulating the performance of a boundary layer ingesting propulsor. Whilst the method is presented with application to the N3-X propulsors, the method is a generic workflow in a modular framework that can be applied to any BLI configuration. The section also includes a description of a new workflow for simulating the performance of a BLI propulsion system at off-design.

In addition to BLI propulsors, the N3-X propulsion system consists of a pair of turbomachines that provide power to the array through a superconducting electrical system. Simulations of this turbo-electric system require the definition of a method to estimate performance of the system as a whole. The size of the turbomachinery is based on the power requirement and hence size of the propulsor array. This then produces the performance of the N3-X propulsion system at design point. Off-design simulations must link the performance of the propulsor array with the performance of the turbomachinery at the specified operating point. In the turbo-electric system case, the link between these systems is the power demand from the array and the available power from the turbomachinery. This necessitates a matching process between the two systems to ensure the power demand matches the available power and vice versa. Section 3.2 details the development of a modelling procedure for the N3-X turbo-electric propulsion system. The remaining sections present analyses of the N3-X propulsion system design variables and the factors that influence its performance. Finally, a ‘baseline’ propulsion system configuration was defined against which alternative propulsion system configurations for the N3-X can be compared.

## 3.1 Boundary Layer Ingestion

Aircraft concepts are being developed that make use of novel configurations to achieve improvements in efficiency through performance benefits to the airframe and propulsion system. Boundary layer ingestion (BLI) is one such technology that has been implemented in a number of conceptual designs. In an aircraft, the boundary layer contributes to drag and results in a momentum deficit, or wake, and is therefore detrimental to performance. The boundary layer can be similarly detrimental to the propulsion system, as a turbulent boundary layer gives rise to non-uniformities in the flow which negatively impact performance. Conventional propulsion system design therefore typically seeks to avoid ingesting any boundary layer flow. This is generally achieved by methods such as bleeding/diverting the boundary layer away from an inlet or with podded engines well outside the airframe’s boundary layer. However, boundary layer ingestion provides a way in which the boundary layer may be used to improve the overall efficiency of the aircraft and reduce fuel consumption. Rather than ingesting only free-stream

### 3. Propulsion System Modelling

---

flow, a BLI propulsor ingests some or all of the boundary layer (Figure 2.4). The resulting lower average velocity of the boundary layer flow reduces the momentum drag at the inlet of a propulsion system. The same thrust may therefore be produced using less power than an equivalent propulsion system in free-stream flow [20]. Boundary layer or wake ingestion as a concept is already implemented in marine propulsion, and research suggests that it can provide similar benefits to efficiency in aviation applications [90]. Research has shown that fuel savings in the region of 5-10% can be achieved by using boundary layer ingestion as opposed to a conventional free-stream propulsion system [56, 90, 91].

Simulating the performance of a boundary layer ingesting propulsion system presents a number of challenges. In a conventional podded engine configuration, the airframe and engine may be easily differentiated. This supports conventional thrust-drag bookkeeping, where the forces resulting from each system may be relatively easily identified. However, in a BLI system, the propulsion system is closely integrated with the airframe. The propulsion system influences airflow over the airframe and vice versa, therefore complicating conventional propulsion system bookkeeping. To circumvent the difficulty of drag bookkeeping in an integrated BLI system, analyses can instead assess the system as a whole, rather than differentiating the propulsion system and airframe. Previous research on the simulation of BLI systems can therefore be broadly split into two categories: whole system analyses and methods that define control volumes to separate the two systems. A further split can be made between computational fluid dynamic (CFD) analyses of the problem, and lower-order analytical methods. CFD methods are useful for the analysis of the combined aircraft and propulsion system. However, it is important to be able to predict the performance of the propulsion system at a preliminary design stage without expensive experimental methods or complex and time-consuming simulations. This is especially important during the evaluation of a set of competing technologies or during configuration down-selection. It is therefore useful to have a rapid, low-order analytical method which is suitable for simulations of the overall performance of an air vehicle with an integrated BLI system.

There are a number of factors that should ideally be represented in a BLI simulation. The boundary layer has a deficit in mass flow, momentum and kinetic energy relative to free-stream flow. This deficit is due to a variation in pressure, velocity and density from the no-slip surface of the boundary layer. The distorted flow may also result in a reduction in fan or compressor efficiency and an increased total pressure loss in the intake. Evaluation of the influence of the boundary layer on performance is therefore a key aspect of a BLI model. The boundary layer itself may be modelled with simple correlations, integral boundary layer equations or a case-specific CFD analysis. These representations have been used in internal force control volumes to estimate the performance of the propulsion system [20, 92, 93]. These control volumes typically deal with the propulsion system as an isolated or uninstalled system in a similar manner to conventional propulsion system analysis. A challenge of the integral boundary layer or one-dimensional control volume method is that flow distortion due to the boundary layer and the influence of the boundary layer on fan or compressor performance is not directly represented. This may instead be estimated by a parallel compressor / parallel stream method [20, 94]. The method splits the flow into a number of streams to assist in prediction of asymmetric flow's impact on a compressor [95].

To circumvent the difficulty of thrust-drag bookkeeping in an integrated BLI system, the power balance method developed by Drela assesses the aircraft system as a whole [96]. A similar method was presented by Arntz et al that uses an exergy analysis of the aircraft and propulsion system [97]. Methods that simulate the aircraft and engine as a combined system avoid the challenges of separately simulating the two components of an integrated system. However, such methods are reliant on a more detailed knowledge of the configuration, which

### 3. Propulsion System Modelling

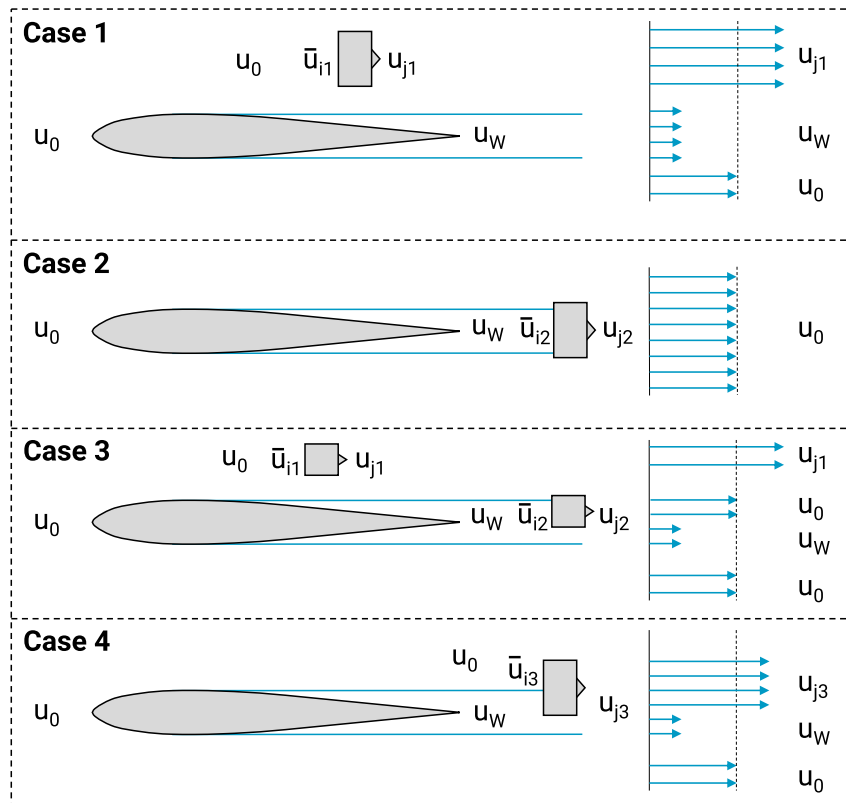


**Figure 3.1:** Example cases comparing conventional and boundary layer ingesting propulsion systems

is less suited to the conceptualisation of a propulsion system configuration. In addition, conventional point mass based aircraft performance models are typically reliant on the ability to separate the thrust and drag of the aircraft and propulsion system. Methods based on more conventional force control volumes are therefore useful at the early stages of design, particularly as aircraft and propulsion system design will typically be conducted by different design groups.

The previous methods for BLI simulation have drawbacks in that they rely either too little on the aircraft configuration (in the case of the uninstalled performance methods), or too much on the configuration (in the case of the exergy and energy methods). Nonetheless, conventional force control volume methods are more suitable for the purposes of both preliminary design and integration in aircraft performance analyses. Previous force control volume methods use a thrust and drag accounting system similar to the uninstalled performance calculations for conventional podded engines. However, BLI systems are inherently integrated and must include aspects of the aircraft configuration to sufficiently represent performance. The integration factor in a BLI system is considered to be a vital part of the system simulation.

Typically, research on performance of BLI systems focuses on proving and identifying the benefits of a BLI system and hence focuses on design point sizing and performance. However, the research does not address the requirements of simulating the performance of a BLI propulsion system at off-design. As research progresses on BLI systems, a more complete assessment of performance at a range of operating points is vital to fully understand performance. In addition, modelling methods are required to predict the mission performance of aircraft utilising BLI propulsion systems as part of the conceptualisation process. There is therefore a gap in research on tools for off-design simulation of a BLI propulsion system.

A novel method is therefore required that includes the integration aspects of the system, whilst remaining flexible enough to accommodate design changes or to be used for different

### 3. Propulsion System Modelling

configurations. A key requirement is the ability to consistently compare different configurations by defining a method that is applicable to any layout or system architecture. The model builds on previous force control volume methods to attempt to address the identified gaps in research through the following work scope:

- Represent a boundary layer ingesting propulsion system using an *installed perspective*
  - Control volume suitable for an integrated boundary layer ingesting propulsion system
  - Location-specific difference in flow characteristics
- Develop a workflow for simulating the performance of a boundary layer ingestion propulsion system at *off-design*
- Represent performance results in *suitable form for use in conventional point mass-based aircraft performance models*
- Develop a *generic method that is able to consistently compare* different configurations and system architectures

#### 3.1.1 Performance Benefits from BLI

Previous research has identified that boundary layer ingestion can be beneficial to an aircraft's performance. The source of this benefit may be identified by assessing a selection of theoretical cases (Figure 3.1). The first case is a conventional configuration with podded engines in free-stream flow. The second case is a boundary layer ingesting propulsor sized to ingest the entire airframe wake. Finally, the third and fourth cases are a combination between the two cases, with a propulsor sized to ingest half the wake, with the remaining thrust provided by a free-stream propulsor. In the examples, Subscript 1 refers to free-stream only, Subscript 2 to boundary layer only, and Subscript 3 to mixed free-stream and boundary layer flow.

Each propulsor (or pair of propulsors in case 3) is sized to produce thrust equal to the drag of the body during flight. There are a number of velocities relevant to the cases. The first is the free-stream flight velocity,  $u_0$ , which is constant for a given flight condition.  $u_w$  is the velocity of the wake, whilst  $\bar{u}_i$  is the average velocity at the inlet of the propulsor. The actual value of  $\bar{u}_i$  depends on where the propulsor is located. A propulsor entirely in the free-stream has  $\bar{u}_i$  equal to  $u_0$ , whilst a propulsor located partially in free-stream and partially in boundary layer air  $\bar{u}_i$  equal to the average velocity of the incoming streamtube of air. Finally,  $u_j$  is the exhaust velocity of the propulsor.

For a simple propulsor, its size and performance may be calculated using the method flowchart in Figure 3.2. In this example process, the mass flow required to produce the requisite net thrust is unknown. The gross thrust is therefore non-dimensionalised by the

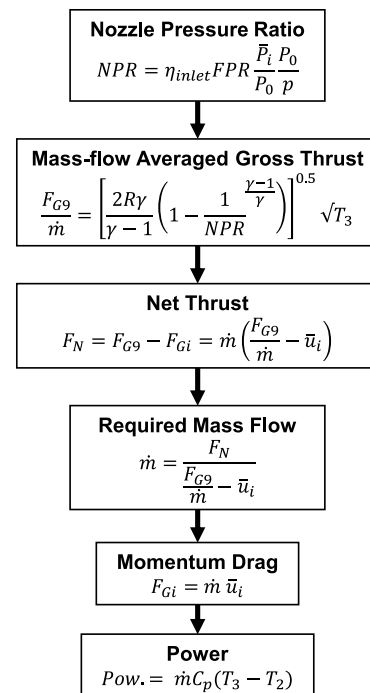


**Figure 3.2:** Simple propulsor performance calculations

### 3. Propulsion System Modelling

---

mass flow to allow the non-dimensional gross thrust to be calculated as a function of propulsor performance variables only. In a conventional propulsion system, Case 1, average incoming velocity,  $\bar{u}_{i1}$ , is equal to the free-stream velocity,  $u_0$ . The exhaust jet velocity,  $u_{j1}$ , depends on the propulsion system configuration (in this case, the fan pressure ratio, FPR). The mass flow entering the propulsor,  $\dot{m}_1$  is then determined by the sizing requirement to achieve the requisite thrust.

In Case 2, the BLI propulsor, the mass flow entering the propulsor can be determined by assuming that the propulsor ingests the entire wake. Similarly, the average incoming velocity,  $\bar{u}_{i2}$ , is equal to the wake velocity,  $u_w$ . These two factors influence the requisite gross thrust,  $F_{G9}$  and hence the fan pressure ratio required to provide the target net thrust. This then leads to the identification of one of the core benefits of a boundary layer ingesting propulsion system. Assuming the same fan pressure ratio (or propulsion system configuration) there is a key difference between a free-stream and BLI propulsor: the average velocity of the incoming streamtube. In a BLI propulsor, the average velocity is lower than free-stream leading to a lower momentum drag than for a free-stream propulsor with the same size. As a result, the gross thrust required from the propulsor is lower than for a free-stream propulsor. In the free-stream propulsor, the higher momentum drag necessitates a higher gross thrust and a higher mass flow than in the BLI propulsor. As a result, the power demand of a free-stream propulsor is higher than a BLI propulsor. The relevant relationships for this description are shown below:

$$\dot{m} = \frac{F_N}{\frac{F_{G9}}{\dot{m}} - \bar{u}_i} \quad (3.1)$$

$$\text{Power} = \dot{m} C_p \Delta T \propto \dot{m} \quad (3.2)$$

For a fixed propulsion system configuration:

$$\frac{F_{G9}}{\dot{m}} = \text{Constant} = f(\text{FPR})$$

$$\bar{u}_{i,\text{BL}} < u_0$$

Therefore:

$$\dot{m}_{\text{BL}} < \dot{m}_{\text{FS}}$$

Power demand for the BLI propulsor is therefore lower, as the enthalpy change ( $C_p \Delta T$ ) over the propulsor fan is constant for a fixed fan pressure ratio.

A difference in average velocity at the intake is not the only difference in between a BLI and freestream propulsion system as the boundary layer leads to pressure, velocity and momentum deficits versus the same area in free-stream flow. The total pressure deficit of the streamtube due to the presence the boundary layer,  $\bar{P}_i/P_0$ , lowers the overall pressure ratio through the propulsor and hence leads to a slightly lower gross thrust than would be produced by a free-stream propulsor with the same fan pressure ratio. The momentum deficit leads to the result that mass flow through a unit area of the boundary layer is lower than the same unit area in free-stream flow. In addition, the mass flow through the area depends on where in the boundary layer flow and how much of the boundary layer is ingested. Research nevertheless suggests that the power required for a BLI propulsor is lower than for a free-stream propulsor, as a result of the momentum deficit. However, excessively high total pressure losses will negate any benefits from ingesting the boundary layer. Similarly, flow distortion will decrease component efficiency and will therefore increase power demand versus a conventional free-stream propulsion system [20].

In Case 3, the system combines a free-stream and BLI propulsion system. The system is

### 3. Propulsion System Modelling

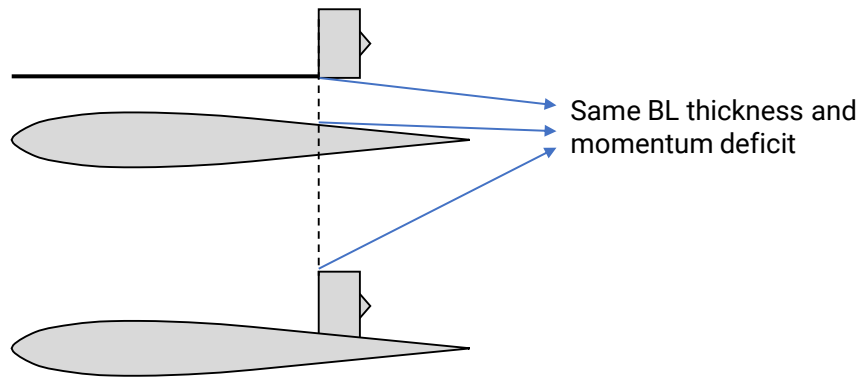


**Figure 3.3:** Boundary layer ingestion with an added plate versus fuselage boundary layer

therefore not as efficient as BLI only system, due to the introduction of a free-stream propulsor. However, the presence of a BLI propulsor leads to a lower power requirement than for a system ingesting only free-stream flow. For a BLI propulsor ingesting more than the entire boundary layer, Case 4, the average velocity at the inlet,  $\bar{u}_i$  is still less than the free-stream flow velocity,  $u_0$ . The required gross thrust,  $F_{G9}$  and mass flow for the system is therefore lower than for the free-stream system and hence leads to a lower power requirement than for a free-stream system. However, the average incoming velocity is higher than that of a system ingesting the boundary layer only. A mixed flow system therefore has a higher power requirement than a BLI only system. Nevertheless, a mixed flow or combined system is useful for aircraft applications, as it is generally not feasible to ingest the entire airframe boundary layer. Benefits can therefore be gained by using a boundary layer ingesting propulsor to produce some thrust, with the remainder produced with free-stream flow (either mixed flow or a separate system).

As much of the benefit of BLI lies in taking advantage of the momentum deficit, a question arises as to whether similar benefits can be gained by, for example, mounting a plate in front of the propulsion system to slow down approaching flow (Figure 3.3). Assuming the same momentum deficit as the fuselage boundary layer is achieved, there will be the same reduction in momentum drag of the propulsion system as a system ingesting the fuselage boundary layer. However, the introduction of the flat plate increases the drag of the aircraft, hence increasing the net thrust requirement. There is therefore no net benefit for the system. In contrast, a net benefit can be achieved if the propulsion system utilises the pre-existing momentum deficit of the fuselage.

Depending on the perspective, BLI can also be presented as an airframe benefit. In a case where flow is accelerated up to or beyond the free-stream velocity, the BLI system is a wake re-energising system. This wake re-energisation balances out the drag from momentum deficit that would otherwise result from a body moving in a fluid. This can be represented as reduction in airframe drag. The previous descriptions have presented BLI in terms of the propulsion system benefit by reducing the momentum drag of the intake. This assumes a propulsion system control volume which starts at or close to the propulsion system's intake, implying that the momentum drag of the propulsion system is influenced by the presence of the boundary layer. If the propulsion system control volume begins in free-stream ahead of the intake, momentum drag is the same as for a free-stream system. The benefit of BLI now moves to the airframe as a 'drag recovery' term. In this perspective, BLI is purely detrimental to the propulsion system due to flow distortion and the total pressure deficit. This control volume presents some difficulties for separating the propulsion system and airframe performance, as a portion of the airframe drag is included in the propulsion rather than airframe control volume. Designing a wake re-energising system defines a propulsion system size and configuration, as

### 3. Propulsion System Modelling

---

the entire boundary layer must be ingested (defining mass flow into the system) and accelerated to free-stream velocity (defining exhaust velocity and hence FPR for a simple propulsor).

Another useful perspective to take is to compare frames of reference for aircraft simulation. In the conventional frame of reference, the aircraft is still and air moves at the flight velocity. From this perspective, the presence of the viscous surface slows the flow velocity: the momentum deficit of the boundary. A more realistic frame of reference is to consider that the air is static and the aircraft is moving. From this perspective, the presence of the viscous surface imparts a velocity to otherwise static air to form the wake. This implies that energy has been provided to the air from the aircraft to form a wake travelling at a portion of the aircraft velocity. In a BLI propulsion system, a portion of this energy is recovered by re-ingesting this boundary layer flow, rather than 'losing' the energy in the wake.

#### 3.1.2 Thrust and Drag Accounting

The forces produced by an aircraft in flight can be split to belong to either a propulsion system or an airframe force accounting system in support of conventional descriptions of aircraft performance [98]. In steady level flight, the net thrust produced by a propulsion system should be adequate to counter the drag of the combined airframe and installed engine. Differentiating these forces is a relatively simple matter for an aircraft with podded engines, as there is limited interaction between the engine and airframe. However, for aircraft with more integrated architectures it becomes more difficult to differentiate between the airframe and the propulsion system [91]. This is typically the case in a military aircraft, where the engines may be embedded in the airframe. However, it is nonetheless useful to separate the force accounting of the engine and airframe, as the design of the two components will generally not be combined and will be performed by different groups at a preliminary design stage. Typically, thrust is defined as a 'standard net thrust' term, the difference between the gross thrust at the nozzle exit and the gross thrust far upstream. However, a boundary layer ingesting propulsion system is an integrated system that is reliant on the airframe for performance. In an integrated or installed system, additional terms may also be assigned to the propulsion system thrust-drag bookkeeping. Performance may instead be represented by a Net Propulsive Force (NPF), which includes the force terms associated with the engine cowl and afterbody, spillage drag, and interference drag.

In a BLI system, flow entering the intake has passed over the surface of the aircraft fuselage. It could therefore be argued that the entire fuselage section prior to the intake is a part of the propulsion system control volume. This leads to the requirement to define an appropriate control volume for an integrated BLI propulsion system. There are two potential definitions of control volume for a boundary layer ingesting propulsion system, defined here as an internal and external control volume (Figure 3.4).

In an internal control volume, the control volume covers the propulsion system alone. There are two challenges to highlight with this definition. Firstly, the airframe drag ahead of the intake is now influenced by the suction of the propulsion system. Airframe drag estimates therefore rely on the propulsion system operating point, as drag when the propulsion system is at high power will differ from drag when the propulsion system is at lower power. In addition, the behaviour of the boundary layer and streamtube as it expands or is compressed into the intake is unknown. For a mass flow ratio of one, streamtube height and hence boundary layer thickness can be assumed to be constant from where engine suction begins to influence air flow up to the intake. However, for other mass flow ratios, streamtube size will change as flow enters the intake. Boundary thickness before air enters the propulsion system's region of influence is known. However, boundary layer thickness at the start of the propulsion system control volume



### 3. Propulsion System Modelling

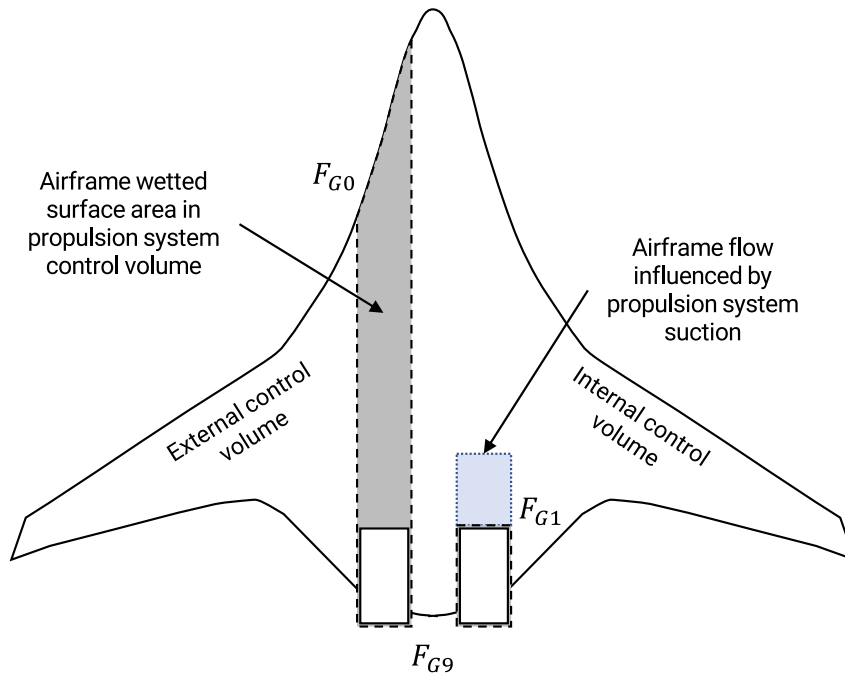


**Figure 3.4:** Comparison sketch of two propulsion system control volumes for a BLI propulsion system

(i.e. the inlet highlight in this case) is unknown, unless a capture area ratio for the propulsion system is assumed.

In an external control volume, the control volume starts at the leading edge in free-stream flow, covering the entire region ahead of the intake. However, this control volume includes all the skin friction drag ahead of the propulsion system intake. Propulsion system performance calculations therefore include airframe drag, which must be removed from the airframe control volume and added to the propulsion system. Wake re-energisation therefore leads to an airframe rather than propulsion system benefit, as the only impact on propulsion system performance calculations results from total pressure deficit and loss in performance due to distorted flow. As with the internal control volume, some knowledge of the boundary layer behaviour is required in order to determine total pressure entering the propulsion system and other boundary layer-influenced parameters.

Both of these control volumes complicate performance calculations, as propulsion system and airframe control volume elements are combined. Instead, a suitable interface point,  $i$ , can be chosen which indicates the region where engine thrust and drag can be separated from the aircraft flight conditions, and vice versa (Figure 3.5). This is estimated to lie approximately two inlet heights ahead of the highlight [99, 100]. In some cases, the definition of a local free-stream station,  $0_i$ , can also be useful, that defines the flow conditions just above the boundary layer. With this control volume it becomes easier to split propulsion system and airframe-influence parameters. In addition, the boundary layer thickness and characteristics can be estimated independently from the propulsion system as it is influenced by the airframe only up to the start of the propulsion system control volume.

As with a conventional propulsion system, the net thrust produced by the propulsion system should counterbalance the aircraft drag in steady level flight. However, the control volume is defined to begin slightly ahead of the inlet at station  $i$ . Therefore, the net propulsive force for a BLI system may be defined as follows (Figure 3.5):

$$\text{NPF} = F_{G9} - F_{Gi} - \tau_{w,i} S_{\text{wet},i} - D_{\text{nacelle}} = D_{\text{aircraft, clean}} \quad (3.3)$$

### 3. Propulsion System Modelling

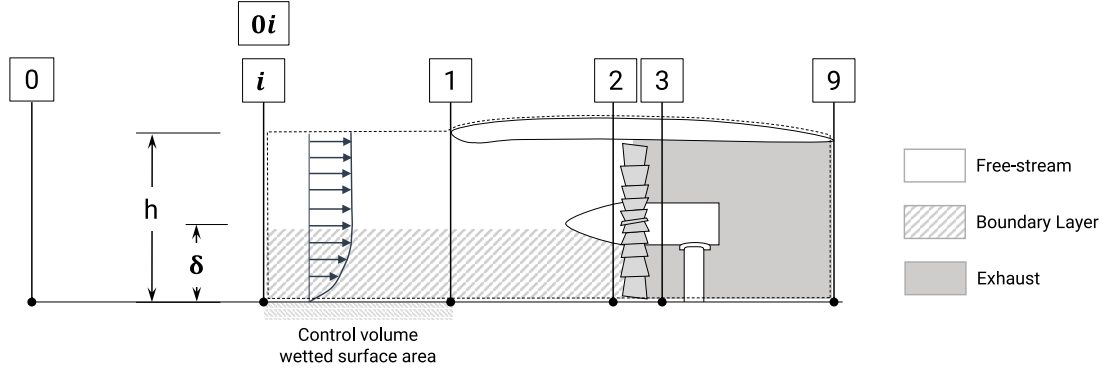


**Figure 3.5:** Propulsion system control volume and station definition.

Where  $F_{G9}$  is the nozzle gross thrust,  $F_{Gi}$  is the momentum drag,  $\tau_{w,i}S_{wet,i}$  is the skin friction of the surface from the interface point to the inlet, and  $D_{nacelle}$  is the nacelle drag. The difference between  $F_{G9}$  and  $F_{Gi}$  is analogous to the conventional net thrust term used in propulsion system performance reporting. For a free-stream propulsor, the velocity is equal to the free-stream velocity and hence  $F_{Gi}$  is equal to  $F_{G0}$ . In addition the skin friction is no longer a part of the control volume. The definition of NPF for the BLI system therefore becomes equal to the conventional definition for a free-stream system.

An additional modification to the formula should also be applied. In many configurations, the BLI propulsion system is mounted on the fuselage surface. In the clean aircraft case, the drag of the surface that would otherwise be covered by the propulsion system is accounted for in the airframe drag calculation. Once the propulsion system is included, the drag of this surface is now covered by the propulsion system control volume. This portion of the fuselage drag should therefore be removed from the total airframe drag. To ensure that the airframe drag calculation remains independent from the propulsion system definition, this drag term may instead be added on to the propulsion system's NPF definition as a  $\Delta D$  term:

$$NPF = F_{G9} - F_{Gi} - \tau_{w,i}S_{wet,i} - D_{nacelle} + \Delta D = D_{aircraft,clean} \quad (3.4)$$

This  $\Delta D$  term is equal to the skin friction drag of the surface covered by the propulsion system control volume.

In the formulation shown in Equation 3.4, an installed perspective is taken and the skin friction within the control volume and nacelle drag are therefore included on the propulsion system side of the equation. For an aircraft of a fixed size (i.e. fixed  $D_{aircraft,clean}$ ), the net propulsive force required from the system is constant. For a net thrust formulation, the net thrust requirement would otherwise change based on the size of the propulsor. This enables analysis of the installed BLI system performance independently from the aircraft performance. This formulation also supports the use of conventional aircraft performance methods by maintaining a separation between the airframe and propulsion system.

#### 3.1.3 Boundary Layer Flow Characteristics

Equations which describe the flow in a boundary layer can be derived from the Navier-Stokes equations for viscous flow. These equations reduce to a more easily solvable form than the full Navier-Stokes equations through the application of appropriate limits to the integrals and with the use of velocity profile approximations [101]. The  $1/n^{\text{th}}$  power law relationship provides one form of velocity profile approximation, where a typical value used to approximate a fully developed boundary layer is  $n = 7$  [102]. A number of methods are also available for estimation

### 3. Propulsion System Modelling

of the boundary layer thickness,  $\delta$ , and characteristics. One such boundary layer thickness estimation is a simple turbulent flat plate approximation of the boundary layer [103]. The flow regime for the case under consideration determines whether laminar or turbulent boundary thickness assumptions should be applied. Alternative functions may provide more suitable estimations of the boundary layer thickness for the specific configuration and flow regime at which the system operates. A number of additional dimensions that define the boundary layer are available. These are the displacement thickness ( $\delta^*$ ), momentum thickness ( $\theta$ ), and energy thickness ( $\theta^*$ ) [104]:

$$\frac{\delta^*}{\delta} = \int_0^\infty \left[ 1 - \frac{\rho_y u_y}{\rho_0 u_0} \right] dy \quad (3.5)$$

$$\frac{\theta}{\delta} = \int_0^\infty \frac{\rho_y u_y}{\rho_0 u_0} \left[ 1 - \frac{u_y}{u_0} \right] dy \quad (3.6)$$

$$\frac{\theta^*}{\delta} = \int_0^\infty \frac{\rho_y u_y}{\rho_0 u_0} \left[ 1 - \left( \frac{u_y}{u_0} \right)^2 \right] dy \quad (3.7)$$

Each boundary layer thickness term represents the distance by which the surface would have to be displaced in an inviscid flow in order to result in the same mass flow, momentum or kinetic energy as the viscous flow. By making use of these definitions, the boundary layer flow characteristics may be represented as non-dimensional parameters [100]:

$$MAG = \frac{\dot{m}_{BL}}{\rho_0 u_{0i} \delta w} = \int_0^1 \frac{\rho_y u_y}{\rho_0 u_0} d(y/\delta) = 1 - \frac{\delta^*}{\delta} \quad (3.8)$$

$$MOG = \frac{mom_{BL}}{\rho_0 u_{0i}^2 \delta w} = \int_0^1 \frac{\rho_y}{\rho_0} \left( \frac{u_y}{u_0} \right)^2 d(y/\delta) = 1 - \frac{\delta^*}{\delta} - \frac{\theta}{\delta} \quad (3.9)$$

$$KEG = \frac{KE_{BL}}{0.5 \rho_0 u_{0i}^3 \delta w} = \int_0^1 \frac{\rho_y}{\rho_0} \left( \frac{u_y}{u_0} \right)^3 d(y/\delta) = 1 - \frac{\delta^*}{\delta} - \frac{\theta^*}{\delta} \quad (3.10)$$

The non-dimensional terms represented in Equations 3.8–3.10 are referred to as the mass flow group (MAG), the momentum group (MOG), and the kinetic energy group (KEG). The groups define the flow characteristics in a unit area ( $\delta w$ ) of the boundary layer flow relative to the flow characteristics of the same unit area in a free-stream flow. Each of the boundary layer flow characteristics,  $\dot{m}_{BL}$ ,  $mom_{BL}$  and  $KE_{BL}$ , is subject to a deficit relative to the equivalent free-stream flow characteristics. In addition to deficits in the mass flow, momentum and kinetic energy, flow in the boundary layer experiences a certain measure of total pressure deficit. This can be calculated as a mass flow-averaged value:

$$\frac{\bar{P}_{BL}}{P_0} = \frac{1}{\dot{m}_{BL}} \int_{BL} \frac{P_y}{P_0} d\dot{m} \quad (3.11)$$

$$\frac{\bar{P}_{BL}}{P_0} = \frac{1}{MAG} \int_0^1 \frac{P_y u_y \rho_y}{P_0 u_0 \rho_0} d(y/\delta) \quad (3.12)$$

The average velocity of flow through the boundary layer may be defined in a similar integral manner:

$$\frac{\bar{u}_{BL}}{u_0} = \frac{1}{\dot{m}_{BL}} \int_{BL} \frac{u_y}{u_0} d\dot{m} \quad (3.13)$$

$$\frac{\bar{u}_{BL}}{u_0} = \frac{1}{MAG} \int_0^1 \frac{u_y^2 \rho_y}{u_0 \rho_0} d(y/\delta) \quad (3.14)$$

### 3. Propulsion System Modelling

The primary purpose of this step in the process is to output three relevant boundary layer characteristics: the mass flow, average velocity, and the average total pressure relative to the free-stream total pressure. Any of the numerous methods available for determining the boundary layer flow characteristics may be applied, provided that they produce the required boundary layer characteristics.

In the case of incompressible flow, the relationships for  $\delta^*$ ,  $\theta$ ,  $\theta^*$  and the average boundary layer velocity can be simplified, as density is constant. Assuming an  $n^{\text{th}}$  power law profile and incompressible flow, the following relationships for the flow can be applied [100]:

$$\frac{\delta^*}{\delta} = \frac{1}{n+1} \quad (3.15)$$

$$\frac{\theta}{\delta} = \frac{n}{(n+1)(n+2)} \quad (3.16)$$

$$\frac{\theta^*}{\delta} = \frac{2n}{(n+1)(n+3)} \quad (3.17)$$

$$\frac{\bar{u}_{BL}}{u_0} = \frac{n+1}{n+2} \quad (3.18)$$

A number of additional definitions are also useful in determining the boundary layer flow characteristics:

$$\frac{\rho_y}{\rho_0} = \left[ 1 + \frac{\gamma-1}{2} M^2 \left[ 1 - \left( \frac{y}{\delta} \right)^{\frac{2}{n}} \right] \right]^{-1} \quad (3.19)$$

$$\frac{P_y}{P_0} = \left[ 1 + \frac{\gamma-1}{2} M^2 \left[ 1 - \left( \frac{y}{\delta} \right)^{\frac{2}{n}} \right] \right]^{-\frac{\gamma}{\gamma-1}} \quad (3.20)$$

#### 3.1.4 Inlet Flow Characteristics for a BLI System

Depending on the propulsion system's size, flow ingested by the propulsion system may be more or less than the entire boundary layer flow. If only the boundary layer is ingested, the streamtube height is automatically fixed to equal the boundary layer thickness and the resultant flow characteristics are the average for the boundary layer. However, ingesting more or less than the entire boundary layer will change the average flow characteristics for the streamtube. Hence, an additional step is required to establish the flow characteristics of the streamtube actually ingested by the propulsion system. Assuming a rectangular streamtube with height  $h$  and width  $w$  and constant boundary layer thickness  $\delta$ , there are three possible options that can be considered:

1. Ingest only the boundary layer ( $h/\delta = 1$ ).
2. Ingest free-stream and the boundary layer ( $h/\delta > 1$ ).
3. Ingest a portion of the boundary layer ( $h/\delta < 1$ ).

In the first case, the average flow characteristics of the ingested flow can be derived using the equations summarised in the previous subsection for the boundary layer. In the case of an inlet which ingests only a portion of the boundary layer, the upper limit of the integrals of Equations 3.8–3.10, Equation 3.12 and Equation 3.14 becomes  $h/\delta$ , the ratio of streamtube height to boundary layer thickness, where  $h/\delta < 1$ . If the intake starts above the surface (e.g. if some of the boundary layer is bled off), the lower limit of the integral must also be changed

### 3. Propulsion System Modelling

to  $h_l/\delta$ , where  $h_l$  is the height of the intake lower lip above the surface and where  $h_l/\delta > 0$ . In the final case, ingested flow characteristics must take into account the combination of both free-stream and boundary layer flow.

Given the definition of station  $i$ , the boundary layer flow characteristics are independent of the size of the propulsion system and streamtube size. The boundary layer flow characteristics and profile can therefore be calculated without defining a streamtube size  $h$ . However, average flow characteristics for the entire streamtube will tend towards free-stream flow characteristics as the ratio  $h/\delta$  increases. The total mass flow of the streamtube is the sum of mass flow through both the free-stream area  $(h - \delta)w$  and boundary layer area  $\delta w$ :

$$\dot{m}_{\text{total}} = \dot{m}_{\text{FS}} + \dot{m}_{\text{BL}} \quad (3.21)$$

$$\dot{m}_{\text{total}} = \rho_0 u_{0i} \delta w \left[ \frac{(h - \delta)}{\delta} + \text{MAG} \right] \quad (3.22)$$

$$\frac{\dot{m}_{\text{total}}}{\rho_0 u_{0i} \delta w} = \left( \frac{h}{\delta} - 1 \right) + \text{MAG} \quad (3.23)$$

Likewise for the momentum and kinetic energy of the streamtube:

$$\frac{\text{mom}_{\text{total}}}{\rho_0 u_0^2 \delta w} = \frac{\text{mom}_{\text{FS}} + \text{mom}_{\text{BL}}}{\rho_0 u_0^2 \delta w} = \left( \frac{h}{\delta} - 1 \right) + \text{MOG} \quad (3.24)$$

$$\frac{\text{KE}_{\text{total}}}{0.5 \rho_0 u_0^3 \delta w} = \frac{\text{KE}_{\text{FS}} + \text{KE}_{\text{BL}}}{0.5 \rho_0 u_0^3 \delta w} = \left( \frac{h}{\delta} - 1 \right) + \text{KEG} \quad (3.25)$$

Unlike mass flow, the total pressure deficit and average velocity of the flow are terms that are averaged over the entire inlet stream. Calculation of each of these flow characteristics follows on from the definitions established in Equation 3.11 and Equation 3.13. Therefore, the combined total pressure deficit of the boundary layer and free-stream flow is a mass flow-averaged value integrated over the entire stream (Equation 3.26). However, total pressure for flow outside the boundary layer is constant ( $P_y = P_0$ ). This splits the integral into boundary layer ( $y$  between 0 and  $\delta$ ) and free-stream flow sections ( $y$  between  $\delta$  and  $h$ ). The solution to the total pressure integral of the inlet flow may be represented in the non-dimensional form of Equation 3.28.

$$\frac{\bar{P}_i}{P_0} = \frac{1}{\dot{m}_{\text{total}}} \int_0^h \frac{P_y}{P_0} d\dot{m} \quad (3.26)$$

$$\frac{\bar{P}_i}{P_0} = \frac{1}{\dot{m}_{\text{total}}} \left[ \int_0^\delta \frac{P_y}{P_0} d\dot{m} + \int_\delta^h d\dot{m} \right] \quad (3.27)$$

$$\frac{\bar{P}_i}{P_0} = \frac{\left( \frac{h}{\delta} - 1 \right) + \text{MAG} \left( \frac{\bar{P}_{\text{BL}}}{P_0} \right)}{\left( \frac{h}{\delta} - 1 \right) + \text{MAG}} \quad (3.28)$$

The average velocity in the combined stream may be likewise calculated by integrating over the entire inlet stream (Equation 3.29). Similar to the total pressure deficit, the velocity outside of the boundary layer in the local free-stream flow is constant ( $u_y = u_0$ ), which splits the integral into free-stream and boundary layer flow components.

$$\frac{\bar{u}_i}{u_0} = \frac{1}{\dot{m}_{\text{BL}}} \int_0^h \frac{u_y}{u_0} d\dot{m} = \frac{\left( \frac{h}{\delta} - 1 \right) + \text{MAG} \left( \frac{\bar{u}_{\text{BL}}}{u_0} \right)}{\left( \frac{h}{\delta} - 1 \right) + \text{MAG}} \quad (3.29)$$

### 3. Propulsion System Modelling

Each of the equations represents the terms non-dimensionally. The streamtube flow characteristics equations are functions of  $h/\delta$  and the relevant average/total boundary layer flow characteristic. Boundary layer flow characteristics can therefore be calculated separately from the propulsion system sizing or performance process and then used to estimate the average streamtube flow characteristics. The three defined terms,  $\dot{m}_{\text{total}}$ ,  $\bar{u}_i$ , and  $\bar{P}_i/P_0$ , are necessary to determine the performance of a propulsion system following 1D gas dynamics methods. Whilst total temperature is also required, it is assumed that flow is isentropic and hence that the streamtube total temperature is equal to the free-stream total temperature. They are also required for the net propulsive force calculation through the definition of  $F_G$ :

$$F_G = \dot{m}u + A(p - p_0) \quad (3.30)$$

The representation of each of the terms as averaged and total values for the stream enables the integration of the boundary layer characteristics within conventional methods for propulsion system performance.

#### 3.1.5 Design Point Sizing

Similar to a conventional propulsion system, the size of a propulsor is determined by the propulsive force required. The required mass flow for a free-stream propulsion system can be reasonably simply obtained as performance is independent from its size. However, in the case of a BLI system, changes to the propulsor and inlet dimensions will influence the averaged flow characteristics at the interface point by changing  $h/\delta$ . Estimation of the size of a BLI propulsor using the method developed in this research therefore necessitates a procedure to solve for the propulsor size that produces the required net propulsive force (Figure 3.6 and Appendix B):

1. Establish the local flow characteristics:

- Reynolds number,  $Re$
- Boundary Layer thickness,  $\delta$
- Local free-stream velocity,  $u_{0i}$

2. Determine the boundary layer flow characteristics:

- Mass flow,  $\dot{m}_{\text{BL}}$ , Equation 3.8
- Average total pressure deficit,  $\bar{P}_{\text{BL}}/P_0$ , Equation 3.12
- Average velocity,  $\bar{u}_{\text{BL}}/u_{0i}$ , Equation 3.14

3. Guess streamtube height,  $h$ , and hence obtain  $h/\delta$

4. Determine streamtube flow characteristics:

- Mass flow,  $\dot{m}_i$ , Equation 3.23
- Average total pressure deficit,  $\bar{P}_i/P_0$ , Equation 3.28
- Average velocity,  $\bar{u}_i/u_{0i}$ , Equation 3.29

5. Estimate installation terms:

- Skin friction drag of surface from station  $i$  to intake highlight,  $\tau_{w,i}S_{\text{wet},i}$
- Nacelle drag,  $D_{\text{nac}}$
- Drag of airframe wetted surface area covered by propulsion system control volume,  $(S_{\text{wet},i} \text{ and } wL_{\text{nacelle}})$ ,  $\Delta D$

### 3. Propulsion System Modelling

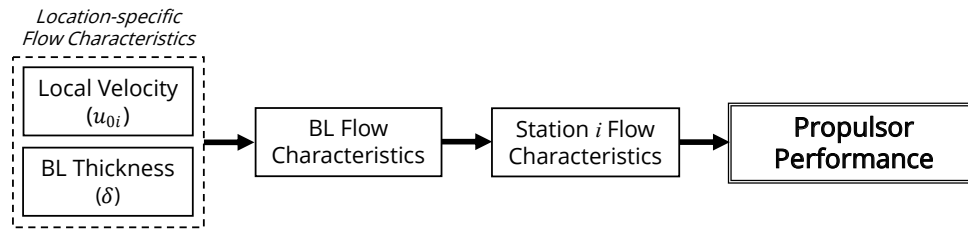


Figure 3.6: BLI propulsor simulation method at design point

6. Estimate propulsion system performance and check net propulsive force, NPF (Figure 3.7 for a propulsor consisting of intake fan and nozzle)
7. Return to Step 3 until target net propulsive force is met

This procedure is a generic workflow that can be applied to any propulsion system configuration or architecture. In order to simplify the analysis, it is assumed that the thickness of the boundary layer does not vary significantly over the width of the inlet streamtube. In addition, a square streamtube cross-section has been assumed throughout. However, this assumption may break down depending on the configuration of the aircraft and propulsion system. Unlike 2- or 3D methods, additional inlet pressure loss due to the boundary layer and compressor efficiency loss due to distortion are not directly represented. These are instead introduced into performance calculations of Step 6 as averaged numerical approximations. For the purposes of this research, the specific heat coefficient for air as a function of temperature was determined using ESDU 00.01.08 data. Gross and net thrust calculations follow AGARD 237 [98]. The gross thrust is scaled by a  $C_v$ , the ratio of actual specific thrust to the ideal specific thrust.

Whilst boundary layer flow characteristics may be assumed to be fixed for a fixed flight condition, they will be dependent on the propulsor location. A propulsor located at the trailing edge of a fuselage will ingest a significantly thicker boundary layer than a propulsor located near the leading edge. The local velocity of the free-stream flow entering a propulsor will also depend on the aircraft configuration due to the velocity profile over the fuselage. For blended wing body type configurations, the aerofoil cross-section leads to a flow acceleration and subsequent deceleration from the leading to trailing edges. Non-lifting fuselages such as the fuselage of a tube-and-wing will experience a deceleration of flow due to the skin friction (leading to the aircraft wake). Propulsion system performance therefore cannot be determined entirely independently from the aircraft and will rely on an estimate of the aircraft configuration. Location and configuration factors will play a significant effect on the performance of a propulsor. Each propulsor should be individually sized for the best performance given its location [105]. Determining the local flow characteristics is therefore the first step in sizing the propulsion system, shown in Step 1 of the above process. The most favourable location can then be selected as a part of the sizing and design process.

The method in Figure 3.7 presents the relationship for performance of a propulsor with critical exhaust flow. It is possible that the nozzle pressure ratio will not be equal to the critical value, and that the exhaust flow will therefore be slightly under or over-expanded. However, for the low pressure ratios considered in this research the exhaust is close to fully expanded. Performance calculations for fully expanded flow were therefore assumed to be applicable for the purposes of this research.

Nacelle drag estimation is an additional factor for the integrated engine performance and the NPF model. For the purposes of this research a simple nacelle design was implemented for nacelle drag estimation. This included a NACA-1 forebody and a circular arc afterbody. An overview of the sizing process is shown in Figure 3.8 including the assumptions made for the

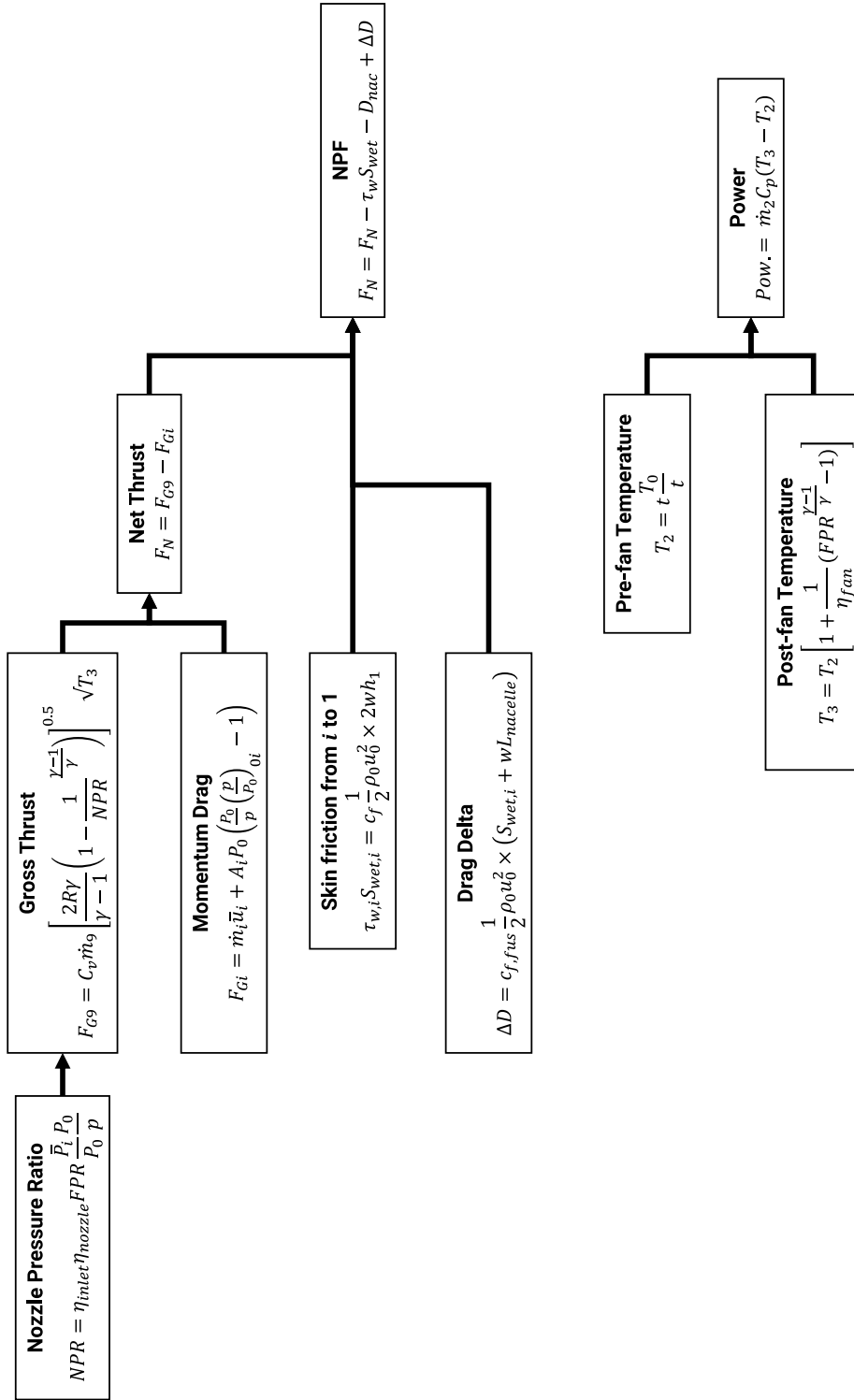
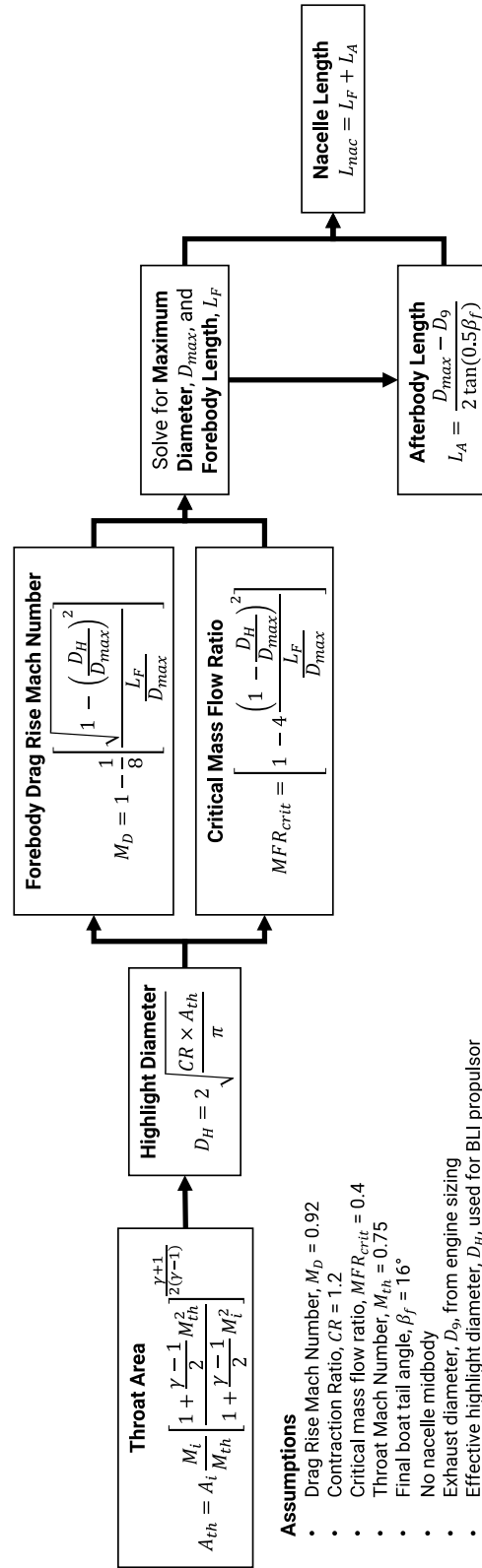


Figure 3.7: Propulsor performance flowchart





**Figure 3.8:** Nacelle sizing flowchart to provide an estimate of nacelle dimensions, NACA-1 forebody and circular arc afterbody, with assumptions

### 3. Propulsion System Modelling

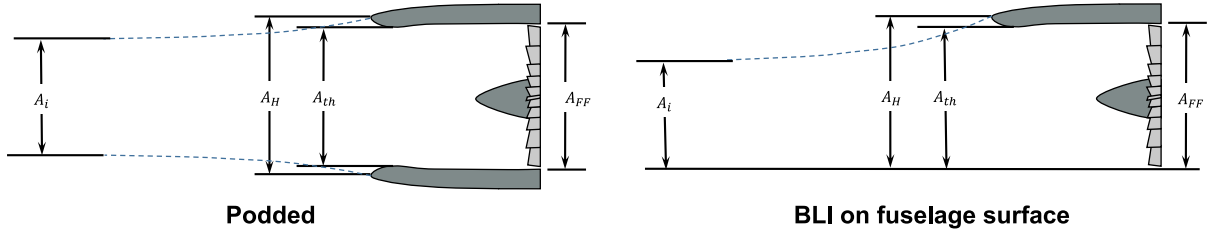


Figure 3.9: Definition of key intake areas

sizing process. Due to the integrated configuration, the lower surface of a BLI system is embedded in the airframe. The nacelle drag for a BLI propulsor is therefore estimated assuming that the nacelle consists only of the upper nacelle surface with wetted surface area approximately equal to the nacelle length,  $L_{nacelle}$  multiplied by the propulsor intake width,  $w$ . The two propulsors at the extreme edges of the array have an additional nacelle component due to the end wall with a wetted surface area approximately equal to  $L_{nacelle}$  multiplied by the highlight height.

A number of key areas can be used to define the size of the intake and the propulsors (Figure 3.9). The intake throat, highlight, and fan face areas may be sized by defining fixed Mach numbers for the throat and fan face and a contraction ratio between the throat and the highlight. The propulsor sizing process produces the area of the incoming streamtube,  $A_i$ . The area of each section of the intake may then be estimated by using the area ratio  $A/A^*$ . Mach number at station  $i$  is assumed to equal the mass flow average Mach number for the incoming streamtube. In order to ensure that the throat will not be choked or close to choking, a throat Mach number of less than one should be selected. A contraction ratio, CR, must also be selected between the throat and the highlight. The mass flow ratio of the propulsors at design point is therefore less than one, as the highlight area,  $A_H$ , is greater than the area of the streamtube at station  $i$ . Intake areas relative to the streamtube area at station  $i$  may be obtained using the area ratio for isentropic flow:

$$\frac{A}{A_i} = \frac{M_i}{M} \left( \frac{1 + \frac{\gamma-1}{2} M^2}{1 + \frac{\gamma-1}{2} M_i^2} \right)^{\frac{\gamma+1}{2(\gamma-1)}} \quad (3.31)$$

Subsequently, the highlight area,  $A_H$  can be obtained given an assumed contraction ratio from the throat area  $A_{th}$ .

$$A_H = CR \times A_{th} \quad (3.32)$$

The fan area,  $A_{ff}$ , resulting from the selected fan face Mach number may be used to estimate the fan diameter by including an assumed hub-to-tip ratio,  $\lambda_{fan}$ :

$$D_{fan} = 2 \sqrt{\frac{A_{ff}}{\pi(1 - \lambda_{fan}^2)}} \quad (3.33)$$

#### 3.1.6 Off-Design Extension

A key aspect of developing a new model for simulating a boundary layer ingesting propulsion system was to enable the use of the model over the full aircraft mission profile. The reviewed literature presented at the beginning of the chapter does not provide a method for simulating BLI propulsion systems at off-design. Therefore, this section will detail the extension of the design point method detailed in the previous sections for use at off-design and hence any altitude, Mach number, or propulsion system power setting.

### 3. Propulsion System Modelling

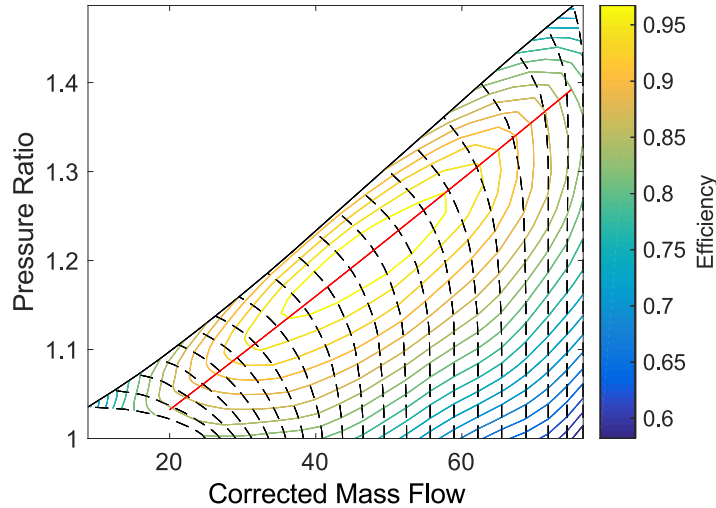


**Figure 3.10:** Generic scaled fan/compressor map with peak efficiency running line

The performance of a propulsion system at off-design can be represented by maps that relate pressure ratio, mass flow, rotational speed and/or efficiency of each propulsion system component. At off-design, the change in mass flow demanded by a propulsor may be represented by the selected component running lines. This depends on the configuration of the components, such as nozzle area, or variable subcomponents such as inlet guide vanes. The mass flow demand may be presented as a non-dimensional mass flow (NDMF) that is independent from the flight conditions:

$$\text{NDMF} = \frac{\dot{m}\sqrt{T}}{P} \quad (3.34)$$

The running line of the component provides a relationship between the mass flow through the component, its pressure ratio, rotational speed, and efficiency (Figure 3.10). The selected component maps will dictate the performance of a component. The mass flow demanded by the operating point of each component must be matched to the operating point of other components within the propulsion system. The nozzle area is a dominant factor in determining the overall operating point of the propulsion system. Assuming a fixed nozzle area, the non-dimensional mass flow of upstream components is dictated by the non-dimensional mass flow of the nozzle. For example, the non-dimensional mass flow of a choked nozzle is constant. This then provides a point to which the operating point of upstream components must be matched. A floating nozzle area will remove the nozzle as a factor that dictates performance of the propulsion system. In particular, research on the N3-X identified a variable area fan nozzle as a necessary requirement to ensure fan stability at the low pressure ratios considered for a BLI propulsor [24, 56].

The size of the inlet stream varies depending on the mass flow demand, with a high mass flow demand resulting in a larger cross-sectional area for the incoming streamtube of air. This can be linked to the capture area ratio (CAR) term: the ratio of inlet area to the streamtube area. The capture area ratio of a propulsion system may be defined as follows:

$$\text{CAR} = \frac{A_i}{A_H} \quad (3.35)$$

For an engine operating in free-stream flow, the mass flow can be obtained from the non-dimensional mass flow without estimating the streamtube size. The total pressure term in non-

### 3. Propulsion System Modelling

dimensional mass flow and the velocity of the capture streamtube are functions of the flight velocity and altitude. For a BLI system, the size of the streamtube will have a noticeable effect on the characteristics of the flow entering the intake. An engine operating with a high capture area ratio will ingest predominantly free-stream air, with a very high ratio of  $h/\delta$ . In contrast, a propulsor operating with a low capture area ratio may ingest predominantly boundary layer. The boundary layer thickness is also a function of the flight velocity, amongst other factors. A slow-moving or static aircraft will have a negligible boundary layer thickness. A propulsor operating at sea-level static conditions may therefore perform very similarly to a conventional free-stream propulsor. The flow characteristics required for the non-dimensional mass flow are therefore a function of the size of the inlet streamtube and hence the capture area ratio or mass flow demand. This is particularly apparent for the total pressure term, as the (mass flow-averaged) total pressure deficit resulting from the boundary layer is a function of the boundary layer flow characteristics and the ratio  $h/\delta$  (Equation 3.28). For example, the pressure term at the fan face can be determined as a function of  $h/\delta$ :

$$P_2 = \eta_{\text{inlet}} \frac{\bar{P}_i}{P_0} \frac{P_0}{p} p \quad (3.36)$$

$$P_2 = \eta_{\text{inlet}} \left[ \frac{(\frac{h}{\delta} - 1) + \text{MAG}(\frac{\bar{P}_{BL}}{P_0})}{(\frac{h}{\delta} - 1) + \text{MAG}} \right] \frac{P_0}{p} p \quad (3.37)$$

Where  $\eta_{\text{inlet}}$  is the total pressure loss through the inlet and  $P_2$  is a function of  $h/\delta$  through  $\bar{P}_i$ . Depending on the configuration, an additional term may be required to determine the total pressure loss due to separation of the incoming flow at the lip or of the boundary layer. Note that it has been assumed that the flow is isentropic and that there is therefore no loss in total temperature:

$$T_2 = \frac{T_0}{t} t \quad (3.38)$$

Given the definition of station  $i$ , the boundary layer flow characteristics are determined by the Mach number and altitude, regardless of the propulsion system power setting. These may therefore be calculated independently from the streamtube flow characteristics, without knowing the value of  $h/\delta$  that matches mass flow demand to the streamtube mass flow. Given this relationship between flow characteristics and the size of the inlet stream, a mass flow-matching procedure is required to match the upstream mass flow and streamtube size to the mass flow demanded by the propulsor. The procedure follows a similar flow to the design point sizing and performance process, except the goal is now to match mass flow rather than meet a target thrust. For a known operating point, the procedure to obtain performance of a BLI propulsor at off-design is as follows (Figure 3.11):

1. Obtain the propulsor and component operating speed line (follow standard procedures for mass flow matching of conventional propulsion system components)
2. Obtain the fan non-dimensional mass flow, NDMF, at the given operating point
3. Determine the boundary layer flow characteristics:
  - Mass flow,  $\dot{m}_{BL}$ , Equation 3.8
  - Average total pressure deficit,  $\bar{P}_{BL}/P_0$ , Equation 3.12
  - Average velocity,  $\bar{u}_{BL}/u_{0i}$ , Equation 3.14
4. Guess streamtube height,  $h$ , and hence obtain  $h/\delta$

### 3. Propulsion System Modelling

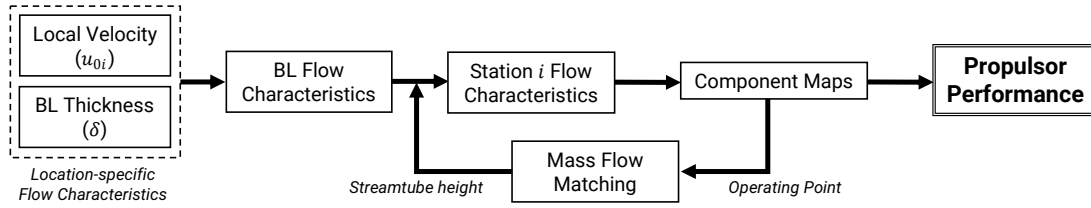


**Figure 3.11:** BLI propulsor simulation method at off-design

5. Determine streamtube flow characteristics:

- Mass flow,  $\dot{m}_i$ , Equation 3.23
- Average total pressure deficit,  $\bar{P}_i/P_0$ , Equation 3.28
- Average velocity,  $\bar{u}_i/u_{0i}$ , Equation 3.29

6. Estimate total pressure and temperature at the fan face, Equations 3.37 and 3.38

7. Calculate mass flow at the fan face from the mass flow demand, NDMF, Equation 3.34

8. Return to Step 4 until streamtube mass flow in Step 5 matches the propulsor system mass flow demand in Step 7

9. Estimate propulsor system performance using streamtube flow characteristics from Step 5 and the engine component operating points (Figure 3.7 for a propulsor consisting of intake fan and nozzle)

The mass flow matching method is a generic workflow that is intended to be applicable for any propulsor system configuration. This procedure should be included within the matching process for the component operating points to determine the engine's overall operating point. The non-dimensional mass flow for each component is a function of the engine's operating point. Iterative loops may therefore also be required to find the point where the component operating points are matched and  $h/\delta$  matches the resulting mass flow demand. Once the engine's operating point has been determined and the mass flow matching procedure is complete, the performance of the propulsor system may be estimated by following conventional 1D gas dynamics methods, as with the design point method. The goal of the above process is to determine inlet flow characteristics, given that the capture area ratio and hence  $h/\delta$  is initially unknown.

A number of additional general assumptions are applied consistent with the assumptions used for the design point method:

- Flow at interface point is independent of propulsor demand
- Constant ratio of free stream to boundary layer air,  $h/\delta$ , from the interface point onwards
- Streamtube flow characteristics are averaged from the interface point onwards
- Square streamtube cross-section of constant width
- Each propulsor in an array operates independently, streamtubes are unconstrained by adjacent fans

Given the constant width cross-section assumption, the capture area ratio of the propulsor may be defined as follows:

$$\text{CAR} = \frac{A_i}{A_H} = \frac{h}{h_H} \quad (3.39)$$

#### 3.1.7 Intake Duct Total Pressure Loss

An ingested turbulent boundary layer can give rise to total pressure and swirl non-uniformities which can have a negative impact on the performance of an engine. The distortion in the inlet can lead to higher total pressure loss in the inlet than for an engine that ingests laminar free-stream flow. In some cases, the adverse pressure gradient through an intake may lead to boundary layer separation. Boundary layer ingesting systems are often paired with S-duct intakes, to allow for greater integration in the airframe. This configuration is particularly at risk of separation, and research has been conducted to determine how best to limit inlet distortion [22, 106].

Previous research has shown that the efficiency of BLI propulsors is sensitive to the total pressure loss in the inlet [94]. This is particularly apparent for low pressure ratio propulsors, as the total pressure loss lowers the effective pressure ratio. The propulsor must therefore ingest more mass flow to produce the required thrust, and will therefore be larger than a system with a lower total pressure loss in the inlet. A larger system may also be required to ingest more free-stream mass flow, hence tending inlet flow characteristics to free-stream and reducing BLI benefits.

A method was developed by Seddon to predict the total pressure loss in an inlet ingesting boundary layer air [107]. The method estimates the total pressure loss as a function of the intake and inlet stream areas and the boundary layer capture ratio. Whilst it is possible that boundary layer control techniques can reduce total pressure loss through the inlet, the method provides a preliminary estimate of total pressure loss. For subsonic flow and the mail-slot configuration, this may be estimated as follows:

$$\frac{\Delta P_1}{P_0} = QK\Phi \quad (3.40)$$

$$Q = 1 - \left( \frac{A_i}{A_{ff}} \right)^3 \quad (3.41)$$

$$K = \frac{\theta}{h} \frac{A_1}{A_{ff}} \left[ 0.6 + 2.4 \left( \frac{A_m}{A_1} - 1 \right) \right] \quad (3.42)$$

Where  $\Phi$  is an empirical function of the boundary layer (Figure 3.12),  $A_1$  is the highlight area,  $A_{ff}$  is the fan face area, and  $A_m$  is the area of the midpoint between the highlight and the fan face. For subsonic Mach numbers,  $\Phi$  can be approximated by the following polynomial:

$$\Phi \equiv f(M_i) = 5.045M_i^3 - 4.753M_i^2 + 1.878M_i - 0.276 \quad 0.35 < M_i < 1.0 \quad (3.43)$$

Assuming that the duct area may be approximated as a straight taper from the fan face to the highlight, total pressure loss through the inlet can be obtained from Seddon's formulation:

$$\eta_1 = 1 - \Phi \frac{\theta}{h} \left( 1.2 - 0.6 \frac{A_1}{A_{ff}} \right) \left[ 1 - \left( \frac{A_i}{A_{ff}} \right)^3 \right] \quad (3.44)$$

The area  $A_i$  is equal to the cross-sectional area of the streamtube at station  $i$ . The highlight area  $A_1$  is a function of the contraction ratio between the intake's throat and the highlight, where the throat is sized for a set (average) Mach number at design point. Both  $A_1$  and  $A_{ff}$  are therefore functions of the Mach numbers for which the intake is sized. To ensure reasonable estimates are produced for  $\eta_1$ , it may be assumed that  $\Phi$  is never less than zero (i.e.  $\Phi = 0$  when  $M < 0.35$ ) and that  $\eta_1$  will never be greater than one. Following these assumptions,

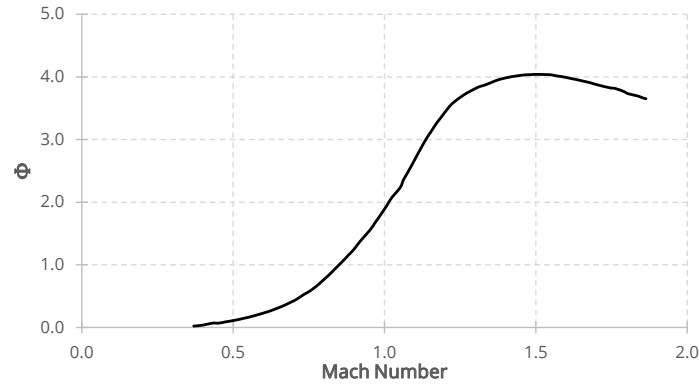


**Figure 3.12:** Boundary layer function for inlet total pressure loss (Seddon, 1970) [107]

intake pressure recovery is 100% for Mach numbers less than 0.35.

#### 3.1.8 Fan/Compressor Efficiency

The non-uniform flow of the boundary layer will negatively impact the efficiency of components ingesting the boundary layer. Depending on the type of distortion, the non-uniform flow may lead to surge in certain sections of the propulsor, requiring a fan with an appropriate surge margin [20]. The non-uniform flow will also impact the mechanical integrity of the fan blades [108].

The developed method does not directly represent the loss of efficiency that results from an ingested turbulent boundary layer. Alternative methods such as the parallel compressor method may be used to estimate the average efficiency of compression [94]. Later simulations suggests that the efficiency of a BLI propulsor is less sensitive to fan efficiency than to the total pressure loss in the inlet (Section 3.3). A loss in efficiency leads primarily to a step increase in power consumption, with little change in the thrust produced.

#### 3.1.9 Representing the Efficiency of a BLI System

Measures of efficiency are a necessary component of the assessment of a propulsion system. For a BLI system in particular, the performance relative to a conventional propulsion system must be improved by a sufficient margin to justify the adoption of the technology. However, appropriate representations of efficiency are required to define the efficiency of a BLI system. Propulsive efficiency,  $\eta_{\text{propulsive}}$ , contributes to the overall efficiency parameter of a conventional propulsion system. In the standard form used in propulsion system performance, propulsive efficiency quantifies the useful propulsive power output as a percentage of the power available from the free-stream flow. For a conventional propulsion system, this can be calculated using the following formula:

$$\eta_{\text{propulsive}} = \frac{2u_0}{u_0 + u_j} \quad (3.45)$$

The formula highlights one of the drivers of propulsion system design: maximising the propulsive efficiency necessitates minimising the exhaust jet velocity. However, this is associated with a reduction in the specific thrust of the propulsion system. In the case of a BLI propulsion system there are three velocities that define the propulsive efficiency, as the flow entering the propulsion system is not equal to the flow available in the free-stream. These velocities are the velocity of the air entering the inlet,  $\bar{u}_i$ , the velocity of the exhaust jet,  $u_j$ , and the velocity of the free-stream flow,  $u_0$ . The propulsive efficiency of a boundary layer ingesting system is therefore

### 3. Propulsion System Modelling

not defined in the same manner as that of a free-stream engine. As the useful propulsive power is in terms of the local inlet stream, the propulsive efficiency of the system is defined relative to these terms [109]:

$$\eta_{\text{propulsive,BL}} = \frac{2u_0}{\bar{u}_i + u_j} \quad (3.46)$$

In the case of a purely wake filling BLI propulsor, the exhaust velocity is equal to the free-stream velocity ( $u_j = u_0$ ). However, unlike a conventional propulsion system, the inlet velocity is less than the free-stream ( $\bar{u}_i < u_0$ ). The denominator of the propulsive efficiency equation is therefore less than the numerator, as  $\bar{u}_i + u_j$  is equal to  $\bar{u}_i + u_0$ , which is less than  $2u_0$ . In this configuration the propulsive efficiency as defined in Equation 3.46 is greater than 100%. An increase in the momentum deficit leads to further reductions in  $\bar{u}_i$  which results in an increase in propulsive efficiency. Even in a BLI system with a higher exhaust velocity, the propulsive efficiency will be greater than that of an equivalent propulsion system in free-stream flow. This is due to the discrepancy between  $u_0$  and  $\bar{u}$  ( $\bar{u}_i < u_0$ ) and the fact that, for the same specific thrust,  $u_j$  for a BLI propulsion system is lower than that of a propulsion system in free-stream flow.  $\bar{u}_i$  tends to  $u_0$  as the ratio  $h/\delta$  increases, and the propulsive efficiency returns to the conventional definition.

Propulsive efficiency is not the only descriptor of performance and efficiency. A high propulsive efficiency in a BLI system may result from a thick boundary layer with a high momentum deficit. However, this may be matched by distortion related inefficiencies elsewhere which are detrimental to the overall system performance. The performance benefit of a BLI system can instead be represented in terms of a power saving coefficient (PSC), as proposed by Smith (Equation 3.47) [90]. This enables the assessment of the benefits of the propulsion system as a whole relative to a comparable system in free-stream flow.

$$\text{PSC} = \frac{P_{\text{ref}} - P_{\text{BLI}}}{P_{\text{ref}}} \quad (3.47)$$

Where  $P_{\text{ref}}$  indicates the power consumption of a propulsion system operating in freestream flow required to propel an aircraft with drag  $D_{\text{aircraft, clean}}$ .  $P_{\text{BLI}}$  indicates the power consumption of a BLI propulsion system required to propel the same aircraft. A positive power saving coefficient represents a BLI system with a power consumption that is lower than that of a free-stream propulsion system. The power saving coefficient representation of efficiency encompasses any losses within the system, and is able to represent the changes of a BLI system relative to an equivalent free-stream option. Smith found that in some cases that the PSC for propulsion system could be in the region of 7%, for the configurations considered [90]. Plas notes that the power saving coefficient will reduce as system loss is increased and can negate the benefit of a BLI system. Nonetheless, the configuration considered had the potential for a power saving of up to approximately 10% when 25% of the airframe drag was ingested [20]. A system that results in a PSC less than zero may be concluded to be non-viable, as a free-stream propulsion system would be a more efficient option.

The power saving coefficient is useful as a comparative term against a conventional system, however, it is also useful to have an efficiency metric that may be used without defining a system against which BLI must be compared. A metric analogous to the thrust specific fuel consumption (SFC) will be used here; a ‘thrust specific power consumption’ (SPC):

$$\text{SPC} = \frac{P}{\text{NPF}} \quad (3.48)$$

This metric presents the power,  $P$ , required by a propulsor per unit propulsive force produced. Whilst specific fuel consumption can be used for fuel-burning systems, power is the more useful



term for electrically driven systems. As with SFC, a lower SPC implies a more efficient system that uses less power. It is also possible to make use of the  $h/\delta$  ratio to predict efficiency. A higher proportion of ingested free-stream air (high  $h/\delta$ ) implies a system with inlet flow characteristics tending to free-stream, and may therefore be less efficient than a system ingesting the boundary layer only.

## 3.2 N3-X Propulsion System Simulation Methodology

The performance of the N3-X propulsion system has been simulated in numerous bodies of research. This research attempts to address some perceived gaps in research by including location-specific aspects in the simulations and a clearly defined off-design performance procedure. In order to ensure a reasonably consistent comparison, it is important to define a simulation methodology and the design variables used in designing and simulating the propulsion system. It is important to define a procedure for simulating the elements of the propulsion system (turbomachinery and BLI propulsor array) in the combined turbo-electric system. Performance of the two systems combines to produce the performance of the system as a whole. A simulation procedure is particularly important at off-design, where the performance of the two systems will diverge from design point performance.

### 3.2.1 N3-X Propulsion System Definition

The propulsor array has an inlet set at 85% of the centreline chord and parallel to the trailing edge [24]. A combination of the highly swept fuselage leading edge and the angled nature of the propulsor array results in a significant change in chord length and local Mach number between the centreline propulsor and the propulsors at the extreme edges of the array. Due to the nature of the aircraft shape and airflow, each propulsor inlet is subject to different boundary layer and air flow characteristics at the interface point (Figure 3.13). The inclusion of these span-related parameters means that each fan in the propulsor array performs differently dependent on the location and configuration. These differences introduce an additional level of complexity into the simulation of the propulsor array, simplified with the assumption that conditions are mirrored about the centreline. Nonetheless, this does imply that each propulsor must be individually designed if optimisation of the propulsion system performance is required. As the original N3-X design does not specify a swan neck or S-duct for the propulsors, direct ingestion with a straight duct is assumed.

The case study made use of publicly available data and research on the aircraft: the aircraft and propulsor array configuration [24], and the boundary layer profiles at the centreline of the airframe [56]. The aircraft configuration provided the reference lengths ( $x$ , distance from the aircraft leading edge) necessary for estimation of the boundary layer thickness. As an initial estimate, the turbulent flat plate assumption was applied. To account for the discrepancy between the flat plate assumption and the actual aircraft configuration, the boundary layer thickness was scaled by a constant to match the available boundary layer profiles. The boundary layer profiles also provided an estimation of the local free-stream velocity at the edge of the boundary layer on the aircraft centreline. The velocity profile provided the local free-stream Mach number at the edge of the boundary layer from  $x/c = 0.6$  to  $x/c = 1.0$ , where  $c$  is the centreline chord length. In the absence of a full CFD data analysis of the airframe, the velocity profile was extended to encompass the entire airframe. This included the assumption that the local free-stream velocity at the edge of the boundary layer would be equal at any axial distance  $x_0$  from the aircraft nose. A more detailed estimate of airframe boundary layer and velocity distribution may be calculated using a more complete analysis of the airframe. However, the publicly available data was ap-

### 3. Propulsion System Modelling

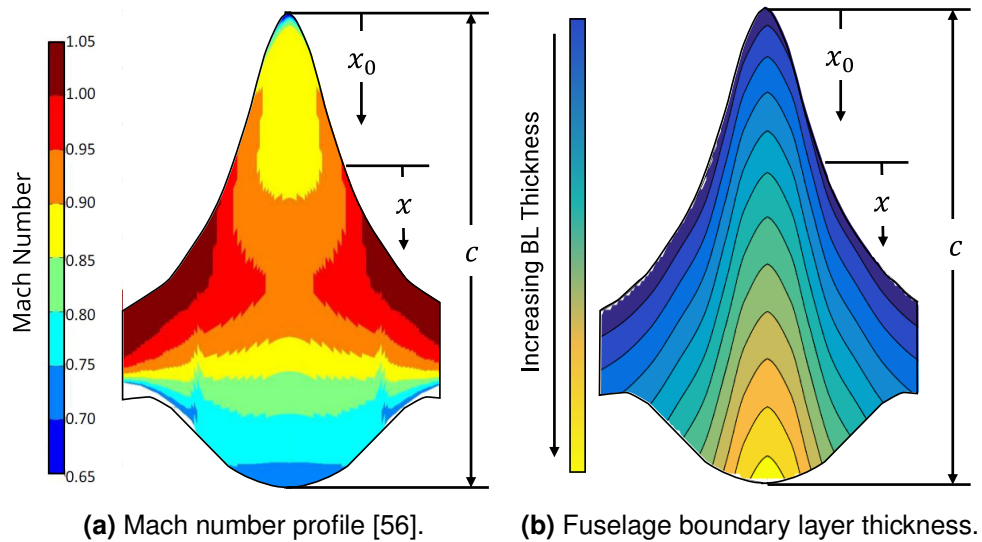


**Figure 3.13:** N3-X airframe Mach number profile and BL thickness.

plied to demonstrate the analysis possible using the limited information that might be available at an early design stage. This is in keeping with the intended application of the method as a preliminary design tool. Further information on the relationships used to approximate the flow over the N3-X airframe is shown in Appendix C.

In order to support the off-design simulations, it was assumed that the turbulent flat plate scaled to the N3-X configuration may be used to estimate the boundary layer thickness at any of the simulated flight conditions. Difference in flow angle resulting from a change in aircraft incidence was neglected, with the assumption that the fuselage acts as a ‘flow straightener’, and hence the inlet stream lies parallel to the fuselage surface once it reaches the interface point. It is assumed that the velocity profile for the airframe at design point may be scaled to the Mach number at the off-design flight condition.

CFD analyses are computationally expensive and time consuming to repeat. This research therefore relies on limited CFD data for the N3-X airframe which is then extended to encompass the entire aircraft and different flight conditions by applying assumptions. This is used to enable rapid analyses, however, the use of assumptions implies a reduction in fidelity versus dedicated analysis at each flight condition and for the entire airframe. Turnbull *et al.* present one such alternative to a full high fidelity CFD analysis [110]. In the method, a flow solution is created for the model in order to determine the streamlines that enter the propulsion system. These streamlines lead to the local flow conditions established as important parameters for this analysis (local Mach number/velocity and boundary layer thickness). Flow characteristics for the streamtube are then averaged, as with the method used in this research. As with CFD, a reasonable level detail is required for the aircraft design to establish flow characteristics over the airframe, however, computational time is lower. Integrating such a tool into the method developed in this research may be a route to moving to higher fidelity in the analysis, although the time to establish a reasonable solution will still limit the feasibility of multiple rapid analyses.

#### 3.2.2 Main Engines

Turbomachinery simulations were performed using *Turbomatch*, an in-house tool for gas turbine simulation [111]. Using the software, a model of the engine can be created from a selection of modules in order to simulate the thermodynamic performance and predict gas properties of the individual gas turbine components. Engine modules include inlets, compressors, turbines,

### 3. Propulsion System Modelling

combustors, bleeds and nozzles. This in turn allows for a detailed simulation of the overall engine performance. *Turbomatch* includes functionality to simulate the design point, off-design and transient performance of gas turbines. Models can also be created to simulate the performance of engines using alternative fuels, multiple spools, and advanced/hybrid cycles.

The design point power demand of the array and the propulsive force required from the engines determines the required size of the turbomachinery. The default configuration of the N3-X turbomachinery as simulated in previous research is a pair of turbogenerators. Each gas turbine produces half of the total power requirement, plus an additional amount to account for transmission efficiency of the superconducting electrical system (baseline value of 99.8% [56]). The baseline N3-X configuration's turbogenerators are sized at design point for zero net thrust, however, some additional thrust may be produced at off-design. The turbogenerator design is based on previous research for the N3-X propulsion system. The engine is assumed to be a twin spool design with a free power turbine. The engine produces enough gross thrust at design point to counterbalance its momentum drag. Compression is split between the low and high pressure compressors such that the enthalpy change over each compressor is the same [56]. A selection of key engine design parameters are shown in Table 3.1. Note that these values are taken from the engine design as established by previous research. No conclusions are made as to the feasibility of these design parameters (e.g. by ensuring that blade and annulus size is reasonable for the chosen configuration).

The present research also assessed potential alternative configurations for the N3-X propulsion system with particular focus on the split of thrust between the propulsor array and the main engines. This leads to a thrust split (TS) design variable, the ratio of propulsive force produced by the propulsor array to the total propulsive force:

$$TS = \frac{NPF_{array}}{NPF_{total}} \quad (3.49)$$

As a part of this thrust split design variable, turbojet and turbofan configurations were considered for the main engines. The configuration of turbojet is essentially the same as that of the turbogenerators, however, the engines are required to produce a certain amount of thrust, depending on the design point thrust requirement. A range of configurations were considered for the turbofan engine. The primary design parameters listed in Table 3.1 were maintained, however, a fan and bypass were added. The bypass ratio and fan pressure ratio were treated as design variables, with the pressure ratio of the low and high pressure compressors adjusted to account for the compression performed by the fan. The equal enthalpy change design was maintained for the low and high pressure compressors. As an initial assumption, the polytropic efficiency of the fan was assumed to be equal to the polytropic efficiency of the compressors. Power to drive the fan was assumed to be provided through the low pressure spool. The turbofan was assumed to be separate exhaust design, however, a mixed exhaust configuration may be necessary to more closely represent the performance of an embedded engine. The engine layouts are illustrated in Figure 3.14.

A new engine was sized for each simulated configuration of the propulsor array in order to determine the required engine size. Engine size was determined by solving for the engine mass flow that produced the required auxiliary power and net thrust. In the turbojet/turbogenerator configurations, the only design variable was the engine core mass flow, as all other design parameters were based on previous research. In the case of the turbofan configuration, each bypass ratio has an optimum fan pressure ratio. Therefore, an additional process was required to determine the optimum configuration for a defined bypass or fan pressure ratio configuration. Increasing the bypass ratio of the turbofan configuration would lead to an improvement in the engine's specific fuel consumption, however, the maximum size of the bypass is limited by the

### 3. Propulsion System Modelling

**Table 3.1:** N3-X engine design parameters [56]

DP Altitude	30,000 ft
DP Mach Number	0.84
Overall Pressure Ratio	64
DP Turbine Entry Temperature (K)	1811
Max. Turbine Entry Temperature (K)	1867
Compressor Polytropic Efficiency	0.9325
Turbine Polytropic Efficiency	0.93
Power Turbine Polytropic Efficiency	0.924

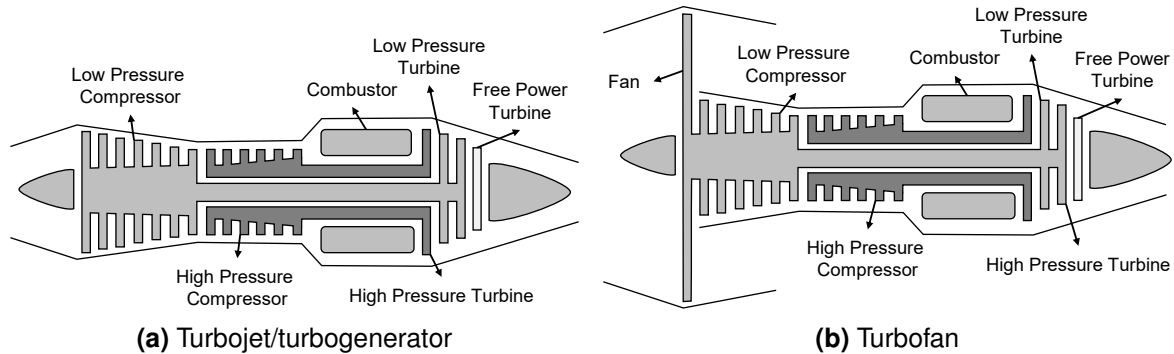


**Figure 3.14:** Representative general engine configurations for the N3-X main engine

available volume within the airframe (assuming an embedded configuration). Turbofans will not be used for 100% thrust split configurations, as no net thrust is required from the main engines and there is therefore no benefit from including a bypass. However, once thrust is required from the main engines at thrust splits less than 100%, there may be a benefit to including a bypass.

#### 3.2.3 Propulsor Array and Propulsors

Each fan in the N3-X's propulsor array must be individually sized to account for the different inlet flow characteristics along the array length. Whilst the overall requirements of the array are fixed (i.e. a fixed net thrust requirement and maximum size), there are a number of degrees of freedom in selecting design variables for the individual fans and the array. The primary design variables include:

- Fan pressure ratio
- Net propulsive force per fan
- Inlet aspect ratio
- Number of propulsors

When considering the propulsion system as a whole, these design variables must be further combined with the thrust split parameter to identify the optimum configuration.  $C_v$  is taken as 0.997 for the N3-X propulsors, based on previous research [24]. Fan adiabatic efficiency,  $\eta_{fan}$ , was assumed to be 0.9535, also based on previous research [24]. The fan face was sized for a Mach number of 0.65. The resultant fan area,  $A_{ff}$  was then used to estimate the fan diameter by including an assumed hub-to-tip ratio,  $\lambda_{fan}$ , of 0.3 [24]. In order to ensure that the throat will not be choked or close to choking, a throat Mach number of 0.75 was selected. A contraction ratio of 1.2 (CR) was selected between the throat and the highlight.

### 3. Propulsion System Modelling

A number of assumptions have been used in simulating the propulsor array of the N3-X at off-design. The primary assumption is that the propulsors have a variable area nozzle. This is assumed to be a ‘floating’ variable area nozzle that is able to achieve any target area based on the fan’s operating point. This requirement was defined in previous research on the N3-X to ensure fan stability given the low fan pressure ratios being used for the propulsors [24]. Off-design mass flow matching is therefore required only between the fan and the mass flow of the inlet stream. The propulsors are assumed to operate on a peak efficiency running line and will have a constant non-dimensional mass flow for a fixed rotational speed. The analyses use a generic fan/compressor map scaled to the size of the N3-X propulsors. This was deemed appropriate given the preliminary nature of the design. However, component maps that more closely match the fan design should be selected as research progresses. It should be noted that, due to the nature of boundary layer flow distortion, the actual running line of the fan will depend on the flow and blade location. Certain segments of the fan may therefore operate closer towards or further from surge than other segments [20, 94]. Different segments may also operate with different efficiencies and pressure ratios, assuming a fixed geometry fan. For the purposes of this research, a single running line for the fan is assumed. The running line and a generic scaled fan/compressor was used to provide an estimate of fan efficiency and fan pressure ratio at the requisite operating point.

#### 3.2.4 Combined Propulsion System

The propulsion system of the N3-X consists of the propulsor array linked to a pair of turbogenerators through a superconducting electrical system. The performance of the propulsor array is therefore linked to the power available from the turbogenerators, whilst the performance of the turbogenerators is linked to the power demand from the propulsor array. The performance of the array as a whole can be represented as a power demand and a net propulsive force. When connected to the main engines, this power demand must be fulfilled by the main engines. Where the power demand cannot be fulfilled by the engines, the rotational speed of the array must be spooled down to match the available power.

Overall propulsion system efficiency must account for the performance of the gas turbines in combination with the propulsor array. As the energy to drive the turboelectric propulsion system is produced through combustion of conventional jet fuel, overall efficiency may be represented through specific fuel consumption. For the purposes of the N3-X propulsion system, specific fuel consumption will be represented with an effective specific fuel consumption (eSFC) term, the ratio between total fuel consumption of the gas turbines and the total net propulsive force (including any thrust produced by the gas turbines):

$$\text{eSFC} = \frac{\dot{m}_{f,\text{total}}}{NPF_{\text{total}}} \quad (3.50)$$

An effective bypass ratio (eBPR) term will also be used, the ratio between the total bypass mass flow (i.e. the mass flow through the propulsor array and turbofan bypass) and the core mass flow (i.e. the mass flow passing through the gas turbine core and entering the combustor):

$$\text{eBPR} = \frac{\dot{m}_{\text{bypass}} + \dot{m}_{\text{array}}}{\dot{m}_{\text{core}}} \quad (3.51)$$

For the purposes of simulation, the performance of the propulsion system is calculated as one of two modes; an engine power matching mode (Mode 1) and a propulsive force matching mode (Mode 2). For the power matching mode, an engine power setting is established (turbine entry temperature is used here), with propulsor array performance dictated by the available power

### 3. Propulsion System Modelling

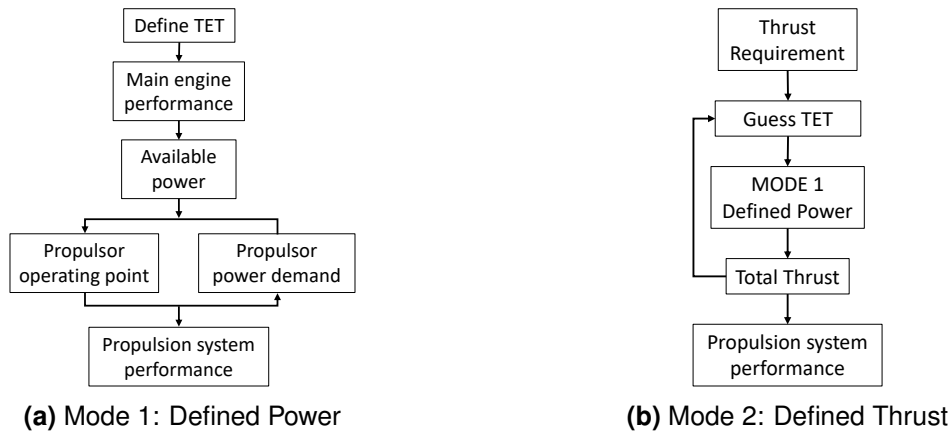


**Figure 3.15:** Simulation procedure for N3-X propulsion system operating modes

produced by the main engines. Unless otherwise stated, it is assumed that all propulsors in the array operate at the same rotational speed, with power distributed accordingly. Therefore, the rotational speed (and hence operating point) of the propulsors in the array is iterated until the power demand of the array as a whole matches the total power available through the superconducting electrical system (Figure 3.15a). An alternate simulation methodology would be to assume that each propulsor is provided with the same power, and iterate the rotational speed of each propulsor independently to determine their operating point.

The propulsive force matching mode is used to calculate the propulsion system performance where the net propulsive force requirement is known, such as the thrust equal to drag requirement for steady level flight during cruise. At off-design, the array and the gas turbines may produce varying amounts of propulsive force. The split between thrust produced by the main engines and the propulsor array is unknown. Therefore, engine power (i.e. turbine entry temperature in this case) is instead iterated until the total propulsive force produced by the combined system equals the required value (Figure 3.15b).

#### 3.2.5 BLI Model Validation

In order to assess the applicability of the model, a validation procedure was performed. The N3-X propulsor array has previously been simulated using a control volume method by Felder *et al.*, the results of which were used to perform a preliminary validation [89]. The reference N3-X simulation did not include location-related or integration parameters. Therefore, in order to allow a like-for-like analysis, the propulsor performance was calculated assuming operation of an array of net thrust-producing (rather than NPF) propulsors at the centreline of the airframe.

A primary component of the developed method was the estimation of local properties using a boundary layer theory-based method, as opposed to a more complex CFD analysis. Therefore, the validity and accuracy of the predicted inlet stream characteristics was assessed. Reference [89] provides the average Mach number and total pressure deficit relative to free-stream for inlet streams of various heights, obtained from CFD data. An equivalent procedure to estimate flow characteristics was performed over the range of streamtube heights provided by the reference. The results of this validation are shown in Figure 3.16. Comparison of the inlet stream properties to the NASA results shows an average difference in Mach number of 0.015 and an average 0.2% difference in boundary layer total pressure loss. This demonstrates that the inlet stream properties predicted by the analytical method closely correspond to those predicted by the CFD derived results.

Subsequently, the net thrust,  $F_N$ , was compared to a sizing procedure performed in the

### 3. Propulsion System Modelling

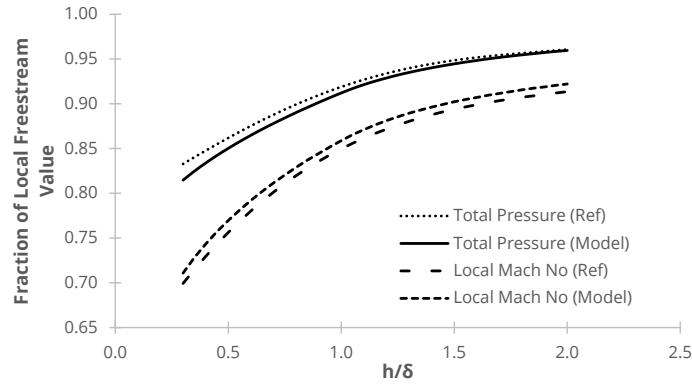


**Figure 3.16:** Validation of stream flow characteristics against NASA data

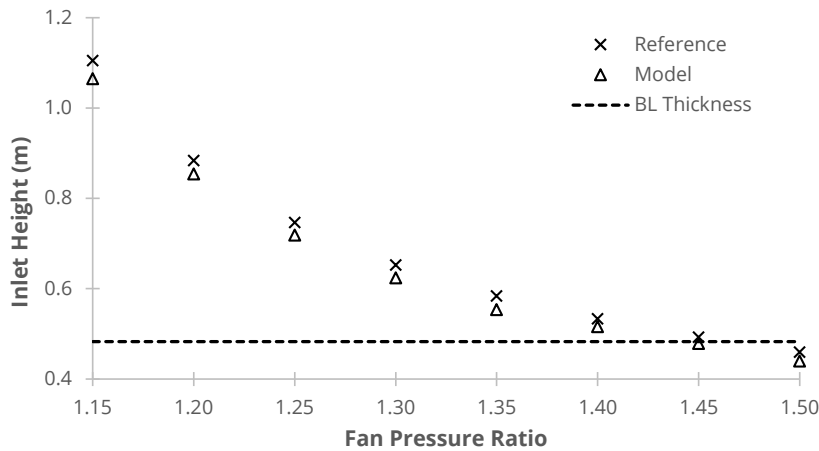


**Figure 3.17:** Validation of BLI propulsor inlet height against NASA data

reference [89]. The simulations performed in the reference attempted to predict the size of a BLI propulsor with a fixed thrust requirement. The reference method used a net thrust control volume combined with inlet flow characteristics derived from the CFD output in Figure 3.16 [92]. As has been noted, changing the size of the propulsors modifies the average inlet flow characteristics. Therefore, a procedure was required to solve for the inlet stream height  $h$  which produces the required thrust, given the propulsor design parameters. In order to perform the comparison, a number of parameters were set to equal those reported in the reference for each simulation point: Total array thrust, fan pressure ratio, number of fans in the array (from which the net thrust of each propulsor may be calculated), inlet aspect ratio, and fan efficiency. The inlet height predicted by the model was found to match the trend shown by the NASA predictions with an average difference in the height of the propulsion system inlet stream of 3.8% (Figure 3.17). Both the reference method and the developed method apply a force control volume for performance calculation. Therefore, the validation demonstrated that the discrepancy in estimated inlet characteristics has only a minor impact on performance calculations.

### 3.3 Propulsor Array Design Variables

The following analyses present considerations for the design point sizing of the propulsor array. Unless otherwise stated, the design point analyses assume that each propulsor is sized to produce the same net propulsive force. The propulsor array is sized to produce 119 kN at

### 3. Propulsion System Modelling

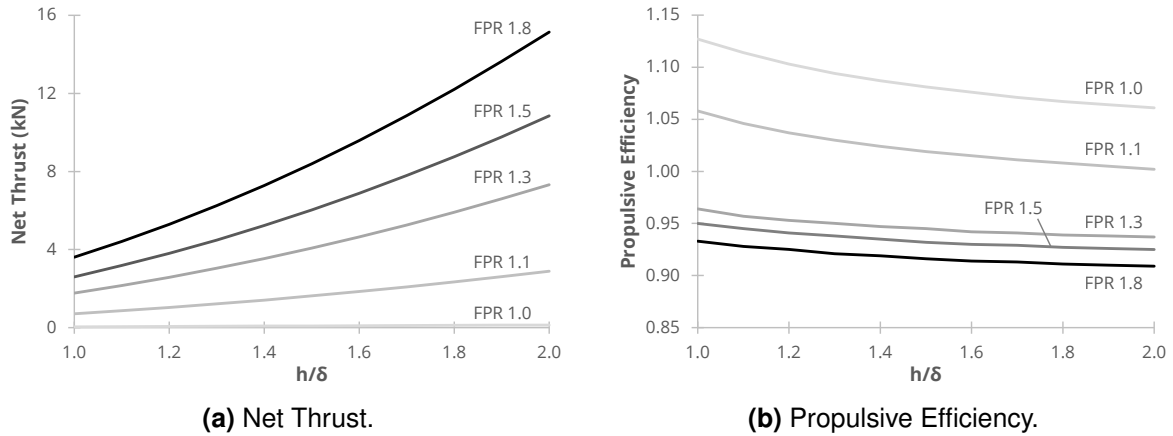


**Figure 3.18:** Design charts for a propulsor at M0.84 and 30,000 ft.

Mach 0.84, 30,000 ft from an array of 15 propulsors. In addition, each propulsor is sized to have a width equal to the fan diameter plus a spacing of 10 cm between each propulsor [56].

#### 3.3.1 Individual Propulsor Design

The thrust produced by a propulsor in the array can be influenced in a number of ways. Assuming the same operating conditions and propulsor efficiency, an increase in propulsor size will increase the mass flow ingested by the propulsion system and therefore increase the total thrust. However, inlet flow characteristics are a function of the ratio of inlet height to boundary layer thickness. Hence, an increase in mass flow by an increase in inlet height will tend the performance towards that of a free-stream propulsion system (assuming a constant boundary layer thickness). Alternatively, thrust can be increased with an increase in the fan pressure ratio. These two options are demonstrated in Figure 3.18. Note that as the results of this subsection are in terms of net thrust, the nacelle drag and installation related factors of the NPF equations are neglected.

A higher fan pressure ratio increases the exhaust velocity of the propulsion system. This results in an increase in specific thrust with a corresponding decrease in propulsive efficiency. The propulsive efficiency for the BLI system nonetheless remains high, and is greater than 100% for the simulated pressure ratios of 1.0 and 1.1. An increase in the inlet height increases the average velocity  $\bar{u}_i$  at the inlet until it approaches the free-stream velocity  $u_0$ . This results in a drop in propulsive efficiency asymptotically approaching the point where  $\bar{u}_i$  is equal to  $u_0$  (Equation 3.29) and the propulsive efficiency is equal to that of a propulsion system in free-stream flow.

The design charts demonstrate one of the challenges in designing a thrust-producing BLI propulsor. Thrust increase obtained by simply increasing the mass flow (via scaling of the propulsor) results in a reduction in boundary layer benefit. A similar conclusion can be made from results shown by Liu *et al.* [94], which demonstrates an increase in power saving coefficient as the BLI ratio (ratio of boundary layer mass flow to total mass flow, and related to the inverse of  $h/\delta$ ) is decreased. Conventional propulsion system performance also dictates that a higher exhaust jet velocity through a higher fan pressure ratio will reduce system efficiency. A balance is therefore required between the two options.



#### 3.3.2 Boundary layer-related Losses

The inherently distorted flow of the boundary layer will have a negative impact on propulsor performance, as additional inefficiencies and losses are introduced that would not be present with ingestion of only free-stream flow. The first of these is a loss in total pressure through the intake duct. This term accounts for the turbulent nature of the boundary layer, which may result in total pressure loss through the intake greater than the losses that would normally occur in a free-stream intake. The second loss is a decrease in fan efficiency due to the flow distortion at the fan face. The inlet flow has a non-uniform velocity and pressure profile introduced by the ingested boundary layer. This non-uniform flow can negatively impact the fan performance, especially for a fan that is not distortion tolerant (such as by including variable pitch or sweep to account for a pressure/velocity profile along the blade).

As would be expected, an increase in the total pressure loss through the intake leads to an increase in the propulsor's power consumption (Figure 3.19a). Assuming a low total pressure loss, the general trend demonstrates a reduction in PSC as the fan pressure ratio increases, similar to the analysis performed by Liu *et al.* [94] (Figure 3.20a). The extent to which the power saving coefficient and power consumption is influenced by the intake total pressure loss depends on the propulsor's fan pressure ratio. The power consumption of low fan pressure ratio propulsors (FPR 1.1–1.2) is strongly influenced by the total pressure deficit in the propulsor, and there is a sharp increase as the deficit increases. In order to achieve the required thrust, the propulsion system requires an increasingly large mass flow to compensate for a reduction in effective fan pressure ratio brought about by the inlet pressure loss. This is obtained by an increase in propulsor size (and hence inlet height), which increases the ratio  $h/\delta$  and brings the inlet average flow characteristics closer to free-stream. A higher fan pressure ratio reduces the mass flow required by the propulsion system and hence decreases the propulsion system size. However, power consumption is increased, as it is a function of both mass flow and enthalpy change. Nonetheless, a higher pressure ratio is more beneficial to power consumption in cases of high inlet pressure loss. For a low total pressure loss (e.g. the 0.2% value quoted in the original research on the N3-X), the propulsor with the lowest power and highest PSC is the one with the lowest fan pressure ratio. However, an optimum fan pressure ratio begins to emerge as the total pressure loss increases, defining the configuration with the lowest power consumption. For a BLI propulsor, the optimum develops due to the tradeoff between the negative effects of a propulsor with a large size and high fan pressure ratio. In contrast to the low total pressure loss case, the configuration with the highest PSC is one with a relatively higher fan pressure ratio. However, it should be highlighted that this is not the same fan pressure ratio as the minimum power configuration. For example, assuming a total pressure loss in the intake of 1%, a minimum power configuration is achieved for a fan pressure ratio of 1.15. However, a higher power saving coefficient is achieved for fan pressure ratios above 1.6.

Decreasing the efficiency of the fan results in an increase in the enthalpy change across the fan. However, there is little change in the thrust produced and hence no compensation by a change in mass flow ratio is required. This results in only a step increase in the power requirement of the propulsor as fan efficiency is decreased (Figure 3.19 and Figure 3.19). Unlike the intake total pressure loss term, a change in fan efficiency does not influence the overall power or PSC trend and there is no apparent optimum.

Although research has shown that ingesting a larger portion of airframe drag is beneficial for the power saving coefficient, specific design factors - such as the fan pressure ratio - will also have an influence. Low pressure ratio propulsors have a lower power requirement than high pressure ratios, and have the potential to ingest a larger percentage of the boundary layer. However, low pressure ratio propulsors can be less efficient in high loss cases than alternative

### 3. Propulsion System Modelling

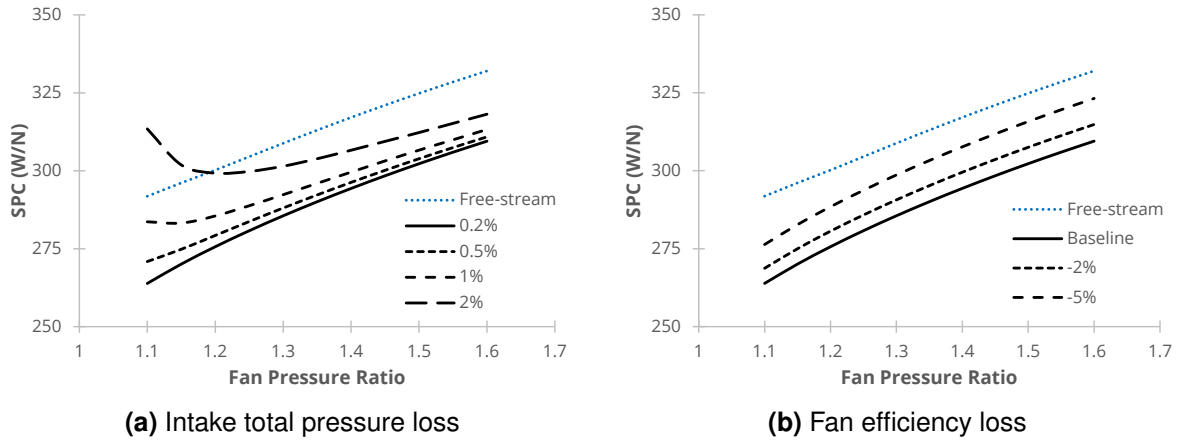


**Figure 3.19:** Influence of efficiency loss on specific power consumption for a propulsor on the N3-X airframe centreline at M0.84 and 30,000 ft (neglecting nacelle drag).

configurations and there is a point beyond which the free-stream propulsor is more efficient than a BLI propulsor. However, if one assumes that inlet and fan efficiency losses can be kept low, the power consumption of a BLI propulsor is lower than that of a propulsor producing the same net thrust from free-stream flow. This reflects conclusions drawn from previous research, which demonstrate a positive PSC for low loss BLI systems [20, 112].

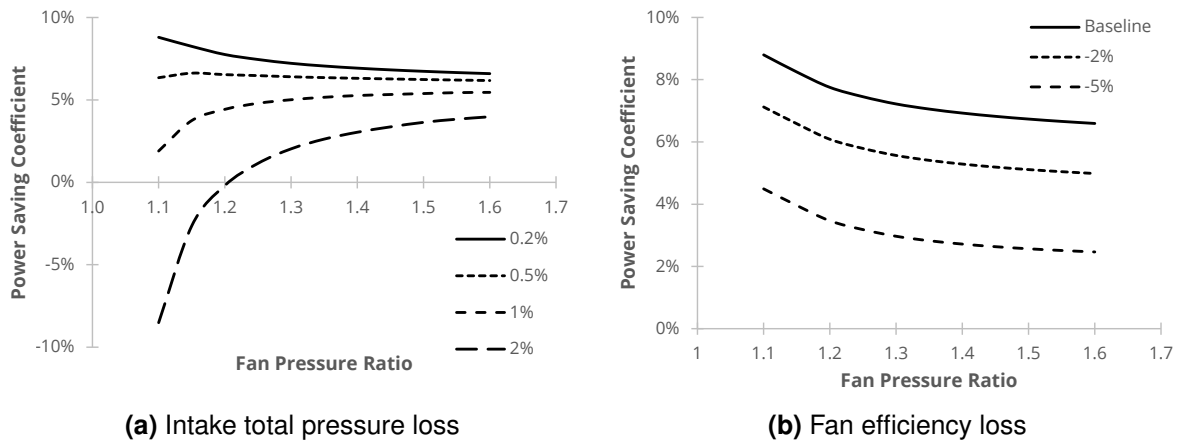


**Figure 3.20:** Influence of efficiency loss on power saving coefficient for a propulsor on the N3-X airframe centreline at M0.84 and 30,000 ft (neglecting nacelle drag).

Whilst the design point system analyses have assumed a total pressure loss of 0.2% through the intake, Seddon’s method provides an alternative viewpoint on the total pressure loss through a BLI inlet. For the N3-X propulsor array, Seddon’s method predicts an inlet total pressure recovery between 99.4%–99.6% for a propulsor at the centreline, depending on the propulsor size (i.e. fan pressure ratio in this case). These estimates are close to the value previously assumed for the N3-X. However, the slight increase in total pressure lost in the inlet will lead to an increase in the propulsion system’s power consumption (Figure 3.19a). The magnitude of the pressure recovery is dependent on the inlet configuration, the mass flow ratio and the ratio  $h/\delta$ , with a lower ratio of  $h/\delta$  leading to a higher total pressure loss (Figure 3.21).

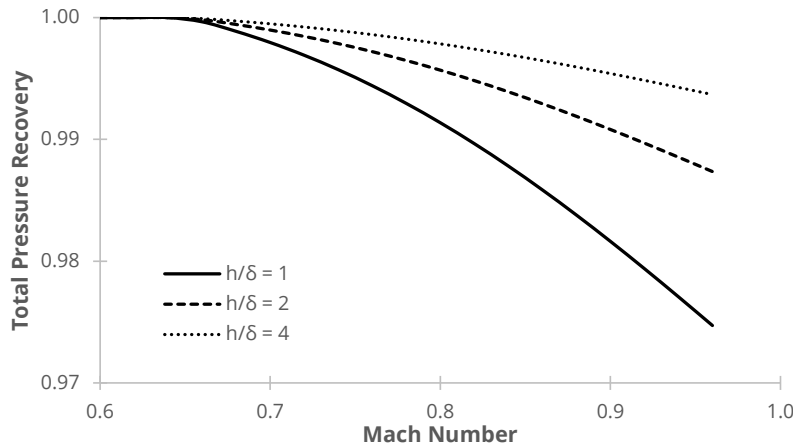


**Figure 3.21:** Inlet total pressure recovery as a function of  $h/\delta$  (CAR = 0.8)

### 3.3.3 Propulsor Location

A propulsor's inlet flow characteristics are dependent on its location on the airframe, with different locations resulting in a different boundary layer thickness or local velocity. A propulsors at the centreline of the airframe will be more efficient than a propulsors at the outer edges of the array, as the centreline has the thickest boundary layer and the lowest local velocity (Figure 3.13). Whilst the boundary layer does result in a reduction in the average velocity at the intake of the propulsors, a high local velocity will eventually cancel out any reduction in velocity versus the free-stream flow. In addition, a thin boundary layer means the benefits from ingesting the boundary layer are small, as inlet flow characteristics tend towards the free-stream (assuming a fixed size propulsor). The reduction in efficiency as a propulsor is moved from the centreline outwards may be seen by simulating performance at a number of locations along the fuselage (Figure 3.22). As the propulsor is moved further away from the airframe centreline, its specific power consumption increases. A point is reached where the power consumption of the propulsor exceeds that of a propulsor operating in free-stream flow. The point where the BLI propulsor is less efficient than a free-stream propulsor will define the maximum sensible length of the array. Propulsors further from the centreline will negatively effect the performance of the system due to a high power consumption, and there is therefore no benefit gained from locating propulsors in this region.

The analysis in Figure 3.22 assumed a fixed inlet total pressure loss of 0.2% [56]. However, Seddon's method identifies that the total pressure loss will be a function of the intake dimensions, the mass flow ratio and the boundary layer capture ratio [107]. All the simulated propulsor configurations operate with a mass flow ratio in the region of 0.8. In addition, the aspect ratio of each inlet is approximately equal, with an intake width 1.18 times its height. The key difference between different configurations is the boundary layer capture ratio. Higher fan pressure ratios lead to a smaller ratio of  $h/\delta$  (higher boundary layer capture ratio), and hence increase the total pressure loss resulting from Seddon's method. However, as the propulsor is moved further from the centreline, the boundary layer thickness reduces and hence  $h/\delta$  increases. This therefore leads to a reduction in total pressure loss in the intake Figure 3.23. The resulting total pressure loss in the inlet is consistently higher than the 0.2% assumed as a baseline value for this research, and leads to an overall increase in power consumption for the propulsors. However, the total pressure loss for propulsors at the outer edge of the array is lower than for the centreline propulsors.

### 3. Propulsion System Modelling

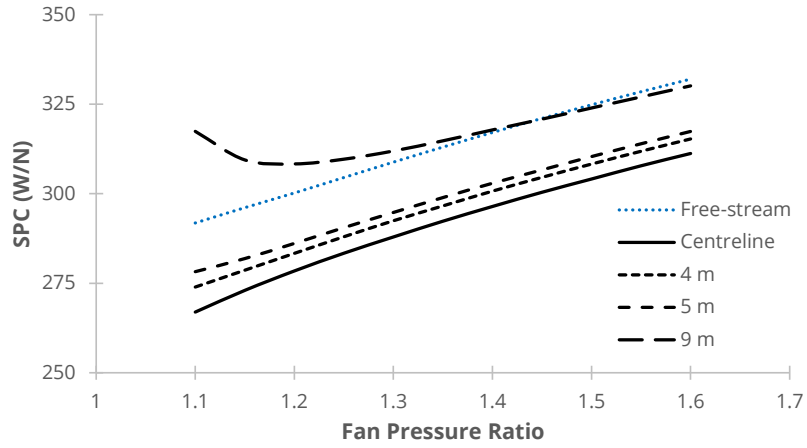


Figure 3.22: Propulsor specific power consumption as a function of distance from the airframe centreline

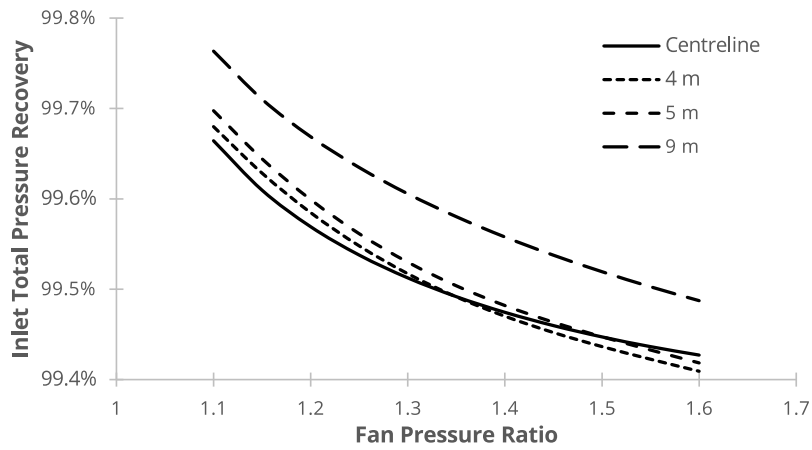


Figure 3.23: Propulsor intake total pressure recovery using Seddon's method

#### 3.3.4 Whole Array Design

The previous two results section have shown the performance of a single propulsor operating at the centreline of the aircraft and various spanwise distances from the centreline. The full array performance must account for all fans in the array. The spanwise variation in flow characteristics adds an additional consideration to the design process, as the size of the propulsor will influence performance. The thinner boundary layer and higher speed flow at the array edges has a negative impact on the efficiency of the propulsor and results in an increase the array power requirement (Figure 3.24). It should be highlighted that the magnitude of the results are dependent on the trends used to estimate the local flow conditions for each propulsor. Three fictitious cases were simulated to demonstrate how the span-related flow characteristics influence performance:

- No Span Effects – Each propulsor in the array ingests the same inlet flow conditions. This case is equivalent to each propulsor being located at the centreline of the airframe. Boundary layer thickness and local free-stream velocity at the edge of the boundary layer are constant.
- $M_{0i}$  Variation Only – Boundary layer thickness  $\delta$  along the length of the array is equal to the centreline boundary layer thickness. The only spanwise variation in flow characteristics is due to the velocity profile over the airframe .
- $\delta$  Variation Only – Local Mach number at the edge of the boundary layer is equal to the centreline local Mach number. The only spanwise variation in flow characteristics is due to the change in boundary layer thickness as a result of the variation in chord length prior to the inlet.

Each configuration is sized for the same net propulsive force and has the same length. The intake total pressure loss is calculated as a function of the inlet configuration following Seddon's method. A reduction of the boundary layer thickness along the array length results in an increase in the power requirement of the array (Figure 3.24). This increase in power requirement results from the increase in  $h/\delta$  along the array length, which tends the inlet flow characteristics to the characteristics of the free-stream flow. An increase in Mach number along the array length will also increase the power consumption of the array as a higher local free-stream velocity results in an increase in momentum drag,  $F_{Gi}$ . This relationship between size and local flow characteristics is presented visually in Figure 3.25. The combination of the two spanwise flow characteristics works to reduce the efficiency of the system as a whole. As the fan pressure ratio increases, the size of each propulsor in the array decreases, leading to a decrease in  $F_{Gi}$  and  $h/\delta$ . However, the higher fan pressure ratio will increase the power consumption of the propulsion system. An minimal power configuration begins to become apparent as fan pressure ratio for the array is varied. This is more apparent when observing the SPC for each individual propulsor (Figure 3.26).

Fan pressure ratio can also be combined with array length as a variable to obtain a low power configuration (Figure 3.27). An increase in fan pressure ratio reduces the mass flow necessary to produce the NPF required from the array. This can be used to set a shorter array length which avoids the high speed, thin boundary layer flow at the array outer edge, or a lower ratio of  $h/\delta$ . In addition, it can lead to a more favourable intake configuration with respect to reducing the total pressure lost as calculated by Seddon's method.

The nacelle drag of the propulsion system is an additional factor in a full NPF assessment. Sizing the propulsion system with the full NPF equation increases the power consumption of the array, as each propulsor must compensate for the installation terms whilst still providing thrust.

### 3. Propulsion System Modelling

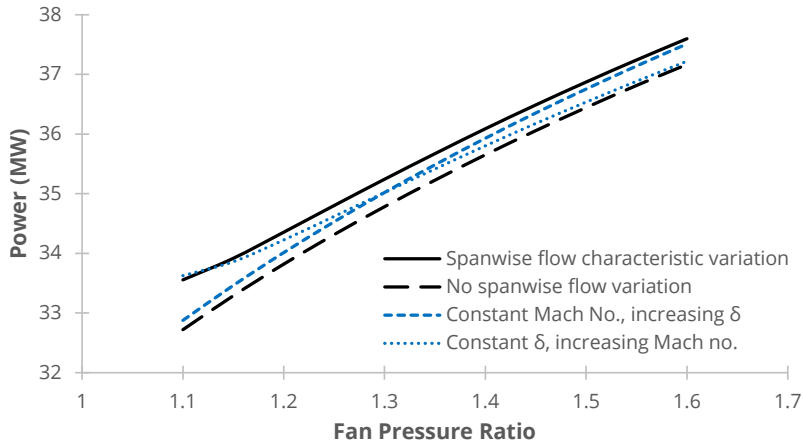


**Figure 3.24:** Influence of span-wise flow characteristic variation on power requirement of an array with 15 fans at M0.84 and 30,000 ft (neglecting nacelle drag).

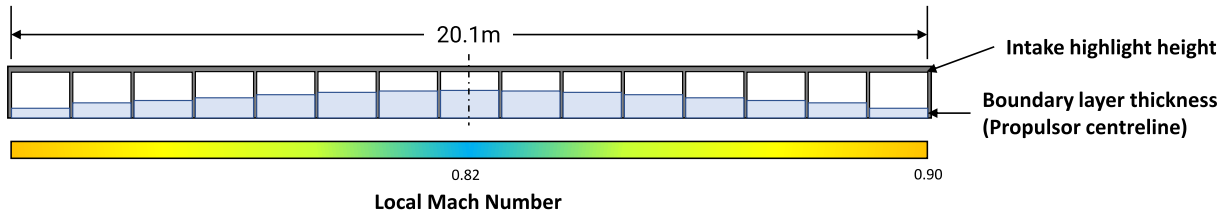


**Figure 3.25:** Sketch indicating propulsor array size and local flow conditions for a 15 fan array with fan pressure ratio of 1.3 and length of 20.1 m

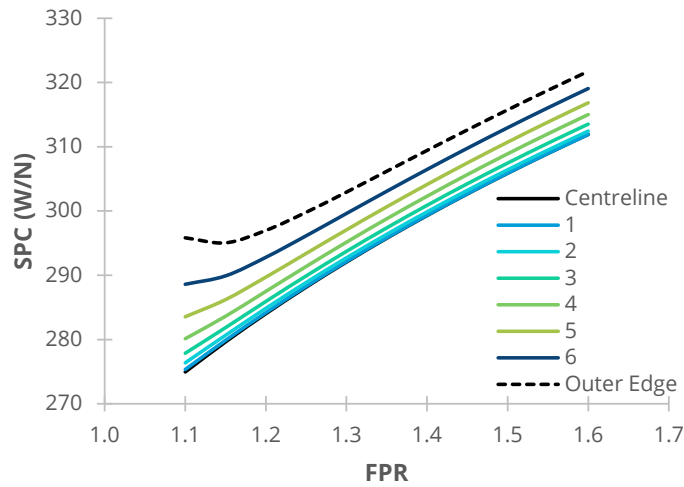


**Figure 3.26:** Influence of fan pressure ratio on individual performance of propulsors in an array (20.1 m array, neglecting nacelle drag)

### 3. Propulsion System Modelling

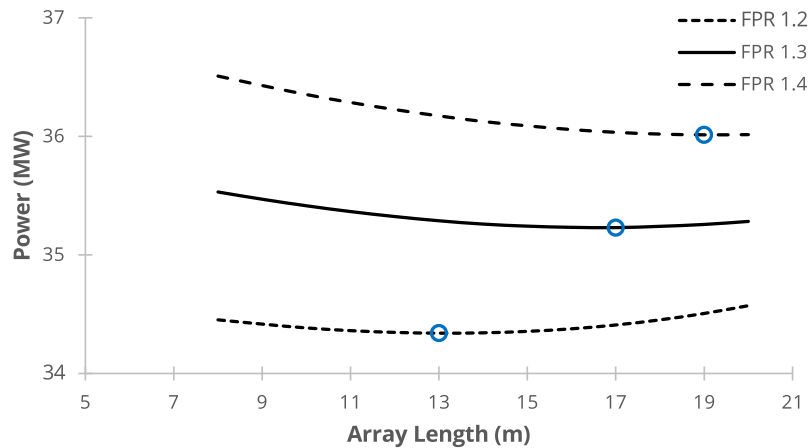


**Figure 3.27:** Influence of array length on power requirement of an array with 15 fans at M0.84 and 30,000 ft (neglecting nacelle drag).

Research suggests that flow on the nacelle of the BWB may be prone to separation [113], therefore, an optimised nacelle configuration is a necessary component of the design. The trade-off between array size and fan pressure ratio can lead to a configuration which minimises power consumption.

In addition to fan pressure ratio, the array configuration also includes parameters such as the number of propulsors and the aspect ratio of each propulsor intake. Tall, narrow inlets increase the ratio  $h/\delta$ , but will reduce array length, which avoids the flow on the outer edges of the fuselage. In contrast, short, wide inlets will bring the inlet height closer to the boundary layer height and ingest a relatively greater portion of the airframe drag. However, this will increase the array length. In addition, the inlet configuration will influence the total pressure recovery through the intake. The trade-off between these costs and benefits determines the ideal configuration in terms of aspect ratio. A similar set of considerations are applicable for the number of propulsors in the array. A greater number of propulsors reduces the average height of each propulsor, as the inlet area is spread over a greater array length. However, this extends the array into the relatively higher speed, thin boundary layer flow (high  $h/\delta$ ) at the fuselage edge, which may be detrimental to the overall power consumption of the array. Array length, propulsor aspect ratio, and number of fans are all linked variables, as they influence the size of the array and the individual propulsors. Each variable can be used to design a minimum power configuration by balancing the same set of considerations.

From an array performance perspective, the number of fans variable will influence the length and height variables for the array. However, the number of propulsors variable will also correspond to the array weight. A larger number of propulsors in the array can lead to an increase in weight, as there are more motors and fans in the system. Therefore, the number of propulsors as a variable must be considered in combination with the propulsion system weight.

To summarise the key factors of a low power array design for the N3-X:

- Array length
  - Local flow velocity
  - Local boundary layer thickness
- Inlet configuration (leading to total pressure recovery in the intake duct)
- Nacelle configuration

## 3.4 Weight Estimation

The weight estimation tools used in this research are intended to provide a preliminary estimate of the propulsion system weight. The tools allow an insight into how changes to the propulsion system design will influence the overall weight. This may then be used to adjust the aircraft's operating empty weight based on the propulsion system design.

### 3.4.1 Turbomachinery

The weight of the gas turbines is estimated using *Atlas*, an in-house tool for the prediction of turbomachinery weight [114]. The tool predicts the overall weight of the gas turbine on a component-by-component basis, including the weight of ducts, shafts, and turbomachinery blades and disks. The tool is applied to predict the weight of both the main engines and the fans in the propulsor array. In the full aircraft analysis, these weights are added to the base airframe weight to produce the aircraft's operating empty weight.

### 3.4.2 Superconducting Electrical System

The superconducting electrical system consists of a number subcomponents (assuming cooling is performed using liquid hydrogen rather than cryocoolers):

- Fan motors
- Generators
- Transmission Cables
- Inverters

In the absence of publicly available or established design tools for superconducting electrical systems, it is difficult to estimate the weight of each of these components. Instead, this research makes use of previous data used in estimating the weight of the N3-X's electrical systems. The weight of the motors and generators was estimated based on a trend relating weight to the shaft horsepower (Figure 3.28 [24]), assuming that generators may be treated similarly to motors for weight purposes [46]. The weight estimate is split into low and high power equations:

$$\log(W_{\text{motor}}) = 0.1990 \log(P) + 0.8632 \quad P \leq 883.8\text{kW} \quad (3.52)$$

$$\log(W_{\text{motor}}) = 0.8497 \log(P) - 1.1866 \quad P > 883.8\text{kW} \quad (3.53)$$

Where  $W_{\text{motor}}$  is the weight of the motor or generator and  $P$  is the shaft power required. The crossover between the two equations occurs for a shaft power of approximately 883.8 kW. Whilst the weight estimated may be considered optimistic [46], it provides an initial estimate of potential technology in the 2035+ entry into service period. A flat weight of 453 kg (1000 lb) was added to account for the transmission lines, based on previous weight estimations performed for the N3-X [56]. The inverter weight is similarly taken as a flat weight of 90.7 kg (200 lb). The electrical system was sized for the maximum power requirement expected during rolling take-off (0ft, Mach 0.25). As each propulsor has a different power requirement, each motor will have a different weight. Sizing the motors and generators for the power requirement at the aerodynamic design point would lead to a lower weight for the electrical system. However, the array performance at off-design would need to be matched to the maximum motor power and available power from the generators. In addition, power from the power turbine would need



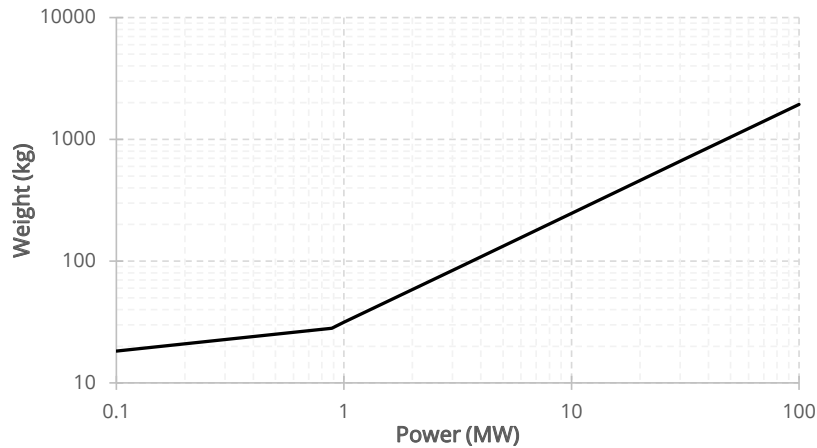


**Figure 3.28:** Weight of superconducting equipments as a function of power [56]

to be matched to the maximum generating capacity of the generators. This could either lead to a lower engine temperature (i.e. lower power setting), or higher thrust produced from the turbomachinery (assuming a fixed power setting). A point for further research may be to predict the propulsor array performance if the array power and net thrust is limited by the power of motors sized for the propulsion system design point.

### 3.5 Baseline Propulsion System

A baseline propulsion system configuration was established for the array to enable comparison to alternative configurations. The design of this baseline array was based on previous research on the N3-X propulsion system [56, 89]. The baseline configuration consists of a 15-fan propulsor array with a fan pressure ratio of 1.3 for each propulsor. The width of each propulsor inlet is assumed to equal the fan diameter with 10 cm spacing between each. The fans were sized for a fan face Mach number of 0.65 and with a hub-to-tip ratio of 0.2. The intake throat was sized for a Mach number of 0.75 and the contraction ratio from the highlight to the throat was assumed to be 1.2. Total pressure recovery through the inlet was calculated following Seddon's method and fan efficiency was assumed to be 0.9535. Each propulsor was sized to produce the same NPF totalling 119 kN for the array as a whole.

Design and performance parameters for each propulsor in the array are shown in Table 3.2, where the propulsors are numbered 0 – 7 from the centreline to the outer edge. Propulsors are mirrored about the centreline (Propulsor 0). The main engines follows the design parameters established in Table 3.1. The propulsion system was simulated at four points; the aerodynamic design point (ADP), a sample point during cruise, rolling take-off (RTO), and sea-level static (SLS). The control parameter for these points was the engine power (in terms of turbine entry temperature following reference [89]), i.e. the propulsion system was simulated in a power matching mode. Where required, the rotational speed of the fans in the array was spooled down to match the power available from the turbogenerators. Performance parameters for the propulsors, engine, and combined propulsion system at each of the operating points are shown in Table 3.2 and Table 3.3. At the cruise power setting, the net thrust from the turbomachinery is slightly negative, and the propulsor split term is therefore 100.1%, as the array must compensate for the increase in momentum drag (see definition of thrust split, Equation 3.49).

A propulsion system design was also created for the LH<sub>2</sub> variant. The system was sized for the same net propulsive force and design parameters for the two engines are assumed to be the same. The present research does not cover the detailed design changes that would be

### 3. Propulsion System Modelling

**Table 3.2:** Performance parameters for individual fans in the baseline N3-X propulsor array at the aerodynamic design point

	0	1	2	3	4	5	6	7
Power (MW)	2.31	2.31	2.32	2.34	2.35	2.37	2.41	2.48
Mass Flow (kg/s)	107.9	107.9	108.3	108.9	109.8	110.8	112.6	115.7
Highlight Height (m)	1.010	1.009	1.007	1.003	0.998	0.993	0.986	0.982
SPC (W/N)	291.6	291.7	292.6	294.4	296.7	299.4	304.2	312.7
$\eta_{\text{inlet}}$	0.9951	0.9951	0.9951	0.9953	0.9957	0.9960	0.9960	0.9961
$\eta_{\text{propulsive}}$	0.941	0.940	0.937	0.933	0.927	0.921	0.908	0.893
$h/\delta$	1.68	1.70	1.78	1.97	2.29	2.71	3.20	3.95

necessary within the engine (such as a change in combustor design) to account for the change in fuel type. The only point of difference between the two engines is therefore the smaller main engine size and performance difference due to a different fuel type (Table 3.4).

It is interesting to note that the main engines sized for LH<sub>2</sub> fuel are able to produce more power than the kerosene engines at sea level static conditions. The LH<sub>2</sub> configuration is therefore able to produce a 1.4% more thrust at SLS than the kerosene variant. There is naturally a difference in fuel consumption between the two configurations, due to the different fuel types. In terms of energy consumption, the LH<sub>2</sub> engines use approximately 3% less fuel energy per newton second than the kerosene engines at ADP, as the core mass flow is 8% less than that of the kerosene engines.

The total weight of the propulsion system may be broken down into individual components (Table 3.5). For the baseline design, each propulsor in the array is individually designed based on local flow conditions. Propulsors at the outer edge are therefore larger and require higher power motors than those near the centreline. The average weight for the fans of each propulsor is approximately 360 kg, with motors averaging 114 kg each. Each of the two generators for the electrical system weighs 690 kg. In addition, the two turbogenerators weigh 1,114 kg each and have an estimated length of 1.05m. Including the miscellaneous weight of HTS wires and inverters, the total weight of the electrical system is approximately 3,635 kg. The total weight of the turbomachinery (turbogenerators and propulsor fans) is 7,680 kg, leading to a total propulsion system weight of 11,312 kg (not including nacelles and pylons for the propulsors). This weight estimate is within 10% of the estimate produced by previous research, which predicts a total weight of 12,330 kg [56] (not including nacelles and pylons for the propulsors). The propulsor array and its electrical system account for approximately 75% of the total propulsion system weight.

The propulsor array's maximum power requirement is dependent on the maximum power available from the main engines. The electrical system can therefore be sized for a slightly lower maximum power that would be required to operate the propulsors at 100% rotational speed at sea level. The motors and generators would otherwise be heavier than necessary.

#### 3.5.1 Final Design Conclusions

The design of the baseline propulsor array for the N3-X allows a number of conclusions to be made for the design of the N3-X propulsion system:

- Local flow conditions may differ substantially along the length of an array installed on the fuselage of a blended wing body airframe. In this situation, each propulsor in the array must be individually designed to account for the different local conditions.
- Different local flow conditions lead to different performance characteristics for each propul-

### 3. Propulsion System Modelling

**Table 3.3:** Performance of the baseline N3-X propulsion system configuration

	ADP	Cruise	RTO	SLS
Altitude (ft)	30000	40000	0	0
Mach Number	0.84	0.84	0.25	0
Engine				
TET (K)	1811	1728	1895	1922
Net Thrust (kN)	0.0	0.0	4.1	8.6
Power (MW)	17.8	10.8	31.5	32.7
Mass Flow (kg/s)	25.40	16.31	48.15	48.89
Fuel Flow (kg/s)	0.706	0.427	1.401	1.459
Array				
NPF (kN)	118.9	74.5	404.8	625.5
Mass Flow (kg/s)	1655.6	1060.3	3151.9	3153.8
Power Consumption (MW)	35.6	21.7	62.9	65.4
Specific Power Consumption (W/N)	299.2	290.7	155.5	104.5
Propulsor RPM	100.0%	100.0%	90.7%	93.2%
Length (m)	20.1			
Propulsion System				
eSFC (mg/Ns)	11.88	11.45	6.78	4.54
eBPR	32.6	32.5	32.7	32.3
eST (N/kg)	69.7	68.2	127.2	197.7
NPF (kN)	118.9	74.5	413.1	642.7
Thrust Split	100.0%	100.0%	98.0%	97.3%

**Table 3.4:** Performance of the LH<sub>2</sub> variant propulsion system configuration

	ADP	Cruise	RTO	SLS
Altitude (ft)	30000	40000	0	0
Mach Number	0.84	0.84	0.25	0
Engine				
TET (K)	1811	1728	1895	1922
Net Thrust (kN)	0.0	0.0	3.9	8.1
Power (MW)	17.6	10.6	31.7	33.1
Mass Flow (kg/s)	23.22	14.77	44.29	45.23
Fuel Flow (kg/s)	0.245	0.146	0.491	0.515
Array				
NPF (kN)	118.9	73.7	406.7	630.1
Mass Flow (kg/s)	1640.2	1045.1	3140.5	3153.5
Power Consumption (MW)	35.2	21.2	63.3	66.3
Specific Power Consumption (W/N)	296.4	287.5	155.7	105.2
Propulsor RPM	100.0%	99.7%	91.2%	93.9%
Length (m)	20.1			
Propulsion System				
eSFC (mg/Ns)	4.12	3.98	2.37	1.59
eBPR	35.3	35.4	35.5	34.9
eST (N/kg)	70.5	68.5	128.3	199.2
NPF (kN)	118.9	73.6	414.4	646.2
Thrust Split	100.0%	100.1%	98.1%	97.5%

### 3. Propulsion System Modelling

**Table 3.5:** Overall weight of the baseline propulsion system configuration

Component	Weight	% of Total
Distributed Propulsors (total)	5452 kg	48%
Turbogenerator	1114 kg	10%
HTS Generator	691 kg	6%
Motors (total)	1707 kg	15%
Misc. HTS	545 kg	5%
Total Weight	11312 kg	

sor in the array. There may therefore be a reasonably noticeable difference in performance characteristics at off-design.

- Assuming each propulsor is operated at the same rotational speed, propulsors in flow with the thinnest boundary layer and fastest local flow (outer propulsors) are less efficient than those with a thick boundary layer and slow local flow (inner propulsors).
- Assuming each propulsor is operated at the same rotational speed, efficiency of individual propulsors at off-design converges as the boundary thickness reduces and mass flow ratio increases.
- The design presented herein assumes that each propulsor is sized to produce the same net propulsive force. As a result, the highlight area of each propulsor differs based on the mass flow for which the propulsor is sized. This may lead to different fan diameters (where each is designed for the same Mach number at the fan face), or different fan face Mach numbers (where each fan is designed with the same diameter). Relevant intake areas may be sized differently, depending on the Mach numbers for which they are designed. In the case of the baseline N3-X array design, the highlight height of the outer propulsor is 2.8% smaller than that of the centreline propulsor. This is due to a combination of the difference in mass flow and the average stream velocity (and hence Mach number).
- Where each propulsor is sized for the same net propulsive force, propulsor at the outer edge of the array have the potential to produce the greatest thrust at SLS, as they are sized for a larger non-dimensional mass flow. Inner propulsors are sized for a smaller non-dimensional mass flow and so produce less thrust at SLS.
- Different boundary layer capture ratios for different propulsors will influence the total pressure recovery in the intake duct.
- Different performance characteristics lead to the potential for individual control of propulsor for the best outcome. Outer propulsors may be used to produce more thrust at low speed, high mass flow ratio flight. Inner propulsors are more efficient in flight conditions where boundary layer thickness is high.

These conclusions can also be extended to apply to other configurations that utilise boundary layer ingestion.

## 3.6 Propulsor Array Performance

### 3.6.1 Individual Propulsors

The previous section presented the overall performance of the baseline propulsion system design at a number of key operating points. It is also useful to break down the performance

### 3. Propulsion System Modelling

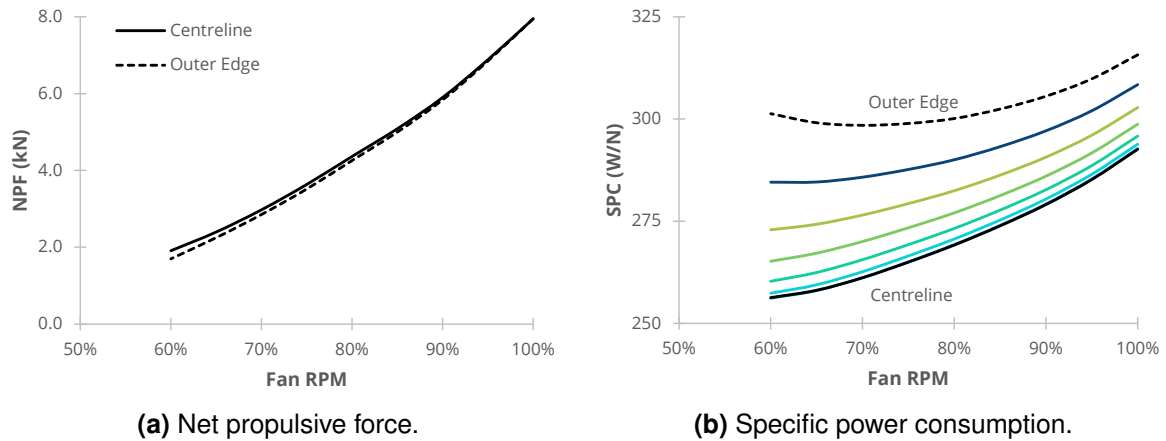


**Figure 3.29:** ADP performance of propulsors at the centreline and end of the propulsor array as a function of rotational speed.

of individual propulsors in the array to identify the differences in performance as a function of the propulsor's location. Whilst each propulsor is sized to produce the same net propulsive force at design point, they will perform differently at off-design conditions due to differences in propulsor size and location. To demonstrate this difference, the performance of two propulsors in the array, the centreline propulsor and the propulsor at the far end of the array, was simulated at the ADP flight conditions (Figure 3.29) and sea level static (Figure 3.30) for a range of fan rotational speeds.

Both propulsors are sized for the same NPF at design point, therefore, the reduction in net propulsive force as the fan RPM reduces is very similar (Figure 3.29a). However, the centreline fan produces slightly more net propulsive force than the end fan as the rotational speed reduces. Both fans operate on the same fan map (scaled to their respective non-dimensional mass flows). Their running line is therefore similar, with the same relationship between rotational speed, fan pressure ratio, and efficiency. The difference therefore arises due to the different flow characteristics of the two propulsors. Net thrust produced by the propulsors reduces for both propulsors as the rotational speed is reduced. However, as the ratio of  $h/\delta$  for the centreline propulsor is lower, its momentum drag is lower (lower average velocity at station  $i$ ). The centreline propulsor is therefore able to produce more net thrust than the outermost propulsor. As the fan at the centreline has a lower ratio of  $h/\delta$  and a higher propulsive efficiency than a propulsor at the end of the array, the SPC of the centreline propulsor is consistently better than propulsors further along the span (Figure 3.29b). Reducing the rotational speed of the propulsor reduces its power consumption and increases its propulsive efficiency (due to a lower exhaust velocity), hence SPC improves as the rotational speed is reduced. In addition,  $h/\delta$  decreases as the fan rotational speed reduces, due to a lower mass flow demand and hence a lower mass flow ratio. A minimum SPC point becomes apparent for the propulsors at the edge of the array. This is similar to the trend which would be observed for a typical turbofan engine, where a minimum SFC point can be found as engine power is reduced.

At sea level static, the differences between the two propulsors reduce (Figure 3.30). The aircraft is static and the airframe boundary layer is negligible, meaning location-specific differences do not play a part in performance. In addition, the high mass flow ratio of sea level static operation means that the ratio of  $h/\delta$  is high enough to make any ingested boundary layer negligible in comparison to the ingested free-stream flow. As both propulsors are effectively operating with free-stream air at a Mach number less than 0.35, the inlet total pressure recovery predicted from Seddon's method is 100%. Therefore, the only difference in performance

### 3. Propulsion System Modelling

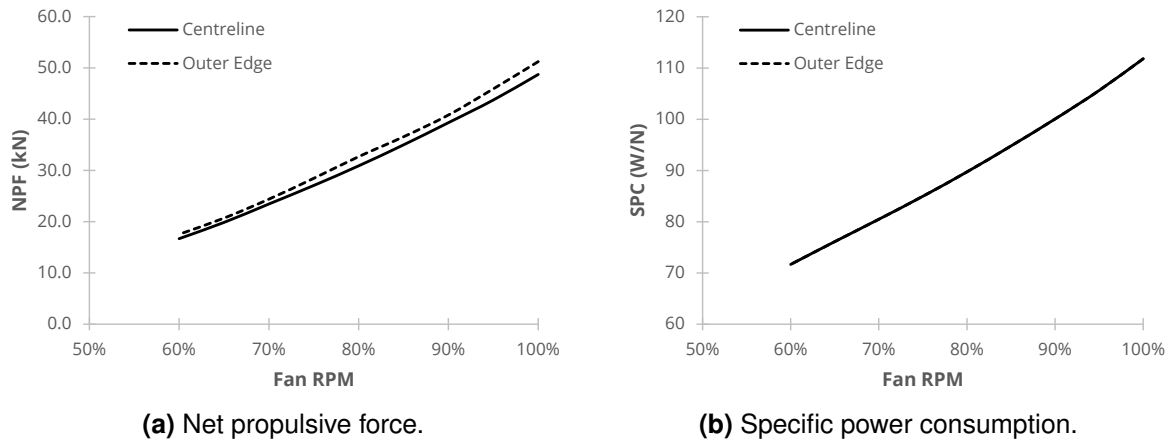


**Figure 3.30:** Sea level static performance of propulsors at the centreline and end of the propulsor array as a function of rotational speed.

between propulsors is the difference resulting from their size. As the performance benefits of the boundary layer do not contribute at static conditions, both propulsors have the same trend linking the decrease in rotational speed to a decrease in specific power consumption (Figure 3.30b). However, the difference between the two propulsors is apparent in their net propulsive force. The propulsor at the array end is larger than the centreline propulsor, as it is sized for a larger non-dimensional mass flow in order to produce the required net propulsive force at ADP. The propulsor at the array end is therefore able to produce more thrust than the centreline propulsor at sea level static conditions.

As the free-stream flow speed increases, the boundary layer begins to play a larger part in performance and the efficiency of the propulsors in the array begins to diverge (Figure 3.31b). As with the change in rotational speed, the centreline propulsor is more efficient, due to the benefits of ingesting a thicker boundary layer. As the flight velocity reduces, the capture area ratio of the propulsor increases. This is matched by a similar increase in the ratio  $h/\delta$ , which tends the inlet flow characteristics, and hence performance, towards that of a free-stream propulsor (Figure 3.32). Flow characteristics as modelled are asymptotic to their free-stream values, however, for the simulated flight altitude of 30,000 ft, average total pressure and velocity reach 99% of their free-stream value at a mass flow ratio of approximately 4, and 99.9% of their free-stream value at a mass flow ratio of approximately 50.

As the rotational speed of the fan is reduced, its mass flow demand also reduces. A low mass flow demand (below 1.0) implies an adverse pressure gradient, which leads to the risk of separation of the boundary before the inlet. The mass flow ratio is also linked to operating conditions (altitude and Mach number), with an increase in speed leading to a decrease in capture area ratio. For the simulated configuration of the propulsor array, the propulsors at the outer edges operate at a lower capture area ratio. However, the outer propulsors also operate with a thinner boundary layer, which may counterbalance the separation risk. The risk of boundary layer separation at low capture area ratio must be addressed for BLI propulsion systems operating at high velocity and low power settings, such as flight idle during descent.

#### 3.6.2 Whole Array

The discrepancy between the propulsor array and main engine performance means that the propulsor array will rarely operate at a point where maximum power demand exactly matches the maximum available power from the free power turbines at the defined engine power setting (Figure 3.33). At lower altitudes the maximum power demanded by the array at 100% rotational

### 3. Propulsion System Modelling

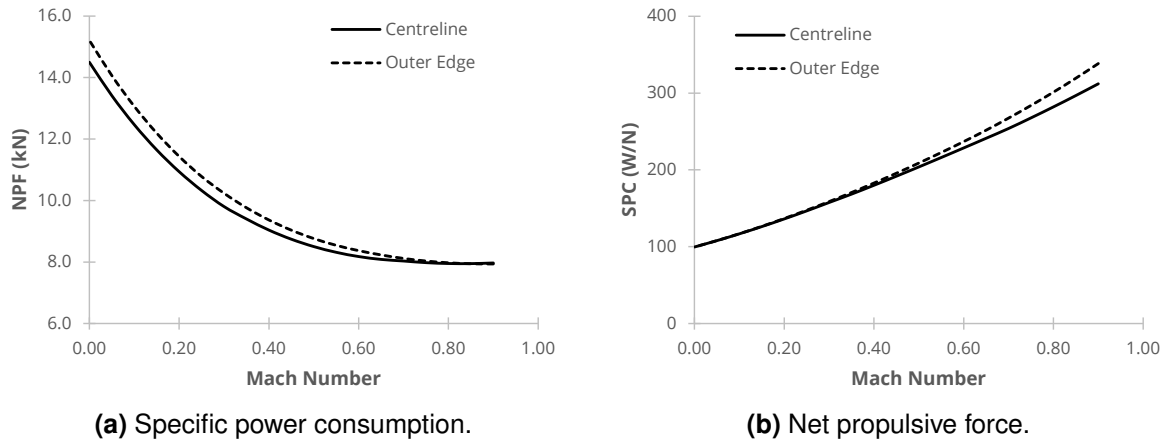


**Figure 3.31:** Performance of propulsors at the centreline and end of the propulsor array at 30,000ft as a function of Mach number

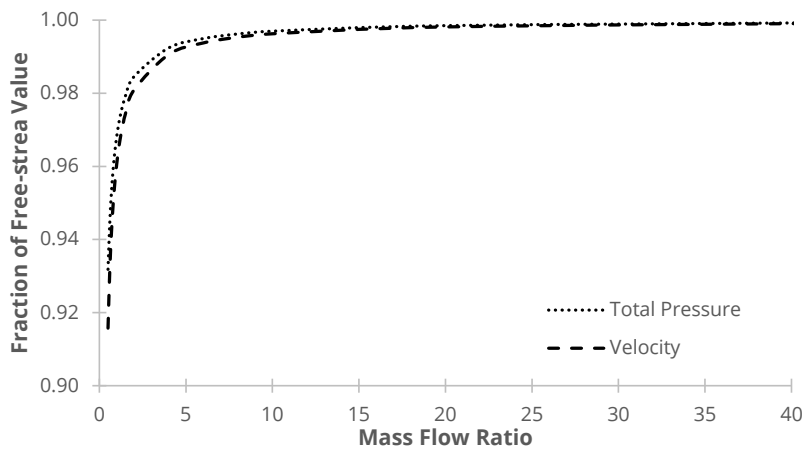


**Figure 3.32:** Mass flow-average total pressure and velocity of inlet stream as a function of mass flow ratio (85% chord)

### 3. Propulsion System Modelling

---

speed exceeds the available power. In contrast, at higher altitudes the available power from the main engines at the ADP power setting exceeds the maximum power demand of the propulsor array operating at 100% RPM. The power deficit at low altitude is significantly greater than the power excess at high altitudes. The higher engine power settings of take-off and climb will reduce the power deficit, but the power demand from the propulsor array is nevertheless greater than the power the main engines are able to supply. The 0 power deficit contour marks the flight conditions where power demand from the propulsor array exactly matches the available power from the turbomachinery.

Whilst the outcome is represented as a power 'deficit', it is an expected aspect of operating different systems and turbomachinery components together. At off-design, the spools in a conventional turbomachine will also settle at a rotational speed that matches the performance of linked components and spools up or down depending on operating point and power requirements. The modelling process for the N3-X turbo-electric system highlights that the same requirement will apply for systems that are connected through an electrical transmission system.

Initially, the performance of the propulsor array has been presented without considering the remainder of the propulsion system (i.e. the electrical system and turbomachinery). The performance of the main engines and the power link between the main engines may therefore be neglected and the propulsors in the array may run at a fixed rotational speed. This allows a map of the potential maximum net propulsive force of the propulsor array at full power (Figure 3.34a). The specific power consumption reduces as altitude and Mach number reduces, similar to the specific fuel consumption trend for conventional propulsion systems. The performance of the array as a whole must account for each propulsor in the array, where the total net propulsive force and power demand is the sum of all array components. At the aerodynamic design point, the lower efficiency of propulsors at the outer edges of the array reduces the overall efficiency of the array as a whole.

As was demonstrated with the individual propulsors, the thin boundary layer/high mass flow ratio at low speed and low altitude results in a potentially high net propulsive force. The potential maximum net propulsive force for the propulsor array at sea level static is 740 kN, or 530 kN at Mach 0.25, the rolling take-off speed. This suggests that the propulsor array would be fully capable of providing sufficient propulsive force for take-off. However, the power demand to run the propulsor array at maximum rotational speed at sea level static conditions would be approximately 83.0 MW. As has already been established in Section 3.5, the main engines as modelled are not capable of providing the full power requirements to run at propulsor array at SLS and the maximum rotational speed. The fans in the propulsor array must therefore be spooled down to a lower rotational speed.

After accounting for the power deficit at low altitudes, a map of the overall propulsion system performance may be created (Figure 3.35). The actual net propulsive force available at low altitudes and Mach numbers is significantly lower than that of the array at maximum rotational speed. However, a measure of additional propulsive force is produced by the main engines that slightly increases the propulsion system's total net propulsive force. As the overall propulsion system performance is being presented, the effective specific fuel consumption may be used as opposed to the specific power consumption. As with a conventional propulsion system, the specific fuel consumption reduces for low speed, low altitude flight.

Finally, the assumption that the fan motors cannot 'overspeed', i.e. will not operate above their maximum RPM, may be applied. This reduces the available thrust at higher altitudes where there is a power excess (Figure 3.36). The main engines may then be operated at a lower power setting to match the cap on the propulsor array performance and hence the slightly lower power demand Figure 3.36. Alternatively, the excess power at high altitudes may be used for



### 3. Propulsion System Modelling

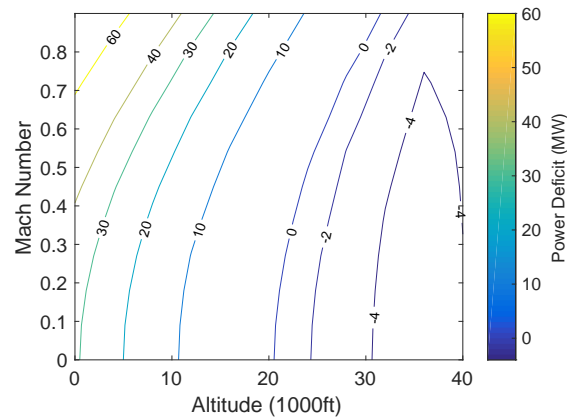


**Figure 3.33:** Power deficit in MW between propulsor array and main engines at ADP power setting as a function of altitude and Mach number

other aircraft subsystems or battery charging. The point where the array performance is capped by the maximum rotational speed limit is clearly visible as a kink in the specific fuel consumption trends with altitude and Mach number. Similarly, the point where array performance is capped by the maximum available power is visible where the net propulsive force trend begins to diverge away from the maximum net propulsive force predicted in Figure 3.34a. Note that the results present the regions that are mathematically possible, however, not all operating points may be physically possible.

### 3. Propulsion System Modelling

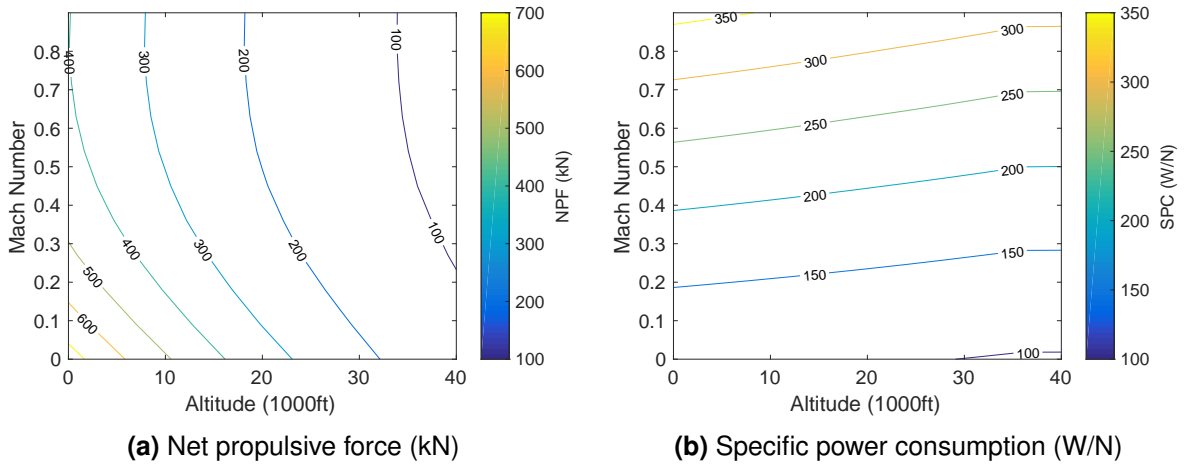


**Figure 3.34:** Propulsor array performance as a function of altitude and Mach number at 100% rotational speed

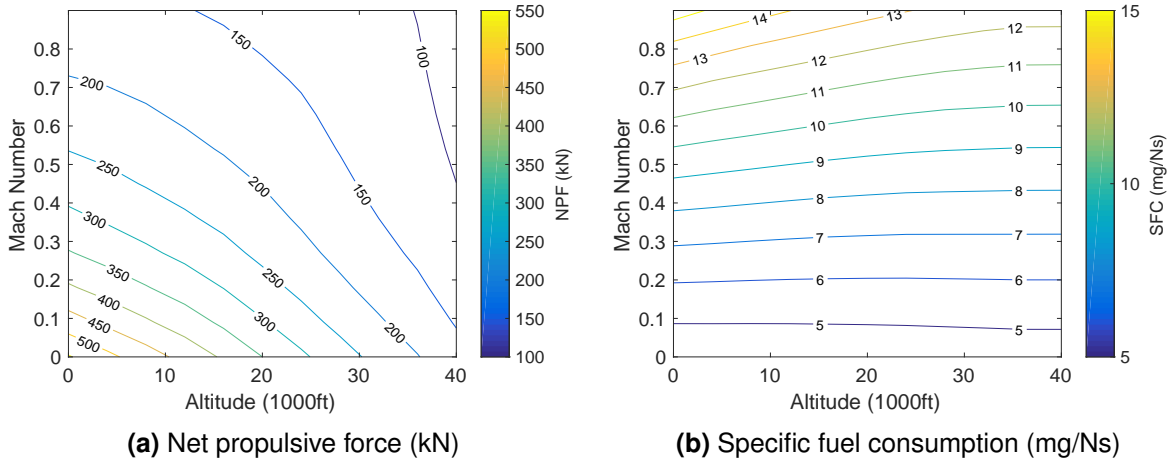


**Figure 3.35:** Propulsion system performance as a function of altitude and Mach number (ADP engine power setting: TET = 1811 K)

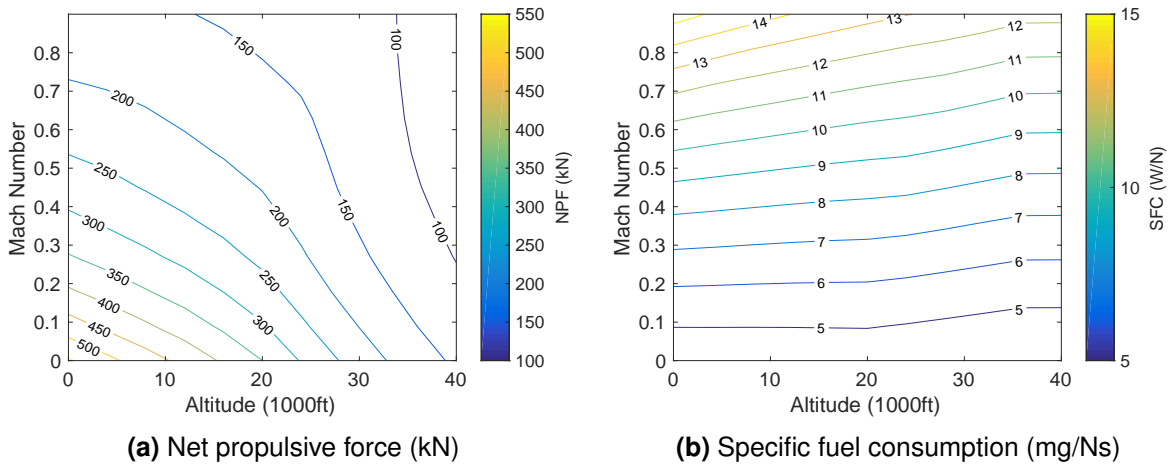


**Figure 3.36:** Propulsion system performance as a function of altitude and Mach number (Array capped at 100% design rotational speed, ADP engine power setting until propulsor array speed cap)

## 4. Aircraft Modelling

A key aspect of simulating the N3-X and similar novel configurations is the development of an aircraft performance model that is able to support the integration of the novel propulsion system model presented in the previous section. The propulsion system model was developed with the goal of being integrated within conventional point mass based aircraft performance simulation methods. Aircraft forces are therefore split into propulsive force and airframe drag. The propulsion system's performance is presented using an integrated net propulsive force perspective. Airframe drag can therefore be calculated completely independently from the propulsion system design. This is a key aspect in developing the aircraft performance model, as it simplifies the interactions between different modules. The key functions of the aircraft performance model were as follows:

- **Mission performance** – The core of the model is the mission performance tool. The model uses a point-mass approximation of an aircraft to predict performance during the flight. A mission is broken down into flight phases consisting of a number of segments. The main outputs required from the model are the block time, fuel burn, and CO<sub>2</sub> emissions. Further outputs are available for performance during the course of the flight, including rates of climb, lift to drag ratio, thrust, and drag. The model is able to simulate a mission with either a defined range, defined take-off weight, or for a given trajectory. In addition, the model is able to produce a payload-range chart.
- **Aircraft drag** – The aircraft drag module estimate the drag of conventional tube-and-wing or blended wing body airframes. The drag estimate makes use of an input file defining the aircraft dimensions to predict drag. The resultant drag value is provided to the core model for each segment of the flight.
- **Propulsion system performance** – A propulsion system performance module is integrated within the main aircraft mission performance model to simulate the propulsion system's performance at each segment of the flight. The module combines the in-house gas turbine simulation tool *Turbomatch* with a tool to simulate the performance of a BLI system. The BLI performance tool follows the model presented in Chapter 3.

This chapter describes the development of the aircraft performance model and details the core modules that combine to estimate mission performance. Aircraft performance models typically use engine decks to provide a lookup table for propulsion system performance. However, the aircraft performance model developed for this research directly integrates the propulsion system performance model to allow performance to be directly calculated at any point during the mission.

One of the goals of this research was to assess the potential of LH<sub>2</sub> as a fuel for the N3-X. As LH<sub>2</sub> is a pressurised cryogenic fuel, it requires dedicated tanks to maintain the requisite temperature and pressure. A model was therefore required to estimate the size and weight of

## 4. Aircraft Modelling

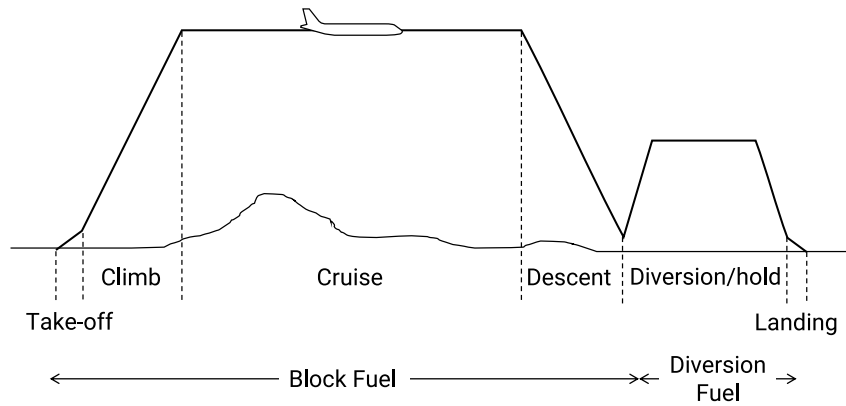


**Figure 4.1:** Mission segments in the aircraft performance model

the LH<sub>2</sub> tanks. Section 4.2 covers the development of a model to provide a preliminary sizing process for LH<sub>2</sub> tanks.

Following development of each of the modules for the aircraft performance models, the performance of the N3-X and the baseline aircraft could be predicted. Models were created for both aircraft using publicly available data (Section 4.4). Finally, the aircraft were simulated for a range of missions to identify the overall energy saving of the N3-X versus the baseline aircraft (Section 4.7). The N3-X aircraft model makes use of the baseline propulsion system defined in Section 3.5 for the kerosene and LH<sub>2</sub> aircraft variants.

### 4.1 Aircraft Performance Model Development

The two key components of the aircraft performance model are a module to estimate airframe drag during the course of the mission ( $D_{\text{aircraft, clean}}$ ) and modules to represent aircraft performance during each flight phase (Figure 4.1):

- Taxi
- Take-off
- Climb
- Cruise
- Descent
- Landing
- Diversion
- Hold

The important outputs for the aircraft model are the fuel consumption, CO<sub>2</sub> emissions, block fuel burn, and block flight time. These outputs may then be fed into the techno-economic phase of the analysis.

#### 4.1.1 Aircraft Drag

The drag of the airframe is assumed to consist of three components: Profile drag, lift induced drag, and transonic parasitic drag term. Aircraft planforms are approximated using basic shapes (Figure 4.2) to simplify drag prediction.

##### Profile Drag

Airframe profile drag,  $C_{D0}$ , is estimated using a drag build-up method which combines all the aircraft components to predict the total profile drag:

## 4. Aircraft Modelling

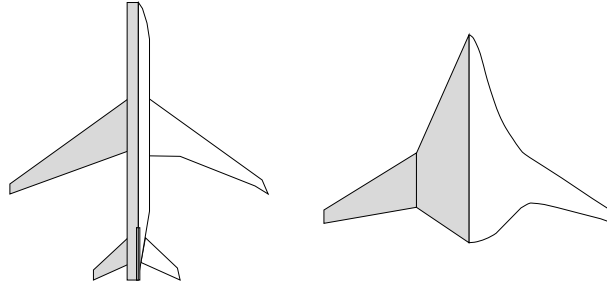


**Figure 4.2:** Simplified planforms for a tube and wing (left) and blended wing body airframe (right)

- |   |  |
|---|--|
| <ul style="list-style-type: none"> <li>• Wing</li> <li>• Fuselage</li> <li>• Horizontal &amp; vertical tail</li> <li>• Nacelle</li> </ul> | <ul style="list-style-type: none"> <li>• Undercarriage</li> <li>• High-lift systems</li> <li>• Secondary items (installation terms, surface finish, etc.)</li> </ul> |
|---|--|

The total airframe profile drag is obtained by the summation of individual component profile drags. Profile drag estimation for each component follows the empirical relationships detailed by Jenkinson *et al.* [115]. Profile drag for the main aircraft components uses the following general relationship:

$$C_{D0,i} = C_{f,i} F_i Q_i \left( \frac{S_{\text{wet},i}}{S_{\text{ref}}} \right) \quad (4.1)$$

- $C_{D0,i}$  = Profile drag of component  $i$
- $C_{f,i}$  = Skin friction coefficient of component  $i$
- $F_i$  = Form factor of component  $i$
- $Q_i$  = Interference factor of component  $i$
- $S_{\text{wet},i}$  = Component wetted surface area
- $S_{\text{ref}}$  = Reference area (wing aerodynamic area)

Form and interference factors depend on the component in question (Table 4.1). The wetted surface area is calculated based on the dimensions for each component. Reference area is assumed to be the aerodynamic wing area, equal to the wing planform area for a conventional tube and wing. Blended wing bodies are treated as flying wings. The aerodynamic wing area is therefore assumed to equal the fuselage and wing planform area, as the fuselage can also act as a lifting surface. For a blended wing body, fuselage wetted surface area and drag calculations make use of the same equations as the wing.

The skin friction coefficient,  $C_f$ , is dependent on the flow regime, where the flow over an aircraft will be predominantly turbulent. For turbulent flow, the skin friction coefficient has been predicted as follows:

$$C_{f,\text{turbulent}} = \frac{0.455}{(\log R_e)^{2.58} \left[ 1 + 0.144 M_{\text{flight}}^2 \right]^{0.65}} \quad (4.2)$$

- $R_e$  = Component Reynolds number
- $M_{\text{flight}}$  = Flight Mach number

The turbulent skin friction coefficient includes a Mach number correction factor which tends to one in low subsonic flight. The characteristic length for the Reynolds number depends on the component in question (e.g. fuselage length or wing mean chord). For wing drag calculations, it is assumed that flow is not turbulent over the full wing chord. The model therefore takes a user-specified value to define the percentage of the wing area that is subject to laminar flow.

## 4. Aircraft Modelling

**Table 4.1:** Interference and form factors for profile drag calculation [115]

	Interference Factor, $F_i$	Form Factor, $Q_i$
Wing	$(F^* - 1) \cos \Lambda_{0.5c} + 1$  $F^* = 1 + 3.3 \frac{t}{c} - 0.008 \left(\frac{t}{c}\right)^2 + 27.0 \left(\frac{t}{c}\right)^3$	1.0
Fuselage	$1 + 2.2 \left(\frac{l_f}{D_f}\right)^{-1.5} - 0.9 \left(\frac{l_f}{D_f}\right)^{-3.0}$	1.0
Tail Surfaces	$(F^* - 1) \cos \Lambda_{0.5c} + 1$  $F^* = 1 + 3.52 \frac{t}{c}$	1.2
Nacelle	1.25	1.0

The skin friction coefficient for the laminar section is defined as follows:

$$C_{f,\text{laminar}} = \frac{1.328}{R_e} \quad (4.3)$$

The skin friction coefficient for the wing as a whole is assumed to equal the area-weighted average of the skin friction coefficient:

$$C_{f,\text{wing}} = C_{f,\text{laminar}} \frac{S_{\text{wet,laminar}}}{S_{\text{wet}}} + C_{f,\text{turbulent}} \left(1 - \frac{S_{\text{wet,laminar}}}{S_{\text{wet}}}\right) \quad (4.4)$$

This skin friction coefficient is then used to estimate the wing profile drag. Raymer notes that a typical value for laminar flow is 10–20% of the wing and almost fully turbulent fuselage [116]. However, he also notes that the value can be as much as 50% of the wing and 20–35% of the fuselage for a modern composite aircraft. This research will assume 20% laminar flow over the wings, although current research is assessing the possibility of natural laminar flow wings [8]. As there is no data to predict the laminar-turbulent split for the N3-X fuselage, the turbulent skin friction coefficient was used for the entire fuselage as an initial assumption.

Undercarriage and high-lift systems drag terms are applied only during relevant flight phases (LTO, start of climb, end of descent). The remaining secondary items drag component is a function of the profile drag coefficients of the relevant components:

$$C_{D0,\text{secondary}} = 0.06C_{D0,\text{wing}} + 0.09C_{D0,\text{fuselage}} + 0.12C_{D0,\text{nacelle}} \quad (4.5)$$

The total profile drag is the sum of the profile drag for each of the components. A final increment of 3% is added to the total profile drag to cater for the systems drag.

### Lift induced Drag

Lift induced drag,  $C_{Di}$  is assumed to be produced by the wings alone (or the entire lifting body in the case of a blended wing body). Assuming that lift is equal to weight, the lift coefficient is calculated as follows:

$$C_L = \frac{L}{0.5\rho u^2 S_{\text{ref}}} = \frac{W}{0.5\rho u^2 S_{\text{ref}}} \quad (4.6)$$

## 4. Aircraft Modelling

Lift induced drag is correlated to the aircraft lift-coefficient,  $C_L$ , through the following relationship:

$$C_{Di} = kC_L^2 = \frac{C_L^2}{\pi AR e} \quad (4.7)$$

Where AR is the aspect ratio of the wing. The term  $e$  is the Oswald span efficiency and is a correction factor that accounts for the difference in lift distribution between an actual wing and an ideal wing with an elliptical lift distribution. There are many methods available for estimating  $e$  for a wing. A common method is to split the factor into viscous and inviscid components [117]:

$$e = \frac{1}{Q + P\pi AR} \quad (4.8)$$

The following relationships for  $Q$  and  $P$  by Kroo were selected as it provided the best match when validating the performance model [118]:

$$Q = \frac{1}{e_{\text{theoretical}} K_{e,f}} \quad (4.9)$$

Kroo defines the theoretical Oswald span efficiency factor,  $e_{\text{theoretical}}$  as 0.99. The value of  $e_{\text{theoretical}}$  may also be determined from an empirical function of the wing taper ratio,  $\lambda$  [117]:

$$e_{\text{theoretical}} = \frac{1}{1 + f(\lambda)AR} \quad (4.10)$$

$$f(\lambda) \approx 0.0524\lambda^4 - 0.1500\lambda^3 + 0.1659\lambda^2 - 0.0706\lambda + 0.0119 \quad (4.11)$$

The term  $K_{e,f}$  is a correction factor linked to the fuselage and aircraft dimensions:

$$K_{e,f} = 1 - 2 \left( \frac{D_f}{b} \right) \quad (4.12)$$

Where  $D_f$  is the fuselage diameter, and  $b$  is the wing span. For a blended wing body, this factor is equal to 1, as the airframe is treated as a flying wing with  $D_f$  equal to zero. The remaining viscous part is defined as a function of the profile drag coefficient:

$$P = 0.38C_{D0} \quad (4.13)$$

For blended wing bodies, an equivalent planform is used to reflect the flying wing assumption. The relevant aspect ratio for the induced drag calculation is therefore the aspect ratio of the equivalent planform (Figure 4.3):

$$AR_{\text{equiv}} = \frac{b_{\text{total}}}{S_{\text{aerodynamic}}} \quad (4.14)$$

Where  $b_{\text{total}}$  is the total aircraft span from wingtip to wingtip and  $S_{\text{aerodynamic}}$  is the aerodynamic wing area. The aerodynamic wing area may not equal the geometric wing area,  $S_{\text{total}}$ , as the fuselage may not be as effective a lifting body as the wings. The taper ratio for the equivalent planform is calculated as follows:

$$\lambda_{\text{equiv}} = \frac{c_{\text{tip}}}{2 \left( \frac{S_{\text{total}}}{b_{\text{total}}} \right) - c_{\text{tip}}} \quad (4.15)$$

Where  $c_{\text{tip}}$  is the wing tip chord.

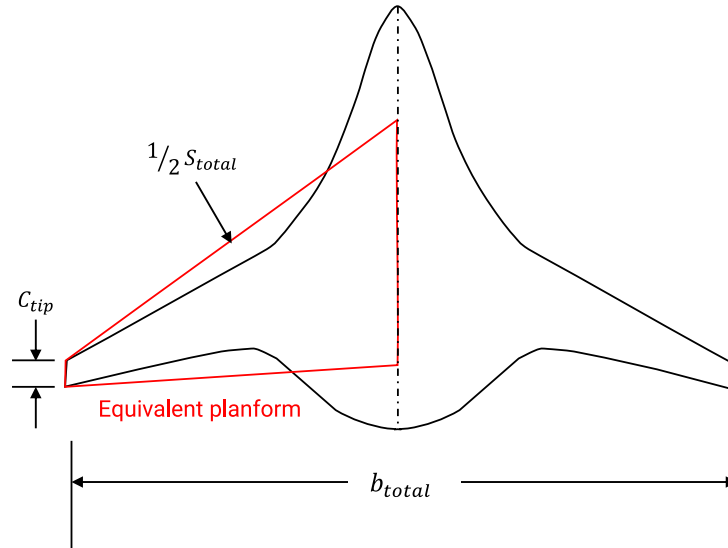


**Figure 4.3:** Aerodynamic equivalent planform for a blended wing body

### Transonic Parasitic Drag

Transonic wave drag components are introduced when the flight Mach number exceeds the aircraft critical Mach number (the Mach number for which shocks occur and begin to influence drag). There are a number of methods available for estimating transonic wave drag. This research uses the graphical approximation technique for the estimation of transonic parasitic drag by Raymer [116]. Five points are used to create an estimation of the wave drag coefficient as a function of Mach number (Figure 4.4). Drag for Point A (Mach 1.2) is determined using an empirical wave drag function applicable only for speeds of Mach 1.2 or greater:

$$\left(\frac{D}{q}\right)_w = E_{WD} \left[ 1 - 0.386 (M_{\text{flight}} - 1.2)^{0.57} \left( 1 - \frac{\pi \Lambda_{LE}^{0.77}}{100} \right) \right] \left(\frac{D}{q}\right)_{\text{Sears-Haack}} \quad (4.16)$$

$$C_{Dw} = \frac{1}{S_{ref}} \left(\frac{D}{q}\right)_w \quad (4.17)$$

Where  $\Lambda_{LE}$  is the leading edge sweep in degrees and  $E_{WD}$  is a correction factor to account for aircraft that do not have a Sears-Haack perfect volume distribution. For a commercial transport aircraft, Raymer suggests a value of 4.0. Wave drag for a Sears-Haack body is estimated as follows:

$$\left(\frac{D}{q}\right)_{\text{Sears-Haack}} = \frac{9\pi}{2} \left(\frac{A_{\text{max}}}{l}\right)^2 \quad (4.18)$$

Where  $A_{\text{max}}$  is the maximum aircraft cross-sectional area and  $l$  is the aircraft length excluding portions of constant cross-sectional area.

Wave drag for Point B at Mach 1.05 is assumed to be equal to that at Mach 1.2. Wave drag at Point C, Mach 1.0, is approximately half the wave drag at Mach 1.05. The drag divergence Mach number,  $M_{DD}$ , defines the point where shocks begin to significantly influence drag and is defined by Boeing as the point where the wave drag component is equal to 0.002. This point may be estimated according the following function:

$$M_{DD} = M_{DD0} LF_{DD} - 0.05 C_{l,\text{design}} \quad (4.19)$$

Both  $M_{DD0}$  and  $LF_{DD}$  are interpolated from graphical functions of the wing quarter chord



## 4. Aircraft Modelling

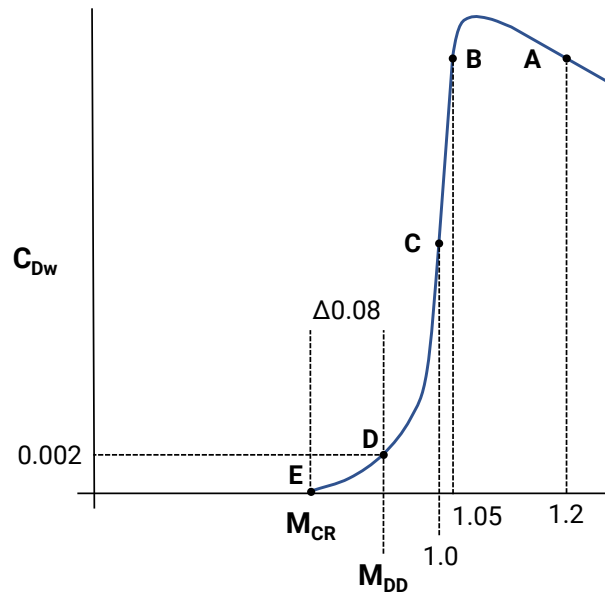


**Figure 4.4:** Simplified approximation for the wave drag coefficient [116]

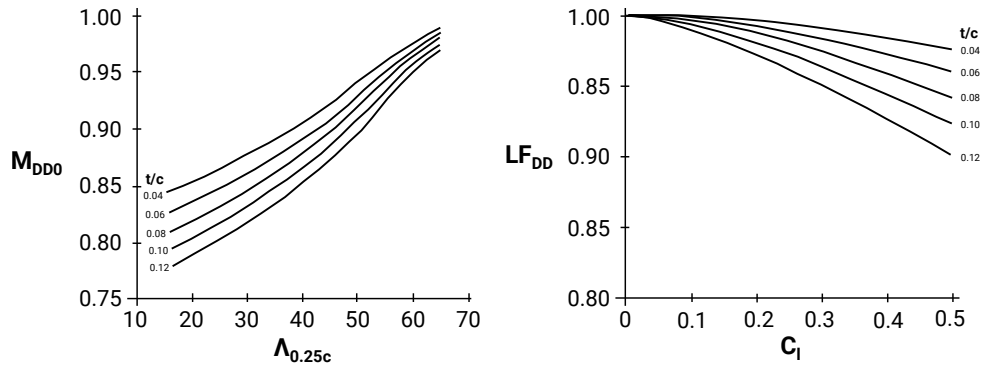


**Figure 4.5:** Correlations for  $M_{DD0}$  and  $LF_{DD}$

sweep, thickness-to-chord ratio, and flight lift coefficient provided by Raymer (Figure 4.5). Assuming supercritical aerofoil design, the thickness-to-chord ratio must be multiplied by 0.06 before being used to estimate  $M_{DD}$ . In the absence of an approximation of the design lift coefficient  $C_{l,design}$ , the design lift coefficient is assumed to equal the lift coefficient at cruise. The difference between  $M_{DD}$  and  $M_{CR}$  is approximately 0.08. The relationship between the Mach number and wave drag component is created by creating a smooth curve interpolation between points E, D, and C and a linear increase between points C and B. Subsequently, the transonic parasitic drag for Mach numbers above the critical Mach number can be estimated by interpolating between the points.

### Winglet Drag Correction Factor

Winglets are typically implemented on aircraft as a way of reducing the airframe induced drag. As a result of the lift produced by the aircraft, trailing vortices are shed behind the aircraft. A major source of induced drag results from the vortices shed by the wingtips. Wingtip devices increase the effective span and aspect ratio of the wing. They increase the lift produced at the wingtips and are therefore a method of controlling these vortices. However, they also increase the profile drag and will increase aircraft weight. As a result of the reduction in wingtip vortices, wingtip devices can reduce the induced drag of the aircraft and hence may can lead to a

reduction in fuel consumption [119].

Niță and Scholz present a method for obtaining an estimate of the induced drag of an aircraft with wingtip devices [117]. However, performance results with the method did not correspond to a validation against a sample aircraft equipped with wingtip devices. Therefore, the influence of wingtip devices is instead accounted for as a correction factor to the aircraft drag. Sample drag reduction values for aircraft equipped with winglets range from 3.5–4.5% less than the airframe drag without winglets [120].

### Total Drag

The overall drag coefficient for the airframe is the summation of the three components of profile, induced, and parasitic drag:

$$C_D = C_{D0} + C_{Di} + C_{Dw} \quad (4.20)$$

Finally, the aircraft drag and hence the lift to drag ratio can be calculated:

$$D = C_D 0.5 \rho u^2 S_{\text{ref}} \quad (4.21)$$

### 4.1.2 Propulsion System Thrust

Point-mass based aircraft performance models require an accounting system that splits the airframe drag from the propulsion system thrust. This is a reasonably simple task for the typical tube-and-wing aircraft configuration, where engines are mounted on pylons away from the airframe. However, Section 3.1.2 identified that differentiating the airframe and engine is more difficult for integrated architectures. An appropriate thrust-drag split is nevertheless necessary to simulate the mission performance of an aircraft.

A cores aspect of the research was the development of a modelling tool for a BLI propulsion system, presented in Chapter 3. An aspect of the model was the development of a method that could support the thrust-drag split required for a point-mass aircraft performance model. Chapter 3 identified that the usual definition of net thrust cannot be used for a BLI propulsion system, as it is integrated in the airframe. This necessitates the definition of a new control volume with a net propulsive force formulation, rather than net thrust as is typically used (Section 3.1.2):

$$\text{NPF} = F_{G9} - F_{Gi} - \tau_{w,i} S_{\text{wet},i} - D_{\text{nacelle}} + \Delta D \quad (4.22)$$

This presents a control volume that splits the airframe and propulsion system at an interface point,  $i$ . This interface point is defined as the point where the propulsion system suction no longer influences airflow over airframe. Chapter 3 also identified two alternative control volumes for a BLI propulsion system, defined here as an internal (propulsion system only) and external (propulsion system and airframe surface up to the leading edge) control volume. In an internal control volume, the airframe drag ahead of the intake is influenced by the suction of the propulsion system. Airframe drag estimates therefore rely on the propulsion system operating point. In an external control volume, the control volume starts at the leading edge of the airframe, starting in free-stream flow and covering the entire region ahead of the intake. However, this control volume includes all the skin friction drag ahead of the propulsion system intake. Propulsion system performance calculations therefore include airframe drag, which must be removed from the clean airframe drag estimate. The definition of station  $i$  resolves these difficulties and supports an easier split between the propulsion system and airframe forces than is possible from internal or external control volumes.

The above net propulsive force formula contains two sub-components: a term analogous to net thrust (the difference between  $F_{G9}$  and  $F_{Gi}$ ) and installed propulsion system terms. The

## 4. Aircraft Modelling

installed terms cover the skin friction drag from the start of the control volume to the highlight and the nacelle drag. In addition, it includes a  $\Delta D$  term that accounts for the fact that the propulsion system control volume covers some of the wetted surface area of the airframe. This term is assigned to the propulsion system force accounting as it would otherwise need to be removed from the airframe drag estimate. In this way, the aircraft drag can be calculated as the clean airframe drag,  $D_{\text{aircraft, clean}}$ , (drag without the propulsion system) without needing to refer to the propulsion system configuration.

The definition of this force control volume supports the typical thrust-drag split used in aircraft performance models. Airframe drag may be calculated independently from the propulsion system using the previously detailed method for profile drag, lift induced drag, and transonic parasitic drag. The ‘thrust’ term for a BLI propulsion system is calculated using the above net propulsive force equation. This then produces the thrust and drag terms needed in a point-mass aircraft performance model.

For the N3-X, two performance ‘modes’ were created to estimate the net propulsive produced by the combined propulsion system. These are the thrust-matching and power-matching modes. The process for calculating performance in each of these modes is presented in Section 3.2. Performance of conventional propulsion systems was produced using *Turbomatch* (Section 3.2.2).

### 4.1.3 Mission Performance

The aircraft mission is split into a number of segments: taxi, take-off, climb, cruise, descent, and landing in addition to diversion and hold time (Figure 4.1). Block fuel burn and time for the mission is equal to the total fuel burn and time spent in the main flight segments. A diversion segment is also included in the mission performance calculation to provide an estimate of the diversion reserve fuel required on board the aircraft.

Flight performance calculations follow the methods described by Raymer [116] and Jenkinson *et al.* [115]. Drag calculations at each flight phase are performed using a drag module which makes use of the calculations described in the previous section. Engine performance is calculated using a propulsion system performance module where performance is calculated for each point in the mission. Relationships for atmospheric properties as a function of altitude may be found in Appendix D. The following section will briefly summarise the main relationships used for simulating the performance of the aircraft. A fully detailed method can be found in Raymer and Jenkinson *et al.* [115, 116].

There are a number of different definitions for the speed of an aircraft:

- **Calibrated air speed**,  $V_{\text{CAS}}$ , the airspeed indicated by the aircraft instruments corrected for instrument and position errors
- **True air speed**,  $V_{\text{TAS}}$ , calibrated air speed corrected for altitude
- **Mach number**,  $M$

The following functions are applied to convert between each representation of speed:

$$V_{\text{TAS}} = \left[ \frac{2P\gamma}{\rho(\gamma-1)} \left[ \left[ 1 + \frac{P}{P_0} \left[ \left( 1 + \frac{(\gamma-1)\rho_0 V_{\text{CAS}}^2}{2P_0} \right)^{\frac{\gamma}{\gamma-1}} - 1 \right] \right]^{\frac{\gamma-1}{\gamma}} - 1 \right] - 1 \right]^{0.5} \quad (4.23)$$

$$M = aV_{\text{TAS}} \quad (4.24)$$

## 4. Aircraft Modelling

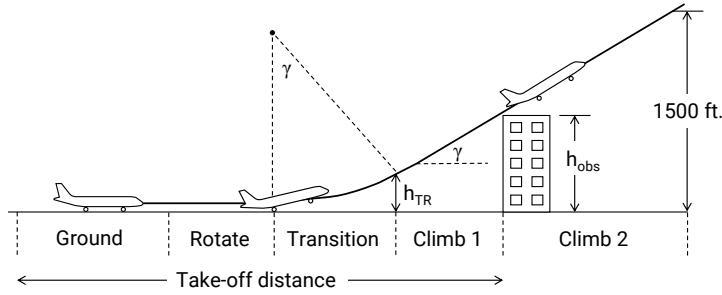


**Figure 4.6:** Take-off segments

### Take-off

Take-off is split into a number of segments (Figure 4.6). For each segment, the distance covered,  $d$ , and the time taken,  $t$ , are calculated. Engine performance is calculated for each of the segments. Fuel consumption during each segment is approximated as the multiple of fuel mass flow rate of the segment by the segment time. Segment time is assumed to be the distance covered divided by the average velocity over the segment.

**Ground Acceleration** The aircraft accelerates from rest to 1.15 times the aircraft stall velocity,  $V_{TO}$ . Aircraft stall velocity is calculated based on the maximum aircraft lift coefficient,  $C_{l,max}$ :

$$V_{stall} = \sqrt{\frac{W}{0.5\rho S_{ref} C_{l,max}}} \quad (4.25)$$

Engine performance is the averaged performance for the ground roll segment, which occurs at 70% of the segment velocity increase. Relevant equations for ground roll are as follows:

$$d_{ground} = \frac{1}{2gK_A} \ln \left[ \frac{K_T + K_T v_{ground,2}^2}{K_T + K_A v_{ground,1}^2} \right] \quad (4.26)$$

$$K_T = \frac{T}{W} - \mu \quad (4.27)$$

$$K_A = \frac{\rho}{2(W/S)} (\mu C_L - C_{D0} - K C_L^2) \quad (4.28)$$

Where  $T/W$  is the thrust to weight ratio,  $\mu$  is the rolling friction coefficient for the runway terrain, and  $v_{ground,1}$  and  $v_{ground,2}$  are the velocities at the start and end of ground roll, respectively. Velocity at the end of ground roll is assumed to be 1.15 times the stall velocity.

**Rotation** The aircraft rotates to the take-off angle of incidence. Rotation time depends on the pilot and aircraft, however, a 3 second rotation time assumption is applied for commercial aircraft. It is assumed that velocity is roughly constant during this segment.

**Transition and Climb 1** The aircraft accelerates from the take-off velocity,  $V_{TO}$ , to the initial climb velocity,  $V_{CL1}$ , with an average transition velocity of  $V_{TR}$ . The distance covered during the segment is described by an arc of length  $R$  from horizontal to the climb angle. During this segment, the lift coefficient is equal to  $0.9C_{l,max}$ . The transition segment is combined with the following obstacle climb segment (Climb 1). In the Climb 1 segment, the aircraft climbs up from transition to the obstacle height,  $h_{obs}$ . The distance covered during the transition phase

#### 4. Aircraft Modelling

depends on whether the aircraft transition climb exceeds the obstacle height, which is 35 ft. for commercial aircraft. If the obstacle height is exceeded during transition, the distance covered during this segment is zero. Relevant equations for transition and Climb 1 are as follows:

$$n = \frac{L}{W} = \frac{0.5\rho S (0.9C_{Lmax}) (1.15V_{stall})^2}{0.5\rho S C_{Lmax} V_{stall}^2} \approx 1.2 \quad (4.29)$$

$$R = \frac{V_{TR}^2}{g(n-1)} \quad (4.30)$$

The climb angle at the end of transition and the start of Climb 1 depends on the engine power:

$$\sin\gamma = \frac{T-D}{W} \quad (4.31)$$

Subsequently, the height covered during transition can be obtained. This must be checked against the obstacle height of 35ft.

$$h_{TR} = R(1 - \cos\gamma) \quad (4.32)$$

If the obstacle height is cleared during transition, the horizontal distance covered during transition is calculated as follows:

$$d_{TR} = \sqrt{R^2 - (R - h_{TR})^2} \quad (4.33)$$

The obstacle height must be cleared during Climb1 if it is not cleared during transition. The horizontal distance covered during these phases is as follows:

$$d_{TR} = R\sin\gamma \quad (4.34)$$

$$d_{climb1} = \frac{h_{obs} - h_{TR}}{\tan\gamma} \quad (4.35)$$

**Climb 2** The second initial climb segment includes climb up to 1,500 ft. above the airport altitude. The segment is split into two subsections, an acceleration up to the second climb velocity,  $V_{2+10}$ , followed by a climb at constant velocity. The velocity during the second climb segment,  $V_{2+10}$ , is assumed to equal the velocity at the end of transition,  $V_{CL1}$ , plus 10 kts.

The distance covered during the acceleration phase of Climb 2 is described by the hypotenuse of a triangle:

$$a_{initial} = \frac{T-D}{W} \quad (4.36)$$

$$R_{arc} = \frac{V_{2+10}^2 - V_2^2}{2a_{initial}} \quad (4.37)$$

Where the angle of this climb segment is obtained from performance values at the end of transition:

$$\tan\theta = \left[ h_{TR} \frac{R(T-D)}{W} \right] \quad (4.38)$$

This hypotenuse distance  $R_{arc}$  and climb angle  $\theta$  can be used to extract the horizontal and vertical distances,  $d_{init}$  and  $h_{init}$  covered during the initial acceleration. The remainder of the Climb 2 segment is conducted at a constant velocity and covers the vertical distance from the end of the acceleration to 1,500 ft above the airport altitude. The vertical distance that must be covered during this segment,  $h_{climb2}$ , depends on the altitude of the airport and the vertical

## 4. Aircraft Modelling

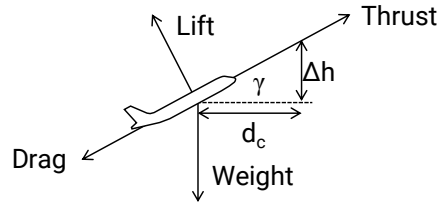


**Figure 4.7:** Forces on an aircraft during steady climb and descent

distance covered during the previous segments. The distance covered during this segment is as follows:

$$d_{1500ft} = \frac{h_{climb2}}{\tan\theta} \quad (4.39)$$

The total distance covered during Climb 2 is the sum of  $d_{init}$  and  $d_{1500ft}$ .

**Overall Take-off Performance** Take-off segment time and fuel burn is the sum of results for each of the take-off segments. The take-off field length includes the horizontal distance covered during the initial roll, rotation, transition, and obstacle climb segments. The balanced take-off field length includes a 15% increase to account for variations in operation as required by JAR/FAR certification rules.

### Climb / Descent

Aircraft performance during steady climbing and descending flight is described by the forces during flight and the angle of climb,  $\gamma$  (Figure 4.7). Climb occurs where the engine thrust,  $F_N$ , exceeds the aircraft drag,  $D$ , which results in a positive rate of climb (RoC).

$$\sin(\gamma) = \frac{F_N - D}{W} \quad (4.40)$$

$$\text{RoC} = \frac{dh}{dt} = \frac{1}{F_a} \frac{F_N - D}{W} V_{TAS} \quad (4.41)$$

The climb segment is split into a number of sub-segments from the end of the take-off segment up to the cruise altitude. The velocity during climb is defined by a speed schedule which defines the aircraft calibrated airspeed up to a maximum Mach number. The aircraft transitions from a constant calibrated airspeed defined velocity to a constant Mach number defined velocity at the transition altitude,  $h_{trans}$ . A factor,  $F_a$ , is applied to the rate of climb to account for the acceleration of the aircraft along the flight path that results from a constant speed definition with changing altitude (ESDU 81046 [121]). The relevant calculation for the acceleration factor depends on whether the climb profile specifies fixed  $V_{CAS}$ ,  $V_{TAS}$ , or fixed Mach number climb as well as the altitude. Engine performance during climb is calculated at the start of each sub-segment, where the engine power setting is defined by the climb schedule. Splitting climb into more sub-segments will increase fidelity, however it will also increase computational time.

### Cruise

Cruise is assumed to be at constant altitude and Mach number. During this phase the engine thrust is equal to the aircraft drag. Engine power setting in the performance calculations is therefore matched to the value that provides the requisite thrust per engine. The relevant output for engine performance is the specific fuel consumption,  $C$ . The Breguet range equation is applied by splitting cruise into a number of smaller subsections of length  $R$ . The aircraft fuel

## 4. Aircraft Modelling

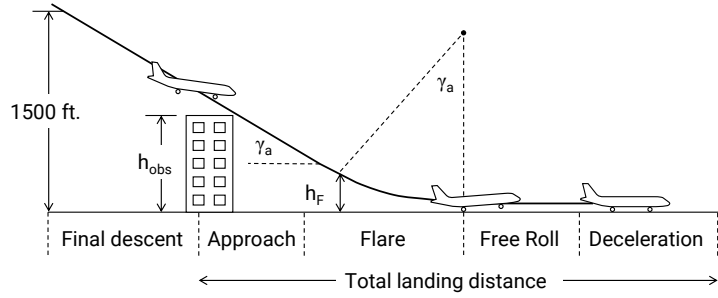


**Figure 4.8:** Landing segments

consumption during each cruise segment may be estimated by using the weight fraction:

$$\frac{W_{\text{initial}}}{W_{\text{final}}} = e^{-\left(\frac{RgC}{V_{\text{TAS}} L/D}\right)} \quad (4.42)$$

$$W_{\text{fuel}} = W_{\text{initial}} \left(1 - \frac{W_{\text{initial}}}{W_{\text{final}}}\right) \quad (4.43)$$

### Landing

Landing follows a similar procedure to the take-off phase and is split into similar segments (Figure 4.8).

**Final Descent** The aircraft descends from the end of the descent segment to the obstacle height,  $h_{\text{obs}}$ . The obstacle height for the landing phase is 50 ft. (as opposed to 35 ft. in climb). The final descent velocity  $V_D$  is defined as 1.3 times the aircraft stall speed. Final descent performance calculations otherwise follow the previously described climb and descent calculations.

**Approach** The aircraft descends from the obstacle height to the flare height,  $h_F$ . The approach angle,  $\gamma_a$ , for a commercial aircraft is defined as being no steeper than 3 degrees. Estimating performance during approach first requires a definition of the flare height. Calculation of flare height follows similar calculations to take-off:

$$h_F = R(1 - \cos\gamma_a) \quad (4.44)$$

Where  $R$  can be calculated using the relationship defined for take-off Climb 1 using the average velocity during approach,  $V_F$ . The aircraft is assumed to touchdown at 1.15 times the stall speed of the aircraft,  $V_{\text{touchdown}}$ . Approach starts at the final descent velocity.

$$V_F = 0.5(V_{\text{touchdown}} + V_D) \quad (4.45)$$

Horizontal distance covered during this segment depends on the vertical distance covered,  $h_{\text{approach}}$ :

$$d_{\text{approach}} = \frac{h_{\text{approach}}}{\tan\gamma_a} \quad (4.46)$$

**Flare** The aircraft flare begins at the flare height,  $h_F$ , and ends at aircraft touchdown. Flare height and velocity,  $v_F$ , are calculated as a part of the previous segment. The distance covered

## 4. Aircraft Modelling

during flare is obtained from the following relationship:

$$d_F = R \sin \gamma_a \quad (4.47)$$

**Free roll** The aircraft rolls for a short time before the pilot applies the brakes. This is assumed to last for 3 seconds. Free roll is assumed to be at a constant speed equal to the touchdown speed. The distance covered during this segment can be obtained following this assumption.

**Ground deceleration** Braking is split into two subsections. In the first, the aircraft applies thrust reversers, which provide a reverse force of approximately 50% of the maximum forward thrust, until the aircraft reaches the thrust reversal cut-off speed (50 knots). In the second subsection, thrust is equal to the idle thrust and the aircraft decelerates from the cut-off speed to rest. Rolling resistance during landing is increased through applying the aircraft brakes. The distance covered the two phases during ground deceleration is obtained from the same relationships as those described for take-off ground roll. Values of  $K_T$  and  $K_A$  appropriate for both phases of ground deceleration should be calculated. As with take-off ground roll, thrust should be calculated as the average at 70% of the speed change for each deceleration phase. A typical rolling friction coefficient,  $\mu$ , for an aircraft with brakes on is 0.7. The total distance covered during ground deceleration is the sum of the distance covered during the thrust reverser active and inactive phases.

**Overall Landing Performance** Landing segment time and fuel burn is the sum of results for each of the Landing segments. The Landing field length includes the horizontal distance covered during flare, ground roll, and ground deceleration. The landing distance also includes a 2/3 increase to allow for pilot technique, as defined by the FAA.

### Diversion and Hold

The diversion is approximated as a single climb segment from the airport altitude followed by cruise at the diversion cruise altitude, and finally a single descent segment to the diversion airport. A hold time over the airport at a fixed altitude and Mach number can also be included.

### Fuel Onboard

Block fuel burn is equal to the sum of the fuel burn for each segment in the flight. The diversion and hold time fuel mass is included in the aircraft reserve fuel mass. An additional reserve mass is included as a percentage of the usable fuel on the aircraft. This percentage is assumed to be 5% of the fuel onboard the aircraft. The total fuel onboard is therefore calculated as follows:

$$M_{f,\text{onboard}} = M_{f,\text{block}} (1 + \%_{\text{reserve}}) + M_{f,\text{diversion}} + M_{f,\text{hold}} \quad (4.48)$$

## 4.2 Liquid Hydrogen Implementation

The baseline design of the N3-X specifies conventional kerosene as a fuel source. However, alternative fuels are being considered as an aspect of further research into green aviation technologies. Liquid hydrogen (LH<sub>2</sub>) is an alternative to hydrocarbon fuel sources that could lead to a zero carbon industry (neglecting possible CO<sub>2</sub> emissions from production of the fuel). A small amount of liquid hydrogen is already expected to be carried on board the aircraft to act as a cryocoolant for the superconducting electrical system. This cryocoolant could therefore also theoretically be used to fuel the aircraft propulsion system. LH<sub>2</sub> is a cryogenic, pressurised



## 4. Aircraft Modelling

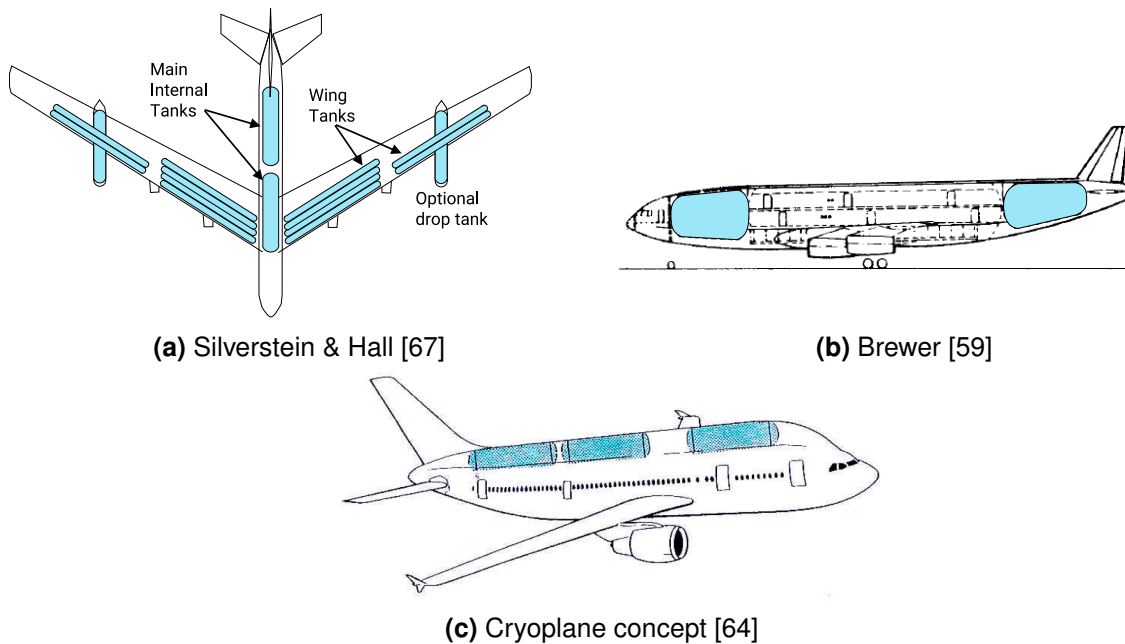


**Figure 4.9:** LH<sub>2</sub> tube-and-wing aircraft concepts from previous research (fuel tanks in blue)

fluid, therefore it must be stored in special pressurised and insulated tanks. A sizing process is therefore necessary in order to both estimate the tank weight and predict the volume of fuel the aircraft is able to carry, given volume constraints within the airframe.

There are a number of areas where an aircraft such as the N3-X may be a good platform to implement LH<sub>2</sub> fuel. The blended wing body fuselage can potentially accommodate cylindrical fuel tanks more easily than tube-and-wing planforms. Whilst tube and wing concepts have been developed for use with LH<sub>2</sub> as fuel, the design of the aircraft is typically heavily influenced by the need to fit cylindrical pressure vessels (Figure 4.9). This will either lead to a loss in usable passenger/cargo volume, or a change in the fuselage configuration which may increase weight and drag and negate the benefits of a lighter fuel. A blended wing body can potentially have a higher volume for the same size aircraft, which could support the use of more fuel tanks without changing the aircraft configuration.

As the efficiency of an aircraft increases, its energy requirements will likewise reduce. The volume of fuel it is required to carry on board is therefore similarly reduced. As a result, a high efficiency aircraft like the N3-X would be required to use less internal volume for tanks than an older, less efficient aircraft. Low volumetric density fuels such as LH<sub>2</sub> may therefore become more feasible as aircraft efficiency increases and the required fuel volume for a defined mission range decreases.

Lower fuel weight may also be beneficial from a structural perspective, as it will reduce the necessary maximum take-off weight of the aircraft, which may lead to a reduction in operating empty weight. The propulsion system for a lighter aircraft may also be a smaller size, as the drag has the potential to be lower, assuming the airframe wetted surface area does not increase dramatically. Alternatively, assuming the maximum take-off weight for an LH<sub>2</sub> aircraft was kept in a similar region to that of a conventional kerosene aircraft, a LH<sub>2</sub> aircraft could accommodate a heavier payload.

### 4.2.1 Liquid Hydrogen Tank Requirements

The requirements for a LH<sub>2</sub> tank differ from those of the conventional kerosene tanks used on commercial aircraft as the fuel must be pressurised and maintained at a low temperature.

## 4. Aircraft Modelling

---

Colozza identifies a number of constraints for the aircraft fuel storage system [66]:

- Maintain constant tank pressure of approximately 1.45 bar
- Insulation suitable for maintaining storage temperature of approximately 20 K for an appropriate length of time to avoid fuel boil-off
- Tank material that is resistant to both embrittlement and fuel permeation
- Airtight tank and fuel lines to minimise boil-off and avoid blockage by frozen air
- Time limitations on storage due to fuel boil-off

The low boiling temperature of hydrogen establishes fuel boil-off as a key design factor in the application of liquid hydrogen fuel. A high boil-off rate will lead to a significant loss in fuel over the course of a flight. Limiting the fuel boil-off therefore supports a higher range and endurance. Alternatively, excess fuel and hence excess volume may be required in order to compensate for any fuel lost to boil-off. As the insulation thickness required to entirely eliminate boil-off can be prohibitive, some boil-off is inevitable. Colozza suggests an excess tank volume of approximately 7.2% is required, in order to maintain a constant tank pressure and provide volume for the boil-off gas [66].

Tank pressure may be maintained by appropriately sizing the tank walls based on the storage requirements and using an appropriate safety factor. Lightweight composites are ideal for maintaining pressure whilst reducing tank weight compared to a metallic tank. However, such materials are more prone to permeation problems and would require a metallic liner. Including a metallic liner introduces additional problems, as the difference in the coefficient of thermal expansion of the tank and liner may result in liner fracture or separation. Aluminium liners have been shown to perform well when applied to cryogenic storage, however, alternative polymer and elastomer options have been considered as options that avoid an excessive coefficient of thermal expansion difference [122]. Whilst metallic tanks avoid the necessity of a tank liner, the higher weight in comparison to composite materials may be detrimental to performance. All-composite 'Type IV' tanks with a composite liner and linerless 'Type V' composite tanks are under development. An all-composite tank would reduce weight in comparison to a tank with a metallic structure, however, a suitable liner or tank material that resists fuel permeation over the tank lifetime is required [123].

In addition to fuel permeation, hydrogen embrittlement can result in failure well below a material's ultimate strength. Certain materials are more susceptible to embrittlement than others, which limits the potential materials available for use in the tank wall. Most metals will be influenced by hydrogen embrittlement to a certain extent, however, materials that are especially likely to incur damage include high strength steels and nickel alloys [124]. Appropriate materials must therefore be selected that avoid embrittlement due to hydrogen.

The insulation component of the tank balances the heat transfer into and out of the tank given the temperature difference between the inside and outside of the tank. This temperature difference is in the region of 200K for a liquid hydrogen tank, assuming the external temperature is equal to the air temperature at cruise. The required thickness of insulation is dependent on the insulating properties of the material selected and the allowable boil-off established for the tank [66]. Increasing the liner thickness will reduce the tank boil-off rate, with a corresponding increase in weight.

In addition to the selection of appropriate tank materials, a suitable tank configuration must be selected. Single walled tanks are an option with a low manufacturing complexity. However, single walled configurations limit the insulation options. A double walled construction is higher complexity, but also enables more forms of insulation, such as vacuum insulation. By making

## 4. Aircraft Modelling

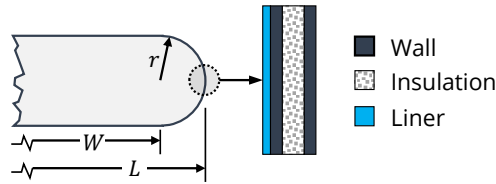


**Figure 4.10:** Liquid hydrogen tank structure

use of a double walled tank, the insulating material may be placed in a location that is protected from both external impacts and exposure to the cryogenic fuel [122]. Vacuum insulated tanks minimise heat conductivity, however, failure of the insulation results in a rapid loss of fuel through boil-off [125]. Whilst alternative insulation methods, such as foam, may be less efficient, they are more easily and safely implemented for aerospace applications. However, alternative materials such as aerogel may also become more common for insulation purposes [122].

### 4.2.2 Tank Configuration

The ideal configuration for a pressurised vessel is a spherical tank, as this avoids any stress concentration points that can result in the failure of the wall. However, spherical tanks are not ideal when attempting to minimise wasted volume, as there is significant volume wasted in between tanks. A better use of space for an aircraft is obtained by utilising cylindrical tanks with hemispherical end caps. The cylindrical tank configuration reduces wasted space, whilst still limiting stress concentration. The tank configuration considered herein consists of a cylindrical tank with four distinct layers. The innermost layer is a tank liner (assuming a tank wall constructed from composite materials), followed by an inner tank wall, the insulation material, and finally, the external tank wall (Figure 4.10) [126]. Tank sizing is based on the method used by Colozza [66] and the tank sizing work flow developed during research by Mari [127] (see also Appendix A). Each tank wall component is treated individually in order to assess the required skin thickness. The tank wall thickness is calculated with the assumption that it may be treated as a single skin, rather than two separate layers.

### 4.2.3 Mechanical Sizing

The tank wall must be sized to resist the pressure load of the stored hydrogen, assuming that the liner and insulation do not provide any structural strength. Tank volume is determined including the excess volume required for boil-off, necessitating a slightly larger, heavier tank than would otherwise be used. For a given mass of LH<sub>2</sub> the volume of the tank,  $V_t$ , is therefore as follows:

$$V_t = \frac{M_{\text{LH}_2}}{\rho_{\text{LH}_2}}(1 + V_e) \quad (4.49)$$

Where  $V_e$  represents the percentage of excess volume required for the tank. For a cylindrical tank with hemispherical end-caps the tank volume is a function of the length of the cylinder section,  $W$ , and radius,  $r$ , of the tank:

$$V_t = \frac{4\pi r^3}{3} + \pi r^2 W \quad (4.50)$$

## 4. Aircraft Modelling

For a cylindrical pressure vessel with hemispherical end caps, the wall thickness may be determined for a known internal pressure,  $P_{LH2}$ :

$$t_{\text{wall}} = \frac{r P_{LH2}}{2\sigma_y} F_oS \quad (4.51)$$

The exact thickness depends on the yield strength of the wall material,  $\sigma_y$ , and the design factor of safety, FoS, assumed to be 1.5 for this research. Finally, the weight of the tank depends on the tank configuration and material:

$$M_{\text{wall}} = \rho_{\text{wall}} \left[ \frac{4\pi(r + t_{\text{wall}})^3}{3} + \pi(r + t_{\text{wall}})^2 W - V_t \right] \quad (4.52)$$

### 4.2.4 Thermal Sizing

The thermal sizing process balances the heat entering tank insulation from the external surroundings via convection,  $Q_{\text{conv}}$ , and radiation,  $Q_{\text{rad}}$ , against the heat conducted into the tank,  $Q_{\text{cond}}$  (Equation 4.53 and Equation 4.54). It is assumed that the tank is in an isolated environment, where all heat transfer occurs naturally [66]. In addition, it is assumed that the tank wall does not act as an insulator, i.e. there is no temperature gradient through the tank structural wall. Insulation thickness is based on an acceptable boil-off rate, where the boil-off is related to heat conducted into the tank (Equation 4.58). Figure 4.11 illustrates the heat transfer processes and temperature variation through the insulation of the tank. The temperature transitions from the external temperature,  $T_{\infty}$ , to the insulation surface temperature,  $T_s$ , and finally, the internal tank temperature,  $T_{LH2}$ . Internal tank temperature and external surrounding temperature are fixed by storage and operating requirements, whilst the insulation surface temperature is dependent on the properties of the insulation and the insulation thickness,  $t_i$ . It will be assumed that the aircraft spends a minimal amount of time on-ground in comparison to the time spent at cruise altitude. Therefore the relevant external temperature would be the air temperature at the cruise altitude. Sizing the tank insulation for the temperature on ground would result in an increase in insulation thickness and a tank that was oversized for cruise conditions.

$$Q_{\text{in}} = Q_{\text{conv}} + Q_{\text{rad}} \quad (4.53)$$

$$Q_{\text{out}} = Q_{\text{cond}} \quad (4.54)$$

Each of the heat transfer terms may be calculated as follows:

$$Q_{\text{conv}} = h(T_{\infty} - T_s) \quad (4.55)$$

$$Q_{\text{rad}} = \varepsilon\sigma(T_{\infty}^4 - T_s^4) \quad (4.56)$$

$$Q_{\text{cond}} = \frac{T_s - T_{LH2}}{R_{th}} \quad (4.57)$$

Table 4.2 demonstrates the equations required to calculate each of the heat transfer terms [66]. The mass flow rate of hydrogen lost to boil-off may be calculated as a function of the heat conduction:

$$\dot{m}_{\text{boiloff}} = \frac{Q_{\text{cond}}}{h_{fg}} \quad (4.58)$$

## 4. Aircraft Modelling

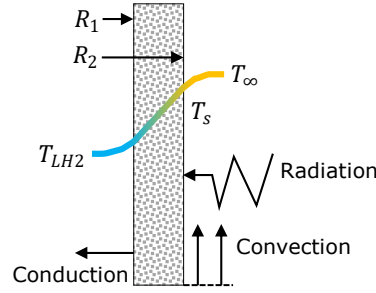


**Figure 4.11:** Heat transfer through tank insulation layer

Additional relevant constants are:

- $\varepsilon$  = Emissivity of the insulation, dependent on insulation material
- $\sigma$  = Stefan-Boltzmann constant,  $5.67 \times 10^{-8} \text{ W/m}^2 \text{ K}^4$
- $K$  = Thermal conductivity of insulation, dependent on insulation material
- $K_g$  = Thermal conductivity of air, function of air temperature,  $0.0196 \text{ W/mK}$  at cruise altitude
- $h_{fg}$  = Latent heat of vaporisation,  $446592 \text{ J/kg}$  for liquid hydrogen
- $g$  = Gravitational acceleration,  $9.80665 \text{ m/s}^2$

Both the tank's internal and external temperatures are known terms in the calculation that depend on the operating conditions and the storage temperature of the fuel. However, the insulation thickness and tank surface temperature are unknowns. Therefore, an insulation thickness must be found that balances the heat into and out of the tank whilst also meeting a specified boil-off rate. The total heat through the tank insulation is the sum of that passing through the walls of the cylindrical and spherical sections. Therefore, the heat transfer through the cylindrical and hemispherical sections may be calculated separately and then subsequently summed.

**Table 4.2:** Heat transfer terms for cylinders and spheres

	Sphere	Cylinder
Thermal Resistance, $R_{th}$	$\frac{1}{4\pi K} \left[ \frac{1}{R_1} - \frac{1}{R_2} \right]$	$\frac{1}{2\pi KW} \ln \left( \frac{R_2}{R_1} \right)$
Convection Coefficient, $h$		$\frac{\text{Nu}K_g}{D}$
Nusselt Number, $\text{Nu}$	$2 + \frac{0.589R_{ad}^{1/4}}{\left[ 1 + \left( \frac{0.469}{\text{Pr}} \right)^{9/16} \right]^{4/9}}$	$\left[ 0.6 + \frac{0.387R_{ad}^{1/6}}{\left[ 1 + \left( \frac{0.559}{\text{Pr}} \right)^{9/16} \right]^{8/27}} \right]^2$
Rayleigh Number, $R_{ad}$		$\frac{8g(T_\infty - T_s)R_2^3}{\nu\alpha T_\infty}$
Prandtl Number, $\text{Pr}$		$\frac{\alpha}{\nu}$
$\alpha$		$-3.119 \times 10^{-6} + 3.541 \times 10^{-8}T_\infty + 1.679 \times 10^{-10}T_\infty^2$
$\nu$		$-2.079 \times 10^{-6} + 2.777 \times 10^{-8}T_\infty + 1.077 \times 10^{-10}T_\infty^2$

The tank surface temperature is a function of the tank wall thickness. The inner insulation radius,  $R_1$  is a function of the tank internal radius,  $r$ , and the thickness of the tank wall,  $t_{\text{wall}}$ :

$$R_1 = r + t_{\text{wall}} \quad (4.59)$$

## 4. Aircraft Modelling

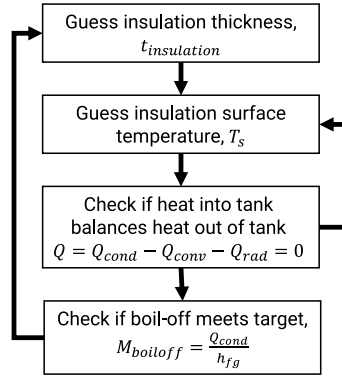


**Figure 4.12:** Iterative process to solve for the required LH<sub>2</sub> tank insulation thickness

The outer insulation radius is then a function of the inner insulation radius and the insulation thickness,  $t_{insulation}$ :

$$R_2 = R_1 + t_{insulation} \quad (4.60)$$

As there are two unknown values that must be found ( $T_s$  and  $t_{insulation}$ ), a set of iterations are required to solve for the requisite tank thickness to meet the target boil-off rate (Figure 4.12). Following calculation of the required insulation thickness, the mass of the insulation may be calculated in a similar manner to the tank wall mass:

$$M_{insulation} = \rho_{insulation} \left[ \frac{4\pi(R_2^3 - R_1^3)}{3} + \pi(R_2^2 - R_1^2)W \right] \quad (4.61)$$

### 4.2.5 Tank Liner

The tank liner is a necessary part of the construction when using a permeable structural material. The selected material must provide a barrier to prevent permeation of hydrogen through the tank wall, whilst also remaining resistant to damage by hydrogen embrittlement. In the absence of a formal method for determining the liner thickness for a liquid hydrogen tank, a liner thickness was assumed. Liner thickness for compressed hydrogen tanks is in the region of 5-12mm for Type III/Type IV tanks [128], with the required thickness depending on the storage pressure. However, metallic tank liners of a thickness down to 0.5mm have been developed [123]. A tank liner thickness of 1.7mm will be assumed [126], however, future development of linerless tanks may eliminate the need for the liner. Given the tank liner thickness and the density of the material used, the weight of the liner may be calculated as follows:

$$M_{liner} = \rho_{liner} \left[ \frac{4\pi [r^3 - (r - t_{liner})^3]}{3} + \pi [r^3 - (r - t_{liner})^3] W \right] \quad (4.62)$$

## 4.3 Liquid Hydrogen Tank Sizing Results

The following tank materials were selected for the tank sizing calculations based on research by Sekaran *et al.* for a similar application [126]:

- Polyethylene tank wall
- Polymethacrylimide Foam
- Aluminium alloy liner (Al-Mg 5086)

## 4. Aircraft Modelling

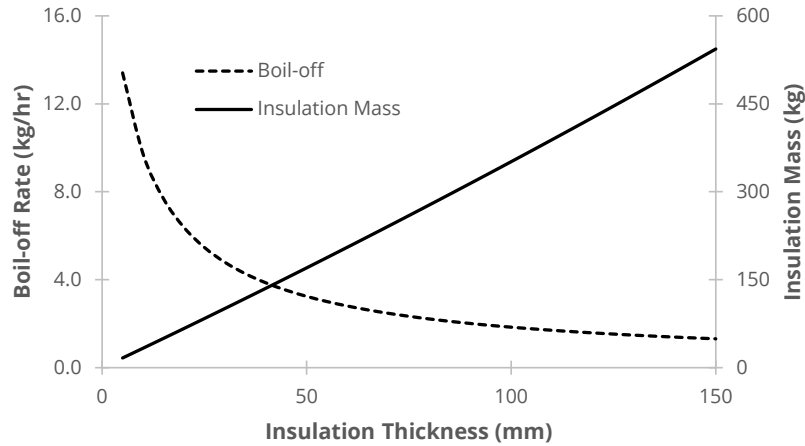


**Figure 4.13:** Influence of insulation thickness on insulation weight and boil off rate (example tank with  $r = 2\text{m}$  and  $W = 5\text{m}$ )

Tanks were sized for a maximum cruise boil-off rate of 0.1% of the initial tank  $\text{LH}_2$  mass per hour, unless otherwise stated.

### 4.3.1 Tank Boil-off

Limiting the boil-off of fuel is an important factor in designing a fuel tank as it reduces the fuel wasted during the course of a flight. Increasing the insulation thickness of the tank reduces the boil-off rate, however, this is matched by an increase in tank weight due to a greater volume of insulating material. An increase in insulation thickness therefore increases both the tank weight and the tank size. In addition, there are diminishing returns from an increase in insulation thickness (Figure 4.13). As space is limited and a large increase in operating empty weight is not desirable, the tank design must define an acceptable boil-off rate which balances lost fuel against the insulation weight and tank size.

The tank's insulation is sized for the conditions experienced at cruise, where the difference in temperature between the inside and outside of the tank is relatively lower than at ground level. However, temperatures whilst the aircraft is on ground and during other flights phases will be higher, and hence the fuel boil-off will be higher than during cruise. As an example, a tank with an internal diameter of 2 m and a cylinder length of 5 m was sized for a boil-off rate of 0.1% of the initial tank  $\text{LH}_2$  mass per hour at cruise conditions. For this design, the required insulation thickness is approximately 25 cm. On ground at ISA temperature, the boil-off rate is equal to 0.14% of the initial tank  $\text{LH}_2$  mass per hour. A long period of time spent on ground at a hot airport could therefore potentially lead to a significant loss of fuel due to boil-off. However, sizing the insulation for ground conditions would lead to unnecessarily heavy insulation given the diminishing returns of increasing insulation thickness (Figure 4.13).

Tank weight can be reduced by sizing for a higher boil-off rate and carrying a larger quantity of fuel to compensate. However, this would increase the fuel volume required, leading to a larger tank. In addition, boil-off at ground level would be correspondingly higher.

### 4.3.2 Tank Dimensions

The combined mass of all the tank wall elements is a function of the tank dimensions. For a fixed tank volume, the tank cylinder length or radius may be varied, where a cylinder length of 0 m would represent a spherical tank. For a given tank capacity, an optimum configuration emerges that leads to a minimum tank weight (Figure 4.14). This optimum is a result of the summation

## 4. Aircraft Modelling

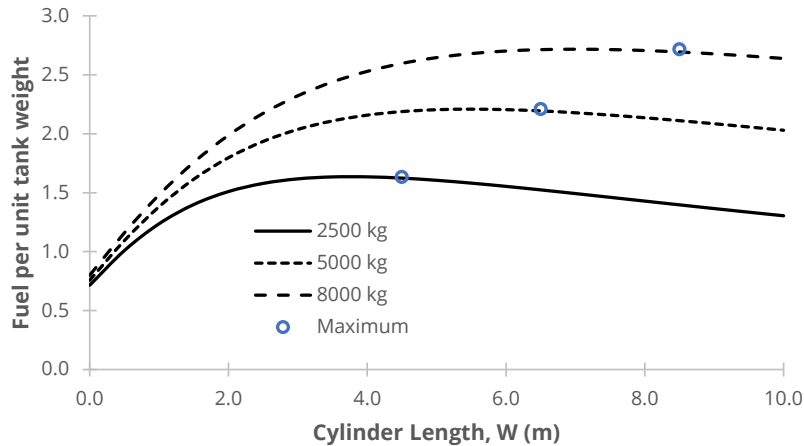


**Figure 4.14:** Unit of LH<sub>2</sub> fuel carried per unit of tank mass for varying tank capacities

of the weights of each of the tank structural components (Figure 4.15). The reasoning behind the minimum may be found by assessing the two key dimension parameters that result from a variation in the tank cylinder length. As the tank cylinder length is increased, the tank radius must be decreased in order to maintain a constant tank volume (Equation 4.50). Therefore, the thickness of the tank wall reduces with an increase in the tank length, as it is a function of radius (Equation 4.51). Hence, the tank weight is predominantly influenced by the radius, and to a lesser extent by the tank length (Equation 4.52). In contrast, the tank insulation thickness is more greatly influenced by the tank surface area. A higher surface area implies that more heat is able to enter the tank, necessitating a greater insulation thickness. Similarly, the tank liner weight is a function of the surface area. The liner thickness is kept constant, regardless of the tank dimensions. Therefore, the higher the tank surface area, the more material is required to provide a complete liner for the tank and the heavier the liner. The tank surface area is a function of both the tank radius and the tank cylinder length, with the minimum surface area combination of radius and cylinder length depending on the tank volume. Both the tank liner and the tank insulation weight demonstrate a minimum which approximately corresponds with the configuration with the minimum surface area to volume ratio. A higher surface area to volume ratio leads to a tank which is able to carry more fuel per unit tank weight. The combination of these factors leads to a configuration with a minimum total weight.

As the tank volume increases, the required dimensions will naturally also increase along with the total weight. Likewise, the optimum magnitude of the length and radius of the tank increases as the tank volume increases. The ideal tank is not simply the one with the lowest weight, but the one with the best ratio of fuel carried to total tank weight. Therefore, despite a higher tank weight, larger tanks are better, as they are able to carry more fuel per unit tank weight (Figure 4.14). The least efficient tanks from a weight perspective are those with a relatively low cylinder length. The weight trend flattens as the cylinder length is further increased. A cylinder length greater than the optimum therefore has less of an impact on weight than selecting a cylinder length lower than the optimum.

### 4.3.3 Tanks for the N3-X

The combination of the cylindrical tank configuration and low volumetric density of LH<sub>2</sub> means that the quantity of fuel that can be carried by the N3-X is limited by the available volume in the aircraft. Whilst kerosene fuel can be stored in wing-based tanks with theoretically any size or shape, LH<sub>2</sub> tanks must be stored in a dedicated space with sufficient volume for a



## 4. Aircraft Modelling

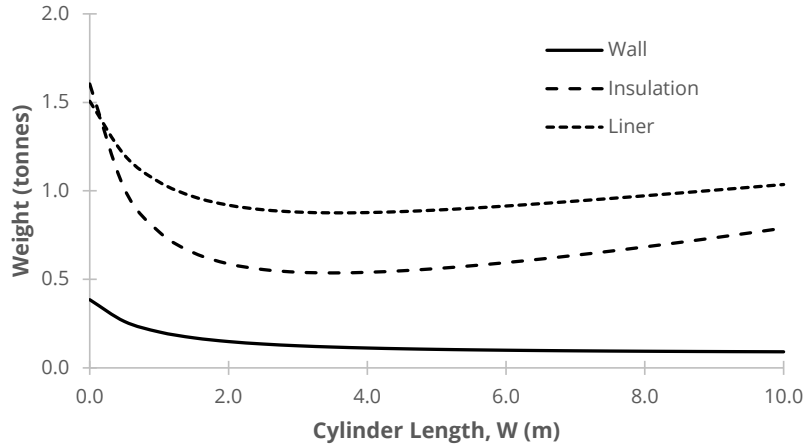


**Figure 4.15:** Breakdown of components of tank weight for a tank with a 2500 kg LH<sub>2</sub> capacity

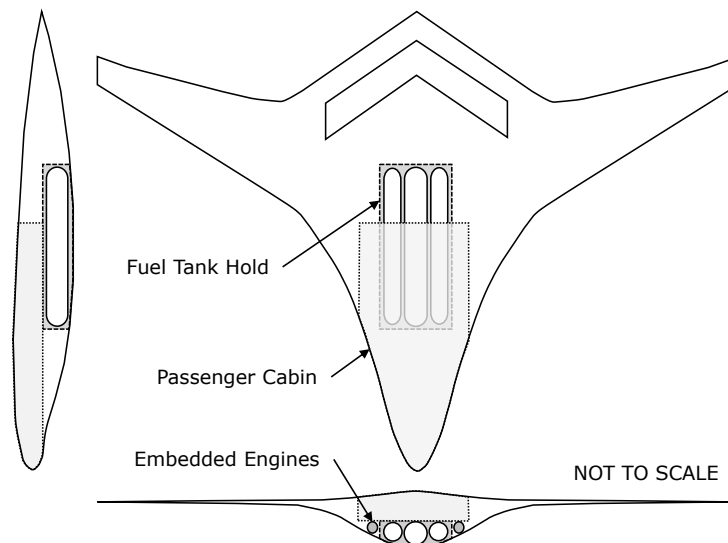


**Figure 4.16:** Potential internal configuration for the N3-X showing locations for the passenger cabin and fuel tank hold

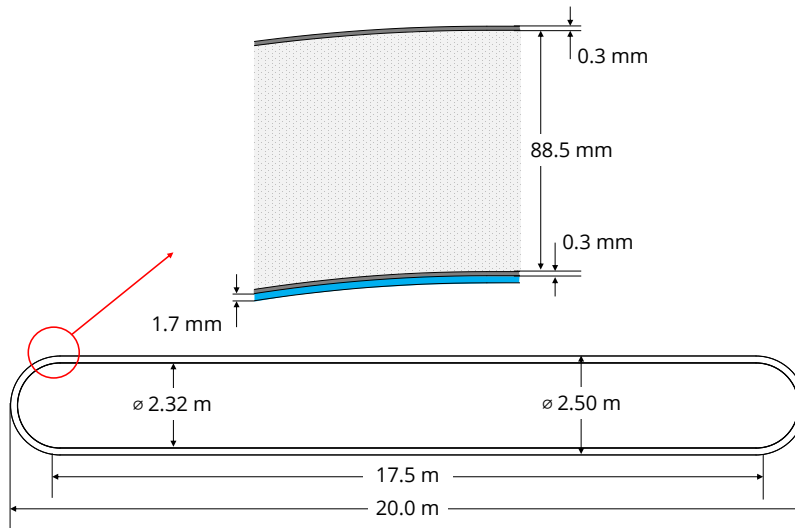
reasonable quantity of fuel. The fuel tanks were assumed to be stored within the fuselage of the N3-X, below the passenger cabin (Figure 4.16). This defines a fixed volume for storing tanks with a length of approximately 20 m and a width of 8.8 m. The space can be best used by implementing a small number of large tanks. Many small tanks would lead to a larger overall weight due to a higher total surface area for the tanks and would lead to wasted space in between the tanks. The centreline of the fuselage is able to accommodate a tank with a maximum diameter of 2.5 m, with two adjacent tanks with a diameter of 2.2m. The tanks must be sized such that the outer tank diameter fits within the available volume of the hold. The tank internal diameter (which defines the fuel volume) will therefore be less than the maximum hold diameter.

Table 4.3 details the key dimensions that describe the two tank sizes. A scaled diagram of the central tank is shown in Figure 4.17. Both tanks are significantly longer than required for minimum tank weight given their volume (Figure 4.14), where the smaller tank is further from its minimum weight dimensions. The relatively higher surface-area-to-volume ratio of the side tanks leads to thicker insulation (40% thicker than the central tank), which reduces the tank capacity, given the fixed outer diameter. The outer tanks therefore carry significantly less fuel per unit tank weight than the larger central tank. The total weight for the tanks is 5,479

## 4. Aircraft Modelling

**Table 4.3:** Key design parameters for the N3-X LH<sub>2</sub> fuel tanks

	Centre Tank	Side Tanks	Total
Number of tanks	1	2	3
Inner Diameter (m)	2.32	1.96	-
Outer Diameter (m)	2.50	2.20	-
Cylinder Length (m)	17.5	17.8	-
Tank Weight (kg)	1841	1819	5479
Fuel Capacity (kg)	5256	3827	12910



**Figure 4.17:** Diagram of tank dimensions for the larger N3-X liquid hydrogen tank

kg (increasing the N3-X OEW by 5%), with a capacity for 12,910 kg of fuel. For both tanks, insulation is the dominant portion of the tank weight. Alternative insulating materials may lead to a lighter tank weight, such as aerogel insulation, which is both light and has low thermal conductivity [122]. It is also possible that the insulation can contribute to the structural strength of the tank to reduce tank wall thickness and weight.

Tanks with a lower cylinder length would be closer to a minimum tank weight configuration, assuming a fixed radius. However, larger tanks generally have a better ratio of fuel weight to tank weight (Figure 4.14). A larger tank size is therefore better from a fuel capacity perspective. In addition, there would be more wasted space between tanks if many smaller tanks were used. Nevertheless, using many smaller tanks presents the possibility for more flexibility by creating a configuration with removable tanks. With a removable tank configuration, operating empty weight can be reduced by using only as many tanks as is required to carry the mission fuel. Range extension can also be considered through the use of external tanks. Alternatively, a dual fuel configuration can be considered, with the aircraft carrying both LH<sub>2</sub> and kerosene. The internal volume provided for fuel tanks may also be increased, such as by placing tanks perpendicularly located in front of and behind the main fuel tanks.

### 4.4 Aircraft Case Study Definition

In order to appropriately model the N3-X and the baseline aircraft, it is necessary to define the aircraft configuration. Data was gathered from publicly available resources to create models of both aircraft that were then integrated in the aircraft performance mode. In the case of

## 4. Aircraft Modelling

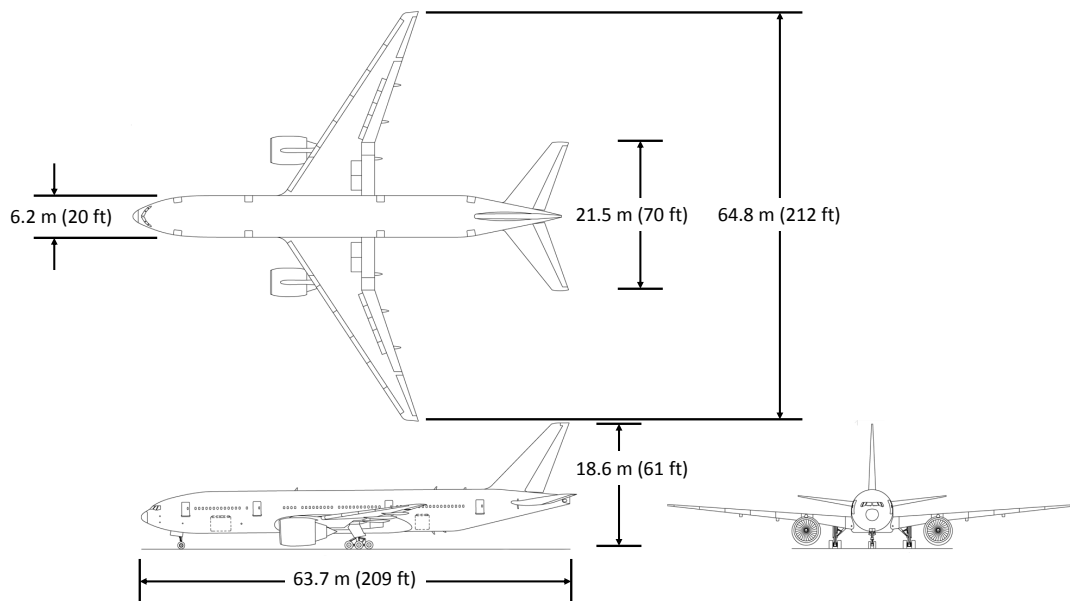


**Figure 4.18:** Plan drawing of the B777-200LR (Image Source: Wikimedia Commons)

the baseline aircraft, a model was also created for the aircraft's engines. As with the N3-X turbogenerators, the baseline aircraft's engines were modelled in *Turbomatch*, an engine modelling tool for gas turbine simulation (Section 3.2.2).

### 4.4.1 Baseline Aircraft

The N3-X is designed with the goal of achieving at least 60% energy saving versus a 2005 EIS best-in-class aircraft. For this and previous research, the baseline has been Boeing's 777-200LR. The B777-200LR is a member of the 777 series of aircraft developed by Boeing and designed for long-haul and ultra long-haul commercial applications. The aircraft has a 301-passenger capacity and is designed for a 7500 nautical mile mission with maximum payload. The aircraft's key dimensions were obtained from scaled diagrams of the aircraft and publicly available data [129–131] (Table 4.4). Propulsive power is provided by a pair of General Electric GE90-115B engines. The engines are two-spool turbofans with a maximum thrust at sea level static conditions of 514 kN (115,100 lbf). There is a limited amount of data available on component design parameters for the engine. An optimiser was therefore used to match an engine model to the available data. The optimiser was used to determine component efficiencies, fan and compressor pressure ratio, and cooling mass flows for the engine with matching data from publicly available resources [132]. The resulting design parameters were then used to create a model approximating the performance of the baseline aircraft's engines (Table 4.5). Subsequently, the aircraft and engine models were used to validate the performance model (Section 4.6).

### 4.4.2 N3-X

The N3-X was designed for the range and payload of the B777-200LR in mind. The aircraft therefore also has a design range of 7,500 nautical miles with a 301-passenger capacity and 54,570 kg total payload capacity. The aircraft's dimensions were obtained from a scaled Open-VSP model of the N3-X [133] (Table 4.6). For the purposes of drag estimation, the airframe was split into wing and fuselage sections. The total span of the aircraft from wing-tip to wing-tip is 65.5 m (215 ft), with the fuselage defined as the central 28.1 m of this span (Figure 4.19).

## 4. Aircraft Modelling

---

**Table 4.4:** Key dimensions parameters for the B777-200LR [129–131]

<b>Wing</b>	
Area (m <sup>2</sup> )	484.3
Span (m)	60.9
Aspect Ratio	8.75
Taper Ratio	0.149
Sweep Angle (°)	31.60
<b>Horizontal Tail</b>	
Area (m <sup>2</sup> )	101.26
Span (m)	21.35
Aspect Ratio	4.5
Taper Ratio	0.30
Sweep Angle (°)	35.0
<b>Vertical Tail</b>	
Area (m <sup>2</sup> )	53.23
Span (m)	9.24
Aspect Ratio	4.5
Taper Ratio	0.29
Sweep Angle (°)	46.0
<b>Fuselage</b>	
Diameter (m)	6.20
Length (m)	62.94
<b>Nacelle</b>	
Diameter (m)	3.96
Length (m)	6.23
Number	2
<b>Weights</b>	
Maximum Take-off (kg)	347,450
Operating Empty (kg)	155,530
Maximum Fuel (kg)	162,750
Maximum Payload (kg)	53,570

## 4. Aircraft Modelling

**Table 4.5:** Key design and performance parameters for engine model approximating the configuration of the GE90-115B [132]

Design Point	
Altitude (ft)	35,000
Mach Number	0.85
Thrust (kN)	72.1
Overall Pressure Ratio	42
Bypass Ratio	7.8
Total Mass Flow (kg/s)	646.7
Combustor Exit Temperature (K)	1380
SFC (mg/Ns)	14.94
Fan Efficiency	0.901
Low Pressure Compressor Efficiency	0.932
High Pressure Compressor Efficiency	0.873
High Pressure Turbine Efficiency	0.915
Low Pressure Turbine Efficiency	0.926
Sea Level Static	
Combustor Exit Temperature (K)	1755
Thrust (kN)	514.3
Total Mass Flow (kg/s)	1675.0
SFC (mg/Ns)	4.29

The fuselage sweep varies from the nose to the start of the wing section. Sweep was therefore assumed to be the average sweep of the entire fuselage section. The aircraft operating empty and payload weights are taken from previous research on the N3-X [56]. The array nacelle drag is included within the propulsion system control volume rather than as a part of airframe drag calculations. To support a low-noise configuration for the N3-X, Berton and Haller assume that the turbogenerators are embedded within the airframe and that the wingtip turbogenerators are replaced with winglets [88]. There is therefore no nacelle drag for the turbogenerators. In the absence of a size estimate of the winglets, they are assumed to reduce airframe drag by 3.9% [120]. In addition, the aircraft has no tail surface. Therefore, the only major components of airframe drag are from the wings and fuselage. For induced drag purposes, the aircraft is treated as a flying wing with an aspect ratio of 4.90 (aerodynamic equivalent planform, Figure 4.3).

The maximum take-off weight and maximum fuel weight of the aircraft were not defined in previous research, as the focus was on the target 7,500 nautical mile mission. As a component of this research, an estimate was made for the payload-range chart of the aircraft. Rough estimates of the maximum take-off weight and maximum fuel capacity of the aircraft were therefore required. The following section summarises the assumptions used to obtain a maximum take-off weight assumption for the aircraft (Section 4.5). The N3-X was assumed to store fuel in the wing volume, as with conventional aircraft. The maximum fuel capacity was therefore taken from an estimate of the wing volume as 148,500 litres, or 120,285 kg of kerosene, assuming a fuel density of 810 kg/m<sup>3</sup>. This is more than ten times the fuel weight of LH<sub>2</sub> assumed for the aircraft, or 3.4 times the fuel energy. The N3-X propulsion system model follows the method detailed in Chapter 3.

### 4.5 Maximum Take-off Weight Estimates

It can be useful to present the performance of an aircraft in terms of a payload-range chart to identify the range of missions available to an aircraft. However, an estimate of the aircraft's

## 4. Aircraft Modelling

**Table 4.6:** Key dimensions parameters for the N3-X [133]

<b>Wing</b>	
Area (m <sup>2</sup> )	197.7
Span (m)	37.4
Aspect Ratio	7.08
Taper Ratio	0.287
Sweep Angle (°)	28.96
<b>Fuselage</b>	
Area (m <sup>2</sup> )	679.4
Span (m)	28.13
Aspect Ratio	1.16
Taper Ratio	0.213
Sweep Angle (°)	60.8
<b>Equivalent Planform</b>	
Area (m <sup>2</sup> )	877.1
Span (m)	65.5
Aspect Ratio	4.90
<b>Weights</b>	
Maximum Take-off (kg)	<i>267,400</i> Estimate
Operating Empty (kg)	121,290
Operating Empty (with LH <sub>2</sub> tanks) (kg)	126,770
Maximum Kerosene Fuel (kg)	<i>120,284</i> Estimate
Maximum LH <sub>2</sub> Fuel (kg)	<i>12,910</i> Estimate
Maximum Payload (kg)	53,570

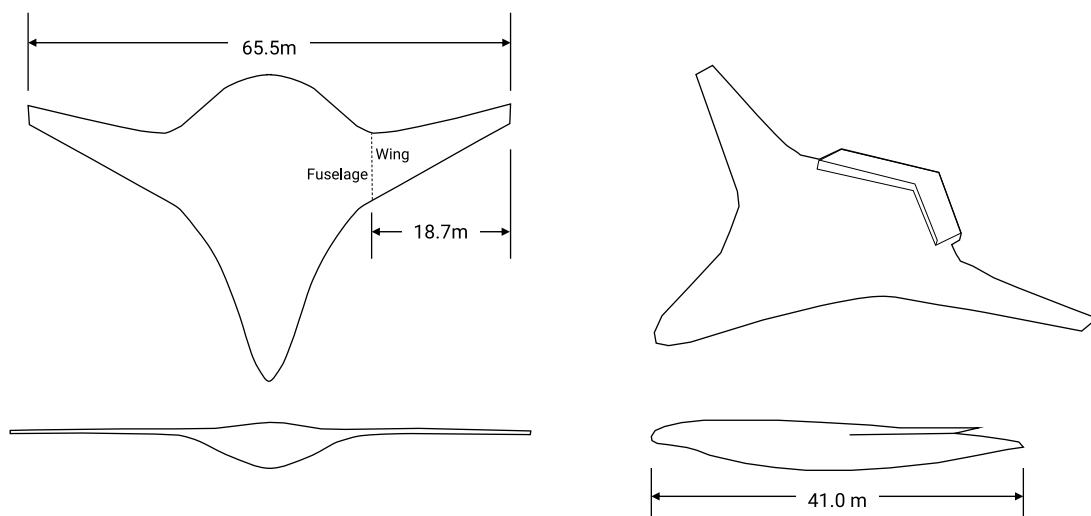


**Figure 4.19:** Plan drawing of the N3-X

## 4. Aircraft Modelling

---

maximum take-off (MTOW) weight is required to create a payload-range chart. There are two routes to obtaining a maximum take-off weight estimate. The aircraft's performance may be calculated for a design mission, with the sum of operating empty weight (OEW), fuel, and payload for the mission leading to an assumption for the maximum take-off weight. Alternatively, maximum take-off weight can be estimated by taking the typical ratio of operating empty weight to maximum take-off weight for commercial aircraft as a target value. For large aircraft, the typical ratio of operating empty weight to maximum take-off weight is between 0.4 and 0.6 [134]. Both estimates have limitations; a MTOW-OEW ratio estimate may under or overestimate the aircraft's capabilities, whilst selecting the TOW from a design mission may underestimate the aircraft's actual capabilities.

It is difficult to accurately predict an aircraft's maximum safe take-off weight without also including aspects of structural design. A higher MTOW generally implies a higher operating empty weight, as a heavier structure is required to withstand the greater maximum aircraft load. There are numerous models available for estimating the operating empty weight of an aircraft during the conceptual design stage. Two aircraft weight models were identified to perform a preliminary estimate of the airframe weight, Raymer [116], and Roskam [135]. Both models break the weight of an aircraft into its groups, including the main structural components (wings, fuselage, empennage etc.) and smaller components such as hydraulics, control systems, and interiors. However, the models do not include weight estimation methods for blended wing body fuselages. A weight estimation relationship developed by Bradley [136] was therefore used for the N3-X fuselage. The N3-X operating empty weight can otherwise be estimated by following the two identified methods. The two models were validated against known weight data for the B777-200LR. Roskam's model produced an estimate within 3% of the actual aircraft weight, whilst Raymer's model resulted in a larger 12% error, primarily due to a lower predicted fuselage weight.

In both models, operating empty weight is a function of the maximum take-off weight, which is itself a function of operating empty weight (as MTOW is the sum of OEW, maximum payload, and maximum fuel). The heavier an aircraft's maximum take-off weight, the heavier the airframe structure must be to support that weight. Therefore, estimating the operating empty weight first requires an assumption for the aircraft's maximum take-off weight. Assuming the maximum take-off weight is unknown, a brief iterative procedure can be used to match an initial OEW guess against the final OEW result. For a known payload and fuel weight:

1. Guess maximum take-off weight
2. Calculate operating empty weight using aircraft weight model
3. Calculate MTOW:  $MTOW = OEW + M_{\text{payload,max}} + M_{\text{fuel,maxrange}}$
4. Repeat Steps 2 and 3 until MTOW estimate converges

In this way, the maximum take-off weight of an aircraft can be linked to an operating empty weight. However, as a result, a reasonable guess for maximum take-off weight is useful to ensure that the aircraft is able to meet its design mission range. An iterative process may therefore be necessary to ensure that the aircraft meets this target range.

The baseline aircraft has a relatively low ratio of operating empty weight to maximum take-off weight ( $\approx 0.45$ ). Using an operating empty weight model it is possible to identify how much a change in this ratio will influence the final operating empty weight. A similar iterative process may be followed as above, however, in this case the maximum take-off weight can be estimated by using the assumed ratio of OEW to MTOW. For an aircraft with the same dimensions as the baseline aircraft, a large change in the ratio of operating empty weight to maximum take-off

## 4. Aircraft Modelling

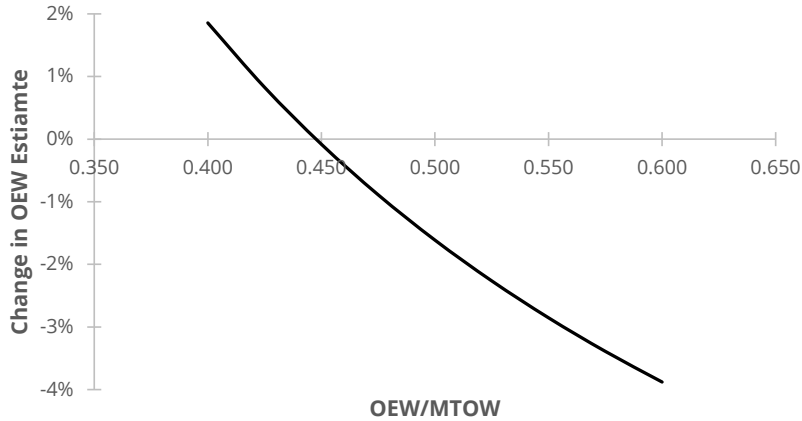


**Figure 4.20:** Operating empty weight estimate for the baseline aircraft as a function of the ratio of operating empty weight to the maximum take-off weight

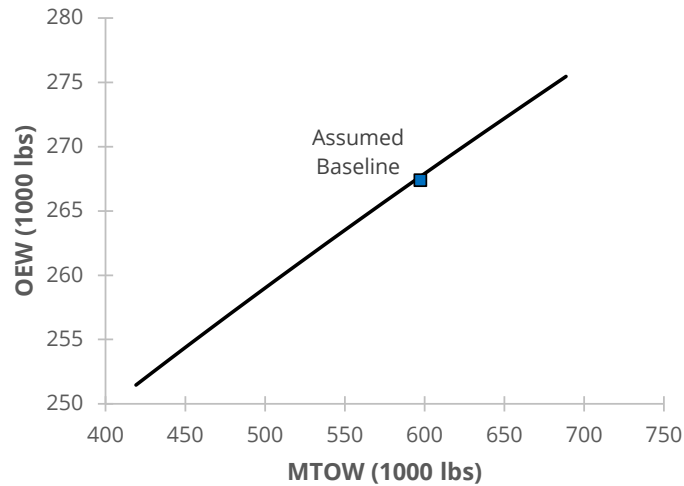


**Figure 4.21:** Operating empty weight estimate for the N3-X as a function of the maximum take-off weight (using an assumed ratio of OEW/MTOW)

weight leads to a relatively small change in the final operating empty weight estimate (Figure 4.20). The operating empty weight estimate for the baseline aircraft for the upper and lower ends of the typical OEW/MTOW range is between -3.88% and +1.86% the baseline value.

The OEW estimates produced and the corresponding relationship to MTOW are preliminary values, and a more complete structural analysis of the aircraft would be required for a more accurate weight estimate. The relationships may nevertheless be used to obtain a preliminary estimate of MTOW and OEW. Previous research predicted an operating empty weight of 121,290 kg for the N3-X. To obtain a rough estimate of maximum take-off weight, a ratio of operating empty weight to maximum take-off weight equal to that of the baseline aircraft was assumed as a starting point. Operating empty weight could then be scaled as a function of the ratio OEW/MTOW using the above aircraft weight models (Figure 4.21). The influence of the assumed MTOW on the aircraft's range was then assessed in Section 4.7.1.

### 4.6 Performance Model Validation

The aircraft performance model was validated against published payload range charts for two actual aircraft; the Boeing 777-200LR [137] (the baseline aircraft) and the Boeing 737-800



## 4. Aircraft Performance Results

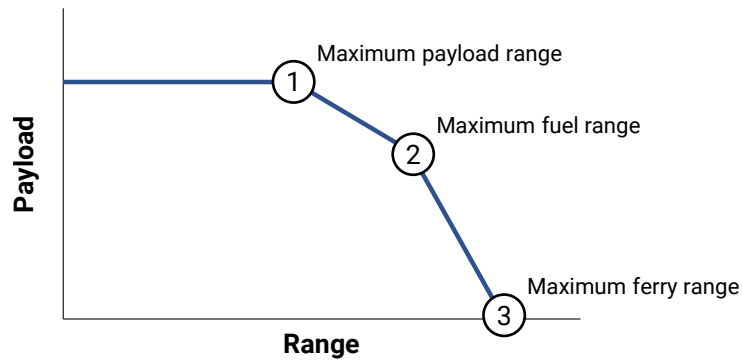


**Figure 4.22:** Example payload-range chart

**Table 4.7:** Aircraft model validation data for the B777-200LR

	Payload (kg)	Model (nmi)	Actual (nmi)	Error
Max. Payload Range	53,570	7678	7500	2.4%
Max. Fuel Range	29,170	9464	9300	1.8%
Max. Ferry Range	0	10366	10500	-1.3%

[138]. In both cases, aircraft weights and dimensions were taken from publicly available sources and aircraft diagrams [84, 137, 138]. As the N3-X propulsion system model for this research differs from the model used in previous research, the N3-X mission performance could not be validated against previous results.

A payload-range chart demonstrates the trade-off between payload and fuel weight in an aircraft, as the maximum take-off weight typically precludes carrying both a full payload and the maximum fuel load. A payload range chart generally consists of three points (Figure 4.22):

1. **Maximum payload range** – The maximum achievable range when the aircraft is carrying the maximum payload. Fuel on board is limited by the maximum take-off weight of the aircraft.
2. **Maximum fuel range** – The maximum achievable range when the aircraft is fully loaded with fuel. Payload on board is limited by the maximum take-off weight of the aircraft.
3. **Maximum ferry range** – The maximum achievable range with no payload and the maximum fuel load. Take-off weight is less than the maximum take-off weight.

The line between the maximum payload and fuel ranges follows the aircraft's maximum take-off weight. The aircraft's take-off weight then reduces as the aircraft moves along the chart from the maximum fuel range to the maximum ferry range and for points within the limits of the chart.

In both cases, the models produce an error for the three points that is well below 5% (Table 4.7, Table 4.8 and Figure 4.23). The performance model was therefore concluded to be able to adequately represent an aircraft's performance for the purposes of this research.

**Table 4.8:** Aircraft model validation data for the B777-200LR

	Payload (kg)	Model (nmi)	Actual (nmi)	Error
Max. Payload Range	21,319	2155	2150	0.2%
Max. Fuel Range	16,520	3072	3065	0.2%
Max. Ferry Range	0	3748	3800	1.4%

## 4. Aircraft Performance Results

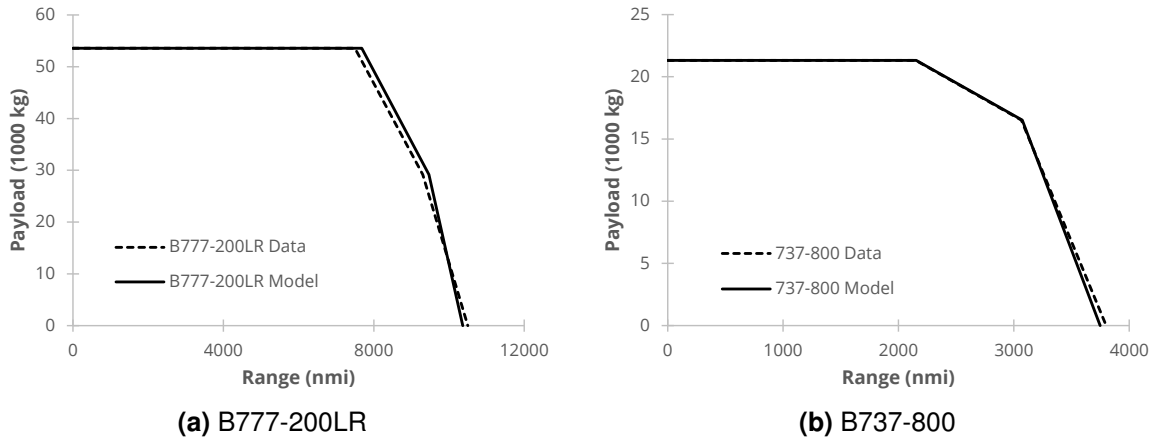


**Figure 4.23:** Aircraft model validation using payload range chart data

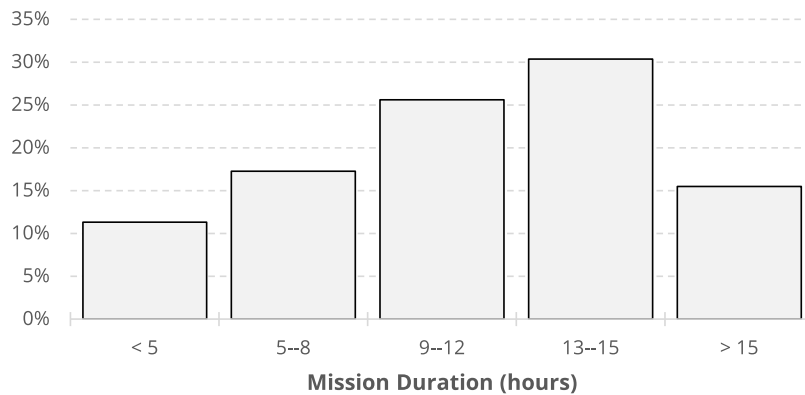


**Figure 4.24:** Flight duration for B777-200LR flights in three 24-hour periods (Data Source: flightaware.com)

## 4.7 Aircraft Performance Results

The primary performance goal of the N3-X is to improve fuel consumption by at least 60% in comparison to the baseline aircraft for the design mission. However, aircraft are rarely operated at their maximum payload-range capabilities. It is therefore also useful to identify the fuel consumption and hence fuel saving for different mission ranges and payload capacities.

Assuming that the N3-X could act as a direct substitute for an aircraft such as the B777-200LR, the 'average' mission can be identified by observing trends in the flights for which the aircraft is typically used. Data from 106 B777-200LR flights over the course of three separate 24-hour periods suggests that the mean flight duration is 10.7 hours (Figure 4.24). This corresponds to a mission range of approximately 5000 nautical miles. Payload for a typical commercial flight of the B777-200LR (especially with respect to cargo on board the aircraft) is harder to identify. IATA's Air Passenger Market Analysis for July 2017 [139] quotes an overall passenger load factor of 81.3% for the global market in 2017. For the B777-200LR, this represents approximately 245 out of an assumed maximum capacity of 301 passengers. Taking an average passenger weight of 86 kg (190 lb) with an average checked baggage weight of 13 kg (28.9 lbs) [140], this leads to a total payload weight of 24326 kg, 45% of the maximum payload. The average freight load factor for aviation is 44.6% [141] for the global market in 2017 to date. Taking this as a percentage of the maximum aircraft payload, it will be assumed that the average aircraft flies at approximately 90% of its full payload capacity. The average mission for the N3-X is therefore assumed to take the following characteristics:

## 4. Aircraft Performance Results

- 5000 nautical mile range ( $\approx 10.7$  hours)
- 245 passengers
- 48,210 kg payload (passengers and freight)

For aircraft using the same fuel and carrying the same payload, comparisons can be reasonably easily made in terms of the difference in fuel burn between the two aircraft for the same mission. However, for different fuel types, difference in fuel mass is less relevant as the fuels have different energy and volumetric densities. Therefore, in cases where fuel type or mission payload differ, it is useful to have an alternative metric for comparison. Performance in this research has been compared in terms of the difference in energy consumption and the energy to revenue work ratio, ETRW of the aircraft. This metric presents the energy consumed by the aircraft whilst carrying payload over a given distance, where a lower ETRW implies a more efficient aircraft that consumes less energy [142]:

$$\text{ETRW} = \frac{\text{LHV}_{\text{fuel}} M_{\text{fuel}}}{g R M_{\text{payload}}} \quad (4.63)$$

Where  $\text{LHV}_{\text{fuel}}$  is the fuel lower heating value,  $M_{\text{fuel}}$  is the mission fuel burn,  $g$  is gravitational acceleration,  $R$  is the flight range, and  $M_{\text{payload}}$  is the flight payload. This metric may also be used for an aircraft that relies on stored energy such as batteries by replacing the numerator with the stored energy consumed during the mission.

### 4.7.1 Payload Range Assessment

The payload range chart is a useful way of comparing the maximum range capability of the aircraft in comparison to the baseline. Operating empty weight and maximum payload weight are known values for the N3-X, however, an estimate is required for the maximum take-off weight and maximum fuel weight. Section 4.5 identified an estimate of the N3-X maximum take-off weight based on the assumption that the ratio of OEW to MTOW is the same as for the baseline aircraft. In addition, it was assumed that fuel would be stored within the aircraft wings, as with conventional aircraft designs. Maximum fuel capacity for the LH<sub>2</sub> variant is defined by the tank volume and sizing in subsection 4.3.3 as 12,910 kg of fuel. In terms of stored energy on board the aircraft, volume restrictions mean that the LH<sub>2</sub> N3-X carries 30% of the energy on board the kerosene N3-X. The weights used to predict the payload-range capabilities of the N3-X are shown in Table 4.6.

Given the MTOW assumption, and as the N3-X is a more efficient aircraft than the baseline, it has the potential to achieve a higher range than the baseline aircraft, up to 12,650 nautical miles with maximum payload (Figure 4.25). Commercial operators would not need to make use of such high range capability, as it exceeds typical flight duration by a large margin. In addition, no city pair is separated by a large enough distance to require the maximum possible range of the aircraft. However, the increase in range suggests potential for changes in the mode of operation or the application of the aircraft, to take advantage of the increased endurance. The chart is used primarily to demonstrate the potential of the N3-X variant of aircraft, as opposed to setting an expected payload-range chart for the aircraft.

As the fuel capacity of the LH<sub>2</sub> fuelled N3-X is limited, the maximum achievable range is approximately 5400 nautical miles, lower than for the kerosene variant and below the 7500 nmi design range. Fuel capacity for at least 17,940 kg of fuel would be required to achieve the design range (including reserve fuel), a 40% increase in fuel capacity. It was assumed that the maximum take-off weight of the LH<sub>2</sub> variant is the same as that of the kerosene aircraft, as the structure is effectively unchanged. The total weight of fuel, fuel tanks, and maximum payload is therefore less than the assumed maximum take-off weight. As a result, the maximum fuel and

## 4. Aircraft Performance Results

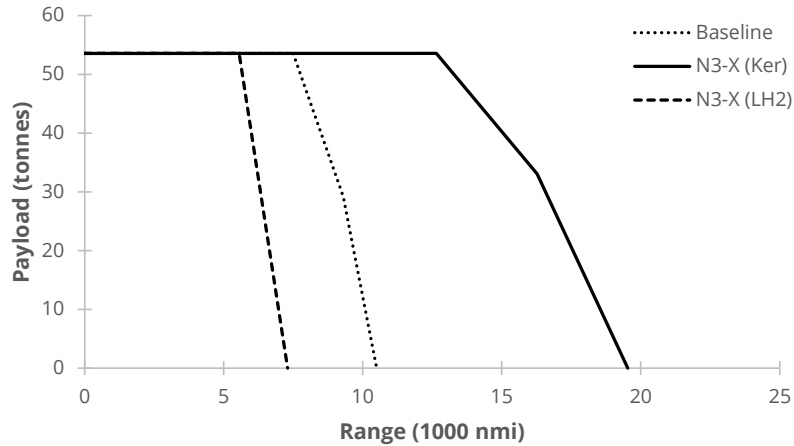


**Figure 4.25:** Payload-range chart prediction for the baseline aircraft and N3-X

maximum payload ranges coincide. There is therefore no trade-off between maximum payload and maximum fuel capacity that is typically found in a payload-range chart. As the assumed maximum take-off weight is never reached for the LH<sub>2</sub> N3-X, the possibility arises of increasing the aircraft's payload capacity to take advantage of the additional weight capability of the aircraft (Section 5.3). Although the possible maximum payload is higher, the LH<sub>2</sub> variant is unable to reach the design 7500 nmi range. Modifications would be necessary to increase range up to the target value. This research considers the possibility of a dual fuel kerosene-LH<sub>2</sub> option for the aircraft in Section 5.3 to extend range past the 5400 nautical mile maximum for the LH<sub>2</sub>-only variant.

### 4.7.2 Mission Performance

Aircraft performance was simulated for a range of mission lengths up to the design range of 7500 nautical miles. The high efficiency of the N3-X configuration leads to a significant difference in fuel burn and energy efficiency between the kerosene variant and the baseline aircraft (Figure 4.26 and Figure 4.27). The energy saving of the kerosene N3-X versus the baseline is therefore 60.4%, exceeding the 60% energy saving target for the design mission (Figure 4.28). This energy saving is achieved through the combination of a higher lift-to-drag ratio airframe (cruise L/D of 25 in comparison to 19 for the baseline aircraft), and the lower specific fuel consumption (cruise SFC of ~10 in comparison to ~15 for the baseline aircraft). However, fuel savings reduce as the mission range is reduced, due to a lower fuel consumption by mass. Energy saving falls below the 60% target for mission ranges lower than approximately 6500 nautical miles (assuming maximum payload for the mission). Although a lower payload decreases the energy efficiency of the aircraft in terms of ETRW (Figure 4.30), the efficiency reduces less rapidly for the N3-X than the baseline line. Therefore, the energy saving of the N3-X versus the baseline aircraft increases as the payload is reduced (Figure 4.29). As a result, for the defined average mission, the N3-X fuel saving versus the baseline aircraft is 60.7%.

The lower density of LH<sub>2</sub> in comparison to kerosene naturally leads to a lower fuel consumption by weight (Figure 4.26). Despite a higher operating empty weight, the energy to revenue work ratio for the LH<sub>2</sub> variant is lower than that of the kerosene N3-X, due to a lower in-flight weight. Energy saving of the LH<sub>2</sub> aircraft versus the baseline is therefore 64.7%, higher than that achieved for the kerosene N3-X (Figure 4.28). Energy saving falls below the 60% target for mission ranges lower than approximately 3000 nautical miles (assuming maximum payload for the mission). Although ETRW and energy saving has been presented for a full range of

## 4. Aircraft Performance Results

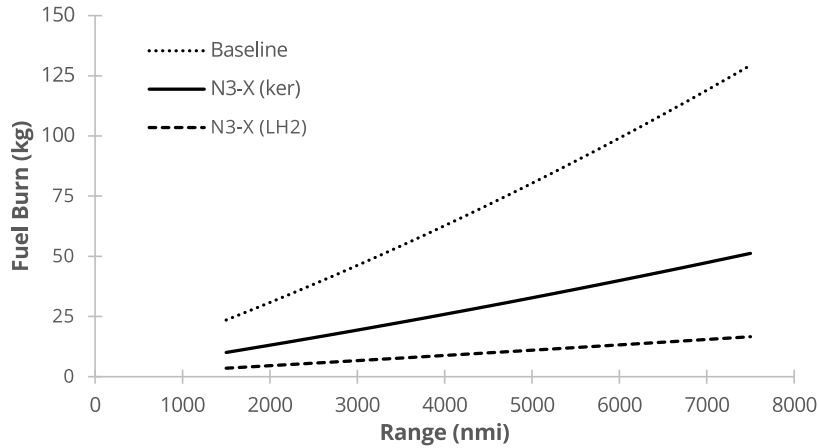


**Figure 4.26:** Fuel burn of the baseline aircraft and N3-X variants up to the 7500 nautical mile design range (maximum payload)

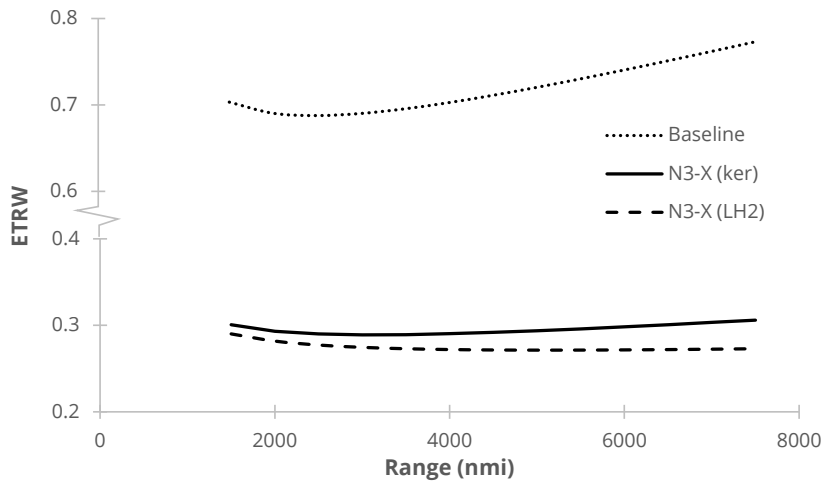


**Figure 4.27:** Aircraft energy-to-revenue-work ratio as a function of mission range (maximum payload)

missions up to the design range of 7500 nmi, the maximum fuel capacity of the LH<sub>2</sub> tanks limits the feasible maximum range of the LH<sub>2</sub> variant to 5400 nmi (subsection 4.7.1).

Both the ETRW and energy saving trends diverge for the two fuel variants of the N3-X as the aircraft range is increased, due to the difference in aircraft weight during flight. The energy saving of using a lighter fuel becomes increasingly apparent as mission range increases, as less fuel is on board and hence less fuel is required. However, this difference in fuel burn is dependent on the LH<sub>2</sub> tank configuration and tank materials. Heavy tanks can potentially increase the OEW of the aircraft to a point where the LH<sub>2</sub> variant is heavier than the kerosene aircraft for a given mission, leading to higher energy consumption and a less efficient aircraft. A 'break even' tank weight can therefore be determined, i.e. the maximum LH<sub>2</sub> tank weight beyond which the LH<sub>2</sub> variant is less efficient than the kerosene variant. As the mission range increases, the difference in fuel weight becomes much more significant for the two fuel options, due to the higher energy density by weight of the LH<sub>2</sub> as fuel. However, for short range missions where fuel consumption is low, the difference in fuel weight on board the aircraft is much lower. The maximum tank weight is therefore significantly less. For example, the break even tank weight for a 2000 nmi mission is approximately 15,000 kg, whilst the break even tank weight for a 5000 nmi mission is approximately 19,000 kg. Given the tank weight estimates produced by

## 4. Aircraft Performance Results

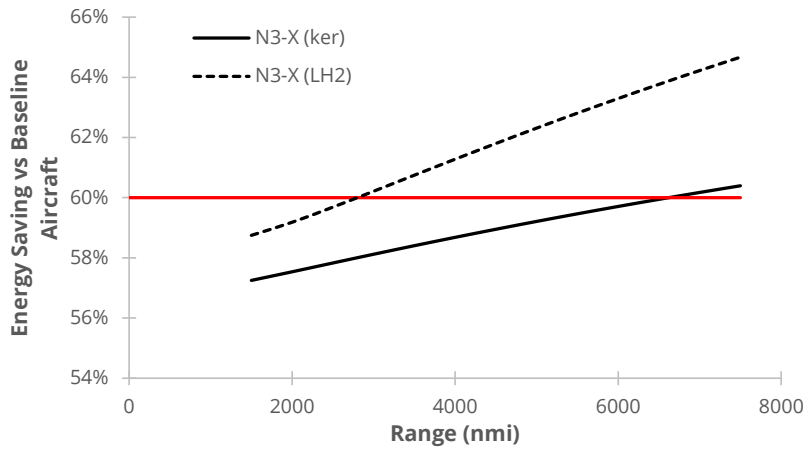


**Figure 4.28:** N3-X energy saving versus the baseline aircraft as a function of range with 60% savings target marked (maximum payload)

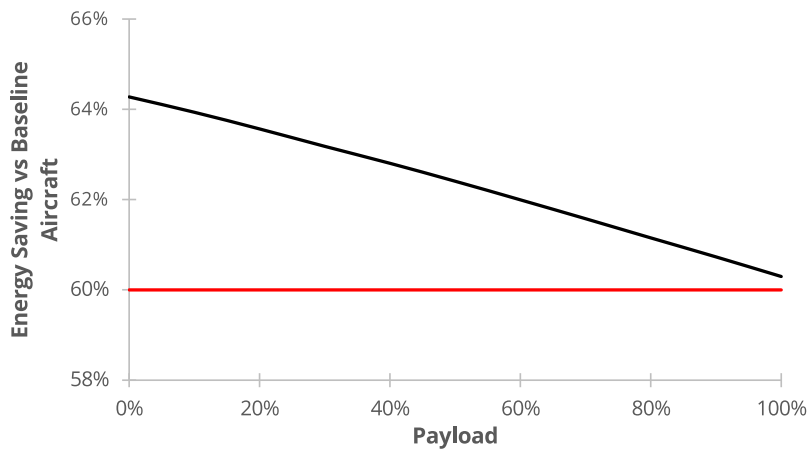


**Figure 4.29:** N3-X energy saving versus the baseline aircraft as a function of payload with 60% savings target marked (Kerosene aircraft, 7500 nmi range)

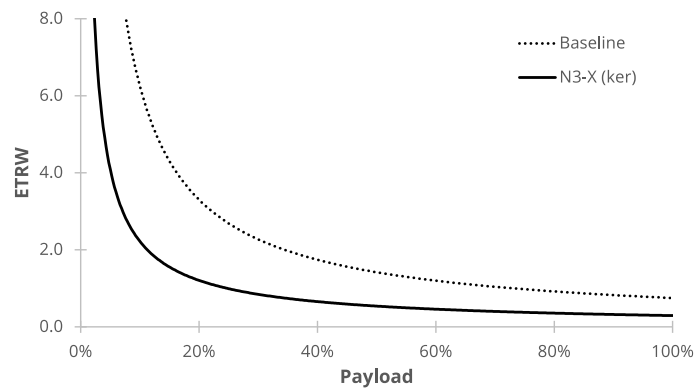


**Figure 4.30:** Aircraft energy-to-revenue-work ratio as a function of payload (7500 nmi range)

## 4. Aircraft Performance Results

the previous section, it is reasonable to assume that the LH<sub>2</sub> N3-X variant will have a consistently lower energy consumption than the kerosene variant. However, it is possible that higher weight tank materials will be required, or that the internal support structure for the LH<sub>2</sub> tanks will increase the operating empty weight and hence increase the aircraft's energy consumption.

As LH<sub>2</sub> is lighter than kerosene, the weight of the aircraft (and hence the drag of the aircraft) during flight varies less than the kerosene aircraft. This leads to less of variation in engine power during the course of the flight. In addition, for the same mission length and same payload, the landing weight of the LH<sub>2</sub> aircraft will typically be higher, due to a higher operating empty weight. This assumes that the weight of reserve kerosene on board the aircraft is less than the weight of the LH<sub>2</sub> tanks. The LH<sub>2</sub> variant is generally lighter than the kerosene aircraft during climb, enabling a faster time to climb than the kerosene variant, assuming the same engine rating and climb schedule (for a 7500 nmi mission: 22 minutes versus 29 minutes). Operational requirements may necessitate a different climb schedule to ensure an appropriate climb rate for the lighter LH<sub>2</sub> variant. Although landing weight of the LH<sub>2</sub> aircraft is generally higher than that of the kerosene variant, the aircraft's weight during the early stages of descent will be lower, due to the lower aircraft weight. As a result, performance characteristics of the two variants during each flight phase may be noticeably different, despite an outwardly similar configuration.

The previous analyses of the N3-X utilised a propulsion system designed for the same thrust requirement for both variants of the N3-X. Both aircraft therefore have the same size propulsor array with the only difference in design being the fuel type. The LH<sub>2</sub> variant's propulsion system therefore runs at a lower power setting than that of the baseline kerosene N3-X for most of the cruise segment. However, the lower weight and drag of the LH<sub>2</sub> variant suggests that the propulsion system may be sized for a smaller thrust rating. A resized propulsion system is created in Section 5.3.

Subsection 4.5 demonstrated that the aircraft's maximum take-off weight is a function of its operating empty weight (Figure 4.21). Therefore, operating empty weight will be different for different ratios of OEW to MTOW (i.e. different assumed maximum take-off weights). A lower ratio of OEW to MTOW will lead to a lower operating empty weight, and will therefore reduce the fuel consumption for the design mission (Figure 4.31a). However, reducing the ratio of OEW to MTOW also implies a lower maximum take-off weight, which will reduce the aircraft's maximum payload range (Figure 4.31b). A maximum ratio of OEW to MTOW can be defined, above which the aircraft is no longer able to achieve its design range of 7500 nmi with maximum payload. Given the assumptions made, this ratio is approximately 0.53 (compared to 0.45 assumed for the N3-X). It should be highlighted that this analysis is reliant on the MTOW assumption and the relationship between MTOW and OEW as determined by the weight models.

### 4.7.3 Cruise-climb

The previous analyses assumed that the aircraft cruises at a fixed altitude for the duration of a flight. However, this is generally not the most efficient cruise option for an aircraft. During the course of cruise, an aircraft's weight reduces during as fuel is consumed. The aircraft's lift must therefore likewise reduce to maintain the requirement that lift is equal to weight:

$$W = L = C_L \frac{1}{2} \rho u^2 S_{\text{ref}} \quad (4.64)$$

The right hand side of the equation can be split roughly into three aspects: angle of attack ( $C_L$ ), altitude ( $\rho$ ), and speed ( $u^2$ ). There are three potential cruise methods that can be used to maintain lift equal to weight:

- **Constant angle of attack and constant Mach number:** The aircraft climbs over the

## 4. Aircraft Performance Results

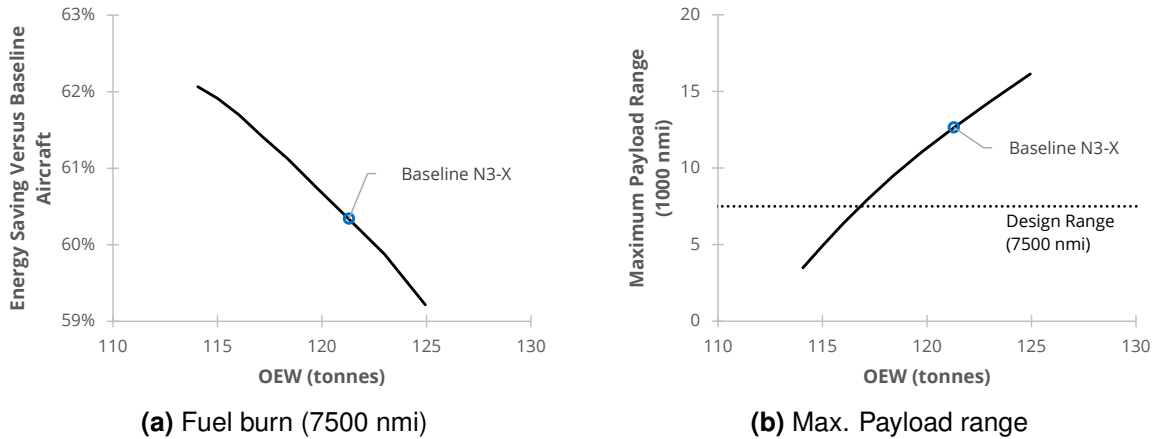


**Figure 4.31:** N3-X performance as a function of operating empty weight (where OEW is a function of OEW/MTOW)

course of the cruise segment as the aircraft weight reduces.

- **Constant angle of attack and constant altitude:** The aircraft airspeed reduces over the course of flight, leading to a reduction in lift.
- **Constant altitude and constant Mach number:** The aircraft angle of attack decreases during the course of the flight, leading to a reduction in the aircraft lift coefficient.

Speed is typically set in the interest of ensuring a reasonable flight time, ruling out a reduction in speed as a way of reducing lift. In addition, air traffic management requirements typically dictate a cruise altitude for an aircraft. Commercial aircraft therefore operate with a varying angle of attack during the course of a flight. As the aircraft's cruise altitude and velocity is fixed, the cruise lift-to-drag ratio is generally lower than maximum achievable value for a given flight condition or aircraft weight. For any given aircraft weight, there is an altitude at which the lift-to-drag ratio is maximised (Figure 4.32). Similarly, at a fixed altitude there is an aircraft weight at which a maximum lift-to-drag ratio is achieved. Therefore, for cruise at a fixed altitude, lift-to-drag ratio is maximised for only a brief portion of the flight. To maximise lift-to-drag ratio for the entire flight, it would be necessary to climb throughout the flight as the aircraft weight reduces. In reflection of this, aircraft typically operate a stepped climb, whereby cruising altitude is increased in steps as and when allowed by air traffic management. In this way, efficiency is improved over operating at a fixed altitude for the entirety of the cruise segment. Further improvements are possible if the aircraft is instead allowed to climb during the course of the flight whilst maintaining a constant velocity. The aircraft lift-to-drag ratio may then be maximised for any stage of the flight, rather than changing with the aircraft weight. In addition to an increase in lift-to-drag ratio, the reduction in drag as the aircraft ascends enables a lower specific fuel consumption during the flight. The overall effect is an improvement in the aircraft's fuel consumption. Current air traffic management rules do not support cruise-climb, instead allowing aircraft to ascend in fixed steps at certain intervals. However, improvements to air traffic management in the future may make optimised cruise a possibility, enabling improvements to efficiency.

A brief analysis was conducted for the N3-X to compare the differences in cruise-climb operation that would result from the two N3-X fuel variants. The previous section identified that the in-flight weight of the LH<sub>2</sub> N3-X is lower than that of the kerosene N3-X. In addition, the aircraft's weight changes less during the course of the flight as the fuel weight is lower. As a result, the variation in altitude and lift-to-drag ratio of the two aircraft will be noticeably different.



## 4. Aircraft Performance Results

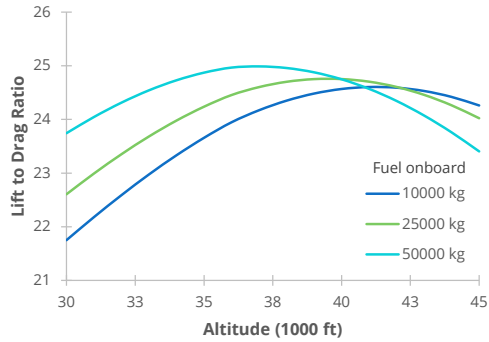


**Figure 4.32:** N3-X lift to drag ratio as a function of altitude for varying values of fuel on board (maximum payload, 7500 nmi mission)

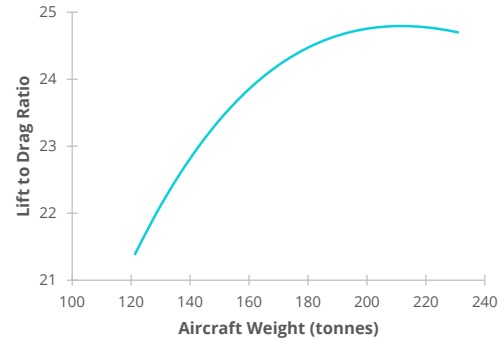


**Figure 4.33:** N3-X lift to drag ratio as a function of aircraft weight at a fixed altitude of 35,000 ft

The cruise-climb type flight was simulated by selecting the altitude which provides the maximum lift to drag ratio for each segment of the cruise simulation. The design 7500 nautical mile range was simulated for both the baseline N3-X and the LH<sub>2</sub> variant. Previous results suggest that the chosen LH<sub>2</sub> configuration cannot achieve the target range of 7500 nmi. These simulations are therefore used only to provide a point of comparison. The cruise-climb version of the cruise performance simulation was allowed to select a cruise starting altitude which corresponded to the maximum lift-to-drag ratio for the defined weight and at the cruise Mach number. The climb segment therefore ends at a lower altitude than for the fixed altitude cruise segment. In this case, the starting altitude for the cruise segment was approximately 37,000 ft, 3,000 ft below the defined cruising altitude for the aircraft (Figure 4.34a). As the LH<sub>2</sub> aircraft variant is lighter at the end of climb than the kerosene aircraft, the starting altitude for climb is just 100 ft below the defined cruising altitude. Both aircraft end cruise at a similar altitude (41,380 ft for the kerosene N3-X vs 41,400 for the LH<sub>2</sub> N3-X), as the difference in weight at the end of cruise is small. Whilst the kerosene N3-X has a higher weight of fuel on board for descent, the weight of the LH<sub>2</sub> tanks results in a similar end of cruise weight for the LH<sub>2</sub> variant for the design mission range.

Whilst the aircraft's lift to drag ratio still decreases as the flight progresses, it is consistently higher than that achieved for the constant altitude cruise (Figure 4.34b). In addition, a shorter time spent at the climb engine power rating reduces fuel burn during the climb segment. The overall reduction in aircraft weight during the mission in combination with a more efficient flight profile leads to an improvement of approximately 2% in mission fuel burn for the design mission range. Further fuel benefits will also be possible for a fully optimised flight path including the climb segment.

Although a reasonable fuel saving is achieved for the kerosene variant, fuel saving for the LH<sub>2</sub> variant is less than 1%. As weight of the LH<sub>2</sub> aircraft changes less during cruise, the improvement in lift-to-drag ratio is minimal in comparison to that observed for the baseline kerosene N3-X (Figure 4.34b). There is therefore less benefit to cruise-climb operation for the LH<sub>2</sub> N3-X. Although there is little fuel benefit to adjusting altitude during cruise, there may be benefits elsewhere. Research by Svensson *et al.* on the Cryoplane LH<sub>2</sub> aircraft concept showed that a significantly lower cruising altitude may be advantageous for their concept [143]. As altitude has less influence on the LH<sub>2</sub> variant's fuel consumption than the kerosene variant, there will be less of a performance penalty to flying at a favourable altitude to reduce the occurrence of contrails. This may be important for an aircraft where the primary exhaust product is water.

## 4. Aircraft Performance Results

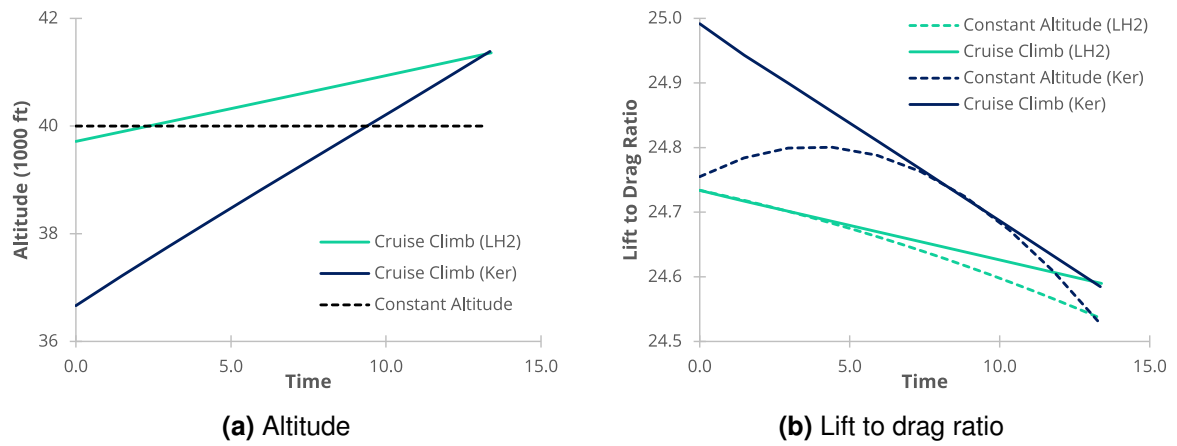


**Figure 4.34:** Cruise climb comparison to fixed altitude cruise

## 5. Alternative Propulsion System Configurations

The previous sections have focused on the baseline configuration for the N3-X as designed by NASA. However, there are a number of degrees of freedom in the design of the aircraft and its propulsion system that have the potential to provide further improvements in efficiency. It is therefore useful to perform a design space exploration to identify those degrees of freedom that have the greatest potential. These factors may then be taken forwards as a part of the technology roadmap for N3-X. This research focuses predominantly on the propulsion system design, as the more modular nature of the system provides a wider design search space. Whilst the design parameters explored herein focus on the N3-X configuration, many of the conclusions and design drivers are applicable to alternative configurations using similar technologies.

The N3-X propulsion system is comprised of three subsystems:

- Turbomachinery (power source)
- Propulsor Array (thrust source)
- Superconducting electrical system (power transmission)

These systems cover the power source, thrust source, and energy transmission elements of the propulsion system. In a conventional turbofan, all three aspects are combined in a single system. However, the modular configuration of a turbo-electric system provides more degrees of freedom in design. Each subsystem presents a number of variables that are useful to explore. Section 3.3 looked briefly at a number of design variables for the propulsion system, including the influence of location, size, and fan pressure ratio on a propulsor's performance. The simulations demonstrated that, even with only these few variables, there are opportunities for optimisation or improving performance.

In addition to the design variables for the propulsor array (such as fan pressure ratio, thrust per propulsor, inlet aspect ratio), the whole system design offers variables for optimisation. The baseline N3-X propulsion system design assigns all thrust producing capability to the propulsor array, with the turbogenerators producing power only. However, it may be beneficial to consider splitting the source of thrust between the turbomachinery and propulsor array. In addition, once the turbomachinery is producing thrust, it may be beneficial to make use of a turbofan rather than turbojet. This research focuses on the turbomachinery and propulsor array design. The superconducting electrical system also offers a wide range of design variables to explore. The focus of this research is on the propulsion system design in terms of the propulsor array and turbomachinery. More information may be found in other research on the design and configuration of the superconducting electrical system [46, 48, 144].

This research has assessed the potential of a LH<sub>2</sub> N3-X variant. However, the performance analysis in Chapter 4 identified that limitations on maximum fuel volume will limit the aircraft's range. Alternative configurations can therefore be considered to assess what design changes may be applied to increase the aircraft's range up to the design range. A number of alternative configurations were also considered for the LH<sub>2</sub> N3-X in Section 5.3 to explore the possibilities

offered by a  $\text{LH}_2$  variant of the N3-X.

The propulsor array presents a large number of design variables that it may be useful to explore. However, it is also useful to explore alternative propulsion system integration architectures. The analysis briefly compares the difference in performance that may result from utilising embedded rather than podded engines. Subsequently, the performance of an 'intermediate' N3-X option was simulated. This configuration simplifies the design by using conventional turbofans rather than the novel turbo-electric propulsion system used in the design of the N3-X. The configuration is treated as an intermediate step from a conventional tube-and-wing to a blended wing body, and finally to the N3-X with its novel propulsion system and airframe configuration.

### 5.1 Array Configurations

#### 5.1.1 Thrust Split

The baseline configuration focuses on a design where the entirety of the propulsive force is produced by the propulsor array at design point. Whilst some thrust may be produced by the turbomachinery at off-design (Table 3.3), the majority of the aircraft's thrust will be produced by the propulsor array for the duration of a flight. However, performance benefits may be possible by splitting the source of thrust between the propulsor array and the main engines. This introduces the thrust split parameter defined in Equation 3.49. Although the electrical transmission efficiency of a superconducting system is high in comparison to conventional electric machines, there is still power lost in the transmission system. Energy is also lost in the power turbine, as the turbomachinery is not 100% efficient. Benefits may therefore be gained by instead directly converting some energy into thrust in the turbomachinery, rather than losing energy in the generation and transmission of power. This also leads to a smaller propulsor array, as its thrust requirement is lower. Depending on how the array is scaled, this can avoid high speed flow at the extreme edges of the array and/or reduce the array height, with the associated performance benefits.

The net propulsive force produced by the propulsor array will depend on the selected thrust split. The remaining propulsive force requirement for the aircraft must be provided through the turbomachinery. For relatively high thrust splits, a turbojet may still provide reasonable efficiency. However, as a turbojet is not the most efficient configuration for producing thrust, turbofan configurations will be necessary as more thrust is required from the main engines. A turbofan configuration adds an additional optimisation parameter, as any given bypass ratio and engine configuration will have a fan pressure ratio that minimises the engine's specific fuel consumption. This minimum specific fuel consumption for the engines is not the same as the minimum effective specific fuel consumption for the propulsion system as a whole. Although there may be benefits to thrust split, reducing the thrust split will reduce the propulsor array size, and hence will reduce the high effective bypass ratio that results from a distributed propulsor array. A very low thrust split is therefore unlikely to be beneficial without compensating by including a high bypass ratio turbofan.

Depending on design-related factors such as intake total pressure loss, a fan pressure ratio that provides a minimum power configuration can be identified (Figure 3.19a). However, for the thrust split analysis, a constant fan pressure ratio of 1.3 was assumed and array length was kept equal to the length of baseline array. In each case, the net propulsive force required from the propulsion system as a whole is constant. The primary design variable is therefore thrust split and the main engine size. Any reduction in thrust from the propulsor array is obtained by reducing the height of the propulsors. In addition to a turbojet thrust split configuration, three

## 5. Alternative Propulsion System Configurations

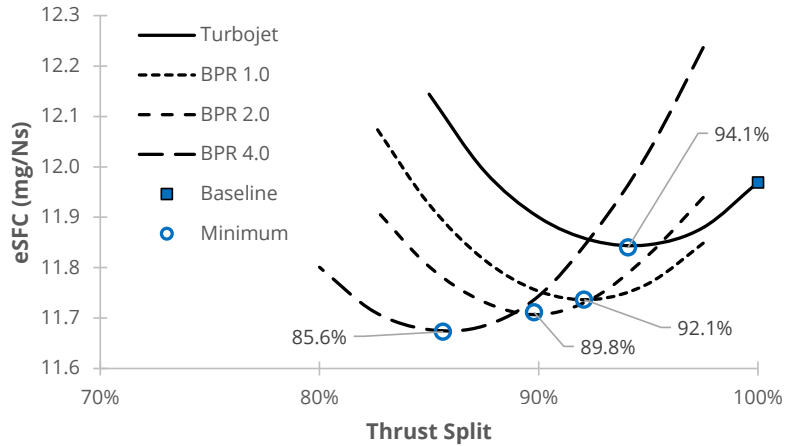


**Figure 5.1:** Specific fuel consumption as a function of thrust split and turbomachinery bypass ratio

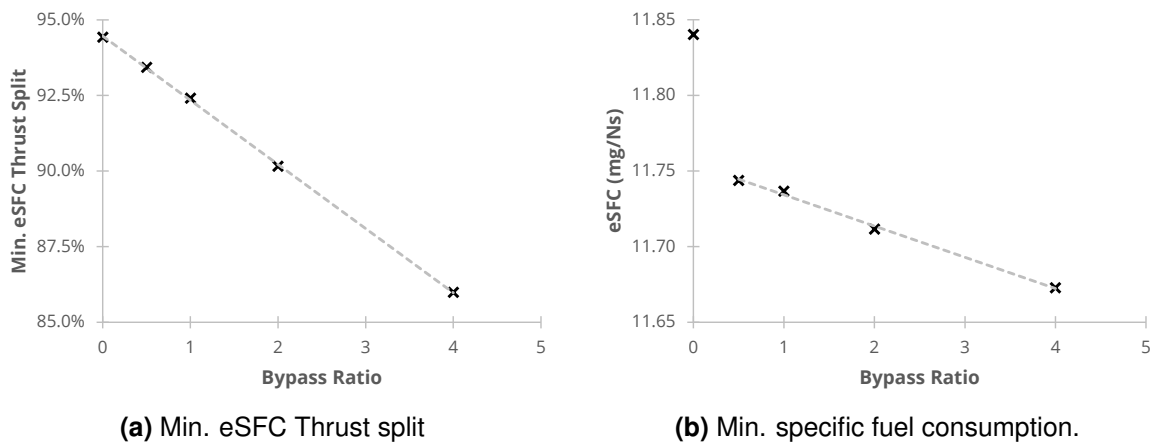


**Figure 5.2:** Bypass ratio influence over optimum thrust split and effective specific fuel consumption

turbofan sizes were considered with bypass ratios of 1.0, 2.0, and 4.0. In each thrust split case and for each turbofan configuration, an increase in thrust from the turbomachinery is obtained by increasing the mass flow and hence size of the engine. Fan pressure ratio for the turbofans in each case is selected to minimise the engine's specific fuel consumption. All other design variables are kept the same as for the baseline configuration of the N3-X turbojet (Table 3.1). As with the baseline turbogenerators, power and thrust required from the main engines are split equally between each of the two turbomachines.

By combining the use of thrust split with the optimum array fan pressure ratio, efficiency may be improved in comparison to the baseline configuration. For the turbojet configuration, specific fuel consumption is minimised at a thrust split of 94.1% (Figure 5.1). At this thrust split, the effective specific specific fuel consumption is approximately 1% lower than the effective specific fuel consumption of the baseline N3-X propulsion system. The thrust split for minimum eSFC decreases linearly with an increase in the bypass ratio (Figure 5.2a). A reasonable improvement in eSFC is provided in the jump from a turbojet to a turbofan, however, the eSFC levels off for further increases in turbofan bypass ratio. For turbofan configurations, the effective specific fuel consumption decreases linearly with an increase in bypass ratio (Figure 5.2b). For the purposes this study, the maximum bypass ratio is limited to values that may be compatible with an embedded engine configuration, as estimated from a model of the aircraft [145]. However, further efficiency improvements may be gained by further increases in bypass ratio for the main engines.

## 5. Alternative Propulsion System Configurations

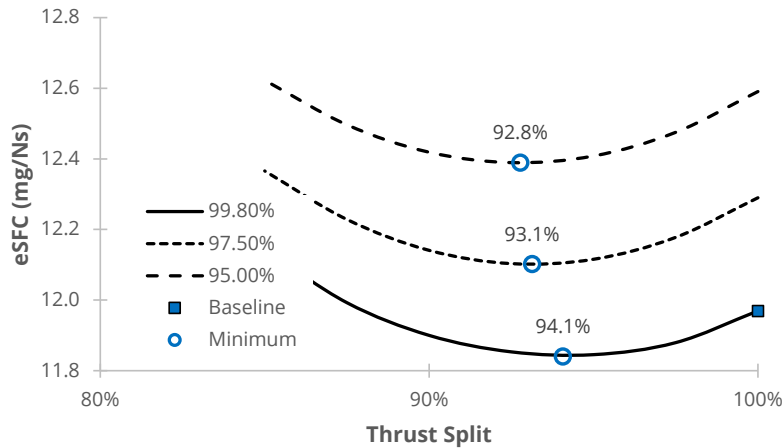


**Figure 5.3:** Effective specific fuel consumption as a function of thrust split and electrical transmission efficiency for a turbojet configuration

An optimum can be found with respect to thrust split due to the balance between the efficiency boost offered by the propulsor array, the efficiency of producing and transmitting power to the array, and the efficiency of producing thrust directly from the main engines. Increasing electrical transmission losses or reducing the power turbine efficiency will therefore reduce the minimum eSFC thrust split (Figure 5.3). Conversely, a more efficient electrical transmission system and power turbine will increase the minimum eSFC thrust split, as less power is 'wasted'. The main goal of the thrust split variable is to find a balance between the high efficiency offered by a distributed BLI propulsor array and an electrical power production/transmission system. If the production and transmission of power was 100% efficient, there would be little benefit to producing thrust from the main engines as opposed to the array (assuming minimal distortion or location-specific performance loss).

A different thrust split will lead to a change in the weight of the propulsion system. A dominant aspect of this change is the fact that a lower thrust split reduces the size of the propulsor array and the weight of the electrical power system, which accounts for approximately 75% of the propulsion system's weight (Table 3.5). Given the relationships used, the electrical system weight decreases linearly with thrust split. The propulsor weight similarly decreases linearly with a decrease in thrust split (assuming all other array design variables are kept the same). It is worth highlighting here that propulsors with a lower fan pressure ratio would be heavier, due to an increase in size. However, their lower power consumption would reduce the electrical system weight. As the array weight is the main component of the propulsion system weight, a reduction in thrust split leads to a reduction in the total weight of the propulsion system. A turbofan is heavier than a turbojet due to the addition of a fan bypass, leading to a higher weight than a turbojet for the same thrust split (Figure 5.4). The optimum configuration from the aircraft perspective must include the influence of thrust split over both the total weight and eSFC of the propulsion system. A configuration may be selected that minimises eSFC, however, this will not correspond to a minimum weight configuration. The influence of thrust split over mission fuel consumption can be found by combining both factors (Figure 5.5). For the turbojet configuration, fuel consumption can be reduced by 1.6% by using a 93.7% thrust split. This minimum fuel thrust split is slightly lower than the 94.1% thrust split that provides the minimum eSFC, as a slight benefit in fuel consumption is gained by reducing the propulsion weight at the expense of a slight increase in eSFC. Although the turbofan configurations have a higher weight than the turbojet configurations, the relatively larger eSFC improvement leads to an overall decrease in mission fuel consumption. In each case, the minimum fuel thrust split is approximately 1%

## 5. Alternative Propulsion System Configurations

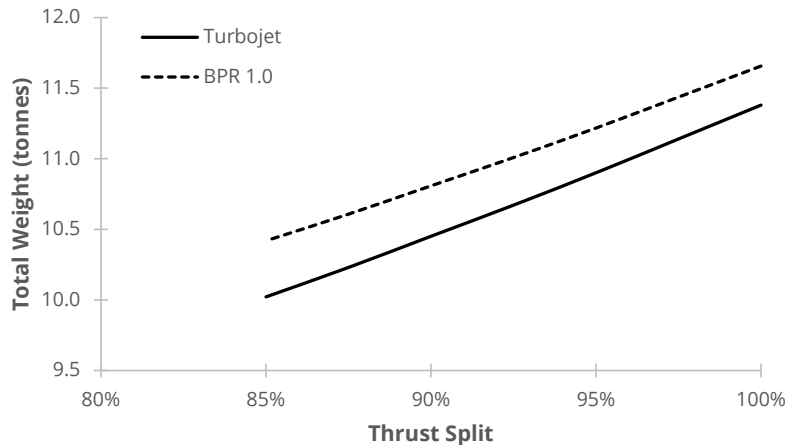


**Figure 5.4:** Total propulsion system weight as a function of thrust split

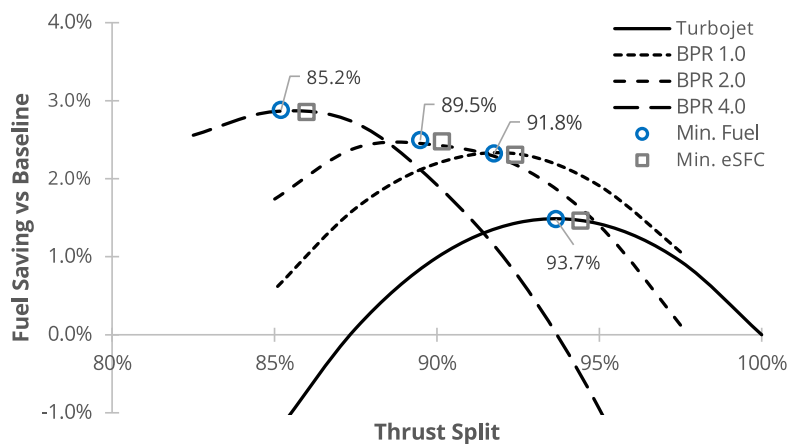


**Figure 5.5:** Fuel saving for a 7500 nmi mission as a function of thrust split

below the minimum eSFC thrust split. However, as the peak of the trend is relatively flat, the actually net difference in fuel consumption is less than 0.5%. As with the eSFC trend, there is a relatively large jump in fuel savings from a turbojet to turbofan configuration. Subsequently, fuel savings increase linearly with an increase in bypass ratio. The increase in weight from turbojet to turbofan means that the jump in fuel savings is not as large as the reduction in eSFC.

Performance of an example thrust split configuration may be compared to the performance of the baseline over the key operating points identified from previous research (Table 3.3). A configuration with a BPR 4.0 turbofan was selected, with thrust split and turbofan fan pressure ratio selected to minimise the specific fuel consumption (Table 5.1). The array is sized for a lower net propulsive force than the baseline array, and hence produces a lower net propulsive force at the key operating points. The slightly lower thrust of the propulsor array is counter-balanced by the higher thrust capability of the turbofans. The reduction in propulsor array size leads to a reduction in its specific power consumption for each operating point. Although a reduction in the propulsor array's size will reduce the effective bypass ratio, the introduction of the turbofans returns the effective bypass ratio to a similar level to the baseline propulsor array. Although the net propulsive force produced by the propulsion system is lower at SLS and RTO, the thrust produced still exceeds the take-off thrust targets established in previous research. This lower thrust is the result of a smaller propulsor array. Overall, the configuration leads to a lower eSFC than the baseline and a 2.3% improvement in the specific fuel consumption during cruise. In combination with a lower weight due to a reduction in array size (Table 5.2), this will

## 5. Alternative Propulsion System Configurations

**Table 5.1:** Performance of a sample thrust split propulsion system (Turbofan BPR = 4.0, Array FPR = 1.3)

	ADP	Cruise	RTO	SLS
Altitude (ft)	30000	40000	0	0
Mach Number	0.84	0.84	0.25	0
Engine				
TET (K)	1811	1728	1895	1922
Net Thrust (kN)	8.5	5.3	28.4	42.3
Power (MW)	15.2	9.2	27.6	27.6
Mass Flow (kg/s)	124.04	79.52	220.17	206.99
Fuel Flow (kg/s)	0.690	0.417	1.383	1.401
Array				
NPF (kN)	101.9	63.9	353.6	530.1
Mass Flow (kg/s)	1411.4	903.7	2728.6	2686.9
Power Consumption (MW)	30.3	18.5	55.3	55.2
Specific Power Consumption (W/N)	297.6	289.1	156.3	104.1
Propulsor RPM	100.0%	100.1%	91.4%	92.8%
Length (m)	20.1			
Propulsion System				
eSFC (mg/Ns)	11.60	11.19	6.74	4.56
eBPR	32.4	32.4	32.4	32.2
eST (N/kg)	71.7	70.1	129.5	198.3
NPF (kN)	118.9	74.5	410.4	614.8
Thrust Split	85.7%	85.8%	86.2%	86.2%

**Table 5.2:** Overall weight of a thrust split propulsion system (Turbofan BPR = 4.0, Array FPR = 1.3)

Component	Weight	% of Total
Distributed Propulsors (total)	4410 kg	40%
Turbofan (×2)	1650 kg	30%
HTS Generators (×2)	609 kg	11%
Motors (total)	1500 kg	14%
Misc. HTS	545 kg	5%
Total Weight	10980 kg	

reduce the fuel consumption of the aircraft.

### 5.1.2 Boundary-Layer Only

In the baseline propulsor array design, the array is required to ingest a portion of free-stream air in order to meet a propulsive force design requirement. However, given the profile of boundary layer flow, much of the momentum deficit is in the lower portion of the boundary layer. Ingesting free-stream air tends inlet flow characteristics towards the characteristics of free-stream air. Efficiency of the propulsor array is therefore lower than that of an array ingesting boundary layer air only. Hence the greatest boundary layer benefit is gained by ingesting only the boundary layer or slightly less than the entire boundary layer. It is therefore useful to consider whether there is any benefit to an array configuration designed to ingest only the boundary layer air.

A boundary layer-only array establishes a fixed size for each propulsor in the array equal to the thickness of the boundary layer. However, the array length and propulsor fan pressure ratio remain as design variables for the array. As with the previous analyses, the boundary



## 5. Alternative Propulsion System Configurations

---

layer thickness is assumed to be approximately constant along the width of each individual propulsor. An additional requirement that was applied to the designs is to assume that exhaust velocity must be greater than or equal to the free-stream velocity. This ensures that wake re-energisation takes place for the design. This limitation sets a minimum fan pressure ratio for each propulsor (FPR between 1.07 and 1.08, depending on location, for the N3-X configuration). Although the inlet stream height for the propulsors is fixed, the inlet width remains a design variable. A higher aspect ratio (wider) inlet enables more boundary layer to be ingested, bringing the associated downsides and advantages of a longer array. It will be assumed that the array length is equal to the length of the baseline array configuration to ensure that the same proportion of the boundary layer is ingested as the baseline array configuration. The only remaining variable is therefore the fan pressure ratio of the propulsors.

For an array sized to ingest only the boundary layer, the mass flow that may be ingested by the array is a fixed value and can only be influenced by a change in the array length. For a fixed array size, the net propulsive force can be increased only by increasing the fan pressure ratio (Figure 5.6a). The remaining propulsive force requirement for the aircraft must be provided through the turbomachinery. As the boundary layer-only propulsors are smaller than those sized for the fixed thrust requirement propulsors (119 kN, each propulsors produces 7.93 kN), their net propulsive force capability is lower. However, ingesting only boundary layer air leads to a more efficient array in terms of specific power consumption than an array ingesting a portion of free-stream air (Figure 5.6b). For example, the fan pressure ratio is 1.3 for the baseline array design. At this fan pressure ratio, the specific power consumption of the boundary layer-only array is 5.2% lower. Fan pressure ratio for a boundary layer-only array can increase up to approximately 1.5 before its specific power consumption exceeds that of the baseline array design.

Neglecting any change in distortion-related performance changes, specific power consumption will increase as the ratio of  $h/\delta$  is increased. For the propulsors sized for a fixed thrust, increasing the fan pressure ratio will decrease  $h/\delta$ , which is beneficial in terms of power consumption. The difference in specific power consumption between the two propulsors therefore reduces as fan pressure ratio increases. In both cases, an increase in fan pressure ratio leads to an increase in power consumption. In the case of the fixed thrust array, a clear minimum SPC fan pressure ratio is apparent. Although specific power consumption is lower, the high aspect ratio inlets (resulting from a fixed array length and inlet height) and low ratio of  $h/\delta$  will lead to a higher inlet total pressure loss. The boundary layer-only array is consistently more efficient than the fixed thrust array in terms of specific power consumption. However, there is a large thrust deficit, particular at low fan pressure ratios (Figure 5.6a), that means a reasonable percentage of the aircraft's thrust must be produced by the turbomachinery.

Location-specific difference in flow conditions mean that each propulsor in the array will perform differently as a function of its location (Figure 5.7), as was also observed for the baseline N3-X propulsor array configuration. The centreline propulsor is subject to the lowest speed local flow and the thickest boundary layer. The thicker boundary layer means a larger size propulsor, whilst lower speed local flow means a lower momentum drag. As a result, a propulsor at the airframe centreline is able to produce the most net propulsive force and has the lowest specific power consumption. As propulsors at the extreme edges of the array are smaller, the net propulsive force produced by each is lower than the inner propulsors (Figure 5.7a). For the outer propulsors, an optimum SPC configuration becomes apparent (Figure 5.7b). This is similar to the trend that begins to emerge in results for the fixed thrust array configuration and follows the same conclusions on the balance between power consumption due to location-specific flow characteristics and fan pressure ratio (Figure 3.26).

The boundary-layer only propulsor array configurations present a way of increasing the ar-

## 5. Alternative Propulsion System Configurations

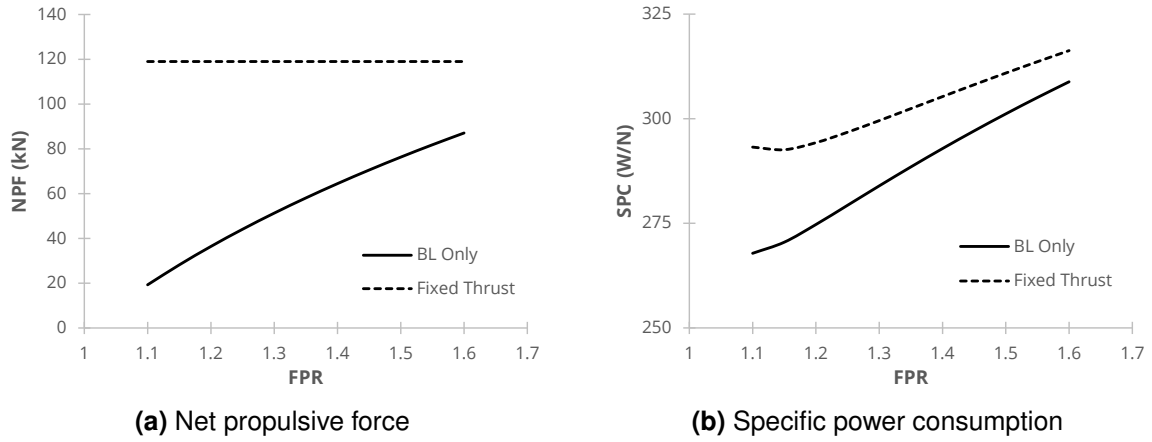


**Figure 5.6:** Performance of an array sized to ingest the boundary layer only compared to a fixed thrust array (20.1 m array)

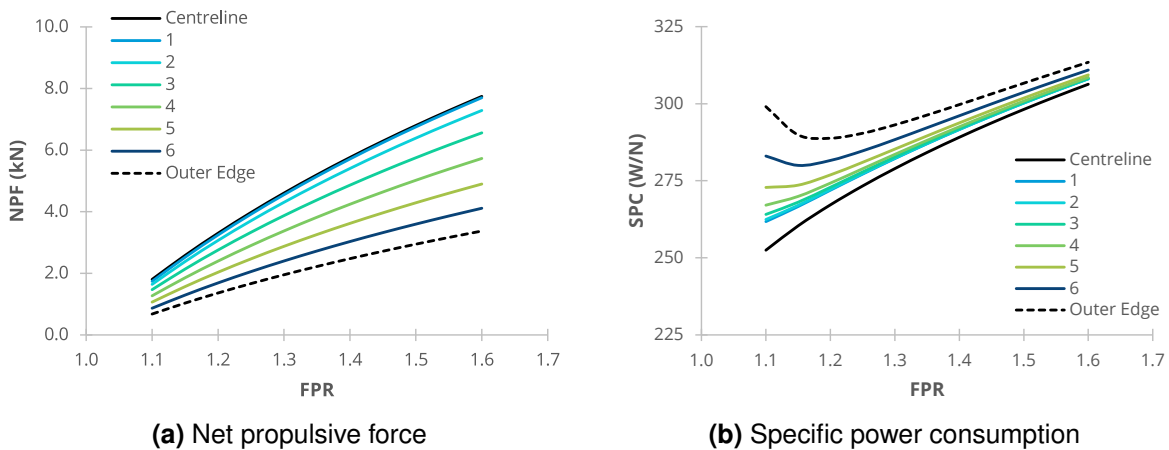


**Figure 5.7:** Individual fan performance for an array sized to ingest the boundary layer only (20.1 m array)

## 5. Alternative Propulsion System Configurations

---

ray's efficiency by reducing the specific power consumption. However, the smaller array leads to a reduction in the effective bypass ratio which will lead to a reduction in the overall efficiency of the propulsion system. Assuming a turbojet configuration, this loss in effective bypass mass flow is likely to lead to an increase in effective specific fuel consumption in comparison to the baseline array configuration. An additional bypass may therefore need to be introduced to compensate for the loss in efficiency by replacing the turbojets with a turbofan configuration. This is especially important for the low fan pressure ratio configurations, where the thrust requirement from the main engines is high.

Design decisions for a boundary layer-only configuration are comparable to the thrust split analysis in Section 5.1.1. As the array fan pressure ratio is decreased, the thrust split similarly decreases. Assuming a fan pressure ratio equal to that of the baseline array configuration (FPR 1.3), the resultant thrust split is 43%. However, Section 5.1.1 identified that the optimal thrust split in terms of eSFC is between 85% and 95%, for the considered range of turbofan bypass ratios. A higher array fan pressure ratio will increase the thrust split closer to this region, however, this will also increase the power consumption of the array. As a result, combining a boundary layer-only array with a turbojet results in a lower efficiency propulsion system than the baseline array configuration. The turbojet is required to produce a significant percentage of the total thrust, even where a reasonably high fan pressure ratio is selected for the array. Lower array fan pressure ratios reduce the thrust split and lead to a reduction in efficiency, whilst a high array fan pressure ratio leads to an increase in array power consumption. The effective specific fuel consumption for the turbojet configuration is minimised at an array fan pressure ratio of approximately 1.8 (Figure 5.8), corresponding to an 86% thrust split. However, this minimum eSFC is 7.8% greater than the eSFC of the baseline configuration. Although the array efficiency is higher than the baseline, the overall propulsion system efficiency is lower, as a larger percentage of the thrust is produced through the main engines. In addition, the fan pressure ratio of 1.8 for the propulsors means that the overall specific power consumption of propulsors in the array is higher than the baseline array with a fan pressure ratio of 1.3, even after accounting for the benefits of ingesting only the boundary layer (Figure 5.6b).

Introducing a bypass leads to a decrease in both the specific fuel consumption and the optimum thrust split. The optimum in terms of the array fan pressure ratio can therefore be lower. The reduction in specific fuel consumption is due to a combination of a lower fan pressure ratio for the array and the introduction of a turbofan to produce the remaining thrust. By extending the trend in Figure 5.8, the propulsion system could achieve an eSFC equal to the baseline value for a system combining turbofans with a bypass ratio of 10.5 and an array with a fan pressure ratio of approximately 1.55 (70% thrust split). This high bypass ratio engine could not feasibly be embedded within the airframe and would necessitate a change in configuration.

As with the thrust split system configuration, weight must also be taken into consideration for the overall performance of the aircraft. Although the simulated configurations have a higher eSFC than the baseline, they have lower weight (calculated using the method defined in Section 3.4). The smaller array power demand leads to a smaller, and hence lighter electrical system. In addition, the propulsors themselves will be significantly smaller and lighter. However, the main engines will be heavier due to a higher thrust requirement and hence larger size. The overall weight reduction nevertheless proves beneficial to the fuel consumption and performance of the aircraft during the course of a mission (Figure 5.9). Despite a weight benefit, the simulated configurations have a higher mission fuel consumption than the baseline N3-X configuration, due to the higher eSFC. In addition, the engine's weight increases as bypass ratio is increased. Therefore, fuel benefits achieved by increasing bypass ratio level off as bypass ratio is increased. By extending the trend in Figure 5.9 it is possible to observe that there is no configuration which can provide a positive fuel saving.

## 5. Alternative Propulsion System Configurations

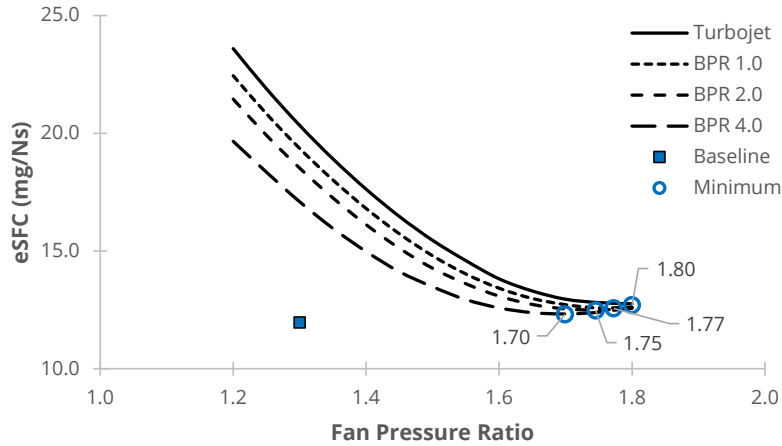


**Figure 5.8:** Effective specific fuel consumption for a fixed height array equal to boundary layer thickness

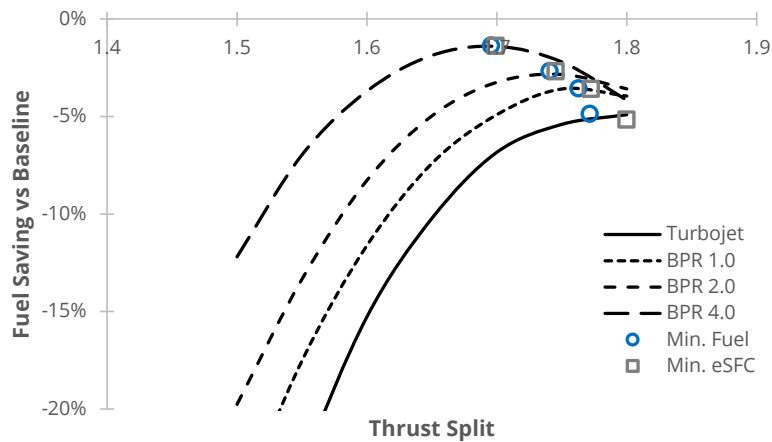


**Figure 5.9:** Fuel saving versus the baseline configuration for a fixed height array equal to boundary layer thickness

General conclusions can be drawn by combining the boundary layer-only configuration results with the thrust split results. For most thrust split configurations, it is more efficient to use a turbofan, as thrust can be more efficiently produced by a turbofan than turbojet. In addition, a reduction in thrust split, however it is gained, reduces loss of power due to inefficiencies in the power turbine or electrical transmission system. However, a large propulsor array provides a high effective bypass ratio (low specific thrust) as a result of the distributed propulsion system. A high thrust split is therefore generally better for performance as it implies a larger distributed propulsor array. The outcome suggests that there is little benefit to sizing the array to ingest boundary layer only. A boundary layer-only array increases the performance gains from ingesting the boundary layer, however, it reduces the performance gains from a large distributed propulsion system with a resultant high effective bypass ratio.

It is also useful to compare the design point configuration and off-design performance of the baseline array to that of an example BLI-only configuration: BPR = 4.0 turbofan with array FPR = 1.7 (Table 5.3 and Table 5.4). As the BL-only propulsor array does not ingest free-stream air, efficiency of each propulsor has the potential to be greater than the baseline design. However, the high fan pressure ratio necessary to reach a minimum eSFC leads to an overall increase in SFC versus the baseline array configuration.

Whilst the ADP and cruise NPF of the baseline and BL-only configurations is approximately the same, there is a noticeable divergence in performance at the RTO and SLS operation points

## 5. Alternative Propulsion System Configurations

**Table 5.3:** Performance parameters for individual fans in a propulsor array sized to equal the boundary layer thickness, FPR = 1.7, at the aerodynamic design point

	0	1	2	3	4	5	6	7
Power (MW)	2.70	2.68	2.55	2.30	1.97	1.66	1.42	1.17
Mass Flow (kg/s)	59.9	59.4	56.5	51.0	43.7	36.8	31.4	25.8
Highlight Height (m)	0.588	0.583	0.553	0.497	0.425	0.357	0.300	0.243
SPC (W/N)	315.4	315.4	315.5	315.6	315.8	316.2	317.3	319.9
$\eta_1$	0.9938	0.9938	0.9935	0.9931	0.9927	0.9921	0.9903	0.9877
$\eta_{\text{propulsive}}$	0.940	0.939	0.938	0.936	0.934	0.930	0.921	0.909
$h/\delta$	1.00	1.00	1.00	1.00	1.00	1.00	1.00	1.00

(Table 5.4). The propulsive force produced by the BL-only configuration is significantly lower than that of the baseline, leading to a higher specific fuel consumption. This is due to the difference in array size between the two configurations. As has been previously discussed, at very low speeds and high mass flow ratios, the benefits from boundary layer ingestion are negligible. The baseline propulsors are larger, due to their sizing requirements. They are therefore capable of producing significant propulsive force in the absence of the boundary layer. In contrast, the propulsors of the BL-only array are sized for the boundary layer thickness, and their maximum thrust is therefore lower. The additional thrust produced by the turbofan engines is not able to compensate for the lower thrust capability of a smaller propulsor array.

### 5.2 Propulsion System Optimisation

Previous configurations have simulated the propulsor array assuming that each propulsor is sized using the same key design variables and for the same net propulsive force per propulsor. However, as each propulsor is subject to different flow conditions, a more efficient configuration may be found by sizing each propulsor individually to minimise the power consumption. A number of these design variables have been addressed individually in Section 3.3. Based on these simulations, a number of conclusions can be drawn regarding the influences and benefits of the design variables. The main design variables for propulsor array that can be used as part of an optimisation are:

- Propulsor fan pressure ratio
- Propulsor inlet aspect ratio
- Net propulsive force per propulsor
- Number of propulsors
- Array length

Given the modelling assumptions, some of the design variables will lead to similar results from a performance analysis perspective. Inlet aspect ratio, the number of propulsors, and the propulsor array length are all interrelated variables that determine the propulsor array's size. They therefore tie into the overall trade-off between extending the propulsor array either up into free-stream flow, or along to the outer edges of the fuselage. Differences will arise between the design variables when considering factors such as the propulsion system weight (due to the number of motors/propulsors) or the pressure loss in the duct (following Seddon's formulation [107], or due to the transition from a rectangular to circular cross-section duct).

For the following analyses, a fixed number of propulsors was assumed. In addition, as reducing the array length would reduce the ingested drag percentage, the array length will be fixed to equal the length of the baseline propulsor array. The combination of these two assumptions removes the propulsor's inlet aspect ratio as a design variable. Inlet aspect ratio will

## 5. Alternative Propulsion System Configurations

**Table 5.4:** Performance of a propulsion system configuration with array sized to equal the boundary layer thickness (Turbofan BPR = 4.0, Array FPR = 1.7)

	ADP	Cruise	RTO	SLS
Altitude (ft)	30000	40000	0	0
Mach Number	0.84	0.84	0.25	0
Engine				
TET (K)	1811	1728	1895	1922
Net Thrust (kN)	11.8	7.4	34.0	48.8
Power (MW)	15.1	9.2	28.4	28.4
Mass Flow (kg/s)	131.89	84.56	234.12	220.10
Fuel Flow (kg/s)	0.733	0.443	1.471	1.490
Array				
NPF (kN)	95.3	59.8	288.5	379.2
Mass Flow (kg/s)	669.9	428.1	1340.1	1321.9
Power Consumption (MW)	30.2	18.4	56.8	56.8
Specific Power Consumption (W/N)	317.2	308.1	197.0	149.7
Propulsor RPM	100.0%	100.2%	90.5%	91.9%
Length (m)	20.1			
Propulsion System				
eSFC (mg/Ns)	12.32	11.88	8.25	6.25
eBPR	16.7	16.6	16.9	16.7
eST (N/kg)	127.5	124.9	197.1	270.5
NPF (kN)	118.9	74.6	356.5	476.7
Thrust Split	80.1%	80.2%	80.9%	79.5%

**Table 5.5:** Overall of a propulsion system configuration with array sized to equal the boundary layer (Turbofan BPR = 4.0, Array FPR = 1.7)

Component	Weight	% of Total
Distributed Propulsors (total)	1430 kg	18%
Turbofan (×2)	1650 kg	41%
HTS Generators (×2)	630 kg	16%
Motors (total)	1550 kg	19%
Misc. HTS	545 kg	7%
Total Weight	8085 kg	

## 5. Alternative Propulsion System Configurations

---

instead be determined by changes to the propulsor size resulting from changes to the remaining design variables. For the following propulsor array optimisations, a turboshaft configuration will be assumed with all thrust produced by the propulsor array. This enables the optimised configuration to be compared most easily against the baseline propulsor array configuration. As the propulsion system's thrust requirement is fixed, the net propulsive force is a constraint for the optimisation process.

There are three separate goals that can be used for the optimisation process, looking at either the propulsor array, the propulsion system as a whole, or the entire aircraft system. This means optimising in terms of specific power consumption, effective specific fuel consumption, and fuel burn, respectively. The previous analyses have shown that these may be conflicting goals, as a low specific power consumption may not equate to the minimum effective specific fuel consumption, which may not correspond to a minimum fuel configuration. Assuming that the engine design remains otherwise the same, a lower power consumption array will reduce effective specific fuel consumption. However, this is not the case where the engine design must be changed, such as with the use of thrust split. The following sections therefore compare the difference in outcomes between a configuration optimised in terms of the propulsor array performance alone (i.e. power consumption), and the aircraft performance (i.e. fuel consumption).

The optimisation presented in Section 5.2.3 makes use of an NSGA-II optimiser developed in previous research by Nalianda [146].

### 5.2.1 Array Fan Pressure Ratio

Assuming that all propulsors operate with the same fan pressure ratio, there may be an optimum fan pressure ratio for the propulsors that minimises the specific power consumption of the array as a whole (Section 3.3). However, each propulsor in the array is subject to different flow conditions. By applying the same fan pressure ratio to the entire propulsor array, some fans operate with a lower power demand than the baseline, and others with a higher power demand. The net outcome is a lower power consumption than the baseline propulsor array configuration. However, it is instead possible to optimise the fan pressure ratio for each propulsor individually. In this optimisation, a fan pressure ratio is selected that minimises the individual propulsor's power consumption and hence the total power consumption of the array. Each propulsor was assumed to produce the same thrust. Therefore, changing the propulsor's fan pressure ratio will lead to a change in the propulsor size. The minimum fan pressure ratio was capped at 1.1. The feasibility of very low pressure ratio propulsors is not assessed in this section. However, this may set a higher cap on fan pressure ratio than the values shown here.

The optimisation shows that the ideal fan pressure ratio increases from a low value at the airframe centreline (Propulsor 0) up to a maximum at the far end of the array (Figure 5.10). The propulsor at the centreline is therefore the largest, whilst the propulsor at the end of the array is the smallest. The fan pressure ratio for propulsors 0–3 meets the FPR cap set in the optimisation. The optimisation would otherwise lead to lower fan pressure ratios for the innermost propulsors. The highest power saving in comparison to the baseline is achieved by the propulsors nearest the centreline, as those deviate the furthest from the baseline fan pressure ratio. With this configuration, the total power saving versus the baseline configuration is 3.0%. In comparison, with a fixed fan pressure ratio of 1.13 for the entire array, the power saving is 2.4% versus the baseline. Individual fan optimisation therefore provides a relatively small performance boost over whole array optimisation. The best benefit is seen for the outermost propulsors. With a fan pressure ratio optimised for the array as a whole, this propulsor would have a higher fuel consumption than the baseline array configuration. However, there is a positive saving where fan pressure ratios are individually optimised. A lower fan pressure

## 5. Alternative Propulsion System Configurations

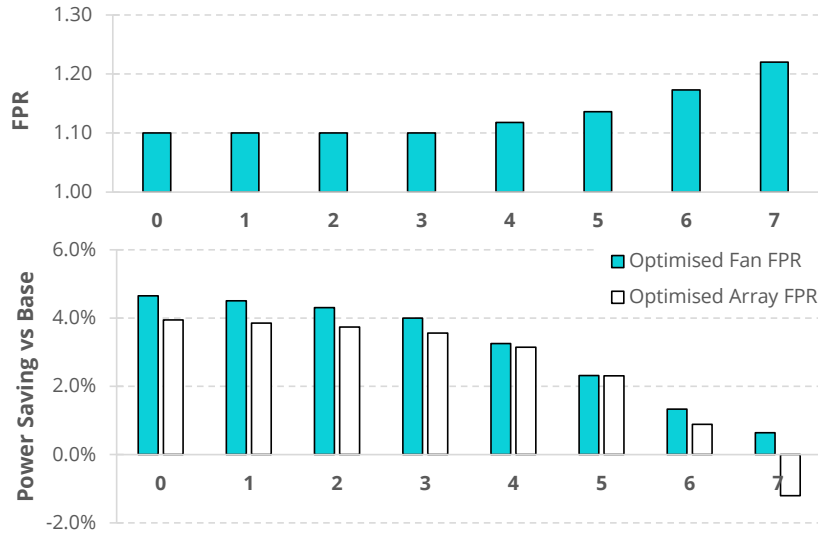


**Figure 5.10:** Optimum fan pressure ratio for individual fans and a 100% TS array in comparison to the baseline configuration and an optimum array fan pressure ratio configuration

ratio reduces the enthalpy change across the fan, leading to a decrease in power consumption. However, it also leads to an increase in the intake height and hence an increase in the ingested free-stream flow. As  $h/\delta$  is already reasonably low for the inner propulsors, there is less of a penalty to increasing their size than for the outer propulsors. The optimum fan pressure ratio is therefore higher for the outer propulsors, as this balances a change in  $h/\delta$  against the power demand resulting from a change in fan pressure ratio.

The lower power consumption would lead to a corresponding decrease in the effective specific fuel consumption of the propulsor array. However, although the low fan pressure ratio enables a lower power demand for the array (and hence lighter motors and generators), the low fan pressure ratio also leads to larger, heavier fans. The overall system weight is therefore 22611 kg, close to double the weight of the baseline propulsion system's weight which leads to a 9% increase in the aircraft's weight. As a result, the fuel consumption of the aircraft increases by approximately 6% versus the baseline configuration for the N3-X propulsion system. Given the influence of weight over the performance of the aircraft, propulsor weight is a vital part of a complete optimisation, as the weight increase will negate the benefits of the eSFC improvement.

The optimum fan pressure ratio is dependent on a wide range of other design and performance factors. In particular, inlet total pressure loss was identified as a parameter that leads to a lower effective fan pressure ratio, and hence increases the optimum fan pressure ratio. Higher total pressure loss in the propulsor intakes would therefore increase the optimum fan pressure ratio for each individual fan. As low pressure ratio fans are sensitive to distorted flow, this is a key factor to assess for further research on optimising the propulsor array.

### 5.2.2 Array Weight

There are two conflicting goals when considering the array design. A low eSFC is achieved by an array design with a low fan pressure ratio, as demonstrated in the previous analysis. However, a low fan pressure ratio implies larger and therefore heavier propulsors. In contrast, a higher fan pressure ratio will reduce the propulsor size and hence will reduce propulsor weight in exchange for a higher weight electrical system due to the increased power requirement. With



## 5. Alternative Propulsion System Configurations

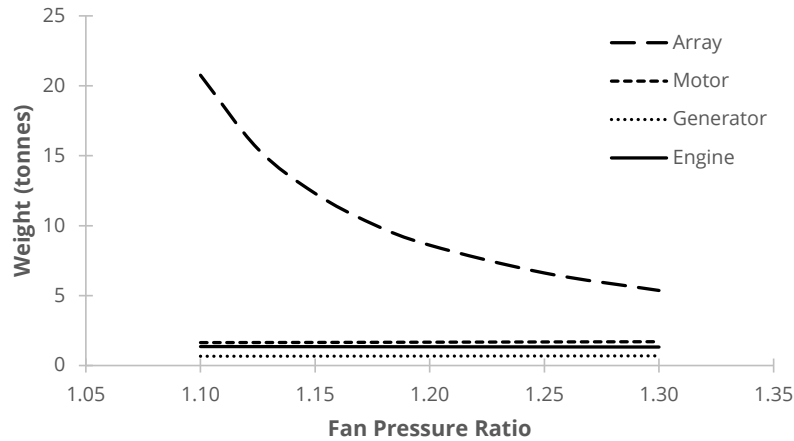


**Figure 5.11:** Influence of array fan pressure ratio on propulsion system weight

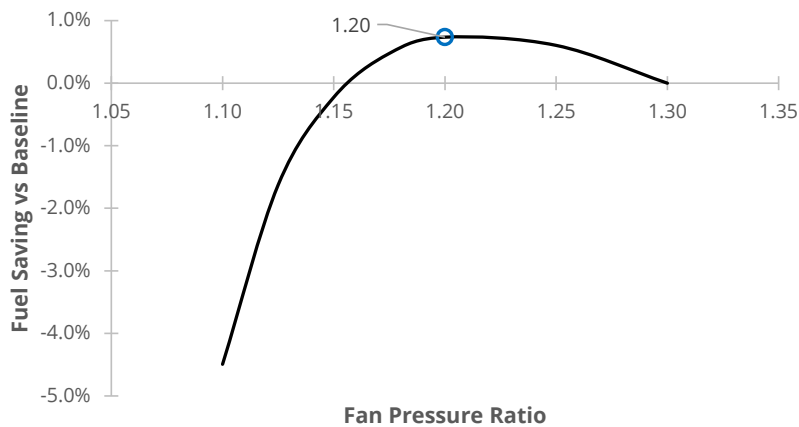


**Figure 5.12:** Influence of array fan pressure ratio on mission fuel consumption for a 7500 nmi flight

the weight relationships used, the decrease in electrical system weight is proportional to the decrease in the array power demand and hence the decrease in the propulsor fan pressure ratio (Figure 5.11). The main engine weight also decreases proportionally with the decrease in power requirement. However, the weight of the propulsors rapidly increases with a decrease in fan pressure ratio. As the propulsors are the dominant part of the overall propulsion system weight for a 100% thrust split configuration, the overall effect is an increase in the total weight of the propulsion system. In combination, there is no clear minimum weight configuration for the propulsor array.

Although a low fan pressure ratio system offers the best eSFC, the significantly higher weight is detrimental for fuel consumption. The optimum configuration from a fuel burn perspective will therefore be an array with a slightly higher fan pressure ratio than that which gives the minimum effective specific fuel consumption. This configuration has a lower weight at the expense of an increase in eSFC. Assuming each propulsor has the same fan pressure ratio and for the 100% thrust split configuration, the best fuel saving can be obtained for a fan pressure ratio of approximately 1.2 (as opposed to FPR 1.13 for minimum eSFC). However, this configuration reduces fuel consumption by less than 1%. Fuel consumption increases sharply with further decreases in fan pressure ratio, due to the higher overall weight and despite a lower eSFC (Figure 5.12).

## 5. Alternative Propulsion System Configurations

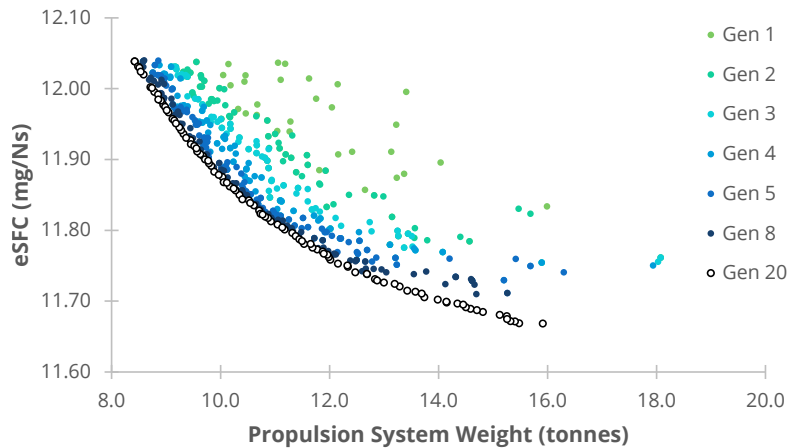


**Figure 5.13:** Pareto front of individual propulsor fan pressure ratio optimisation for minimum eSFC and array weight

### 5.2.3 Optimisation for Fuel

Both the effective specific fuel consumption and the aircraft weight will have an impact on the overall fuel burn on the aircraft. However, the previous two analyses have demonstrated that weight and eSFC are two conflicting goals, as a minimum eSFC configuration has a higher weight. Both Section 5.2.1 and Section 5.2.2 demonstrated that a configuration that minimises eSFC or the array's power consumption is therefore not the same as the configuration that minimises fuel consumption. This trade-off can be demonstrated by optimising the fan pressure ratio of each individual propulsor in the array with low fuel burn as the target, rather than eSFC or weight.

An NSGA-II optimiser developed by Nalianda [146] was used to assess the trade-off between eSFC and weight. As low weight and eSFC are conflicting goals, the combined analysis leads to Pareto front of results (Figure 5.13). The minimum weight that can be reached by the optimiser is limited by the maximum power that can be produced by the main engines at ADP, given the engine's design assumptions. As minimum weight corresponds to high fan pressure ratio and hence high power demand, there are some configurations for which the engine is unable to produce sufficient power. This point is visible as a cut-off point in the upper end of results for eSFC above approximately 12.04 mg/Ns. The results clearly demonstrate the trade-off between minimising the eSFC and minimising weight, as the goals cannot be achieved simultaneously.

A combination of low weight and low eSFC will lead to a minimum fuel burn configuration. The best configurations can be identified by predicting how weight and eSFC influence the fuel consumption for the design 7500 nmi mission (Figure 5.14). Better fuel savings are achieved by the low weight systems, despite a relatively higher eSFC. Whilst a low eSFC does lead to a fuel saving, array weight increases sharply with a decrease in fan pressure ratio (Figure 5.11). This increase in weight means fuel consumption quickly approaches that of the baseline N3-X configuration.

The best fuel saving is achieved by a configuration that balances a minimum eSFC against a minimum weight configuration. This configuration achieves a 1.4% fuel saving versus the N3-X baseline configuration. From the dataset of simulated configurations, the best fuel saving is achieved by using fan pressure ratios that are higher than those from the previous eSFC optimisation (Figure 5.15). The optimisation results in a relatively higher fan pressure ratio for the end and centre propulsors. Unlike the optimum from an eSFC only perspective, the lowest fan pressure ratio propulsor is in the half-span of the array, rather than the centreline of

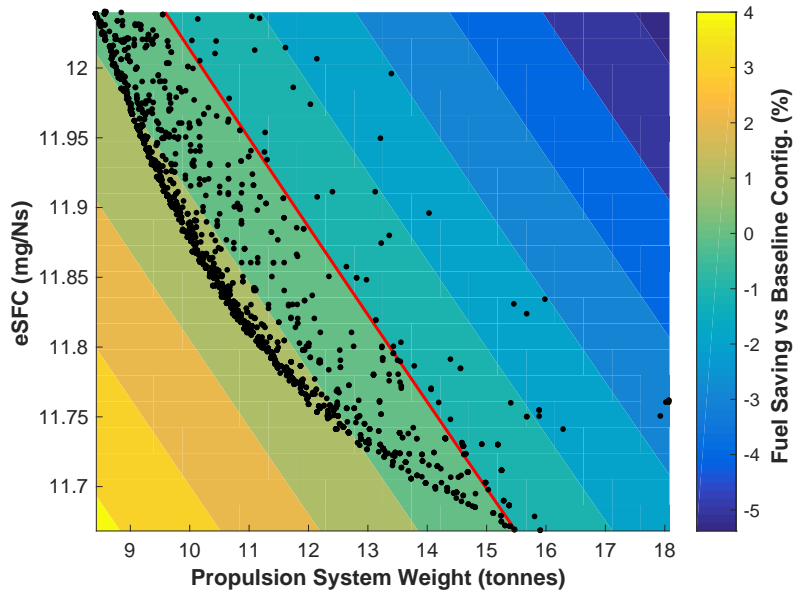


**Figure 5.14:** Pareto front of individual propulsor fan pressure ratio and fuel saving versus baseline N3-X configuration

the array. End propulsors are sized for the greatest mass flow and are hence the largest and heaviest. Therefore, a higher fan pressure ratio will provide the greatest benefit to weight. In addition to a lower weight, the smaller size means a lower ratio of  $h/\delta$  and hence a small increase in efficiency. In contrast, the centreline propulsors are the smallest and most efficient. As these propulsors have the lowest SPC, a slight increase in fan pressure ratio is less detrimental to overall performance than the same increase for propulsors further along the span. Therefore, their fan pressure ratio may be slightly increased to provide a weight improvement at the expense of a slight loss in performance. Propulsors in the middle of the array half-span trade off these two factors and hence have relatively lower fan pressure ratios than the end and centreline propulsors. These propulsors are smaller than the end propulsor, but have a lower efficiency than the centerline propulsor. The optimum fan pressure ratio is therefore relatively lower, as performance can be improved at the expense of an increase in weight.

The two extreme ends of the pareto front provide low weight and low eSFC configurations for the propulsor array, with the minimum fuel configuration combining elements of both. Higher fan pressure ratios leads to smaller, lighter propulsors. The minimum weight configuration from the pareto front therefore has the highest fan pressure ratios. The low eSFC configuration demonstrates the opposite, as a low fan pressure ratio leads to a lower eSFC (Figure 5.10). All three selected configurations demonstrate a similar trade-off between performance and weight as a function of location.

### 5.2.4 Combining Propulsion System Options

Excluding the boundary layer-only and podded engine configurations, many of the alternative propulsor array configurations presented in this section provide relatively small fuel burn improvements in the order of 1–3%. However, a more significant improvement can potentially be gained by combining the options assessed in each alternative configurations. Of the alternatives that have been assessed, there are three options that it may be useful to combine:

- Thrust split between main engines and propulsor array
- Turbofan replacement for turbogenerators (in combination with thrust split)

## 5. Alternative Propulsion System Configurations

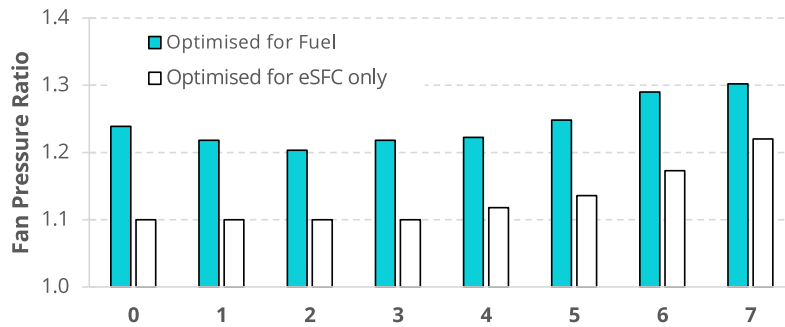


**Figure 5.15:** Fan pressure ratio for individual fans for a minimum fuel configuration in comparison to an eSFC minimum configuration

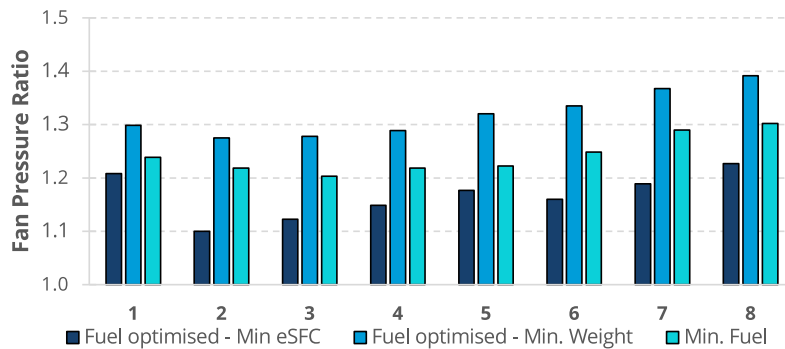


**Figure 5.16:** Fan pressure ratio for individual fans for a minimum fuel configuration in comparison to minimum weight and minimum eSFC configuration from the Pareto front

- Individually sized propulsors

Assuming each configuration option's fuel saving can be compounded, a turbofan (BPR 4.0) configuration with an optimised array (for both weight and eSFC) would improve fuel consumption by 3.5% versus the baseline N3-X configuration. This would lead to a further 1.5% improvement in energy usage versus the baseline B777-200LR aircraft model.

### 5.3 Alternative LH<sub>2</sub> Aircraft Configurations

Chapter 2 identified that liquid hydrogen has the potential to be a useful fuel for aircraft in the future. In addition to being a zero carbon emissions fuel, Section 4.7 demonstrated that the energy consumption of the LH<sub>2</sub> fuelled N3-X may be lower than that of the kerosene fuelled N3-X. This is primarily due to a reduction in in-flight weight of the aircraft during the course of a mission. In the sizing process for the propulsion system of the LH<sub>2</sub> N3-X, the propulsion system was assumed to be sized for the same net propulsive force as that of the kerosene aircraft (Section 3.5). However, a lighter aircraft implies that the propulsion system may be sized for a smaller thrust. Therefore, the following section will briefly assess a resized propulsion system for the LH<sub>2</sub> N3-X.

The tanks required to store LH<sub>2</sub> will increase the aircraft's operating empty weight, however, the dedicated fuel tanks do allow for some flexibility in how many tanks are carried on board the aircraft. It may therefore be useful to consider a configuration with removable tanks, whereby the number of fuel tanks on board the aircraft depends on the quantity of fuel required for the specific flight length. Although the energy consumption with LH<sub>2</sub> as a fuel has the potential to be lower, the maximum range of the configuration assessed in Chapter 4 is approximately 5400

## 5. Alternative Propulsion System Configurations

nmi. Whilst the LH<sub>2</sub> is a good low-energy alternative to the kerosene variant for missions up to this range, it cannot achieve the design range. It is therefore also useful to identify how the aircraft's range can be extended. For this research, a dual fuel configuration was considered. In this configuration, kerosene was utilised to extend the range of the aircraft up to the design range of 7500 nmi.

### 5.3.1 Resized Propulsion System

As the weight of the LH<sub>2</sub> N3-X is less than the kerosene N3-X during cruise, the aircraft's drag is lower. In addition, a lower weight enables a faster climb rate, assuming the same power setting is used for the propulsion system during the climb segment. As a result, the LH<sub>2</sub> variant can make use of a smaller propulsion system to provide similar performance to the kerosene N3-X. For the purposes of this analysis, it was assumed that the propulsion system should be sized to achieve the same climb rate as the baseline N3-X propulsion system at the aerodynamic design point (30,000 ft, Mach 0.84) and for the design 7500 nautical mile mission. At this flight condition, the climb rate of the kerosene N3-X is approximately 740 feet per minute. The LH<sub>2</sub> variant at the same point and for the same mission range achieves a climb rate of 1060 feet per minute. The remaining engine design parameters were assumed to otherwise remain the same as the baseline N3-X engine configuration (Table 3.1). Array design parameters are also retained from the baseline configuration, excluding the assumption that the width of each propulsor intake is equal to the fan diameter. The resized array is instead assumed to be the same length as the length of the baseline array, to ensure that the same proportion of the airframe drag is ingested. This resized propulsor array therefore has shorter intakes and hence a lower ratio of  $h/\delta$  than the baseline N3-X propulsor array. This is the main source of an eSFC benefit for resizing the propulsion system, as the engine design parameters remain otherwise the same.

In order to achieve the target rate of climb, the net propulsive force of the LH<sub>2</sub> N3-X array must be reduced by 10%. This reduces the effective specific fuel consumption at ADP by less than 1% (Table 5.7). The smaller array size also means the thrust produced at off-design is lower. For example, sea level static thrust reduces by 10%, in line with the 10% reduction in design point thrust. However, the smaller array size also reduces the propulsion system weight by approximately 1000 kg (Table 5.8), which partially compensates for the increase in weight resulting from the LH<sub>2</sub> tanks.

Although the resized propulsion system offers a reduction the effective specific fuel consumption, the resultant fuel consumption for the resized propulsion system is 0.8% higher than that observed for the larger propulsion system. This is a result of the assumptions made for the climb segment and the climb schedule. As both aircraft were modelled with the same climb schedule and engine power during climb, the larger systems is able to climb to cruising altitude more quickly than the smaller size propulsion system. As the difference in SFC between the two systems is minimal, the resized propulsion system does not provide enough of a fuel saving during the cruise segment to compensate for the increased fuel burn during climb. Therefore, given the modelling assumptions made, there is no benefit to resizing the propulsion system for the design mission. However, changes to the climb profile may change this result, as the resized propulsion system otherwise provides a lower weight and slight improvement in specific fuel consumption in comparison to the larger propulsion system.

As the requirements of the LH<sub>2</sub> and kerosene N3-X variants are different, it is likely that propulsion system design optimisation for the two systems would lead to different results. The present research has focused on the baseline kerosene fuelled configuration. Design space exploration for the LH<sub>2</sub> propulsion system is the subject for further research.

## 5. Alternative Propulsion System Configurations

**Table 5.6:** Performance parameters for individual fans in the resized propulsor array at the aerodynamic design point for the LH<sub>2</sub> variant

	0	1	2	3	4	5	6	7
Power (MW)	2.07	2.07	2.08	2.09	2.10	2.12	2.13	2.15
Mass Flow (kg/s)	96.6	96.7	97.0	97.5	98.1	98.7	99.2	100.4
Highlight Height (m)	0.911	0.911	0.910	0.909	0.907	0.905	0.903	0.900
SPC (W/N)	290.2	290.3	291.2	292.7	294.5	296.3	297.9	301.4
$\eta_1$	0.9948	0.9948	0.9950	0.9953	0.9958	0.9962	0.9967	0.9978
$\eta_{propulsive}$	0.944	0.944	0.942	0.939	0.936	0.933	0.930	0.925
$h/\delta$	1.52	1.54	1.62	1.78	2.04	2.36	2.76	4.25

**Table 5.7:** Performance of the resized propulsion system configuration for the LH<sub>2</sub> N3-X variant

	ADP	Cruise	RTO	SLS
Altitude (ft)	30000	40000	0	0
Mach Number	0.84	0.84	0.25	0
Engine				
TET (K)	1811	1728	1895	1922
Net Thrust (kN)	0.0	-0.1	3.4	7.2
Power (MW)	15.8	9.5	28.4	29.7
Mass Flow (kg/s)	20.82	13.24	39.71	40.56
Fuel Flow (kg/s)	0.220	0.131	0.441	0.462
Array				
NPF (kN)	107.0	66.4	365.0	565.4
Mass Flow (kg/s)	1471.2	937.2	2823.2	2834.9
Power Consumption (MW)	31.6	19.0	56.8	59.4
Specific Power Consumption (W/N)	295.4	286.5	155.6	105.1
Propulsor RPM	100.0%	99.7%	91.1%	93.8%
Length (m)		20.1		
Propulsion System				
eSFC (mg/Ns)	4.11	3.96	2.37	1.59
eBPR	35.3	35.4	35.5	35.0
eST (N/kg)	70.7	68.7	128.1	198.9
NPF (kN)	118.9	66.2	371.9	579.9
Thrust Split	100.0%	100.2%	98.1%	97.5%

**Table 5.8:** Overall weight of the baseline propulsion system configuration

Component	Weight	% of Total
Distributed Propulsors (total)	4585 kg	45%
Turbogenerator	1114 kg	22%
HTS Generator	629 kg	12%
Motors (total)	1550 kg	15%
Misc. HTS	545 kg	5%
Total Weight	10350 kg	

## 5. Alternative Propulsion System Configurations

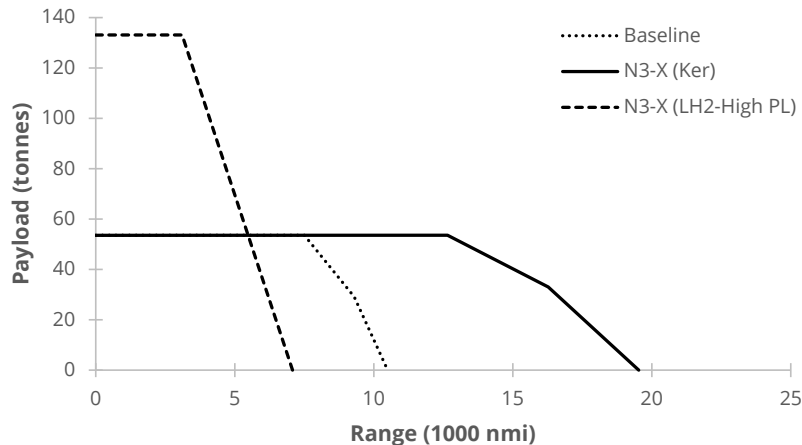


Figure 5.17: Payload-range chart prediction for the extended payload LH<sub>2</sub> N3-X

### 5.3.2 Extended Payload Capacity

The payload-range analysis for the LH<sub>2</sub> and kerosene N3-X showed that there is a significant difference in the maximum range of the two aircraft (Figure 4.25). However, it was assumed that both aircraft have the same maximum safe take-off weight as both aircraft have effectively the same structure (assuming the presence of the LH<sub>2</sub> fuel tanks and their support structure does not negatively impact the structural capabilities of the airframe). As the maximum weight of LH<sub>2</sub> on board the aircraft is significantly lower than the maximum weight of kerosene, there is significant additional capability for an increase in payload capacity for the LH<sub>2</sub> N3-X. It is therefore useful to consider an alternative configuration for the LH<sub>2</sub> N3-X that takes advantage of this additional weight allowance by extending the payload capacity up to the assumed maximum take-off weight of the aircraft.

Given the assumption made for the maximum take-off weight of the N3-X, a maximum payload of up to 133,100 kg (293,440 lb) may be possible for LH<sub>2</sub> N3-X. This more than doubles the payload capacity of the aircraft. With this payload and maximum take-off weight, the payload range achieved by the LH<sub>2</sub> N3-X is approximately 3110 nautical miles. As is to be expected, this is less than the 5400 nautical mile range achieved with the design payload of 58,570 kg.

A higher payload will naturally increase the mission energy consumption and hence reduce the energy saving versus the baseline aircraft. However the higher payload is more efficient from an energy-to-revenue-work ratio perspective, as a significantly higher payload is carried for a relatively smaller increase in energy consumption (Figure 5.18). From an ETRW perspective, saving versus the baseline aircraft is therefore greater for the extended payload LH<sub>2</sub> N3-X than for the standard payload LH<sub>2</sub> N3-X. However, as the extended payload N3-X is unable to achieve anywhere close to the design mission range of 7500 nautical miles, the configuration is unable to achieve the 60% savings target for the design mission.

The physical cargo space of the LH<sub>2</sub> variant may be limited by the presence of fuel tanks in the aircraft hold. It is nevertheless possible that the aircraft could be used for high volumetric density cargo. Nevertheless, the high payload capacity and low energy-to-revenue-work ratio suggest that a LH<sub>2</sub> variant may be applicable in high capacity cargo transportation applications for short- to medium-haul flights. The simulation suggests that a freighter variant of the aircraft could be a useful application for either the LH<sub>2</sub> N3-X, or for other LH<sub>2</sub> aircraft, as the low fuel weight enables a higher payload than kerosene aircraft.

## 5. Alternative Propulsion System Configurations

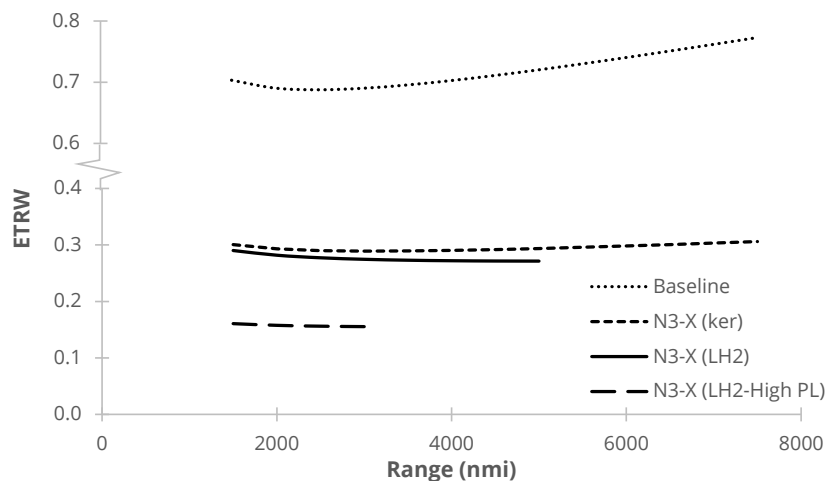


**Figure 5.18:** Aircraft energy-to-revenue-work ratio as a function

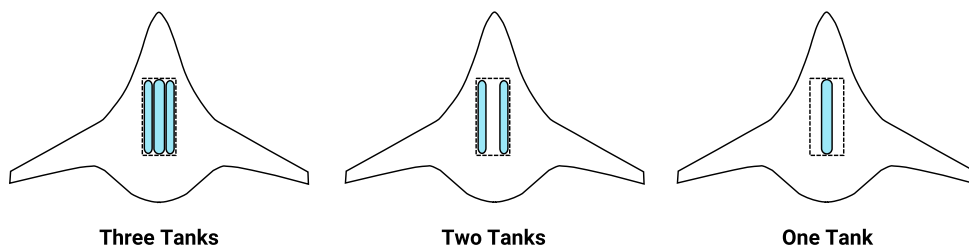


**Figure 5.19:** Sketch of removable tank configurations for the LH<sub>2</sub> N3-X

### 5.3.3 Removable Tanks

In the LH<sub>2</sub> N3-X, the LH<sub>2</sub> tanks add to the aircraft's operating empty weight, leading to an increase in energy consumption. For short range missions, it is likely that not all fuel tanks would be required to carry the fuel needed for a mission. As a result, there would be some mission ranges at which there would be unnecessary or useless weight on board the aircraft. However, the LH<sub>2</sub> fuel tanks are dedicated vessels, rather than incorporated in the wing structure as for a kerosene aircraft. These dedicated fuel tanks present the opportunity for an aircraft with removable tanks. In this configuration, fuel tanks could be removed when not needed, which would reduce the aircraft's weight during flight and hence reduce its energy consumption. The aircraft configuration could therefore be adapted to best suit the range over which it is to be operated.

The LH<sub>2</sub> tank configuration created for the aircraft consists of three tanks, one large tank at the aircraft's centreline, and two smaller tanks on either side. In order to ensure a centre of gravity at the aircraft centreline, it would be necessary to maintain a symmetric distribution of fuel tanks around the aircraft. Therefore, there are two potential sub-configurations: a single-tank configuration with only the central tank, and a two-tank configuration with the two side tanks (Figure 5.19). Each configuration would have a maximum range for which it was applicable, with the single-tank configuration being suited to short haul flights less than 2030 nautical miles, and the full three-tank configuration for medium/long haul flights from 3095 nautical miles up to the maximum 5380 nautical mile range (Table 5.9).

The reduction in aircraft weight leads to a decrease in the aircraft's fuel burn and hence a decrease in the energy to revenue work ratio Figure 5.20. There is a step increase in the energy-to-revenue-work ratio where the aircraft is required to swap between configurations. A removable tank configuration leads to an energy saving between 1–3% in comparison to



## 5. Alternative Propulsion System Configurations

**Table 5.9:** Fuel capacity and tank weight for removable tank configurations

	Three Tanks	Two Tanks	One Tanks
LH <sub>2</sub> Capacity (kg)	12,910	7,654	5,256
Tank Weight (kg)	5,480	3,640	1,841
Maximum Payload Range (nmi)	5,380	3,095	2,030

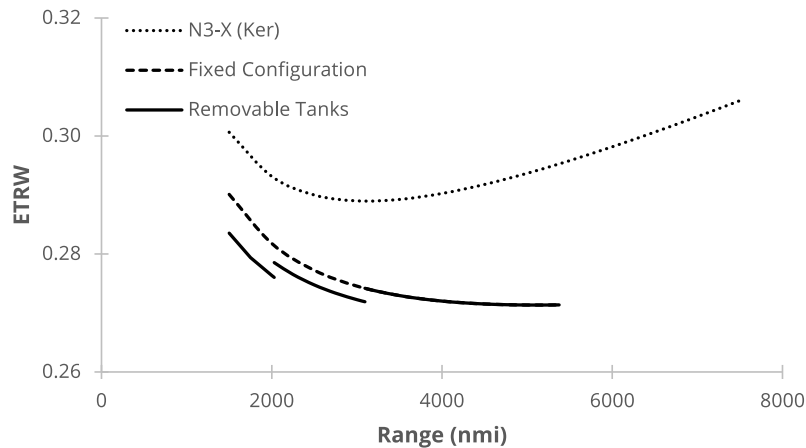


**Figure 5.20:** Energy to revenue work ratio for a removable LH<sub>2</sub> tank aircraft configuration

the fixed tank LH<sub>2</sub> N3-X, depending on the range and tank configuration Figure 5.20. There may therefore be a benefit to considering a removable tank configuration for the LH<sub>2</sub> aircraft. However, this assumes that the weight and cost of an aircraft with removable tanks is not significantly greater than the weight of an aircraft with a fixed configuration. Whilst this analysis has looked at the three-tank configuration from Section 4.3.3, further flexibility may be offered by offering a range of tank layouts to provide a good energy saving for a range of missions.

### 5.3.4 Dual Fuel

Subsection 4.7.1 demonstrated that the LH<sub>2</sub> aircraft variant would not be able to achieve the design range of 7500 nautical miles. One option for increasing the aircraft's range would be to add external fuel tanks to the aircraft or assign additional internal volume for the fuel tanks and hence increase the aircraft's fuel capacity. However, an alternative option is to consider a dual fuel aircraft configuration. In this configuration, additional kerosene could be carried on board the aircraft to extend the aircraft's range beyond the 5400 nmi maximum of the LH<sub>2</sub> aircraft. Alternatively, a fuel mixture of LH<sub>2</sub> and kerosene could be used throughout the flight to decrease specific fuel consumption of the kerosene N3-X and reduce the aircraft's weight during flight.

A mixed fuel configuration is outside the scope of the present research. This research therefore does not intend to make any suggestions as to the feasibility of an engine that is able to switch between different fuel types during the course of a flight. However, it is possible to estimate how much kerosene would be required to extend the aircraft's range up to the design range of 7500 nautical miles. In order to make this estimate, it was assumed that the aircraft first burns all of its kerosene fuel, then switches to LH<sub>2</sub> fuel. In addition, it was assumed that the diversion reserve is LH<sub>2</sub> rather than kerosene. In this way, the heavier fuel is used first, with less of the flight spent at a relatively higher aircraft weight. However, additional reserve fuel would be required for both LH<sub>2</sub> and kerosene (equal to 5% of the block fuel). The aircraft would therefore be required to carry a small amount of reserve kerosene during the entire flight.

The estimate assumes that the aircraft would first take off, climb and cruise initially using

## 5. Alternative Propulsion System Configurations

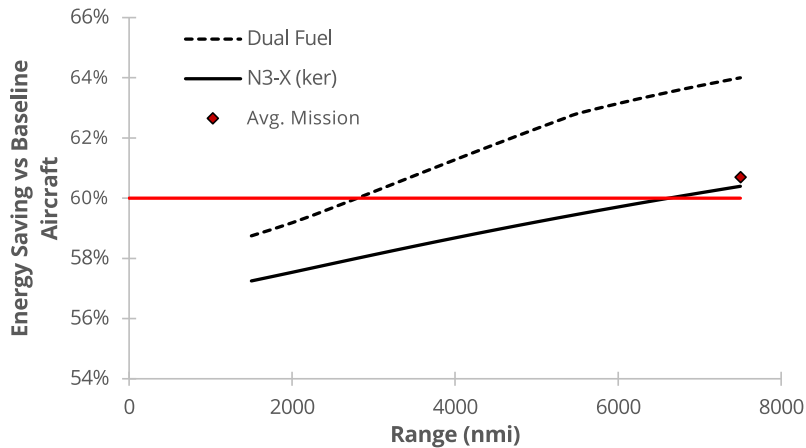


**Figure 5.21:** Energy saving versus the baseline aircraft for a dual fuel N3-X variant in comparison to the baseline N3-X

kerosene. Subsequently, the remainder of cruise along with descent and landing would use the LH<sub>2</sub> on board the aircraft. Therefore, the first stage of the analysis is to predict the maximum payload range of the aircraft using LH<sub>2</sub> and excluding the take-off and climb segments. Subsequently, the kerosene fuel required to carry the aircraft, payload, LH<sub>2</sub> tanks, and fuel LH<sub>2</sub> fuel load over the remaining distance can be estimated. The fully LH<sub>2</sub> N3-X variant is 2120 nautical miles short of the design 7500 nautical mile range (Figure 4.25). In the dual fuel case, the aircraft is only required to cruise, descend and land with LH<sub>2</sub> fuel, cutting out the fuel consumed during take-off and landing, as fuel used during these segments would be kerosene. However, it is also assumed that the aircraft would be required to carry reserve kerosene equal to 5% of the block kerosene fuel burn. This will increase the aircraft's weight during the second half of the flight and reduce the aircraft's range. The kerosene on board the aircraft is a function of the additional range that must be covered. An iterative procedure is therefore required to find the range that can be covered by the aircraft using LH<sub>2</sub> fuel whilst accounting for the additional weight of reserve kerosene carried during the second half of the flight:

1. Select a mission range
2. Guess kerosene on board aircraft
3. Calculate reserve kerosene (5% of block kerosene)
4. Calculate aircraft range covered by the aircraft burning LH<sub>2</sub> in cruise, descent, and landing
5. Calculate additional range to be covered by aircraft with kerosene
6. Calculate kerosene required to cover the additional range, assuming kerosene is used during take-off, climb, and part of cruise
7. Return to Step 3 until range covered by the aircraft matches the target range

This process is only required for ranges greater than the maximum range of the LH<sub>2</sub> variant. Ranges below this would be covered by LH<sub>2</sub> only, and so would not require additional fuel on board the aircraft.

Without accounting for the weight of the reserve kerosene, the aircraft is able to travel 5670 nautical miles if cruising, descending, and landing only. This range reduces to 5580 nautical miles once reserve kerosene is carried on board the aircraft, 1920 nautical miles short of the

## 5. Alternative Propulsion System Configurations

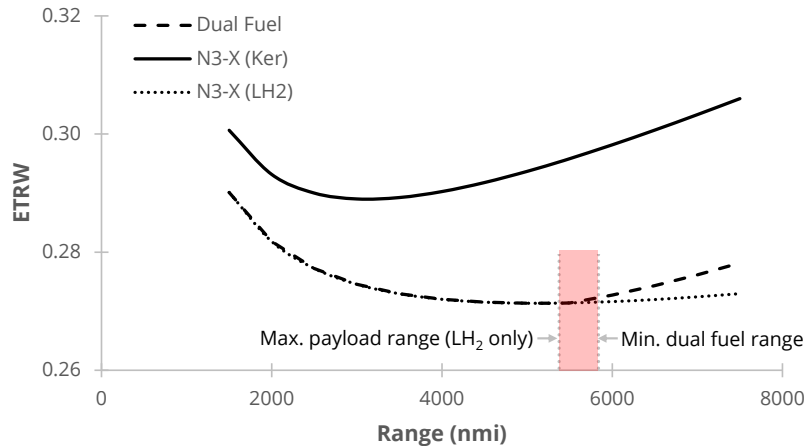


**Figure 5.22:** Energy to revenue work ratio for a dual fuel N3-X variant in comparison to LH<sub>2</sub> only and baseline N3-X (inapplicable ranges marked)

design range. In order to fly this initial 1920 nautical miles, 14,540 kg of kerosene would be required (not including the reserve fuel). In terms of kerosene fuel consumption, this configuration reduces fuel burn by 89% and energy consumption by 64% in comparison to the baseline aircraft for the design mission (Figure 5.21). The dual fuel variant is lighter during flight than the kerosene-only N3-X, as the majority of the flight is operated using LH<sub>2</sub> rather than kerosene. The resultant energy-to-revenue-work ratio is therefore significantly lower for the dual fuel configuration than for the kerosene only configuration (Figure 5.22). The higher weight of kerosene means that the energy to revenue work ratio diverges from the trend for a LH<sub>2</sub> only variant once kerosene is introduced to extend the aircraft's range. The dual fuel configuration nevertheless has a lower energy consumption than the kerosene-only configuration. Whilst this analysis focuses on a primarily LH<sub>2</sub> fuelled aircraft, the performance of a mixed fuel configuration will lie somewhere between that of the dual fuel configuration simulated in this section and the kerosene N3-X. The exact energy saving would be dependent on the split between LH<sub>2</sub> and kerosene on board the aircraft. Given the possible benefits of a mixed fuel configuration, this is a promising option for implementation on the N3-X or similar aircraft as it has the potential to provide a large reduction in hydrocarbon fuel consumption. It is possible that there is an optimal split between kerosene and N3-X that leads to the best combination of range capability and energy consumption.

The LH<sub>2</sub> variant would be able to operate using LH<sub>2</sub> only for distances up to the maximum LH<sub>2</sub> range of the aircraft. An increasing amount of kerosene would then be required as range increased above the maximum LH<sub>2</sub> aircraft range. The analysis in this research assumes that the fuel switch can occur during cruise only, in order to ensure that there would be no loss in power or rate of climb capability in the more critical climb segment. There are therefore mission ranges between 5376 nmi and 5830 nmi over which the dual fuel N3-X variant could not be used, as the fuel switch would occur during climb.

### 5.4 Alternative Integration Architectures

A pair of brief indicative studies were performed to provide an approximate estimate of performance changes due to alternative integration architectures. The following analyses use simplified propulsion system integration physics to provide an insight on performance. Future work should develop these analyses further.

The original N3-X configuration presented by Felder *et al.* proposed an aircraft with podded

## 5. Alternative Propulsion System Configurations

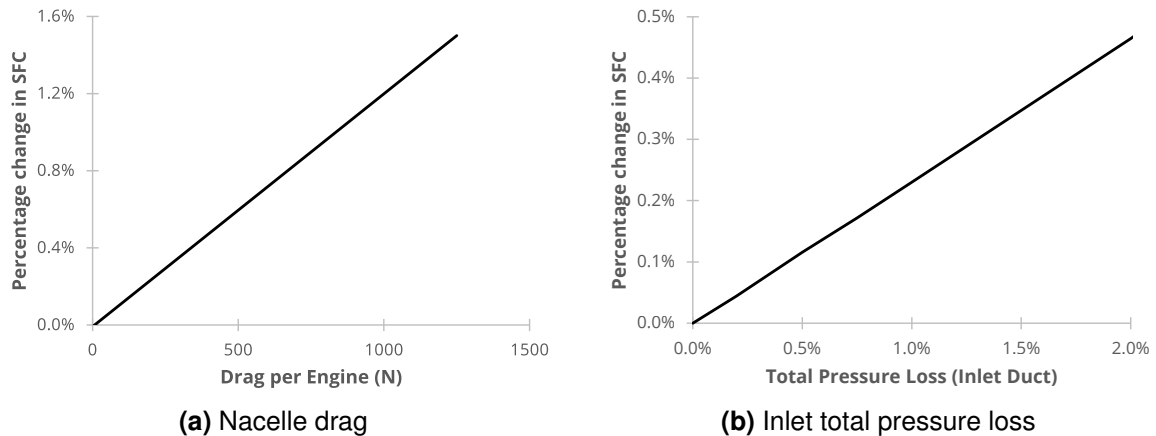


**Figure 5.23:** Influence of nacelle drag and engine inlet total pressure loss on specific fuel consumption of the baseline N3-X configuration

engines mounted on the aircraft's wingtips (2009 [24]). Further updates to the design by Berton and Haller in 2014 proposed a change to embedded engines to reduce the noise produced by the aircraft [88]. In a podded configuration, the engine nacelles produce drag that will contribute towards the total drag of the aircraft. In comparison, embedded engines have no nacelles and so can initially be assumed to contribute no drag to the airframe. However, depending on the length and configuration of the intake, there may be a total pressure loss from the free-stream flow to the engine face. Both nacelle drag and total pressure loss in the intake will negatively impact the performance of the aircraft and increase the specific fuel consumption. From this perspective, there is no obvious advantage for one engine configuration over another. It is therefore necessary to compare how either nacelle drag or total pressure loss in the intake duct will influence the propulsion system's efficiency.

The magnitude of the total pressure loss for an embedded inlet or drag for a turbogenerator nacelle will be depend on its configuration, the design of which is beyond the scope of this research. However, the nacelle drag estimate and resulting influence on specific fuel consumption can be used to identify a maximum acceptable total pressure loss. Any total pressure loss beyond this value would be more detrimental to efficiency than the nacelle drag, whilst any total pressure loss below this value would be less detrimental to efficiency than the nacelle drag. This enables a configuration to be selected that is less detrimental to the overall performance of the propulsion system and aircraft (Figure 5.23).

Further research and a more detailed design study would be required to identify the intake duct configuration and hence the duct total pressure loss to be expected for the embedded turbogenerators. However, a prospective location for the embedded engines was considered in the outer portion of the airframe fuselage to identify possible duct length for the embedded engine (Figure 5.24). The location was selected to ensure sufficient diameter for the turbogenerators and volume for the LH<sub>2</sub> fuel tanks (Figure 4.16). In the selected location, the embedded portion provided a length of approximately 9.1m for the engines. This location would therefore lead to a long intake and/or exhaust duct. The aerofoil shape of the fuselage also would also lead to a significant wetted surface area before and after the duct. An ideal location would have to bear in mind the importance of minimising or reducing total pressure loss resulting from a long duct and long wetted surface area ahead of the intake.

It is worth highlighting that, assuming a constant array length, the nacelle drag of the array does not change as noticeably for an increase in array size (i.e. height). The majority of the array's nacelle drag results from the upper nacelle surface, as the propulsors are embedded

## 5. Alternative Propulsion System Configurations

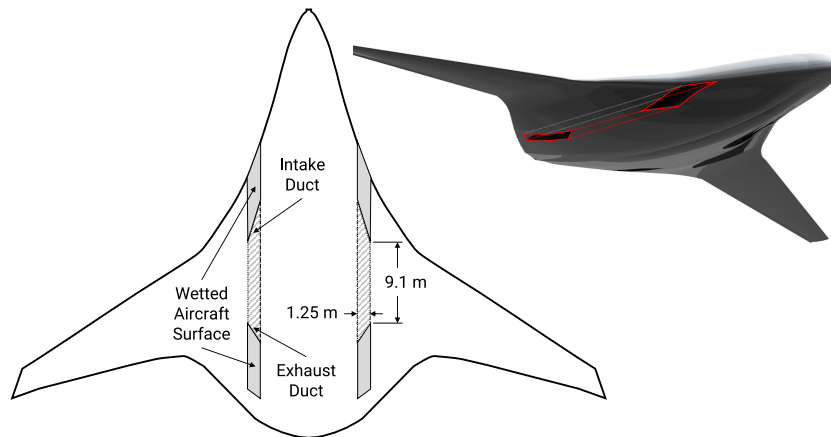


**Figure 5.24:** Representative sketch of embedded engine location and duct for the N3-X

in the airframe. Only the propulsors on each end of the array will contribute drag from nacelle side walls. Therefore, if the array length is kept constant, the nacelle drag changes little with a change in size. In contrast, change to the design of the turbomachinery will have a significant influence over the resultant nacelle drag. This is particularly apparent for a change from turbojet to turbofan, as the introduction of a bypass will increase the engine diameter for the same thrust, leading to a greater nacelle surface area and hence an increase in nacelle drag. This higher nacelle drag will naturally have a larger impact on the specific fuel consumption of the engines.

As an alternative configuration, an N3-X with a pair of podded turbofans can be considered, similar to the N2A configuration [24]. This configuration will be labelled the N3-I for the purposes of this research. Whilst a podded engine configuration will forfeit any benefits received from the distributed BLI propulsion system, it reduces the aircraft's level of complexity by utilising a conventional propulsion system. This was considered as a potential intermediate configuration that would enable development of the novel systems in the aircraft to take place in stages. In particular, low TRL technologies such as superconducting electrical systems for aircraft and boundary layer ingestion could be introduced and certified separately from blended wing body type airframes for aircraft (which are at a higher TRL level). This may also be advantageous from a cost perspective, as the development and ownership costs of a conventional propulsion system are likely to be lower than those of a novel propulsion system. This intermediate configuration also enables the performance benefits of the airframe configuration to be assessed reasonably independently from the propulsion system configuration.

A brief analysis was performed for the N3-I with a pair of high bypass turbofans. The airframe's configuration was kept unchanged from the configuration of the baseline N3-X. The propulsion system was replaced with a pair of high bypass turbofans producing the same propulsive force requirement for the airframe as was required from the baseline configuration (119kN). It was assumed that the engine's design variables remained predominantly unchanged, including the number of spools, component efficiencies, operating pressure ratio, and the design point altitude and Mach number (Table 3.1). In addition, the assumption of an equal enthalpy split between the high and low pressure compressors was maintained. The embedded turbojets/turbogenerators used for the N3-X would not be suitable for the N3-I configuration. A turbofan with a suitable bypass ratio must therefore be selected for the engine. As the efficiency of a turbofan increases in line with an increase in bypass ratio, there is no optimum value of bypass ratio that can be selected for the design. A bypass ratio of 10 was selected for the engines, consistent with the bypass ratios of modern or upcoming large turbofans in 2017 such as the GE9X, in development to improve upon the GE90-115B engines and intended for the next aircraft in the 777-series [147]. No other assumptions were made for the technology within

## 5. Alternative Propulsion System Configurations

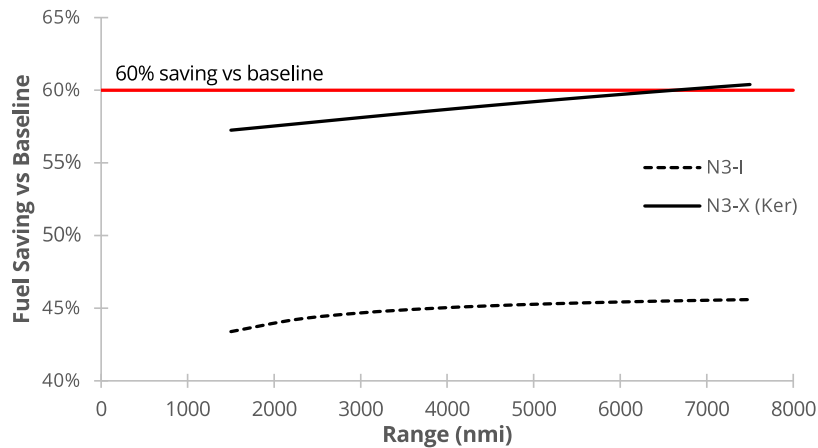


**Figure 5.25:** Fuel saving of the N3-I versus the baseline aircraft

the engine, such as a geared fan or combined cycles. A fan pressure ratio of approximately 1.5 and turbine entry temperature of 1485 K was selected at the aerodynamic design point for a minimum specific fuel consumption configuration. Nacelles were sized using the process presented in Figure 3.8, with drag calculated as part of the aircraft drag estimate (Section 4.1).

Previous analyses have shown that the baseline N3-X configuration has the potential to exceed the 60% energy saving target versus the baseline aircraft. A portion of this fuel benefit is the result of the BLI propulsor array, as the distributed propulsion system with boundary layer ingestion improves performance over a more conventional turbofan. For the design 7500 nautical mile mission, the N3-I reduces fuel consumption versus the baseline by 45.6%, rather than the 60.4% reduction achieved by the baseline N3-X configuration. This is due to the higher weight and lower efficiency of the two turbofan engines assumed for the configuration. Although the specific fuel consumption of the turbofans is higher than the N3-X effective specific fuel consumption, the N3-I turbofans nevertheless have a higher efficiency than the baseline engines, primarily due to a higher bypass ratio. The ‘evolutionary’ turbofans used for the N3-I therefore offer an 18% improvement in specific fuel consumption versus the baseline aircraft’s engines at cruise. In combination with the 30% improvement in lift-to-drag ratio, the fuel benefit versus the baseline aircraft is still significant. Therefore, as with the baseline N3-X design, the fuel saving achieved by the N3-I is a combination of both the higher lift-to-drag ratio of the airframe and a more efficient propulsion system turbofans. Note that this is a brief indicative study. For example, the analysis does not include the additional trim drag that may be result from providing an appropriate trim for an aircraft with a high thrust line.

## 6. Cost and Techno-economic Modelling

At the conceptual phase of aircraft such as the N3-X, the main focus of research is ensuring that the aircraft is able to meet technological performance targets and that technology can be brought to a suitable standard. For the purposes of this research, the target is a fuel consumption target versus a baseline aircraft. The previous chapters have identified the fuel consumption benefits of a conceptual aircraft, NASA's blended wing body N3-X. In addition, the possible performance improvements that may be gained by a selection of alternative configurations have been identified. However, a key aspect of the research is to establish whether these performance benefits can also lead to financial benefits. From an operator's perspective, the running costs of an aircraft are one of the most important factors to consider and aircraft must remain profitable to ensure a sustainable business. However, fuel is not the entire story once costs are taken into account. Operating costs account for a wide range of other factors such as maintenance costs or administrative costs. An aircraft may offer large fuel savings in comparison to alternatives, however, exorbitant costs elsewhere may entirely negate any cost benefits gained from a reduction in fuel consumption. An aircraft manufacturer will therefore aim to ensure that their new product is economically attractive for the customer. Costs are also very important from a manufacturer's perspective. The lower the manufacturing and development costs of an aircraft, the more easily a manufacturer is able to make a profit. In addition, a lower aircraft cost will be attractive to a customer, as it will be easier to make a good return on their investment.

Numerous new concepts and technologies are being proposed to achieve the challenging goals for the development of future aircraft. With so many concepts being created, there is a degree of uncertainty in determining where research focus is best placed and what the best option is for further development. For a commercial application, cost and economics are the dominant decision factor in selecting new technology. It is here that a techno-economic analysis becomes necessary. Chapter 2 identified a selection of perspectives and studies encompassed by the techno-economic analysis heading. However, there is a key challenge when attempting to perform the techno-economic analysis of a novel aircraft. For evolutionary aircraft, many costs can be predicted based on historical trends and engineering best guesses. For novel concepts, especially those that are not implemented in aviation, costs are almost entirely unknown as there is no historical value from which data can be extrapolated. In addition, the development costs associated with bringing a novel technology up from low TRL to commercial implementation may be significant. In many cases, such as superconducting machinery, the technologies do not exist at anything close to the level necessary for implementation on an aircraft. It is nevertheless vital to consider costs at the early development stage to ensure that technologies are economically feasible. This is especially true given that many costs are locked in at the preliminary design phase [69].

The focus of this section of the research was therefore on developing a model suitable

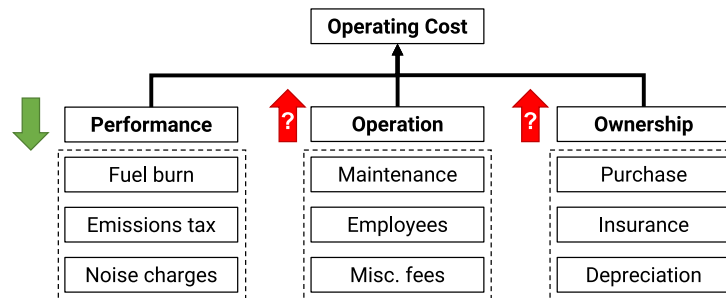


**Figure 6.1:** Sketch of operating costs for a novel aircraft

for assessing and comparing novel aircraft from a techno-economic perspective. However, as has been identified, there are many unknown costs in the development and operation of a novel aircraft. The chapter therefore first details the cost components that comprise the operating cost of a commercial aircraft (Section 6.2). This is then connected to an investment cost analysis methodology that assess the return on investment that an investor would receive from a new aircraft (Section 6.3). As costs for a novel aircraft are uncertain, this included a sensitivity analysis to identify how operating cost and return on investment are influenced by two key unknown costs: acquisition price and maintenance cost. Subsequently, acquisition price and maintenance cost estimates were created for the aircraft to identify where a novel aircraft might lie in the sensitivity analysis (Section 6.4 and Section 6.5). This also included the requirements and assumptions for modelling the N3-X. The cost estimates may then be used to determine whether a novel aircraft is likely to be economically viable, i.e. provide a good return on investment for an operator. Finally, the results for modelling the acquisition price and maintenance cost of the N3-X were identified (Sections 6.6).

### 6.1 Operating Cost in a Novel Aircraft

Operating costs may be roughly split into three groupings with a rough guess on how they change relative to a conventional aircraft (Figure 6.1). Performance costs include costs such as fuel consumption or emissions charges. As novel aircraft are designed to strict targets for energy use and emissions, it is a given that these will be lower than a conventional aircraft. These costs may be reasonably easily obtained via performance modelling to obtain fuel consumption and CO<sub>2</sub> emissions levels for the novel aircraft. The next grouping is the operations cost, covering costs that result from the day-to-day operation of the aircraft such as maintenance costs, landing costs, and employee salaries. It is reasonable to assume that operations costs, and particularly maintenance costs will be higher for a novel aircraft than a conventional one. Finally, there are ownership costs that must be paid regardless of whether an aircraft is flown daily or not. This includes costs such as those related to the purchase of the aircraft (e.g. interest repayment on the purchase) and insurance of the aircraft. These are again likely to increase for a novel aircraft. These can be reduced to two key factors: acquisition price and maintenance cost [78]. It may be reasonably safe to assume that both these costs will be higher than those of a conventional aircraft until novel technologies become well established.

The magnitude of cost for each of these two cost factors is unknown and will remain uncertain until concepts advance past the preliminary design phase. However, as cost has already been identified as an important factor in decision-making, a method is required that can be used to account for costs. Here a reverse approach becomes useful. Whilst costs are unknown, it is still possible to determine the costs for which an aircraft is no longer an attractive concept. For an aircraft such as the N3-X, this is the acquisition and/or maintenance price at which savings



## 6. Direct Operating Cost

---

due to a reduction in fuel consumption are cancelled out. A manufacturer may then set a target cost and determine whether such a cost is likely to be feasible. This perspective considers performance benefits from an operator's or financier's perspective by presenting the financial value of a performance benefit. The greater the performance benefit versus a baseline aircraft, the higher price that can be charged by a manufacturer whilst still presenting an attractive product.

A vital aspect of the complete techno-economic analysis of the N3-X or any aircraft is a suitable operating cost estimate. The first stage in creating an analysis is therefore to create an operating cost model encompassing the main cost factors in the operation of an aircraft (Section 6.2). The goal of an investment is not only to make a profit, but to make enough of a profit to justify the initial investment cost. The goal is that an investment should provide a larger return than investing the funds elsewhere. The greater the return, the more attractive the product. This return on investment can then be a proxy for the viability of a product. It is therefore useful to present an investment cost analysis perspective when considering the economic benefits of a product (Section 6.3). An investment cost analysis takes a long term view over the entire life of the aircraft to identify whether potentially high initial investment is justifiable. In the case of a novel aircraft, the costs needed to establish the direct operating costs and return on investment are unknowns. However, it is possible to identify the sensitivity of operating cost and economic viability to the unknown costs. A sensitivity analysis can then produce an estimate of where the aircraft would no longer be attractive for an operator and hence where it would no longer be economically viable.

The sensitivity analysis forms the core of the economic viability assessment of the aircraft. A higher maximum viable cost for the aircraft implies that a manufacturer has greater margin for increased costs during development and manufacture, whilst still retaining an attractive aircraft for a customer. An operator can also be more certain whether there is value to investing in the aircraft. The margin is a useful measure of the financial value of performance benefits, as a higher performance benefit can lead to a higher sale price for the aircraft and hence greater profits for the manufacturer. From the operator's perspective, performance benefits can be measured as a potential return on investment or operating cost benefit.

### 6.2 Direct Operating Cost

The economic performance of a product or project may be represented by identifying the operating cost and revenue produced. Operating cost may be split into two components, direct and indirect costs [13]. Direct costs can be easily associated with a project, such as materials, labour, or maintenance. Indirect costs are typically more difficult to attribute to a single project, and will include administrative staff salaries, advertising costs, and similar miscellaneous costs [148]. Although indirect operating costs must be included in a company-wide assessment, it includes costs which may be distributed over a range of projects. Therefore, direct operating cost is more useful as a point of comparison between individual aircraft. For the present study, the project in question is the purchase and operation of a novel aircraft concept from the perspective of an airline operator. Costs related to such a project are therefore the purchase, ownership, and running costs of an aircraft [13]:

- Fuel
- Emissions taxation
- Maintenance (engine and airframe)
- Insurance
- Depreciation
- Interest repayment (Amortisation)
- Crew salary

## 6. Investment Cost Analysis

Direct operating costs may also include landing and service fees, however, these are airport and country specific. This represents one business model for the operation of aircraft. Other avenues of aircraft operation are also prevalent, such as leasing. Aircraft may also be financed partially by investing capital rather than entirely through debt. For the purposes of this research, direct operating cost has been split into three sub-groups: time, fuel, and emissions costs (Figure 6.2). Fuel and CO<sub>2</sub> emissions costs are inter-related, with both being a function of the aircraft energy efficiency, fuel consumption, and engine characteristics. Both costs can be determined from aircraft mission simulation and depend on the mission type alone. The emissions taxation component enables the simulation of alternative scenarios and policies, such as carbon taxation. The time cost component consists of costs associated with the purchase and ownership of an aircraft, including insurance cost, crew salary, interest, depreciation and maintenance. These components are financial rather than performance related and can contribute around three quarters of the overall aircraft operating cost [13]. Assuming the aircraft is purchased through financing - rather than leased - interest on the purchase cost must be repaid over the aircraft life. Depreciation is not a direct outflow of money, however, it represents the decrease in value of the aircraft over its life. Assuming a straight-line depreciation method, the depreciation cost per year of an aircraft with value  $X$  at the start of its life may be calculated as follows [13]:

$$C_{\text{depreciation}} = \frac{X(1 - \text{residual}\%)}{\text{life}} \quad (6.1)$$

The useful economic life and residual value of an aircraft at the end of its life depends on aircraft type and operator policy. The economic life of aircraft will typically lie anywhere between 5 and 30 years with a residual value from 5–20% of the aircraft's initial value [149]. For this research, residual aircraft value was assumed to be 10% of the initial value over a 20-year useful economic life. Insurance cost depends on the risk of operation, and was assumed to be 0.5% of the aircraft value per year for the present research [13]. The costs in the time cost grouping are generally per unit time costs rather than per flight costs, and the cost assigned per flight cycle will therefore depend on the number of flights the operator runs per year as well as the mission type. For example, interest, insurance, depreciation and crew salary are yearly terms. The cost per flight will therefore depend on the aircraft's utilisation. More flights per year means these costs can be more widely distributed over the total yearly flights.

The overall direct operating cost per flight cycle (FC) is the sum of all the cost components:

$$\text{DOC} = M_f C_{\text{fuel}} + M_{\text{CO}_2} C_{\text{CO}_2} + C_{\text{maint}/\text{FH}} \text{FH} + \frac{X}{\text{FC}} \left[ \text{insurance}\% + \text{interest}\% + \frac{1 - \text{residual}\%}{\text{life}} \right] + \frac{C_{\text{crew}}}{\text{FC}} \quad (6.2)$$

Performance model outputs can be used to provide the fuel cost as the multiple of block fuel burn,  $M_f$ , and the current fuel price,  $C_{\text{fuel}}$ , and the CO<sub>2</sub> emissions cost as the multiple of block CO<sub>2</sub> emissions,  $M_{\text{CO}_2}$ , and the current charge per unit CO<sub>2</sub>,  $C_{\text{CO}_2}$ . Maintenance cost is the multiple of the maintenance cost per flight hour,  $C_{\text{maint}/\text{FH}}$ , and the flight block hours, FH. The remaining terms are the yearly insurance cost, interest repayment, and depreciation. Insurance, interest, and residual are all represented as percentage values of the aircraft acquisition price,  $X$ . Finally,  $C_{\text{crew}}$  is the total crew salary per year.

### 6.3 Investment Cost Analysis

Investment cost analyses are often performed to assist in project and investment decisions. Amongst some of the methods available, the application of the concept of Net Present Value

## 6. Investment Cost Analysis

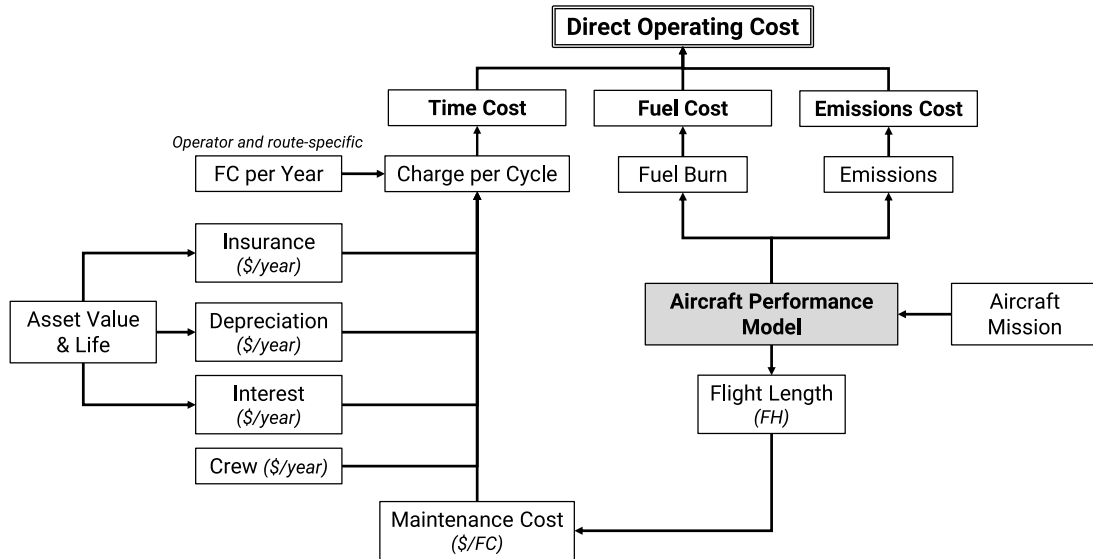


**Figure 6.2:** Breakdown of direct operating cost model components for an aircraft ownership model

(NPV, Equation 6.3) is quite prevalent. In a basic sense, a project offering the best net income over time should be the most attractive option. However, this is not always the case, as money has a time value. In many cases, an income of \$100 today is better than the same money provided a year in the future or over the course of a number of months. This is due to the fact that money now may be used or invested elsewhere, whilst money in the future is not yet available. Equally, expenditures in the future are less significant than expenditures required now. The net present value is therefore a way to represent opportunity cost of a project, i.e. the loss of an opportunity to invest in an alternative project. NPV is an economic valuation concept that weights profit and loss according to their distance in the future by making use of a discount factor,  $r$ , for the cash flow term:

$$NPV = \sum_{n=0}^{\text{life}} \frac{C_n}{(1+r)^n} \quad (6.3)$$

Where  $C_n$  is the cash flow in each year of the project or product life cycle. In general, the discount factor in a net present value analysis represents the return on investment that is required from a project for it to be attractive. A value such as the interest rate can therefore be used, as this would represent the return that would be achieved if the money was instead invested in a location such as a bank or savings account. Often, the discount factor applied is the weighted average cost of capital (WACC). Generally, finance is obtained through a combination of debt (e.g. borrowed money) and equity (e.g. stocks and shares). WACC is an average of these two finance methods, weighted by their use within the company [13]:

$$WACC = r_d \left[ \frac{\text{Debt}}{\text{Debt} + \text{Equity}} \right] + r_e \left[ \frac{\text{Equity}}{\text{Debt} + \text{Equity}} \right]$$

The value then represents how much a company owes to its debt and equity holders, where a higher WACC means that more income is owed to investors. The weighted average cost of capital is therefore useful in an investment cost analysis, as it sets a minimum acceptable rate of return. Any rate of return lower than this value implies that a project is not profitable, as more money would be paid out for the financing cost than is being made from the project. For example: a project is financed by a \$100 investment with a 50:50 split of capital from lenders and shareholders. The lenders require repayments of 10% of the initial money lent

## 6. Investment Cost Analysis

**Table 6.1:** Example net present value analysis with a 10% discount factor and \$500 initial investment

Year	Cash Flow (\$)		
	Project 1	Project 2	Project 3
0	-500	-500	-500
1	1000	220	0
2	0	220	0
3	0	220	0
4	0	220	0
5	0	220	1200
<b>Profit (\$)</b>	500	600	700
<b>NPV (\$)</b>	409.09	333.97	245.11
<b>IRR</b>	100%	33.7%	19.1%

to the company and the shareholders are promised a 20% return on their investment. For every \$100 earned, the company therefore owes \$5 to the lender (i.e.  $0.5 \times 0.1 \times 100$ ) and \$10 to the shareholders (i.e.  $0.5 \times 0.2 \times 100$ ). The total outgoing money to repay the initial investment is \$15, with a weighted average cost of capital of 15%. In this case, a project would require a minimum return of at least 15%, as anything lower would mean more money paid out to debt and equity holders than made by the company. Where WACC is available, it is a useful measure of a project's profitability. However, it can be difficult to calculate depending on the mix of finance sources. In addition, a company's WACC may not accurately represent the financing of a particular project. It is nevertheless useful to have a consistent value for comparison purposes.

As an alternative to net present value, the Internal Rate of Return (IRR) may be calculated. This value is the rate for which the project NPV breaks even, i.e. expenditures exactly cancel out revenue. The IRR of a project should ideally exceed the minimum required return rate in order to be considered a suitable investment. This minimum can be represented by the WACC, which is typically 7–8% for the airline industry [12].

When comparing a selection of investments, the one offering the highest NPV or the highest internal rate of return is the one most likely to be selected, as it offers the best weighted income. Projects may have similar net present values whilst having a very different split of cash flow over time or covering very different durations. In addition, projects with higher net income over a longer period of time may have a lower net present value than a smaller income over a shorter time period, due to the inclusion of the discount rate to represent the time value of money. The best project from a net present value perspective may therefore be very different to the best project from a net income perspective. A number of example projects are shown in Table 6.1. Whilst Project 3 has the highest net income, it has the lowest net present value and lowest IRR of the three options, as the investor must wait five years before receiving any income. Project 1 has the lowest net income, but all profit is made in the first year. This results in the highest net present value and a good return. A quick return on a project gives the investor the opportunity to invest in a new project the following year, i.e. the opportunity cost for the project is low.

For long term projects, inflation may also have an effect, as it will influence the real value of money over time. The effect of inflation may be included in the NPV calculation by either modifying the cash flow or the rate of return. In the first case, the cash flow,  $C_n$ , in each time step of the calculation is inflated using the current inflation rate and discounted using a money or nominal rate of return. In the second case, the cash flow is left in terms of the real cash flow

## 6. Investment Cost Analysis

value at the project start, and the inflation correction applies to the discount factor as a real rate of return [150]. Including inflation becomes increasingly relevant in the case of projects with long life cycles. In the present study, the real cash flow and rate of return will be used. Therefore, the inflation rate is assumed to be covered within the rate of return term, whilst the cash flow values are in terms of the value of money at the start of the aircraft life. The nominal (inflation independent) rate of return may be calculated from the real term using Equation 6.4, where  $r_n$  and  $r_r$  are the nominal and real rates of return, respectively, and  $i$  is inflation [150]:

$$(1 + r_n) = (1 + r_r)(1 + i) \quad (6.4)$$

The technologies in the N3-X concept create a unique challenge for an economic assessment of the aircraft, as they are not currently in commercial use and also incorporate a number of new concepts. The two key uncertainties with relation to direct operating cost are the acquisition price (leading to the cost of interest repayment, insurance, and depreciation), and the maintenance cost. Exact values for these two terms are unknown for a novel aircraft, and conventional methods for estimating these costs will have limited accuracy. However, a sensitivity analysis method can be used to assess the influence of changes in acquisition price and maintenance cost over the direct operating cost. In combination with a NPV analysis, additional estimates may also be made for the regions where the novel aircraft provides a reasonable rate of return. This method allows a range of viable costs to be identified at the preliminary design stage [78]. These costs estimates may then be used to inform conclusions on the economic viability of the novel aircraft concept. Such analysis provides a useful perspective for an aircraft manufacturer, as a target cost can be identified to ensure that the new concept will be attractive for operators.

In this research, no assumptions were made as to the revenues earned by the novel and baseline aircraft. Instead, revenues were assumed to be equal for the two aircraft, as the aircraft would operate on the same routes with similar passenger numbers and with no change in ticket prices for a route. Therefore, the only economic difference between the novel concept and the baseline would be the difference in direct operating cost. Therefore, the profitability of the novel concept is the difference in direct operating cost when compared to the baseline aircraft. Following this assumption, the NPV analysis was made in terms of the difference in direct operating cost, as opposed to revenue. The project IRR was subsequently calculated based on this operating cost difference, with a NPV formulation as follows [78]:

$$\Delta X = \sum_{n=1}^{\text{life}} \frac{\Delta \text{DOC}}{(1 + \text{IRR})^n} \quad (6.5)$$

In this formulation,  $\Delta X$  is equal to the difference in aircraft purchase cost (the difference in the initial investment),  $\Delta \text{DOC}$  is the difference in direct operating cost, and IRR is the real rate of return for which the project NPV is equal to zero. The term  $n$  represents the years in the aircraft's economic life, up to the assumed maximum of 20 years. Direct operating cost was calculated as a cost per flight and then multiplied by the assume number of flights per year to produce the yearly profit versus the baseline. Flight cycles per year were scaled based on flight length and reference data on the B777-200LR [151] (Figure 6.3). Crew salary was assumed to be a yearly expenditure, distributed over the number of flights per year. The N3-X and B777-200LR were assumed to be crewed by two pilots and 13 cabin crew paid the average US\$ yearly salary for their respective occupations [152]. Aircraft and engine maintenance cost per flight hour is dependent on the mission length, where cost per flight hour is generally higher for aircraft flying many short range mission rather than fewer long missions. Section 6.5 details the model used to account for this effect.

## 6. Investment Cost Analysis

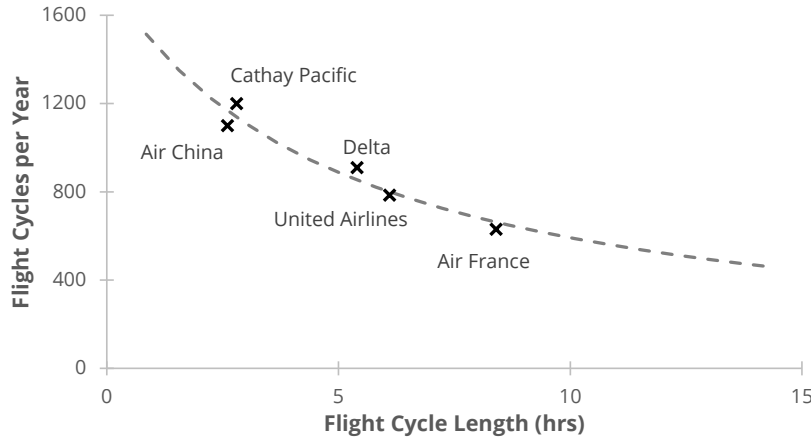


Figure 6.3: Flight cycles per year for the Boeing 777-200LR [151]

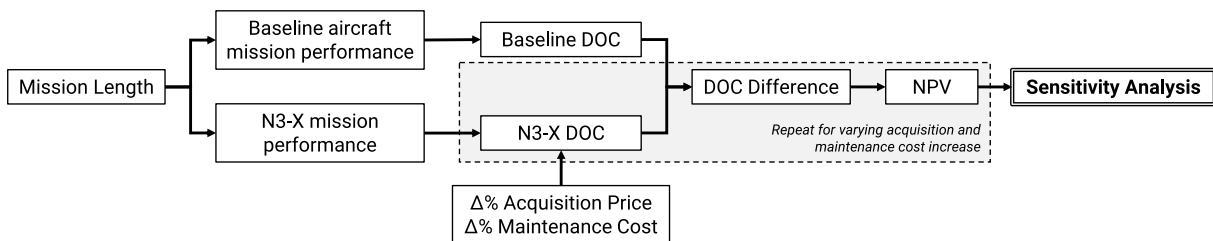


Figure 6.4: Flowchart for direct operating cost sensitivity analysis

In the sensitivity analysis, the influence of changes in acquisition price and maintenance cost on the direct operating cost benefit must be identified. The change in direct operating cost was estimated by scaling acquisition price and maintenance cost as a percentage increase in comparison to the baseline aircraft, with the costs of the baseline aircraft as a starting point (Figure 6.4). For example:

$$X = X_{\text{baseline}} (1 + \Delta\%)$$

By estimating the change in direct operating costs over a range of values, a map of the direct operating cost versus the baseline may be created. Figure 6.5 presents a sample of the sensitivity analysis, consisting of three distinct regions marked by the two indicated trend lines:

**Trend A: Equal DOC** – Direct operating cost for the proposed technology is equal to that of the baseline aircraft.

**Trend B: IRR equal to WACC** – Points lying on this line have an IRR that matches the defined minimum (WACC in this case). The IRR = WACC line marks the maximum increases in acquisition price and maintenance cost for a proposal to remain attractive.

**Region 1: Non-profitable** – In this region, the direct operating costs of the proposed concept exceed those of the baseline aircraft. Any benefits obtained by improvements in fuel consumption or other efficiencies are outweighed by significant added costs per flight cycle from the other elements of direct operating cost. There is little justification for developing or purchasing the technology should the proposal lie within this region.

**Region 2: Profitable, inadequate IRR** – In this region, direct operating costs are lower than those of the baseline aircraft. However, the technology does not provide a sufficient return on investments, as determined by the operator's WACC. The size of the region will vary

## 6. Acquisition Cost Estimation

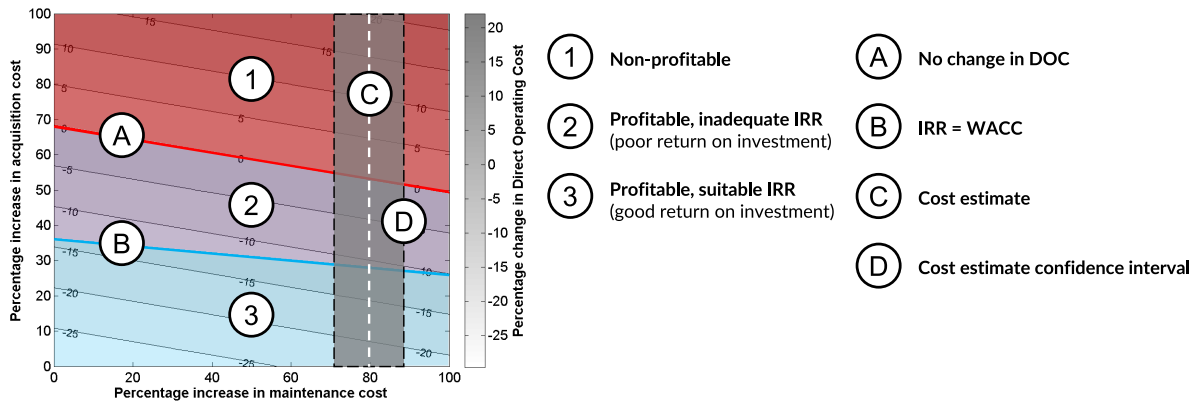


**Figure 6.5:** Example output from the economic sensitivity analysis.

depending on the customer's WACC. Whilst the proposal is profitable in this region, it should still be avoided as it will not be as attractive for the customer.

**Region 3: Profitable, suitable IRR** – Ideally a proposal should lie within this region, as technology here will be economically attractive. The technology is both more profitable than the baseline, and sees a higher return on investment than the minimum defined value.

The sample also includes an overlay that represents a maintenance cost estimate (C) with a confidence interval (D). The sensitivity analysis leads to a prediction of the viable cost margins for the aircraft in a given economic scenario, with maximum values defined by the IRR = WACC trend. This trend can be used by a manufacturer to define a target cost beyond which the concept is no longer attractive to a customer. However, the sensitivity analysis does not provide any indication as to where a concept may lie on the analysis, but rather suggests the ideal cost. The aircraft's actual costs may lie anywhere on the plotted region and potentially beyond the plot's boundaries. As the IRR = WACC trend defines the maximum viable cost, it is useful for a manufacturer to determine whether such costs are feasible. As has previously been identified, predicting the cost of a novel aircraft is difficult, given that much of the technology is not in commercial use for the aviation industry. However, a preliminary acquisition price or maintenance cost estimate can be produced using conventional tools and combined with the sensitivity analysis. It is then possible to identify whether the aircraft's predicted cost is likely to coincide with the economically viable region identified by the sensitivity analysis. If a cost estimate is produced that is well above the maximum viable cost, it is highly likely that the aircraft will not be economically viable as the likelihood of underestimating cost is small. In contrast, an initial cost estimate well below the maximum viable cost suggests that there is still potential for an economically viable aircraft.

### 6.4 Acquisition Cost Estimation

As a commercial product, cost is a vital component in the development of an aircraft. High production or research & development costs for the manufacturer can lead to a high cost product for customers, which will limit the economic attractiveness of a concept, regardless of what novel technologies it contains. However, optimising for a low acquisition cost will run counter to other goals such as minimising fuel consumption or emissions [71, 153]. A minimum acquisition cost aircraft will look very different to a concept concerned only with increasing efficiency. For example, a simple aircraft manufactured entirely from low cost steel would be cheaper than an

## 6. Acquisition Cost Estimation

---

advanced composite aircraft, however, the fuel costs of such an aircraft would be prohibitive. One particular case that can be presented is the Airbus A380, which required modifications during design to reduce noise and meet night time noise restrictions. A low noise design resulted in a higher drag aircraft, and hence an increase in fuel consumption [71]. Such a case demonstrates the conflicting nature of different design goals. This will become increasingly challenging as noise, emissions and energy savings goals tighten. It is likely that the novel technologies required to meet these goals will require expensive development programs and may cost more than previous technologies. It is therefore vital to perform cost analyses to ensure that the concept is viable for both manufacturers and operators.

In addition to conflicting design goals, the cost committed to development escalates rapidly as a design progresses [69]. Design changes at late stages of development will therefore cost significantly more than those made at the preliminary design stage. Literature suggests that 70-80% of product cost is determined by decisions made during the conceptual phase [154]. Whilst designers have the greatest freedom to make changes early in the design stage before decisions are finalised, there is limited design information available at the preliminary stage.

The present research focuses on techno-economic analysis for aircraft at the preliminary design phase. The selected methods and models must therefore suit this phase of research. However, it is difficult to estimate the cost of conceptual aircraft that incorporate novel technologies, as there is limited historical data against which a comparison can be made. In addition, the level of detail necessary for an accurate component-by-component cost breakdown is not available. Cost estimates are therefore bound to be inaccurate. Any given framework or cost estimating method is not suited to every phase of development. Different cost estimating methods can therefore be applied as development progresses from conceptual design through to production [69].

### 6.4.1 Cost Model Classification

The cost of a new aircraft at the earliest stages of conception can often be best predicted based on an intuitive estimate based on expert judgement using previous knowledge. However, as the project progresses further, more detailed calculation based methods become useful [155]. Calculation-based cost models can generally be split into two categories: Parametric Cost Models (PCM) and Manufacturing Process Cost Models (MPCM) [156]. These two categories of model attempt to overcome the difficulties of estimating the cost of an engineering project from different perspectives and at different levels of fidelity.

#### Parametric Cost Models

Parametric cost models make use of historical data to establish a statistical relationship between variables. In the case of cost estimation, this will be between the cost of the aircraft and the design parameter or parameters found to correlate well with cost. The relationship between the dependent variable cost and its independent variables can be determined using a regression analysis to create a cost estimating relationship (CER). Such relationships are strongly reliant on the size and suitability of the historical database used to create the relationship, in addition to the independent variables selected. The availability of data is also a key factor in the creation of a suitable CER, as program or component manufacturing cost data will typically be proprietary information. Previous research has found a number of parameters that are suitable for use as CER variable, such as aircraft empty weight or aircraft flight speed [157, 158]. Aircraft empty weight in particular shows a clear correlation to list price (Figure 6.6), as aircraft cost is a function of the cost of materials and manufacture and hence is closely linked to the aircraft size.



## 6. Acquisition Cost Estimation

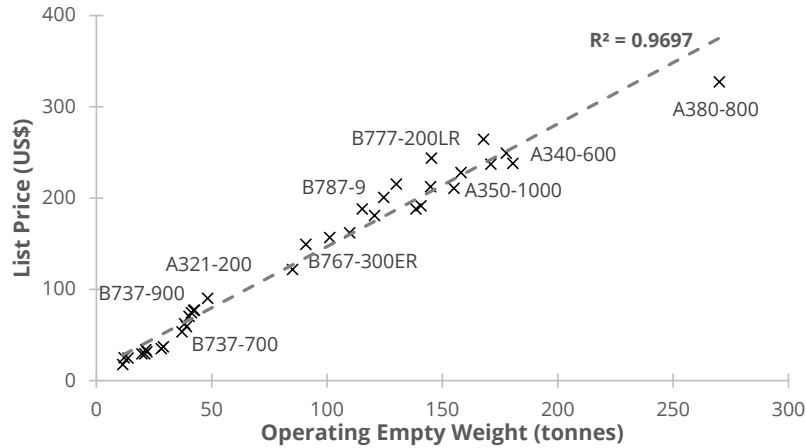


Figure 6.6: Aircraft list price versus operating empty weight [159]

The fastest method to predict cost is to create a relationship to list price based on aircraft design parameters or that may be obtained from publicly available data. However, a list price estimation limits the inclusion of novel factors such as new engine designs or other concepts as estimates the aircraft price as a whole product without the nuances of a more detailed breakdown. Simple single-variable relationships can be limited in applicability, for example, a weight-based cost estimation model will predict the same cost for two components of the same weight, regardless of material expense or component complexity. Similarly, speed is not suitable as a single-variable predictor of cost, as commercial aircraft typically fly within the same range of cruise Mach numbers but will nonetheless have significantly different costs. Relationships therefore employ multiple variables to account for the various factors that correlate with cost. Additionally, it is important to select a variable that has a strong relationship with cost, rather than a variable that correlates only loosely or by chance alone.

As CERs are based on correlations and data fits, a certain measure of uncertainty will always be present. Selection of a suitable model relies on identifying the model with the best fit, or the highest value of  $R^2$ , known as the coefficient of determination. In a best case scenario  $R^2 = 1$ , implying a perfect fit. A basic form of regression analysis relationship is a simple linear relationship between cost and the independent variable [160]:

$$Y = \beta_0 + \beta_1 X + E \quad (6.6)$$

Where  $\beta_0$  and  $\beta_1$  represent the y-intercept and gradient, respectively. The parameter  $E$  represents the model error and provides a random factor to the equation which accounts for uncertainty. Such a factor emphasises that a cost model will never perfectly predict cost. As an alternative to a linear relationship, a non-linear power law CER may be used. As it is common to use more than one variable to describe cost, a regression model using multiple linear and non-linear components, or a combination, will often be used.

Rais-Rohani and Dean [156] describe a simplified general expression for cost using a power law relationship:

$$\text{Cost} = e^q \prod x^a \quad (6.7)$$

Each product term represents a parameter contributing to the cost of the product through the power relationship  $x^a$ . Complexity is identified as a key cost contributor by the use of the term  $q$ , representing the manufacturing complexity. The complexity term represents factors such as part count, tolerance, machining difficulty, and surface finish. It follows that relaxing these requirements will reduce cost. As this is a generalised form, suitable data to define the

## 6. Acquisition Cost Estimation

---

relationship for both the complexity and the overall CER is required.

A selection of historic parametric equations for aircraft are available. Roskam separates the cost estimation of an aircraft into a number of subcomponents, split between manufacturing, production, and labour costs [158]. Cost is estimated using power law CERs based on data from a number of sources. These relationships are based on multiple regression formulae originally using data for 29 post-1945 aircraft obtained from the Aeronautical Manufacturers Planning Report, with a database modified over time. The relationships developed by the RAND corporation were used to create the Development and Procurement Costs of Aircraft model (DAPCA) [161]. As the model was based on conventional aircraft for the time, it underestimates the cost of advanced and non-aluminium designs [116]. With a sample set primarily constituted by military aircraft and particularly fighters, the equations are better suited to prediction of military fighter aircraft costs [162]. Additional components not included in the DAPCA equations are accounted for in Roskam's cost estimation procedure, including the cost of interiors and avionics. Costs reported by such models must be adjusted for inflation in order to represent current value of money, however, it has been noted that the same inflation rate might not apply to all sections of production [163]. As commercial aircraft are produced in reasonably large numbers, models often produce the costs estimate as a cumulative cost for a 'lot' of aircraft, from which an average unit cost can be obtained [157, 164].

Sample size and homogeneity have been identified as key factors that influence models [160]. Aircraft with common characteristics ensure homogeneity of the database, however this also limits the data points for a regression analysis, and certain classes of aircraft may be more challenging to define than others [162]. The applicability of a PCM becomes more limited for new technology that is not represented in the historical database. A key issue in the application of old PCM models to current and future aircraft is the increasing use of composite materials, unlike the primarily metallic structure of the historical databases. Added complexity and higher material cost can increase the overall aircraft cost, despite a lower weight [165], a factor partially accounted for by a complexity factor such as the one mentioned by Rais-Rohani and Dean [156].

The most accurate PCM estimation will rely on proprietary data from similar aircraft using a manufacturer's experience from previous projects. In the absence of both historical data and detailed manufacturer cost information, the accuracy of a PCM cost estimation is limited. However, the collection of data can be a challenging task due to either the unavailability of internal cost records for commercial projects, or the over-abundance of information in the case of publications for public defence projects [166]. It is also important to ensure the accuracy of the data used in the model, as any inaccuracy will introduce further errors into a model entirely reliant on historical data. Cost model inaccuracy will also be compounded by uncertainty in aircraft weight estimates at the preliminary design stage, the primary parameter for cost estimations. Despite the availability and repeatability of results obtained through a CER, the use of the cost estimator's own expert judgement is a useful part of analyses, especially as errors in formula-based cost estimation of up to 770% have been reported [154].

CERs in the sector of aircraft engine cost estimation are also available, such as those developed by the RAND corporation for military engine programs [167]. The same regression techniques as for airframe are applied, however, the CER descriptor variables will be parameters such as turbine entry temperature, thrust rating or shaft horsepower [159].

It is worth noting that many of the sources for acquisition cost CERs rely on data obtained from military aircraft, highlighting the need to determine how applicable the models are for commercial projects. Finizie notes in a comparison between contractor and navy cost methods that contractor engines can cost 25% less than navy engines based on their respective estimation methods [168].

### Manufacturing Process Cost Models

MPCM models support a bottom-up design process, which assess each component and the processes required for its manufacture, building up to an estimation of the total aircraft cost. A MPCM model may be alternatively known as an activity based cost method (ABC), as cost is comprised of the activities required for manufacture. Many studies consider its application to composite components which can require a large number of processes to manufacture. The Advanced Composite Cost Estimating Model (ACCCEM) creates a methodology to estimate the recurring costs of fabrication of composite parts [169]. Cost is comprised of three modules: factory labour standards estimation, support function estimation, and cost projections. The cost of a component is built up based on the processes required to manufacture it. Similarly, Gutowski *et al.* [170] outline a model for predicting the cost of advanced composite components by building up a set of tasks. The time total taken for these tasks may be used to predict the cost based on a cost per hour value. Castagne *et al.* [171] break down the cost of manufacturing a component into associated material, fabrication, and assembly costs. Such methods apply to the more detailed cost estimation of an advanced development stage, rather than the general top-down estimations of the concept phase that are associated with the PCMs of the previous section, although regression models may still be used.

The bottom-up style of cost estimation is best suited to projects at a more advanced stage of development, where cost details are known. This can limit their usefulness in design projects seeking to limit costs from an early stage, as the details necessary for the estimation are unknown. A MPCM estimation is also prone to underestimating costs, as it is inevitable that certain factors will either not be foreseen or are difficult to estimate (such as the cost of overrunning deadlines) [166]. The use of a high fidelity model will not be suitable at the preliminary design stage, as it would require many assumptions of the aircraft configuration that would introduce unnecessary errors into the estimate.

### Combined Methods

Both of the summarised methods have advantages and drawbacks that mean their applicability is dependent on the stage of development. Newnes *et al.* identify that cost estimation software users would prefer options for both parametric and more detailed bottom-up design estimation models [69]. At the early conceptual design stage the detail required for a MPCM cost estimation is unavailable, ruling out such an estimation procedure. However, the applicability of conventional PCM estimation tools is limited when considering novel aircraft, especially for the publicly available tools such as the relationships presented by Raymer [116].

Scanlan *et al.* propose a hybrid procedure that can be expanded as development progresses from the conceptual design phase to the detail design phase [172]. The aircraft is represented as an exemplar which contains all the parameters for a detailed design of the aircraft. At the conceptual design stage this structure is defined using default characteristics which can be defined as development progresses and detailed parameters become known. Design uncertainty at the early stage is represented by a cost uncertainty which reduces as more parameters are defined.

It is difficult to make an accurate cost estimate for a novel aircraft at the early design stage using either a PCM or MPCM. A combined method is nonetheless useful as research progress, as a cost estimate can be refined once further design detail becomes available. This research will make use of a PCM in reflection of the preliminary stage of development. However, refining the cost estimate is a necessary aspect of reducing uncertainty in the design and increasing the accuracy of an economic viability analysis. The goal of a cost estimate with respect to this research is to narrow down the region in the sensitivity analysis where a novel aircraft is

expected to lie. This will necessitate the use of more accurate cost predictions where possible and once they may be suitably applied.

### 6.4.2 Airframe Acquisition Cost Model Selection

Aircraft manufacturers will have well-developed models for predicting the cost of a new project and setting a list price for the aircraft. However, these acquisition cost models, and more advanced modern models, have not been made available for public use. The publicly available parametric models rely on older data to develop trends, and will therefore introduce a large measure of uncertainty into the cost prediction. This is especially true for a novel conceptual aircraft with an entry into service more than 30 years after the year in which many of the available models were released. In order to reduce the estimate uncertainty, it was important to select cost models which include factors that may be used to adjust for novel aircraft concepts. Two publicly available models were selected with this form of support (models detailed in Appendix E):

- RAND Corporation (Resetar *et al.*, 1991 [173] updated by Younossi *et al.*, 2001 [174])
- Roskam, 1990 [158]

The RAND Corporation cost models divide the aircraft cost into a number of groups covering the aircraft development program. It should be noted that the RAND model database consists predominantly of military aircraft, including fighter aircraft. However, Hess and Romanoff note that breaking the database up to cover only transport aircraft does not benefit the cost prediction models [162]. Resetar *et al.*'s models were used to provide the parametric cost functions, which consist of the the following groups:

- Development program cost,  $C_{\text{development}}$ 
  - Non-recurring engineering hours
  - Non-recurring tooling hours
  - Development support cost
  - Flight test cost
- Manufacturing cost,  $C_{\text{manufacture}}$ 
  - Recurring engineering hours
  - Recurring tooling hours
  - Recurring labour hours
  - Recurring manufacturing material cost
  - Recurring QA hours

The cost of the development program is classified as a non-recurring cost and is spread out over a first lot of aircraft. The manufacturing cost applies to each aircraft and would continue after the development program cost had been paid off following the sale of the first lot. Resetar *et al.* provide cost functions for the aircraft development program and manufacturing process, including material weight factors to adjust for the use of advanced materials [173]. The more recent models provided by Younossi *et al.* add more up to date cost factors which may be used to extrapolate the change in the cost of manufacturing with various material types over time [174]. The RAND corporation models also include a learning curve correction for manufacturing cost

## 6. Acquisition Cost Estimation

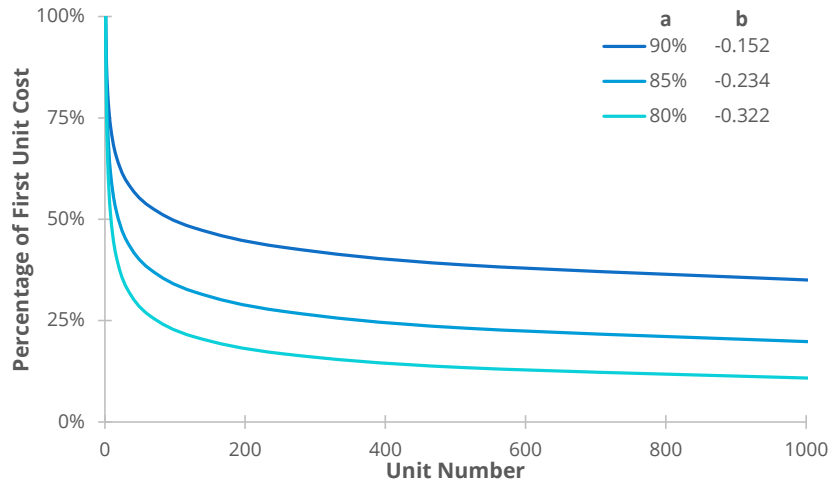


**Figure 6.7:** Example learning curves for the manufacturing cost of an airframe

that accounts for the fact that the cost of production reduces as more aircraft are manufactured (Figure 6.7):

$$X_n = aX_{n-1} = X_1n^b \quad (6.8)$$

Where  $a$  is the learning slope,  $b$  is the learning exponent,  $X_1$  is the manufacturing cost of the first item, and  $X_n$  is the manufacturing cost of the  $n^{\text{th}}$  item.

The cost per aircraft is the total of the cost estimate for the development program and manufacture of the first lot of aircraft, divided by the number of aircraft in the first lot:

$$X = \frac{C_{\text{development}} + C_{\text{manufacture}}}{N_{\text{aircraft}}} \quad (6.9)$$

The cost is created for a fixed first lot of  $N_{\text{aircraft}}$ . As the actual manufacturing cost for a single aircraft is a function of the learning curve, the value of  $X$  incorporates the average manufacturing cost of aircraft in the first lot. It is assumed that the development program will be paid off after the first lot is sold. The price  $X$  therefore represents the ‘break even’ cost for the aircraft, i.e. the sale price for which costs are exactly covered. As the development program is a finite cost, the manufacturer will begin to make a profit on the aircraft once the development program is paid off after the sale of the first lot of aircraft. The manufacturing learning curve means that aircraft manufacturing costs reduce as more aircraft is produced. However, it may be expected that not all of these savings will be passed on to the customer. Instead, the lower manufacturing cost can be used to provide a profit for the manufacturer. It may therefore be assumed that the sale price  $X$  would remain unchanged after the sale of the first lot of aircraft.

Roskam’s models follow a similar cost estimation procedure to the RAND Corporation models. Although no material cost factors are presented, the models do include aircraft ‘difficulty’ factors which may be used to adjust for novel or new aircraft. Roskam’s cost model breaks the aircraft cost into a similar set of components to the RAND Corporation methods. Aircraft cost is again estimated based on a set of parametric cost functions for the development program and the aircraft manufacturing cost. Roskam also notes that the unit price of an aircraft will include a margin to allow for a profit to be made on the aircraft. By neglecting the profit term of the aircraft cost estimate, the break even aircraft price may be estimated. Roskam’s cost functions consist of the following groups:

## 6. Acquisition Cost Estimation

---

- Finance cost, with rate  $r_{\text{finance}}$
  - Development program cost,  $C_{\text{development}}$ 
    - Airframe engineering and design
    - Development support and testing
    - Flight test aircraft cost
      - \* Engine and avionics
      - \* Manufacture
      - \* Material
      - \* Tooling
- Manufacturing cost,  $C_{\text{manufacture}}$ 
    - Airframe engineering and design
    - Engine and avionics
    - Interior
    - Manufacture
    - Material
    - Tooling
    - QA

Roskam's models include a financing cost term which accounts for the cost of funding the manufacturing and development program for the aircraft. Roskam suggests a value of 10% of manufacturing and development cost for the aircraft is suitable for the finance rate [158]. Roskam's parametric cost functions estimate the manufacturing cost for a single aircraft, unlike the relationships developed by the RAND corporation which include a learning factor and estimate the cumulative cost for an aircraft lot. The development cost must therefore be distributed as a cost per aircraft by dividing by the total number of aircraft. The concept of a first lot of aircraft may be introduced here to define the total number of aircraft after which the development program is paid off. The break even acquisition price can finally be calculated as the sum of the development and manufacturing costs, multiplied by the financing cost:

$$X = \left[ \frac{C_{\text{development}}}{N_{\text{aircraft}}} + C_{\text{manufacture}} \right] (1 + r_{\text{finance}}) \quad (6.10)$$

The cost estimates produced by both models link to the number of aircraft sold in the first lot. The more aircraft in the first lot, the smaller the percentage contribution of the development program to the total cost, as it is distributed over a larger number of aircraft. A larger number of aircraft sold in the first lot therefore leads to a lower cost per aircraft. The RAND corporation models also include a learning curve for manufacturing cost. The manufacturing cost per unit therefore decreases as more aircraft are produced. In both cases, it is assumed that the development program is paid off following the sale of the first lot of aircraft. Sales beyond the first lot of aircraft are assumed to make a profit, as the development program has been paid off (assuming the acquisition price has not changed). The first lot has been used here as a target number of initial sales for the aircraft to break even and is used to establish a list price for the aircraft. In both cases, cost estimates must be scaled to the current value of money using the rate of inflation between the dollar year of the model and the current year.

### Acquisition Cost Model Modifications

Both the Roskam and RAND Corporation models include factors that are useful in predicting the cost of a novel aircraft. As both models break costs down into similar groups, it is possible to combine elements from each to cover factors not covered by one or another of the models. The RAND corporation model provides materials cost weighting factors which are especially useful for a modern aircraft with increasingly high composite material use. The Roskam models include a program difficulty factor, and also covers the cost of financing the development program and the cost of aircraft interiors. These elements were combined in each cost model to create two modified cost models which could then subsequently be used to create two cost predictions for the aircraft.

## 6. Acquisition Cost Estimation

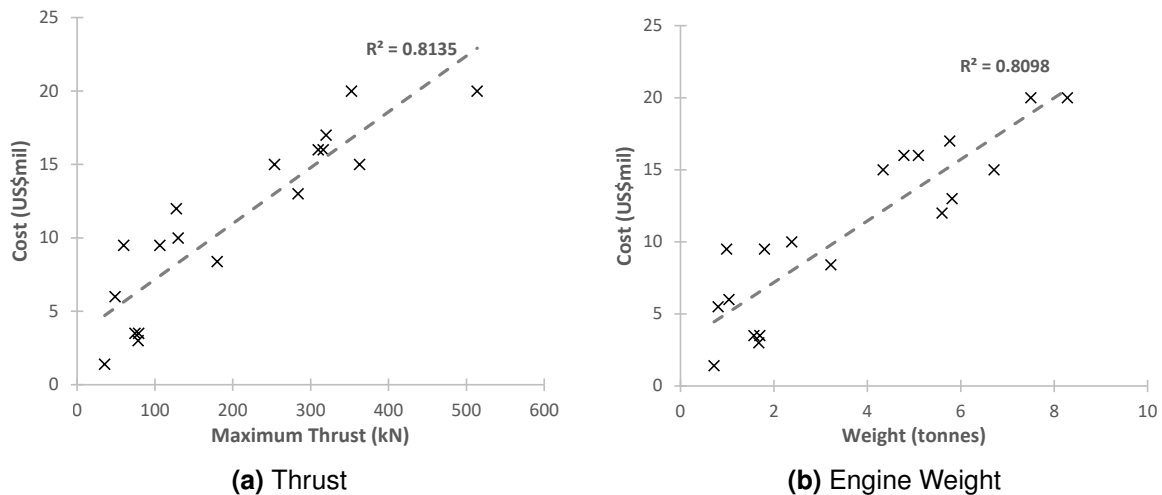


**Figure 6.8:** Engine price correlation with thrust and weight

By combining aspects from each model, the aim is to cover perceived gaps in each of the models. In combination, the models offer the following features:

- Program finance cost
- Development program cost
- Manufacturing cost
- Scale factors for advanced materials in manufacture
- Program difficulty scale factor for development and manufacturing cost
- Cost of aircraft interiors

### 6.4.3 Engine Acquisition Cost Model Selection

Although the airframe cost is the dominant component of an aircraft's acquisition cost, the engine will also contribute to the total cost. Section 6.4 identified that models can be split into PCM and MPCM models, and that parametric cost models are better suited to the cost estimation of preliminary designs. This conclusion also holds for the propulsion system, as detailed component design will not have been performed at the preliminary design stage. As with the airframe, there are key variables that are useful in predicting cost. For an engine, these are the thrust or weight, as both relate to engine size and hence correlate reasonably well with cost (Figure 6.8).

Two publicly available models were selected to estimate the acquisition cost of the main engines (see Appendix E):

- Birkler *et al.*, 1982 [175]
- Younossi *et al.*, 2002 [167]

Both models are developed by the RAND corporation. However, the methods used by Birkler *et al.* and Younossi *et al.* differ in the relationships and inputs used. Birkler *et al.*'s model splits the cost estimate into development program and production costs [175]. The development program cost includes the costs to bring the engine to the model qualification test (MQT) stage plus additional costs to correct engine problems during service and the cost of performance

## 6. Acquisition Cost Estimation

and reliability improvement over time. MQT is defined as a series of tests that is used to demonstrate that the engine is production-ready. The relationships do not include the cost of demonstrator or flight test engines. The cost estimating relationships use maximum thrust and maximum turbine inlet temperature as inputs to estimate both the development,  $C_{\text{development,eng}}$ , and manufacturing cost,  $C_{\text{manufacturing,eng}}$ . Maximum turbine inlet temperature in particular was identified as a variable that closely ties to cost, as it is typically linked to an engine's technology level. Maximum turbine inlet temperature can therefore serve as a proxy for the developmental costs of factors such as advanced materials and engine performance improvements. As with the airframe cost models, the development cost is distributed over the first lot. As there are multiple engines per aircraft, it is assumed that the first lot of engines is equal to the number of engines per aircraft,  $N_{\text{engines}}$ , multiplied by the number of aircraft in the first lot,  $N_{\text{aircraft}}$ . Total cost for the engine is the sum of the manufacturing cost and the development cost, distributed over the number of engines in the first lot:

$$C_{\text{engine}} = C_{\text{manufacturing,eng}} + \frac{C_{\text{development,eng}}}{N_{\text{engines}}N_{\text{aircraft}}} \quad (6.11)$$

Younossi *et al.*'s model also splits costs into relationships for the development program and the manufacture of engines [167]. Relationships are provided for the cost of developing an engine derivative versus the development cost of a new engine. The development program cost includes the costs incurred during the design, development, and testing of an engine. The method uses a learning slope to estimate the cost of the first engine and the  $n^{\text{th}}$  engine. Hence the average manufacturing cost of engines in the first lot can be obtained:

$$C_{\text{manufacturing,eng}} = \frac{1}{N_{\text{engines}}} \sum_{n=1}^{N_{\text{engines}}} C_{\text{manufacturing,eng},n} n^b \quad (6.12)$$

Where  $b$  is the learning curve exponent, with an assumed 80% learning curve for engine manufacture. Maximum turbine inlet temperature, maximum engine thrust, engine weight, and specific fuel consumption at sea level are used as inputs for the cost estimating relationships. As with the previous model, the total engine cost is the sum of the average manufacturing cost per engine and the development cost, distributed over the number of engines in the first lot.

Both sets of cost estimating relationships were developed using a database of military aircraft engines. As has previously been identified by Finizie, military engine costs estimates are typically higher than cost estimates for civil engines [168]. The estimates are nevertheless useful to provide a preliminary value of cost. In addition, engine cost is a reasonably small percentage of the total cost. Therefore, errors in engine cost estimates contribute a relatively smaller error to the overall acquisition cost estimate.

Publicly available engine acquisition cost estimation models are typically focused on conventional propulsion system configurations: turbojets and turbofans. However, the main engines of the N3-X are predominantly power producing, rather than thrust producing. Therefore, these models are more difficult to apply to the N3-X case study. Instead, an 'equivalent engine' was defined for use in the cost estimating relationships. This equivalent engine has the same design variables as the N3-X main engines (i.e. mass flow, component efficiencies, maximum temperature), however, the auxiliary power requirement is defined as 0MW. The equivalent engines are therefore thrust producing turbojets, as opposed to power producing turbogenerators. The maximum sea level thrust produced by the equivalent engine could then be used in the cost estimating relationships.

In addition to the above described cost models, cost estimates were produced by simple correlations of cost to engine thrust and weight. A correlation of cost to weight bypasses the



## 6. Acquisition Cost Estimation

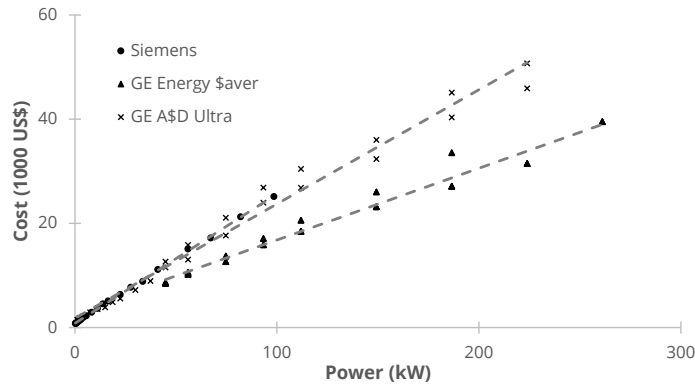


Figure 6.9: Motor cost correlations for three commercial motor classes

requirement for an equivalent engine to be defined, and was used as a point of comparison against cost estimates from the selected models (Figure 6.8).

### Miscellaneous Propulsion System Components

The N3-X propulsion system also includes the propulsor array and the superconducting electrical system, which will also contribute towards the total cost of the aircraft. It was assumed that the cost of the propulsors in the array could be estimated in a similar manner to the cost of a propulsor fan or propeller using relationships by Roskam [158]. The cost estimating relationship correlates cost to shaft horsepower and provide estimates for both composite and metal blades. Composite blades were assumed for the N3-X propulsor array, with a cost estimating relationship as follows:

$$C_{\text{fan}} = 10^{(0.7746 + 1.1432 \log_{10} P_{\text{shaft}})} \quad (6.13)$$

The maximum power at RTO was used to determine the shaft horsepower,  $P_{\text{shaft}}$ , for the cost-estimating relationship. In the absence of an alternative method for the cost of individual propulsor fans, this relationship was used to provide a estimate, as the propulsor fans would be superficially similar to fans in conventional propulsion systems.

A superconducting electrical system presents the biggest challenge for a cost estimate of the N3-X, as there are currently no superconducting electrical systems available for commercial aviation. In addition, the 2–3 MW motors required for each propulsor in the array have a higher power rating than most conventional motors. There is therefore no historical data on which to base a cost estimate. As a preliminary assumption, the cost of the motors and generators was taken from a simple correlation of motor power to cost, using costs for commercially available electrical motors [176, 177]. The cost values were extrapolated out to the requisite power level, although this lies well outside of the available data set. The motor/generator cost was assumed to be the average cost estimated by the three data sets correlated to the power (Figure 6.9).

It is highly likely that there will be a significant and non-quantifiable error in the motor and generator cost estimate. However, a preliminary estimate is necessary in the absence of validation data for the cost of high power superconducting systems. Cost estimates for superconducting systems in aviation applications are a subject for further work as research on superconductivity and high power electrical systems progresses.

#### 6.4.4 Cost Model Validation

The cost estimates produced by the two selected models were validated against the quoted list price for the baseline aircraft; \$320.7 million for 2017 [178]. Material composition by weight for

## 6. Acquisition Cost Estimation

**Table 6.2:** Aircraft unit cost estimates for the baseline aircraft (2017 US\$mil)

	Price	Error	SEE
Actual List Price	\$320.7	-	-
Roskam	\$337.7	5.3%	-
RAND	\$329.2	2.6%	±\$112.6

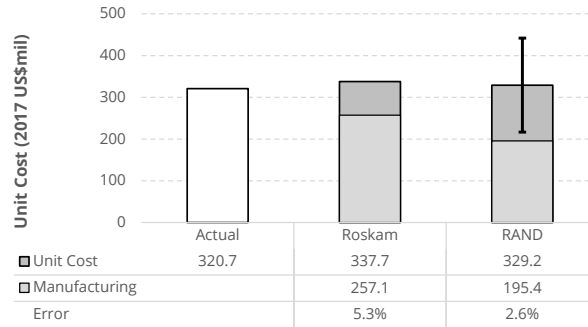


**Figure 6.10:** Cost model validation on the baseline aircraft, including standard error of estimate

the B777-200LR was taken to be 70% aluminium, 11% composite, 7% titanium, and 11% steel [179]. It was assumed that the first lot of aircraft is equal to the aircraft sales prior to its entry into service. This is equal to 154 aircraft for the B777 series [180]. The two models produce a reasonable estimate of the aircraft cost with an average error of approximately 4% (Table 6.2). Whilst the two cost estimates produce similar values, the split between unit manufacturing cost and development program is different, with the RAND model attributing more of the cost to the development program than Roskam’s model (Figure 6.10). Although the error for both models was low, the RAND model was selected for further use to provide a cost estimate for the N3-X. This is primarily due to the availability of the standard error of estimate term, which allows a confidence interval to be produced for the acquisition price estimate. However, elements from the Roskam model were combined with the RAND model, as identified in Section 6.4.2. The RAND model applied herein was therefore modified to include the cost of aircraft interiors, a program difficulty factor, and the financing cost of the aircraft program.

Cost estimates for the engines of the baseline aircraft were validated against a publicly available price quoted for the GE90-115B engines: \$24mil [181]. The selected cost models underestimate the engine price by up to 18% (Table 6.3). However, it should be highlighted that engines are generally sold as an option in combination with an airframe, and it is therefore difficult to identify the cost of the engine alone. The engine cost estimate will be taken as the averaged value.

**Table 6.3:** Engine unit cost estimates for the baseline aircraft (2017 US\$mil)

	Price	Error	SEE
Actual List Price	\$24	-	-
Birkler	\$19.6	18.1%	±\$1.12
Younossi	\$22.3	6.9%	±\$3.44
Weight Correlation	\$20.8	13.2%	±\$2.63
Thrust Correlation	\$22.9	4.5%	±\$2.62

## 6. Maintenance Cost Estimation

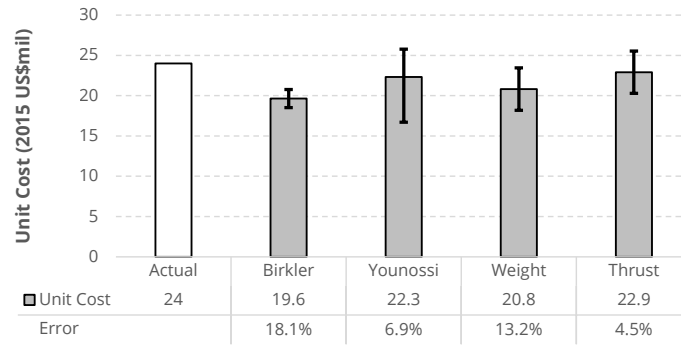


**Figure 6.11:** Cost model validation on the baseline aircraft's engines, including standard error of estimate

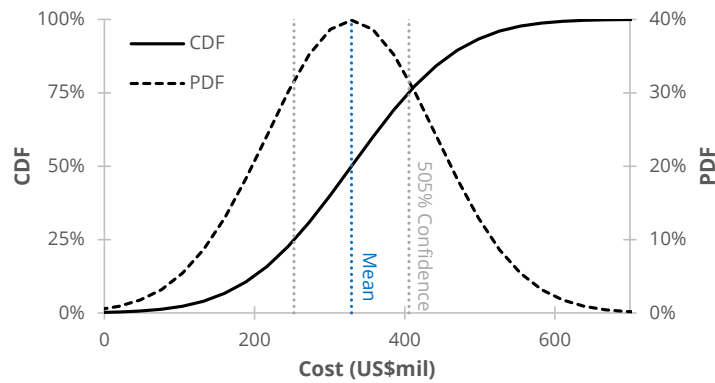


**Figure 6.12:** Probability and cumulative distribution functions for the baseline aircraft cost estimate (normal distribution)

### Model Uncertainty

As the cost estimates are reliant on regression analyses to create the cost estimating relationships, a degree of uncertainty is inevitable. The RAND models provide the standard errors of estimate (equivalent to the standard deviation in a statistical analysis), that may be used to create confidence intervals for the cost estimate. Assuming a normal distribution, the cost is 95% certain to lie within  $\pm$  two standard deviations of the estimate and 99.7% certain to lie within  $\pm$  three standard deviations of the estimate. Given the relatively high standard error for the costs estimate, a smaller confidence interval is more useful. In addition, using the full 99.7% confidence interval would lead to an unrealistically low value for the lower end of the confidence interval. Instead, a 50% confidence interval has been used, contained within  $\pm$  0.675 times the standard deviation.

It is more likely that the cost of an aircraft would overrun than that it would be lower than expected. Alternative distributions include the lognormal distribution, which can favour values greater than the mean estimate (Figure 6.13). The skewness of the lognormal distribution depends on the variance of the estimate, with a higher variance leading to a greater skew (Figure 6.14). The variance can be estimated if a set of data is available. Alternatively, the variance for a normal distribution is equal to the square of the standard deviation. As there is no data set for the cost estimate, a variance would have to be assumed. The lognormal distribution produces larger upper limits for the 50% confidence interval. However, a lognormal distribution is difficult to apply to the cost estimate without knowing the variance of the data. Based on the information available and the scope of the research, a normal distribution will therefore be retained for this research.

## 6. Maintenance Cost Estimation

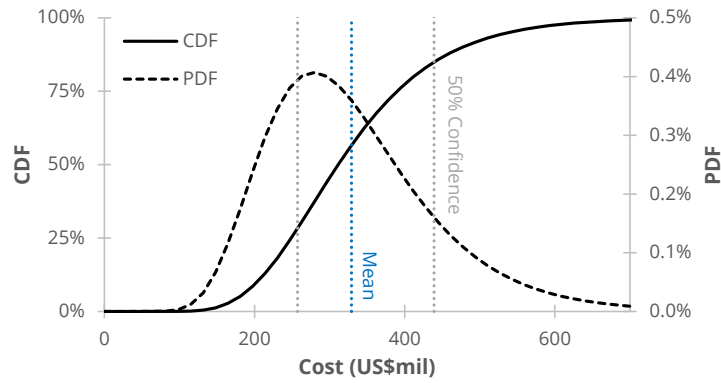


**Figure 6.13:** Probability and cumulative distribution functions for the baseline aircraft cost estimate (lognormal distribution,  $\text{Var}(X) = \sigma^2$ )

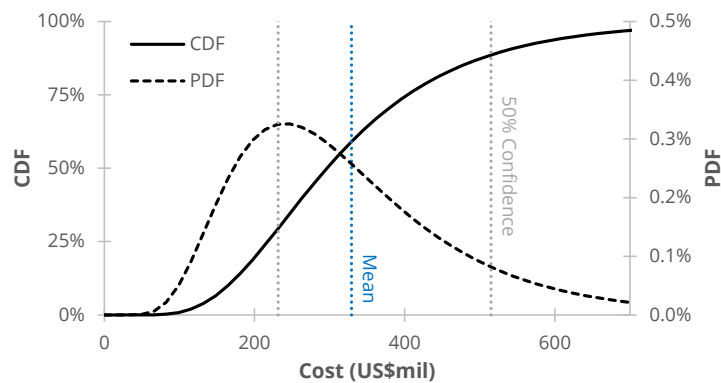


**Figure 6.14:** Probability and cumulative distribution functions for the baseline aircraft cost estimate (lognormal distribution,  $\text{Var}(X) = 2\sigma^2$ )

### 6.5 Maintenance Cost Estimation

As with acquisition cost estimation tools, maintenance cost estimation tools can be split into activity-based (such as maintenance workscoping) and parametric cost estimating relationships. There are additional levels of detail available within the parametric cost grouping from estimating a simple cost per flight hour to estimating the cost of shop visits and part replacements. A detailed maintenance cost estimate necessitates reasonable workscoping capability to predict the activities and hence costs of maintenance visits throughout an aircraft or engine's life. However, as with acquisition cost modelling, there are alternative cost estimating tools that are better suited to the limited information available for preliminary designs. Many of the conclusions made regarding the acquisition cost models can be similarly applied to maintenance cost models. At the preliminary phase, the level of design detail required for a thorough workscope and component based cost estimate is unavailable. In addition, many of the publicly available models rely on older databases of aircraft and engines, reducing their usefulness for far-future concepts. The models may nevertheless be used to provide an initial cost estimate.

The exact activities that take place during an aircraft or engine's shop visit will depend on the use the aircraft or engine has seen. For the engine, there are several causes for a shop visit [182]:

- **Exhaust gas temperature (EGT) margin deterioration** – The exhaust gas temperature margin is an indicator of the engine's performance degradation as it ages. Wear and damage to components during the course of an engine's life will reduce efficiency and increase the temperature at which the engine must operate. High exhaust gas temperatures can be indicative of a degraded engine, and can result in further component damage due to high temperatures within the engine. An engine manufacturer will establish a maximum exhaust gas temperature to be used in determining the EGT margin. As the engine reaches its EGT margin, a shop visit will be required to restore performance. Parts will be inspected for wear and replaced or repaired as necessary.
- **Life limited part (LLP) replacement** – Many engine components have lives that are limited to a set maximum number of flight cycles before they must be repaired or replaced. The number of flight hours until the parts must be replaced will depend on the mode of operation. Short haul aircraft operating many flight cycles generally approach the life limit of LLPs more quickly than long haul aircraft, as they will operate more flight cycles per year.
- **Hardware deterioration** – Engine components will deteriorate over the course of operation due to the conditions in which they operate. This is particularly the case for high pressure turbine components, which are subject to high temperatures and high rotational speeds (fatigue and creep damage).
- **Unscheduled removals** – Events during the engine's life may necessitate unexpected maintenance. A common cause is foreign object damage, such as bird strikes or ingested particulates such as ash. These events may necessitate the replacement of engine components and hence additional costs. However, the unexpected nature of these events means that they would not be included in basic cost estimating relationships for maintenance.

The main cause of engine removals is dependent on the primary mode of operation. Engines operating regularly on short routes will typically fly a larger number of flight cycles per year and will therefore be subject to faster degradation of EGT margins and LLPs. Longer haul engines

## 6. Maintenance Cost Estimation

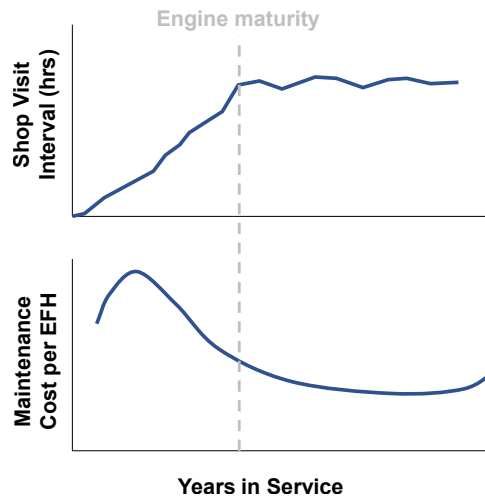


**Figure 6.15:** Engine maintenance cost per flight hour as an engine ages

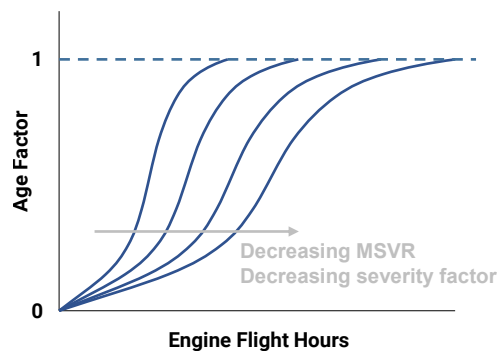


**Figure 6.16:** Engine ageing and age factor

will also require removals due to EGT margin deterioration in addition to hardware deterioration, such as creep damage. The primary cause of engine removal will also depend on an engine's age, with mature engine removals being dominated by different factors to new engines undergoing their first shop visit [182]. The costs of an engine's shop visit will also therefore depend on its age. In particular, early shop visits for an engine are often different to later shop visits, and may occur more often than shop visits for mature engines [162] (Figure 6.15). In this case, mature engines are defined as those with a roughly constant time in between overhauls. Figure 6.15 demonstrates the cost of a sample engine over the course of its life. In this sample, early engine maintenance costs are high where early design problems become apparent. Subsequently, a mature cost trend can be established as early problems are ironed out, maintenance programs are improved for the new engine, and the interval between shops visits reduces. Finally, shop costs begin to increase as engine ageing becomes apparent and LLPs reach the end of their lives [183].

Another perspective on engine maturity defines an engine as mature when it reaches the end of its life (Figure 6.16). An engine's maturity may also be linked to the severity factor of operation. Engine's with higher severity factors, such as those operating many short cycles and those operating in hot or corrosive environments, will age faster than engines operating fewer cycles [184]. The mature shop visit rate (MSVR, number of shop visits per engine flight hour) may be linked to this, with a high severity factor reducing the interval between shop visits.

Performance restoration is not a dominant contributing factors for the maintenance of the airframe. Airframe maintenance instead focuses on part wear due to factors such as fatigue or corrosion damage. The rate of deterioration due to these two factors will depend on the mode of

## 6. Maintenance Cost Estimation

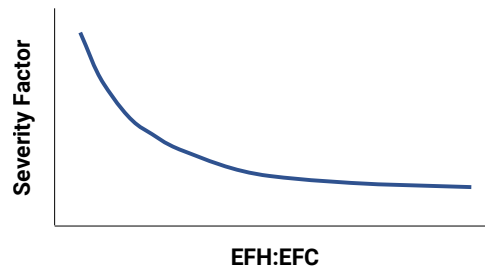


**Figure 6.17:** Engine severity factor as a function of engine flight hours per flight cycle

operation. For example, fatigue damage will propagate much faster on aircraft operating many short haul flight cycles per year than on long haul aircraft. This can be further exacerbated by corrosive environments, such as the salty air on ocean routes. However, composite materials are seeing increased use on aircraft and are influenced less by fatigue and corrosion damage. Maintenance of an airframe covers the following activities [185]:

- Servicing of parts to reduce deterioration rate
- Visual, operation or function checks to identify possible degradation or failure
- Restoration of components
- Replacement of parts outside their expected lifespan

As with engines, unexpected events such as friendly foreign object damage (e.g. due to damage on the ground during aircraft loading) may also necessitate maintenance activities. However, due to their unpredictable nature, they are generally not accounted for in basic cost estimating relationships.

A useful preliminary assumption for maintenance cost is to scale a baseline maintenance cost value using severity and ageing factors to account for the mode of operation or age:

$$C_{\text{maint}} = C_{\text{maint,base}} \times SF \times AF \quad (6.14)$$

A severity factor trend can be assumed which accounts for how the ratio of engine flight hours per flight cycle (Figure 6.17) and engine age (Figure 6.16) influences maintenance cost. Scale factors can also be applied to account for hot or corrosive environments [182]. However, a baseline cost is necessary to represent the maintenance cost of the engine or airframe which can then be scaled using the relevant factor. This must be obtained by using published data for currently operating engines or by creating a baseline cost estimate using other methods.

In the absence of a baseline cost or assumed severity factors, cost estimating relationships may be used. More detailed methods may be used to estimate the maintenance cost of engines that link the cost estimate to the performance of each component [186]. Such methods must be linked to engine performance models. Further detail may be added through the use of activity based costing methods, however, the overall costs in these methods will similar combine to the labour, materials, and maintenance burden cost components [187]. For a preliminary design, the level of detail in an activity based costing method is unnecessary. However, simpler parametric cost estimating relationships can be applied.

For both the airframe and engine, a simple way to estimate maintenance cost is to break it down into three components: labour, materials, and maintenance burden [54, 188]. The labour cost accounts for the man-hours spent on maintenance activities. Material cost accounts for the parts or materials required during the course of maintenance. Finally, the maintenance burden accounts for indirect factors such as administrative costs. Cost estimating relationships

## 6. Maintenance Cost Estimation

---

for maintenance rely on a number of key parameters that correlate reasonably well to the maintenance cost. For the airframe, useful variables are its weight and acquisition price, as these correlate to the size of the aircraft and the cost of materials used in its manufacture. Weight and cost are also useful parameters for estimating the engine's maintenance cost for similar reasons, in addition to the engine's maximum thrust.

Many of the publicly available maintenance cost models for airframes are pre-2000 models that rely on older aircraft databases to create cost estimating relationships. However, aircraft are using increasing quantities of composite materials in their manufacture, as opposed to conventional metals such as aluminium. The common causes of failure for composite structures differ to those of metallic structures, with the damage caused by impacts being the main cause, rather than fatigue of metal structures [185]. Depending on the composite materials used, the repair of composite structures will also differ to the methods for repairing a metallic structure. Research by Raman *et al.* on the influence of advanced materials on the maintenance cost of the F/A-18 concluded that composite materials are generally more expensive than conventional materials [189]. However, the cost was identified to be dependent on the material and part type. Boeing claims that the predominantly composite B787 has a lower maintenance cost than metallic structures due to reduced fatigue and corrosion damage, and that the aircraft can be repaired in a similar manner to conventional metallic structures [190]. With the increasing use of composites in airframe structures, it may be reasonable to conclude that composite structures in the 2035 EIS period will not be noticeably more expensive than aluminium structures.

### 6.5.1 Maintenance Cost Model Selection

A detailed workscope for engine maintenance will naturally be the most accurate predictor of engine maintenance cost. However, this form of analysis is more applicable to in-service engines with a known operating procedures, known part cost, and requisite maintenance activities. Maintenance cost per year or flight cycle is then the result of a detailed schedule of work for engine maintenance. This detailed analysis is not useful for a preliminary cost estimate, and parametric cost estimating relationships are once again the most feasible option. In addition, detailed component design is not available for a preliminary design configuration. This rules out component-based maintenance cost estimates. Although a detailed maintenance cost estimate is not feasible, it is still important for the model to be able to represent maintenance cost as a function of engine operation. As identified in the previous section, maintenance requirements are dependent on factors such as local environment (e.g. hot airports) and flight cycle length. Flight cycle length is a particularly important aspect that must be represented if the cost of missions other than the baseline design mission is to be simulated. For a novel aircraft, maintenance cost cannot be estimated by scaling a known baseline cost, as there is no data from which a baseline value can be obtained. Applicable methods must therefore rely on regression analyses to identify how maintenance cost is related to known engine design variables such as thrust and temperature.

A selection of maintenance cost estimating relationships were chosen for the propulsion system and airframe. The combination of models provides a wider range of values for comparative purposes. Of the selected models, four covered the maintenance cost of engines and two covered the maintenance cost of the airframe. The following models were used to provide estimates from a range of time periods:

- ATA, 1967 (Airframe and engine models) [188]
- Liebeck *et al.*, 1995 (Airframe and engine models) [54]
- Kang *et al.*, 2008 (Engine model) [186]



## 6. Maintenance Cost Estimation

**Table 6.4:** Inputs for the selected cost estimating relationships

	ATA	Liebeck	Kang	Seemann
Airframe				
Airframe Weight	X	X	-	-
Block Speed	X		-	-
Aircraft Cost	X		-	-
Flight Hours (FH)	X	X	-	-
Engine				
SLS Thrust	X	X		X
Engine Weight				X
Engine Cost	X			
Component Performance			X	
Component Stages			X	
Component Diameters			X	
Engine Flight Hours (EFH)	X	X	X	X

- Seemann *et al.*, 2011 (Engine model) [191]

The cost estimating relationships presented by ATA, and Liebeck *et al.* break costs down into labour, materials, and maintenance burden to create an overall cost per trip or cost per flight hour. Separate relationships are provided for the airframe and engine. The relationships presented by Kang *et al.* and Seemann *et al.* estimate maintenance cost by predicting the interval between shop visits, the shop visit cost, and the cost of life-limited parts. Subsequently, these values can be used to estimate the average cost per flying hour or the cost per trip. The relationships provided by Kang *et al.* use the performance and dimensions of the fan, compressors and turbines during SLS operation (temperatures, pressures, tip speeds, number of stages and diameter) to create a cost estimate. An estimate of the engine dimensions is therefore required. This was obtained using in-house software for gas turbine sizing (Section 3.4.1). The model by Seemann *et al.* relies on a simpler relationship linking maintenance cost to the engine's thrust and weight. Table 6.4 breaks down the inputs required for each of the selected cost estimating relationships. None of the models provide standard errors of estimate. Therefore, confidence intervals cannot be produced for the maintenance cost estimates. The influence of flight time on the engine maintenance cost per flight hour may be presented as on a maintenance cost severity curve [182]. As each model includes the number of flight hours as an input, they may be used to produce severity curves similar to the example shown in Figure 6.17 by varying the input flight length.

It was assumed that a novel airframe configuration would not have significantly higher maintenance costs than a conventional planform, and hence that current models would be able to create a reasonable estimate. However, the selected models do not account for the potentially higher maintenance cost attributable to the use of a composite structure. The airframe maintenance cost models are predominantly a function of airframe weight. Therefore, a lighter airframe would lead to a lower cost estimate, even where a lighter airframe is the result of using advanced materials. Section 6.4 identifies that the RAND acquisition cost model includes materials weighting factors to scale the estimate based on the use of advanced materials. These materials weighting factors account for the fact that low weight can be the result of more expensive or novel materials. It is useful to incorporate a similar functionality in the airframe maintenance cost models. Both airframe maintenance cost models break the cost estimate into comparable groupings to the acquisition cost estimate: labour and materials. It was therefore be assumed that similar materials weighting factors may be applicable for the maintenance cost

## 6. Maintenance Cost Estimation

---

models. As an initial estimate, the material weighting factors from the acquisition cost modelling section were used. The two relevant factors are the materials and labour scale factors for airframe manufacture from Resetar *et al.* [173] and Younossi *et al.* [174]. The baseline aircraft is manufactured primarily from aluminium, with a small percentage of composite materials. The resultant material cost factors for the baseline aircraft therefore lead to a reduction in maintenance labour cost (WMCF = 0.932) and an increase in material cost (WMCF = 1.039). These materials weighting factors were used to provide an initial estimate of the influence of advanced materials on the cost estimate.

### Maintenance Cost for the N3-X

Predicting maintenance cost for a future novel aircraft is one of the main challenges in the techno-economic analysis. The selected engine maintenance cost models are derived from data for conventional turbojet and turbofan configurations. It can therefore be assumed that a reasonable estimate would be produced for the maintenance cost of the baseline aircraft's engines. However, these models will become less applicable as propulsion system configurations diverge further from current engines and as new components are added. This is especially true for the turbo-electric propulsion system of the N3-X, which incorporates a superconducting electrical system and multiple propulsors, rather than two to four individual propulsion units. As a result, the engine maintenance cost models are less applicable to the novel propulsion system configuration of the N3-X.

However, it can be assumed that a cost estimate could be produced for the turbomachinery, as these would likely be a similar configuration to more conventional propulsion systems. As the main engines are closer to turbogenerators than turbojets, they do not produce a thrust term suitable for the cost estimating relationships by Liebeck *et al.*, Seemann *et al.*, and Kang *et al.* As a preliminary estimate, the equivalent thrust-producing engine could therefore be used instead to represent the turbogenerators for a maintenance cost estimate. Whilst industrial gas turbine models may also be applicable for a power-producing engine, aero gas turbine models were used to ensure a consistent estimate between thrust-producing and non thrust-producing variants of the N3-X main engines.

The remaining two sub-systems are more challenging when creating a cost estimate. Superconducting electrical machinery is not currently used in commercial aircraft applications. At the time of the study, there is therefore no information available in literature on predicting its maintenance cost. In addition, industrial electric machines are at a difficult scale to electrical machines for an aircraft. Industrial maintenance cost models were therefore concluded to be unsuitable for the purposes of this research. Predicting the maintenance cost of an array of distributed fans is equally difficult, as such a configuration is not currently used on aircraft. Of the selected models, the maintenance cost for a fan is generally encompassed within the overall maintenance cost estimate for a turbofan engine.

These electrical system and propulsor array are key subsystems in the propulsion system. However, no information is available at this point in time to create a maintenance cost estimate for these two subsystems. Creating a maintenance cost estimate for the turbomachinery alone would therefore lead to an estimate that is likely to be unreasonably low, as it would neglect a large portion of the propulsion system. In order to obtain a preliminary cost estimate accounting for the whole system, the thrust and weight of the propulsion system as a whole was used (i.e. including the electrical system and propulsor array), as opposed to the thrust and weight of the equivalent engine. An alternative assumption may be to assume that the propulsor array needs minimal maintenance, as it simply consists of a number of fans. However, an additional cost model would still be required to predict the maintenance cost of the electrical system.

Therefore, given the scope of the study and the modelling fidelity requirement, this assumption is believed to be suitable. However, further work may wish to develop cost estimates for a turbo-electric propulsion system.

### 6.5.2 Maintenance Cost Model Validation

The maintenance cost estimates produced by the two selected models were validated against publicly available data for the maintenance cost of the baseline aircraft and its engines. Data was not available for the airframe maintenance cost of the B777-200LR. Instead, it was assumed that the airframe maintenance cost would be similar to that of other aircraft in the B777 series. Airframe maintenance cost per flight hour values were available for two flight cycle lengths: 7.5 hours for the B777-200ER and 3.0 hours for the B777-200/-300 (2008 data). Maintenance cost per flight hour data was available for the GE90-115B and the GE90 series of engines for a selection of flight cycle lengths from 2.8 to 10 hours (2012 data) [192]. Both data sets were scaled by the inflation rate to provide estimates for the the maintenance cost per flight hour at the current value of money. In some cases, the reference data is provided as a range of values. The mean value was therefore assumed to be applicable.

#### Airframe

Of the two models used to predict the airframe cost, the model by Liebeck *et al.* provides an estimate that closely matches the costs quoted by the reference source (Figure 6.18). The severity curve trend produced by the model fits closely to the two available data points. However, the ATA model significantly overestimates the airframe maintenance cost per flight hour. The two methods use similar components to estimate the overall airframe maintenance per flight hour and lead to similar severity curve trends. However, the ATA model estimate produces a labour time estimate that is twice that of the Liebeck model, leading to higher labour costs per flight hour. In addition, the prediction of the maintenance materials cost is higher. As the error in the ATA estimate is high, the model was not utilised for the N3-X cost estimate.

Including the materials weighting factors from the airframe acquisition price estimate provides a more accurate maintenance cost estimate than neglecting the factor. For a 7.5 flight hour mission, the reference data quotes a maintenance cost per flight hour between \$650 and \$732 (\$834.5 to \$741.0 in 2017 US\$) [193]. Without the materials scaling factors, the model by Liebeck *et al.* predicts a maintenance cost of \$897.3 per flight hour (7.5% to 21.1% error). After incorporating the materials cost factors, the maintenance cost per flight hour reduces to \$843.84 per flight hour, closer to the value from reference data (1.1% to 13.9% error). Whilst the model still overestimates cost, the factors were concluded to be a useful addition to the airframe maintenance cost estimate.

The maintenance severity curve produced by the model by Liebeck *et al.* was used to predict the impact of flight cycle length on the maintenance cost per flight hour. This severity curve was used to obtain a value for the airframe maintenance cost per flight hour of the baseline aircraft to be used as an input in the direct operating cost model (Figure 6.2).

#### Engine

The engine maintenance cost models by Liebeck *et al.* and Kang *et al.* noticeably underestimate the engine maintenance cost per flight hour (Figure 6.19). As with the airframe maintenance cost estimate, the ATA model significantly overestimates the engine maintenance cost per flight hour. Of the four selected models, the model by Seemann *et al.* produces an estimate that most closely reflects the maintenance cost values and severity curve. The largest error

## 6. Maintenance Cost Estimation

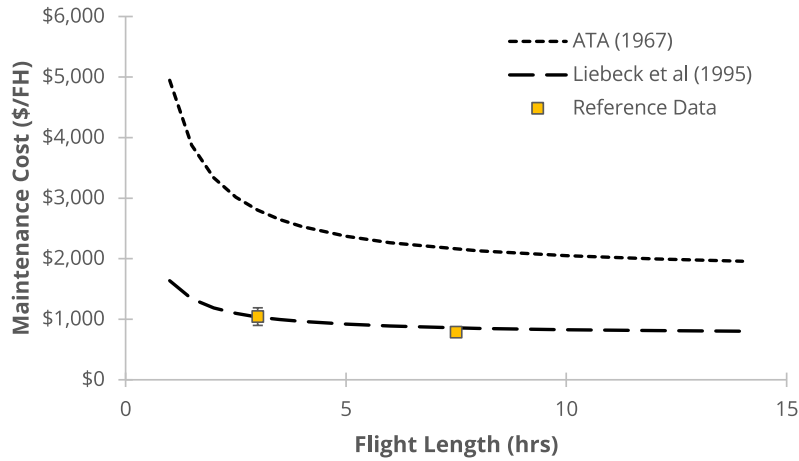


**Figure 6.18:** Airframe maintenance severity curve estimate for the baseline aircraft

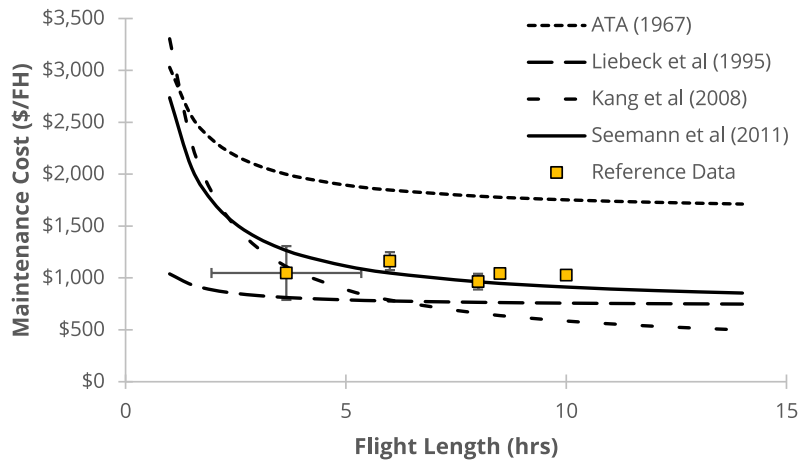


**Figure 6.19:** Engine maintenance severity curve estimate for the baseline aircraft

is for the lowest length flight where cost is overestimated, however, this may be a result of the wide range of values covered by this data point (flight length between 2.8 and 4.5 hours, cost from \$425 to \$545 per flight hour). Cost is slightly underestimated for the remaining points (0.15% to 9.9% error). Of the selected maintenance cost models, Kang *et al.* and Seemann *et al.* produce similar relatively steeper trends for the maintenance severity curve at shorter flight lengths. In contrast, Liebeck *et al.*'s model produces a much flatter severity curve. Excluding the 2.8 to 4.5 hour reference data point, the severity curve is most closely matched by Seemann *et al.* for longer range missions. It is difficult to conclude which trend is most accurate in the absence of more data points for very short flights. However, the most important range to cover is medium to long-haul flight lengths, as this is the typical operating range of the baseline aircraft. The closest cost estimate was provided by Seemann *et al.*. In addition, the model by Seemann *et al.* is the most recent of the selected models. It therefore follows that the model should reflect current maintenance costs for aircraft engines more accurately than the older models. This model was selected to provide an engine maintenance cost estimate using the resulting severity curve.

## 6. Maintenance Cost Estimation

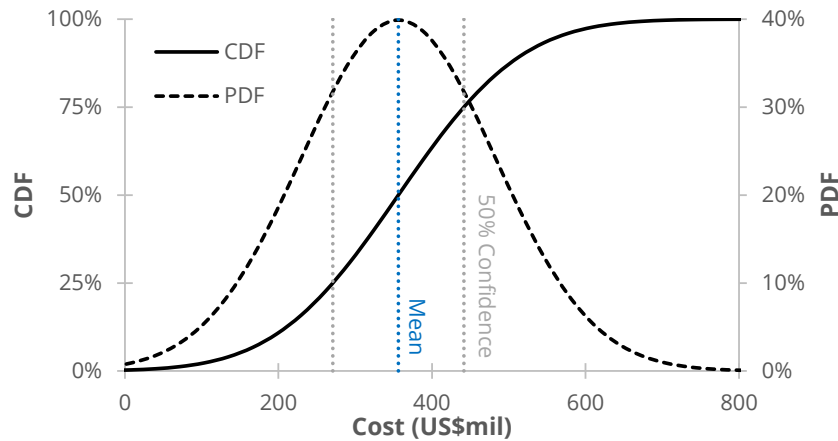


**Figure 6.20:** Probability and cumulative distribution functions for the N3-X aircraft cost estimate (normal distribution)

### 6.6 Application to the N3-X

The models selected in the previous two sections were used to predict the acquisition price and maintenance cost per flight hour as a function of the flight cycle length for the N3-X. For all the following estimates it must be highlighted that the values produced are preliminary values that are reliant on the assumptions made (e.g. application of material cost factors). It is likely that actual costs for the N3-X would differ from the values predicted in the following subsections. The values will be taken only as preliminary values to be used in combination with the direct operating cost sensitivity analysis.

#### 6.6.1 Acquisition Price

The N3-X was assumed to be a predominantly composite aircraft. As an initial estimate, the N3-X was assumed to be manufactured by the same materials by weight as the B787, a current aircraft manufactured from primarily composite material. Material composition by weight for the N3-X was taken to be 55% composite, 20% Aluminium, 15% titanium, and 10% steel [190]. For the initial cost estimate, it was assumed that the first lot of aircraft is equal to the number of aircraft for the B777-200LR lot (154 aircraft). A program difficulty factor of 1.5 was selected for the model. The model predicts an acquisition price of \$356.2mil (11% higher than the baseline aircraft cost), with a standard error of estimate equal to  $\pm$ \$126.6mil. Therefore, within a 50% confidence interval, the N3-X may cost between \$270mil and \$441mil, assuming a normal distribution (Figure 6.20).

The engine acquisition price model by Younossi *et al.* predicts a higher cost for the N3-X main engines than that of the baseline aircraft's engines. The remaining engine cost estimates produce similar results for the acquisition price of the N3-X main engines. Assuming the cost may be taken from the remaining three models, the main engines are predicted to cost between \$5.3mil and \$6.1mil, with a mean cost of \$5.73mil. Cost of the remaining components is \$2.27mil for the propulsor array and \$25.3mil for the electrical system. The total propulsion system cost is therefore predicted to be in the region of \$39.0mil. The total propulsion system cost for the baseline aircraft is in the region of \$48mil. As the N3-X is a lighter, more efficient aircraft with lower thrust requirement, it is to be expected that its propulsion system would be smaller and hence cheaper than an older system. However, the estimate does not account for the potentially high costs of a novel system (especially superconducting systems) and the development costs of its constituent technologies.

## 6. Maintenance Cost Estimation

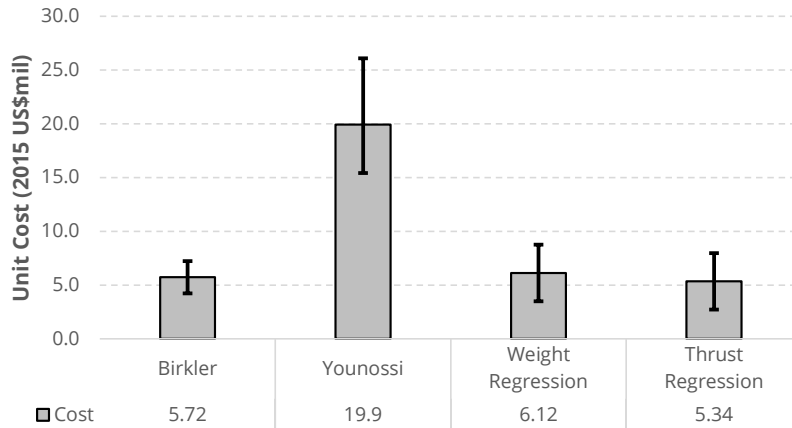


Figure 6.21: N3-X gas turbine engine cost estimates, including standard error of estimate

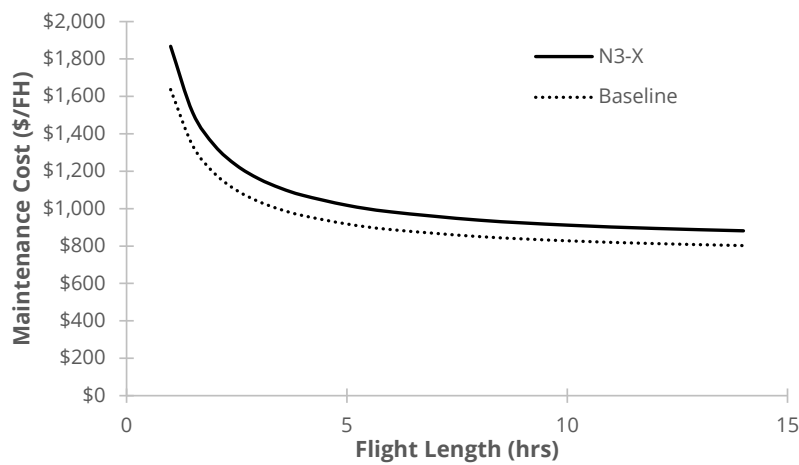


Figure 6.22: Airframe maintenance severity curve estimate for the N3-X versus the baseline aircraft

### 6.6.2 Maintenance Cost

The maintenance cost model predicts a slightly higher maintenance cost per flight hour for the N3-X than the baseline aircraft (Figure 6.22). However, this difference is due to the higher material cost factors used to modify the cost estimating relationships. The N3-X is a lighter aircraft than the baseline aircraft due to the use of composite materials and a different airframe configuration. As the airframe maintenance cost estimate uses weight as an input, the estimate would otherwise produce a lower maintenance cost per flight hour than the baseline aircraft. However, the material and labour costs for composite materials are currently higher than for conventional aluminium airframes, as identified in the acquisition cost modelling section (section 6.4). The materials scale factors therefore account for this difference in material type. For the N3-X, a predominantly composite airframe leads to a higher labour (WMCF = 1.010) and material cost (WMCF = 1.597).

The thrust and weight of the propulsion system as a whole was used in the engine maintenance cost model. In the absence of maintenance cost estimates for propulsor fans and superconducting, this provides a potentially more reasonable propulsion system maintenance cost estimate. The engine maintenance cost model would otherwise produce a low cost estimate, due to the low maximum thrust and weight of the turbogenerator equivalent engine in comparison to the baseline aircraft's engines.

Despite including the entire propulsion system, the maximum thrust and weight of the N3-X

## 6. Maintenance Cost Estimation

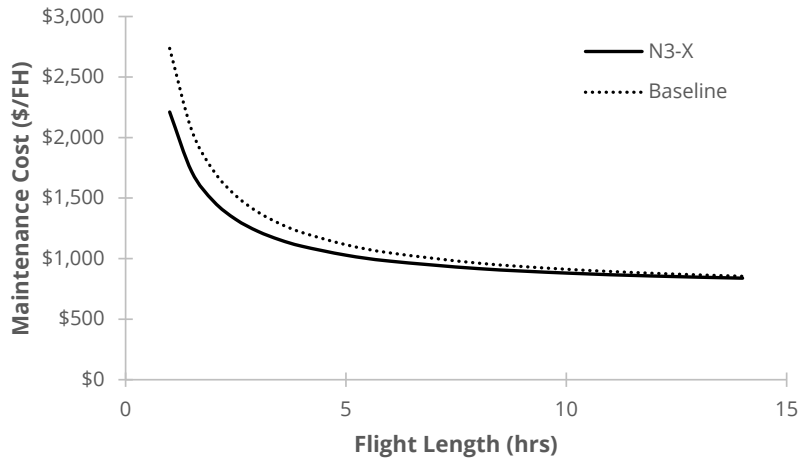


**Figure 6.23:** Engine maintenance severity curve estimate for the N3-X versus the baseline aircraft

propulsion system system is lower than the baseline aircraft. The resultant engine maintenance cost per flight hour is therefore lower than that of the baseline aircraft (Figure 6.23). This presents one of the key difficulties in applying a conventional maintenance cost model to a novel configuration. Cost models are functions of well-correlated values such as thrust and weight. For an efficient configuration such as the N3-X, thrust requirements are relatively lower than they would be for an aircraft of similar size, hence necessitating a smaller propulsion system. This will result in a lower cost estimate for maintenance. However, the maintenance cost will also be a function of the novelty or complexity of a system, as a highly complex system with many parts may need more frequent part replacement. Given the novelty of the N3-X propulsion system and its multiple sub-systems, it is likely that actual maintenance costs will be higher than predicted. A 'complexity' factor may be needed to scale costs for novel configurations containing multiple sub-systems and components. In addition, maintenance cost models for the superconducting electrical system must be developed. The values produced for the maintenance cost estimate are therefore useful only to provide a very rough idea of the cost region in terms of maintenance cost per flight hour.

## 7. Techno-economic Analysis

Performance analyses for the N3-X have demonstrated that energy savings in the region of 60% are possible in comparison to the baseline. For a conventional aircraft, fuel contributes in the region of 30% to the total direct operating cost for an operator. A 60% fuel saving will therefore reduce direct operating cost by 18%. As fuel price increases, the percentage contribution of fuel to direct operating cost increases and hence the resultant savings provided by the aircraft will increase. However, Chapters 2 and 6 identified that fuel is not the whole story once the costs of an aircraft are being assessed. This leads to one of the key questions addressed by this research: *Will a high efficiency aircraft translate into an economically viable concept?* The techno-economic analysis method described in Chapter 6 provides a method to assess the economic viability of an aircraft concept and a way to identify the financial value of fuel savings offered by a high-efficiency aircraft. Greater fuel savings will lead to a greater financial value to the manufacturer, enabling a higher sale price for the aircraft. This can either provide a greater margin for a high cost development program or, in the best case scenario where development and manufacturing costs are low, provide a good profit margin for the manufacturer. The techno-economic analysis attempts to identify the point where the high fuel saving of a future aircraft concept is able to translate into an economically viable product. As a part of the analysis, the techno-economic framework can be used to identify the maximum viable cost of the aircraft, representing the financial value of a high efficiency aircraft. This financial value is closely linked to the economic environment, particularly fuel price, as low fuel price decreases the economic value of fuel savings versus an older aircraft.

Before moving on to a techno-economic analysis of the aircraft, it is important to identify key costs that will factor into the analysis. A core aspect of the economic analysis for an aircraft is the price of fuel. As the cost of fuel varies over time, a fixed value will be selected for the following techno-economic analyses unless otherwise stated. The selected price is the fuel price as of 14<sup>th</sup> of July 2017: \$477.2 per metric tonne of kerosene (60.6 \$/bbl). The LH<sub>2</sub> variant of the aircraft has also been included in the techno-economic analysis. However, the future cost of liquid hydrogen as an aviation fuel is unknown, particularly if industry focus is turned towards the development of zero carbon fuels. An initial estimate of the fuel price of LH<sub>2</sub> was made based on targets for hydrogen production. This establishes a price point of \$2.00 per kilogram LH<sub>2</sub> (target for 2020, LH<sub>2</sub> production through water electrolysis) [194]. This value is set as an expected value for 2035, however, current estimates for the price per kilogram of LH<sub>2</sub> are significantly higher at around \$6.90 per kilogram LH<sub>2</sub> [194].

Additional parameters used for the analysis are an interest rate of 5.5% per year and an insurance cost per year equal to 0.5% of the aircraft's initial value. The exact insurance and interest rates will be operator, aircraft and/or route specific, however, these represent feasible values for aviation [13]. The weighted average cost of capital for the airline industry varies year on year between 7–8%, but was assumed to be 8% for the purposes of the analysis [12]. Exact values will be operator-specific, however, this is a representative value for the industry as a whole. Pilot salary was assumed to be US\$105,720 per year and crew salary was assumed to



be US\$48,500 per year [152].

### 7.1 Direct Operating Cost

It is first useful to identify the influence that fuel consumption has over the direct operating cost of the aircraft as a function of mission length. As an initial point of reference, direct operating cost will be compared assuming that the N3-X has the same acquisition price and maintenance cost per flight hour as the baseline aircraft. Chapter 6 identified that an aircraft's direct operating cost is influenced by a range of factors. A reasonable fuel saving therefore translates into a smaller direct operating cost saving (assuming all other costs remain equal). Therefore, for the kerosene N3-X and at the July 2017 fuel price, a fuel saving of just over 60% for the design missions leads to a DOC saving of 21.1%, with a lower DOC saving for shorter mission ranges (assuming all other costs remain equal, Figure 7.1). Despite a large saving in fuel consumption, the overall cost benefits are relatively lower. This reason for this outcome may be found by identifying the percentage contribution of each cost component to the overall direct operating cost (Figure 7.2). At the July 2017 fuel price, fuel burn accounts for approximately 36% of the total direct operating cost estimate for the baseline aircraft. As the flight range reduces, the total fuel burn reduces, and fuel therefore contributes less to direct operating cost than for long range missions. In addition, there is a non-linear relationship for the difference in fuel burn between the baseline and the N3-X (Figure 4.26). As a result of these two trends, the net difference in fuel consumption reduces with the mission range, leading to a non-linear reduction in direct operating cost saving as the mission range is reduced. The fuel saving offered by the N3-X increases as the aircraft payload is reduced (Figure 4.29). However, the change in fuel consumption is less significant between different payload capacities than different mission ranges. In addition, a reduction in fuel burn means that the percentage contribution of fuel to direct operating cost reduces slightly as a function of the payload (Figure 7.3). The direct operating cost saving therefore increases only slightly as the payload is reduced. For the 7500 nautical mile mission, reducing payload from the maximum to zero payload improves the energy saving by +4% but increases the direct operating cost saving by only +1%.

Acquisition-related costs such as interest and depreciation contribute a significant percentage to the overall direct operating cost (Figure 7.2). A small percentage increase in the aircraft's acquisition price would therefore lead to a noticeable increase in direct operating cost. Maintenance, the other key unknown cost, contributes a relatively smaller percentage to the total direct operating cost, and therefore has a smaller influence over the direct operating cost.

As fuel consumption (or fuel price) decreases, the contribution of fuel cost to direct operating cost decreases and the percentage contribution of the remaining cost components increases. Even when assuming the same acquisition price and maintenance cost as the baseline aircraft, the costs related to acquisition price outweigh the cost of fuel. For a high efficiency and novel aircraft such as the N3-X, maintenance cost and acquisition price are likely to be higher than for a conventional aircraft, whilst fuel costs will be lower. Maintenance may therefore contribute more to the total direct operating cost of a future novel aircraft than fuel. This suggests that there may be a shift in focus in the future from developing more fuel-efficient technology to developing low maintenance or low cost technology as fuel becomes a negligible component of direct operating cost.

The influence that fuel consumption has over direct operating cost is naturally a function of the current fuel price, with a high fuel price meaning that fuel contributes more to the total direct operating cost. Historically, a high fuel price has encouraged investment in new aircraft, as the penalties of operating less efficient aircraft are high. This can be demonstrated by identifying how historical fluctuations in fuel price influence the direct operating cost estimate (Figure 7.4a).

## 7. Techno-economic Analysis

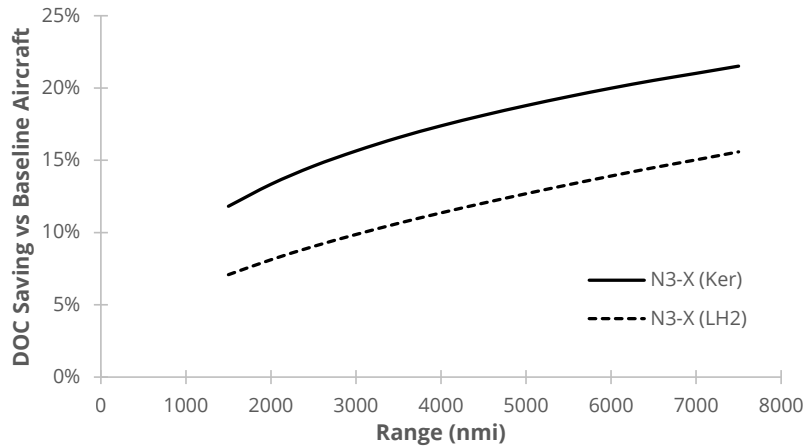


**Figure 7.1:** Direct operating cost comparison for the N3-X and baseline aircraft (assuming acquisition and maintenance equal to the baseline)

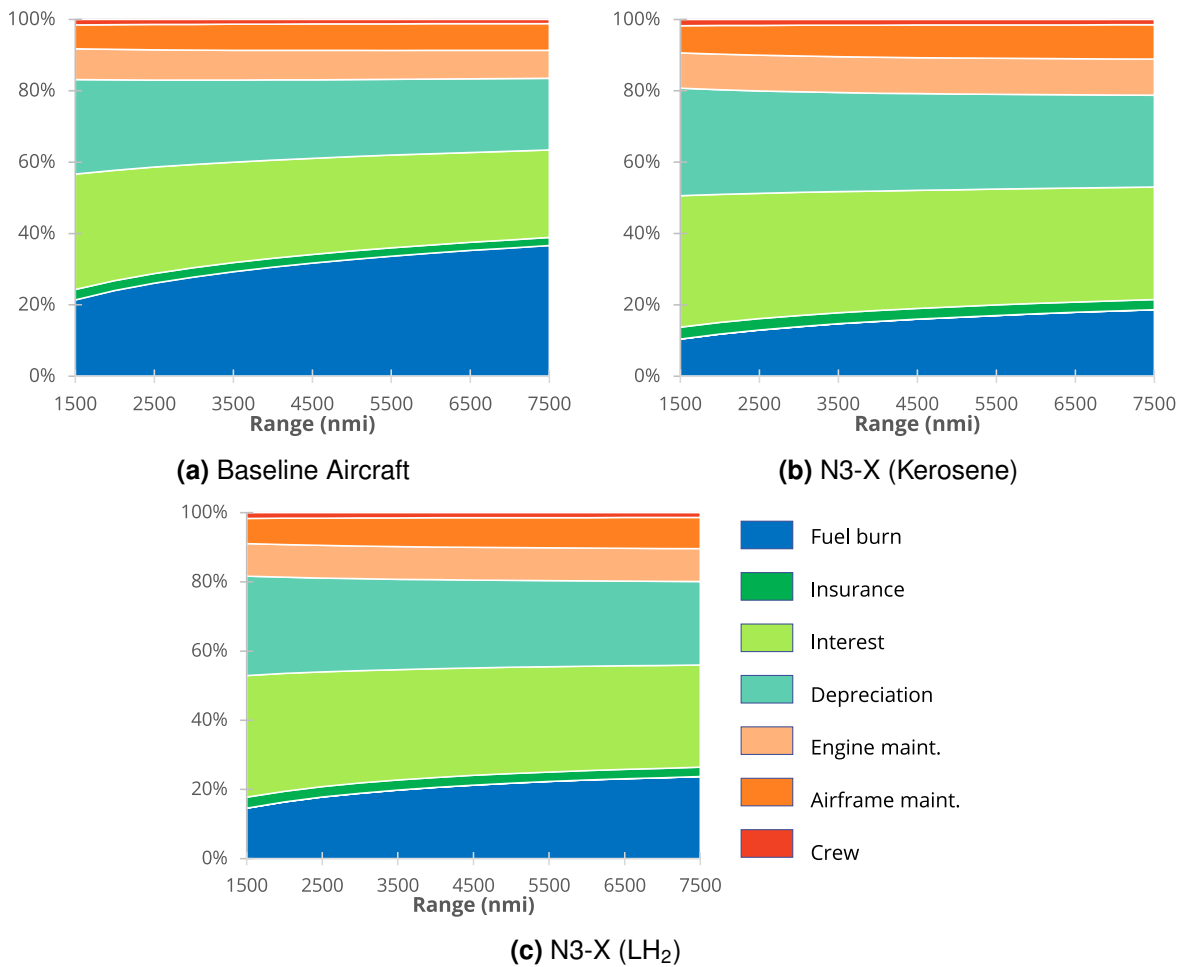


**Figure 7.2:** Breakdown of direct operating cost components as a function of mission range

## 7. Techno-economic Analysis

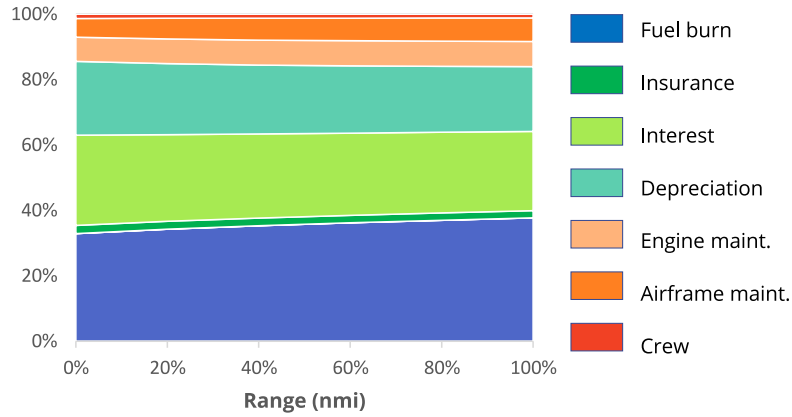


**Figure 7.3:** Breakdown of direct operating cost components for the baseline aircraft as a function of payload (7500 nmi)

In comparison to the DOC estimate for July 2017, the peak price in March 2012 leads to a 48% increase in direct operating cost for the baseline aircraft. In contrast, direct operating cost for the kerosene N3-X increases by only 34% when using the March 2012 fuel price. This is a result of the lower contribution of fuel to overall direct operating cost in comparison to the baseline. It is also important to highlight that the direct operating cost of the LH<sub>2</sub> variant is assumed to not be subject to fluctuations based on changes in fuel price, as it would not be reliant on the supply and demand of oil. The large fuel savings of the N3-X mean that, in a high fuel price scenario, the direct operating cost saving becomes significant (Figure 7.4b). For the March 2012 fuel price of \$1079.4 per metric tonne, the saving in DOC is 34%, rather than 21% DOC saving at the July 2017 fuel price.

The direct operating cost saving of the LH<sub>2</sub> variant is larger at a high kerosene fuel price than the kerosene N3-X. Conversely, the direct operating cost saving for the LH<sub>2</sub> N3-X is lower when the price of kerosene is low. As the price of LH<sub>2</sub> is assumed to be fixed, the aircraft's direct operating cost is not influenced by changes in the price of kerosene. This is advantageous in periods of relatively high fuel price, as the operating cost is relatively lower than a kerosene fuelled aircraft. However, the fixed fuel price means that operating cost benefits are not evident when the current price of kerosene falls. The operating cost of the kerosene fuelled N3-X is therefore relatively cheaper than that of the LH<sub>2</sub> variant. The analysis also highlights that there is a fuel price combination (LH<sub>2</sub> and kerosene) for which the direct operating cost of the LH<sub>2</sub> N3-X is the same as that of the kerosene N3-X. Equally, there is a fuel price combination for which the direct operating cost of the LH<sub>2</sub> N3-X is the same as that of the baseline aircraft. Therefore, for any current kerosene fuel price, there is a target LH<sub>2</sub> fuel price beyond which the LH<sub>2</sub> aircraft is not advantageous, as fuel costs are higher. In the direct operating cost simulation using July 2017 kerosene fuel price, the direct operating cost of the kerosene N3-X is lower than that of the LH<sub>2</sub> N3-X, given the LH<sub>2</sub> fuel price assumption (Figure 7.4b). However, for fuel prices in the 2012–2015 simulation period, the LH<sub>2</sub> N3-X has a lower direct operating cost. The exact value at which the DOC is equal is dependent on the mission length, as the fuel consumption of the two aircraft does not decrease at an equal rate (Figure 4.26). The LH<sub>2</sub> price per kilogram for which fuel cost of a LH<sub>2</sub> aircraft is equal to the kerosene options is calculated as follows:

$$C_{\text{Breakeven,LH2}} = \frac{M_{\text{Kerosene}}}{M_{\text{LH2}}} C_{\text{Kerosene}} \quad (7.1)$$

The break even fuel price in terms of the total DOC will depend on how much the remaining

## 7. Techno-economic Analysis

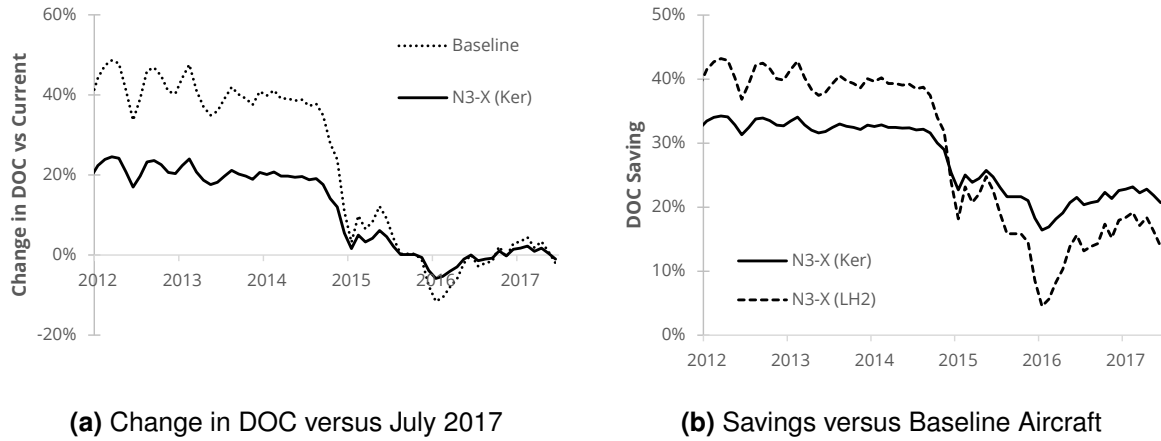


**Figure 7.4:** Influence of historical fuel price changes on the fuel and direct operating cost estimates for a 7500 nmi mission (Fuel price data source: IndexMundi)

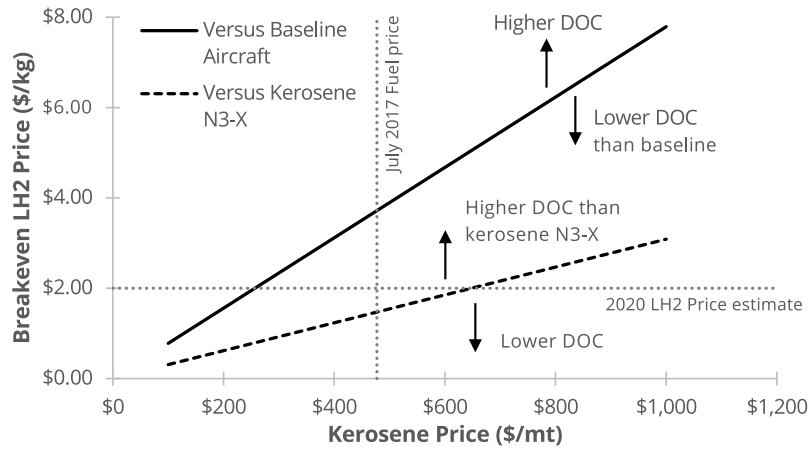


**Figure 7.5:** Hydrogen fuel price for which LH<sub>2</sub> N3-X DOC is equal to DOC for the baseline aircraft and kerosene N3-X (7500 nmi mission)

costs are in comparison to the baseline aircraft or kerosene N3-X:

$$C_{\text{Breakeven,LH2}} = \frac{M_{\text{kerosene}}C_{\text{kerosene}} + \sum C_{i,\text{kerosene}} - \sum C_{i,\text{LH2}}}{M_{\text{LH2}}} \quad (7.2)$$

Where  $C_i$  represents the remaining components of direct operating cost (insurance, maintenance etc.). The higher the remaining costs, the lower the break even LH<sub>2</sub> price will be, as the cost of fuel must be lower to compensate for increased costs elsewhere. The break even LH<sub>2</sub> price increases as kerosene price increases, due to the lower fuel burn by mass of the LH<sub>2</sub> variant (Figure 7.5). The LH<sub>2</sub> variant is therefore able to operate with a higher cost per kilogram of fuel, whilst remaining cheaper than the aircraft with kerosene. The break even LH<sub>2</sub> price is higher when comparing the baseline aircraft and the LH<sub>2</sub> N3-X variant, as the difference in fuel burn by mass is higher. There is a similar outcome as the mission range is varied. The difference in fuel burn by mass is higher for the longer range missions. The break even LH<sub>2</sub> price therefore increases as the mission range increases. In order to match the direct operating cost of the kerosene N3-X, LH<sub>2</sub> price per kilogram would need to achieve a price point of no more than \$1.47 per kilogram of LH<sub>2</sub> fuel. Alternatively, given the current cost estimate for LH<sub>2</sub> of \$2.00 per kilogram of fuel, a kerosene fuel price of \$650 per metric tonne (\$82.5/bbl) would match the direct operating cost of the two fuel variants.

### 7.2 Investment Cost Analysis

For a high efficiency concept such as the N3-X, considering a change in fuel consumption alone will naturally lead to a reduction in cost (Figure 7.1) and therefore an economically attractive product. However, it is unlikely that all other costs will remain the same for a novel aircraft concept. A core part of the techno-economic analysis is therefore to predict the sensitivity of direct operating cost to acquisition price and maintenance cost. In addition, the net present value analysis described in Chapter 7 must be introduced, as the aircraft should offer a good return on investment for the operator. Assuming a fixed income, the return on investment decreases as costs increase. There is therefore a limiting value which represents the maximum cost, beyond which the aircraft is no longer a commercially viable product. This has also been combined with the maintenance cost and acquisition price estimates. It is then possible to identify whether the cost estimate lies within the economically viable region (see Figure 6.5 for a description of the sensitivity analysis output). The cost estimates will be shown as overlays on the sensitivity analysis chart, including a 50% confidence interval for the acquisition price and  $\pm 10\%$  bounds for the maintenance cost (in the absence of a standard error of estimate).

The previous section demonstrated that the influence that fuel savings have over cost is limited by the fact that other costs contribute a relatively larger proportion to the total direct operating cost. In addition, the influence of fuel savings over direct operating cost is lower as mission range is reduced, due to a smaller difference in fuel burn by mass (Figure 7.1). As a result, there is a smaller margin for an increase in acquisition price or maintenance cost for short range missions (Figure 7.6). Two example mission ranges were selected for the sensitivity analysis: a medium haul 2500 nmi flight (Figure 7.6a), and the design 7500 nmi mission (Figure 7.6b). For a short range mission, there is less financial value to the fuel savings offered by the N3-X as other costs outweigh the significance of the cost of fuel (Figure 7.2). For the 7500 nautical mile mission, fuel is 36% of the direct operating cost. In contrast, it is only 26% of direct operating cost for the 2500 nautical mile flight. This is a particularly important aspect when considering the application of the aircraft to high capacity, short haul routes. The low cost margin means that it will be difficult to market the aircraft as a lower cost alternative for such operators, unless the acquisition price and maintenance cost can be kept low. For the design mission and at the July 2017 fuel price, the maximum reasonable increase in acquisition price compared to the baseline aircraft is approximately 24.0% (assuming no change in maintenance cost per flight hour). The maximum reasonable acquisition price increase drops to 13.5% for the shorter 2500 nmi mission, as there is less financial value gained from the fuel saving. Whilst the aircraft would still be profitable for an acquisition price increase of up to 48% for the design mission, the return on investment would no longer be sufficient. As maintenance cost is increased, the maximum reasonable acquisition price decreases. However, maintenance cost has a much smaller influence over cost than acquisition price, as it contributes a smaller percentage to the total direct operating cost.

If the N3-X is targeted at a market operating primarily at missions near the design mission (7500 nmi, maximum payload), this may rule out its attractiveness for short to medium haul markets. The 24% increase in acquisition price is reasonable for the 7500 nmi mission. However, for shorter range missions, this acquisition price would not provide an adequate return on investment for an operator. This may present a difficulty when the majority of the baseline aircraft's missions are operated at less than the maximum range (Figure 4.24). There may therefore be a benefit to targeting a lower range mission as the design mission from a cost perspective. The lower acquisition price target will make the aircraft more attractive for long-haul operators (offering a higher direct operating cost saving), without ruling out the feasibility of the aircraft for medium-haul or high capacity short-haul applications. A design mission should

## 7. Techno-economic Analysis

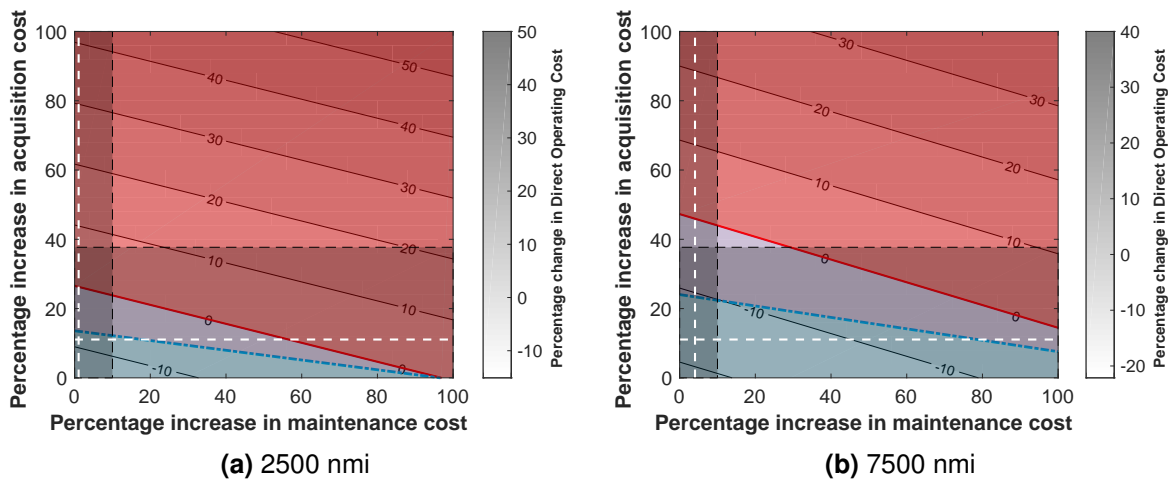


**Figure 7.6:** Direct operating cost sensitivity analysis for the kerosene N3-X in comparison to the baseline aircraft

therefore be selected that will maximise the potential market. At first glance, this may appear to define the lowest likely mission range as the design target, as this will lead to the lowest acquisition price target with the best savings for longer range missions and the widest range of economically viable missions. However, a very low acquisition price target may not be feasible for the manufacturer. This must also be taken into account when defining the economic design mission.

The acquisition cost estimate for the N3-X in Section 6.6.1 produces a cost 11% higher than that of the baseline, well within the maximum reasonable acquisition cost for the two selected missions. As the magnitude of the maintenance cost per flight hour is dependent on the mission range (Figure 6.22 and Figure 6.23), the predicted maintenance cost relative to the baseline aircraft is not constant. Nevertheless, the estimate of the maintenance cost is also well within the maximum reasonable limits. In combination, the cost margins seem reasonable, as the resulting cost lies within the economically viable region of the sensitivity analysis. However, the outer bounds of 50% confidence interval for the acquisition price estimate lie outside the viable region. In the case of the shorter range mission, this enters a region where the N3-X would be more expensive to operate than the baseline aircraft.

There is a reasonable margin for a higher cost when operating the aircraft on longer range missions. For mission ranges of approximately 1000 nautical miles or less, the acquisition price and maintenance cost of the N3-X must equal that of the baseline aircraft in order to be economically viable. This will likely limit the attractiveness of the aircraft as a product for operators with high capacity short haul route, as it is unlikely that the manufacturers could achieve such a price point.

It should be highlighted that the cost estimates are only preliminary values, and are therefore used only to gain an insight as to whether the cost margins are reasonable. The cost estimates lie below the maximum viable cost, suggesting that there is potential for the aircraft to be economically viable. An economically viable aircraft would be much less likely if the cost estimates were to lie above the maximum viable cost, as reducing the acquisition price of a novel aircraft would be challenging. Other measures would be necessary to increase the maximum viable cost (such as taxation) in order to add financial value to a high efficiency aircraft concept and hence justify higher development or manufacturing costs for a manufacturer. Alternatively, a manufacturer would have to operate at a loss to set a lower list price.

For the design 7500 nmi mission, fuel contributes 17% of the total direct operating cost of

## 7. Techno-economic Analysis

---

the N3-X, whilst maintenance cost accounts for 19% of the total direct operating cost (using the cost estimate produced in Chapter 6). In contrast, this split is 36% and 16% for fuel and maintenance components, respectively, of the direct operating cost of the baseline aircraft. In the previous section, it was suggested that high efficiency, low fuel cost aircraft may shift industry focus from improving fuel consumption to reducing maintenance cost. This outcome reinforces the initial suggestion, as fuel is now a smaller component of the N3-X direct operating cost than maintenance cost. This is even more so the case for shorter range missions, where fuel contributes less to the total direct operating cost whilst maintenance cost per flight hour is higher.

Although maintenance cost for the N3-X is a more significant cost than fuel costs, there is also a benefit to aiming for low acquisition price rather than low maintenance cost. Acquisition price of the aircraft links to the largest components of the direct operating cost: depreciation and insurance. In addition, the acquisition price of the aircraft is a sunk cost once the aircraft has been purchased. The resulting depreciation, interest repayments and insurance costs are effectively fixed and will be paid regardless of how often the aircraft is flown. In contrast, maintenance cost has a relatively smaller influence over direct operating cost. Assuming acquisition cost is kept low, the maintenance cost of the N3-X can be more than double that of the baseline aircraft, whilst still offering a lower direct operating cost. An operator also has slightly more control over an aircraft or propulsion system's maintenance costs, such as by improving maintenance practice or by modifying aircraft/engine operation. A high maintenance cost may therefore be considered more acceptable to an operator than a high acquisition price.

From an economic perspective, a lower acquisition price may be considered acceptable even at the expense of an increase in maintenance cost, as this may increase the direct operating cost saving. However, from a research perspective, reducing maintenance costs may become a new dominant driver for the development of future aircraft concepts once low fuel costs become the norm.

### 7.2.1 Alternative Scenarios

The previous sensitivity analysis uses a fuel price equal to the July 2017 fuel price of \$477.2/mt (60.6 \$/bbl) and no carbon taxation. However, it is useful to consider the influence of other fuel price scenarios on the sensitivity analysis. Two sample fuel prices were selected from historical fuel price data: a local peak fuel price in March 2012 of \$1079.4 per metric tonne (\$137.1/bbl) and a local minimum fuel price in January 2016 of \$307.9 per metric tonne (\$39.1/bbl). A low fuel price will reduce the financial value of a reduction in fuel burn, as fuel becomes a minimal aspect of direct operating cost. The reverse is true in a high fuel cost scenario, where the financial penalties of operating a low efficiency aircraft are higher. Fuel price therefore has a noticeable influence on the direct operating cost saving (Figure 7.4) and hence on the maximum economically viable cost (Figure 7.7). For the March 2012 fuel price of \$1079.4 per metric tonne, the maximum reasonable acquisition price increases from 24.0% greater than the baseline aircraft's acquisition price to 54.3% greater (Figure 7.7a). The high fuel price dramatically increases the percentage contribution of fuel consumption to the total direct operating cost of the baseline aircraft. The fuel savings offered by the N3-X therefore lead to a much greater improvement in direct operating cost. The margins for an increase in cost are therefore much larger and acquisition price and maintenance cost estimates lie fully within the viable region. This outcome reflects historical trends for the aviation industry, where high fuel prices encourage investment in new, high efficiency technology, as the fuel savings lead to a larger reduction in operating cost. In contrast, fuel price in January 2016 reached a low of \$307.9 per metric tonne. In this case, the maximum reasonable acquisition price reduces to

## 7. Techno-economic Analysis

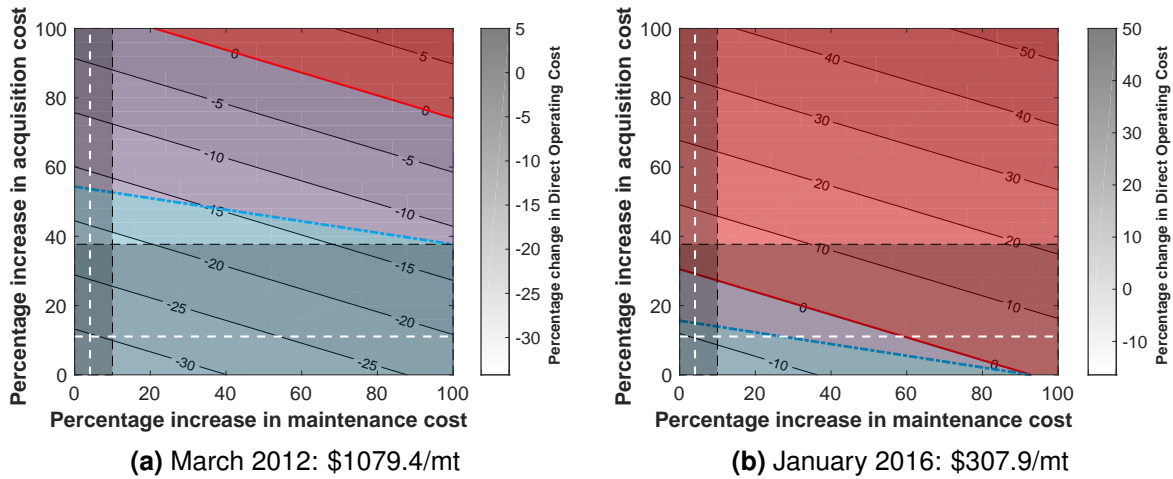


**Figure 7.7:** Direct operating cost sensitivity analysis for the kerosene N3-X in comparison to the baseline aircraft – Alternative fuel price scenarios (7500 nmi)

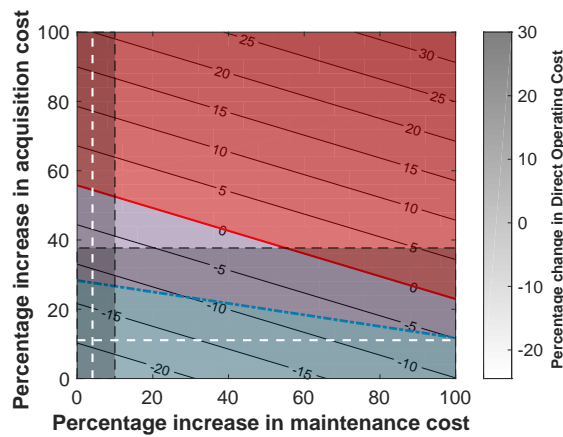


**Figure 7.8:** Direct operating cost sensitivity analysis for the kerosene N3-X in comparison to the baseline aircraft – Carbon tax \$27/mt, Fuel price \$477.2/mt (7500 nmi)

15.6% of the baseline aircraft's value (Figure 7.7b). In this fuel price scenario, it is hard to justify the purchase of a high cost aircraft unless acquisition price and maintenance cost can be kept low. For mission ranges of 3000 nautical miles or less, the acquisition price and maintenance cost of the N3-X must equal that of the baseline aircraft in order to be economically viable. This rules out the N3-X as a commercially viable option for high capacity short- to medium-haul routes.

The previous analyses have assumed that there is no CO<sub>2</sub> emissions taxation. However, it is feasible that a worldwide carbon tax could be introduced to cover aircraft CO<sub>2</sub> emissions. It is difficult to predict an exact value for this carbon tax, however, estimates for the price of CO<sub>2</sub> emissions for 2035 provide a value of between \$30 and \$73 per short ton [195]. As with a high fuel price scenario, emissions taxation penalises the use of less efficient aircraft and would encourage investment in newer aircraft. The cost of CO<sub>2</sub> emissions adds a further element to the aircraft's direct operating cost and would, for CO<sub>2</sub> emissions, increase in proportion with fuel consumption. In a CO<sub>2</sub> emissions taxation scenario there is a wider margin for an increase in acquisition and maintenance cost, as the N3-X would now reduce both fuel and CO<sub>2</sub> emissions costs by 60%. Assuming a taxation scenario of \$30 per short ton CO<sub>2</sub> (\$27/mt CO<sub>2</sub>), the maximum reasonable acquisition price increases to 30% greater than the acquisition price of the baseline aircraft (Figure 7.8). The higher the taxation, the more low efficiency aircraft are



## 7. Techno-economic Analysis

---

penalised. CO<sub>2</sub> emissions taxation is therefore a useful way of encouraging investment in novel high efficiency concepts. This reflects conclusions in previous research, which identified that CO<sub>2</sub> emissions taxation would be useful in encouraging the adoption of novel aircraft concepts [78, 83]. However, relatively lower carbon taxation could be applied, as the large fuel saving of the N3-X provides a good financial incentive to invest.

Two key scenarios have been considered in this section: fuel price and emission taxation. However, there are a number of other variables that may influence viability depending on the scenario. Many are reliant on the business practice of specific operators, as each will have their own unique combination of aircraft utilisation and ownership models. From the factors included in this research, there are a number of additional considerations that will influence viability:

- **Load Factor** – The analyses predominantly focus on an aircraft with 100% load factor and the maximum possible payload. Operating with a lower payload will reduce the mission fuel burn and leads to a higher energy saving versus the baseline aircraft (Figure 4.29). Although energy savings are higher, the percentage contribution of fuel to the direct operating cost of the baseline aircraft reduces as the payload is reduced (Figure 7.3). As a result, payload weight on board the aircraft has a relatively small influence over the direct operating cost saving. A greater advantage is therefore gained in terms of the aircraft's energy saving versus the baseline aircraft than the direct operating cost saving. Nevertheless, the average mission identified in Section 4.7 identified that the typical payload will be less than 90% of the maximum payload. This will improve the direct operating cost saving for the average mission, and hence will increase the maximum viable cost of the aircraft.
- **Flight Length and Flights per Year** – As both the N3-X and the baseline aircraft are assumed to fly at the same cruise speed, there is a negligible difference in flight time between the two aircraft. As a result, the N3-X could theoretically be used as a direct substitute for the baseline aircraft, with no changes to slight scheduling. In this case, the number of flights per year for the two aircraft would be the same. If the flight speed of the aircraft were to differ, different scheduling requirements may be required which would lead to a different number of flight cycles per year for each aircraft. In terms of the cost analysis, the per flight cycle contribution of acquisition cost related terms would vary depending on the number of flight cycles per year. A larger number of flights per year would decrease the per-flight contribution of yearly costs such as depreciation and decrease the total DOC of a flight. This would increase the benefits gained from the fuel savings of the N3-X and hence increase the margins for an increase in cost. In contrast, less flights per year would place a higher burden of acquisition cost-related terms on the DOC of a flight. In addition, maintenance cost is estimated as a per flight hour value. A different flight length would therefore change the mission's maintenance cost.  
  
The number of flights per year is also dependent on the operator. Whilst a general assumption was applied in this research to link flight length to flights per year (Figure 6.3), the actual outcome will depend on the operator's scheduling requirements.
- **Useful/economic Life** – Reducing the aircraft's useful life will increase the aircraft's yearly depreciation (assuming the same residual value at the end of the aircraft's life). This will increase the direct operating cost estimate and reduce the influence of fuel savings. A longer expected life or utilisation period is beneficial for the operator, as it allows more time for a return on potentially high initial investment costs. If the two aircraft being compared in an economic analysis have different lives, the comparison is more difficult as it would be incorrect to use the same period of time for both aircraft.

## 7. Techno-economic Analysis

---

- **Insurance Rate** – Insurance rate depends on the aircraft type and route. Whilst a novel aircraft such as the N3-X could potentially be subject to a higher insurance rate, it is unlikely to diverge significantly from the insurance rate for current aircraft as this would be detrimental for the new aircraft market.
- **Interest Rate** – An increase in interest rate will naturally increase the aircraft's direct operating cost, and hence reduce that influence that fuel savings have over the aircraft's direct operating cost. A high interest rate will also establish a higher target rate of return for the aircraft, as WACC may be higher. This will further reduce the maximum economically viable cost of the aircraft.
- **Magnitude of Initial Investment** – The direct operating cost estimate assumes that the aircraft is fully financed through debt, i.e. the operator borrows money to cover the full cost of the aircraft. It is possible that the operator may choose to finance the purchase through a combination of debt and alternative sources (such as equity or by reinvesting profits in the purchase of new aircraft) or an outright purchase. This reduces the initial cost at the start of the aircraft's life and also reduces the yearly interest repayment. It may also reduce the target rate of return for the aircraft.
- **Ownership Model** – Leasing has become an increasingly common method for the ownership of aircraft, with over 40% of the global aircraft fleet owned by lessors. Although the 2016 outlook suggested that the leasing market may be stagnating [196], leasing is nevertheless an important aspect to consider for aircraft ownership and operation. In a leasing ownership model, the investment cost analysis must expand to include the lessor in addition to the operator and manufacturer perspectives. Related research has been conducted to assess a leasing rather than ownership model for the aircraft [197] (Appendix A).
- **Sale Price** – Whilst the list price provides an estimate of the aircraft's value, the actual sale price can potentially be significantly lower than the list price. Regular customers or operators ordering a large number of aircraft may have the opportunity to purchase at a significant discount, which will therefore reduce the interest repayments on an aircraft purchase. In particular, during the initial launch of an aircraft the manufacturer may be willing to operate a loss in order to attract customers and establish a strong market for a new aircraft product.
- **End of Life** – The analysis does not include an assumption of what happens to the aircraft at the end of its life. The operator could theoretically continue to use the aircraft, or sell the aircraft once it has reached the end of its economic life. Sale of the aircraft at the end of its life would provide an additional income at the end of the aircraft's life equal to its residual value. The economic life quoted for depreciation purposes by an operator may not match up to actual service life, and older aircraft may be brought out of storage at a later date or operated beyond the end of their life. At this point depreciation and interest repayments (depending on repayment period) are no longer be a concern. As the cost burden on an older aircraft is lower, there is less of a financial penalty to leaving them unused for a period of time. In contrast, utilisation of a new aircraft should be maximised to ensure the best value is obtained from it.
- **Depreciation Model** – This research assumes a linear depreciation for the aircraft value over time. Different depreciation models will change the contribution of depreciation to

## 7. Techno-economic Analysis

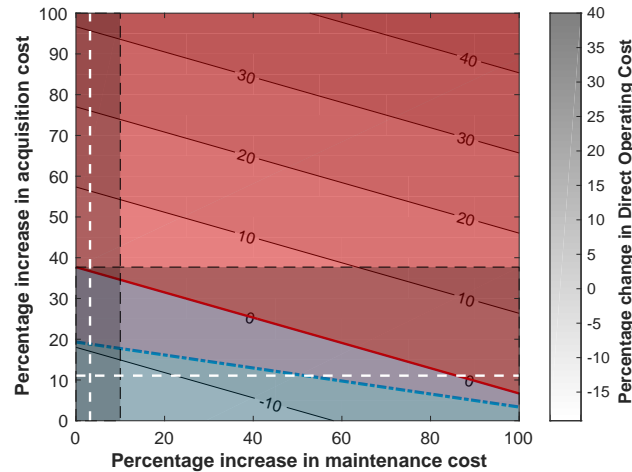


**Figure 7.9:** Direct operating cost sensitivity analysis for the kerosene N3-X in comparison to the baseline aircraft for the 'average' aircraft mission (5000 nmi, 90% max. payload)

the direct operating cost of that year. The sensitivity of direct operating cost to acquisition price may change significantly where depreciation is a non-linear function of the acquisition price.

### 7.2.2 Average Aircraft Mission

It is particularly important to ensure that the aircraft is an attractive economic proposal for operators given the typical or average mission expected for the aircraft. Section 4.7 identified an average aircraft mission for the baseline aircraft as follows:

- 5000 nautical mile range ( $\approx 10.7$  hours)
- 245 passengers
- 48,210 kg payload (passengers and freight)

Although this represents a typical mission, it is important to highlight that whilst a 10.7 hour flight is the mean value, the most common duration is 13–15 hours ( $\approx 6000$ – $7000$  nautical miles) as this covers approximately 30% of flights for the baseline aircraft (Histogram of data in Figure 4.24). Aircraft Commerce also suggests that common flight durations for the B777 series of aircraft are in the 11–16 hour range [193]. It is also likely that these flights will be operated for lower payloads than the assumed value. The definition of the average mission for economic purposes must take into account the most typical mission for the aircraft, but also the most profitable market to target.

Given the typical mission durations for the baseline aircraft, the average direct operating cost saving for the N3-X is likely be lower than the maximum achieved for the design mission range. Whilst lower payloads will slightly compensate for this drop in direct operating cost saving, the influence over the direct operating cost is small. The net result is that the maximum viable acquisition cost drops to 19% (Figure 7.9), lower than the value established for the design 7500 nautical mile mission (Figure 7.6). Whilst the maximum viable acquisition cost is lower for the average aircraft mission, the acquisition price and maintenance cost estimates for the aircraft are still well within the established limits.

Further analysis is required to identify the maximum viable cost by accounting for the histogram of flights for the aircraft. An operator's fleet will be comprised of a number of aircraft that may operate on different routes and with different loading. However, a fixed price point must be established that maximises the aircraft's attractiveness to customers. As the net benefit for

an operator should be positive, a target price must be set that ensures that the aircraft is economically viable for the fleet as a whole, rather than an individual route. This will establish an economic design mission range and loading. Missions above this range or with a lower loading will then provide higher savings to an operator, whilst those at a higher loading or shorter range will provide lower savings. From an energy consumption perspective, it is possible that the overall energy saving for a fleet would not meet the 60% savings target. A fleet-level consideration may therefore also be necessary to establish a performance design mission that ensures the global fleet is able to meet the 60% energy savings target. This aspect is included as a suggestion for further work in Chapter 10.

### 7.2.3 Yearly DOC Variation

The previous analyses assumed that external costs such as fuel price and CO<sub>2</sub> emissions taxation are fixed over the entire economic life of the aircraft. This can be considered as equivalent to selecting an average cost over the lifetime of the aircraft. Fuel price hedging by operators can limit the influence of variable fuel price on income for a set period of time. However, aviation fuel in particular is subject to yearly and monthly variations. Given the long economic life of an aircraft, direct operating cost is guaranteed to change over the course of time. Assuming that all other costs remain fixed, an increase in fuel price over the course of time will increase the direct operating cost saving of a high efficiency aircraft. A higher net direct operating cost saving will therefore lead to an increase in the maximum cost margin. Conversely, decreasing costs will reduce the economic benefit of operating the high efficiency aircraft. It is therefore useful to incorporate variable costs within the analysis to assess how they may influence direct operating cost and the aircraft's viability.

Whilst the investment cost analysis is a whole-life calculation (Equation 6.5), the direct operating cost saving will vary depending on the yearly expenditures (Equation 6.2). Each year in the sum for the net present value analysis must therefore utilise the direct operating cost for that particular year. Extending the analysis to individually assess the direct operating cost for each year creates a three-dimensional data set by adding a time axis. In this variable cost scenario, the direct operating cost contours produced in the sensitivity analysis of Figure 6.5 is able to present either the average DOC saving over the aircraft economic life or the DOC saving for a particular year. As a result, the  $\Delta\text{DOC} = 0$  trend line depends on which year is plotted for the direct operating cost contours. In contrast, the internal rate of return is a single value calculated for the aircraft's lifetime. The resultant  $\text{IRR} = \text{WACC}$  trend is therefore a fixed trend established from the investment cost analysis. The sensitivity analysis as presented in Figure 6.5 is not able to represent how direct operating cost changes each year.

As the sensitivity analysis cannot demonstrate a yearly variation in direct operating cost, it is more difficult to identify the influence of a changing cost on operating cost benefits in the long term. The sensitivity analysis in Figure 6.5 can be used to present the average direct operating cost saving. In a changing fuel price scenario, this would be equivalent to using an average fuel price. However, actual direct operating cost for each year will depend on the current fuel price. A number of examples are shown in Table 7.1. In the first scenario, the cash flow reduces over time (e.g. rising fuel price scenario), in the second the cash flow is constant (e.g. fixed fuel price). Finally, the cash flow increases over time in the third scenario (e.g. falling fuel price). Each example has the same average cash flow, (e.g. same average fuel price). However, the rising cost scenario has the highest net present value, due to higher initial savings. As net present value is weighted towards near-term costs, the long-term outcome of a change in costs may not be clearly identifiable without breaking down costs on a year-by-year basis. Despite the highest net present value, the aircraft would be operating at a loss by the end of the rising

## 7. Techno-economic Analysis

**Table 7.1:** Example net present value analysis with a 10% discount factor, \$500 initial investment and changing yearly costs

Year	Cash Flow (\$)		
	Rising Cost	Constant Cost	Falling Cost
0	-500	-500	-500
1	500	200	-100
2	300	200	100
3	200	200	200
4	100	200	300
5	-100	200	500
<b>Avg. Cash Flow (\$)</b>	200	200	200
<b>Profit (\$)</b>	500	500	500
<b>NPV (\$)</b>	359.0	258.2	157.4

cost scenario. However, using net present value or the average cost alone (i.e. the second scenario) would not clearly represent this. Instead, the first scenario would appear to be the most attractive. The third scenario has the lowest net present value, however, it becomes more profitable over time. In a fuel price scenario, a falling fuel price may have a negative impact on long term profitability versus a conventional baseline that is not represented in the net present value. It is therefore useful to be able to identify how a lifetime change in cost may influence profitability. In a variable cost scenario, it is also useful to identify if or when profitability is likely to be lowest.

The influence of a variable cost on yearly DOC may instead be identified by creating a data snapshot of direct operating cost at either a defined acquisition price or maintenance cost to cover the time axis of the analysis. This snapshot allows a clearly view on what the long term profitability of the aircraft may be, by accounting for changes in direct operating cost in the long-term. This may otherwise not be clearly identifiable by looking at net present value or the profit alone.

A number of sample scenarios were created for the N3-X to demonstrate this capability. Fuel price is a key scenario that must be considered. The first two scenarios were therefore sample fuel price forecasts created using a random delta in fuel price from the \$477.2/mt value used in the previous analyses. A fuel price forecast was created by assuming fuel price will increase or decrease by a random percentage each year, where a normal distribution is assumed to apply to the yearly change in fuel price. Historical fuel price data from the past 20 years was used to estimate the mean and standard deviation for the forecast. Two data sets were selected: a rising fuel price scenario, and a falling fuel price scenario (Figure 7.10). An additional scenario was included with a yearly increase in carbon tax, following the price of CO<sub>2</sub> from 2020 to 2040 as predicted in reference [195]. For all three scenarios, data slices were produced at the maintenance cost and acquisition price predicted for the N3-X in Section 6.6 (+11% in acquisition price and +4% in maintenance cost, respectively).

An increase in fuel costs over the course of an aircraft's life will lead to an increase in lifetime direct operating cost for the baseline aircraft as fuel begins to contribute an increasingly large percentage to the direct operating cost. The direct operating cost saving of the N3-X versus the baseline aircraft is therefore higher, leading to a higher maximum viable acquisition price than the fixed price scenario (Figure 7.11). In contrast, a falling fuel price over the course of the aircraft's life will reduce direct operating cost saving, and hence reduce the maximum

## 7. Techno-economic Analysis

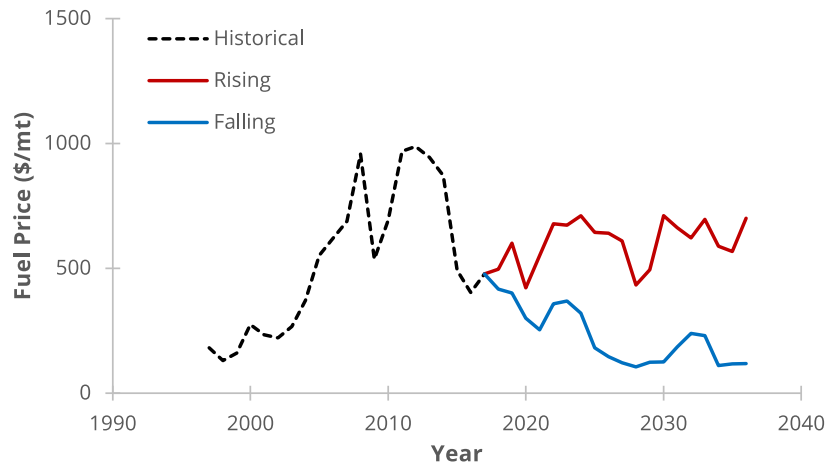


**Figure 7.10:** Sample fuel datasets over time

viable cost (Figure 7.12). Despite the same starting point (i.e. the same initial fuel price), the viability in these two scenarios is very different. In particular, the aircraft would not appear to be economically viable for the falling fuel price scenario, as the acquisition price and maintenance cost estimates lie above the maximum viable costs established by the  $IRR = WACC$  trend.

Yearly direct operating cost saving is dependent on the fuel price, however, the maximum viable cost is dependent on lifetime direct operating cost from the investment cost analysis. The  $IRR = WACC$  trend line may therefore not always correspond to a positive direct operating cost saving for every year of the aircraft life. This is apparent in the falling fuel price scenario, where the  $IRR = WACC$  trend line intersects the  $\Delta DOC = 0$  trend line later in the aircraft's life (Figure 7.12a). A low fuel price for a period of time will reduce the DOC saving, however, this may be counterbalanced by larger savings in other periods of time. The overall direct operating cost saving for the entire aircraft life may therefore be positive, despite periods of low or non-existent direct operating cost savings.

Similar to the rising fuel price scenario, an increase in carbon taxation will lead to an increase in direct operating cost savings over the course of the aircraft's economic life (Figure 7.13). Unlike the fuel price scenarios, carbon tax may be more easily controlled and is less likely to be subject to sudden changes. There is therefore a smooth change in direct operating costs over aircraft life (assuming a fixed fuel price). An increase in carbon tax can be used to incentivise investment in novel aircraft in a falling fuel price scenario. Depending on the fuel price forecast and scenario, the ideal level of taxation or change in taxation level over time can be identified which may encourage investment in new aircraft. An analysis such as that presented in Figure 7.13 allows a suitable schedule of taxation steps to be determined that can incentivise investment in a novel aircraft without imposing a sudden large step change in taxation.

Changing costs over the lifetime of the aircraft can impact viability in ways that are not readily apparent if costs at the beginning of life only are considered. In a rising cost scenario, the aircraft has the potential to be economically viable in the long term even if direct operating cost savings are initially low. A change in cost over the aircraft lifetime may be particularly useful in a taxation scenario, as carbon taxation can be gradually introduced and increased year on year, rather than starting at a relatively higher value. This would support an adjustment period as taxes were increased to the target level, rather than a sudden jump in costs for the operator. The operating cost benefits of a high efficiency aircraft would then become increasingly apparent over the course of time. Starting at a lower level of taxation and increasing over time will reduce the maximum viable acquisition cost in comparison to a higher fixed price scenario, due to lower

## 7. Techno-economic Analysis

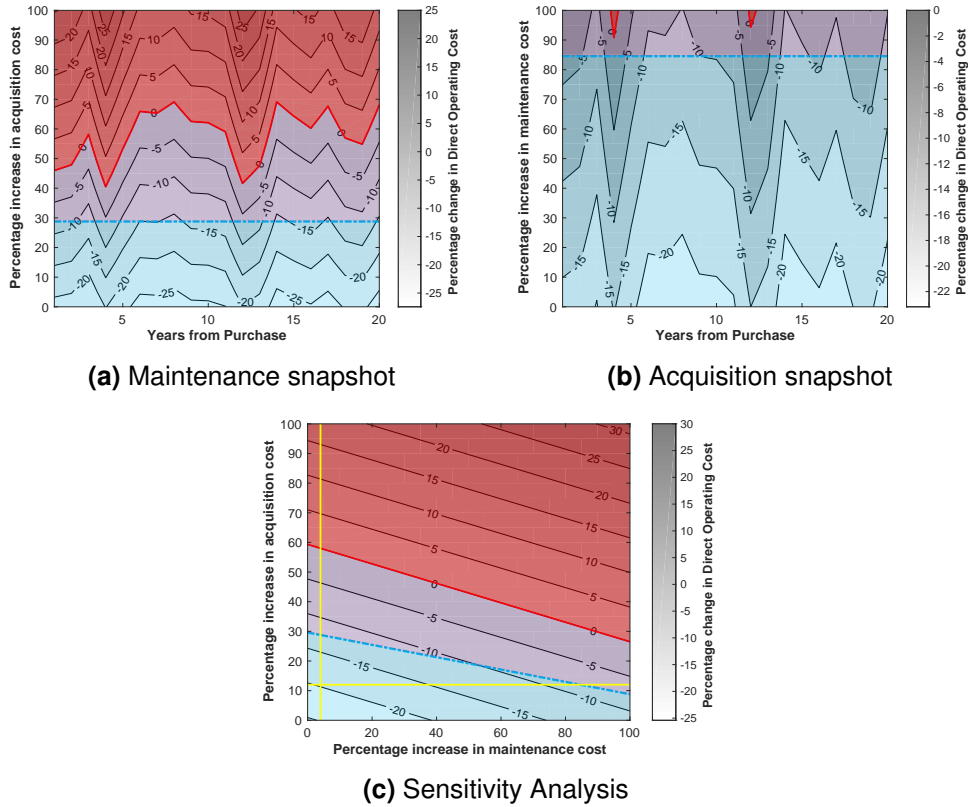


**Figure 7.11:** Direct operating cost time snapshot for a rising fuel price scenario

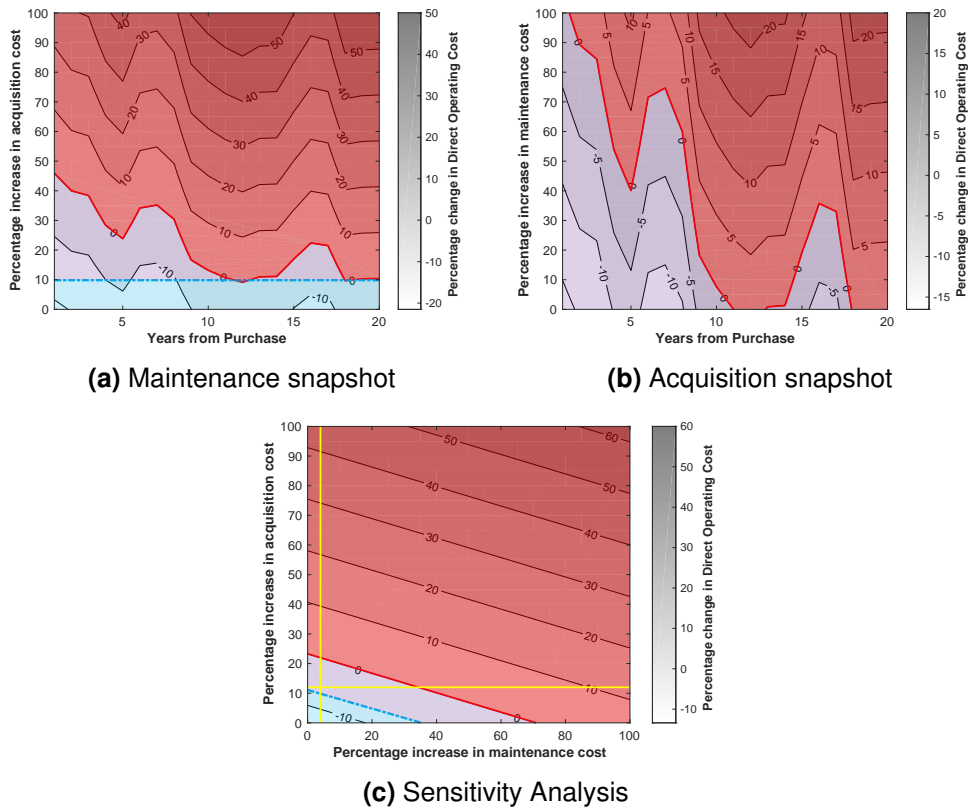


**Figure 7.12:** Direct operating cost time snapshot for a falling fuel price scenario

## 7. Techno-economic Analysis

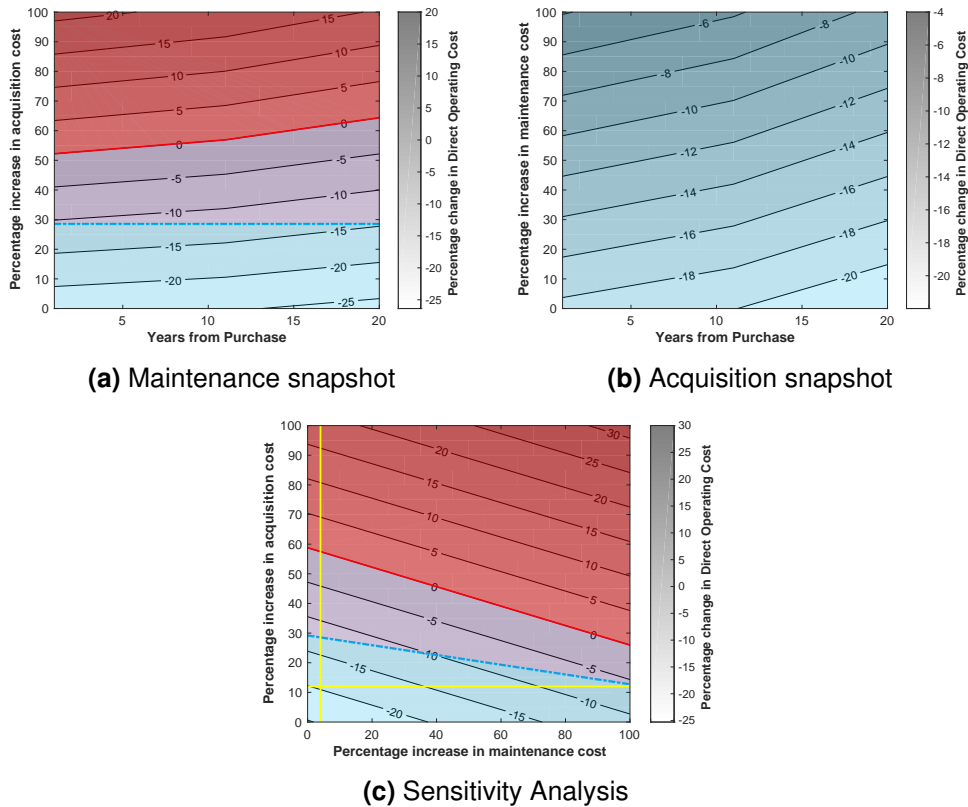


**Figure 7.13:** Direct operating cost time snapshot for an increasing carbon tax scenario

average saving in direct operating cost versus the baseline.

Forecasting of costs such as fuel price will play a part in the viability of the aircraft. The expectation of low fuel price in the future will negatively impact the aircraft's viability, as an operator would benefit less from investing in a high efficiency aircraft. Costs for early adopters of the aircraft may therefore be high relative to competitors who continue to operate older, less efficient aircraft. In contrast, the expectation of rising fuel price or emissions taxation may encourage investment, as the net direct operating saving for early adopters will be relatively higher than those that remain with older aircraft.

These further analyses have demonstrated variable fuel and CO<sub>2</sub> emissions taxation over the course of the aircraft life. It may also be useful to incorporate the change in maintenance costs over time as the aircraft and propulsion system age, as the maintenance characteristics of the novel aircraft may differ to the baseline (Chapter 10 contains an overview of suggested further work).

### 7.3 Aircraft Price & Market

In both the cost estimation models applied in this research, the acquisition price of the aircraft is a function of the number of aircraft in the first lot. The cost estimate is split into two components: development cost contribution, and manufacturing cost. The more aircraft sold in the first lot, the lower the contribution of development cost to the cost estimate, as the development program cost can be spread over a larger number of aircraft sales. The learning curve for the manufacturing cost of the aircraft also leads to a reduction in cost as more aircraft are manufactured. The overall effect is therefore a reduction in the break even price of the aircraft (i.e. the price for which the sale price covers the cost of manufacturing and the development



## 7. Techno-economic Analysis

cost contribution). In this research, the acquisition price of the aircraft is assumed to equal the break even value and the acquisition price will therefore reduce as the number of aircraft sales increases. The original acquisition price estimate created for the N3-X is based on an assumed first lot of aircraft, assumed in this research to be equal to the aircraft orders before delivery of the first aircraft (154 for the baseline aircraft). Further aircraft can be sold following the first lot, and, assuming no change in acquisition price, a profit will be made as the development program has been paid off and manufacturing cost reduces further. Even assuming that manufacturing cost is fixed and independent of the number of aircraft sales, a higher number of aircraft sales enables the aircraft to more quickly break even.

The break even price can be reduced by assuming a large number of aircraft orders. However, the aviation market is able to support only a finite number of new aircraft. It is therefore important to establish whether the acquisition price estimate corresponds with a number of aircraft sales that is feasible for the future aircraft market. The preliminary cost estimate for the N3-X assumed the same number of aircraft in the first lot as the B777 series (assumed to be 154 aircraft). This results in an acquisition price estimate 11% greater than that of the baseline aircraft. It is also possible to work in reverse and estimate the number of aircraft sales necessary to break even at a target price. The following general trend may be used to estimate the relationship between the number of aircraft and the sale price (Figure 7.14):

$$X = a_1 n^b + a_2 \pm E \quad (7.3)$$

Where  $X$  is the aircraft's acquisition price,  $n$  is the number of aircraft,  $a_1$ ,  $a_2$ , and  $b$  are constants, and  $E$  is an error term that accounts for the confidence intervals of the cost estimate. The previous sections identified that, at the July 2017 fuel price, the maximum reasonable acquisition price for an economically viable aircraft is 24.0% greater than that of the baseline aircraft, assuming that there is no change in maintenance cost. This corresponds to 120 aircraft sales (Figure 7.14). However, the estimate must also account for the upper and lower bounds of the confidence interval. In real terms, the upper bound represents a case where costs overrun and more aircraft sales are required to break even. The reverse applies for the lower bound of the interval where costs are lower than expected. In this case, the aircraft program is able to break even more quickly than expected. A 50% confidence interval was applied to the N3-X acquisition cost estimate. At the upper bound of the confidence interval, 200 aircraft sales would be required to break even. A cost underrun would mean the aircraft could break even after only 70 aircraft sales. The maximum reasonable acquisition price reduces as the mission range is reduced. Therefore, if the aircraft were to be targeted at markets operating the aircraft over shorter ranges, a lower acquisition price would be necessary, and hence the manufacturer would require a larger number of aircraft sales to break even. For the sample 2500 nmi mission, the maximum reasonable acquisition price increase is 15.8% greater than the baseline aircraft. This corresponds to 140 aircraft sales, with an upper and lower bound of 240 and 80 aircraft respectively. As the acquisition price trend flattens out, the upper and lower bounds for the number of aircraft widen and there is more uncertainty in the estimate.

A high fuel price scenario leads to a higher maximum reasonable acquisition price, which will correspond to a lower number of aircraft sales to break even. It is easier for a manufacturer to sell a new aircraft product in a high fuel price scenario, as operators are more willing to invest in more expensive aircraft technology. In contrast, the low fuel price scenario will necessitate more aircraft sales, as the target acquisition price would be lower. Similar conclusions can be made for other scenarios. The wider the margin for increases in cost, the easier it is for a manufacturer to break even quickly as it is able to offer the aircraft at a higher cost whilst retaining an economically attractive product.

## 7. Techno-economic Analysis

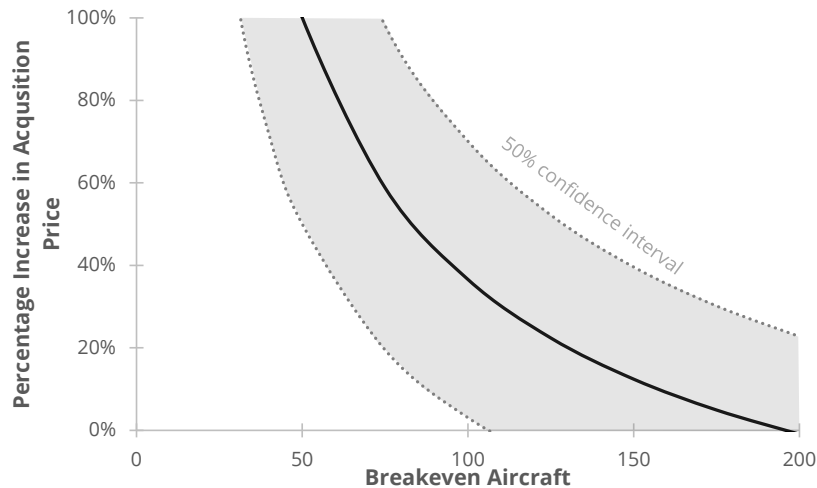


**Figure 7.14:** N3-X acquisition price versus the baseline aircraft as a function of the number of aircraft in the first lot

It is important to identify whether the target number of aircraft sales is a reasonable number based on the expectation for the aircraft market. As has been identified, there were around 154 initial orders for B777 series. Therefore, the 120 aircraft sales target for the N3-X would appear reasonable. However, the upper bounds of the estimate may be more challenging, especially if the cost limit from a long range mission is applied. Boeing predicts that there is a market for 530 new large widebody aircraft sales by 2035, many of which would be replacements for older, less efficient aircraft [3]. The N3-X would therefore need to capture 22% of the future large widebody market to meet the target price. This would appear reasonable, especially if the market is expanded to include the medium widebody aircraft market.

The number of aircraft to break even is reliant on the accuracy of the acquisition cost estimate. In addition, it is reliant on assumptions for how manufacturing cost is influenced by the number of aircraft manufactured. There is therefore an inherent degree of inaccuracy in the estimates of break even aircraft number. Higher fidelity cost models would need to be applied to increase the accuracy of the estimate, especially for those factors not adequately covered by current cost models. The analysis nevertheless provides a further view on the aircraft's viability from a manufacturer's perspective by accounting for what makes the aircraft attractive to customers and what the aircraft market is able to support.

## 8. Technology Roadmap and Risk Assessment

Far future aircraft concepts have the potential to offer substantial improvements in performance and efficiency in comparison to modern aircraft. Previous research on the N3-X, in combination with performance analyses, has demonstrated that the aircraft would appear to meet performance targets (Chapter 3). Based on this outcome in combination with direct operating cost and investment cost analysis, the aircraft would appear to be economically viable (Chapter 7). However, the development of far future aircraft concepts cannot be performed without a range of assumptions which result in uncertainty in the design. Errors may then subsequently be compounded across the entire techno-economic analysis. This design uncertainty has the potential to result in an end product which under-performs or, in a best case scenario, over-performs in comparison to original predictions. Much of the uncertainty in predicting the end product will result from the difficulty of forecasting the design of an aircraft or technology over time lines that may span 10–20 years of research, development, and testing. Forecasting how much the final product may differ from the preliminary design is naturally a highly challenging task. It can also be difficult to predict the time and investment required to achieve the requisite technology readiness level for early concepts. A risk assessment is a necessary component of the TERA framework to identify factors that are most likely to influence the outcomes of the analysis and hence viability. These factors will then feed into the roadmap for future development of the aircraft and its constituent technologies.

For the N3-X and similar aircraft, there are two key factors that are necessary to ensure a viable aircraft. The first is to ensure that the aircraft is able to meet performance targets. The N3-X and other aircraft are designed for CO<sub>2</sub> emissions and energy consumption standards that must be met. Design changes at the early development stage can be used to influence the performance of the final aircraft. However, unexpected changes later in development or under-performance for certain components will negatively impact the aircraft ability to meet design targets. The second factor is the aircraft's economic viability, represented in this research as the sensitivity analysis and cost analysis framework presented in Chapter 7. Performance changes will naturally influence viability, as this will lead to a change in fuel consumption or CO<sub>2</sub> emissions. Factors such as a change in flight speed will also influence economics, depending on whether changes to the flight schedule and number of flights per year would be required. In addition, there may be design changes that have a negligible impact on performance whilst having a more significant impact on cost. In these cases, it is advantageous to assess whether design decisions can be made that lead to a lower cost without significantly influencing performance.

Each of the aircraft systems and subsystems will have some influence over the performance and economic viability of the aircraft. The influence of each parameter and the risk of it preventing the aircraft from becoming viable. Design factors can be reduced to a number of key terms with relevance to the complete techno-economic analysis:

## 8. Risk Assessment

---

- Weight
- Specific Fuel Consumption
- Drag
- Acquisition Price
- Lift to Drag Ratio
- Maintenance Cost

These parameters may be derived from the primary equations used to obtain the aircraft fuel consumption and direct operating cost, the Breguet range and direct operating cost equations (design-related parameters in **bold**):

$$R = \frac{V}{\text{SFC}} \frac{C_L}{C_D} \ln \left( \frac{W_{\text{initial}}}{W_{\text{final}}} \right) \quad (8.1)$$

For the N3-X, the aircraft's flight speed is assumed to be equal to that of the baseline aircraft. A lower flight speed may enable a lower mission fuel consumption, however, this may lead to secondary effects influencing the direct operating cost of the aircraft. The final result of the remaining variables depends on the aircraft's actual performance in comparison to predictions. Many of the variables are linked, for example, a change in propulsion system design may influence SFC and the propulsion system's weight. As a result, the aircraft operating empty weight and hence the lift-to-drag ratio during flight will change.

$$\text{DOC} = \mathbf{M}_{\text{fuel}} C_{\text{fuel}} + \mathbf{M}_{\text{CO}_2} C_{\text{CO}_2} + \mathbf{C}_{\text{maint}/\text{FH}} \text{FH} + \frac{\mathbf{X}}{\text{FC}} \left[ \text{insurance}\% + \text{interest}\% + \frac{1 - \text{residual}\%}{\text{life}} \right] + \frac{C_{\text{crew}}}{\text{FC}} \quad (8.2)$$

In the direct operating cost equation, the fuel burn and CO<sub>2</sub> emissions will depend on the aircraft's performance, whilst the maintenance cost and acquisition price of the aircraft will depend on the design. The price of fuel and CO<sub>2</sub> emissions in addition to the cost of insurance, interest rate, and depreciation (residual and life) will influence viability, but are external factors that are not directly a function of the aircraft's design. Design changes that influence performance will typically have an impact on cost. For example, the acquisition cost estimate is a function of the airframe weight. An increase in weight would therefore increase both the acquisition price,  $X$ , and the fuel consumption,  $M_{\text{fuel}}$ . Although viability has been split into performance and economic aspects, it is also worth highlighting that the energy consumption target is itself a sub-term of the aircraft's viability. An increase in fuel consumption will therefore negatively impact the aircraft's ability to meet the performance target and may also reduce its economic viability through an increase in fuel costs. However, a design decision that increases fuel consumption may reduce other costs, such as reducing the acquisition price of the aircraft.

### 8.1 Overview of Possible Risk Factors

The N3-X can be broken down into a number of key components and subsystems that have a large impact on performance and cost, and hence on viability. The following section presents a mainly qualitative overview of possible risk factors that may arise from each of these aspects of the aircraft's design. Some aspects of the design can be considered low list factors relative to other subsystems on the aircraft, as they are reliant on the evolutionary development of current technology. One such factor is the design of the turbogenerators for the aircraft propulsion system. As turbomachinery design is a well-established process, the risk level is lower than for other factors such as the development of high power superconducting machinery.

It first useful to identify how the previously identified key factors from the Breguet range equation will influence the aircraft's ability to meet performance targets. In reality, the aspects

## 8. Risk Assessment

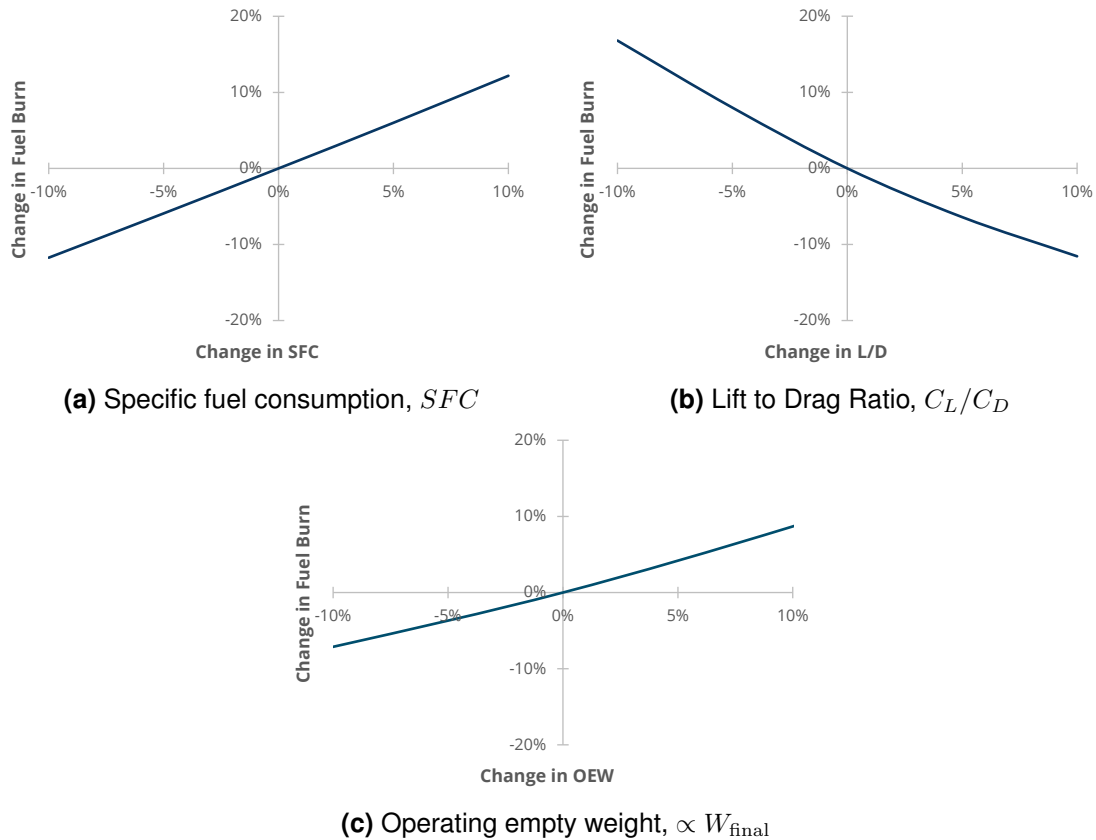


**Figure 8.1:** Key aircraft design factors with an influence over fuel consumption

of the Breguet range equation are interlinked. It is therefore difficult to completely separate one value from another. It is nevertheless possible to gain an overview of the influence of each of the three identified parameters over fuel burn. For each parameter, a percentage change was artificially introduced in the performance simulation of the N3-X, leaving all design variables the same. Of the three key variables, lift-to-drag ratio and specific fuel consumption provide similar increases in total fuel burn of the N3-X per percent change in variable (Figure 8.1a and Figure 8.1b). Operating empty weight leads to a smaller increase in fuel consumption per percent increase in weight (Figure 8.1c).

The techno-economic analysis has already identified that acquisition price has a greater influence over the aircraft's viability than maintenance cost or fuel consumption. The change in direct operating cost with a change in each factor depends on the percentage contribution of each cost component to the total direct operating cost. The significance of each of the design-related factors in the DOC equation is dependent on many of the other assumptions made in the analysis, such as fuel price and interest or insurance rates. It is nevertheless reasonable to assume that acquisition price will remain a dominant part of the DOC for a direct ownership model unless fuel prices spike dramatically. Figure 8.2 breaks down the individual effect of each of these aircraft-related factors. As with the sensitivity analysis, acquisition and maintenance cost have been presented relative to the costs of the baseline aircraft (Figure 8.2a and Figure 8.2b). The cost estimates along with their upper and lower bounds are also included. Fuel consumption is presented relative to the baseline estimate of fuel burn for the kerosene N3-X (Figure 8.2c).

## 8. Risk Assessment

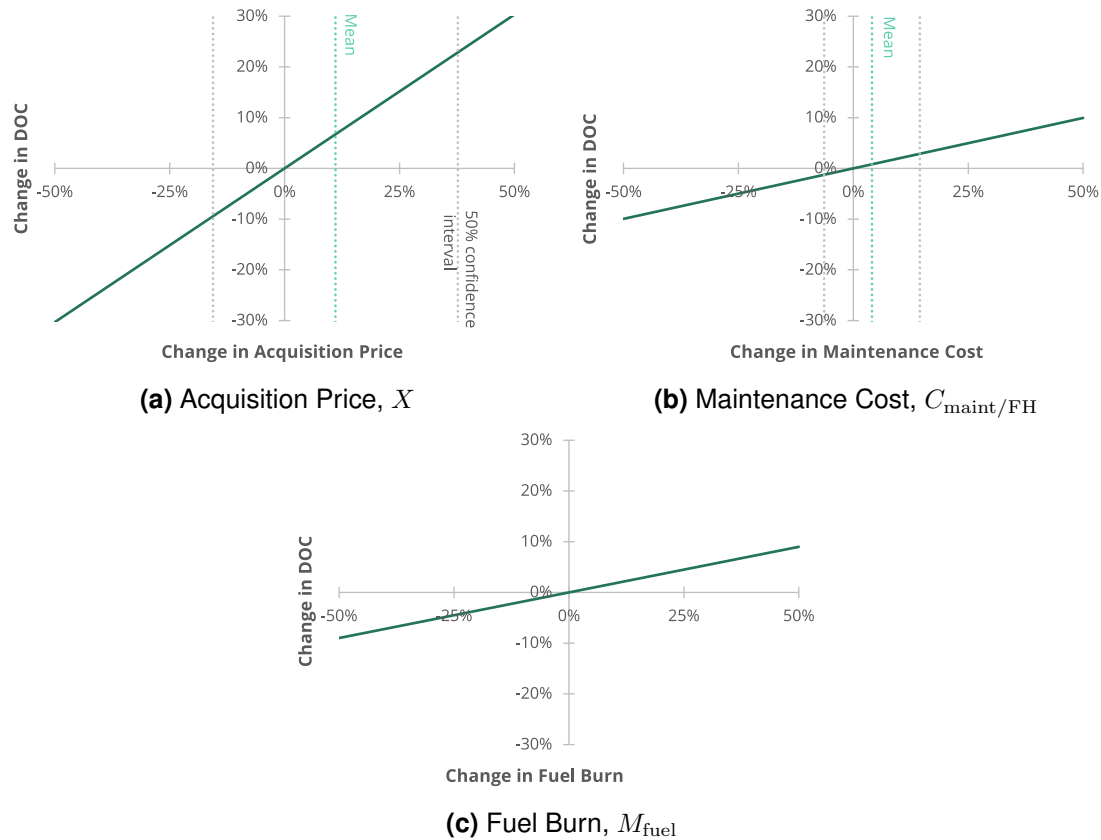


Figure 8.2: Key aircraft design factors with an influence over direct operating cost

### 8.1.1 Airframe Performance and Operating Empty Weight

Whilst there are currently no commercial blended wing bodies, the general concept of a flying wing type airframe is not entirely unknown. Small scale experimental aircraft such as the X-48 suggest a medium technology readiness level for the technology [198]. It is reasonable to expect uncertainty in the operating empty weight estimate for the aircraft, even for well established airframe types, as an exact value is not possible until the design is at an advanced stage. There is also some uncertainty with regards to the materials used in the airframe. However, a largely composite airframe is likely, which will factor into operating empty weight estimates. The expected performance and control requirements are relatively lower risk factors for the design, as they have been covered as an aspect of previous research and experimentation on BWB airframes.

The operating empty weight of the aircraft is a factor in both the aircraft's fuel consumption and the acquisition cost estimation. It is also a parameter with a significant level of uncertainty at the preliminary design phase, compounded by the novel airframe configuration. The N3-X airframe weight as estimated by previous research is approximately 107,590 kg [24] (excluding the propulsion system). However, changes to structural design, internal configuration, or the materials used may influence the aircraft weight with a subsequent impact on performance. Operating empty weight predictions for an aircraft at the preliminary design phase often rely on historical data and trends. For conventional airframes there is a significant pool of data to draw from to create parametric equations which may relatively accurately estimate weight. However, there is more uncertainty in using historical data for weight estimation of alternative aircraft planforms, such as the blended wing body. Uncertainty is unavoidable at the early stages of aircraft development. It is therefore likely that the estimated weight will differ from the final

weight of the aircraft as the details of the design changes.

The airframe weight has a number of impact on aircraft performance. The aircraft's weight during a flight relates directly to the lift induced drag and hence an increase in drag, as a higher weight implies higher lift during cruise. A change in aircraft weight will also have an impact on the lift-to-drag ratio. Although the lift-to-drag ratio does not vary linearly with a change in lift a higher initial weight will negatively impact the fuel consumption of the aircraft, regardless of the change in lift-to-drag ratio. Assuming that the propulsion system design remains the same, the airframe's weight will not directly influence the specific fuel consumption of the propulsion system at design point. However, an increase in drag necessitates a higher engine power setting to provide the requisite thrust. Therefore, specific fuel consumption during a flight increases in line with drag.

The maximum take-off weight is a significant assumption for the aircraft as it is based on historical data only, but it does not factor in to the fuel consumption estimate for the design mission. The MTOW estimate therefore does not directly influence the fuel saving performance indicator. The MTOW assumed in this research enables a maximum range to be achieved that is greater than that of the design mission. Designing for a lower MTOW could lead to a lower operating empty weight, and hence greater mission fuel saving. There may therefore be some flexibility to the final operating empty weight.

The aircraft's acquisition price has a high level of uncertainty due to a combination of factors. Any acquisition cost estimate at an early design stage has an inherent level of uncertainty, as forecasting costs is difficult. This is compounded by the development of a novel aircraft configuration for the commercial industry. In addition, there are a number of ancillary costs for the development of an aircraft for the N3-X which may inflate the development and manufacturing cost of the aircraft. This includes the development of facilities and tools for the manufacture of a blended wing body airframe and potentially a portion of the burden for the development of technologies such as superconductivity up to a suitable TRL. The acquisition price estimate used in this research is predominantly a function of the aircraft's operating empty weight. An increase in weight will therefore lead to an increase in cost, assuming that material use remains the same. However, this also depends on the source of the weight changes, as the use of cheaper, heavier materials will increase weight, but may reduce cost. A similar outcome is evident for the maintenance cost estimate, as a higher airframe or propulsion system weight leads to a higher maintenance cost per flight hour. For the design mission of 7500 nautical miles, the direct operating cost can increase by approximately 8% whilst maintaining an adequate return on investment. This corresponds to an operating empty weight increase of approximately 12%. However, this operating empty weight would lead to a fuel consumption greater than that required to achieve the performance target of a 60% energy saving versus the baseline aircraft.

### 8.1.2 Airframe Material Composition

Previous research on the N3-X did not identify the materials that would be used in its manufacture. However, it is reasonable to assume that the aircraft would use a high proportion of composite materials. The weight estimation models applied in this research use scale factors to account for the use of composite materials in the airframe. It is therefore difficult to identify the extent to which material type changes the weight estimate. The influence of material type on the acquisition cost estimate can be more easily identified, as the material scale factor is dependent on the materials used. The materials used in the airframe are assumed to be a low-risk aspect of the design, as composite materials are becoming relatively more common in commercial aircraft.

### 8.1.3 Aircraft Internal Configuration and Compatibility

The internal design of the aircraft has not been a major focus of this research, with the exception of determining the available volume for the aircraft's LH<sub>2</sub> tanks. However, a more detailed design will require a more complete assessment of the aircraft's cabin configuration and internal structure. Liebeck identifies a number of challenges that must be addressed for a safe and comfortable journey in a blended wing body planform: alternative to windows for passengers in the centre of the fuselage, rapid exit from the aircraft in an emergency, possibly high cabin angles during cruise [51]. However, Liebeck's blended wing body design process suggests solutions to these design challenges which does not rule out the application of the planform as a suitable configuration for a passenger transport.

Another challenge may result from the use of engines embedded within the airframe. Integration of the engines within the airframe without negatively impacting the structural integrity of the airframe will be necessary. Safety will also be a key concern, as engine debris may enter the cabin in the event of an uncontained engine failure. Finally, some form of noise shielding may be necessary to prevent excessive engine noise from entering the cabin.

Compatibility with airport infrastructure is also an important requirement for the design of the aircraft. In an ideal case, a blended wing body would be able to easily interface with current airport infrastructure. This will include compatibility with airport ground support equipment and gate infrastructure. Compatibility also enforces a maximum wingspan limit for the aircraft. The aircraft's taxi weight will also be limited to a value that does not exceed the maximum allowed for the particular pavement grade of the airport taxiways and runway. However, in the case of the N3-X, the aircraft is already designed to a wingspan less than the maximum allowed at a parking stand or on the taxiway. In addition, a BWB aircraft is typically lighter than a conventional tube-and-wing for the same capacity [52]. As a result, size and weight is unlikely to be an issue in terms of compatibility with airport runways and taxiways. Compatibility will be more difficult when also considering the changes to airport infrastructure needed to support a LH<sub>2</sub> rather than kerosene fuelled aircraft. Specialised equipment would be required to refuel the aircraft and, in the case of a removable tank configuration, remove or add tanks as required. Airport capability would be required to support the safe manufacture (assuming fuel was manufactured on-site), distribution, and storage of fuel [59].

### 8.1.4 Superconducting Propulsion System

There is a high level of uncertainty in the integration of a superconducting propulsion system on an aircraft. There are a number of factors that are a source of risk. Primary amongst these is the likelihood of superconducting system being implemented on commercial aircraft by 2035. Current predictions find it unlikely that superconducting systems will be developed to a level of maturity that satisfies certification requirements by the FAA and similar bodies within the next 30 years [16]. Significant investment would therefore be required if it were to be implemented on an aircraft before 2050.

Previous research on the N3-X identified a transmission efficiency between 97.75% and 99.88% for the superconducting system, depending on the cryocoolant type. Higher transmission losses necessitate larger turbomachinery that produces enough power to compensate for losses, leading to higher weight and higher fuel consumption (Figure 5.3). High losses in the transmission system can quickly increase fuel consumption to a point where the energy savings target is no longer met. This is compounded by the possibility that a superconducting system with an adequate efficiency level may not be possible within the required time-frame. The weight of cryocoolers (assuming cryocoolers are used rather than a cryogenic fluid as coolant) is also a risk factor in the design of the superconducting system. Low efficiency or high weight



cryocoolers necessitate a larger propulsion system to compensate for the increase in airframe weight. As a result, larger cryocoolers are needed for a larger, higher power system.

Moving to conventional motors and generators would significantly increase the weight of the electrical system. As with the superconducting system, the weight of conventional motors and generators can be estimated based on a trend relating weight to the shaft horsepower (Figure 3.28) [24]. Using these trends, the weight of an industrial motor would be more than 20 times that of the projections for the superconducting motor. This would increase the propulsion system weight to 5 times the value currently predicted for the N3-X, and would increase the aircraft's operating empty weight by 43% (neglecting increase in turbomachinery weight). This would dramatically increase the aircraft's fuel burn, even before accounting for the increase in SFC as a result of higher transmission losses. In addition, current motor technology does not yet cover the 1 MW+ power range required for systems such as the N3-X. However, motor weight and power rating is projected to improve over the next 20 years. A projection for non-superconducting motor technology estimates power ratings of 1–3 MW and a power density of 9kW/kg [16], with TRL 6 achieved in 20 years and entry into service in 30. It is worth highlighting that there is significant industry focus on hybrid electric aircraft, with demonstrators and experimental aircraft planned for the near future (Section 2.2). This may accelerate the time frame for the development of high power, low weight electrical system. In comparison to requirements for the N3-X, current state of the art non-superconducting motors have a rating of 0.25 MW and power density of 2.2 kW/kg [16]. Using projected motor technology would therefore reduce weight to one fourth of the current weight estimate for conventional motors. It is worth highlighting that there is inconsistency in projections for the power density of electrical systems in general, as weight must also include the packaging requirements for the motors etc.

### 8.1.5 Electrical System Architecture & Safety

Research by Armstrong has looked at a number of different architectures for the design of the N3-X electrical system [48]. The design of the system and the required components will dictate the overall weight of the propulsion system in addition to its reliability and efficiency. As the N3-X propulsion system is entirely reliant on electrical transmission system, the electrical system design will also have to include adequate fault management strategies in the event of a failure. Components may therefore need to be oversized to ensure adequate thrust is maintained throughout the flight [144]. This may necessitate either oversized motors to provide additional power when needed, or oversized propulsors to provide additional thrust when needed, with a resulting increase in weight.

### 8.1.6 Engine Intake Total Pressure Recovery

The N3-X design used in this research focuses on a propulsion system configuration with embedded turbogenerators. Depending on the design of the intake ducts and the location of the engines, it is likely that the total pressure lost in the intake will be higher for the embedded engines than it would be for a standard podded engine. This will lead to a slight increase in the specific fuel consumption of the propulsion system. Section 5.4 briefly covers the how intake total pressure loss will influence the specific fuel consumption. However, the design of intake ducts for propulsion systems is a well-established body of research. It will therefore be assumed that losses can be kept reasonably low, and hence have little impact on performance.

### 8.1.7 Propulsor Array Design and Location

Chapters 3 and 5 detailed a range of alternative configurations and design variables for the N3-X propulsion systems. This creates a design space that demonstrates the change in performance that is possible from using alternative designs. The models used to simulate the propulsion system and aircraft are design tools at a low level of fidelity primarily suitable for the conceptual design process. However, they provide a preliminary insight into how the propulsion system's efficiency can be influenced and how the propulsion system's design influences overall performance. Errors introduced by the assumptions made in preliminary design tools are inevitable. As higher fidelity models become available, more accurate results will become possible. The primary goal of the design space exploration is to provide an insight into where the most benefit can be gained through a change in propulsion system configuration. The models suggest that improvements in the region 3% are possible by combining alternative propulsion system configurations (such as thrust split and turbofans rather than turbogenerators) with an optimised propulsor array.

Given the low fidelity of the models, the propulsor design is identified as a medium risk factor, however, it is expected that further research will be able to increase fidelity and further optimise the design to counterbalance any inaccuracies in initial performance estimates.

### 8.1.8 Boundary Layer Distortion

The flow distortion resulting from the presence of the boundary layer has been represented in this research as two effects: a total pressure loss in the intake duct, and a reduction in fan efficiency. The magnitude of each of these values will dictate whether BLI is actually beneficial in comparison to a free-stream propulsion system. Research agrees that significant distortion is detrimental to performance, and may bring the propulsion system closer to surge [20, 94]. Total pressure recovery in boundary layer ingesting propulsion systems and the design of distortion tolerant fans has already been identified as a key aspect for further research. One focus has been on the design of low-loss S-ducts, as BLI propulsion systems are typically embedded within an airframe [22, 106]. More recent research has also looked at developing a distortion tolerant fan for BLI applications, aiming to design a fan that can withstand the mechanical excitations and aerodynamic stability concerns resulting from operating in boundary layer flow [199]. This design has been tested in experimental research to validate the design procedures for a BLI fan [200].

Total pressure recovery is a high risk factor for the aircraft's performance, as it will strongly influence the propulsion system's performance. Simulations in this research have identified that high total pressure loss will lead to a large increase in power demand, especially for the low pressure ratio fans considered for the N3-X propulsion system design. The simulations assume a total pressure recovery of 99.8% in the propulsor inlet. However, higher total pressure loss in the intake will quickly increase power consumption to a point where there is no benefit to using a BLI system over a free-stream propulsor array. This point is approached more quickly for the low fan pressure ratios that have been considered for the N3-X propulsor array. For the design fan pressure of 1.3, this limit is approached for a inlet total pressure recovery of approximately 97.7% (see also Figure 3.19a). This would increase SFC by 6.5% and hence increase fuel consumption by 7.9%. The aircraft would then no longer be able to achieve its 60% fuel saving target. As a comparison, the models suggest that the minimum total pressure recovery to ensure the performance target is met is 99.6% (Figure 8.3).

Recent experimental research on a boundary layer ingesting propulsor with a fan pressure ratio of 1.35 has found that the total pressure recovery is 96.5% at ADP [200]. For this total pressure loss, and given the assumptions of the model, there is no benefit to be gained by using

## 8. Risk Assessment

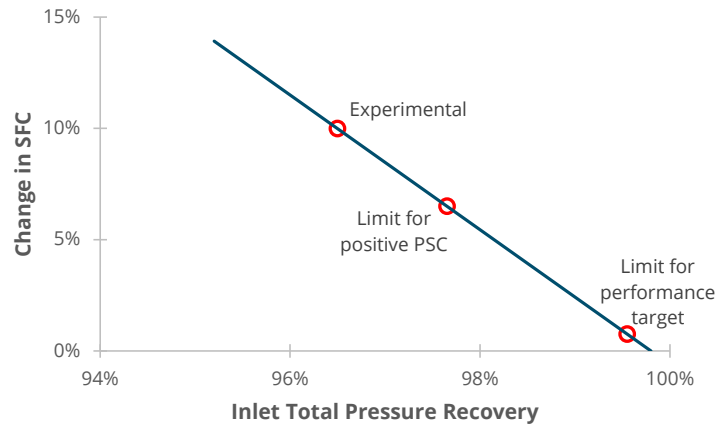


**Figure 8.3:** Influence of intake total pressure recovery in the BLI propulsors on SFC

a boundary layer ingesting propulsion system. Intake design and total pressure recover in the intake is therefore a very high risk aspect of the design of the N3-X. This outcome suggests that intake design for maximum total pressure recovery should be a major aspect of the technology roadmap to ensure that the N3-X is viable and able to meet performance targets.

### 8.1.9 Safety Factors

Safety is a crucial factor to consider during the development of an aircraft. There are numerous safety considerations in the development of any aircraft, regardless of whether or not novel technology is implemented. However, a novel aircraft such as the N3-X incorporates a range of technologies that are not currently implemented on commercial aircraft. There are therefore a number of additional safety factors on top of those that will already feature in the design process.

Many of the design decisions made at the conceptual phase have safety factors that may begin to play a larger part as research progresses. Amongst other safety factors, there are a number key safety aspects of the design that will need to be addressed. The first is the use of a blended wing body rather than tube-and-wing airframe. A conventional tube-and-wing is designed to allow relatively easy egress of passengers in the event of an emergency. Whether the aircraft is a wide- or narrow-body, the aisles between the seats have direct access to an exit at multiple locations along the length of the fuselage. In the case of a blended wing body, the fuselage surface area available for emergency exits is lower, whilst the internal volume is relatively higher. However, Liebeck suggests that appropriately designed aisles would allow passengers a direct view of and easy access to emergency exits [51]. The different aircraft layout would nonetheless necessitate the development of new emergency evacuation procedures.

Engine installation is a second major safety factor to consider. The engines are embedded within the fuselage of the aircraft. As a result, there is a high risk that engine debris may either enter the passenger cabin or damage critical components of the airframe structure. This is a vital safety factor to consider during the design of a commercial passenger aircraft.

The use of LH<sub>2</sub> rather than conventional kerosene will also contribute to safety requirements for the aircraft. There is a public perception of LH<sub>2</sub> as a dangerous fuel that stems from historical cases such as the Hindenburg disaster. However, research has shown that LH<sub>2</sub> fuel leaks may be less dangerous than kerosene fuel leaks in the event of a fire [60]. As LH<sub>2</sub> is gaseous once tank pressure is lost, the fuel quickly dissipates, assuming there is sufficient ventilation. In contrast, kerosene is liquid and therefore spreads, rather than being localised to the point of the

leak. The use of LH<sub>2</sub> will nevertheless require additional safety factors to consider both on board the aircraft and on ground at an airport. As LH<sub>2</sub> is a flammable fuel with different characteristics to kerosene, appropriate new safety procedures will be necessary during refuelling.

Embedded engines lead to an additional safety factor for the LH<sub>2</sub> N3-X variant. It is possible that the LH<sub>2</sub> fuel tanks would be stored adjacent to the embedded engines (Figure 4.16). It is therefore possible that engine debris could damage or pierce the LH<sub>2</sub> fuel tanks. Damage to the fuel tanks in the event of a critical engine failure would lead to a loss in pressure and the rapid boil-off of fuel. In contrast, damage to kerosene tanks would lead to a slower loss in fuel. The LH<sub>2</sub> N3-X design selected in this research utilises three fuel tanks. Whether tanks are damaged due to engine debris or other reasons, loss in pressure in a single tank would lead to the loss of a large percentage of the fuel on board the aircraft. This would significantly reduce the aircraft's range and potentially limit the number of available destinations for an emergency landing. It may therefore be necessary to use many smaller tanks rather than fewer large tanks to ensure that less fuel would be lost if a single tank were to fail.

Current research suggests that high voltage levels will be required for the power levels on a more-electric or turbo-electric aircraft. There are design-related factors that must be addressed for high voltage equipment such as the requirement for thicker insulation and the breakdown of the airgap that can lead to discharge at high altitude [48]. The use of electrical machines with a high power and high voltage level will necessitate appropriate safety procedures during repair or maintenance activities.

### 8.2 SWOT Analysis

The previously identified some of the risks and technology challenges for the aircraft that should be addressed over the course of development of the N3-X or similar aircraft. In a techno-economic analysis, it is important to also take a wider viewpoint to identify possible challenges for the aircraft's viability. A qualitative analysis can identify the strengths, weaknesses, opportunities & threats for the N3-X (SWOT analysis). A SWOT analysis can be used to provide an evaluation of a project and the possible factors that either help or hinder its ability to meet objectives. The SWOT analysis splits the evaluation of a project into internal and external factors, and helpful or harmful factors (Figure 8.4). For this research, the project in question is the development of the N3-X, a novel aircraft concept. Strengths and weaknesses refer to internal factors, in this case relating to the design of the aircraft. In contrast, opportunities and threats refer to external factors that may influence the aircraft and its viability, such as policy decisions, competitors, and the economic environment. The main goals for the development of the N3-X are to achieve performance targets and create an economically viable aircraft concept. In this case, the SWOT analysis is applied to provide a wider overview of potential challenges or advantages for the aircraft and avenues for further research. The N3-X itself may not be the final selection for further development as a green aviation aircraft concept. Nevertheless, the conclusions made in the SWOT analysis may be used to target areas of research or blockers for the development of similar aircraft. Ideally, harmful factors should be converted to helpful factors for the aircraft and its constituent technologies or manufacturers and operators. However, in many cases this may not be possible. These then become factors that may require further research or mitigation in the future.

The following section will provide an overview of a SWOT analysis of the aircraft. The analysis is by no means comprehensive, however, it is intended to highlight some of the points that have become apparent during the course of the research. The points made for the following analyses take the perspective of a commercial entity with the assumptions that decisions cannot be altruistic. Any beneficial or harmful factors are therefore in terms of more economic

## 8. Risk Assessment

	Helpful Factors	Harmful Factors
Internal Factors (Aircraft design, technology)	Strengths	Weaknesses
External Factors (Policy makers, competitors)	Opportunities	Threats

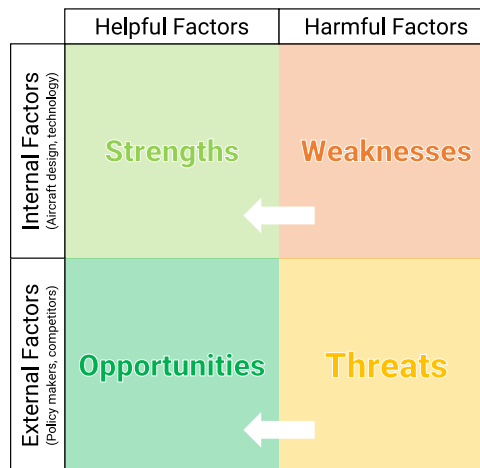


**Figure 8.4:** Strengths, weaknesses, opportunities & threats (SWOT) analysis matrix

outcomes such as the marketability or profitability of the aircraft, rather than in terms of the aircraft's ability to meet performance targets.

### Strengths

- The N3-X offers large fuel savings and low CO<sub>2</sub> emissions in comparison to the baseline aircraft. Boeing and Airbus identify in the market forecast that approximately 40% of new aircraft orders up to 2035 will be replacements for older, less efficient aircraft [3, 4]. As the N3-X offers in the region of 60% versus one such older aircraft, it is an ideal candidate for this market. A large increase in efficiency versus older aircraft will be beneficial in the long term as the likelihood of regulations that penalise less efficient aircraft increases. The introduction of carbon taxation will further increase the demand for replacement aircraft that are able to dramatically reduce performance-related costs.
- The N3-X has the potential to translate fuel savings into a large direct operating cost saving for customers, assuming other costs can be kept low. This will lead to a good return on investment for customers, potentially increasing the attractiveness of the aircraft for customers. This return could exceed the industry average WACC of 7–8% and the average industry return on capital of ≈9% [12]. The aircraft could therefore increase the profit margin of the aviation industry, assuming ticket prices remained approximately constant. This is important for an industry where capital investment is high. Depending on the economic environment, the demand for high efficiency / low cost aircraft concepts may also be high, providing a large market for a manufacturer.
- The aircraft's relatively lower fuel consumption will act as a buffer against the impact of fuel price fluctuations, as fuel accounts for a smaller percentage of costs in comparison to current aircraft. A change in fuel price will therefore have less influence over direct operating cost. Fuel accounts for approximately 36% of the baseline aircraft direct operating cost for the design mission. A 10% increase in fuel price therefore increases direct operating cost by 3.6%. In contrast, assuming all other costs remain equal, the direct operating cost of the N3-X would increase by only 2.3%. The significance of fuel cost in decisions is therefore lower in comparison to an older aircraft.
- A distributed propulsion system removes concerns about engine ground clearance. A propulsion system can be more easily scaled by, for example, adding additional propulsors to the array. There is therefore less concern about increasing propulsion system size

## 8. Risk Assessment

---

should the manufacturer wish to develop an aircraft family starting from the N3-X as a base.

- A distributed and turbo-electric propulsion system provides a more modular framework for improvements or upgrades. Propulsion systems can potentially be incrementally upgraded in a more modular fashion, rather than an expensive re-engine option. This is beneficial for the operator, as it will spread costs over a wider period of time. As with the above point, the modular configuration also enables a more easily scalable propulsion system for a family of aircraft.
- A turbojet/turbogenerator is likely to be a lower complexity system than alternative advanced turbofan concepts. This has the potential to reduce maintenance, material, and overhaul costs versus current systems. In addition, the turbomachinery is primarily intended to act as a power source rather than thrust source. This may support operating the turbomachinery at a more constant power setting over the course of a flight and avoid transient operation. Excess power not used by the propulsor array can then be used to charge batteries or power on-board systems. This will reduce large peaks in shaft speed and engine temperature and hence increases the life of the turbomachinery. As a result, maintenance costs will be lower as part replacement is less frequent. In contrast, there is a significant variation in power setting for current propulsion systems, as thrust requirements vary over the course of a flight.
- A large jump in efficiency, rather than gradual increments, has the potential to slow the demand for constant improvements in fuel consumption. The costs associated with developing increasingly more complex machines may therefore not be as necessary. Research focus will likely instead move towards developing low cost technologies, as fuel becomes a negligible part of an operator's direct operating cost. This may also be presented as an opportunity for manufacturers to develop new products with a different design focus.
- A large reduction in fuel requirements for a mission will reduce the amount of fuel that must be loaded onto the aircraft before a flight. This has the potential to reduce the time required for loading fuel on the aircraft and hence may allow a slight reduction in turnaround time for aircraft. However, the B777-200LR airport planning document identifies that aircraft fuelling is typically not the longest on-ground activity [129]. This is therefore likely to be an advantage for only a limited number of scenarios.
- The N3-X is designed for a similar capacity to the baseline aircraft, however the different aircraft planform leads to a smaller footprint (shorter fuselage). This may prove advantageous in airports.

### Weaknesses

- The aircraft relies on many low TRL concepts, such as BLI propulsion systems and superconductivity. Significant investment is therefore needed to bring the technologies to a level suitable for integration on an aircraft. There is also the risk that reaching target efficiencies may be difficult or impossible without a costly research and development program. If the entire program cost were to be assigned to one aircraft program, the necessary list price to pay off the development program would be excessive. However, the cost burden is unlikely to lie fully on one aircraft program and preliminary research up to mid TRL would not be conducted by a manufacturer alone.
  - **Threat** – Competitors will also be able to leverage the technology for similar benefits.

## 8. Risk Assessment

---

- **Opportunity** – Once developed, the technologies applied for the aircraft can be applied to other aircraft at a much lower cost. This creates the opportunity for a new family of aircraft. Many of the constituent technologies and concepts in the N3-X have already been proposed for use on aircraft that open up new markets for the aviation industry.
- Initial investment for manufacturers will be necessarily high to manufacture the aircraft and market an aircraft concept. Current aircraft manufacturing facilities and resources are geared towards conventional aircraft configurations. A new aircraft will require significant investment from manufacturers to build new facilities suitable for a novel configuration. The high investment requirements will necessitate a higher return for the manufacturers than for a conventional aircraft or a new addition to an aircraft family. As a result, it may be more difficult to pay off investment costs without raising the aircraft's list price or capturing a large percentage of the market.
- A potentially higher acquisition price will necessitate a significant initial investment cost for operators. This will negatively impact profitability of the aircraft, which will reduce its attractiveness for an operator. A novel aircraft concept is a high risk proposition for an operator. Benefits may need to be significant in order to encourage investment.
  - **Strength** – Early adopters may be able to leverage novelty factor and a reduction in cost to increase profits versus competitors.
- There is continuous improvement in the optimisation of maintenance practice and the maintenance of conventional turbomachinery is a well-established field. However, common maintenance practice is not yet available for complex turbo-electric propulsion systems. Novel technologies and system architectures are highly likely to be more costly to maintain than current systems. The running costs of the aircraft are therefore likely to be high until a larger knowledge base is developed for the maintenance of new subsystems such as superconducting electrical machinery. In particular, maintenance hours may be high for novel technologies.
- There may a number of passenger comfort issues to address with the configuration. Embedded engines in close proximity to the passenger cabin may increase cabin noise. A blended wing body fuselages may also be less practical for passenger comfort (e.g. access to windows), safety, and loading, as a longer distance to exits may slow passenger entry and exit.
- There may be safety risks to embedded engines in the event of an uncontained failure. The engines are likely to be in closer proximity to the passenger cabin than a conventional podded engine. As a result, the likelihood of engine components penetrating the cabin following a failure is high.
- The expense of developing a LH<sub>2</sub> infrastructure may limit the potential of the LH<sub>2</sub> aircraft variant. Significant investment would be required from airports to develop storage and fuelling capabilities for the fuel.
- Public perception of LH<sub>2</sub> as a fuel may prevent its application on a passenger aircraft, despite proven safety.

### Opportunities

- A reduction in operating costs over time has allowed airline operators to reduce ticket prices. Air travel has therefore become a feasible activity for a much wider market than in the early days of commercial travel. A further reduction in ticket price may open up a much wider market for air travel, particularly in regions where the aviation market is still developing such as Asia and Africa. This presents the potential for a significant increase in revenue for operators of aircraft with a low running cost.
- Thrust vectoring has been proposed as a potential additional application for distributed propulsion systems. In addition, the blended wing body airframe is a higher lift configuration than a conventional tube-and-wing. These two factors in combination offer the potential for a reduction in runway length. This may open up more airport destinations for operators, assuming the airports have the capacity and facilities to support large aircraft. This may also offer the opportunity for a more point-to-point operating model as opposed to the hub-and-spoke network typical for operators currently.
- A range of novel technologies are required as subsystems in the N3-X. The technologies developed during the process of conceptualising the N3-X can be leveraged to develop new aircraft programs. Current research has already proposed the expansion of a 'thin-haul' aircraft market that is well suited to hybrid-/turbo-/all-electric propulsion systems. The smaller capacity aircraft market is one that is not typically covered by the two dominant large aircraft manufacturers. However, this may become an increasingly profitable market for further investment by leveraging technologies developed for larger applications.
- It is likely that carbon taxation and charges related to noisy operation or airport NO<sub>x</sub> will increase over time. The financial penalties of operating older aircraft will therefore increase over time. This gives the aircraft and its constituent technologies long-term viability that may increase the market for manufacturers over time.
- A reduction in noise may extend operating hours and enable more flights per day. In addition, it may remove some barriers to the expansion and extension of airports. A reduction in airport noise may also provide long term benefits to surrounding communities.
- Developing and operating a low fuel aircraft ahead of competitors could be beneficial for operators and manufacturers as they will be able to offer a significantly more attractive product.
- The blended wing body planform has a significantly different internal configuration to a conventional aircraft. This change in configuration may lead to a higher belly capacity with resulting higher maximum payload weight for a freighter option. The payload-range chart prediction suggests a high maximum range for the aircraft, given the maximum take-off weight assumption. An increase in the maximum allowable weight could allow a very high payload capacity aircraft, trading off range for payload. The different internal configuration may also support cargo types that are not currently feasible to transport as air cargo. This also applies to the LH<sub>2</sub> variant, as the low weight of the fuel on-board the aircraft will increase the payload capacity. This may prove advantageous for the air freight market.
- The novelty factor and green credentials of the aircraft could increase market share. In addition, there may be PR or marketing value to being perceived as a green airline or manufacturer.



### Threats

- The viability of any new aircraft is closely tied to current fuel price. It is difficult to encourage operators to invest in a high efficiency aircraft technology when costs are low. The aircraft is economically viable when costs are high, however, if fuel prices fall over time, the benefit of the aircraft becomes negligible for operators. As the wider global community moves to low or zero hydrocarbon technologies, the demand for hydrocarbon fuels will fall. As a result, the cost of fuel may fall as there is a larger supply available. This may negatively impact viability without an alternative external driver to discourage the use of older aircraft.
- There is an industry-wide push towards the development of green aircraft using novel technologies. There are therefore many competing options under development that have the potential to meet performance targets. As a result, it is possible that competing aircraft concepts will emerge that offer similar efficiency levels at a lower price point.
- Aiming for a very high efficiency aircraft concept is likely to lead to a high cost development program, and hence a high acquisition price for the aircraft. Competing options may offer lower efficiency improvements at a lower price. This may be more attractive to customers in the short term, despite the long term benefits of a higher efficiency option.
  - **Opportunity** – Lower fuel savings will limit long term viability, and there is therefore the opportunity to jump ahead of competitors by developing a higher efficiency aircraft ahead of others.
- Whilst major airports may be willing to develop infrastructure to support blended wing body aircraft, smaller airports may be less willing to invest until the blended wing body market is larger. As a result, the number of possible destination may be limited in the short to medium term.
- In the long term, it is possible that legislation may attempt to encourage a zero carbon aviation industry. This will limit the lifetime of any aircraft that is reliant on hydrocarbons as a fuel source.
  - **Opportunity** – The technologies developed for an aircraft such as the N3-X (including distributed propulsion systems, superconductivity and BLI) will be applicable to electric aircraft or alternative fuels. The developed technologies can therefore be advanced to zero carbon concepts following their use on the N3-X.
- There is a high perception of risk inherent in novel technologies. As profit margins in the aviation industry are low, this high risk may deter investment. Historically, certain manufacturers have found that the choice to invest in potentially risky projects led to high costs or products with no market willing to purchase. The perception of risk in novel technology may limit investment by operators before the technology has been proven to be safe and profitable.

## 9. Conclusions

**Overview** A wide range of technologies are currently being researched to address challenging developmental goals for the aviation industry. These goals are performance-oriented, such as a reduction in CO<sub>2</sub> emissions, noise and energy consumption. Hence, research focus is predominantly on establishing whether these technologies can achieve performance goals. Chapter 2 presented reviewed literature on novel aircraft technologies that highlights a focus on predicting performance. The benefits of a new technology are presented in terms of factors such as a reduction in specific fuel consumption or power requirement. However, this leaves a number of key questions at the research level that must be answered. From an operator's perspective, one of the dominant deciding factors in technology selection is cost. However, a performance parameter cannot necessarily be easily translated into a cost benefit for the operator. In addition, competing concepts are designed with similar performance goals in mind. Hence, the performance expected from them is similar. How then can an operator differentiate these competing concepts? Economic viability then becomes the deciding factor in whether a technology is adopted. It is therefore a major consideration that must factor into the development of novel technology. This leads to a second challenge. Research and methods are available to quantify costs and hence predict economic viability for known and evolutionary technologies. However, it is difficult to quantify costs for a novel aircraft that utilises revolutionary technology, as there is no historical data on which a cost estimate can be based. Therefore, how can the economic viability of a novel aircraft concept be assessed from the operator's or manufacturer's perspective?

Research on revolutionary aircraft concepts predominantly focuses on performance simulation and defining propulsion system or aircraft configurations. As a result, there is limited research that attempts to identify the financial benefit of the concepts currently under investigation. It was therefore necessary to develop a way to translate performance benefits into a form suitable for a financier's perspective: operating cost benefits and a return on investment. The goal of the process is to quantify the financial value of a revolutionary technology. As there is significant uncertainty in predicting the cost of a novel aircraft, a reverse approach to the economic viability question has been used [146]. Rather than predicting a cost for the aircraft and then assessing financial benefits, maximum cost boundaries can be identified, beyond which there is no longer any financial benefit for an operator to adopt the technology. A manufacturer may then extract a maximum economically viable cost for the aircraft concept. However, an insight is also required into whether this maximum economically viable cost is feasible for the manufacturer. The research therefore develops a process to identify whether it is possible to achieve the target price-point and whether the aircraft market could support the number of aircraft sales necessary to achieve a reasonable price-point.

**Model Development** This research focused on assessing the economic viability of NASA's N3-X, a blended wing body aircraft with a turbo-electric distributed propulsion system and boundary layer ingestion (BLI). In order to prove the economic viability of a novel aircraft, a

## 9. Conclusions

---

full mission analysis must be performed to predict mission-level performance of the concept. The science of boundary layer ingesting propulsion systems is a well-understood topic. There are numerous bodies of research available that prove the potential performance benefits of BLI on a range of different aircraft configurations. However, previous modelling procedures for BLI propulsion systems tend to present only design point performance benefits [20, 24], with the assumption that the majority of a flight is spent in cruise. In order to provide a holistic view, it is then necessary to develop an analytical methodology for a BLI propulsion system to assess performance over a whole mission. Because of this requirement, the methodology requires a higher level of fidelity than previously available whilst remaining generic and flexible enough to support alternative configurations and propulsion system architectures. The requirement for the techno-economic analysis is to predict the mission fuel burn benefit of a BLI propulsion system such that a performance benefit can be translated into a mission economic benefit for an operator.

The main contribution of the research is therefore to develop a methodology to assess the economic viability of an aircraft that utilises a novel BLI propulsion system at a higher level of fidelity than previously available. Based on the identified gaps in literature, a detailed methodology was created to address the following major points:

- A generic work flow to simulate the performance of a boundary layer ingesting propulsion system at a range of flight conditions, suitable for use with aircraft performance simulation methods
- A methodology to assess the economic viability of a novel aircraft and propulsion system concept by identifying its maximum viable cost and then predicting whether the target price point is feasible for the manufacturer and the future aircraft market

Providing an economic perspective to a novel concept can assist in technology down-selection and helps identify the technologies most likely to be attractive to investors or operators. If a configuration is likely to not be economically viable, design changes to increase the attractiveness of the concept can be identified. For each configuration that is considered, the performance benefit of a design change or novel technology can be translated into the financial value provided to an operator. A method to assess the economic viability of a novel aircraft is a vital aspect of ensuring an economically sustainable industry in the future. This aspect of novel technology development forms the core of the techno-economic and environmental risk assessment method developed in this research.

To achieve the stated goals of the research, work was split into three phases. In the first phase, modelling procedures were developed to simulate the performance of the aircraft and its propulsion system. In the second phase, the economics of the aircraft was modelled in terms of the direct operating cost for an operator and the internal rate of return for the investment. The performance models developed during the research were also used to explore the aircraft design search space to identify the variables most likely to be beneficial. Of those assessed, thrust split and the individual optimisation of fans in the array would appear to be promising. The final phase combined a risk assessment with the performance and techno-economic aspects of the study to create a technology roadmap for the aircraft.

**Performance** The focus of the performance simulation phase of the research was primarily to establish the fuel consumption of the case study aircraft for any defined mission. The main performance goal for the aircraft is to achieve an energy saving of at least 60% in comparison to the baseline aircraft for the design mission. The N3-X was simulated as a kerosene option and a LH<sub>2</sub> variant, both using the propulsion system design parameters defined by previous research on the aircraft. Performance simulation of the N3-X suggests that the aircraft will achieve an energy saving of 60.4% versus the baseline aircraft for the design mission. The

## 9. Conclusions

---

energy saving for shorter range missions is lower, whilst the energy saving for the 'average' aircraft mission (5000 nmi, 90% payload) is 60.7%. The outcome therefore reinforces conclusions made in previous research that the N3-X can achieve its design goal. The LH<sub>2</sub> N3-X variant design used in the research was found to be capable of achieving a range of approximately 5,400 nautical miles, less than the 7,500 nautical mile maximum range for which the aircraft is intended. Additional fuel capacity would therefore be necessary to achieve the target range. The LH<sub>2</sub> variant nevertheless has a lower energy consumption than the kerosene N3-X, due to a lower weight during flight. The low fuel weight may also make the LH<sub>2</sub> an attractive prospect for use as a freight aircraft, due to a potentially high maximum payload weight in combination with a low energy-to-revenue-work ratio.

**Economic Viability** Direct operating costs saving for the N3-X was found to be lower than the fuel saving, as fuel does not account for the entirety of an aircraft's direct operating cost. Assuming all other costs remain equal, the kerosene N3-X was found to offer a direct operating cost saving of 21.1% versus the baseline aircraft for the design mission (July 2017 fuel price). As a result, the aircraft's acquisition price could increase to up to 24% more than that of baseline aircraft, whilst still remaining profitable. However, the maximum cost margins reduce for lower mission lengths, as fuel contributes less to the aircraft's direct operating cost. Acquisition cost estimation suggests that around 120 aircraft sales would be needed for the N3-X to break even, approximately 22% of the future large wide-body market. A higher number of sales would be required if a lower acquisition price was to be targeted. The aircraft is less viable when aimed at short- to medium-haul markets, as the potentially high costs of the aircraft outweigh the smaller saving in direct operating achieved by the aircraft's 60% fuel saving. The return on investment is low for short-haul range, and it may therefore be difficult to offer the aircraft as an attractive product for high capacity short-haul markets.

**Risk Assessment** Finally, the risk assessment identified a number of aspects that will have the most significant impact over the aircraft's viability. This includes the development of super-conducting machines and the development of distortion tolerant and low loss BLI propulsion systems. These will feature as a key part of the aircraft's technology roadmap and are currently research topics in the wider aerospace research community.

## 10. Further Work

This research has covered a wide range of areas from performance to economics. This leads to a range of different topics that may be useful to take forwards in further research. The topics presented here differ from the technology roadmap topics covered in Chapter 8 which will be covered by research as the technologies advance to higher TRL. Instead, the topics presented here cover aspects of either the techno-economic research or the design space exploration that may have potential.

**Propulsion System Design and Optimisation** This research has demonstrated the large number of variables available for the design of the N3-X propulsion system. As research progresses on the design of an aircraft such as the N3-X, it will be important to select the most useful variables for the development of the propulsion system. Analyses performed in this research suggest that it is useful to modify the propulsion system design to a configuration using thrust split and turbofan engines, rather than the initial turbogenerator and propulsor array combination. Introducing a turbofan into the propulsion design will necessitate additional research in optimising the turbofan and propulsion system's design.

As is currently found in the development of more conventional turbofans, specific fuel consumption can be improved by moving to increasingly higher bypass ratios. The same result can be observed for the turbomachinery component of the N3-X propulsion system, as a higher bypass ratio system is more efficient for producing thrust. Instead, other design factors will establish a limit on the ideal or maximum feasible bypass ratio of the system. A major factor that will influence the design is the available volume within the N3-X airframe for embedded engines. Embedded turbofans are generally low bypass ratio, which reduces the system's volume requirement. However, the available volume within the N3-X airframe is likely to be larger than the volume typically available for aircraft using embedded engines (especially military applications). In addition, introducing a turbofan increases the level of complexity of the turbomachinery, which will influence costs. A turbofan and thrust split design option is nevertheless proposed to be a useful avenue of research for improving the system's efficiency.

As the design progresses, it will also be useful to further develop aspects of research focusing on the individual design and sizing of the array. The optimisations presented in this research have shown that there is a reasonable scope for improving the performance of the propulsor array. By focusing on the design of individual propulsors and optimising each based on its location, a reasonable decrease in power consumption can be achieved. It will therefore be useful to further develop the individual design and optimisation aspects of research for the design of the N3-X.

**Individual Fan Control** The results from the propulsor array simulation suggest that those propulsors at the outside of the array are less efficient, but are able to produce more thrust due to a larger size (given the sizing assumptions). In contrast, the inner propulsors are more efficient, due to a slower local flow and thicker boundary layer. This suggests that it will also

## 10. Further Work

---

be useful to consider the possible benefits of individual control of propulsors within the array. Spooling certain propulsors in the array up or down may provide useful benefits, depending on the in-flight requirements. One such possible option is to disable the outer propulsors in the array when thrust requirements are low and to use only the more efficient central propulsors (such as during descent). Alternatively, propulsors with the highest risk of flow separation during low power conditions may be disabled to prevent separation in the adverse pressure gradient from the interface point to the intake. As a related option, it may be useful to consider a configuration option where propulsors may be wind-milled to produce power when not in use.

**Variable Area Floating Nozzle** In keeping with previous research on the N3-X, this research has assumed that the area of the N3-X exhaust nozzles is floating. The nozzle area of each propulsor is therefore assumed to dynamically adjust during the course of the flight to accommodate the peak efficiency running line used to simulate the fans. However, it is possible that a floating area nozzle may be mechanically too complex or heavy to incorporate on the aircraft. In this case, a simpler fixed area nozzle may be necessary. It may also be useful to consider a nozzle with limited variable area capability to support a number of key flight conditions, without being a fully floating nozzle area. It will therefore be important to assess the influence that a fixed or limited variable area exhaust will have on the propulsion system and hence the aircraft's performance. With a fixed exhaust area and assuming that the nozzle is choked, the non-dimensional mass flow of the nozzle is constant. The non-dimensional mass flow of the nozzle will only reduce once the nozzle is no longer choked. The fan's operating point is now dictated by the nozzle, rather than the running line assumed in this research. The new running line of the fan follows a path that ensures that the area condition is met for the exhaust. For example, for a defined rotational speed, the operating point moves along the speed line on the map to meet the constant area and constant non-dimensional mass flow requirement.

For the BLI propulsor, an iterative loop is already required to determine the inlet stream height that meets the mass flow demand of the fan. However, for a fixed area exhaust, an additional iteration is required to find the fan operating point based on the nozzle operating requirements. An approximate representation of the change in running line is shown in Figure 10.1. In this example, a high fan pressure ratio is selected at design point to ensure that the nozzle remains choked for the chosen speeds. For each point, the following procedure was used: with fan speed as the defined starting point, the non-dimensional mass flow was iterated by following the speed line. For each iteration the propulsor operating point changes (i.e. fan pressure ratio, efficiency, and mass flow demand) were obtained. Subsequently, the stream-tube height which met the fan mass flow demand was found (see the procedure described in Section 3.1.6). Finally, the resultant exhaust area was calculated. The iteration was repeated, moving along the speed line until nozzle area converged to the target value. For the selected example, the operating line moves further away from the surge line and towards very low fan pressure ratios that may not support stable operation. This outcome supports the original design decision for the N3-X to use a variable area nozzle for fan stability. It is worth highlighting that the actual running of a BLI fan or compressor will be closer to surge than the running line applied here [20]. It is nevertheless possible to conclude that a fixed nozzle area would be detrimental to performance.

If the floating area nozzle is to be retained, there are additional factors that will need to be included to increase the fidelity of the analysis. Large reductions in nozzle area may imply a large boat-tail angle for the exhaust which will result in an increase in boat-tail drag for the nacelle. This increase in drag will need to be accounted for in the installed net propulsive force term. Simulation data for the N3-X over the 7500 nautical mile mission suggests that the nozzle area during climb and cruise varies is within 5% of the design exhaust area. However, exhaust

## 10. Further Work

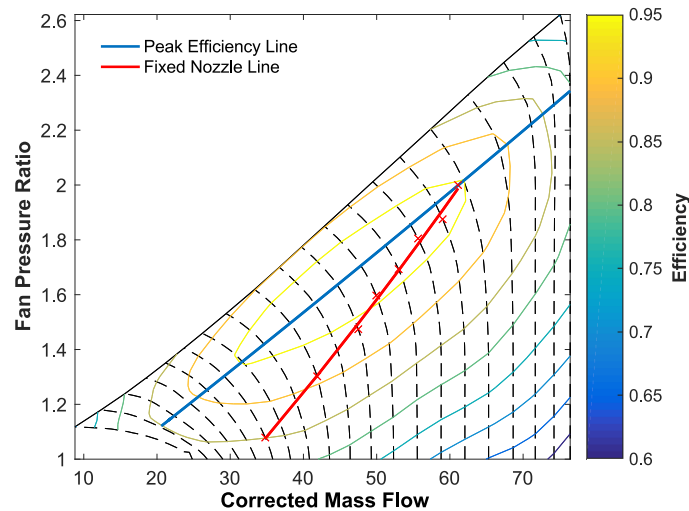


**Figure 10.1:** Approximate running line for a sample BLI propulsor with a fixed area nozzle

area is 12% greater than the design nozzle area at sea level static, and is 50% of the design point exhaust area during descent. It is possible that higher drag during descent may be useful, enabling a steeper rate of descent on an otherwise high-lift airframe.

**Superconducting Electrical System** This research focused on the performance of the turbomachinery and propulsor components of the propulsion system. However, further development is necessary to address the simplified assumptions used to approximate the superconducting power system. The models presented in this research represent the superconducting system primarily as a fixed transmission efficiency term. Further development will be needed to model the system on a more detailed component level. Of particular importance for a study such as the one presented herein, it is important to identify how the efficiency of the electrical system will vary based on power demand and operating conditions (e.g. propulsor and hence motor rotational speed).

**Liquid Hydrogen Aircraft Options** The research presents primarily performance estimates of a hypothetical aircraft variant for the N3-X that burns both LH<sub>2</sub> and kerosene during a mission. This was applied to provide a range increase for the LH<sub>2</sub> variant of the N3-X. However, further research would be required to identify the feasibility of a gas turbine that can swap between different fuel types. Alternatively, it may be useful to assess the feasibility of a variant that burns a mixture of LH<sub>2</sub> and kerosene.

It is possible that a minimum energy split between LH<sub>2</sub> and kerosene may exist for the design mission. By reducing the size of the LH<sub>2</sub> tanks, the weight of the aircraft would be reduced, and therefore the required energy for the flight would reduce. However, this would lead to less LH<sub>2</sub> and hence more kerosene on board, leading to an increase in weight. There may therefore be a point which minimises the required energy by balancing the quantities and split between each fuel type.

It is also possible that a dual fuel configuration may prove beneficial from an economic perspective. Current cost estimates for LH<sub>2</sub> as fuel lead to a higher direct operating cost for the LH<sub>2</sub> variant than the kerosene variant, despite a lower fuel burn by mass. Combining fuel types could potentially lead to a low cost solution by reducing the kerosene fuel burn and reducing the energy consumed by the aircraft. However, the high cost of LH<sub>2</sub> could also lead to an increase in overall fuel cost. As with energy consumption, there may be a split which minimises

## 10. Further Work

---

the overall life cycle costs for the aircraft. This analysis would also need to account for the additional costs of developing, manufacturing and owning a dual fuel aircraft.

**Trajectory optimisation** Improved air traffic management has been proposed as one of the routes towards reducing the carbon emissions of the aviation industry [8]. This research has looked briefly at cruise-climb as an alternative to a fixed altitude cruise to improve fuel consumption. Complete trajectory optimisation can provide further benefits to the fuel consumption of the aircraft, over and above that provided by the high efficiency airframe. In addition, trajectory optimisation may be useful to minimise contrail formation, although this will likely conflict with a low fuel trajectory.

**Defining the ‘jumping-in’ point** Assuming an established product line, a manufacturer can remain profitable in the short term by continuing to sell current products and providing services to its customers. However, at a certain point it becomes necessary for a manufacturer to invest in the development of new products to stay ahead of competitors and ensure that products remain attractive to customers. It is therefore important for a manufacturer to define the point at which it is most profitable to invest heavily in the development of a new product. Too early, and there is a risk that the new product will push the manufacturer’s other products out of the market before demand has reduced. Too late, and the manufacturer risks a period where current products are not attractive to customers and better competing options are available. For a large scale development program like the N3-X, it is useful to be able to define at what point it is most profitable for a manufacturer to invest in order to reap the greatest benefits. Justin *et al.* [201] presents one such perspective by assessing development timelines to identify the most profitable portfolio of products. Similarly, from an operator’s perspective, it is useful to define when it is best to invest in the purchase of new aircraft. In this case it is important not only to predict the actual costs of the aircraft, but also to predict opportunity costs and possible loss in sales through competition.

**Change in Aircraft Market** A high efficiency aircraft such as the N3-X should ideally lead to operating cost savings for an operator. The operator may take advantage of the increase in profits that results. Alternatively and depending on the location, lowering ticket prices may increase the passenger market, leading to a net increase in sales. This may lead to an increase in profits, despite lower ticket prices. It will therefore be useful to combine the aircraft’s techno-economic analysis with a market analysis to predict if lower operating costs can be leveraged to provide further advantages for an operator. Low cost operators already apply such a concept to remain profitable by reducing their operating costs (such as by not offering in-flight entertainment system or meals) and selling lower cost tickets.

Analysis of global population and the number of aviation passengers suggests that there is a large untapped market in regions such as Africa and Asia. Even without a change in ticket price, markets such as Africa and Asia will continue to grow, and may have different aviation requirements than the well-established North American and European Markets [3]. In particular, the Asian market requires more high capacity, short haul routes, whereas high capacity aircraft are generally designed for long haul routes. As a result, an aircraft intended for these growing markets may require a substantially different design (e.g. lower cruise speed).

**Optimum Technology Mix** The N3-X combines a wide selection of technologies to achieve the 60% energy savings target. Each of these technologies will naturally imply certain costs that will influence the final operating cost of the aircraft. There will therefore be a technology mix which maximises profitability for an operator. Certain design decisions may also have a



## 10. Further Work

---

relatively minor impact on performance whilst having a large impact on cost. It will therefore be useful to expand the analyses to consider a set of different options and identify the most viable combination that achieves the performance target and limits cost for manufacturers and operators.

**Change in Design Outlook** Currently, components on an aircraft are designed for long lives and are replaced only occasionally. This generally implies high cost components, as lives must be long. A change in perspective may prove advantageous for the industry by moving from components designed for long life to components designed to be cheaply and quickly replaced. In combination with economies of scale, mass producing components to be regularly replaced may lead to lower costs overall for the aircraft. Component cost could be reduced, as the requirement for long life would be reduced. In addition, as components may be easily replaced, maintenance time can be reduced, as there is less of a requirement for detailed inspection for damage.

Distributed propulsion systems such as that applied for the N3-X make use of many small propulsors, rather than few, complex turbomachines. It is possible economies of scale may be applied here to lead to a reduction in costs through the mass production of many relatively simple items. Epstein [31] suggests that the concept of many small engines may be a useful business model in the future, where thrust is sold as a commodity and the number of propulsion units provided is a function of the aircraft's thrust requirement. This perspective in combination with an economy of scale and easily replaceable units may be an option for lower costs for both manufacturers and operators.

**Competing Options** Numerous competing aircraft options have been proposed in research both in parallel with the N3-X at NASA and as research by other entities. It will be useful to apply the techno-economic framework to the competing aircraft options in order to rank and compare each concept. This will assist in identifying the optimal research area for investment and further research. It will also be able to identify commonalities between the concepts in terms of a technology level that is required by all the concepts to reach target performance levels.

**Lifetime Maintenance Costs** The maintenance cost of an aircraft and propulsion system varies over the course of the aircraft life. The techno-economic analysis assumed a fixed cost per flight hour over the entire aircraft life. However, it may also be useful to incorporate a model that is able to adjust maintenance cost per flight hour over the course of the aircraft's life. In particular, it will be useful to identify whether the maintenance cost per flight hour is similar for the baseline aircraft and novel aircraft, or whether design decisions lead to a divergence in cost over time. Where cost increases over time, it will be useful to identify if any design changes will be required to reduce the lifetime costs of the aircraft.

In addition to lifetime maintenance cost, it is important to identify the additional cost of maintenance time. Complex aircraft may require significant time in the shop to perform maintenance actions. This will reduce the availability of the aircraft, which may negatively impact costs, as replacement aircraft must be found to cover the flight schedule.

**Cost of Noise** Noise has not been considered as a component of this research. However, reducing noise is a key aspect of development for both current and future aircraft. CAEP noise levels establish maximum noise levels for new engines which have become increasingly stringent over time. In addition, noise is included in developmental targets for future aircraft. Noise is a limiter on both aircraft operations and aircraft expansion. Investment in new runways or

## 10. Further Work

---

airport infrastructure must ensure that noise is kept at a reasonable level for local communities. Quieter aircraft can therefore lead to an increase in operating hours and potentially less resistance to airport expansion. Whilst it is relatively easier to identify the benefits of extending operating hours thanks to a reduction in noise, it is harder to identify the economic cost of noise. Tam *et al.* identify that a low noise aircraft can provide wider benefits to the local community, with a resulting increase in economic growth [83]. It follows that a high noise aircraft incurs some economic cost. A wider techno-economic analysis should encompass the benefits to the community that result from low noise aircraft operation. This may be useful to establishing noise taxation levels to encourage the development of low noise aircraft.

**Aircraft NO<sub>x</sub> Emissions** The research has focused on the requirement for aircraft to reduce their Carbon Dioxide emissions. However, it is equally important to consider the significance of NO<sub>x</sub> for an aircraft such as the N3-X both on-ground and during flight. The baseline design of the N3-X engines assumes a high combustor exit temperature, this may imply high NO<sub>x</sub> emissions. However, the N3-X also has lower thrust requirements than the baseline B777-200LR due to the introduction of BLI and an airframe with a high lift-to-drag ratio. The overall impact on NO<sub>x</sub> emissions must therefore be considered.

**Fleet Analysis** The performance and techno-economic analyses in this research have focused predominantly on single aircraft operating a single mission length for its entire life. In reality, an operator will own a large number of aircraft operating on numerous routes. As has already been identified, the fuel and direct operating cost saving of the aircraft depends on the mission range. It will therefore also depend on the city pairs between which the aircraft is operated. A full fleet analysis will be necessary to establish whether there is a net benefit for an operator with a fleet of N3-X aircraft. In addition, it is important to determine whether this fleet as a whole is able to meet the fuel burn target. If the majority of aircraft are operated significantly below the design range, it is possible that the net fuel benefit may fall below the 60% target. A sample 'average' fleet should therefore be selected to assess the fleet benefits and performance of the N3-X.

**Non-linearities in Cost Modelling** The current models assume that the two unknown costs (acquisition price and maintenance cost) are independent from each other. However, it is likely that there will be some form of relationship between an aircraft's maintenance cost and acquisition price. For example, advanced materials imply a high acquisition price and are also likely to lead to higher maintenance costs due to a higher material cost. The extent to which these two parameters are related is another unknown factor in the analysis that would add an additional dimension to the cost sensitivity. A cost function may therefore be a useful development to relate how the sensitivity analysis will change as the relationship between different cost factors becomes increasingly non-linear.

# 11. Publications

This final chapter summarises the publications that have been produced over the course of the doctoral research program.

## 2015

- Chana Goldberg, Devaiah Nalianda, and Riti Singh. (2015) "Techno-economic and environmental risk assessment of a blended wing body with distributed propulsion." In *51<sup>st</sup> AIAA/SAE/ASEE Joint Propulsion Conference*. AIAA 2016-4024. [doi:10.2514/6.2015-4024](https://doi.org/10.2514/6.2015-4024)
- C. Goldberg, D. Nalianda, R Singh and Rubén Del Rosario, (2015). "A Techno-Economics Perspective to Facilitate Future Implementation of Turbo-Electric Distributed Propulsion Systems", Special session in *22<sup>nd</sup> International Symposium on Air Breathing Engines*. ISABE-2015-20287
- Chana Goldberg, Eleftherios Giakoumakis, and Devaiah Nalianda. (2015). "Assessment of Propulsive Airframe Integration Issues of a Conceptual Aircraft using Distributed Propulsion and Boundary Layer Ingestion", In *22<sup>nd</sup> International Symposium on Air Breathing Engines*. ISABE-2015-20072.

## 2016

- **Inlets, Nozzles and Propulsion Systems Integration session Best Paper.** Chana Goldberg, Devaiah Nalianda, Pericles Pilidis, David MacManus, and James Felder. (2016). "Installed Performance Assessment of a Boundary Layer Ingesting Distributed Propulsion System at Design Point", In *52<sup>nd</sup> AIAA/SAE/ASEE Joint Propulsion Conference*. AIAA 2016-4800. [doi:10.2514/6.2016-4800](https://doi.org/10.2514/6.2016-4800).

## 2017

- Chana Goldberg, Devaiah Nalianda, Pericles Pilidis, and Riti Singh. (2017). "Economic Viability Assessment of NASA's Blended Wing Body N3-X Aircraft." In *53<sup>rd</sup> AIAA/SAE/ASEE Joint Propulsion Conference*. AIAA 2017-4604. [doi:10.2514/6.2017-4604](https://doi.org/10.2514/6.2017-4604)
- Chana Goldberg, Devaiah Nalianda, Panagiotis Laskaridis, and Pericles Pilidis. (2017). "Performance Assessment of a Boundary Layer Ingesting Distributed Propulsion System at Off-Design." In *53<sup>rd</sup> AIAA/SAE/ASEE Joint Propulsion Conference*. AIAA 2017-5055. [doi:10.2514/6.2017-5055](https://doi.org/10.2514/6.2017-5055)
- C. Goldberg, J. Felder, D. Nalianda, V. Sethi, P. Pilidis and R. Singh. (2017). "Turbo-electric Vehicle Study - A techno-economic and environmental risk assessment of the N3-X" In *23<sup>rd</sup> International Symposium on Air Breathing Engines*. ISABE-2017-22535.

## 11. Bibliography

---

- C. Goldberg, D. Nalianda, V. Sethi, P. Pilidis and R. Singh. (2017). Liquid Hydrogen Fuel for a Blended Wing Body Aircraft: Case Study on the N3-X In *23<sup>rd</sup> International Symposium on Air Breathing Engines*. ISABE-2017-21470.
- Chana Goldberg, Devaiah Nalianda, and Pericles Pilidis. (2017). Installed Performance Assessment of an Array of Distributed Propulsors Ingesting Boundary Layer Flow. In *ASME Turbo Expo 2017*. ASME GT2017-63917. [doi:10.1115/GT2017-63917](https://doi.org/10.1115/GT2017-63917) (**accepted for publication in ASME Journal of Engineering for Gas Turbines and Power, GTP-17-1588**)

### 2018

- C. Goldberg, D. Nalianda, V. Sethi, P. Pilidis, R. Singh and K. Kyprianidis. (2018) Assessment of an energy-efficient aircraft concept from a techno-economic perspective, *Applied Energy*, 221:229-238. [doi:10.1016/j.apenergy.2018.03.163](https://doi.org/10.1016/j.apenergy.2018.03.163).
- C. Goldberg, D. Nalianda, D. MacManus, P. Pilidis and J. Felder. (2018, accepted for publication). Method for simulating the performance of a boundary layer ingesting propulsion system at design and off-design. *Aerospace Science and Technology*.

# Bibliography

- [1] Air Transport Action Group. Flightpath, 2013. ICAO 38th Assembly.
- [2] IATA. Airlines finance monitor, 2016. URL <http://www.iata.org/publications/economics/Pages/index.aspx>. Accessed: June 2016.
- [3] Boeing. Current market outlook 2016–2035, 2016.
- [4] Airbus. Airbus Global Market Forecast: Growing Horizons 2017 – 2036, 2017.
- [5] IATA. Profitability and the air transport value chain, 2013. IATA Economics Briefing No. 10.
- [6] Boeing. Boeing Current Market Outlook 2017–2036, 2017.
- [7] IATA. IATA fact sheet - fuel, 2017. URL [https://www.iata.org/pressroom/facts\\_figures/fact\\_sheets/Documents/fact-sheet-fuel.pdf](https://www.iata.org/pressroom/facts_figures/fact_sheets/Documents/fact-sheet-fuel.pdf). Accessed: September 2017.
- [8] International Civil Aviation Organization. ICAO Environmental Report 2016 Aviation and Climate Change, 2016.
- [9] The right flightpath to reduce aviation emissions, 2010. UNFCCC Climate Talks.
- [10] Clean Sky. European Aeronautics: A Vision for 2020. URL <http://www.cleansky.eu/history>. Accessed: September 2017.
- [11] National Aeronautics and Space Administration. New Aviation Horizons Initiative and Complementary Investments, 2017.
- [12] IATA. Economic performance of the airline industry: Mid 2017, 2017. URL <http://www.iata.org/whatwedo/Documents/economics/IATA-Economic-Performance-of-the-Industry-mid-year-2017-report.pdf>. Accessed: June 2017.
- [13] Paul Clark. *Buying the big jets: fleet planning for airlines*. Ashgate Publishing, Ltd., 2007.
- [14] Flight International. Whatever happened to propfans? URL <https://www.flightglobal.com/news/articles/whatever-happened-to-propfans-214520/>. Accessed: September 2017.
- [15] E.M. Greitzer, P.A. Bonney, E. De la Rosa Blanco, C.S. Dorbian, M. Drela, D.K. Hall, R.J. Hansman, J.I. Hileman, R.H. Liebeck, J. Lovegren, P. Mody, J.A. Pertuze, S. Sato, Z.S. Spakovszky, C.S. Tan, J.S. Hollman, J.E. Duda, N. Fitzgerald, J. Houghton, J.L. Kerrebrock, G.F. Kiwada, D. Kordonowy, J.C. Parrish, J. Tylko, E.A. Wen, and W.K. Lord. N+3

## 11. Bibliography

---

- Aircraft Concept Designs and Trade Studies and Final Report: Volume 1. Technical Report NASA/CR-2010-216794/VOL1, Massachusetts Institute of Technology, Aurora Flight Sciences, and Pratt & Whitney, 2010.
- [16] Division on Engineering and Physical Sciences Committee on Propulsion and Energy Systems to Reduce Commercial Aviation Carbon Emissions, Aeronautics and Space Engineering Board. *Commercial Aircraft Propulsion and Energy Systems Research: Reducing Global Carbon Emissions*. The National Academies Press, 2016.
- [17] Flightglobal. Aircraft paint suppliers explore sharkskin coating, 2013. URL <http://www.flightglobal.com/news/articles/aircraft-paint-suppliers-explore-sharkskin-coating-381646/>. Accessed: 2015-04-28.
- [18] Flightglobal. EasyJet turns to nanotechnology to save fuel, 2011. URL <http://www.flightglobal.com/news/articles/easyjet-turns-to-nanotechnology-to-save-fuel-353148/>. Accessed: 2015-04-28.
- [19] A M O Smith and Howard E Roberts. The Jet Airplane Utilizing Boundary Layer Air for Propulsion. *Journal of the Aeronautical Sciences (Institute of the Aeronautical Sciences)*, 14(2):97–109, 1947. doi: 10.2514/8.1273.
- [20] A P Plas, M A Sargeant, V Madani, D Crichton, E M Greitzer, T P Hynes, and C a Hall. Performance of a Boundary Layer Ingesting (BLI) Propulsion System. In *45th AIAA Aerospace Sciences Meeting and Exhibit, 8 - 11 January 2007, Reno, NV, USA*, number AIAA 2007-450, 2007. doi: 10.2514/6.2007-450.
- [21] Arne Seitz, Julian Bijewitz, Sascha Kaiser, and Guido Wortmann. Conceptual investigation of a propulsive fuselage aircraft layout. *Aircraft Engineering and Aerospace Technology*, 86(6):464–472, 2014. doi: 10.1108/AEAT-06-2014-0079.
- [22] Susan Althoff Gorton, Lewis R Owens, Luther N Jenkins, Brian G Allan, and Ernest P Schuster. Active flow control on a boundary-layer-ingesting inlet. In *42nd AIAA Aerospace Sciences Meeting and Exhibit, Reno, NV, USA*, number AIAA 2004-1203, 2004. doi: 10.2514/6.2004-1203.
- [23] Martin Rein, Stefan Koch, and Markus Rutten. Experimental Investigations on the Influence of Ingesting B.L. into a Diverterless S-Duct Intake. In *52nd Aerospace Sciences Meeting, National Harbor, MD, USA*, number AIAA 2014-0373, 2014. doi: 10.2514/6.2014-0373.
- [24] James L Felder, Hyun Dae Kim, and Gerald V Brown. Turboelectric distributed propulsion engine cycle analysis for hybrid wing body aircraft. In *47th AIAA Aerospace Sciences Meeting, Orlando, FL, USA*, number AIAA 2009-1132, 2009. doi: 10.2514/6.2009-1132.
- [25] Cesare A Hall and Daniel Crichton. Engine design studies for a silent aircraft. *Journal of Turbomachinery*, 129(3):479–487, 2007.
- [26] Jason Welstead and James L Felder. Conceptual Design of a Single-Aisle Turboelectric Commercial Transport with Fuselage Boundary Layer Ingestion. In *54th AIAA Aerospace Sciences Meeting, San Diego, CA, USA*, number AIAA 2016-1027, 2016. doi: 10.2514/6.2016-1027.

## 11. Bibliography

---

- [27] Amir S Gohardani, Georgios Doulgeris, and Riti Singh. Challenges of future aircraft propulsion: A review of distributed propulsion technology and its potential application for the all electric commercial aircraft. *Progress in Aerospace Sciences*, 47(5):369–391, 2011.
- [28] Arun K Sehra and Woodrow Whitlow. Propulsion and power for 21st century aviation. *Progress in Aerospace Sciences*, 40(4):199–235, 2004.
- [29] Hyun Dae Kim. Distributed propulsion vehicles. In *27th International Congress of the Aeronautical Sciences, Nice, France*, 2010.
- [30] George R Seyfang. Fanwing—developments and applications. In *28th Congress of the International Council of the Aeronautical Sciences*, number ICAS 2012-1.3.3, 2012.
- [31] Alan H Epstein. Aeropropulsion for commercial aviation in the twenty-first century and research directions needed. *AIAA journal*, 2014.
- [32] A<sup>3</sup> / Airbus. Welcome to Vahana, 2016. URL <https://vahana.aero/welcome-to-vahana-edfa689f2b75>. Accessed: September 2017.
- [33] Lilium. The Lilium Jet. URL <https://lilium.com>. Accessed: September 2017.
- [34] Volocopter GmbH. Volocopter. URL <https://www.volocopter.com/en/>. Accessed: September 2017.
- [35] Askin T Isikveren, Arne Seitz, Julian Bijewitz, Arthur Mirzoyan, Alik Isyanov, Richard Grenon, Olivier Atinault, J-L Godard, and Stefan Stückl. Distributed propulsion and ultra-high by-pass rotor study at aircraft level. *The Aeronautical Journal*, 119(1221):1327–1376, 2015.
- [36] Marty K Bradley and Christopher K Droney. Subsonic Ultra Green Aircraft Research: Phase I Final Report. Technical Report NASA/CR-2011-216847, Boeing Research and Technology, 2012.
- [37] Charles Lents, Larry Hardin, Jonathan Rheume, and Lee Kohlman. Parallel hybrid gas-electric geared turbofan engine conceptual design and benefits analysis. In *AIAA Propulsion and Energy Forum, Salt Lake City, UT, USA*, 2016.
- [38] Ralph Jansen, Cheryl Bowman, Amy Jankovsky, Rodger Dyson, and James Felder. Overview of nasa electrified aircraft propulsion (EAP) research for large subsonic transports. In *53rd AIAA/SAE/ASEE Joint Propulsion Conference, Atlanta, GA, USA*, number AIAA 2017-4701, 2017.
- [39] NASA. NASA Electric Research Plane Gets X Number, New Name. URL <https://www.nasa.gov/press-release/nasa-electric-research-plane-gets-x-number-new-name>. Accessed: September 2017.
- [40] Aurora Flight Sciences. XV-24A Lightning Strike. URL <http://www.aurora.aero/lightningstrike/>. Accessed: September 2017.
- [41] Anusha Harish, Christian Perron, Daniel Bavaro, Jai Ahuja, Melek Ozcan, Cedric Y Justin, Simon I Briceno, Brian J German, and Dimitri Mavris. Economics of advanced thin-haul concepts and operations. In *16th AIAA Aviation Technology, Integration, and Operations Conference*, 2016. AIAA 2016-3767.

## 11. Bibliography

---

- [42] Alan Epstein. Aircraft Propulsion: What does the future bring?, 2017. Plenary Session at 53rd AIAA/SAE/ASSEE Joint Propulsion Conference, Atlanta, GA, USA.
- [43] Aviation Week. Airbus Drops Electric Light Aircraft For Larger E-Fan X, 2017. URL <http://aviationweek.com/commercial-aviation/airbus-drops-electric-light-aircraft-larger-e-fan-x>. Accessed: September 2017.
- [44] Randy Bowman. Electrical materials research for nasa's hybrid electric commercial aircraft program, 2017. Presented at the Interagency Advanced Power Group Electrical Materials panel session.
- [45] Cesar A Luongo, Philippe J Masson, Taewoo Nam, Dimitri Mavris, Hyun D Kim, Gerald V Brown, Mark Waters, and David Hall. Next generation more-electric aircraft: a potential application for hts superconductors. *IEEE Transactions on Applied Superconductivity*, 19(3):1055–1068, 2009.
- [46] Gerald V Brown. Weights and efficiencies of electric components of a turboelectric aircraft propulsion system. In *49th AIAA aerospace sciences meeting including the new horizons forum and aerospace exposition, Orlando, Florida, USA*, number AIAA 2011-225, 2011.
- [47] Airbus Group and Rolls-Royce. E-Thrust: Electrical distributed propulsion system concept for lower fuel consumption, fewer emissions and less noise, 2016.
- [48] Michael J Armstrong, Christine AH Ross, Mark J Blackwelder, and Kaushik Rajashekara. Propulsion system component considerations for nasa n3-x turboelectric distributed propulsion system. *SAE International Journal of Aerospace*, 5(2012-01-2165):344–353, 2012.
- [49] Frederick Berg, Joseph Palmer, Paul Miller, and Graham Dodds. HTS system and component targets for a distributed aircraft propulsion system. *IEEE Transactions on Applied Superconductivity*, 27(4):1–7, 2017.
- [50] Benjamin T Schiltgen, Jeffrey L Freeman, and David W Hall. Aeropropulsive interaction and thermal system integration within the eco-150: A turboelectric distributed propulsion airliner with conventional electric machines. In *16th AIAA Aviation Technology, Integration, and Operations Conference*, 2016. AIAA 2016-4064.
- [51] Robert H Liebeck. Design of the blended wing body subsonic transport. *Journal of aircraft*, 41(1):10–25, 2004. doi: 10.2514/1.9084.
- [52] AL Bolsunovsky, NP Buzoverya, BI Gurevich, VE Denisov, AI Dunaevsky, LM Shkadov, OV Sonin, AJ Udzhuhu, and JP Zhurihin. Flying wing – problems and decisions. *Aircraft design*, 4(4):193–219, 2001.
- [53] Ning Qin, Armando Vavalle, Alan Le Moigne, M Laban, K Hackett, and P Weinerfelt. Aerodynamic considerations of blended wing body aircraft. *Progress in Aerospace Sciences*, 40(6):321–343, 2004.
- [54] Robert H Liebeck, Donald A Andrastek, Johnny Chau, Raquel Girvin, Roger Lyon, Blaine K Rawdon, Paul W Scott, and Robert A Wright. Advanced subsonic airplane design and economic studies. Technical Report NASA CR-195443, McDonnell-Douglas Aerospace.



## 11. Bibliography

---

- [55] JI Hileman, ZS Spakovszky, M Drela, MA Sargeant, and A Jones. Airframe design for silent fuel-efficient aircraft. *Journal of aircraft*, 47(3):956, 2010.
- [56] James Felder, Gerald Brown, Hyun Kim, and Julio Chu. Turboelectric Distributed Propulsion in a Hybrid Wing Body Aircraft. In *20th International Society for Airbreathing Engines, Gothenburg, Sweden*, number ISABE-2011-1340, 2011.
- [57] Simon Blakey, Lucas Rye, and Christopher William Wilson. Aviation gas turbine alternative fuels: A review. *Proceedings of the combustion institute*, 33(2):2863–2885, 2011.
- [58] Mitch R Withers, Robert Malina, Christopher K Gilmore, Jonathan M Gibbs, Chris Trigg, Philip J Wolfe, Parthasarathi Trivedi, and Steven RH Barrett. Economic and environmental assessment of liquefied natural gas as a supplemental aircraft fuel. *Progress in Aerospace Sciences*, 66:17–36, 2014.
- [59] GD Brewer. The prospects for liquid hydrogen fueled aircraft. *International Journal of Hydrogen Energy*, 7(1):21–41, 1982.
- [60] Bhupendra Khandelwal, Adam Karakurt, Paulas R Sekaran, Vishal Sethi, and Riti Singh. Hydrogen powered aircraft: the future of air transport. *Progress in Aerospace Sciences*, 60:45–59, 2013.
- [61] Magdalena Momirlan and T Nejat Veziroglu. The properties of hydrogen as fuel tomorrow in sustainable energy system for a cleaner planet. *International journal of hydrogen energy*, 30(7):795–802, 2005.
- [62] US Department of Energy - Fuel Cell Technologies Office. Multi-year research, development, and demonstration plan – hydrogen production, 2015.
- [63] Paul Stadler. Cost evaluation of large scale hydrogen production for the aviation industry. Master's thesis, Ecole Polytechnique Fédérale de Lausanne, 2014.
- [64] Reinhaard Faa. Cryoplane – flugzeuge mit wasserstoffantrieb, 2001. Airbus Deutschland Cryoplane presentation.
- [65] D Daggett, R Hendricks, and R Walther. Alternative fuels and their potential impact on aviation, 2006. NASA/TM-2006-214365.
- [66] Anthony J Colozza and Lisa Kohout. Hydrogen storage for aircraft applications overview. Technical Report NASA/CR – 2002-211867, Analex Corporation, 2002.
- [67] Abe Silverstein and Eldon W Hall. Liquid hydrogen as a jet fuel for high-altitude aircraft, 1955. NACA Research Memorandum.
- [68] Deutschen Zentrums für Luft- und Raumfahrt. Zero-emission air transport first flight of four-seat passenger aircraft HY4, 2016. URL [http://www.dlr.de/dlr/en/desktopdefault.aspx/tabid-10081/151\\_read-19469/#/gallery/24480](http://www.dlr.de/dlr/en/desktopdefault.aspx/tabid-10081/151_read-19469/#/gallery/24480). Accessed: September 2017.
- [69] LB Newnes, AR Mileham, Wai Ming Cheung, Robert Marsh, JD Lanham, ME Saravi, and RW Bradbery. Predicting the whole-life cost of a product at the conceptual design stage. *Journal of Engineering Design*, 19(2):99–112, 2008.
- [70] Ryan P Henderson, Joaquim RRA Martins, and Ruben E Perez. Aircraft conceptual design for optimal environmental performance. *The Aeronautical Journal*, 116(1175): 1–22, 2012.

## 11. Bibliography

---

- [71] Nicolas E Antoine and Ilan M Kroo. Framework for aircraft conceptual design and environmental performance studies. *AIAA journal*, 43(10):2100–2109, 2005.
- [72] Rajeev K Goel and Daniel P Rich. On the adoption of new technologies. *Applied Economics*, 29(4):513–518, 1997.
- [73] Stephen Ogaji, Pericles Pilidis, and Richard Hales. TERA-a tool for aero-engine modelling and management. In *2nd World Congress on Engineering Asset Management and 4th International Conference on Condition Monitoring, Harrogate, UK, 2007*.
- [74] Tomas Grönstedt, Carlos Xisto, Vishal Sethi, Andrew Rolt, Nicolás García Rosa, Arne Seitz, Kyros Yakinthos, Stefan Donnerhack, Paul Newton, Nicolas Tantot, Oliver Schmitz, and Anders Lundblad. Ultra low emission technology innovations for mid-century aircraft turbine engines. In *ASME Turbo Expo 2016: Turbomachinery Technical Conference and Exposition*, 2016. GT2016-56123.
- [75] William Camilleri, Eduardo Anselmi, Vishal Sethi, Panagiotis Laskaridis, Andrew Rolt, and Pedro Cobas. Performance characteristics and optimisation of a geared intercooled reversed flow core engine. *Proceedings of the Institution of Mechanical Engineers, Part G: Journal of Aerospace Engineering*, 229(2):269–279, 2015.
- [76] Pablo Bellocq, Vishal Sethi, Luca Cerasi, Sebastian Ahlefeldt, Riti Singh, and Nicolas Tantot. Advanced open rotor performance modelling for multidisciplinary optimization assessments. In *ASME Turbo Expo 2010: Power for Land, Sea, and Air*, number GT2010-22963, 2010.
- [77] Andrew M Rolt and Konstantinos Kyprianidis. Assessment of new aero engine core concepts and technologies in the eu framework 6 newac programme. In *ICAS 2010 Congress Proceedings*, 2010. ICAS 2010-408.
- [78] DK Nalianda, KG Kyprianidis, V Sethi, and R Singh. Techno-economic viability assessments of greener propulsion technology under potential environmental regulatory policy scenarios. *Applied Energy*, 157:35–50, 2015.
- [79] Mara Vera-Morales, Will Graham, Cesare Hall, and Andreas Schfer. TOSCA - Technology Opportunities and Strategies towards Climate friendly trAnsport: Techno-Economic Analysis of Aircraft, 2011. FP7-TPT-2008-RTD-1.
- [80] Dimitri N Mavris, George C Mantis, and Michelle R Kirby. Demonstration of a probabilistic technique for the determination of aircraft economic viability. In *1997 World Aviation Congress, World Aviation Conference*, 1997.
- [81] Frederic Burgaud, Christopher P Frank, and Dimitri N Mavris. An aircraft development methodology aligning design and strategy to support key decision making. In *57th AIAA/ASCE/AHS/ASC Structures, Structural Dynamics, and Materials Conference*, number AIAA 2016-1661, 2016.
- [82] Lynnette Dray, Antony Evans, Tom Reynolds, Andreas W Schäfer, María Vera-Morales, and Wolfram Bosbach. Airline fleet replacement funded by a carbon tax: an integrated assessment. *Transport Policy*, 34:75–84, 2014.
- [83] Ryan Tam, Peter Belobaba, Karen R Polenske, and Ian Waitz. Assessment of silent aircraft-enabled regional development and airline economics in the uk. In *45th AIAA Aerospace Sciences Meeting and Exhibit, Aerospace Sciences Meetings, Reno, NV, USA*, number AIAA 2007-455, 2007.

## 11. Bibliography

---

- [84] *Jane's All the world Aircraft*. Jane's Information Group, 2016.
- [85] Japan Airlines. JAL Aircraft collection: Boeing 747-400D. URL <https://www.jal.co.jp/en/aircraft/conf/744d.html>. Accessed: November 2017.
- [86] Alex M Stoll and Gregor Veble Mikic. Design studies of thin-haul commuter aircraft with distributed electric propulsion. In *16th AIAA Aviation Technology, Integration, and Operations Conference*, 2016. AIAA 2016-3765.
- [87] Uber. Uber Elevate: Fast-Forwarding to a Future of On-Demand Urban Air Transportation, 2016. URL <https://www.uber.com/elevate.pdf>. White Paper, Accessed: July 2017.
- [88] J Berton and W Haller. A noise and Emissions Assessment of the N3-X Transport. In *52nd Aerospace Sciences Meeting, National Harbor, MD, USA*, number AIAA 2014-0594, 2014. doi: 10.2514/6.2014-0594.
- [89] James L Felder, Hyun Dae Kim, and Gerald V Brown. An Examination of the Effect of Boundary Layer Ingestion on Turboelectric Distributed Propulsion Systems. In *49th AIAA Aerospace Sciences Meeting, Orlando, FL, USA*, number AIAA 2011-300, 2011. doi: 10.2514/6.2011-300.
- [90] Leroy H. Smith. Wake ingestion propulsion benefit. *Journal of Propulsion and Power*, 9(1):74–82, 1993. ISSN 0748-4658. doi: 10.2514/3.11487.
- [91] Larry W Hardin, Gregory Tillman, Om P Sharma, Jeffrey Berton, and David J Arend. Aircraft System Study of Boundary Layer Ingesting Propulsion. In *48th AIAA/ASME/SAE/ASEE Joint Propulsion Conference and Exhibit, Atlanta, GA, USA*, number AIAA 2012-3993, 2012. doi: 10.2514/6.2012-3993.
- [92] JI Felder and Hyun Dae Kim. Control Volume Analysis of Boundary Layer Ingesting Propulsion Systems With or Without Shock Wave Ahead of the Inlet. In *49th AIAA Aerospace Sciences Meeting, Orlando, FL, USA*, number AIAA 2011-222, 2011. doi: 10.2514/6.2011-222.
- [93] Esteban A Valencia, Devaiah Nalianda, Panagiotis Laskaridis, and Riti Singh. Methodology to assess the performance of an aircraft concept with distributed propulsion and boundary layer ingestion using a parametric approach. *Proceedings of the Institution of Mechanical Engineers, Part G: Journal of Aerospace Engineering*, 229(4):682–693, 2015. doi: 10.1177/0954410014539291.
- [94] Chengyuan Liu, Daniel Ihiabe, Panagiotis Laskaridis, and Riti Singh. A preliminary method to estimate impacts of inlet flow distortion on boundary layer ingesting propulsion system design point performance. *Proceedings of the Institution of Mechanical Engineers, Part G: Journal of Aerospace Engineering*, 228(9):1528–1539, 2014. doi: 10.1177/0954410013496750.
- [95] R. Chue, E. M. Greitzer, C. S. Tan, T. P. Hynes, and J. P. Longley. Calculations of Inlet Distortion Induced Compressor Flow Field Instability. *International Journal of Heat and Fluid Flow*, 10(3):211–223, 1989. doi: 10.1016/0142-727X(89)90040-4.
- [96] Mark Drela. Power balance in aerodynamic flows. *AIAA journal*, 47(7):1761–1771, 2009. doi: 10.2514/1.42409.

## 11. Bibliography

---

- [97] Aurélien Arntz, Olivier Atinault, and Alain Merlen. Exergy-Based Formulation for Aircraft Aeropropulsive Performance Assessment: Theoretical Development. *AIAA Journal*, 53 (6):1627–1639, 2014. doi: 10.2514/1.J053467.
- [98] AGARD. Guide to In-Flight Thrust Measurement of Turbojets and Fan Engines. *AGARD 237*, 1979.
- [99] AP Plas. Performance of a boundary layer ingesting (BLI) propulsion system. Master's thesis, 2006.
- [100] Darrell Williams. Application of boundary layer theory to BLI simulation [Personal Communications], 2015.
- [101] J D Anderson. *Fundamentals of Aerodynamics*. McGraw-Hill Education, 1991. ISBN 0072373350. doi: 10.1371/journal.pcbi.1000716.
- [102] B. S. Stratford and G. S. Beavers. The Calculation of the Compressible Turbulent Boundary Layer in an Arbitrary Pressure Gradient-A Correlation of certain previous Methods. Technical Report ARC-3207, Aeronautical Research Council, 1961.
- [103] Hermann Schlichting. Boundary layer theory. part 2 - turbulent flows. Technical Report NACA-TM-1218, Zentrale fuer Wissenschaftliches Berichtswesen, Berlin, Germany, 1949.
- [104] Herrmann Schlichting and Klaus Gersten. *Boundary-layer theory*. Springer, 2000. ISBN 3540662707.
- [105] Jonathan C Gladin, Brian K Kestner, Jeff S Schutte, and Dimitri N Mavris. Engine Design Strategy for Boundary Layer Ingesting Propulsion Systems With Multiple Non-Symmetric Engine Inlet Conditions. In *ASME Turbo Expo 2013: Turbine Technical Conference and Exposition, San Antonio, TX, USA*, number GT2013-95905, 2013. doi: 10.1115/GT2013-95905.
- [106] Bobby L Berrier and Brian G Allan. Experimental and Computational Evaluation of Flush-Mounted, S-Duct Inlets. In *42nd AIAA Aerospace Sciences Meeting and Exhibit, Reno, NV, USA*, number AIAA 2004-764, 2004. doi: 10.2514/6.2004-764.
- [107] J Seddon. *Boundary-layer interaction effects in intakes with particular reference to those designed for dual subsonic and supersonic performance*. Aeronautical Research Council, 1970.
- [108] Panagiotis Laskaridis. Assessment of distributed propulsion systems used with different aircraft configurations. In *51st AIAA/SAE/ASEE Joint Propulsion Conference*, pages AIAA 2015–4029, 2015.
- [109] Andrew Rolt and John Whurr. Optimizing Propulsive Efficiency in Aircraft with Boundary Layer Ingesting Distributed Propulsion. In *22nd International Symposium on Air Breathing Engines, 25 - 30 October 2015, Phoenix, AZ, USA*, number ISABE-2015-20201, 2015.
- [110] Andrew Turnbull, Hugo Jouan, Panagiotis Giannakakis, and Askin T. Isikveren. Modeling boundary layer ingestion at the conceptual level. In *23rd International Society of Air-breathing Engines (ISABE) Conference, Manchester, UK*, number ISABE-2017-22700, 2017.

## 11. Bibliography

---

- [111] JR Palmer. *The Turbomatch scheme for aero/industrial gas turbine engine design point/off design performance calculation*. Thermal Power Group, Cranfield University, 1990.
- [112] Arne Seitz and Corin Gologan. Parametric design studies for propulsive fuselage aircraft concepts. *CEAS Aeronautical Journal*, 6(1):69–82, 2015. doi: 10.1007/s13272-014-0130-3.
- [113] Hyoungjin Kim and Meng-Sing Liou. Flow Simulation of N3-X Hybrid Wing-Body Configuration. In *51st AIAA Aerospace Sciences Meeting, Grapevine (Dallas/Ft. Worth Region), TX, USA*, number AIAA 2012-221, 2013. doi: 10.2514/6.2013-221.
- [114] Periklis Lolis. *Development of a Preliminary Weight Estimation Method for Advanced Turbofan Engines*. PhD thesis, 2015.
- [115] Lloyd R Jenkinson, Paul Simpkin, and Darren Rhodes. *Civil jet aircraft design*. American Insitute of Aeronautics and Astronautics, 1999.
- [116] Daniel P Raymer. *Aircraft design: A conceptual approach*. American Institute of Aeronautics and Astronautics, 1999.
- [117] Mihaela Niță and Dieter Scholz. Estimating the oswald factor from basic aircraft geometrical parameters. *Desutscher Luft- und Raumfahrtkongress 2012*, 2012.
- [118] Ilan Kroo. *Aircraft design: Synthesis and analysis*. Desktop Aeronautics Inc., 2001.
- [119] Robert Fay, Robert Laprete, and Michael Winter. Blended winglets for improved airplane performance. *Aero*, 17:16–31, 2002.
- [120] Boeing. Blended Winglets for Improved Airplane Performance. *Aero*, pages 16–31, 2002.
- [121] ESDU. Acceleration factors for climb and descent rates at constant EAS, CAS, M, 1992. ESDU 81046.
- [122] Subodh K Mital, John Z Gyekenyesi, Steven M Arnold, Roy M Sullivan, Jane M Manderscheid, and Pappu LN Murthy. Review of current state of the art and key design issues with potential solutions for liquid hydrogen cryogenic storage tank structures for aircraft applications. Technical Report NASA/TM – 2006-214346, The University of Toledo, N&R Engineering, and Glenn Research Center, 2006.
- [123] Jinyang Zheng, Xianxin Liu, Ping Xu, Pengfei Liu, Yongzhi Zhao, and Jian Yang. Development of high pressure gaseous hydrogen storage technologies. *International Journal of Hydrogen Energy*, 37(1):1048–1057, 2012. ISSN 0360-3199. doi: <http://dx.doi.org/10.1016/j.ijhydene.2011.02.125>.
- [124] Robert Paul Jewett, RJ Walter, WT Chandler, and RP Frohberg. Hydrogen environment embrittlement of metals. Technical Report NASA CR-2163, Rocketdyne, 1973.
- [125] G Daniel Brewer. *Hydrogen Aircraft Technology*. CRC press, 1991.
- [126] Paulas Raja Sekaran, Amir S. Gohardani, Georgios Doulgeris, and Riti Singh. Liquid hydrogen tank considerations for turboelectric distributed propulsion. *Aircraft Engineering and Aerospace Technology: An International Journal*, 86(1):67–75, 2013.
- [127] Pierre Mari. Techno-Economic and Environmental Risk Assessment of a Blended Wing Body with Distributed Propulsion – Liquid Hydrogen Variant. Master's thesis, 2015.

## 11. Bibliography

---

- [128] TQ Hua, RK Ahluwalia, J-K Peng, Matt Kromer, Stephen Lasher, Kurtis McKenney, K Law, and J Sinha. Technical assessment of compressed hydrogen storage tank systems for automotive applications. *International Journal of Hydrogen Energy*, 36(4):3037–3049, 2011.
- [129] Boeing Commercial Airplanes. 777-200lr / -300er / -freighter airplane characteristics for airport planning, 2015.
- [130] Lloyd R Jenkinson, Paul Simpkin, and Darren Rhodes. Civil jet aircraft design appendices: Data a : Aircraft data file, boeing aircraft, 2001. URL <https://booksite.elsevier.com/9780340741528/appendices/data-a/table-4/table.htm>.
- [131] Boeing. 777-200lr performance summary, 2009.
- [132] *Jane's Aero Engines 2014-2015*. IHS Jane's Information Group, 2014.
- [133] Mark Moore. OpenVSP Model: NASA N3-X Concept, . URL <http://hangar.openvsp.org/vspfiles/59>. Accessed: September 2017.
- [134] Raffi Babikian, Stephen P Lukachko, and Ian A Waitz. The historical fuel efficiency characteristics of regional aircraft from technological, operational, and cost perspectives. *Journal of Air Transport Management*, 8(6):389–400, 2002.
- [135] Jan Roskam. *Airplane Design Part V: Component Weight Estimation*. Roskam Aviation and Engineering Corporation, 1990.
- [136] Kevin R. Bradley. A sizing methodology for the conceptual design of blended-wing-body transports. Technical report, George Washington University; Joint Institute for the Advancement of Flight Sciences; NASA Langley Research Center, 2004. NASA/CR-2004-213016.
- [137] *777-200LR / -300ER / -Freighter: Airplane Characteristics for Airport Planning*. Boeing Commercial Airplanes, 2015.
- [138] *737: Airplane Characteristics for Airport Planning*. Boeing Commercial Airplanes, 2013.
- [139] IATA. Air Passenger Market Analysis (July 2017), 2017. URL <http://www.iata.org/whatwedo/Documents/economics/passenger-analysis-jul-2017.pdf>. Accessed: September 2017.
- [140] Federal Aviation Administration (FAA). Advisory circular: Aircraft weight and balance control, 2005. URL [https://www.faa.gov/documentLibrary/media/Advisory\\_Circular/AC120-27E.pdf](https://www.faa.gov/documentLibrary/media/Advisory_Circular/AC120-27E.pdf). Accessed: September 2017.
- [141] IATA. Air Freight Market Analysis (July 2017), 2017. URL <http://www.iata.org/whatwedo/Documents/economics/freight-analysis-jul-2017.pdf>. Accessed: September 2017.
- [142] DIA Poll. The optimum aeroplane and beyond. *The Aeronautical Journal*, 113(1141): 151–164, 2009.
- [143] Fredrik Svensson, Anders Hasselrot, and Jana Moldanova. Reduced environmental impact by lowered cruise altitude for liquid hydrogen-fuelled aircraft. *Aerospace Science and Technology*, 8(4):307–320, 2004.

## 11. Bibliography

---

- [144] Marie-Claire Flynn, Catherine Jones, Puran Rakhra, Patrick Norman, and Stuart Gal-  
loway. Impact of key design constraints on fault management strategies for distributed  
electrical propulsion aircraft. In *53rd AIAA/SAE/ASEE Joint Propulsion Conference, At-  
lanta, GA, USA, 2017*. AIAA 2017-5034.
- [145] Mark Moore. NASA N3-X Concept - OpenVSP model, . URL <http://hangar.openvsp.org/vspfiles/59>. Accessed: July 2017.
- [146] Devaiah Nalianda. *Impact of Environmental Taxation Policies on Civil Aviation – A  
Techno-Economic Environmental Risk Assessment*. PhD thesis, Cranfield University,  
2012.
- [147] General Electric. GE9X Commercial Aircraft Engine. URL <https://www.geaviation.com/commercial/engines/ge9x-commercial-aircraft-engine>. Accessed: June 2017.
- [148] FAA Office of Aviation Policy and Plans. *Economic Values for FAA Investment and Reg-  
ulatory Decisions: A Guide*. U.S. Federal Aviation Administration, 2016.
- [149] IATA and KPMG. Airline disclosure guide: Aircraft acquisition cost and depreciation,  
2016. IATA.
- [150] Stephen Lumby. *Investment Appraisal and Financial Decisions*. Chapman & Hall, 1991.
- [151] Aircraft Commerce. Owners & operators guide: 777-200/-300. *Aircraft Commerce*, 60:  
6–30, 2008.
- [152] Bureau of Labor Statistics. Occupational outlook handbook: Transporta-  
tion and material moving occupations, 2016. URL [https://www.bls.gov/ooh/  
transportation-and-material-moving/home.htm](https://www.bls.gov/ooh/transportation-and-material-moving/home.htm). Accessed: June 2017.
- [153] Vicki S Johnson. Optimizing conceptual aircraft designs for minimum life cycle cost.  
Technical Report N89-25211, NASA Langley Research Center, 1989.
- [154] Christopher Rush and Rajkumar Roy. Expert judgement in cost estimating: Modelling  
the reasoning process. *Concurrent Engineering*, 9(4):271–284, 2001.
- [155] Christopher Rush and Rajkumar Roy. Analysis of cost estimating processes used within  
a concurrent engineering environment throughout a product life cycle. In *7th ISPE In-  
ternational Conference on Concurrent Engineering: Research and Applications, Lyon,  
France, July 17th-20th, Technomic Inc., Pennsylvania USA, 2000*.
- [156] M Rais-Rohani and EB Dean. Toward manufacturing and cost considerations in multi-  
disciplinary aircraft design. In *37th Structure, Structural Dynamics and Materials Confer-  
ence*, number AIAA 96-1620, 1996.
- [157] G. S. Levenson, H. E. Boren, D. P. Tihansky, and F. Timson. Cost-estimating relationships  
for aircraft airframes. Technical Report R-761-PR, 1972.
- [158] Jan Roskam. *Airplane Design Part VIII: Airplane Cost Estimation*. Roskam Aviation and  
Engineering Corporation, 1990.
- [159] Ihs jane’s all the world’s aircraft: Development & production, 2014.
- [160] Cost estimating handbook. Technical report, NASA, 2015.

## 11. Bibliography

---

- [161] HE Boren Jr. Dapca: A computer program for determining aircraft development and production costs. Technical Report RM-5221-PR, RAND Corporation, 1967.
- [162] Ronald Wayne Hess and HP Romanoff. Aircraft airframe cost estimating relationships. study approach and conclusions. Technical Report R-3255-AF, RAND Corporation, 1987.
- [163] Joseph P Large, Harry G Campbell, and David Cates. Parametric equations for estimating aircraft airframe costs. Technical Report R-1693-1-PA&E, RAND Corporation, 1976.
- [164] Michael N Beltramo, Donald L Trapp, Bruce W Kimoto, and Daniel P Marsh. Parametric study of transport aircraft systems cost and weight. Technical report, Science Applications, Inc and Douglas Aircraft Company, 1977.
- [165] Richard Curran, Mark Price, S Raghunathan, E Benard, S Crosby, S Castagne, and P Mawhinney. Integrating aircraft cost modeling into conceptual design. *Concurrent Engineering*, 13(4):321–330, 2005.
- [166] PG Pugh. Working top-down: cost estimating before development begins. *Proceedings of the Institution of Mechanical Engineers, Part G: Journal of Aerospace Engineering*, 206(2):143–151, 1992.
- [167] Obaid Younossi, Mark V Arena, Richard M Moore, Mark Lorell, and Joanna Mason. Military jet engine acquisition: Technology basics and cost-estimating methodology. Technical report, RAND Corporation, 2002.
- [168] LT Finizie. A comparison of navy and contractor gas turbine acquisition cost. In *ASME 1983 International Gas Turbine Conference and Exhibit*, 1983.
- [169] Donald J LeBlanc. *Advanced composite cost estimating manual*. Northrop Corporation, Aircraft Division, 1976.
- [170] Timothy Gutowski, David Hault, Greg Dillon, Ein-Teck Neoh, Stuart Muter, Eric Kim, and Mawuli Tse. Development of a theoretical cost model for advanced composite fabrication. *Composites Manufacturing*, 5(4):231–239, 1994.
- [171] Sylvie Castagne, Richard Curran, Alan Rothwell, Marc Price, Emmanuel Benard, and Srinivasan Raghunathan. A generic tool for cost estimating in aircraft design. *Research in Engineering Design*, 18(4):149–162, 2008.
- [172] Jim Scanlan, Terry Hill, Rob Marsh, Christophe Bru, Martin Dunkley, and Paul Cleevely. Cost modelling for aircraft design optimization. *Journal of Engineering Design*, 13(3): 261–269, 2002.
- [173] Susan A Resetar, James Curt Rogers, and Ronald W Hess. Advanced airframe structural materials: A primer and cost estimating methodology. Technical Report R-4016-AF, RAND Corporation, 1991.
- [174] Obaid Younossi, Michael Kennedy, and John C Graser. Military airframe costs. the effects of advanced materials and manufacturing processes. Technical Report R-4016-AF, RAND Corporation, 2001.
- [175] John L Birkler, Jeffrey Bruce Garfinkle, and Kenneth E Marks. *Development and production cost estimating relationships for aircraft turbine engines*. RAND Corporation, 1982.



## 11. Bibliography

---

- [176] Siemens. Simotics low-voltage motors, 2015. URL <https://www.industry.usa.siemens.com/drives/us/en/electric-motor/nema-motors/Literature-and-technical-resources/Documents/Pricelist-D81.1-P-March-2015%20Update.pdf>. Accessed: January 2016.
- [177] GE. Extra severe duty motors, 2015. URL <https://www.gepowerconversion.com/sites/gepc/files/product/X%D%20Ultra%20841%20Brochure.pdf>. Accessed: January 2016.
- [178] Boeing. About Boeing Commercial Airplanes, . URL <http://www.boeing.com/company/about-bca/#/prices>. Accessed: May 2017.
- [179] Brian Smith. The boeing 777. *Advanced Materials and Processes*, September:41–44, 2003.
- [180] Boeing. B777 Orders and Deliveries, . URL <http://active.boeing.com/commercial/orders/displaystandardreport.cfm?cboCurrentModel=777&optReportType=AllModels&cboAllModel=777&ViewReportF=View+Report>. Accessed: May 2017.
- [181] Devesh Agarwal. The worlds largest aircraft engine, the ge90-115b, 2015. URL <http://www.bangaloreaviation.com/2009/10/worlds-largest-aircraft-engine-ge90.html>. Accessed: January 2016.
- [182] Shannon Ackert. Engine maintenance concepts for financiers, 2010.
- [183] G Philip Sallee. Economic effects of propulsion system technology on existing and future transport aircraft. Technical Report NASA CR-134645, American Airlines, 1974.
- [184] Hariharan Hanumanthan. *Severity estimation and shop visit prediction of civil aircraft engines*. PhD thesis, Cranfield University, 2009.
- [185] National Research Council. *New materials for next-generation commercial transports*. National Academies Press, 1996.
- [186] Myoungcheol Kang, Stephen Ogaji, Pericles Pilidis, and Changduk Kong. An approach to maintenance cost estimation for aircraft engines. In *ASME Turbo Expo 2008: Power for Land, Sea, and Air*, number GT2008-50564. American Society of Mechanical Engineers, 2008.
- [187] Driss Rchid, Otmane Bouksour, and Zitouni Beidouri. The activity based costing method opportunity to assess and master the aircraft maintenance service cost for third party: a case study. *IJCSI International Journal of Computer Science Issues*, 10(1):609–706, 2013.
- [188] ATA. Standard method of estimating comparative direct operating costs of turbine powered aircraft. Technical report, 1967.
- [189] Raj Raman, John C Graser, and Obaid Younossi. *The effects of advanced materials on airframe operating and support costs*. RAND Corporation, 2003.
- [190] Justin Hale. Boeing 787 from the ground up. *Aero*, 24(4):17–23, 2006.
- [191] Ralf Seemann, Stephan Langhans, Thomas Schilling, and Volker Gollnick. Modeling the life cycle cost of jet engine maintenance. In *Deutscher Luft- und Raumfahrtkongress - DLRK2011*, 2011.

- [192] Aircraft Commerce. Ge90 family maintenance costs. *Aircraft Commerce*, 84:11–18, 2012.
- [193] Aircraft Commerce. Owners & operators guide: 777-200/-300. *Aircraft Commerce*, 60: 6–30, 2008.
- [194] US Department of Energy - Fuel Cell Technologies Office. Multi-year research, development, and demonstration plan – hydrogen production. Accessed: March 2017.
- [195] Patrick Luckow, Elizabeth A. Stanton, Spencer Fields, Bruce Biewald, Sarah Jackson, Jeremy Fisher, and Rachel Wilson. 2015 carbon dioxide price forecast. Technical report, 2015. Synapse Energy Economics, Inc.
- [196] Oliver Clark Flight Global. Lessors unlikely to manage 50% of fleet within 10 years: Ascend, 2016. URL <https://www.flightglobal.com/news/articles/lessors-unlikely-to-manage-50-of-fleet-within-10-ye-425069/>. Accessed: July 2017.
- [197] Francesco De Bosio. Techno-Economic and Environmental Risk Assessment of a Blended Wing Body with Distributed Propulsion – Leasing Model. Master's thesis, 2017.
- [198] NASA. X-48 research: All good things must come to an end, 2013. URL [https://www.nasa.gov/topics/aeronautics/features/X-48\\_research\\_ends.html](https://www.nasa.gov/topics/aeronautics/features/X-48_research_ends.html). Accessed: July 2017.
- [199] William T Cousins, Dmytro Voytovych, Gregory Tillman, and Eric Gray. Design of a distortion-tolerant fan for a boundary-layer ingesting embedded engine application. In *53rd AIAA/SAE/ASEE Joint Propulsion Conference, Atlanta, GA, USA*, 2017. AIAA 2017-5042.
- [200] David J Arend, John D Wolter, Stefanie M Hirt, Andrew J Provenza, John A Gazzaniga, William T Cousins, Larry W Hardin, and Om P Sharma. Experimental evaluation of an embedded boundary layer ingesting propulsor for highly efficient subsonic cruise aircraft. In *AIAA Propulsion and Energy Forum, Atlanta, Georgia*, 2017.
- [201] C Justin, S Briceno, and D Mavris. A competitive and real-options framework for the economic analysis of large aerospace programs. In *28th International Congress of the Aeronautical Sciences, Brisbane, Australia*, 2012.
- [202] Alberto Buonvino. Boundary Layer Flow Field Analysis for a BWB aircraft. Master's thesis, 2017.
- [203] ESDU. Specific heat capacities and their ratio as functions of temperature for several common gases, 1982. ESDU 00.01.08.
- [204] Deagel. Deagel Engine Database, 2017. URL <http://www.deagel.com/Propulsion-Systems.htm>. Accessed: January 2017.

# A. Related Research

The following chapter will summarise contributions from related research that has been conducted during Masters degree research at Cranfield University in connection with the main NASA grant research. The projects covered a combination of techno-economics and performance related subjects to explore additional aspects of the main grant focus or develop models for use in the main body of the research.

## A.1 Liquid Hydrogen Tank Sizing

A segment of the research conducted on the N3-X considered the use of liquid hydrogen as an alternative fuel for the aircraft. As a cryogenic liquid, LH<sub>2</sub> requires specialised tanks to maintain the fuel at the appropriate temperature and pressure. A tool was therefore required to predict the weight of the LH<sub>2</sub> tanks. In addition, it was necessary to determine the volume available within the aircraft for the fuel tanks, as the configuration of a pressure vessel for a cryogenic fuel implies space and volume limitations that are not applicable for a wing-based kerosene tank. Research by Mari in 2015 worked on the development of a method for sizing tanks for a liquid hydrogen aircraft with simulations of the resultant aircraft performance [127]. The LH<sub>2</sub> tank sizing derived from previous research for the sizing of LH<sub>2</sub> tanks ([66, 126]). The research compared a selection of tank materials to identify low weight combinations of material type for the tank wall, insulation, and liner. The research was also used to predict an internal configuration for the aircraft in order to identify the available volume for the fuel tanks (Figure A.1a). This included estimating the cabin volume required for the full complement of 301 passengers in a 3-class layout (Figure A.1b). In addition, the volume available for cargo (standard LD3 containers) was estimated to be 170m<sup>2</sup>, comparable to the 160m<sup>2</sup> capacity of the B777-200LR baseline. This cargo hold was assumed to lie behind the fuel tank hold. Cargo volume was also identified to either side of the passenger cabin, providing an additional 62m<sup>2</sup> of cargo capacity if required. An area suitable for embedded turbogenerators with a diameter of up to 1.5m was also included. The resultant sizing estimate produced a fuel tank hold with a 19m length and 10m width. The maximum height of the fuel tank hold was identified to be 3m. The research made use of a three tank layout with a capacity for 12904 kg of fuel.

The modelling procedure developed in the thesis was implemented in Section 4.2 to develop a sizing process for the tanks and explore the factors with an influence over tank weight. The internal configuration estimates were used in the main body of research to determine the maximum feasible dimensions of the LH<sub>2</sub> tanks, given the size of the N3-X. However, the maximum tank diameter was reduced to 2.5m as an assumption for the space required for the airframe and tank support structure. The fuel hold length was increased from 19m to 20m to compensate for the loss in diameter.

**Pierre Mari (2015) Abstract: [127]** *As times progresses, the air traffic continue to growth, resulting in more emission. Therefore, NASA has created future environmental targets to meet, which they want to meet by working on a revolutionary aircraft, the N3-X Blended Wing Body. However, the assessments of the new technologies from a performance point of view need to be translated into economic benefits. This thesis uses a techno-economic risk assessment (TERA) framework that mixes the flight and economic performance of the NASA N3-X aircraft to assess if the concept is economically viable. A preliminary arrangement of the inside structure of the*

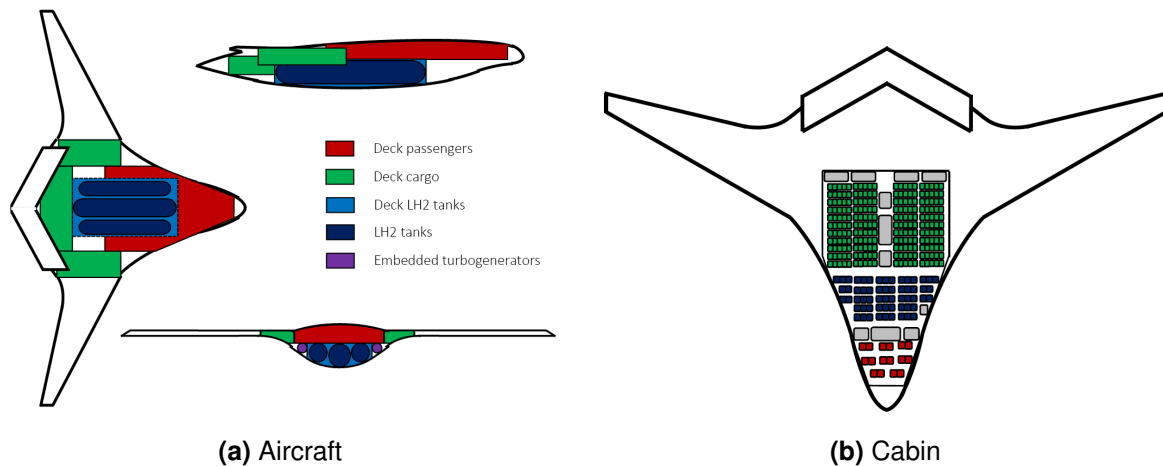


**Figure A.1:** Example internal configuration layout for the N3-X [127]

*aircraft including passenger seats, cargo and LH<sub>2</sub> tanks location is proposed, and the weight of the LH<sub>2</sub> tanks is included in the flight performance and economic study. The thesis finds that the N3-X offers at least 70% fuel savings compared to the Boeing 777-200LR baseline and meaningful operating cost savings. Moreover, it appears that an aircraft fuelled with kerosene can propose further operating cost savings over aircraft fuelled with kerosene if the industry could sell the hydrogen as \$1.00 per pound of fuel.*

## A.2 Leasing Model

It is common for aircraft to be leased rather than purchased outright. This change in ownership model changes the direct operating cost structure for the aircraft, and may therefore change the conclusions of a techno-economic analysis. Research by de Bosio in 2017 worked on the development of a leasing cost model for use within the techno-economic framework [197]. The research compared a number of different ownership models: the direct ownership model used in the main body of research, and a leasing model. The leasing model replaces the time cost group with terms related to lease costs for an aircraft (Figure A.2):

- Initial investment
- Insurance
- Direct maintenance costs
- Periodic payments to the lessor
  - Periodic rental fees (dependent on aircraft value and depreciation)
  - Maintenance reserves

In the leasing model, maintenance costs are split into direct maintenance costs and maintenance reserve costs. Maintenance is split into these two aspects as the lessor remains the owner of the aircraft and will therefore aim to take of the asset to ensure it remains in good condition until the end of the lease agreement. The maintenance reserve costs are therefore used to determine the lease payments required from a lessee. The lessor is also responsible for major maintenance checks and overhauls, which will contribute towards the lease payments. The remaining maintenance is the responsibility of the lessee and is covered by the direct maintenance costs. The lease is also assumed to include a security deposit at the start of the lease term equal to three months of lease payments which is returned at the end of the lease agreement, assuming the terms of the lease agreement have been respected.

Rental fees were assumed to be fixed monthly payments, with an additional charge if the operator were to operate outside what was agreed in the contract. The primary purpose of the

## A. Related Research

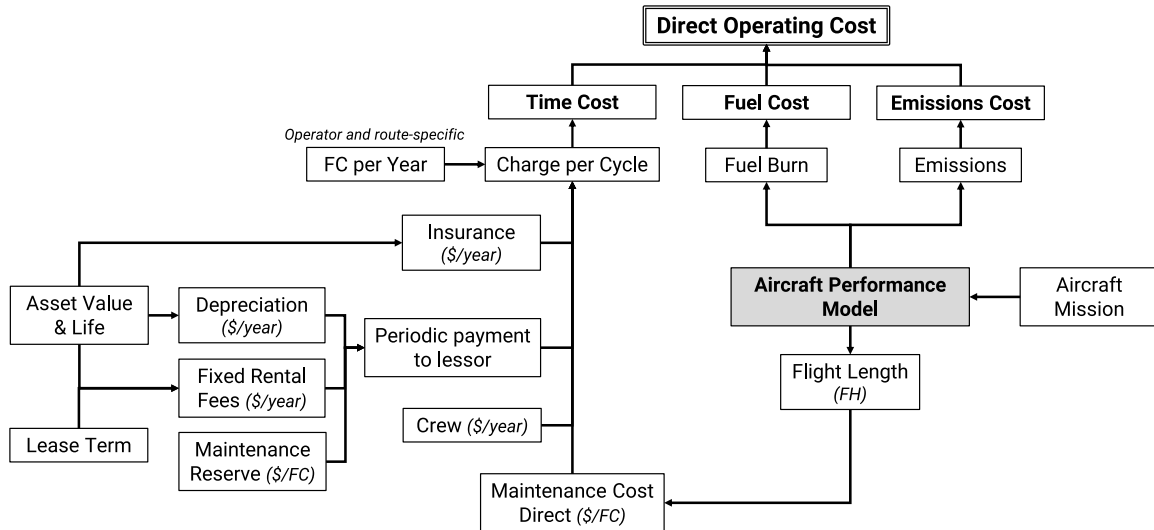


**Figure A.2:** Breakdown of direct operating cost model components for the leasing model [197]

periodic rental fees was assumed to be to cover the loss in asset value due to depreciation. The monthly rental fees are therefore a function of the aircraft value and economic life. The research assumes that the lease requires rentals to be paid one month in advance. The periodic rental fee per month,  $C_{\text{rental/month}}$ , is calculated as follows:

$$C_{\text{rental/month}} = \frac{X}{r_l} \quad (\text{A.1})$$

$$r_l = \frac{1 - (1 + r_i)^{x-n}}{i} + x \quad (\text{A.2})$$

Where  $X$  is the aircraft's initial value,  $r_i$  is the interest rate,  $x$  is the number of rentals payable in advance, and  $n$  is the number of payments in the lease term. This must be added to the maintenance reserve cost contribution to estimate the total monthly lease payment.

Two options were considered for the leasing model. In the first, the operator leases the aircraft for a fixed period and the aircraft then returns to the lessor. In the second, the operator is given the option to purchase the aircraft at the end of the lease period. The purchase price is dependent on the aircraft value at the end of the lease period, i.e. accounting for the depreciated value of the aircraft. In the purchase-after-lease model, the operator pays a fixed sum when the aircraft is purchased. This sum is assumed to come from a combination of the profits earned by the aircraft over the course of the lease period and a loan to cover the remaining cost. The direct operating cost then swaps to an ownership model, however, ownership costs are lower as the investment cost is less than the acquisition price for a new aircraft. After a certain period of time, a loan is no longer required to purchase the aircraft as the purchase cost can be fully covered by the profits made during the course of operation. This will then significantly reduce operating costs of a purchased aircraft, as interest repayments on a loan are no longer necessary. This option was considered as it gives an operator a chance to continue operating an aircraft at the end of the lease period. The operator then has the benefit of gaining ownership of an aircraft asset, rather than a lease-only option where the operator does not retain any assets. The model also includes the benefits of a tax shield for the operator, whereby taxable income is reduced by claiming deductions on cost factors such as interest and depreciation. In a purchase option, a tax shield can be gained on loan payments to repay the debt from the purchase of the aircraft asset. In a lease option, there is less benefit from a

## A. Related Research

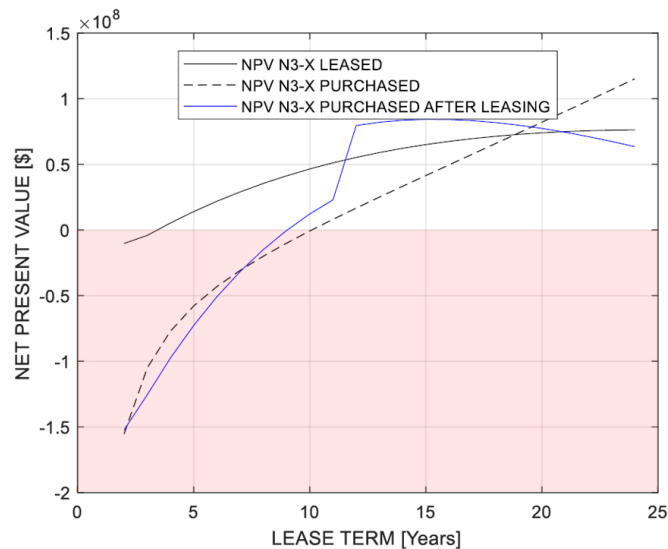


**Figure A.3:** Net present value comparison of N3-X leasing and purchase options as a function of operating period for the design mission range (highest NPV is best) [197]

tax shield as there is no large investment funded by debt.

The research identified that the profits versus the baseline B777-200LR are different for a lease versus operating a directly purchased aircraft. The most attractive option is dependent on the operating period for the aircraft. For the N3-X, an operating period of less than 18 years would favour an aircraft lease, as this would provide a better NPV than ownership. A longer operating period would favour direct purchase of the aircraft. The purchase-after-lease option was found to be most attractive for a lease period between 12–19 years. Either leasing option proves financial attractive over a reasonably long operating period, as the initial investment is significantly lower (Figure A.3). In the long term, the higher payments of a lease contract will outweigh the benefits of the lower initial investment. Therefore, leasing is best for an operating period up to 12 years, then from 12–19 years a purchase-after-lease option is best. Finally, purchase is best if the aircraft is to be operated for a period of 19 or more years. However, the net present value is negative for very short operating periods of less than three years, even for the leasing option, as there is not adequate time to recoup investment costs. As with an ownership model, profitability is low for short range missions. Viability of the aircraft is therefore better if the aircraft is offered primarily for long haul missions, regardless of the ownership model (Figure A.4). However, leasing is slightly better for the short-haul applications than the purchase option, as leasing reduces the impact of a high initial investment cost.

**Francesco de Bosio (2017) Abstract: [197]** *The aircraft industry is becoming significantly aware of environmental concerns and it is developing new increasingly sustainable technologies. For this reason, NASA has been developing the Blended Wing Body project, named N3-X, with distributed propulsion that has been demonstrated to be a revolutionary technology in order to achieve targets such as lower fuel consumption, noise and emissions reduction.*

*In this regard, in the present work, the fuel saving of the N3-X is going to be quantified in comparison to the baseline aircraft Boeing 777-200LR. Moreover, a comparative study between the proposed technology and the baseline is going to be presented, considering two different acquisition methods: purchase and lease. Afterwards, an analysis of sensitivity of the N3-Xs direct operating cost is going to be assessed in order to complete a techno-economic framework of the NASA's proposal.*

*The project is going to be presented in four different sections. Firstly, a comparison between*

## A. Related Research

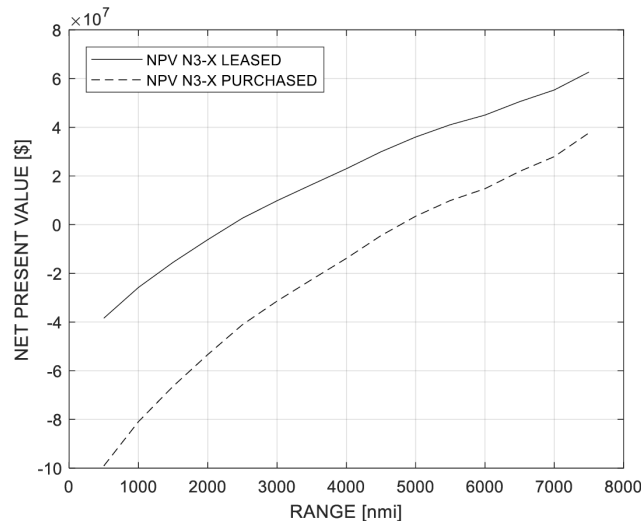


**Figure A.4:** Net present value comparison of N3-X leasing and purchase options as a function of range (19 year operating period) (highest NPV is best) [197]

*the Blended Wing Body N3-X aircraft and the B777-200LR is going to be carried out in order to define the different outcomes in terms of performance due to the technological development. Secondly, the direct operating cost of the two aircraft is going to be determined considering it both under operating lease and under ownership. Moreover, considering the former financial alternative, a reduction about 20% in N3-X's DOC, when compared to the baseline's DOC, is going to be demonstrated. Thirdly, this work shall discuss which acquisition method would be more attractive, from the operators perspective, depending on mission range and lease term or operating period. Finally, the sensitivity of the direct operating cost of the N3-X under operating lease agreement is going to be evaluated in order to assess the profitability of the project and hence the feasibility from an economic perspective. In particular, this work is going to demonstrate that the maximum increase in DOC is 25% whilst maintaining a sufficient margin of profitability.*

### A.3 CFD Analysis of the N3-X Airframe

The main body of research presented herein focuses on the development and application of a BLI simulation method suitable for the conceptualisation and preliminary design phase of research. The stated aim of the developed models was therefore to provide a rapid analysis method with limited reliance on CFD data. Numerous assumptions were therefore required to enable a simulation the propulsion system without performing a time consuming CFD analysis for every iteration of the design space exploration. It is nevertheless useful to identify where there may be inaccuracies in the assumptions made in modelling the propulsion system.

A set of CFD analyses were created by Buonvino [202] for the N3-X to visualise the flow field around the aircraft and in particular in the vicinity of the propulsion system. The research identified that the actual interface point can differ significantly from the assumptions used in this research, depending on flight condition and location. The study suggested that, for a propulsor at 85% of the airframe centreline, the propulsion system influence can extend as far upstream as to 60% of the chord, with a significant flow influence from 70% of the chord. The analysis also reinforced conclusions made in previous research that the array nacelle around the airframe centreline may be prone to developing shocks during flight [113] (Figure A.5). Nacelle design would therefore need to be tailored to reduce the likelihood of flow separation

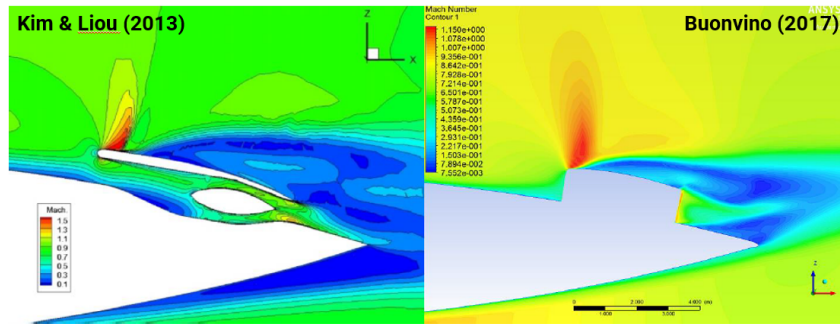


**Figure A.5:** Mach contours over the N3-X nacelle [202] with comparison to previous research by Kim & Liou [113]

and shocks. The research also produced estimates of the trend for the boundary layer and local velocity along the length of the propulsor array. However, as a highly detailed mesh was not used for the airframe, the results were used to portray trends rather than exact values. The boundary layer thickness and local velocity was found to vary noticeably along the length of the array, due to the pressure distribution over the airframe and swept nature of the leading edge. The velocity distribution and boundary layer profiles were also found to vary significantly as a function of flight condition.

The results gained from the analysis by Buonvino were used in Section A.3.1 to assess the following points:

- Actual interface point location and variation from assumptions as a function of location and flight conditions
- Boundary layer thickness as a function of location and flight conditions
- Local flow velocity as a function of location and flight conditions
- Fuselage Mach number profile of the N3-X airframe versus the N2A
- Possible separation during descent

**Alberto Buonvino (2017) Abstract: [202]** *The continuous increase of the amount of the everyday flights has as a consequence a vertiginous growth of the polluting emissions in the world. This urgent phenomenon together with the need of the aviation companies of reducing the fuel expenses is leading to the design of completely new concept airplanes and engine systems.*

*The matter of this work involves the use of Computational Fluid Dynamics (CFD) to study the flow evolution around one of these new concept airplane, the NASA N3-X concept. The contribution to knowledge is of investigating the flow field around the airfoil of this new generation airplane for 8 flight points to validate the preliminary intake design made by Cranfield University with an unidimensional gas dynamic model. This study is preparatory to allow Cranfield University to have the knowledge of the thermodynamics in the proximity of the engines inlet to carry out an optimization study of the nacelles intake aerodynamics.*

### A.3.1 Boundary Layer and Velocity Profile Assumptions

The focus of the BLI method developed in the main body of research is to provide a model that can be used during the preliminary design process with little to no reliance on CFD simulations to provide airframe flow data. The data necessary for the model can be provided by



initial assumptions that may be refined as the design develops. In the analyses presented in this research, limited CFD data was used to provide Mach numbers and the local boundary layer thickness at the centreline of the airframe during cruise. This data was then extended to cover the entire rear of the fuselage by applying the assumptions described in the previous sections. This data was also extended to other flight conditions by again applying a number of assumptions. The model therefore relies only on an initial input of relatively basic CFD data. Reliance on CFD can be removed by instead using analytical methods and approximations to estimate the airframe boundary layer in the relevant locations. Airframe streamline solvers such as the method presented by Turnbull *et al.* are another alternative [110]. Model fidelity can also be increased by introducing more CFD data to replace the assumptions made for the fuselage boundary layer over the full mission. Given the stated aims of the model, adding high fidelity CFD data is less useful, as it is intended for the preliminary design phase rather than high accuracy modelling. Nevertheless, it is useful to assess how the assumptions that were made may differ from reality, and hence identify the possible error.

There are number of key results that are useful to compare to CFD data:

- Actual interface point location and variation from assumptions as a function of location and flight conditions
- Boundary layer thickness as a function of location and flight conditions
- Local flow velocity as a function of location and flight conditions
- Fuselage Mach number profile of the N3-X airframe versus the N2A
- Possible separation during descent

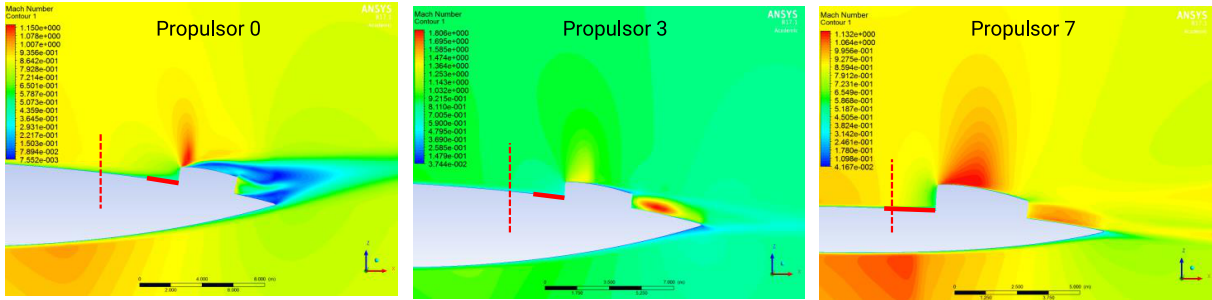
The CFD analyses created by Buonvino can be used to compare the assumptions applied for the BLI model against results from the CFD analysis [202]. The aircraft model was created based on publicly available configuration data as used in the main body of research [145]. The size and location of the propulsor array was based on the baseline configuration created in Section 3.5. Data was then extracted for a number of sections along the length of the array. Previous research has identified that the flow over the N3-X nacelle is prone to shocks and separation at the centre of the array [113]. This was reflected in the analyses created for this research, however, the discussion will focus on flow conditions ahead of the intake, rather than flow over the nacelle and rear of the aircraft as this lies outside the scope of the research.

The region where the propulsion system begins to influence the airframe flow is difficult to identify. However, the CFD data suggests that the propulsion system interface point is further ahead of the intake than assumed (Figure A.6). For cruise conditions and the centreline propulsor, velocity is influenced approximately six highlight heights ahead of the intake. However, boundary layer thickness only begins to change significantly at around the original assumed interface point of two highlight heights ahead of the intake. The location of the interface point changes depending on flight conditions and propulsor location. During descent, velocity begins to change closer to seven highlight heights away from the intake. As with cruise, boundary layer thickness begins to change close to the assumed interface point. The interface point is closer to the assumed region for the outer propulsor. The outcome suggests that a variable control volume size may be necessary for the different flight conditions. The main difference resulting from this assumption will be the portion of fuselage drag that must be included in the propulsion system control volume (Equation 3.3).

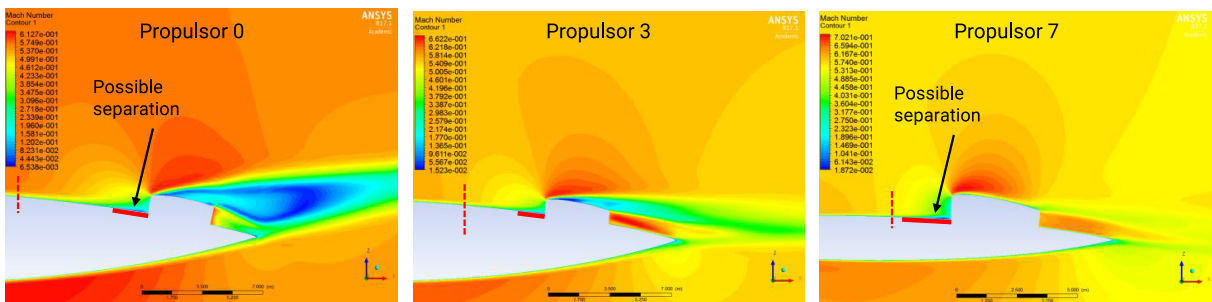
The CFD analysis also suggest that separation may occur during descent (visible on the inner and outer propulsors). However, the flow subsequently reattaches before entering the intake, and the separation bubble is small relatively to the streamtube height.

# A. Related Research

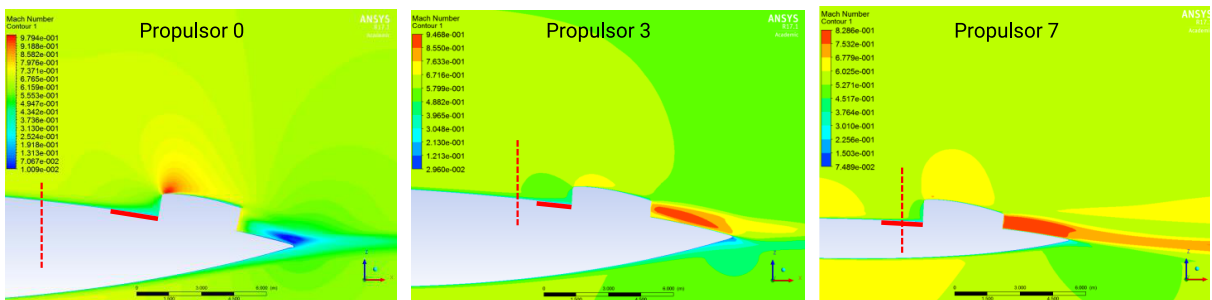
## Cruise 40,000 ft



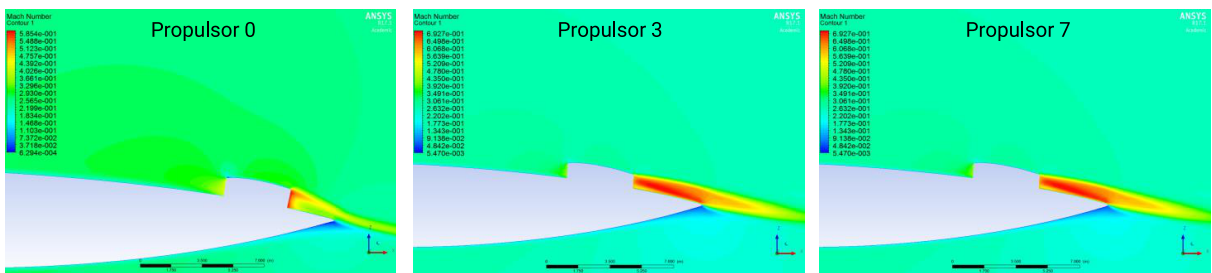
## Descent 10,000 ft



## Climb 10,000 ft



## RTO Sea level, Mach 0.25



**KEY:**  
 2x highlight height distance ————  
 Approximate start of propulsion system influence on airframe - - - - -

**Figure A.6:** CFD for different flight conditions and propulsors with approximate interface point

## A. Related Research

---

The mesh resolution used for the analysis was not high enough to accurately predict boundary layer thickness along the length of the propulsor array at each flight condition. The data could therefore not be used to check the accuracy of the boundary layer thickness assumptions. However, a comparison of the CFD data to model assumptions for the inner (propulsor 0) and outer (propulsor 7) propulsors was made to compare flow assumptions along the array length (Figure A.9). The comparison shows that the assumed boundary layer profile lies reasonably close to that obtained from the CFD analysis. There is a greater difference between the results obtained from the outer propulsor in comparison to the model. This is to be expected, as the assumptions made for the flow profile will break down the further the data extrapolation is taken, as only the velocity profile at the airframe centreline is known. It is worth highlighting that the difference between the assumed and actual interface point will also lead to discrepancies between the calculated and actual boundary layer thickness at the interface point.

The data was also used to compare Mach numbers across the fuselage. One of the main assumptions in the research is that the Mach number profile from simulations of the N2A can be used for the N3-X. A comparison of the N2A data versus the N3-X data shows a superficially similar Mach number profile across the airframe (Figure A.7), as would be expected for similar configurations. However, the local Mach number in the region of the propulsor array appears to increase more rapidly for the N3-X airframe than the N2A configuration. The array therefore approaches flow that is faster than the flight velocity sooner than is assumed for this research.

Data was extracted for the local velocity at the interface point for each propulsor in the array at a number of flight conditions (Figure A.8). The difference in configuration and the different assumptions lead to a higher local Mach number during cruise for the outer propulsors, although the local Mach number is correct for the centreline propulsor. In contrast, local Mach number during climb is lower than the flight Mach number for all but the outermost propulsor. The outcome is similar for the descent phase. Finally, the rolling take-off condition shows that the local Mach number is consistently higher than estimated. This is a result of the suction of the propulsion system, which accelerates flow over the airframe well ahead of the defined interface point (Figure A.6). Although the absolute Mach number values are different for each flight condition, the overall trend is similar, with a dip in local Mach number occurring around Propulsor 5. This suggests that it is not entirely unreasonable to apply the same general profile to local Mach number trends once data is appropriately scaled for the given flight condition.

The actual numerical value of the local Mach number used in the analyses of this report differs from that observed in this research. However, the conclusions made regarding location and local velocity still hold. A high local Mach number will increase momentum drag and outer propulsors will still be less efficient than the innermost propulsors, favouring a shorter array. However, the comparisons shown in this section do highlight the necessity to introduce higher fidelity data as the aircraft and propulsion system design process progresses.

## A. Related Research

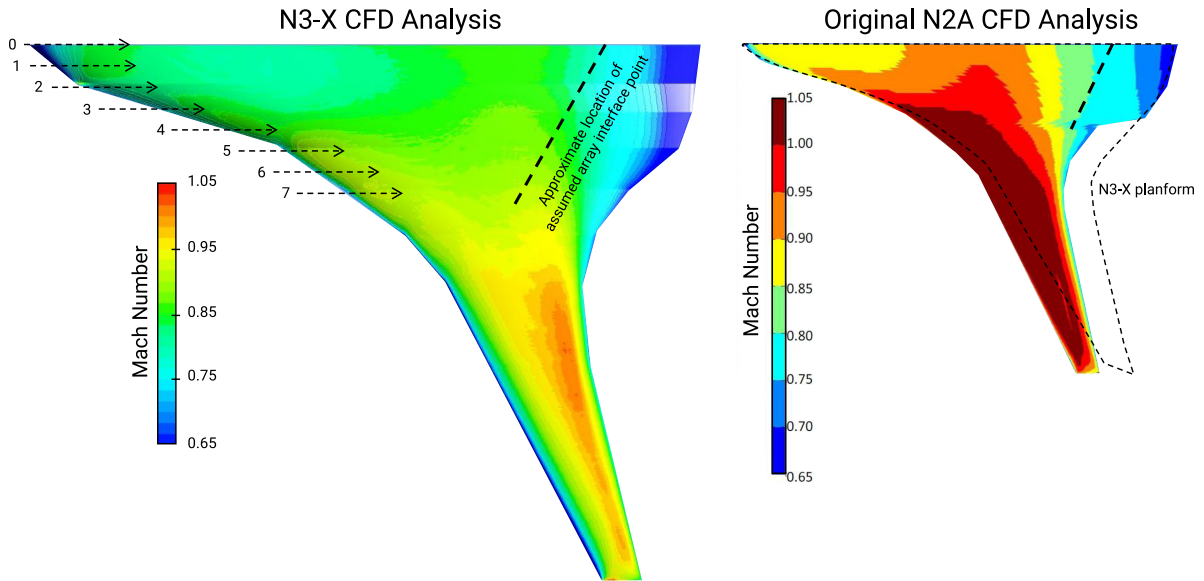


**Figure A.7:** Comparison of CFD data displaying the Mach number over the N3-X fuselage versus N2A fuselage data (Flight Mach number 0.84)

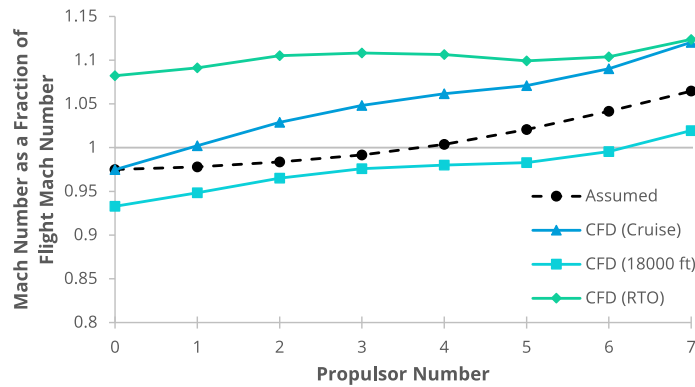


**Figure A.8:** Mach number as a fraction of free-stream Mach number for each propulsor in the array

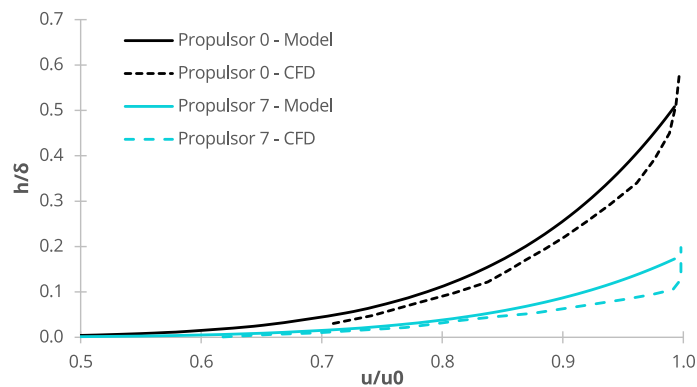
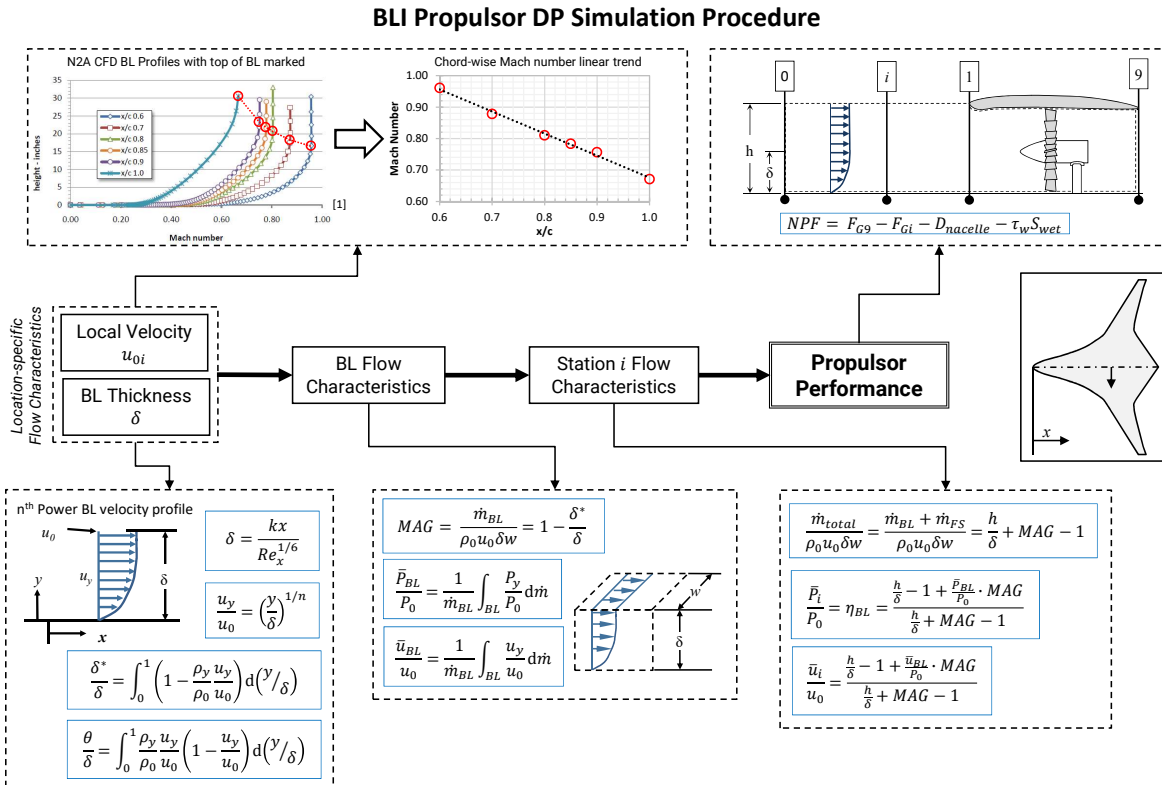


**Figure A.9:** Boundary layer profile comparison to data extracted from CFD analysis

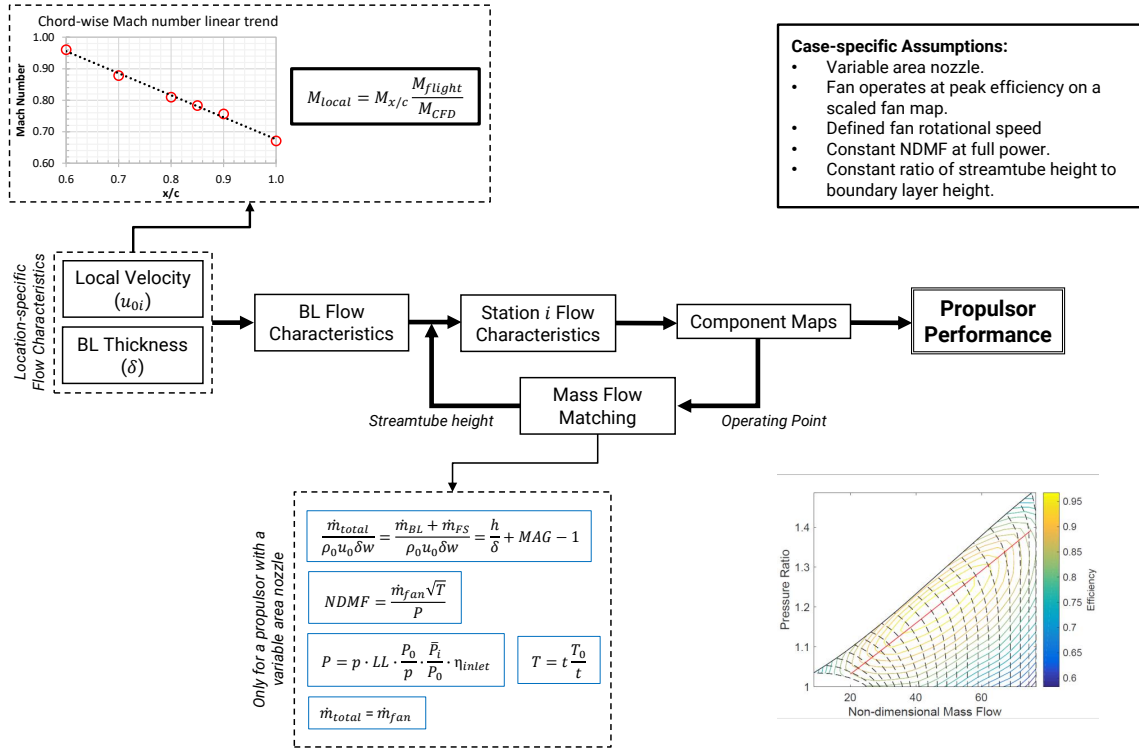
# B. BLI Simulation Method

The following flowcharts demonstrate the methodology used to simulate a BLI propulsion system. The flowcharts include comments specific to the N3-X configuration, however, the general flowchart demonstrates the generic method for simulating BLI propulsion systems at design point and off-design.



[1] Felder, J. L., Brown, G. V., Kim, H. D., & Chu, J. (2011). Turboelectric distributed propulsion in a hybrid wing body aircraft.

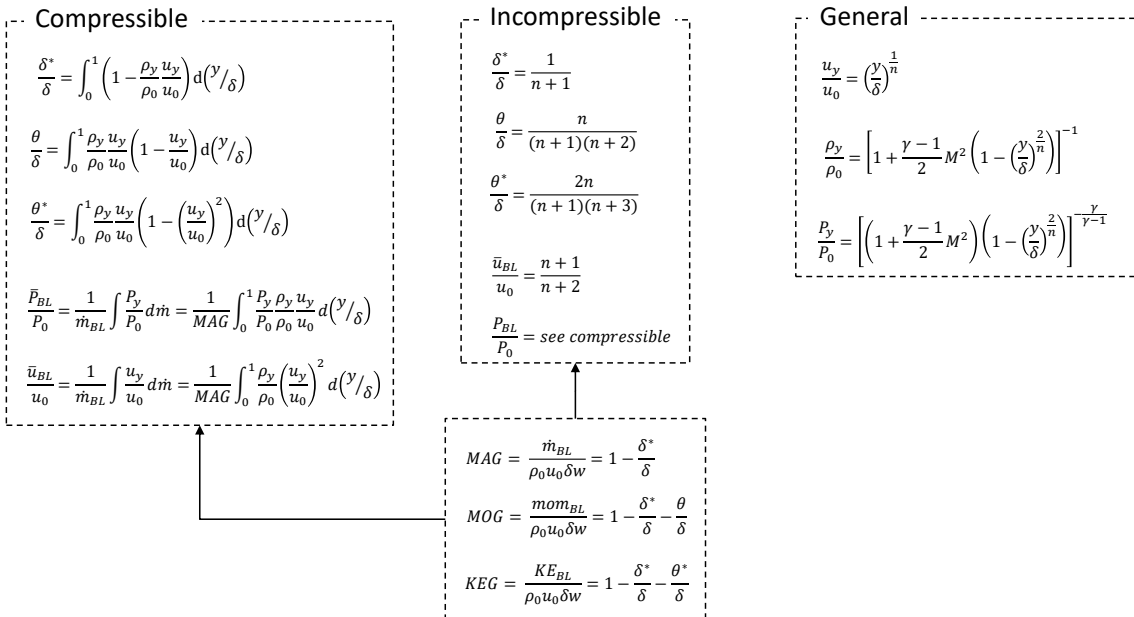
BLI Propulsor OD Simulation Procedure



2

BL Integral

Assuming a power law velocity profile is used



3

## C. Flow Profile over the N3-X

The following appendix provides an overview of the relationships used to approximate the flow over the centreline of the N3-X airframe. The flow profile is extracted from previous research on the N3-X [56]. The research provides boundary layer profiles over the centreline of the N3-X airframe at a number of locations along the rear portion of the fuselage from 60% chord to 100% chord (Figure C.1). This data was used to extract the boundary layer thickness and local Mach number over the airframe (Figure C.2). As the velocity of the boundary layer is asymptotic to the free-stream velocity, the boundary layer thickness is defined as the point above the surface where local velocity is 99% of its free-stream value [104]. The resultant data is expected to have certain percentage error given the accuracy of extracting data from a plotted trend.

The following relationship was produced to predict the local Mach number as a function of  $x/c$ :

$$M_{\text{local}} = -0.6308 \frac{x}{c} + 1.3161 \quad (\text{C.1})$$

A turbulent flat plate correlation was used to predict the boundary layer thickness [102]:

$$\delta = \frac{kx}{Re_x^{1/6}} \quad Re_x > 10^7 \quad (\text{C.2})$$

In the general equation form,  $k$  is equal to 0.23. For the N3-X configuration, the correction factor was taken as a function of the local Mach number (Figure C.3):

$$k = 0.1196M_{\text{local}} + 0.2620 \quad (\text{C.3})$$

The boundary layer thickness diverges at the trailing edge. However, the estimate is only required for  $x/c < 1$ , as the array is mounted ahead of the trailing edge.

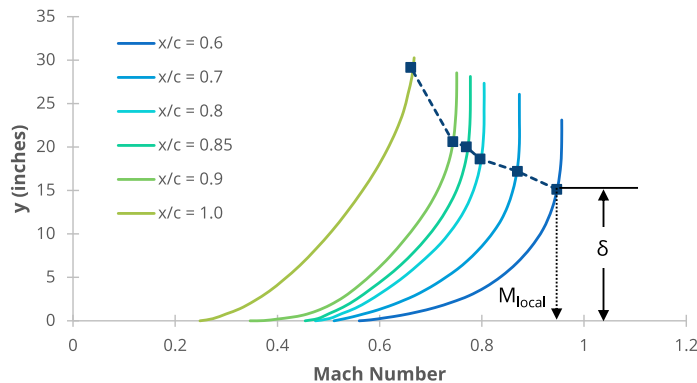


**Figure C.1:** N2A centreline boundary layer and Mach number profiles [24]

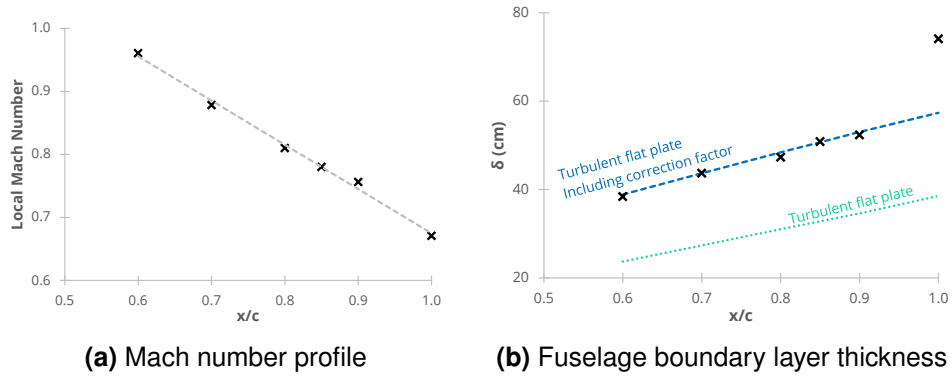


Figure C.2: N3-X airframe Mach number profile and BL thickness at centreline extracted from reference data

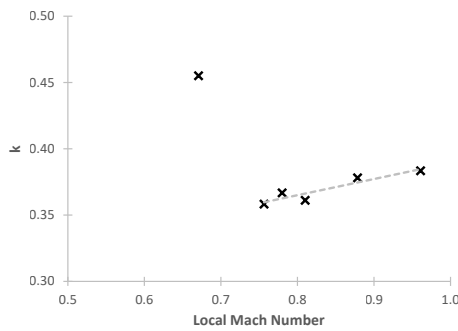


Figure C.3: Correction factor  $k$  for the turbulent boundary layer equation



## D. Atmospheric Properties

Atmospheric properties at altitude follow the US 1976 International Standard Atmosphere (ISA). The heat capacity ratio of air,  $\gamma$ , interpolates data from ESDU 00.01.08 [203].

$$T = T_n + \lambda_n (h - h_n) \quad (\text{D.1})$$

$$P = P_n \frac{T_n^{\frac{g}{R\lambda_n}}}{T} \quad \lambda_n \neq 0 \quad (\text{D.2})$$

$$P = P_n e^{\frac{-g(h-h_n)}{RT_n}} \quad \lambda_n = 0 \quad (\text{D.3})$$

$$\rho = \frac{P}{RT} \quad (\text{D.4})$$

$$a = \sqrt{\gamma RT} \quad (\text{D.5})$$

$$\mu = \mu_0 \left( \frac{T}{T_0} \right)^{1.5} \frac{T_0 - 110.4}{T + 110.4} \quad (\text{D.6})$$

- $a$  = Speed of sound
- $g$  = Gravitational acceleration (= 9.80665 m/s<sup>2</sup>)
- $h$  = Altitude (m)
- $P$  = Pressure at altitude (Pa)
- $P_n$  = Pressure at start of atmosphere level  $n$
- $R$  = Specific gas constant of air (= 287.0579 J / kg K )
- $T$  = Temperature at altitude (K)
- $T_n$  = Temperature at start of atmosphere level  $n$
- $\gamma$  = Specific heat capacity ratio of air
- $\lambda_n$  = Temperature lapse rate (K/m)
- $\mu$  = Dynamic viscosity of air at altitude (Pa.s)
- $\mu_0$  = Dynamic viscosity of air at sea level (= 0.0000181206 Pa.s)
- $\rho$  = Density of air at altitude (kg/m<sup>3</sup>)

**Table D.1:** Atmosphere layers

$n$	Altitude, $h_n$ (km)	Temperature, $T_n$ (K)	Lapse Rate, $\lambda_n$ (K/km)	Pressure, $P_n$ (Pa)
0	0	288.15	-6.5	101325
1	11	216.65	0	22632.1
2	20	216.65	1	5474.89
3	32	228.65	2.8	868.02
4	47	270.65	0	110.91
5	51	270.65	2.8	66.94
6	71	214.65	2	3.96

# E. Acquisition Cost Models

## E.1 Airframe

The Acquisition cost model primarily used functions from Resetar *et al.* [173] with updates from Younossi *et al.* [174] to provide more recent materials cost factors. Modifications are also included from the acquisition cost model from Roskam to account for the cost of aircraft interiors, finance cost, and a program difficulty factor,  $F_{\text{diff}}$ , for the development program of a novel aircraft [158].

The parametric cost functions are presented in terms of two parameters, the aircraft operating empty weight in pounds, OEW, and the aircraft maximum speed in knots,  $V_{\text{max,kts}}$ . The flight test cost also includes the number of test aircraft as a parameter,  $N_{\text{test}}$ . The majority of the cost components are calculated as man hours, which may be converted to costs using the labour rates shown in Table E.1.

Non-recurring engineering hours (thousands):

$$\text{NRENGR} = 0.0168 \text{ OEW}^{0.747} V_{\text{max,kts}}^{0.800} F_{\text{diff}} \quad (\text{E.1})$$

Non-recurring tooling hours (thousands):

$$\text{NRTOOL} = 0.0186 \text{ OEW}^{0.810} V_{\text{max,kts}}^{0.579} F_{\text{diff}} \quad (\text{E.2})$$

Development support cost (thousands of 1990 US\$):

$$\text{DS} = 0.0563 \text{ OEW}^{0.630} V_{\text{max,kts}}^{1.30} \quad (\text{E.3})$$

Flight test cost (thousands of 1990 US\$):

$$\text{FT} = 1.54 \text{ OEW}^{0.325} V_{\text{max,kts}}^{0.822} N_{\text{test}}^{1.21} \quad (\text{E.4})$$

Cumulative recurring engineering hours for first lot of 100 aircraft (thousands):

$$\text{ENGR}_{100} = 0.000306 \text{ OEW}^{0.880} V_{\text{max,kts}}^{1.12} \quad (\text{E.5})$$

Cumulative recurring tooling hours for first lot of 100 aircraft (thousands):

$$\text{TOOL}_{100} = 0.00787 \text{ OEW}^{0.707} V_{\text{max,kts}}^{0.813} \quad (\text{E.6})$$

Cumulative recurring labour hours for first lot of 100 aircraft (thousands):

$$\text{LABR}_{100} = 0.141 \text{ OEW}^{0.820} V_{\text{max,kts}}^{0.484} \quad (\text{E.7})$$

Cumulative recurring material cost for first lot of 100 aircraft (thousands of 1990 US\$):

$$\text{MATL}_{100} = 0.540 \text{ OEW}^{0.921} V_{\text{max,kts}}^{0.621} \quad (\text{E.8})$$

Cumulative recurring QA hours for first lot of 100 aircraft (thousands):

$$\text{QA}_{100} = 0.133 \text{ LABR}_{100} \quad (\text{E.9})$$

The cost functions in Equations E.5–E.9 estimate the cumulative manufacturing cost for the full first lot of aircraft, assuming that the first lot consists of 100 aircraft. The number of aircraft in the first lot may be adjusted for using a learning curve, which modifies a cost by assuming that it reduces as more products are manufactured due to improvements in the process. Learning curves take the general form of a power law. Therefore the cost of item  $n$ ,  $C_n$ , may be predicted from the cost of the first item,  $C_1$  as follows:

$$C_n = C_1 n^b \quad 0 < b < 1 \quad (\text{E.10})$$

The cost estimating relationships in Equations E.5–E.9 are for a first lot of 100 aircraft. The results may be scaled to a user-specified number of aircraft using a learning curve relationship:

$$C_{n,j} = C_{100,j} \left( \frac{n}{100} \right)^b \quad (\text{E.11})$$

Where  $n$  is the actual number of aircraft in the first lot,  $C_{100,j}$  is the cost component from Equations E.5–E.9, and  $b$  is the relevant learning exponent from Table E.1. The resulting values  $C_{n,j}$  are the cumulative cost components scaled for a first lot of  $n$  aircraft. An example case is shown below:

Sample aircraft with a cumulative engineering hours cost of \$1,500 mil for 100 aircraft (average of \$15 mil per aircraft):

$$X_{100,j} = \text{ENGR}_{100} = 1500$$

$$\bar{X}_{100,j} = \overline{\text{ENGR}}_{100} = 15$$

Learning exponent from Table E.1:

$$b = 0.485$$

Cost for the first unit:

$$X_{1,j} = \frac{X_{100,i}}{100^b}$$

$$X_{1,j} = \text{ENGR}_1 = \frac{1500}{100^{0.485}}$$

$$X_{1,j} = \text{ENGR}_1 = 60.7$$

Cumulative engineering hours cost for a lot of 120 aircraft:

$$X_{n,j} = X_{100,i} \left( \frac{n}{100} \right)^b$$

$$X_{n,j} = \text{ENGR}_{120} = 1500 \left( \frac{120}{100} \right)^{0.485}$$

$$X_{n,j} = \text{ENGR}_{120} = 1638.7$$

$$\bar{X}_{n,j} = \overline{\text{ENGR}}_{120} = 13.7$$

Cumulative cost for a lot of 120 aircraft is therefore \$1,638.7 mil (average of \$13.7 mil per aircraft).

Development costs do not need to be scaled by learning curves, as they are assumed to be one-time costs before manufacture of the commercial aircraft product begins.

Material cost factors modify each of the cost components and are calculated as follows

**Table E.1:** Labour rate and learning exponents for aircraft manufacturing and development cost [173].

Component	Labour (1990 US\$)	Learning
Engineering	80.8	0.485
Tooling	70.6	0.546
Labour	66.1	0.641
Materials	-	0.799
QA	65.6	0.641

[174]:

$$\text{WMCF}_j = \sigma_l \sum (S_m W_{\%,m}) + (1 - \sigma_l) \quad (\text{E.12})$$

Where  $S_m$  is the material cost index for the materials used in the aircraft structure (Table E.2) with a percentage by weight of the aircraft structure of  $W_{\%,m}$ . The multiple of these two terms is summed over the total number of materials types used in the airframe.  $\sigma_l$  is a factor which represents the extent to which each cost factor is influenced by weight (structure factors in Table E.2). Resetar *et al.* provide material cost factors,  $S_m$ , for the late 1980s and the mid 1990s, whilst Younossi adds further factors for the late 1990s and projects into mid 2000. An example case is presented below to calculate the materials cost weighting factor (WMCF) for the recurring engineering hours:

Sample aircraft consisting of 80% Aluminium by weight and 20% C-epoxy by weight, assuming a mid-2000 time period. The portion of recurring engineering hours attributable to materials:

$$\sigma_l = 0.42$$

The materials cost factor:

$$\text{WMCF}_j = \sigma_l \sum (S_m W_{\%,m}) + (1 - \sigma_l)$$

$$\text{WMCF}_{\text{ENGR}} = 0.42 \times (0.91 \times 0.8 + 1.18 \times 0.2) + (1 - 0.42)$$

$$\text{WMCF}_{\text{ENGR}} = 0.9849$$

Finally, the engineering hours calculated in Equation E.5 are scaled by the weighting factor:

$$\text{ENGR}_{100} = \text{ENGR}_{100} \text{WMCF}_{\text{ENGR}}$$

Taking the cumulative engineering hours cost of \$1,500mil from the previous example:

$$\text{ENGR}_{100} = 1477.4$$

Similar calculations must be made for the other elements of the cost equation using the factors shown in Table E.2 and Table E.3.

Following the calculation of each individual cost element, the overall aircraft cost may be estimated as follows:

$$X = i \sum_n \frac{C_{n,j}}{n} + C_{\text{engine}} N_{\text{engines}} \quad (\text{E.13})$$

Where  $X$  is the aircraft cost,  $C_{n,j}$  are the manufacturing cost components from Equations E.5–E.9 (scaled to the number of aircraft in the lot and by the materials weighting factor) and development cost components from Equations E.1–E.4 (scaled by the materials weighting factor),

**Table E.2:** Influence of material on cost components,  $\sigma_l$  [173].

Component		$\sigma_l$
Non-recurring		
Engineering		0.45
Tooling		0.87
Recurring		
Engineering		0.42
Tooling		0.82
Labour		0.67
Materials		0.58
QA		0.69

**Table E.3:** Factors,  $S_m$ , for calculating the materials cost weighting factor

Late 1980							
	NRENGR	NRTOOL	ENGR	TOOL	LABR	MATL	QA
Al	1.00	1.00	1.00	1.00	1.00	1.00	1.00
Al-Li	1.10	1.20	1.10	1.10	1.10	2.70	1.10
Ti	1.10	1.40	1.40	1.90	1.60	2.80	1.60
Steel	1.10	1.10	1.10	1.40	1.20	0.70	1.40
C-epoxy	1.40	1.60	1.90	2.20	1.80	4.90	2.40
C-BMI	1.50	1.70	2.10	2.30	2.10	5.50	2.50
C-thermoplastic	1.70	2.00	2.90	2.40	1.80	6.50	2.60
Mid 1990							
	NRENGR	NRTOOL	ENGR	TOOL	LABR	MATL	QA
Al	1.00	1.00	0.90	0.90	0.90	0.80	0.90
Al-Li	1.00	1.10	1.00	1.10	1.00	0.90	1.00
Ti	1.00	1.40	1.20	1.60	1.40	2.70	1.40
Steel	1.10	1.10	1.10	1.40	1.20	0.70	1.40
C-epoxy	1.20	1.40	1.50	2.00	1.50	3.80	1.80
C-BMI	1.30	1.50	1.60	2.10	1.80	4.10	2.10
C-thermoplastic	1.40	1.60	1.40	2.40	1.60	4.40	2.00
Late 1990							
	NRENGR	NRTOOL	ENGR	TOOL	LABR	MATL	QA
Al	1.00	0.97	0.97	0.94	0.94	0.80	0.95
Al-Li	1.00	1.09	1.00	1.06	1.00	0.90	1.04
Ti	1.00	1.38	1.04	1.38	1.40	2.50	1.18
Steel	1.02	1.07	1.03	1.22	1.18	0.70	1.12
C-epoxy	1.14	1.33	1.29	1.54	1.38	3.39	1.62
C-BMI	1.16	1.42	1.32	1.67	1.46	3.45	1.65
C-thermoplastic	1.14	1.59	1.26	1.75	1.50	3.84	1.71
Mid 2000							
	NRENGR	NRTOOL	ENGR	TOOL	LABR	MATL	QA
Al	1.00	0.88	0.91	0.86	0.82	0.75	0.95
Al-Li	1.00	0.99	0.94	0.97	0.87	0.84	1.04
Ti	1.00	1.26	0.97	1.26	1.29	2.37	1.18
Steel	1.02	0.97	1.02	1.12	1.05	0.70	1.12
C-epoxy	1.14	1.21	1.18	1.33	1.17	3.08	1.50
C-BMI	1.16	1.29	1.21	1.44	1.24	3.14	1.52
C-thermoplastic	1.14	1.44	1.15	1.50	1.27	3.48	1.58

and  $n$  is the number of aircraft in the first lot. In order to cover the full aircraft cost, the cost of the engines,  $C_{\text{engines}}$  must also be included.

Additions from the acquisition cost model by Roskam's account provides a simple estimate for the cost of the aircraft interior as follows [158]:

$$C_{\text{interior}} = 2000N_{\text{pax}} \quad (\text{E.14})$$

Including the finance cost with a finance rate of  $r_{\text{finance}}$ , the acquisition price of an aircraft is estimated as follows:

$$X = i(1 + r_{\text{finance}}) \left[ \frac{\sum C_{n,j}}{n} + C_{\text{interior}} \right] + C_{\text{engine}}N_{\text{engines}} \quad (\text{E.15})$$

The factor  $i$  corrects for the inflation rate between the dollar year of the model and the current year. In addition to providing the parametric cost functions, Resetar et al's models quote the standard error of the estimate. These standard errors may be used to estimate the confidence intervals for the cost estimate.

## E.2 Engine

Three methods were used to create an estimate for the acquisition cost of the aircraft propulsion system:

- Birkler *et al.* [175]
- Younossi *et al.* [167]
- Regression analysis of weight and thrust using publicly available data [204]

### E.2.1 Birkler *et al.*

For a subsonic engine, the parametric cost functions are presented in terms of two parameters: the engine maximum thrust in pounds force,  $FN_{\text{max}}$ , and the maximum engine temperature in Fahrenheit,  $T_{\text{max}}$ .

Development cost (millions of 1980 US\$):

$$\text{DEVCOSt} = -525.763 + 0.023FN_{\text{max}} + 0.07T_{\text{max}}$$

Production cost (thousands of 1980 US\$):

$$\text{PROCOST} = -2228.14 + 0.043FN_{\text{max}} + 0.969T_{\text{max}}$$

Following the calculation of each cost element, the overall engine cost may be estimated as follows:

$$C_{\text{engine}} = i \left[ \frac{\text{DEVCOSt}}{N_{\text{engines}}} + \text{PROCOST} \right]$$

### E.2.2 Younossi *et al.*

The parametric cost functions are presented in terms of four parameters: the engine maximum thrust in pounds force,  $FN_{\text{max}}$ , the maximum engine temperature in Rankine,  $T_{\text{max}}$ , the engine specific fuel consumption in lb/hr/lbf,  $\text{SFC}$ , and the engine weight in pounds,  $W_{\text{engine}}$ . An assumption of 6000 test hours,  $H_{\text{test}}$ , is also included for the development program of a derivative engine.

Development cost for a new engine (millions of 2000 US\$):

$$\text{DEVCOSt}_{\text{new}} = \exp[-24.429 + 4.027 \ln(T_{\text{max}})]$$

Development cost for a derivative engine (millions of 2000 US\$):

$$\text{DEVCOSt}_{\text{derivative}} = \exp[-39.422 + 5.066 \ln(T_{\text{max}}) - 1.299 \ln(\text{SFC}) + 0.582 \ln(H_{\text{test}})]$$

The production cost of the first unit (millions of 2000 US\$):

$$\text{PROCOST} = \exp[-10.4 - 8.55 \ln(0.85) + 1.162 \ln(T_{\text{max}}) + 0.262 \ln(W_{\text{engine}})]$$

The production cost is for the first unit only. Subsequent engine costs can be estimated using the assumed 85% learning curve slope (see Equation E.10 and Equation E.11 for scaling cost by a learning curve). The engine cost is therefore calculated as the average for a cumulative set of engines in the first lot. The development cost depends on whether a new or derivative engine is assumed. Following the calculation of each cost element, the average engine cost may be estimated as follows:

$$C_{\text{engine}} = \frac{i}{N_{\text{engines}}} \left[ \sum_{n=1}^{N_{\text{engines}}} (\text{PROCOST} \times n^{-0.234}) + \text{DEVCOSt} \right]$$

### E.2.3 Regression Model

A simple regression analysis for engine cost was created as functions of engine weight in kg,  $W_{\text{engine}}$ , and engine maximum thrust rating in kN,  $\text{FN}_{\text{max}}$ . The regressions were created using publicly available data of the list price of aerospace engines (Table E.4). Separate regressions were produced as a function of thrust and of engine weight (Figure 6.8).

Overall engine cost as a function of maximum thrust may be estimated as follows (millions of 2017 US\$):

$$C_{\text{engine}} = 0.03804\text{FN}_{\text{max}} + 3.3664 \quad R^2 = 0.8135$$

Overall engine cost as a function of weight may be estimated as follows (millions of 2017 US\$):

$$C_{\text{engine}} = 0.002134W_{\text{engine}} + 2.9143 \quad R^2 = 0.8098$$

**Table E.4:** Engine data for regression analysis [204]

<b>Engine</b>	<b>Weight (kg)</b>	<b>Thrust (kN)</b>	<b>Unit Cost (US\$mil)</b>
CFM56-5B	2380	130	10.0
GE90-115B	8283	514	20.0
Trent 1000	5765	320	17.0
F117-PW-100	3221	180	8.4
AE 3007	719	35.45	1.4
CF34-10	1678	78.5	3.0
CF6-80E1	5090	310	16.0
GENx-1B64	5816	284	13.0
GENx-2B	5600	-	12.0
GP7270	6712	363	15.0
PW4062	4340	253.55	15.0
Trent 772	4785	316.3	16.0
Trent XWB	7500	352.5	20.0
F404-GE-IN20	1035	48.9	6.0
Adour	809	-	5.5
AL-31F	1570	74.5	3.5
F100-PW-229	1700	79	3.5
F119-PW-100	1800	106.4	9.5
EJ200	990	60	9.5
LEAP-1A	-	127.5	12.0



# F. Maintenance Cost Models

The following appendix provides an overview of the relationships used to provide a maintenance cost estimate for the baseline aircraft and the N3-X.

## F.1 Airframe

The airframe maintenance cost model developed by Liebeck *et al.* in 1995 [54] was used to estimate the maintenance cost of the baseline aircraft and the N3-X. Materials cost scale factors (WMCF) from the acquisition cost estimate were used to scale the labour and material costs elements (see Appendix E).

The model breaks cost down into the costs of labour, material costs, and maintenance burden. The labour and materials costs are further split into costs per flight hour (FH) and costs per flight cycle (FC). These must be summed to estimate the overall cost per flight. The average cost per trip or per flight hour is represented as a function of airframe weight in pounds (AFW) and flight length. The airframe labour cost (AFLAB) and material cost (AFMAT) per flight hour were scaled by the previously identified material scaling factors. The model assumes a labour rate (RL) of \$25.00 per man hour (1995 US\$). The resulting maintenance cost estimates must be scaled by the rate of inflation from 1995 to the current year.

The following cost estimating relationships were used to estimate airframe maintenance cost (including materials scaling factors where relevant). Labour hours per flight hour:

$$AFLAB_{FH} = 1.260 + (1.774AFW \times 10^{-5}) - 0.1071 (AFW \times 10^{-5})^2 \quad (F.1)$$

Labour hours per flight cycle:

$$AFLAB_{FC} = 1.614 + (0.7227AFW \times 10^{-5}) + 0.1024 (AFW \times 10^{-5})^2 \quad (F.2)$$

Total labour cost per flight (1995 US\$):

$$AFLAB = WMCF_{LAB} (AFLAB_{FH}FH + AFLAB_{FC}) RL \quad (F.3)$$

Material cost per flight hour (1995 US\$):

$$AFMAT_{FH} = 12.39 + (29.80AFW \times 10^{-5}) + 0.1806 (AFW \times 10^{-5})^2 \quad (F.4)$$

Material cost per flight cycle (1995 US\$):

$$AFMAT_{FC} = 15.20 + (97.33AFW \times 10^{-5}) - 2.862 (AFW \times 10^{-5})^2 \quad (F.5)$$

Total material cost per flight (1995 US\$):

$$AFMAT = WMCF_{MAT} (AFMAT_{FH}FH + AFMAT_{FC}) \quad (F.6)$$

Maintenance burden per flight (1995 US\$):

$$AFMAB = 2.0AFLAB \quad (F.7)$$

Total airframe maintenance cost per flight:

$$C_{\text{maint,AF,trip}} = \text{AFLAB} + \text{AFMAT} + \text{AFMAB} \quad (\text{F.8})$$

Total airframe maintenance cost per flight hour:

$$C_{\text{maint,AF}} = \frac{C_{\text{maint,AF,trip}}}{\text{FH}} \quad (\text{F.9})$$

## F.2 Engine

The engine maintenance cost model developed by Seeman et al in 2011 [191] was used to estimate the maintenance cost of the baseline aircraft and N3-X engines. In the case of the N3-X, an 'equivalent' thrust-producing engine was used, as the cost estimating relationships rely on thrust as a variable.

The model differentiates engine maintenance cost estimates for 'first run' and 'mature' engines. In both cases, an interval between shop visits is estimated (in terms of number of flight hours). Subsequently, a shop visit cost is estimated. Maintenance cost per flight hour is then taken to be the average maintenance cost per flight hour, accounting for the maintenance costs of both the first run and mature engine. Costs may be further scaled by severity factors to account for factors such as engine derate and environment. These factors were not applied in the present research, as no derate was used and environmental factors were not required. A severity factor scaling for the number of flight hours is used in the maintenance cost of method. The cost estimating relationships are functions of the engine weight in pounds (ENGW), the engine's maximum thrust in pounds force ( $F_{N,\text{max}}$ ), and the thrust-to-weight ratio (TWR). As with the airframe maintenance cost, the final maintenance cost per flight hour estimate must be corrected for inflation from the model year (2011) to the current year.

The following cost estimating relationships were used to estimate engine maintenance cost. Interval between shop visits in flight hours for first run engine:

$$I_{\text{FR}} = 22539 + 1.433 \times \text{ENGW} - 0.315 \times F_{N,\text{max}} + \left[ (F_{N,\text{max}} - 76305)^2 \times 3.44 \times 10^{-6} \right] \quad (\text{F.10})$$

Interval between shop visits in flight hours for mature engine:

$$I_{\text{MR}} = 34415 - 2759.25 \times \text{TWR} - 0.3663 \times \text{ENGW} + \left[ (\text{AFW} - 12072)^2 \times 1.01795 \times 10^{-4} \right] \quad (\text{F.11})$$

Shop visit restoration cost per flight hour for first run engine (2011 US\$):

$$\text{SVRC}_{\text{FR}} = 7 + 0.00236189 \times F_{N,\text{max}} \quad (\text{F.12})$$

Shop visit restoration cost per flight hour for mature engine (2011 US\$):

$$\text{SVRC}_{\text{MR}} = 46 + 0.00288612 \times F_{N,\text{max}} \quad (\text{F.13})$$

Life limited part cost per flight cycle (2011 US\$):

$$\text{LLP} = -115 + 0.01945 \times \text{ENGW} + 0.003121 \times F_{N,\text{max}} + \left[ (\text{ENGW} - 8608.781)^2 \times 2.69 \times 10^{-6} \right] \quad (\text{F.14})$$

Shop visit cost of first run engine (2011 US\$):

$$\text{SV}_{\text{FR}} = \text{LLP} \times \frac{I_{\text{FR}}}{\text{FH}} + \text{SVRC}_{\text{FR}} \times I_{\text{FR}} \quad (\text{F.15})$$

Shop visit cost of mature engine (2011 US\$):

$$SV_{MR} = LLP \times \frac{I_{MR}}{FH} + SVRC_{MR} \times I_{MR} \quad (F.16)$$

Average maintenance cost per flight hour per engine:

$$C_{\text{maint,ENG}} = \frac{SV_{FR} + SV_{MR}}{I_{FR} + I_{MR}} \quad (F.17)$$